

Univerza
v Ljubljani

Fakulteta za
*gradbeništvo in
geodezijo*



PODIPLOMSKI ŠTUDIJ
GRADBENIŠTVA

DOKTORSKI ŠTUDIJ

Kandidat:

VLADIMIR VUKOBRATOVIĆ, univ.dipl.inž.grad.-master

**VPLIV NELINEARNEGA POTRESNEGA ODZIVA
KONSTRUKCIJ NA ETAŽNE SPEKTRE POSPEŠKOV**

Doktorska disertacija štev.: 245

**THE INFLUENCE OF NONLINEAR SEISMIC
RESPONSE OF STRUCTURES ON THE FLOOR
ACCELERATION SPECTRA**

Doctoral thesis No.: 245

Soglasje k temi doktorske disertacije je dala Komisija za doktorski študij UL
na 18. redni seji, dne 8. junija 2011.

Za mentorja je bil imenovan akad. prof. dr. Peter Fajfar.

Pisanje v angleškem jeziku je odobrila Komisija za doktorski študij UL
na 18. redni seji, dne 8. junija 2011.

Ljubljana, 8. junij 2015

Univerza
v Ljubljani

Fakulteta za
*gradbeništvo in
geodezijo*



Komisijo za oceno ustreznosti teme doktorske disertacije v sestavi:

- akad. prof. dr. Peter Fajfar,
- izr. prof. dr. Matjaž Dolšek,
- prof. dr. Mehmed Čaušević, Univerza na Reki, Gradbena fakulteta,

je imenoval Senat Fakultete za gradbeništvo in geodezijo na 19. redni seji, dne 30. marca 2011.

Poročevalce za oceno doktorske disertacije v sestavi:

- prof. dr. Tatjana Isaković, UL FGG,
- doc. dr. Iztok Peruš, UM FG,
- prof. dr. Mehmed Čaušević, Univerza na Reki, Gradbena fakulteta,

je imenoval Senat Fakultete za gradbeništvo in geodezijo na 18. redni seji, dne 25. marca 2015.

Komisijo za zagovor doktorske disertacije v sestavi:

- prof. dr. Matjaž Mikoš, dekan UL FGG, predsednik,
- akad. prof. dr. Peter Fajfar, mentor,
- prof. dr. Tatjana Isaković, UL FGG,
- doc. dr. Iztok Peruš, UM FG,
- prof. dr. Mehmed Čaušević, Univerza na Reki, Gradbena fakulteta,

je imenoval Senat Fakultete za gradbeništvo in geodezijo na 20. redni seji, dne 27. maja 2015.

IZJAVA O AVTORSTVU

Podpisani **Vladimir Vukobratović** izjavljam, da sem avtor doktorske disertacije z naslovom **Vpliv nelinearnega potresnega odziva konstrukcij na etažne spektre pospeškov**.

Izjavljam, da je elektronska različica v vsem enaka tiskani različici.

Izjavljam, da dovoljujem objavo elektronske različice v repozitoriju UL FGG.

STATEMENT OF AUTHORSHIP

I, undersigned **Vladimir Vukobratović** hereby declare that I am the author of the doctoral dissertation titled **The influence of nonlinear seismic response of structures on the floor acceleration spectra**.

I declare that the electronic version is entirely identical to the printed version.

I declare that I allow publication of the electronic version in the repository of the UL FGG.

Ljubljana, 8. junij 2015

.....
(podpis / signature)

This page is intentionally left blank.

ERRATA

Page	Line	Error	Correction
-------------	-------------	--------------	-------------------

BIBLIOGRAPHIC – DOCUMENTALISTIC INFORMATION AND ABSTRACT

UDC: 624.012.45:624.042.7(043)
Author: Vladimir Vukobratović, M.Sc. in Civil Engineering
Supervisor: Prof. Peter Fajfar, Ph.D.
Title: The influence of nonlinear seismic response of structures on the floor acceleration spectra
Document type: Doctoral dissertation
Notes: 208 p., 8 tab., 127 fig., 34 eq., 8 ann.
Keywords: floor response spectra, direct method, parametric study, response-history analysis, primary structure, secondary structure, equipment, inelastic behaviour, ductility, peak floor acceleration

Abstract

Floor acceleration spectra, which are important for seismic design and assessment of acceleration-sensitive equipment, were studied in the dissertation. A relatively simple practice-oriented method for the determination of floor acceleration spectra directly from the ground motion spectra was developed. Elastic and inelastic structural behaviour was taken into account. Extensive parametric studies were performed on single- (SDOF) and multi-degree-of-freedom (MDOF) structures and a large number of floor acceleration (response) spectra were calculated by using the response-history analysis (RHA). In the case of SDOF structures two different sets of ground records were used, whereas in the case of MDOF structures only one of these sets was considered. The influences of the type, natural period, hysteretic behaviour, and ductility of the primary structure, as well as the influence of the equipment damping, were studied. Additionally, in the case of SDOF structures, the influence of input ground motion characteristics was also investigated. The obtained results confirmed the fact that inelastic behaviour of the primary structure can significantly reduce floor acceleration spectra, especially their peak values. The method for direct determination of floor response spectra was firstly developed for SDOF structures and it was validated by comparing its results with the floor response spectra obtained from the RHA. A good agreement between the results obtained for both elastic and inelastic structural behaviour was observed. The method was extended to MDOF structures and it was coupled with the nonlinear pushover-based N2 method. In the case of elastic structures the method provides floor response spectra which are in very good agreement with the results obtained from the RHA. In the case of inelastic structures, in general, a satisfactory accuracy can be achieved.

BIBLIOGRAFSKO – DOKUMENTACIJSKA STRAN IN IZVLEČEK

UDK: 624.012.45:624.042.7(043)
Avtor: Vladimir Vukobratović, univ. dipl. inž. grad. - master
Mentor: prof. dr. Peter Fajfar
Naslov: Vpliv nelinearnega potresnega odziva konstrukcij na etažne spektre pospeškov
Tip dokumenta: Doktorska disertacija
Obseg in oprema: 208 str., 8 pregl., 127 sl., 34 en., 8 pril.
Ključne besede: etažni spektri odziva, direktna metoda, parametrična študija, časovna analiza odziva, primarna konstrukcija, sekundarna konstrukcija, oprema, neelastično obnašanje, duktilnost, maksimalni etažni pospešek

Izvleček

V disertaciji so obravnavani etažni spektri pospeškov, ki so pomembni za potresno projektiranje in ocenjevanje opreme, občutljive na pospeške. Razvita je razmeroma enostavna za prakso uporabna metoda za določanje etažnih spektrov pospeškov iz spektrov tal. Upoštevano je bilo elastično in neelastično obnašanje konstrukcije. Obsežne parametrične študije so bile izvedene za modele konstrukcije z eno (SDOF) in več prostostnimi (MDOF) stopnjami. S časovno analizo odziva (RHA) je bilo izračunano veliko število etažnih spektrov pospeškov. V primeru SDOF konstrukcij sta bili uporabljeni dve neodvisni skupini akcelrogramov, v primeru MDOF konstrukcij pa je bila upoštevana le ena od teh skupin. Raziskovani so bili vplivi tipa, nihajnega časa, histereznega obnašanja in duktilnosti primarne konstrukcije, in vpliv dušenja opreme. Za SDOF konstrukcije je bil raziskan tudi vpliv karakteristik vhodnih akcelrogramov. Dobljeni rezultati so potrdili dejstvo, da neelastično obnašanje primarne konstrukcije lahko pomembno zmanjša etažne spektre pospeškov, zlasti njihove maksimalne vrednosti. Metoda za direktno določanje etažnih spektrov je bila najprej razvita za SDOF konstrukcije in potrjena s primerjavo njenih rezultatov z etažnimi spektri, dobljenimi z RHA. Opaženo je bilo dobro ujemanje rezultatov, dobljenih za elastično in neelastično obnašanje konstrukcije. Metoda je bila razširjena na MDOF konstrukcije in povezana z nelinearno N2 metodo, ki temelji na potisni analizi. V primeru elastičnih konstrukcij daje metoda etažne spektre pospeškov, ki se zelo dobro ujema z rezultati, dobljenimi z RHA. V primeru neelastičnih konstrukcij je v splošnem mogoče doseči zadovoljivo natančnost.

This page is intentionally left blank.

ACKNOWLEDGMENTS

Undertaking PhD studies has been a big step and a life-changing experience for me. Even though there were times when I doubted whether such a step was right or wrong, I am now totally sure that it was one of the best choices I have ever made.

First, I wish to thank my mentor, professor Peter Fajfar. It has been a great honor to be his student. He has been supportive since the day I started PhD studies at the University of Ljubljana. The road to finish this dissertation was sometimes rough. In both good and bad times, professor Fajfar supported me not only as an academic advisor, but also as a friend. Being his student is not only an honor, but also a big commitment. By setting high standards, he has managed to make me achieve the results of which I am very proud. He was and remains my best role model for a scientist, mentor and teacher.

A lot of love, patience, understanding and support of my family have followed me not only during my PhD studies, but also throughout my whole life. My sister Nataša has always inspired me with her optimism and positive thinking. Her great faith in me is something I can never forget. My mother Ružica is the most responsible for my interests in science. She generously helped me to make my first steps in the scientific field, by spending a great time by my side throughout early days of my education. She has showered me with her care all my life. For everything she has ever done for me, I am forever grateful. My father Goran invested a lot of time, energy and effort to provide me with an opportunity to become a respected part of academic community. He always instructed me on how to distinguish right from wrong, he taught me about honesty, and he made me become a good and decent person. His visions will always illuminate my ways. Without my family, I would never succeed.

Finally, I would like to thank my loving wife Miroslava. She was a perfect fellow traveler for all years behind us and she will remain my biggest inspiration in the time that comes.

This page is intentionally left blank.

TABLE OF CONTENTS

STATEMENT OF AUTHORSHIP	I
ERRATA	III
BIBLIOGRAPHIC – DOCUMENTALISTIC INFORMATION AND ABSTRACT	IV
BIBLIOGRAFSKO – DOKUMENTACIJSKA STRAN IN IZVLEČEK	V
ACKNOWLEDGMENTS	VII
TABLE OF CONTENTS	IX
LIST OF TABLES	XI
LIST OF FIGURES	XII
KAZALO PREGLEDNIC	XVIII
KAZALO SLIK	XIX
SYMBOLS	XXV
ABBREVIATIONS	XXVII
1 INTRODUCTION	1
1.1 The theme of the doctoral dissertation	1
1.2 State of the art at the relevant scientific field	3
1.3 The structure of the doctoral dissertation	10
2 PARAMETRIC STUDY OF FLOOR RESPONSE SPECTRA FOR SINGLE-DEGREE-OF-FREEDOM STRUCTURES	12
2.1 Description of seismic input and structural models	12
2.2 Analysis of structural models	14
2.3 Results of the study	15
3 A METHOD FOR DIRECT GENERATION OF FLOOR RESPONSE SPECTRA FOR SINGLE-DEGREE-OF-FREEDOM STRUCTURES	44
3.1 Original method	44
3.2 Extension and modifications of the original method	45
3.3 Comparison of the original and proposed direct method for elastic structures	51
3.4 Validation of the proposed direct method	52
3.5 Comparison of the proposed method with the provisions of Eurocode 8 (2004)	68
3.6 Comparison of the proposed method with the method proposed by Sullivan et al. (2013)	69
3.7 Example of the application of the proposed method	72
4 PARAMETRIC STUDY OF FLOOR RESPONSE SPECTRA FOR MULTI-DEGREE-OF FREEDOM STRUCTURES	73
4.1 Description of seismic input, structural models and structural analysis	73
4.2 Results of the study	79
4.2.1 Results obtained for structure W03	80
4.2.2 Results obtained for structure W10	85
4.2.3 Results obtained for structure F03	90

4.2.4	Results obtained for structure F10	95
4.2.5	Influence of individual modes on floor response spectra	103
5	PEAK FLOOR ACCELERATIONS IN MULTI-DEGREE-OF-FREEDOM STRUCTURES	115
5.1	Introduction	115
5.2	Estimation of peak floor accelerations in elastic and inelastic MDOF structures	116
5.2.1	Results obtained for elastic MDOF structures	117
5.2.2	Results obtained for inelastic MDOF structures	119
6	A METHOD FOR DIRECT GENERATION OF FLOOR RESPONSE SPECTRA FOR MULTI-DEGREE-OF-FREEDOM STRUCTURES	124
6.1	Formulation of the direct method	124
6.1.1	Direct floor response spectra for individual modes	124
6.1.2	Combination of direct floor response spectra obtained for individual modes	126
6.2	Validation of the proposed method – elastic structures	128
6.3	Validation of the proposed method – inelastic structures	129
7	A STEP-BY-STEP OVERVIEW OF THE METHOD FOR DIRECT GENERATION OF FLOOR RESPONSE SPECTRA FOR MDOF STRUCTURES	168
7.1	Main steps in the application of the direct method	168
7.2	Numerical example of the application of the direct method	170
7.2.1	Modal analysis	170
7.2.2	Application of the N2 method on the fundamental mode	170
7.2.3	Determination of PFAs and floor response spectra for individual modes	172
7.2.4	Combination of PFAs and floor response spectra obtained for individual modes	177
8	CONCLUSIONS	181
8.1	Main findings	181
8.2	Original contributions	186
8.3	Suggestions for further research	187
	POVZETEK	189
	REFERENCES	203
ANNEX A	Derivation of the direct method proposed by Yasui et al. (1993)	
ANNEX B	Application of the reduction factor R_{μ} in the seismic design of equipment	
ANNEX C	Evaluation of the equation for determination of the effective natural period of the structure proposed by Akiyama (1985)	
ANNEX D	Overview of the N2 method	
ANNEX E	Formula for direct generation of floor response spectra outside the resonance region for MDOF structures	
ANNEX F	Overview of modal combination rules proposed by USNRC 1.92 (2006)	
ANNEX G	Derivation of Equation G.1	
ANNEX H	A brief analysis of scatter related to the seismic input and floor response spectra	

LIST OF TABLES

Table 2.1:	Data of the selected set of ground motions which corresponds to soil type B	13
Table 2.2:	Data of the selected set of ground motions which corresponds to soil type D	14
Table 3.1:	Errors of the approximate spectra in comparison to the "exact" inelastic spectra, soil type B	46
Table 3.2:	Errors of the approximate spectra in comparison to the "exact" inelastic spectra, soil type D	47
Table 3.3:	The amplification factors AMP used in the numerical example	72
Table 4.1:	Axial forces (N), yield moments (M_y) and rotations (θ_y) in plastic hinges (frame F03)	77
Table 4.2:	Axial forces (N), yield moments (M_y) and rotations (θ_y) in plastic hinges (frame F10)	79
Table 7.1:	Gupta's coefficients for modal combination (elastic and Q_0 structure F03)	177

LIST OF FIGURES

Figure 1.1:	Illustration of the floor response spectra concept	2
Figure 2.1:	Elastic acceleration spectra (5% damping) of individual records, target and mean spectrum for (a) soil type B (target spectrum with PGA=0.35g) and (b) soil type D (target spectrum with PGA=0.39g)	15
Figure 2.2:	Hysteretic behaviour of (a) elasto-plastic (EP) and stiffness degrading (Q) model with (b) zero (Q_0) and (c) 10% hardening (Q_{10})	15
Figure 2.3:	Mean values of the floor response spectra (A_s) and peak accelerations (A_p) for the structures with natural periods equal to 0.2 and 0.3 s, 5% damping of the structure and soil type B	18
Figure 2.4:	Mean values of the floor response spectra (A_s) and peak accelerations (A_p) for the structures with natural periods equal to 0.5 and 0.75 s, 5% damping of the structure and soil type B	19
Figure 2.5:	Mean values of the floor response spectra (A_s) and peak accelerations (A_p) for the structures with natural periods equal to 1.0 and 2.0 s, 5% damping of the structure and soil type B	20
Figure 2.6:	Mean values of the floor response spectra (A_s) and peak accelerations (A_p) for the structures with natural periods equal to 0.2 and 0.3 s, 5% damping of the structure and soil type D	21
Figure 2.7:	Mean values of the floor response spectra (A_s) and peak accelerations (A_p) for the structures with natural periods equal to 0.5 and 0.75 s, 5% damping of the structure and soil type D	22
Figure 2.8:	Mean values of the floor response spectra (A_s) and peak accelerations (A_p) for the structures with natural periods equal to 1.0 and 2.0 s, 5% damping of the structure and soil type D	23
Figure 2.9:	The ratio of the floor response spectra of the inelastic and elastic structures with natural periods equal to 0.2 and 0.3 s, 5% damping of the structure and soil type B	24
Figure 2.10:	The ratio of the floor response spectra of the inelastic and elastic structures with natural periods equal to 0.5 and 0.75 s, 5% damping of the structure and soil type B	25
Figure 2.11:	The ratio of the floor response spectra of the inelastic and elastic structures with natural periods equal to 1.0 and 2.0 s, 5% damping of the structure and soil type B	26
Figure 2.12:	The ratio of the floor response spectra of the inelastic and elastic structures with natural periods equal to 0.2 and 0.3 s, 5% damping of the structure and soil type D	27
Figure 2.13:	The ratio of the floor response spectra of the inelastic and elastic structures with natural periods equal to 0.5 and 0.75 s, 5% damping of the structure and soil type D	28
Figure 2.14:	The ratio of the floor response spectra of the inelastic and elastic structures with natural periods equal to 1.0 and 2.0 s, 5% damping of the structure and soil type D	29
Figure 2.15:	Floor response spectra normalized to the peak acceleration of the structures with natural periods equal to 0.2 and 0.3 s, 5% damping of the structure and soil type B	30

Figure 2.16:	Floor response spectra normalized to the peak acceleration of the structures with natural periods equal to 0.5 and 0.75 s, 5% damping of the structure and soil type B	31
Figure 2.17:	Floor response spectra normalized to the peak acceleration of the structures with natural periods equal to 1.0 and 2.0 s, 5% damping of the structure and soil type B	32
Figure 2.18:	Floor response spectra normalized to the peak acceleration of the structures with natural periods equal to 0.2 and 0.3 s, 5% damping of the structure and soil type D	33
Figure 2.19:	Floor response spectra normalized to the peak acceleration of the structures with natural periods equal to 0.5 and 0.75 s, 5% damping of the structure and soil type D	34
Figure 2.20:	Floor response spectra normalized to the peak acceleration of the structures with natural periods equal to 1.0 and 2.0 s, 5% damping of the structure and soil type D	35
Figure 2.21:	A comparison of floor response spectra obtained for different Q models, for the structures with natural periods equal to 0.2 and 0.3 s and 5% damping, soil type B	36
Figure 2.22:	A comparison of floor response spectra obtained for different Q models, for the structures with natural periods equal to 0.5 and 0.75 s and 5% damping, soil type B	37
Figure 2.23:	A comparison of floor response spectra obtained for different Q models, for the structures with natural periods equal to 1.0 and 2.0 s and 5% damping, soil type B	38
Figure 2.24:	A comparison of floor response spectra normalized to the peak acceleration of the structure obtained for different Q models, structures with natural periods equal to 0.2 and 0.3 s and 5% damping, soil type B	39
Figure 2.25:	A comparison of floor response spectra normalized to the peak acceleration of the structure obtained for different Q models, structures with natural periods equal to 0.5 and 0.75 s and 5% damping, soil type B	40
Figure 2.26:	A comparison of floor response spectra normalized to the peak acceleration of the structure obtained for different Q models, structures with natural periods equal to 1.0 and 2.0 s and 5% damping, soil type B	41
Figure 2.27:	The amplification factors (<i>AMP</i>) computed in the parametric study for the EP model of the structure	42
Figure 2.28:	The amplification factors (<i>AMP</i>) computed in the parametric study for the Q_{10} model of the structure	42
Figure 2.29:	The amplification factors (<i>AMP</i>) versus the damping of the equipment represented as mean values depending on the ratio T_p/T_C	43
Figure 3.1:	"Exact" and approximate inelastic spectra for soil types B and D (5% damping of the structure)	47
Figure 3.2:	A comparison between (a) the "exact" and (b) the approximate inelastic acceleration spectra for the structure (5% damping) obtained for two different Q models, soil type B	47
Figure 3.3:	Proposed amplification factors and comparison with <i>AMP</i> obtained in the parametric study	49
Figure 3.4:	A comparison of the floor response spectra for elastic structures for soil type B, 5% damping of the structure	51

Figure 3.5:	Floor response spectra for the EP model of the structure, natural periods equal to 0.2 and 0.3 s, 5% damping of the structure, soil type B	53
Figure 3.6:	Floor response spectra for the EP model of the structure, natural periods equal to 0.5 and 0.75 s, 5% damping of the structure, soil type B	54
Figure 3.7:	Floor response spectra for the EP model of the structure, natural periods equal to 1.0 and 2.0 s, 5% damping of the structure, soil type B	55
Figure 3.8:	Floor response spectra for the EP model of the structure, natural periods equal to 0.2 and 0.3 s, 5% damping of the structure, soil type D	56
Figure 3.9:	Floor response spectra for the EP model of the structure, natural periods equal to 0.5 and 0.75 s, 5% damping of the structure, soil type D	57
Figure 3.10:	Floor response spectra for the EP model of the structure, natural periods equal to 1.0 and 2.0 s, 5% damping of the structure, soil type D	58
Figure 3.11:	Floor response spectra for the Q_{10} model of the structure, natural periods equal to 0.2 and 0.3 s, 5% damping of the structure, soil type B	59
Figure 3.12:	Floor response spectra for the Q_{10} model of the structure, natural periods equal to 0.5 and 0.75 s, 5% damping of the structure, soil type B	60
Figure 3.13:	Floor response spectra for the Q_{10} model of the structure, natural periods equal to 1.0 and 2.0 s, 5% damping of the structure, soil type B	61
Figure 3.14:	Floor response spectra for the Q_{10} model of the structure, natural periods equal to 0.2 and 0.3 s, 5% damping of the structure, soil type D	62
Figure 3.15:	Floor response spectra for the Q_{10} model of the structure, natural periods equal to 0.5 and 0.75 s, 5% damping of the structure, soil type D	63
Figure 3.16:	Floor response spectra for the Q_{10} model of the structure, natural periods equal to 1.0 and 2.0 s, 5% damping of the structure, soil type D	64
Figure 3.17:	Floor response spectra for the Q_0 model of the structure, natural periods equal to 0.2 and 0.3 s, 5% damping of the structure, soil type B	65
Figure 3.18:	Floor response spectra for the Q_0 model of the structure, natural periods equal to 0.5 and 0.75 s, 5% damping of the structure, soil type B	66
Figure 3.19:	Floor response spectra for the Q_0 model of the structure, natural periods equal to 1.0 and 2.0 s, 5% damping of the structure, soil type B	67
Figure 3.20:	Floor response spectra obtained by Eurocode 8 (2004) and the proposed method for (a) EP and (b) Q_{10} models with $\mu=2$, T_p equal to 0.3, 0.5, 0.75 and 1.0 s, type 1 spectrum, soil type B, 5% damping, $\alpha_g S=0.30g$	69
Figure 3.21:	Floor response spectra obtained by two direct approaches for the Q_{10} model of the structure, natural periods equal to 0.3 and 1.0 s, 5% damping of the structure, soil type B	70
Figure 3.22:	Floor response spectra obtained by two direct approaches for the Q_{10} model of the structure, natural periods equal to 0.3 and 1.0 s, 5% damping of the structure, soil type D	71
Figure 3.23:	Floor response spectra obtained by the proposed direct method for (a) the elastic model and (b) the Q_{10} model of the structure with 5% damping, soil type B (PGA=0.35g)	72
Figure 4.1:	Elastic acceleration spectra (5% damping) of individual records, modified target and mean spectrum for soil type B	74
Figure 4.2:	Reinforcement at the bottom of the wall W03 (plastic hinge region)	75
Figure 4.3:	Reinforcement of columns and beams in frame F03	77
Figure 4.4:	Reinforcement of columns and beams in frame F10	78

Figure 4.5:	(a) Pushover curves for MDOF and SDOF systems and (b) Capacity diagram for the EP model	80
Figure 4.6:	(a) Pushover curves for MDOF and SDOF systems and (b) Capacity diagram for the Q_0 model	81
Figure 4.7:	Mean values of the floor response spectra normalized with the mean PGA, structure W03 (1% damping of the equipment)	83
Figure 4.8:	Mean values of the floor response spectra normalized with the mean PGA, structure W03 (5% damping of the equipment)	84
Figure 4.9:	(a) Pushover curves for MDOF and SDOF systems and (b) Capacity diagram for the EP model	86
Figure 4.10:	(a) Pushover curves for MDOF and SDOF systems and (b) Capacity diagram for the Q_0 model	87
Figure 4.11:	Mean values of the floor response spectra normalized with the mean PGA, structure W10 (1% damping of the equipment)	88
Figure 4.12:	Mean values of the floor response spectra normalized with the mean PGA, structure W10 (5% damping of the equipment)	89
Figure 4.13:	(a) Pushover curves for MDOF, SDOF and idealized SDOF system and (b) Capacity diagram for the EP model	91
Figure 4.14:	(a) Pushover curves for MDOF, SDOF and idealized SDOF system and (b) Capacity diagram for the Q_0 model	92
Figure 4.15:	Mean values of the floor response spectra normalized with the mean PGA, structure F03 (1% damping of the equipment)	93
Figure 4.16:	Mean values of the floor response spectra normalized with the mean PGA, structure F03 (5% damping of the equipment)	94
Figure 4.17:	(a) Pushover curves for MDOF, SDOF and idealized SDOF system and (b) Capacity diagram for the EP model	95
Figure 4.18:	(a) Pushover curves for MDOF, SDOF and idealized SDOF system and (b) Capacity diagram for the Q_0 model	96
Figure 4.19:	Mean values of the floor response spectra normalized with the mean PGA, structure F10 (1% damping of the equipment)	98
Figure 4.20:	Mean values of the floor response spectra normalized with the mean PGA, structure F10 (5% damping of the equipment)	99
Figure 4.21:	Pushover curves for (a) MDOF and (b) SDOF system (the EP model)	101
Figure 4.22:	Pushover curves for (a) MDOF and (b) SDOF system (the Q_0 model)	102
Figure 4.23:	Absolute floor accelerations obtained for individual modes in the case of structure W03 and Kalamata earthquake	104
Figure 4.24:	Absolute floor accelerations obtained for individual modes in the case of structure W03 and Ionian earthquake	105
Figure 4.25:	Absolute floor accelerations obtained for individual modes in the case of structure W10 and Kalamata earthquake	106
Figure 4.26:	Absolute floor accelerations obtained for individual modes in the case of structure W10 and Ionian earthquake	107
Figure 4.27:	Kalamata elastic spectrum and floor response spectra obtained for MDOF structure, individual modes and by using SRSS and ALGSUM combination rules (structure W03)	110
Figure 4.28:	Ionian elastic spectrum and floor response spectra obtained for MDOF structure, individual modes and by using SRSS and ALGSUM combination rules (structure W03)	111

Figure 4.29:	Kalamata elastic spectrum and floor response spectra obtained for MDOF structure, individual modes and by using SRSS and ALGSUM combination rules (structure W10)	112
Figure 4.30:	Ionian elastic spectrum and floor response spectra obtained for MDOF structure, individual modes and by using SRSS and ALGSUM combination rules (structure W10)	113
Figure 5.1:	Peak floor accelerations of the elastic structures W03, W10, F03 and F10 normalized with the mean PGA, obtained directly (by using the "exact" input) and from the RHA	118
Figure 5.2:	Peak floor accelerations of the elastic structures W03, W10, F03 and F10 normalized with the mean PGA, obtained directly (by using the approximate and "exact" input) and from the RHA	120
Figure 5.3:	Peak floor accelerations of the inelastic structure W03 normalized with the PGA, obtained directly and from the RHA	121
Figure 5.4:	Peak floor accelerations of the inelastic structure W10 normalized with the PGA, obtained directly and from the RHA	122
Figure 5.5:	Peak floor accelerations of the inelastic structure F03 normalized with the PGA, obtained directly and from the RHA	122
Figure 5.6:	Peak floor accelerations of the inelastic structure F10 normalized with the PGA, obtained directly and from the RHA	123
Figure 6.1:	Linking of floor response spectra obtained by USNRC 1.92 (2006) methods and the ALGSUM rule	128
Figure 6.2:	Floor response spectra for the elastic model of the structure W03 normalized with the mean PGA of the input, for 1% damping of the equipment	131
Figure 6.3:	Floor response spectra for the elastic model of the structure W03 normalized with the mean PGA of the input, for 5% damping of the equipment	132
Figure 6.4:	Floor response spectra for the elastic model of the structure W10 normalized with the mean PGA of the input, for 1% damping of the equipment	133
Figure 6.5:	Floor response spectra for the elastic model of the structure W10 normalized with the mean PGA of the input, for 5% damping of the equipment	134
Figure 6.6:	Floor response spectra for the elastic model of the structure F03 normalized with the mean PGA of the input, for 1% damping of the equipment	135
Figure 6.7:	Floor response spectra for the elastic model of the structure F03 normalized with the mean PGA of the input, for 5% damping of the equipment	136
Figure 6.8:	Floor response spectra for the elastic model of the structure F10 normalized with the mean PGA of the input, for 1% damping of the equipment	137
Figure 6.9:	Floor response spectra for the elastic model of the structure F10 normalized with the mean PGA of the input, for 5% damping of the equipment	138
Figure 6.10:	Floor response spectra for the EP model of the structure W03 (ductility $\mu=1.9$) normalized with the PGA of the input, for 1% damping of the equipment	139
Figure 6.11:	Floor response spectra for the EP model of the structure W03 (ductility $\mu=1.9$) normalized with the PGA of the input, for 5% damping of the equipment	140
Figure 6.12:	Floor response spectra for the EP model of the structure W03 (ductility $\mu=4.0$) normalized with the PGA of the input, for 1% damping of the equipment	141
Figure 6.13:	Floor response spectra for the EP model of the structure W03 (ductility $\mu=4.0$) normalized with the PGA of the input, for 5% damping of the equipment	142
Figure 6.14:	Floor response spectra for the Q_0 model of the structure W03 (ductility $\mu=2.0$) normalized with the PGA of the input, for 1% damping of the equipment	143

Figure 6.15:	Floor response spectra for the Q_0 model of the structure W03 (ductility $\mu=2.0$) normalized with the PGA of the input, for 5% damping of the equipment	144
Figure 6.16:	Floor response spectra for the Q_0 model of the structure W03 (ductility $\mu=4.2$) normalized with the PGA of the input, for 1% damping of the equipment	145
Figure 6.17:	Floor response spectra for the Q_0 model of the structure W03 (ductility $\mu=4.2$) normalized with the PGA of the input, for 5% damping of the equipment	146
Figure 6.18:	Floor response spectra for the EP model of the structure W10 (ductility $\mu=2.0$) normalized with the PGA of the input, for 1% damping of the equipment	147
Figure 6.19:	Floor response spectra for the EP model of the structure W10 (ductility $\mu=2.0$) normalized with the PGA of the input, for 5% damping of the equipment	148
Figure 6.20:	Floor response spectra for the EP model of the structure W10 (ductility $\mu=4.0$) normalized with the PGA of the input, for 1% damping of the equipment	149
Figure 6.21:	Floor response spectra for the EP model of the structure W10 (ductility $\mu=4.0$) normalized with the PGA of the input, for 5% damping of the equipment	150
Figure 6.22:	Floor response spectra for the Q_0 model of the structure W10 (ductility $\mu=2.1$) normalized with the PGA of the input, for 1% damping of the equipment	151
Figure 6.23:	Floor response spectra for the Q_0 model of the structure W10 (ductility $\mu=2.1$) normalized with the PGA of the input, for 5% damping of the equipment	152
Figure 6.24:	Floor response spectra for the Q_0 model of the structure W10 (ductility $\mu=4.1$) normalized with the PGA of the input, for 1% damping of the equipment	153
Figure 6.25:	Floor response spectra for the Q_0 model of the structure W10 (ductility $\mu=4.1$) normalized with the PGA of the input, for 5% damping of the equipment	154
Figure 6.26:	Floor response spectra for the EP model of the structure F03 (ductility $\mu=2.0$) normalized with the PGA of the input, for 1% damping of the equipment	155
Figure 6.27:	Floor response spectra for the EP model of the structure F03 (ductility $\mu=2.0$) normalized with the PGA of the input, for 5% damping of the equipment	156
Figure 6.28:	Floor response spectra for the Q_0 model of the structure F03 (ductility $\mu=2.1$) normalized with the PGA of the input, for 1% damping of the equipment	157
Figure 6.29:	Floor response spectra for the Q_0 model of the structure F03 (ductility $\mu=2.1$) normalized with the PGA of the input, for 5% damping of the equipment	158
Figure 6.30:	Floor response spectra for the EP model of the structure F10 (ductility $\mu=2.1$) normalized with the PGA of the input, for 1% damping of the equipment	159
Figure 6.31:	Floor response spectra for the EP model of the structure F10 (ductility $\mu=2.1$) normalized with the PGA of the input, for 5% damping of the equipment	160
Figure 6.32:	Floor response spectra for the EP model of the structure F10 (ductility $\mu=4.1$) normalized with the PGA of the input, for 1% damping of the equipment	161
Figure 6.33:	Floor response spectra for the EP model of the structure F10 (ductility $\mu=4.1$) normalized with the PGA of the input, for 5% damping of the equipment	162
Figure 6.34:	Floor response spectra for the Q_0 model of the structure F10 (ductility $\mu=2.2$) normalized with the PGA of the input, for 1% damping of the equipment	163
Figure 6.35:	Floor response spectra for the Q_0 model of the structure F10 (ductility $\mu=2.2$) normalized with the PGA of the input, for 5% damping of the equipment	164
Figure 6.36:	Floor response spectra for the Q_0 model of the structure F10 (ductility $\mu=4.4$) normalized with the PGA of the input, for 1% damping of the equipment	165
Figure 6.37:	Floor response spectra for the Q_0 model of the structure F10 (ductility $\mu=4.4$) normalized with the PGA of the input, for 5% damping of the equipment	166
Figure 7.1:	Floor response spectra for elastic and Q_0 model (ductility $\mu=2.1$) of the structure F03, for 5% damping of the equipment	179

KAZALO PREGLEDNIC

Preglednica 2.1:	Podatki o izbranem setu akcelerogramov, ki ustreza tipu tal B	13
Preglednica 2.2:	Podatki o izbranem setu akcelerogramov, ki ustreza tipu tal D	14
Preglednica 3.1:	Napake približnih spektrov v primerjavi s »točnimi« spektri, tip tal B	46
Preglednica 3.2:	Napake približnih spektrov v primerjavi s »točnimi« spektri, tip tal D	47
Preglednica 3.3:	Amplifikacijski faktorji <i>AMP</i> uporabljeni v numeričnem primeru	72
Preglednica 4.1:	Osne sile (N), momenti (M_y) in rotacije (θ_y) na meji tečenja v plastičnih členkih (okvir F03)	77
Preglednica 4.2:	Osne sile (N), momenti (M_y) in rotacije (θ_y) na meji tečenja v plastičnih členkih (okvir F10)	79
Preglednica 7.1:	Guptini koeficienti za modalno kombinacijo (elastična in Q_0 konstrukcija F03)	177

KAZALO SLIK

Slika 1.1:	Ilustracija koncepta etažnih spektrov odziva	2
Slika 2.1:	Elastični spektri pospeškov (5% dušenja) posameznih zapisov, ciljni in povprečni spekter za (a) tip tal B (ciljni spekter s $PGA=0.35g$) in (b) tip tal D (ciljni spekter s $PGA=0.39g$)	15
Slika 2.2:	Histerezno obnašanje (a) elasto-plastičnega modela (EP) in modela s padajočo togostjo z (b) nič (Q_0) in (c) 10% utrditve (Q_{10})	15
Slika 2.3:	Povprečne vrednosti etažnih spektrov odziva (A_s) in maksimalnih pospeškov (A_p) za konstrukcije, ki imajo nihajna časa enaka 0.2 in 0.3 s, 5% dušenja konstrukcije in tip tal B	18
Slika 2.4:	Povprečne vrednosti etažnih spektrov odziva (A_s) in maksimalnih pospeškov (A_p) za konstrukcije, ki imajo nihajna časa enaka 0.5 in 0.75 s, 5% dušenja konstrukcije in tip tal B	19
Slika 2.5:	Povprečne vrednosti etažnih spektrov odziva (A_s) in maksimalnih pospeškov (A_p) za konstrukcije, ki imajo nihajna časa enaka 1.0 in 2.0 s, 5% dušenja konstrukcije in tip tal B	20
Slika 2.6:	Povprečne vrednosti etažnih spektrov odziva (A_s) in maksimalnih pospeškov (A_p) za konstrukcije, ki imajo nihajna časa enaka 0.2 in 0.3 s, 5% dušenja konstrukcije in tip tal D	21
Slika 2.7:	Povprečne vrednosti etažnih spektrov odziva (A_s) in maksimalnih pospeškov (A_p) za konstrukcije, ki imajo nihajna časa enaka 0.5 in 0.75 s, 5% dušenja konstrukcije in tip tal D	22
Slika 2.8:	Povprečne vrednosti etažnih spektrov odziva (A_s) in maksimalnih pospeškov (A_p) za konstrukcije, ki imajo nihajna časa enaka 1.0 in 2.0 s, 5% dušenja konstrukcije in tip tal D	23
Slika 2.9:	Razmerje etažnih spektrov odziva neelastičnih in elastičnih konstrukcij, ki imajo nihajna časa 0.2 in 0.3 s, 5% dušenja konstrukcije in tip tal B	24
Slika 2.10:	Razmerje etažnih spektrov odziva neelastičnih in elastičnih konstrukcij, ki imajo nihajna časa 0.5 in 0.75 s, 5% dušenja konstrukcije in tip tal B	25
Slika 2.11:	Razmerje etažnih spektrov odziva neelastičnih in elastičnih konstrukcij, ki imajo nihajna časa 1.0 in 2.0 s, 5% dušenja konstrukcije in tip tal B	26
Slika 2.12:	Razmerje etažnih spektrov odziva neelastičnih in elastičnih konstrukcij, ki imajo nihajna časa 0.2 in 0.3 s, 5% dušenja konstrukcije in tip tal D	27
Slika 2.13:	Razmerje etažnih spektrov odziva neelastičnih in elastičnih konstrukcij, ki imajo nihajna časa 0.5 in 0.75 s, 5% dušenja konstrukcije in tip tal D	28
Slika 2.14:	Razmerje etažnih spektrov odziva neelastičnih in elastičnih konstrukcij, ki imajo nihajna časa 1.0 in 2.0 s, 5% dušenja konstrukcije in tip tal D	29
Slika 2.15:	Etažni spektri odziva normirani na maksimalni pospešek konstrukcij, ki imajo nihajna časa 0.2 in 0.3 s, 5% dušenja konstrukcije in tip tal B	30
Slika 2.16:	Etažni spektri odziva normirani na maksimalni pospešek konstrukcij, ki imajo nihajna časa 0.5 in 0.75 s, 5% dušenja konstrukcije in tip tal B	31
Slika 2.17:	Etažni spektri odziva normirani na maksimalni pospešek konstrukcij, ki imajo nihajna časa 1.0 in 2.0 s, 5% dušenja konstrukcije in tip tal B	32
Slika 2.18:	Etažni spektri odziva normirani na maksimalni pospešek konstrukcij, ki imajo nihajna časa 0.2 in 0.3 s, 5% dušenja konstrukcije in tip tal D	33
Slika 2.19:	Etažni spektri odziva normirani na maksimalni pospešek konstrukcij, ki imajo nihajna časa 0.5 in 0.75 s, 5% dušenja konstrukcije in tip tal D	34

Slika 2.20:	Etažni spektri odziva normirani na maksimalni pospešek konstrukcij, ki imajo nihajna časa 1.0 in 2.0 s, 5% dušenja konstrukcije in tip tal D	35
Slika 2.21:	Primerjava etažnih spektrov odziva izračunanih za različna Q modela, za konstrukcije, ki imajo nihajna časa 0.2 in 0.3 s in 5% dušenja, tip tal B	36
Slika 2.22:	Primerjava etažnih spektrov odziva izračunanih za različna Q modela, za konstrukcije, ki imajo nihajna časa 0.5 in 0.75 s in 5% dušenja, tip tal B	37
Slika 2.23:	Primerjava etažnih spektrov odziva izračunanih za različna Q modela, za konstrukcije, ki imajo nihajna časa 1.0 in 2.0 s in 5% dušenja, tip tal B	38
Slika 2.24:	Primerjava etažnih spektrov odziva normiranih na maksimalni pospešek konstrukcije izračunanih za različna Q modela, za konstrukcije, ki imajo nihajna časa 0.2 in 0.3 s in 5% dušenja, tip tal B	39
Slika 2.25:	Primerjava etažnih spektrov odziva normiranih na maksimalni pospešek konstrukcije izračunanih za različna Q modela, za konstrukcije, ki imajo nihajna časa 0.5 in 0.75 s in 5% dušenja, tip tal B	40
Slika 2.26:	Primerjava etažnih spektrov odziva normiranih na maksimalni pospešek konstrukcije izračunanih za različna Q modela, za konstrukcije, ki imajo nihajna časa 1.0 in 2.0 s in 5% dušenja, tip tal B	41
Slika 2.27:	Amplifikacijski faktorji (<i>AMP</i>) izračunani v parametrični študiji za EP model konstrukcije	42
Slika 2.28:	Amplifikacijski faktorji (<i>AMP</i>) izračunani v parametrični študiji za Q_{10} model konstrukcije	42
Slika 2.29:	Amplifikacijski faktorji (<i>AMP</i>) v odvisnosti od dušenja opreme predstavljeni kot povprečne vrednosti za različna razmerja T_p/T_C	43
Slika 3.1:	»Točni« in približni neelastični spektri za tla tipa B in D (5% dušenja konstrukcije)	47
Slika 3.2:	Primerjava med (a) »točnimi« in (b) približnimi neelastičnimi spektri pospeškov za konstrukcijo (5% dušenja) za dva različna Q modela, tip tal B	47
Slika 3.3:	Predlagani faktorji amplifikacije in primerjava z <i>AMP</i> , ki so izračunani v parametrični študiji	49
Slika 3.4:	Primerjava etažnih spektrov odziva za elastične konstrukcije za tla tipa B, 5% dušenja konstrukcije	51
Slika 3.5:	Etažni spektri odziva za EP model konstrukcije, nihajni časi enaki 0.2 in 0.3 s, 5% dušenja konstrukcije, tip tal B	53
Slika 3.6:	Etažni spektri odziva za EP model konstrukcije, nihajni časi enaki 0.5 in 0.75 s, 5% dušenja konstrukcije, tip tal B	54
Slika 3.7:	Etažni spektri odziva za EP model konstrukcije, nihajni časi enaki 1.0 in 2.0 s, 5% dušenja konstrukcije, tip tal B	55
Slika 3.8:	Etažni spektri odziva za EP model konstrukcije, nihajni časi enaki 0.2 in 0.3 s, 5% dušenja konstrukcije, tip tal D	56
Slika 3.9:	Etažni spektri odziva za EP model konstrukcije, nihajni časi enaki 0.5 in 0.75 s, 5% dušenja konstrukcije, tip tal D	57
Slika 3.10:	Etažni spektri odziva za EP model konstrukcije, nihajni časi enaki 1.0 in 2.0 s, 5% dušenja konstrukcije, tip tal D	58
Slika 3.11:	Etažni spektri odziva za Q_{10} model konstrukcije, nihajni časi enaki 0.2 in 0.3 s, 5% dušenja konstrukcije, tip tal B	59
Slika 3.12:	Etažni spektri odziva za Q_{10} model konstrukcije, nihajni časi enaki 0.5 in 0.75 s, 5% dušenja konstrukcije, tip tal B	60

Slika 3.13:	Etažni spektri odziva za Q_{10} model konstrukcije, nihajni časi enaki 1.0 in 2.0 s, 5% dušenja konstrukcije, tip tal B	61
Slika 3.14:	Etažni spektri odziva za Q_{10} model konstrukcije, nihajni časi enaki 0.2 in 0.3 s, 5% dušenja konstrukcije, tip tal D	62
Slika 3.15:	Etažni spektri odziva za Q_{10} model konstrukcije, nihajni časi enaki 0.5 in 0.75 s, 5% dušenja konstrukcije, tip tal D	63
Slika 3.16:	Etažni spektri odziva za Q_{10} model konstrukcije, nihajni časi enaki 1.0 in 2.0 s, 5% dušenja konstrukcije, tip tal D	64
Slika 3.17:	Etažni spektri odziva za Q_0 model konstrukcije, nihajni časi enaki 0.2 in 0.3 s, 5% dušenja konstrukcije, tip tal B	65
Slika 3.18:	Etažni spektri odziva za Q_0 model konstrukcije, nihajni časi enaki 0.5 in 0.75 s, 5% dušenja konstrukcije, tip tal B	66
Slika 3.19:	Etažni spektri odziva za Q_0 model konstrukcije, nihajni časi enaki 1.0 in 2.0 s, 5% dušenja konstrukcije, tip tal B	67
Slika 3.20:	Etažni spektri odziva dobljeni s pomočjo Evrokoda 8 (2004) in predlagane metode za (a) EP in (b) Q_{10} modela z $\mu=2$, T_p enako 0.3, 0.5, 0.75 in 1 s, tip 1 spektra, tip tal B, 5% dušenja, $a_g S=0.30g$	69
Slika 3.21:	Etažni spektri odziva dobljeni z dvema direktnima pristopoma za Q_{10} model konstrukcije, nihajni časi enaki 0.3 in 1.0 s, 5% dušenja konstrukcije, tip tal B	70
Slika 3.22:	Etažni spektri odziva dobljeni z dvema direktnima pristopoma za Q_{10} model konstrukcije, nihajni časi enaki 0.3 in 1.0 s, 5% dušenja konstrukcije, tip tal D	71
Slika 3.23:	Etažni spektri odziva dobljeni s pomočjo predlagane metode za (a) elastičen model in (b) Q_{10} model konstrukcije s 5% dušenja, tip tal B (PGA=0.35g)	72
Slika 4.1:	Elastični spektri pospeškov (5% dušenja) posameznih zapisov, modificirani ciljni in povprečni spekter za tla tipa B	74
Slika 4.2:	Armatura ob vpetju stene W03 (območje plastičnega členka)	75
Slika 4.3:	Armatura stebrov in gred okvirja F03	77
Slika 4.4:	Armatura stebrov in gred okvirja F10	78
Slika 4.5:	(a) Potisne krivulje za MDOF in SDOF sistema in (b) Diagram kapacitete za EP model	80
Slika 4.6:	(a) Potisne krivulje za MDOF in SDOF sistema in (b) Diagram kapacitete za Q_0 model	81
Slika 4.7:	Povprečne vrednosti etažnih spektrov odziva normirane s povprečnim PGA, konstrukcija W03 (1% dušenja opreme)	83
Slika 4.8:	Povprečne vrednosti etažnih spektrov odziva normirane s povprečnim PGA, konstrukcija W03 (5% dušenja opreme)	84
Slika 4.9:	(a) Potisne krivulje za MDOF in SDOF sistema in (b) Diagram kapacitete za EP model	86
Slika 4.10:	(a) Potisne krivulje za MDOF in SDOF sistema in (b) Diagram kapacitete za Q_0 model	87
Slika 4.11:	Povprečne vrednosti etažnih spektrov odziva normirane s povprečnim PGA, konstrukcija W10 (1% dušenja opreme)	88
Slika 4.12:	Povprečne vrednosti etažnih spektrov odziva normirane s povprečnim PGA, konstrukcija W10 (5% dušenja opreme)	89
Slika 4.13:	(a) Potisne krivulje za MDOF, SDOF in idealizirani SDOF sistem in (b) Diagram kapacitete za EP model	91
Slika 4.14:	(a) Potisne krivulje za MDOF, SDOF in idealizirani SDOF sistem in (b) Diagram kapacitete za Q_0 model	92

Slika 4.15:	Povprečne vrednosti etažnih spektrov odziva normirane s povprečnim PGA, konstrukcija F03 (1% dušenja opreme)	93
Slika 4.16:	Povprečne vrednosti etažnih spektrov odziva normirane s povprečnim PGA, konstrukcija F03 (5% dušenja opreme)	94
Slika 4.17:	(a) Potisne krivulje za MDOF, SDOF in idealizirani SDOF sistem in (b) Diagram kapacitete za EP model	95
Slika 4.18:	(a) Potisne krivulje za MDOF, SDOF in idealizirani SDOF sistem in (b) Diagram kapacitete za Q_0 model	96
Slika 4.19:	Povprečne vrednosti etažnih spektrov odziva normirane s povprečnim PGA, konstrukcija F10 (1% dušenja opreme)	98
Slika 4.20:	Povprečne vrednosti etažnih spektrov odziva normirane s povprečnim PGA, konstrukcija F10 (5% dušenja opreme)	99
Slika 4.21:	Potisne krivulje za (a) MDOF in (b) SDOF sistem (EP model)	101
Slika 4.22:	Potisne krivulje za (a) MDOF in (b) SDOF sistem (Q_0 model)	102
Slika 4.23:	Absolutni etažni pospeški dobljeni za posamezne oblike v primeru konstrukcije W03 in Kalamata potresa	104
Slika 4.24:	Absolutni etažni pospeški dobljeni za posamezne oblike v primeru konstrukcije W03 in Ionian potresa	105
Slika 4.25:	Absolutni etažni pospeški dobljeni za posamezne oblike v primeru konstrukcije W10 in Kalamata potresa	106
Slika 4.26:	Absolutni etažni pospeški dobljeni za posamezne oblike v primeru konstrukcije W10 in Ionian potresa	107
Slika 4.27:	Kalamata elastični spekter in etažni spektri odziva dobljeni za MDOF konstrukcijo, posamezne oblike in z uporabo SRSS in ALGSUM kombinacijskih pravil (konstrukcija W03)	110
Slika 4.28:	Ionian elastični spekter in etažni spektri odziva dobljeni za MDOF konstrukcijo, posamezne oblike in z uporabo SRSS in ALGSUM kombinacijskih pravil (konstrukcija W03)	111
Slika 4.29:	Kalamata elastični spekter in etažni spektri odziva dobljeni za MDOF konstrukcijo, posamezne oblike in z uporabo SRSS in ALGSUM kombinacijskih pravil (konstrukcija W10)	112
Slika 4.30:	Ionian elastični spekter in etažni spektri odziva dobljeni za MDOF konstrukcijo, posamezne oblike in z uporabo SRSS in ALGSUM kombinacijskih pravil (konstrukcija W10)	113
Slika 5.1:	Maksimalni etažni pospeški elastičnih konstrukcij W03, W10, F03 in F10 normirani s povprečnim PGA, dobljeni direktno (ob uporabi »točnega« inputa) in iz RHA	118
Slika 5.2:	Maksimalni etažni pospeški elastičnih konstrukcij W03, W10, F03 in F10 normirani s povprečnim PGA, dobljeni direktno (ob uporabi približnega in »točnega« inputa) in iz RHA	120
Slika 5.3:	Maksimalni etažni pospeški neelastične konstrukcije W03 normirani s PGA, dobljeni direktno in iz RHA	121
Slika 5.4:	Maksimalni etažni pospeški neelastične konstrukcije W10 normirani s PGA, dobljeni direktno in iz RHA	122
Slika 5.5:	Maksimalni etažni pospeški neelastične konstrukcije F03 normirani s PGA, dobljeni direktno in iz RHA	122
Slika 5.6:	Maksimalni etažni pospeški neelastične konstrukcije F10 normirani s PGA, dobljeni direktno in iz RHA	123

Slika 6.1:	Povezava etažnih spektrov odziva dobljenih z USNRC 1.92 (2006) metodo in ALGSUM pravila	128
Slika 6.2:	Etažni spektri odziva za elastičen model konstrukcije W03 normirani s povprečnim PGA inputa, za 1% dušenja opreme	131
Slika 6.3:	Etažni spektri odziva za elastičen model konstrukcije W03 normirani s povprečnim PGA inputa, za 5% dušenja opreme	132
Slika 6.4:	Etažni spektri odziva za elastičen model konstrukcije W10 normirani s povprečnim PGA inputa, za 1% dušenja opreme	133
Slika 6.5:	Etažni spektri odziva za elastičen model konstrukcije W10 normirani s povprečnim PGA inputa, za 5% dušenja opreme	134
Slika 6.6:	Etažni spektri odziva za elastičen model konstrukcije F03 normirani s povprečnim PGA inputa, za 1% dušenja opreme	135
Slika 6.7:	Etažni spektri odziva za elastičen model konstrukcije F03 normirani s povprečnim PGA inputa, za 5% dušenja opreme	136
Slika 6.8:	Etažni spektri odziva za elastičen model konstrukcije F10 normirani s povprečnim PGA inputa, za 1% dušenja opreme	137
Slika 6.9:	Etažni spektri odziva za elastičen model konstrukcije F10 normirani s povprečnim PGA inputa, za 5% dušenja opreme	138
Slika 6.10:	Etažni spektri odziva za EP model konstrukcije W03 (ductility $\mu=1.9$) normirani s PGA inputa, za 1% dušenja opreme	139
Slika 6.11:	Etažni spektri odziva za EP model konstrukcije W03 (ductility $\mu=1.9$) normirani s PGA inputa, za 5% dušenja opreme	140
Slika 6.12:	Etažni spektri odziva za EP model konstrukcije W03 (ductility $\mu=4.0$) normirani s PGA inputa, za 1% dušenja opreme	141
Slika 6.13:	Etažni spektri odziva za EP model konstrukcije W03 (ductility $\mu=4.0$) normirani s PGA inputa, za 5% dušenja opreme	142
Slika 6.14:	Etažni spektri odziva za Q_0 model konstrukcije W03 (ductility $\mu=2.0$) normirani s PGA inputa, za 1% dušenja opreme	143
Slika 6.15:	Etažni spektri odziva za Q_0 model konstrukcije W03 (ductility $\mu=2.0$) normirani s PGA inputa, za 5% dušenja opreme	144
Slika 6.16:	Etažni spektri odziva za Q_0 model konstrukcije W03 (ductility $\mu=4.2$) normirani s PGA inputa, za 1% dušenja opreme	145
Slika 6.17:	Etažni spektri odziva za Q_0 model konstrukcije W03 (ductility $\mu=4.2$) normirani s PGA inputa, za 5% dušenja opreme	146
Slika 6.18:	Etažni spektri odziva za EP model konstrukcije W10 (ductility $\mu=2.0$) normirani s PGA inputa, za 1% dušenja opreme	147
Slika 6.19:	Etažni spektri odziva za EP model konstrukcije W10 (ductility $\mu=2.0$) normirani s PGA inputa, za 5% dušenja opreme	148
Slika 6.20:	Etažni spektri odziva za EP model konstrukcije W10 (ductility $\mu=4.0$) normirani s PGA inputa, za 1% dušenja opreme	149
Slika 6.21:	Etažni spektri odziva za EP model konstrukcije W10 (ductility $\mu=4.0$) normirani s PGA inputa, za 5% dušenja opreme	150
Slika 6.22:	Etažni spektri odziva za Q_0 model konstrukcije W10 (ductility $\mu=2.1$) normirani s PGA inputa, za 1% dušenja opreme	151
Slika 6.23:	Etažni spektri odziva za Q_0 model konstrukcije W10 (ductility $\mu=2.1$) normirani s PGA inputa, za 5% dušenja opreme	152
Slika 6.24:	Etažni spektri odziva za Q_0 model konstrukcije W10 (ductility $\mu=4.1$) normirani s PGA inputa, za 1% dušenja opreme	153

Slika 6.25:	Etažni spektri odziva za Q_0 model konstrukcije W10 (ductility $\mu=4.1$) normirani s PGA inputa, za 5% dušenja opreme	154
Slika 6.26:	Etažni spektri odziva za EP model konstrukcije F03 (ductility $\mu=2.0$) normirani s PGA inputa, za 1% dušenja opreme	155
Slika 6.27:	Etažni spektri odziva za EP model konstrukcije F03 (ductility $\mu=2.0$) normirani s PGA inputa, za 5% dušenja opreme	156
Slika 6.28:	Etažni spektri odziva za Q_0 model konstrukcije F03 (ductility $\mu=2.1$) normirani s PGA inputa, za 1% dušenja opreme	157
Slika 6.29:	Etažni spektri odziva za Q_0 model konstrukcije F03 (ductility $\mu=2.1$) normirani s PGA inputa, za 5% dušenja opreme	158
Slika 6.30:	Etažni spektri odziva za EP model konstrukcije F10 (ductility $\mu=2.1$) normirani s PGA inputa, za 1% dušenja opreme	159
Slika 6.31:	Etažni spektri odziva za EP model konstrukcije F10 (ductility $\mu=2.1$) normirani s PGA inputa, za 5% dušenja opreme	160
Slika 6.32:	Etažni spektri odziva za EP model konstrukcije F10 (ductility $\mu=4.1$) normirani s PGA inputa, za 1% dušenja opreme	161
Slika 6.33:	Etažni spektri odziva za EP model konstrukcije F10 (ductility $\mu=4.1$) normirani s PGA inputa, za 5% dušenja opreme	162
Slika 6.34:	Etažni spektri odziva za Q_0 model konstrukcije F10 (ductility $\mu=2.2$) normirani s PGA inputa, za 1% dušenja opreme	163
Slika 6.35:	Etažni spektri odziva za Q_0 model konstrukcije F10 (ductility $\mu=2.2$) normirani s PGA inputa, za 5% dušenja opreme	164
Slika 6.36:	Etažni spektri odziva za Q_0 model konstrukcije F10 (ductility $\mu=4.4$) normirani s PGA inputa, za 1% dušenja opreme	165
Slika 6.37:	Etažni spektri odziva za Q_0 model konstrukcije F10 (ductility $\mu=4.4$) normirani s PGA inputa, za 5% dušenja opreme	166
Slika 7.1:	Etažni spektri odziva za elastičen in Q_0 model (duktilnost $\mu=2.1$) konstrukcije F03, za 5% dušenja opreme	179

SYMBOLS

A	absolute floor acceleration
a_0	mass coefficient of the Rayleigh damping model
a_1	stiffness coefficient of the Rayleigh damping model
a_g	design ground acceleration on type A ground defined in Eurocode 8 (2004)
AMP	amplification factor for the SDOF primary structure
AMP_i	amplification factor for the mode i of the MDOF primary structure
A_p	peak acceleration of the SDOF primary structure
A_s	floor response spectrum value for the case of the SDOF primary structure
$A_{s,ij}$	floor response spectrum value for the case of the MDOF primary structure for the mode i at the floor j
A_{se}	floor response spectrum value for the case of the elastic SDOF primary structure
d	displacement of the MDOF system
d^*	displacement of the equivalent SDOF system
d_j	displacement of the storey j
d_t	target (roof) displacement of the MDOF system
d_t^*	displacement demand of the equivalent SDOF system
d_y^*	displacement at the yield point of the equivalent SDOF system
E_c	modulus of elasticity of concrete
E_s	modulus of elasticity of steel
F	base shear force of the MDOF system
F^*	base shear force of the equivalent SDOF system
f_1	frequency used in Gupta's combination method
f_2	frequency used in Gupta's combination method
f_i	frequency for the mode i
f_r	the rigid frequency
F_s	horizontal force which should be applied to the non-structural element (equipment)
f_y	yield strength of reinforcement
F_y^*	base shear force at the yield point of the equivalent SDOF system
f_{ZPA}	frequency at which the spectral acceleration returns to the zero period acceleration (ZPA)
g	acceleration of gravity
H	building height measured from the foundation or from the top of a rigid basement
i	mode; variable
I	moment of inertia of the cross section
j	floor (storey)
k	stiffness of the SDOF primary structure
L_w	total height of the wall
m	mass of the SDOF primary structure
M	earthquake magnitude
\mathbf{M}	mass matrix
m^*	effective mass
m_s	mass of the non-structural element (equipment)
M_y	yield moment in the plastic hinge
n	number of modes with frequency below f_{ZPA}
N	axial force; the total number of modes
\mathbf{P}	vector of lateral loads
PFA	peak floor acceleration
PFA_{ij}	peak floor acceleration for the mode i at the floor j
PFA_j	peak floor acceleration at the floor j
$PFA_{mm,j}$	peak floor acceleration related to the missing mass at the floor j
$PFA_{periodic,i}$	periodic part of the peak floor acceleration at the floor j
$PFA_{rigid,i}$	rigid part of the peak floor acceleration at the floor j
PGA	peak ground acceleration
q_s	importance factor of the non-structural element (equipment)
R_μ	reduction factor due to ductility
S	soil factor defined in Eurocode 8 (2004)
S_a	value on the capacity diagram of the equivalent SDOF system
S_{ay}	acceleration at the yield point on the capacity diagram of the equivalent SDOF system
S_e	value in the input elastic acceleration spectrum

$S_e(T_p^*), S_e(T_{p,i}^*)$	value in the input elastic acceleration spectrum which applies to the equivalent SDOF system for the mode i
$S_e(T_{p,1}^*)$	value in the input elastic acceleration spectrum which applies to the equivalent SDOF system for the fundamental mode
$S_e(T_{p,i}, \zeta_{p,i})$	value in the input elastic acceleration spectrum which applies to the elastic MDOF primary structure for the mode i
$S_e(T_p, \zeta_p)$	value in the input elastic acceleration spectrum which applies to the elastic SDOF primary structure
$S_e(T_s, \zeta_s)$	value in the input elastic acceleration spectrum which applies to the elastic SDOF equipment (secondary structure)
SF	scale factor
T	fundamental period of the structure in the direction where acceleration time-history will be applied
$T^*, T_{p,i}^*$	effective natural period of the equivalent SDOF system for the mode i
T_B	lower limit of the constant spectral acceleration branch in Eurocode 8 (2004) elastic spectrum
T_C	upper limit of the constant spectral acceleration branch in Eurocode 8 (2004) elastic spectrum; characteristic period of the ground motion
T_p	natural period of the SDOF primary structure
$T_{p,\mu}$	effective natural period of the SDOF primary structure
$T_{p,1}^*$	effective natural period of the equivalent SDOF system for the fundamental mode
$T_{p,i}$	natural period of the MDOF primary structure for the mode i
$T_{p,i,\mu}$	effective natural period of the MDOF primary structure for the mode i
T_s	natural period of the elastic SDOF equipment (secondary structure)
T_s^*	transfer point
z	height of the non-structural element (equipment) above the level of application of the seismic action (foundation or top of a rigid basement)
ZPA	zero period acceleration
α	ratio of the post-yield and the elastic stiffness
α_i	rigid response coefficient
β	coefficient used in Newmark's integration method
γ	coefficient used in Newmark's integration method
Γ	transformation factor
Γ_i	modal participation factor for the mode i
γ_s	importance factor of the non-structural element (equipment)
η	damping correction factor defined in Eurocode 8 (2004)
θ_v	yield rotation in the plastic hinge
μ	ductility factor
ζ_p	damping coefficient of the SDOF primary structure
$\zeta_{p,i}$	damping coefficient of the MDOF primary structure for the mode i
ζ_s	damping coefficient of the elastic SDOF equipment (secondary structure)
σ	standard deviation
ϕ_{ij}	value of the mode shape component for the mode i at the floor j
ϕ_i	eigenvector for the mode i
ϕ_1^{inel}	vector of inelastic first mode shape
Φ_{OS}	matrix which contains eigenvectors determined in OpenSees
Φ_{SAP}	matrix which contains eigenvectors determined in SAP
$\omega_{p,i}$	natural circular frequency of the MDOF primary structure for the mode i

ABBREVIATIONS

ALGSUM	Algebraična vsota	Algebraic summation rule
ASCE		American Society of Civil Engineers
CV	Koeficient variacije	Coefficient of variation
CQC	Popolna kvadratna kombinacija	Complete Quadratic Combination
DOF	Prostostna stopnja	Degree-of-freedom
EP	Elasto-plastičen model	Elasto-plastic model
ESMD		European Strong-Motion Database
MDOF	Sistem z več prostostnimi stopnjami	Multi-degree-of freedom system
NEHRP		National Earthquake Hazards Reduction Program
OpenSees		Open System for Earthquake Engineering Simulation
PEER		Pacific Earthquake Engineering Research Center
PFA	Maksimalni pospešek etaže	Peak floor acceleration
PGA	Maksimalni pospešek tal	Peak ground acceleration
Q	Model s padajočo togostjo	Stiffness degrading model
Q ₀	Model s padajočo togostjo brez utrditve	Stiffness degrading model with zero hardening
Q ₁₀	Model s padajočo togostjo in 10% utrditve	Stiffness degrading model with 10% hardening
RC	Armirani beton	Reinforced concrete
RHA	Analiza potresnega odziva	Response-history analysis
SAP		Structural Analysis Program
SDOF	Sistem z eno prostostno stopnjo	Single-degree-of-freedom system
SRSS	Geometrijska vsota	Square Root of Sum of Squares
USNRC		U.S. Nuclear Regulatory Commission

This page is intentionally left blank.

1 INTRODUCTION

Experience shows that during earthquakes equipment in buildings may be subjected to large accelerations. The safety of equipment is in many cases the most important issue in the design. In industrial buildings such as nuclear power plants, floor response spectra are usually used for seismic design and evaluation of mechanical and electrical equipment (e.g. piping systems, boilers, turbines, generators, pumps, tanks, ducts, etc.). It has been recognized that the damage of such equipment may represent a threat to life safety and a great economic loss. Therefore, an adequate resistance of equipment during earthquakes is of great importance.

The second half of the 20th century was characterized by mass construction of a great number of nuclear power plants. Seismic analysis of equipment (secondary systems) in such structures was unavoidable. At that time, many researchers made a great deal of effort to develop rational methods for the seismic analysis and seismic design of secondary systems. The development of these methods came as a need to provide sufficient sustainability of critical equipment in industrial structures during earthquakes. It was shown that accurate and efficient analysis of secondary systems may be very difficult and complicated. Different methods of analysis were proposed. Some of them are based on strong empirical facts while others are based on principles of structural dynamics. The fact that primary and secondary structures may have very different dynamic properties and that they are designed by different teams at a different time caused troubles to researchers. Therefore, the development of a reasonably reliable but relatively simple method for seismic analysis of secondary systems represents a big challenge in earthquake engineering.

In the last three decades, construction of new nuclear power plants has not been frequent as in the above mentioned period. On the other hand, all of these structures built in the past have to be reevaluated. Main reasons for that lie not only in the fact that they are old, but also in the fact that current building codes and provisions have significantly changed from the time those structures were designed and built. Modern computer software gives us an opportunity to conduct quite accurate structural analysis, even in complex cases such as analysis of secondary structures attached to primary structures. It is therefore of crucial importance that we use this opportunity, in order to provide maximum safety of industrial structures and their equipment, whose collapse could cause unforeseeable consequences.

1.1 The theme of the doctoral dissertation

Once constructed, primary and secondary structures represent entirety. In order to include all mutual influences, they should be analysed as one unity (coupled system). That kind of system does not possess classical modes of vibration and it is (most often) not classically damped, which makes it very difficult to analyse. Even though such analysis gives more accurate results, it is impractical and unjustified for everyday practice.

Floor response spectra in terms of acceleration, which are also known as in-structure spectra, are usually used for seismic design and evaluation of acceleration-sensitive equipment installed in buildings. The floor response spectra concept is based on a separate (uncoupled) analysis of the structure and its equipment, which means that their dynamic interaction is neglected (see Figure 1.1). It is considered to be sufficiently accurate in cases of equipment whose mass is significantly smaller than that of the structure, by a factor of at least one hundred. If this factor is smaller, the floor response spectra are usually conservative (see e.g. Figure 3.1-2 in ASCE 4-98 2000, Adam and Furtmüller

2008, Adam et al. 2013, Pinkawa et al. 2014). In the dissertation, it was assumed that the mass of equipment is significantly smaller than the mass of the primary structure, i.e. the original floor response spectra concept was considered. Thus, the main steps for the calculation of floor acceleration spectra ("classical approach" in Figure 1.1) are:

- 1) Response-history analysis of the structure by using a set of ground motions;
- 2) Determination of the response of a floor in terms of the absolute floor acceleration;
- 3) Generation of floor acceleration spectrum corresponding to the absolute acceleration response-history determined in step (2).

Many researchers have proposed methods that enable the generation of floor response spectra directly from the design response spectrum ("direct approach" in Figure 1.1) in order to avoid long numerical integrations. Apart from the design response spectrum, input data are also the dynamic properties of primary and secondary structures. Because of their simplicity, these methods are being widely used in practice. Developments of early floor response spectra methods have been based on the assumption that the primary structure and equipment remain in linear elastic region during earthquakes. Even in the case of structures of great importance, such as nuclear power plants, it is justifiable to allow a moderate amount of inelastic behaviour during strong earthquakes. This fact is important, especially in case of the evaluation of existing structures, since neglecting the influence of structural inelasticity on floor accelerations may lead to unrealistic results.

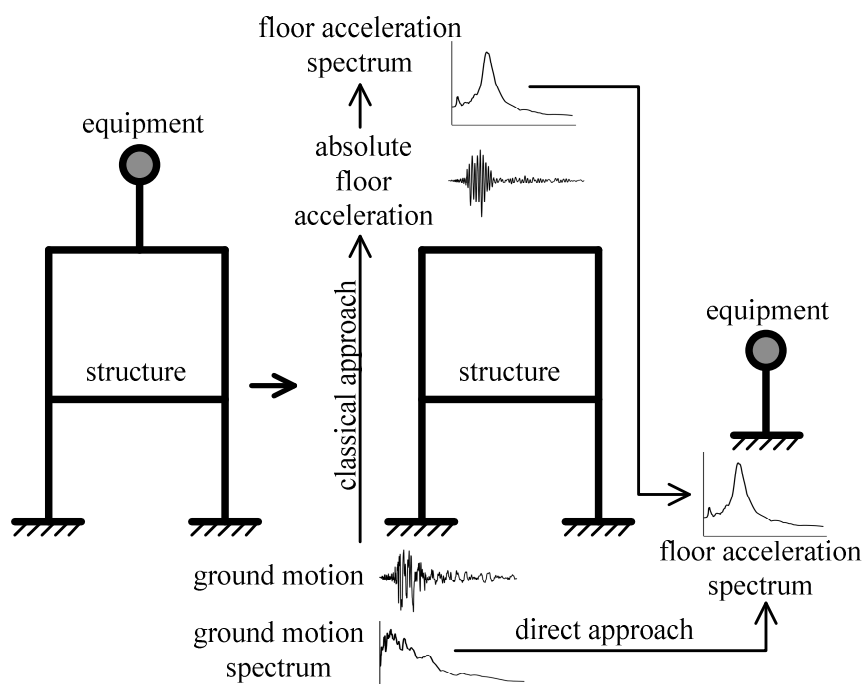


Figure 1.1: Illustration of the floor response spectra concept

Slika 1.1: Ilustracija koncepta etažnih spektrov odziva

Significant reductions in peak values of floor response spectra can be obtained if the inelastic behaviour of the primary or/and secondary structure is taken into account. Neglecting this fact may lead to unrealistic and uneconomical design. Only a few researchers have made an effort to derive simplified methods which include inelastic structural behaviour in the analysis and the lack of such methods is evident. On the other hand, most of the existing proposed methods are either quite complex

and impractical for wider application, or insufficiently accurate. It was therefore concluded that a practice-oriented direct method is still missing.

Recognizing the importance of the influence that inelastic structural behaviour has on the response of secondary systems, the analysis of this influence and the development of a practice-oriented direct method which takes into account the inelastic behaviour of the primary structure were chosen to be the main objectives of the dissertation. The analyses were conducted on uncoupled structure-equipment systems. Inelastic behaviour was assumed only in primary structures, while equipment remained in linear elastic region. Thus, the main goals of the dissertation are:

- investigation of the effects which the inelastic structural behaviour of the SDOF (single-degree-of-freedom) and MDOF (multi-degree-of-freedom) primary structures has on the response of equipment (secondary structures) for various hysteretic models and comparison of the newly obtained findings with the existing ones, and
- development of a new simple practice-oriented method for direct generation of floor response spectra, which takes into account structural inelasticity.

1.2 State of the art at the relevant scientific field

The development of floor response spectra methods started in early 1970s. According to Villaverde (1997), the first progress on the subject was realized by Biggs and Roesset (1970), Amin et al. (1971) and Kapur and Shao (1973). The developed methods represented a very good alternative for time-consuming methods which were based on the response-history analysis and usage of seismic waves as input. In the light of proposed solutions, Peters et al. (1977) developed a new method which was based on the uncoupled analysis of primary and secondary structures. Like the first methods that had been proposed, it also provided the direct generation of floor response spectra from the ground response spectrum. The method distinguishes between resonant and non-resonant cases of primary and secondary structures. Similar research was conducted by Vanmarcke (1977), whose method provided evaluation of the secondary system response directly from the specified ground response spectra. He expressed maximum acceleration of the secondary system by combining individual contributions for all significant modes of the primary structure by using the Square Root of Sum of Squares (SRSS) rule. Singh and Sharma (1983) proposed a method for the direct determination of floor response spectra from the design ground spectrum for elastic MDOF structures that can be affected with high frequency modes. The method is based on mode accelerations and the seismic input is defined in terms of relative acceleration and velocity spectra. The authors implied that the direct methods based on the mode displacement approach (which use pseudo-acceleration spectra as seismic input) can give inaccurate results if the complete set of modes (eigenvalues) is not taken into account. In the proposed method effects of high frequency modes were taken into account implicitly. The study showed that higher modes have the most significant effect on the floor accelerations in lower floors of stiff structures.

At one point, researchers came to the conclusion that floor response spectra methods are in some cases limited and impractical for use in direct analysis of combined primary-secondary systems. Dynamic interaction between two subsystems is neglected and that fact can sometimes lead to conservative results, especially in cases when the mass of equipment is not negligible comparing to the mass of the primary structure. Following already mentioned two main approaches, several modifications were proposed. Since the main objectives of the dissertation do not apply to the analysis of interaction between the two subsystems, the description of the aforementioned modified methods is going to be

brief and restricted to those with most practical significance. Vidic (1988) gave a good insight into the method developed by Der Kiureghian et al. (1983), through the results obtained by a computer program that he designed and based on this method. Igusa and Der Kiureghian (1985) developed a method which more accurately accounts for tuning, interaction and non-classical damping. Modal properties of the coupled system were derived in terms of the known properties of two subsystems by using modal synthesis and perturbation techniques. The direct generation of floor response spectra was conducted by using derived modal properties of the composite system and specified ground response spectrum. A parametric analysis was conducted in order to show the accuracy of the proposed method. Gupta and Jaw (1986) presented a method capable of accounting for various coupling effects on the response of secondary systems. The method uses displacement and velocity spectra at the base of the primary structure as seismic input for generation of the floor response spectra. The results obtained from the proposed method showed very good agreement with the results obtained from response-history analysis. Suarez and Singh (1987) introduced an approach that also incorporated the effect of the interaction between primary and secondary structures. Modal synthesis of the dynamic properties of individual structures was used to obtain modal properties of the coupled system. Seismic input may be defined in terms of smoothed ground spectra. The method is suitable for analysis of both light and heavy secondary systems. Villaverde (1991) proposed simple approximate formulas for determination of the maximum response of secondary systems. Even though primary and secondary structures were considered as one unit, they were expressed in terms of independent dynamic properties. The formulas are restricted to primary and secondary systems which behave linearly and have classical modes of vibrations. George and Gupta (1995) derived closed-form equations for response of secondary systems. The equations can be used for quick evaluation of points of floor response spectra and they are also applicable to MDOF secondary systems.

All of the above mentioned methods were derived on the basis of the assumption of linear elastic behaviour of both primary and secondary structures. It soon became clear that most structures to which secondary systems are attached yield during strong earthquakes. Even in the case of structures of great importance, such as nuclear power plants, it is justifiable to allow a moderate amount of inelastic behaviour during strong earthquakes. This fact is important, especially in the case of the evaluation of existing structures, since neglecting the influence of structural inelasticity on floor accelerations may lead to unrealistic results. In general, significant reductions in peak values of floor response spectra can be achieved if the inelastic behaviour of the primary structure and/or equipment is taken into account.

An early observation of this phenomenon was made by Kelly (1978) who had conducted research on twelve MDOF structures. Several different structural types were taken into account and a height of each structure was varied. As an input, El Centro 1940 N-S component was used. Structural behaviour was assumed to be elastic and inelastic for two different levels of structure yield strength. It was observed that the peak values of absolute floor accelerations significantly decrease in the case of inelastic structural behaviour in comparison to the elastic one.

Lin and Mahin (1985) thoroughly investigated the effects of inelastic deformations, different hysteretic characteristics of the supporting structure and influence of amount of viscous damping of the subsystem. Primary structures were modelled as SDOF systems with elasto-perfectly plastic and stiffness degrading nonlinear behaviour and 5% damping. Maximum displacement ductilities of 1, 2, 4 and 8 were considered. Secondary structures were also modelled as SDOF systems but with linear elastic behaviour and 1% and 5% damping. Ten ground motions were used as seismic input. Quantification of the effects of inelastic deformations on the response of secondary structure was

obtained through the definition of an amplification factor. Thus, the design floor response spectra accounting for yielding of the supporting structure were obtained by using the amplification factors and conventional linear elastic floor response spectra.

Through an extensive study, Sewell et al. (1986) examined the influence of various factors on floor response spectra in nonlinear MDOF primary structures. In the study, the emphasis was on the comparison of equipment response in nonlinear and linear structures. The factors which mostly influence the response of elastic equipment in nonlinear structures are the number of degrees-of-freedom (DOF) of the structure, the localization of inelasticity in the structure, the distribution of strength, location of the equipment in the structure and the characteristics of input ground motion. Other factors, such as damping of the structure and equipment, did not show unusual or unanticipated influence on the response of equipment in inelastic MDOF structures. The study showed that in some cases of nonlinear structures floor response spectra can be greater than the floor response spectra of the corresponding elastic structures. It was shown that this trend is more pronounced when the yielding of structure is localized and the base input is narrow band centered near the fundamental frequency. Study also indicated that the absolute response of equipment can be predicted, for a given amount of structural inelasticity, in a simple manner from the input ground motion spectrum.

A method that fully takes into account interaction between the primary and secondary structure, as well as the inelastic behaviour of the supporting structure, was proposed by Villaverde (1987). The method is appropriate for the analysis of elastic MDOF secondary structures attached to one or two arbitrary points of inelastic MDOF primary structures. Both subsystems were considered as an integrated combined system, which was analysed by using an approximate procedure for modal analysis of multistory structures. The procedure was, however, restricted to primary structures with elasto-plastic behaviour and to those cases in which the secondary system has a small mass comparing to the primary system.

Igusa (1990) examined how nonlinear response differs from linear. Under the assumption of moderate nonlinearities he developed analytical expressions for the wide-band nonlinear response. Primary-secondary system was modelled as 2-DOF system. Nonlinear equations for system's response were solved by using the equations for the linear 2-DOF primary-secondary system, which were previously obtained by Igusa and Der Kiureghian (1985). The effect of nonlinearity has proven to be more important than the effect of interaction between two subsystems.

A very simple method for the direct determination of floor response spectra in elastic SDOF structures was proposed by Yasui et al. (1993). This method represents an important part of the dissertation and it is discussed in more detail in Chapter 3, as well as in ANNEX A.

Novak and Fajfar (1994) conducted a parametric study which was based on uncoupled SDOF inelastic primary and SDOF elastic secondary structure. Natural period of vibration and ductility of the primary structure were varied. Three hysteretic models were assumed: elasto-plastic, bilinear with 10 per cent hardening and stiffness degrading Q-model. Damping ratio for the primary structure was chosen to be 5%. A simplified method for the direct generation of floor response spectra that takes into account the nonlinear behaviour of the primary structure was also proposed. It was concluded that inelasticity of the primary structure reduces peak values of floor response spectra obtained for elastic primary structures. Similar but extended study was conducted by Fajfar and Novak (1995). The basic idea used in those studies (consideration of inelastic structural behaviour) was also used in this dissertation.

Interesting research results were obtained by Singh et al. (1996). The study showed that in some cases floor response spectra in inelastic structures can be greater in the high frequency range than the corresponding floor response spectra in elastic structures. According to the authors, the main reason for this is the phenomenon of internal resonance in nonlinear vibrations. Internal resonance can be observed in the case of structures with concentrated inelasticity, while structures with distributed inelasticity do not show sensitivity to this phenomenon. Analysis showed that higher intensity of seismic input, as well as the higher level of inelasticity, tends to increase the effect of internal resonance. On the other hand, an increase in the damping ratio of the primary and secondary structure tends to diminish it.

Adam and Fotiu (2000) conducted a parametric study where a primary structure was modelled as a four story frame, and a secondary structure as a SDOF oscillator attached to it. Two methods for analysis of coupled primary-secondary systems were proposed. The behaviour of both primary and secondary structures was assumed elastic and bilinear elasto-plastic. The results of uncoupled analysis were also presented for the purpose of comparison. North-south component of El Centro earthquake was used as seismic input. It has been shown that inelastic behaviour significantly reduces the response of the secondary structure. The effect of interaction between primary and secondary structure increases with an increase in the modal mass ratio. Non-classical damping does not affect significantly the response of the secondary subsystem.

Rodriguez et al. (2002) gave an emphasis to the interaction between a building nonlinear response and the magnitude of floor accelerations. Parametric linear and nonlinear response-history analysis of regular cantilever wall buildings with rigid diaphragms was conducted. Analysis showed that the maximum floor accelerations occur in the top floor and that inelasticity significantly reduces them. The authors have also proposed a simple procedure that derives design floor horizontal forces. The procedure is based on the assumption that ductility only affects floor accelerations associated with the first mode of the response of the building.

Miranda and Taghavi (2005) proposed a simple method that can be used for a quick approximate evaluation of peak floor accelerations in elastic or practically elastic buildings subjected to a particular ground motion. In the method, the dynamic properties of multistory buildings are approximated by using an equivalent continuum model consisting of a flexural and shear cantilever beam and the first three modes of vibration are taken into account. The method is also applicable for structures whose stiffness is reduced along the height. Taghavi and Miranda (2005) investigated the accuracy of the proposed approximate method and concluded that the method produces good results with a small computational effort.

Singh et al. (2006) presented formulas that can be used to improve current estimate of the peak floor acceleration defined in 2003 NEHRP Provisions for the design of non-structural components in buildings. This work considered only the elastic behaviour of structures as well as the rigid non-structural components (Part I). Additional work was made on a subject of flexural non-structural components, which was also discussed by Singh et al. (2006) (Part II).

Seismic analysis of non-structural components in buildings can be conducted by an approximate method proposed by Villaverde (2006), which takes into account the nonlinear behaviour of both the primary structure and equipment. Geometric characteristics of the system, weights, target ductilities of the primary structure and equipment, fundamental natural period of the primary structure and the design response spectra are the only information required for the appliance of the method. The results

of comparative study were presented, and although they indicated that in all cases method leads to adequate design of non-structural components, the author suggested that the method needs to be investigated further. This should be achieved by considering non-structural components with different characteristics, mounted on different buildings.

Medina et al. (2006) studied the influences on floor response spectra for light secondary systems mounted on frame structures. This was conducted through numerical simulations on regular frames which represented structures and SDOF oscillator which represented equipment. It was concluded that the most important parameters that affect the shape and magnitude of floor response spectra are modal periods of the structure, location of the equipment in the structure and the damping ratio of the equipment. Distributed inelasticity of the structure reduces maximum floor accelerations, which is of great importance, especially in cases when period of vibration of the equipment is near the fundamental period of the structure. Peak accelerations of the equipment mounted on inelastic frames can be obtained by scaling peak accelerations of the equipment mounted on elastic frames with proposed acceleration response modification factor. Sankaranarayanan and Medina (2007) evaluated the dependence of the proposed acceleration response modification factor. They presented the values of the factor in three different floor response spectral regions. The study showed that both amplification and reduction of the elastic floor response spectra can occur in the different regions. Inelasticity of the structure tends to decrease elastic floor response spectra values when the structure and equipment have similar periods of vibrations. On the other hand, an increase in the floor response spectra values occurs in regions located between any two modal periods of the structure.

Politopoulos and Feau (2007) examined the influence of nonlinear response of SDOF primary structures on the floor response spectra. Secondary structures were also assumed to be SDOF but with linear elastic behaviour. As shown by previous studies, the nonlinear behaviour of the primary structure reduces the peak values of the floor response spectra in most of the range of frequencies. An equivalent linear oscillator can successfully reproduce the effect of elasto-plastic behaviour of the primary structure to the floor response spectra. A method for the design of floor response spectra based on the energy dissipation capacity of the primary structure has been proposed.

Kumari and Gupta (2007) proposed a modal combination rule for estimation of peak values of absolute floor accelerations in multistory shear buildings with linear elastic behaviour. In the proposed approach, seismic input was represented through pseudo-spectral acceleration spectrum. The correlations between the ground acceleration and the relative acceleration in each mode and the correlations between the relative accelerations in various modes were taken into account. It should be noted that is also possible to omit the aforementioned correlations in order to achieve a simpler variant of the proposed combination rule. A numerical study was performed in order to examine the accuracy of the proposed rule. Response-history analysis was conducted on three different structures by using six ground motions and the obtained results indicated that the proposed rule produced satisfying results along the height of the considered buildings.

An extensive parametric study on seismic response of non-structural components in buildings with nonlinear behaviour was conducted by Chaudhuri and Villaverde (2008). The study was divided into two parts. The linear elastic behaviour of non-structural components was assumed in the first and nonlinear behaviour was assumed in the second part. Primary structures were modelled as both flexible and rigid steel frames. Dynamic interaction between the primary and secondary systems was taken into account (coupled analysis). General conclusion was that, in most cases, the nonlinear behaviour of the primary system has the favorable effect on the response of the secondary system. It

was also shown that it is justified to assume linear elastic behaviour of the secondary system. All obtained conclusions are valid for structures with bilinear hysteretic behaviour without stiffness degradation.

Acceleration of non-structural components in low and high-rise ductile frames was examined by Uma et al. (2010). Analysis was conducted for ultimate limit state and serviceability limit state intensities. It has been found that floor spectral response is mostly affected by the behaviour of the structure, especially in cases of tuning. The elastic behaviour of the structure tends to amplify acceleration of the equipment, while inelastic behaviour reduces it. The analysis showed that the intensity of seismic input also has an important influence on floor spectral response.

Oropeza et al. (2010) investigated the response of non-structural components in the case of uncoupled system and the nonlinear behaviour of the primary structure. Both subsystems were modelled as SDOF. Analysis was conducted for different natural frequencies of the primary structure, strength reduction factors, hysteretic models, and 5% damping ratio. As seismic input, a great number of ground acceleration time histories were used. The results obtained for all hysteretic models were generally consistent, except in the case of elasto-plastic model. The results were therefore classified into two groups: for the elasto-plastic and stiffness degrading models. They were presented as plots of amplification and resonance factors for different hysteretic models. The authors suggested possible modification of current design provisions, as well as some possible extensions of the study.

Politopoulos (2010) examined the influence of inelastic behaviour of MDOF structures on the floor response spectra. Inelastic frame structures which were designed by using the capacity design method represented inelastic MDOF structures. It was shown that uniformly distributed plasticity (in comparison with the single-storey plastic mechanisms) significantly attenuates amplification of the contribution of higher modes. Therefore, the study showed that capacity design methods have proven to be beneficial in reducing peak floor accelerations.

A comprehensive analysis of reinforced concrete buildings with different lateral force resisting systems and heights was conducted by Shoostari et al. (2010). The main purpose of the study was to provide a large volume of data which could improve design of operational and functional components of buildings in Canada. The study confirmed amplification of floor response spectra with respect to the ground spectral accelerations. Floor accelerations were highest at the roof level, gradually decreasing towards the first floor. The authors have derived an equation which provides generation of floor response spectra directly from uniform hazard spectra. The equation is applicable for the case of buildings on firm grounds in Canada.

Chaudhuri and Hutchinson (2011) performed a parametric study on stiff and flexible steel frame structures for the cases of elastic and inelastic behaviour. The study showed that in some cases peak floor accelerations in inelastic structures can be greater than in elastic structures. The authors proposed a practical approach for approximate prediction of peak floor accelerations in buildings that are expected to undergo moderate to severe ground excitations. The proposed procedure is empirical, since it is based on linear modal properties of the structure which are combined with modal response modification factors.

Pozzi and Der Kiureghian (2012) developed a response spectrum analysis method for the estimation of peak floor accelerations in elastic MDOF structures. The method is based on the Complete Quadratic Combination (CQC) rule and it approximately accounts for the contribution of truncated higher

modes. The method is able to provide a consistent estimation of peak floor accelerations along the entire height of the structure. In the study, the accuracy of the SRSS combination rule was also discussed, and it was concluded that it may lead to incorrect estimation of peak floor accelerations, especially near the supports of the structure.

Maniatakis et al. (2013) investigated higher mode effects in the case of RC frame structures. These effects turned out to be significant, even in the case of planar structures. It was shown that storey accelerations and inertial forces are strongly influenced by higher mode effects, whereas displacements and inter-storey drifts are not. The existence of the relation between the contribution of higher modes and ground motion characteristics was also shown. The study indicated that the adoption of unique reduction factor for all modes, which is based on the inelastic response in the fundamental mode, may lead to quite a significant underestimate of storey accelerations and inertial forces. In addition, the assumption of linear elastic behaviour for higher modes may lead to an overestimate of the response.

Wieser et al. (2013) conducted a series of nonlinear incremental dynamic analyses on four 3D ductile flexible moment resisting frame buildings in order to investigate floor acceleration responses and to identify the crucial parameters in the determination of acceleration demands on non-structural components. The authors proposed an alternative direct approach for determination of the design acceleration demands on non-structural components, as well as some changes in the current design codes.

Based on the results obtained in the study of inelastic SDOF oscillators, a methodology for estimation of peak floor acceleration demands in inelastic MDOF structures was proposed by Moschen et al. (2013). Effects of positive and negative post yield stiffness, as well as of different damping types were studied. The relationship between elastic spectral acceleration and inelastic peak floor acceleration demands was determined by using a regression analysis, whereas the prediction of peak floor accelerations was based on the first mode approximation procedure. The authors have suggested that there is a need for future testing and enhancement of the methodology.

Sullivan et al. (2013) conducted a study of floor response spectra taking into account SDOF primary structures with elastic and inelastic behaviour, which were subjected to accelerograms of varying seismic intensity. The elastic SDOF system represented equipment. In the paper, some of the current codes for the design of non-structural components were reviewed, and it was concluded that improvements are needed for both SDOF and MDOF supporting structures. The authors presented a new empirical approach in which the natural period and inelasticity of the primary structure define the shape of the floor response spectrum, whereas the damping of equipment defines its magnitude. Calibrated equations for the prediction of floor response spectra in SDOF primary structures were proposed.

The above described research was later extended by Calvi and Sullivan (2014), who proposed a procedure for the estimation of floor response spectra in elastic MDOF primary structures. Floor response spectra obtained from the proposed approach were compared with the floor response spectra obtained from the response-history analysis conducted on spatial RC wall structures of different height by using a set of 47 ground motions. From the presented results, which were obtained for a 20-storey structure, it was observed that the proposed approach provides satisfactory estimation of floor response spectra.

An assessment of several current code provisions which propose simplified formulas for the determination of seismic demands on non-structural components was conducted by Pinkawa et al. (2014), who found that these formulas may not be as straightforward as expected and that they can lead to unsafe design. It was shown that the coupled analysis of the structure-component system should be conducted in cases when the mass of the component is larger than 1% of the total mass of the structure, in order to obtain economic results. By contrast, in the case of light non-structural components, the authors suggested that the application of the floor response spectrum approach is suitable for the design.

Moschen et al. (2014) proposed a modified response spectrum method for the assessment of peak floor accelerations in elastic MDOF structures. The method is based on an extended CQC combination rule, relative accelerations, peak ground acceleration and the cross correlation coefficients between the two latter quantities. The method is not restricted to a specific type of lateral load bearing structure. Application of the method was demonstrated on a very flexible 24-storey frame structure and the obtained results showed satisfactory agreement with the results obtained from the response-history analysis. It was also observed that the SRSS rule produced rather poor results when applied on the considered structure.

1.3 The structure of the doctoral dissertation

The doctoral dissertation has two main objectives: to study, qualify and quantify all main influences that nonlinear seismic response of structures has on the floor acceleration spectra, and to develop a simplified practice-oriented method for generation of floor response spectra directly from ground motion spectra. Thus, the dissertation consists of two main parts, which are conducted separately for SDOF and MDOF primary structures.

In Chapter 2 of the dissertation the results of an extensive parametric study of floor response spectra obtained for SDOF primary structures are presented. Both elastic and inelastic primary structures were taken into account, while an elastic SDOF oscillator represented equipment in all cases. The structure and equipment were always treated as an uncoupled system. In the parametric study, a large number of floor response spectra were calculated. Various influences on floor response spectra were examined: natural period, hysteretic behaviour and ductility of the structure, as well as the damping of the equipment. The influence of the ground motion characteristics was also investigated. Two different sets, consisting of 30 ground records each, were used in the study.

Based on the results obtained and conclusions made in the parametric study (Chapter 2), a method for direct generation of floor response spectra from ground motion spectra for SDOF primary structures was developed in Chapter 3. As a basis for the development of the direct method, a very simple method for the direct determination of floor response spectra proposed by Yasui et al. (1993) was used. The idea for the extension of the original method to the nonlinear range was proposed by Novak and Fajfar (1994). The original method was developed for elastic structures and equipment, which were represented as uncoupled SDOF systems. In order to make the original direct method applicable to the case of inelastic SDOF structures, and to improve its accuracy in the resonance region, some changes were made, which are in detail described in Chapter 3. For the case of elastic SDOF structures, some of the results obtained by using the proposed direct method were compared with the results of the original method proposed by Yasui et al. (1993), as well as with the results obtained in the parametric study, i.e. results obtained by using response-history analysis. In order to validate the proposed direct method for the case of inelastic SDOF structures, the results of the method were

compared with the results obtained in the parametric study, with the results obtained by the procedure provided in Eurocode 8 (2004), as well with the results obtained by the direct method proposed by Sullivan et al. (2013).

Chapter 4 presents the results of an extensive parametric study of floor response spectra for MDOF primary structures, by taking into account elastic and inelastic structural behaviour. In all cases, the elastic behaviour of the SDOF equipment was assumed. Structures and equipment were treated as uncoupled. The influences of the type, natural period, hysteretic behaviour and ductility of the structure, as well as the influence of the damping of the equipment were studied. As the seismic input, a set of 30 ground records was used in the study. This set was also used in Chapter 2. Some issues related to structural modelling were also discussed. In the case of inelastic primary structures ductility demands were determined by using the nonlinear pushover-based N2 method. An interesting analysis of influence of individual modes on the floor response spectra was conducted for the case of elastic primary structures. Based on the obtained results, some general characteristics of floor response spectra were identified and discussed.

In the seismic design of acceleration-sensitive equipment, peak floor acceleration (PFA) represents a very important parameter. The determination of PFA also represents a significant part in the floor response spectrum approach. In Chapter 5 a discussion of PFAs in elastic and inelastic MDOF primary structures is presented, along with the proposed approach for direct determination of PFAs, which is based on a standard modal response spectrum analysis. The proposed approach is applicable for elastic primary structures and, as an approximation, also for inelastic primary structures. The PFAs obtained from the parametric study of floor response spectra for MDOF structures (Chapter 4) were compared with PFAs obtained directly from the proposed approach and the results were discussed.

Based on the direct method previously developed for SDOF primary structures (Chapter 3), and on the results obtained in the parametric study conducted on MDOF primary structures (Chapter 4), a method for direct generation of floor response spectra for MDOF structures was developed and presented in Chapter 6. The most important parts of the proposed method are: the modal superposition (which is an approximation in the case of inelastic structures), modal combination methods which are different in different period ranges of the equipment (methods proposed by USNRC 1.92 2006 and algebraic summation rule), and the N2 method. The proposed direct method was applied to elastic and inelastic MDOF primary structures previously analysed in Chapter 4, and the obtained results were compared with the results obtained from the response-history analyses. The comparison provided a proper evaluation of the method's accuracy.

A step-by-step overview of the proposed method for direct determination of floor response spectra in MDOF structures is presented in Chapter 7. In addition, a numerical example of the application of the method is also shown.

Main findings and conclusions are summarized in Chapter 8, along with original contributions and the suggestions for further research.

2 PARAMETRIC STUDY OF FLOOR RESPONSE SPECTRA FOR SINGLE-DEGREE-OF-FREEDOM STRUCTURES

This chapter presents the results of an extensive parametric study of floor acceleration spectra, taking into account the elastic and inelastic behaviour of primary structures, and the elastic behaviour of the equipment. The structures and equipment were modelled as uncoupled single-degree-of-freedom (SDOF) systems. The main goal of the parametric study was to determine some general characteristics of floor response spectra.

2.1 Description of seismic input and structural models

In the parametric study, a total of 12,240 floor response spectra were calculated by the procedure described in the Section 1.1, i.e. by using response-history analysis. A SDOF model was used for both the elastic and inelastic structures and elastic equipment, which were treated as uncoupled. The influences of the natural period, hysteretic behaviour and ductility of the structure, as well as the influence of the damping of the equipment, were studied. The influence of the ground motion characteristics was also investigated.

Two different sets, consisting of 30 ground records each, were used in the study. The records of each set were chosen so that their mean spectrum matched the target spectrum. The target spectrum was the elastic spectrum defined by Eurocode 8 (2004). Type 1 spectra for soil types B and D (each for one set of records) were used, with the peak ground acceleration (PGA) equal to 0.35g and 0.39g, respectively. Soil type B represented stiff, whereas soil type D represented soft soils. The characteristic periods of the ground motion T_C (i.e. the periods corresponding to the boundary between the acceleration and velocity controlled ranges of the ground motion spectrum) were equal to 0.5 and 0.8 s for soil types B and D, respectively. The selection of ground records was made by using the REXEL program (Iervolino et al. 2010) in the case of soil type B, whereas the software developed by the Baker Research Group (Jayaram et al. 2011) was used in the case of soil type D. The records which correspond to the soil type B were selected from European Strong-Motion Database (ESMD), whereas the records which correspond to the soil type D were selected from PEER Ground Motion Database. The data of the selected records are shown in Tables 2.1 and 2.2 (M denotes magnitude, whereas R denotes epicentral distance), for soil types B and D respectively. It should be noted that the ground motions which correspond to the soil type D were magnified by a scale factor equal to 1.15.

In the case of soil type D the chosen set of records did not contain pulse-like ground motions, whereas in the case of soil type B this was not considered within the process of ground motion selection, since the ESMD does not implicitly indicate whether a ground motion is pulse-like or not. Pulse-like ground motions are a special class of ground motions which contain a pulse in the velocity time-history of the motion and they represent a challenge in seismic performance assessment procedures. The procedure of identification of pulse-like records was proposed by Baker (2007), but the details of the procedure exceed the scope of the dissertation.

The target and mean spectra of the selected sets of records for both soil types are shown in Figure 2.1. It should be noted that, according to Eurocode 8 (2004), no value of the mean 5% damping spectrum of the chosen ground motions should be less than 90% of the corresponding value on the target 5% damping spectrum in the range of periods of $0.2T$ and $2.0T$, where T represents fundamental period of the structure in the direction where acceleration time-history will be applied. This was fully taken into account, i.e. the mean and the target spectra for 5% damping were fitted between 0.15 and 2.5 s. The

mean PGA values of 30 ground motions representing soil types B and D amounted to 0.43g and 0.50g, respectively.

The natural periods of the structures, T_p , used in the parametric study, amounted to 0.2, 0.3, 0.5, 0.75, 1.0 and 2.0 s. Three different hysteretic models were taken into consideration: elasto-plastic (EP), and stiffness degrading (Q) models with zero (Q_0) and 10% hardening (Q_{10}). Structures with strength degradation were not considered in the study. In the case of the Q models (see Q-Hyst model by Saiidi and Sozen 1979), the unloading stiffness degradation coefficient was equal to 0.5. Typical hysteretic behaviour is shown in Figure 2.2. The constant target ductility factor μ was assumed throughout the whole period range. It amounted to 1.0 (elastic structures), 1.5, 2.0 and 4.0. "Mass-proportional" damping amounted to 5% in the case of primary structures, and to 1, 3, 5 and 7% in the case of the equipment.

Table 2.1: Data of the selected set of ground motions which corresponds to soil type B

Preglednica 2.1: Podatki o izbranem setu akceleroogramov, ki ustreza tipu tal B

Event	Waveform / Earthquake ID	Year	Station	M	R [km]	PGA [g]
Montenegro	196/93	1979	ST62	6.9	25	0.31
Montenegro	196/93	1979	ST62	6.9	25	0.45
Montenegro	197/93	1979	ST63	6.9	24	0.24
Montenegro	199/93	1979	ST67	6.9	16	0.38
Montenegro	199/93	1979	ST67	6.9	16	0.36
Duzce 1	1703/497	1999	ST553	7.2	8	0.38
Duzce 1	1703/497	1999	ST553	7.2	8	0.51
Duzce 1	1560/497	1999	ST541	7.2	39	0.80
Duzce 1	1560/497	1999	ST541	7.2	39	0.75
Campano Lucano	290/146	1980	ST96	6.9	32	0.22
Campano Lucano	291/146	1980	ST276	6.9	16	0.18
Campano Lucano	291/146	1980	ST276	6.9	16	0.16
Izmit	1226/472	1999	ST553	7.6	100	0.31
Izmit	1226/472	1999	ST553	7.6	100	0.36
Izmit	1257/472	1999	ST772	7.6	20	0.30
Kalamata	413/192	1986	ST164	5.9	10	0.30
Kalamata	413/192	1986	ST164	5.9	10	0.22
Faial	7329/2343	1998	ST87	6.1	11	0.42
Faial	7329/2343	1998	ST87	6.1	11	0.38
Gazli	74/43	1976	ST27	6.7	11	0.62
Gazli	74/43	1976	ST27	6.7	11	0.72
Umbria Marche	594/286	1997	ST60	6.0	11	0.52
Umbria Marche	594/286	1997	ST60	6.0	11	0.46
Panisler	354/171	1983	ST133	6.6	33	0.13
Panisler	354/171	1983	ST133	6.6	33	0.16
Firuzabad	7162/2313	1994	ST3297	5.9	7	1.00
Firuzabad	7162/2313	1994	ST3297	5.9	7	1.06
Dinar	879/349	1995	ST271	6.4	8	0.32
Ionian	42/30	1973	ST8	5.8	15	0.25
South Iceland	6263/2484	2000	ST2484	6.5	7	0.51

Table 2.2: Data of the selected set of ground motions which corresponds to soil type D

Preglednica 2.2: Podatki o izbranem setu akceleroogramov, ki ustreza tipu tal D

Event	Waveform / Earthquake ID	Year	Station	M	R [km]	PGA [g]
Northridge-01	STC180	1994	Saticoy	6.7	12	0.48
Northridge-01	CNP196	1994	Canoga Park - T. Can.	6.7	15	0.42
Northridge-01	SCE288	1994	Sylmar STA-EAST	6.7	5	0.49
Northridge-01	RO3090	1994	Sun Valley Roscoe B.	6.7	10	0.44
Northridge-01	MUL279	1994	Beverly Hills - 14145	6.7	17	0.52
Northridge-01	ORR360	1994	Castaic Old Ridge Rt	6.7	21	0.51
Northridge-01	MUL009	1994	Beverly Hills - 14145	6.7	17	0.42
Northridge-01	ORR090	1994	Castaic Old Ridge Rt	6.7	21	0.57
Northridge-05	SYL090	1994	Sylmar County Hosp.	5.1	25	0.60
Loma Prieta	HSP000	1989	Hollister South&Pine	6.9	28	0.37
Loma Prieta	G02090	1989	Gilroy Array #2	6.9	11	0.32
Loma Prieta	HDA165	1989	Hollister Diff Array	6.9	25	0.27
Loma Prieta	A01090	1989	Foster City - Apeel 1	6.9	44	0.29
Loma Prieta	STG000	1989	Saratoga Aloha Ave	6.9	9	0.51
Chi-Chi	CHY036-E	1999	CHY036	7.6	16	0.29
Chi-Chi	TCU074-E	1999	TCU074	7.6	14	0.60
Chi-Chi	TCU074-N	1999	TCU074	7.6	14	0.35
Chi-Chi	TCU079-E	1999	TCU079	7.6	11	0.74
Chi-Chi	TCU072-N	1999	TCU072	7.6	7	0.40
Chi-Chi	TCU084-N	1999	TCU084	7.6	11	0.42
Landers	JOS090	1992	Joshua Tree	7.3	11	0.28
Landers	YER270	1992	Yermo Fire Station	7.3	24	0.25
Imperial Valley	H-E04140	1979	El Centro Array #4	6.5	7	0.49
Imperial Valley-06	H-DLT352	1979	Delta	6.5	22	0.35
Superstition Hills	B-IVW360	1987	Wildlife Liq. Array	6.2	18	0.21
Duzce	BOL000	1999	Bolu	7.1	12	0.73
San Salvador	NGI180	1986	National Geogr. Inst.	5.8	7	0.41
Coalinga	H-Z14000	1983	Parkfield - F. zone 14	6.4	30	0.28
Palm Springs	MVH135	1986	Morongo Valley	6.1	12	0.21
Gazli	GAZ090	1976	Karakyr	6.8	6	0.72

2.2 Analysis of structural models

Analysis of response of the primary structures was conducted using the OpenSees 2.2.2, which provides a wide band of options regarding hysteretic models and numeric solvers. Zero-Length element was used to define simple oscillator which represented SDOF primary structures. The behaviour of elastic structures was represented by the Elastic Material, the Steel01 Material was used in the case of EP structures, whereas the Hysteretic Material was used in the case of Q_0 and Q_{10} structures (for material details see Mazzoni et al. 2007). Newmark integration method was used for time-history analyses, taking into account coefficients $\gamma=0.5$ and $\beta=0.25$, i.e. acceleration was taken to be a constant within each time step. For each analysis, time step was taken to be equal to the time step of the applied ground motion. Since the procedure for achieving target ductility is iterative, MATLAB 7.5.0 was used as an input pre-processor. This way, a large number of input parameters could be taken into account at the same time, which significantly reduced time for conducting the parametric study. In

order to validate the results obtained from the OpenSees 2.2.2 and pre-processor input codes, a certain number of control analyses was conducted using the SAP2000 14.0.0 and NONLIN 6.01. A simple code for the calculation of floor response spectra was written in MATLAB 7.5.0 and the aforementioned Newmark integration method was used for time-history analyses of elastic SDOF equipment. Since the results of the parametric study contained a great number of data, MATLAB 7.5.0 was also used as a post-processor, which provided an easy processing of the analyses output. All data obtained in the parametric study was processed in SMI OpenOffice.org 3.0.0 and MS Office Excel 2007.

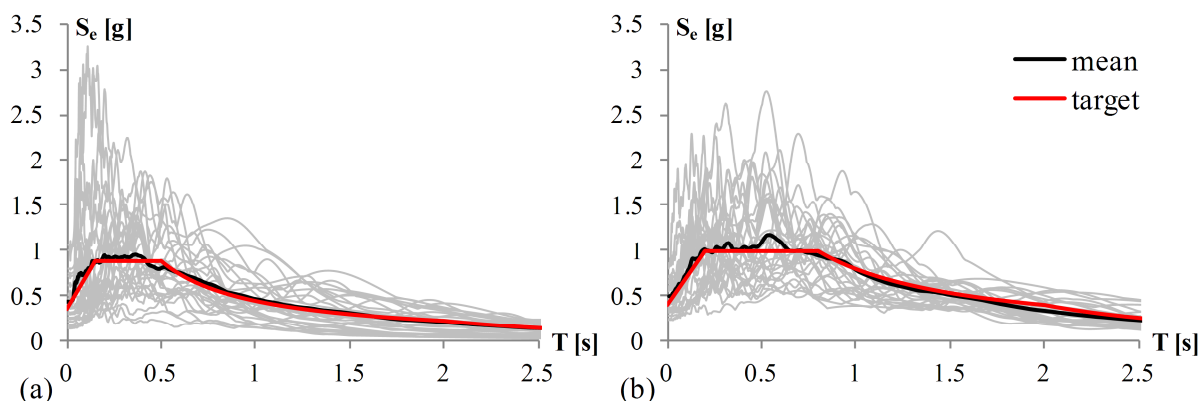


Figure 2.1: Elastic acceleration spectra (5% damping) of individual records, target and mean spectrum for (a) soil type B (target spectrum with $PGA=0.35g$) and (b) soil type D (target spectrum with $PGA=0.39g$)

Slika 2.1: Elastični spektri pospeškov (5% dušenja) posameznih zapisov, ciljni in povprečni spekter za (a) tip tal B (ciljni spekter s $PGA=0.35g$) in (b) tip tal D (ciljni spekter s $PGA=0.39g$)

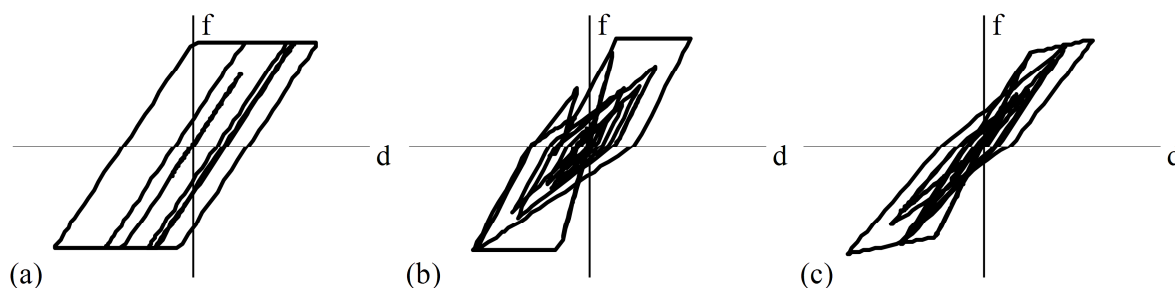


Figure 2.2: Hysteretic behaviour of (a) elasto-plastic (EP) and stiffness degrading (Q) model with (b) zero (Q_0) and (c) 10% hardening (Q_{10})

Slika 2.2: Histerezno obnašanje (a) elasto-plastičnega modela (EP) in modela s padajočo togostjo z (b) nič (Q_0) in (c) 10% utrditve (Q_{10})

2.3 Results of the study

The results obtained in the parametric study provided the basis for the development of the method for the direct generation of floor response spectra for inelastic structures. They showed some trends which can be considered as general characteristics of floor response spectra.

This section presents the most important results and conclusions of the study. The natural periods of the (primary) SDOF structure and of the equipment (the secondary structure) are denoted as T_p and T_s , respectively. The floor acceleration spectra values are denoted as A_s (or A_{s_e} in the special case of an

elastic structure). The peak acceleration of the structure is denoted as A_p . The results shown in Figures 2.3–2.20 were obtained for the sets of ground records which correspond to soil types B and D and for structures with the natural periods equal to 0.2, 0.3, 0.5, 0.75, 1.0 and 2.0 s. In all cases the damping of the structure (ζ_p) amounted to 5%, whereas the damping of the equipment (ζ_s) amounted to 1, 3, 5 and 7%.

The results obtained for the elastic, EP and Q_{10} model are presented. The floor response spectra shown in Figures 2.3–2.8 represent mean values, whereas in Figures 2.9–2.14 the ratios of floor response spectra for inelastic (A_s) and the corresponding elastic structures (A_{se}) are presented. The period range of a floor spectrum can be roughly divided into three regions, depending on the ratio T_s/T_p : the pre-resonance region ($T_s/T_p < 0.8$), the resonance region ($0.8 < T_s/T_p < 1.25$), and the post-resonance region ($T_s/T_p > 1.25$).

It is obvious from Figures 2.3–2.8 that in the pre-resonance and resonance regions, the behaviour of the equipment is strongly influenced by the behaviour of the primary structure. Both regions are characterized by a significant reduction in A_s due to inelastic structural behaviour and the size of the reduction depends on the ductility demand of the structure. This fact is of great importance for the development of the method for direct generation of floor response spectra. In the post-resonance region, the floor response spectrum is controlled by the ground motion spectrum, i.e. the floor response spectrum approaches to the ground motion spectrum as the ratio T_s/T_p decreases, which is also an important fact. Additionally, in the post-resonance region the inelastic structural behaviour has only a small influence on the floor response spectrum. If $T_s \gg T_p$, there is practically no reduction due to inelastic behaviour in the case of the EP model, whereas in the case of the Q_{10} model, some slight amplification can be observed. The same conclusion was made by Fajfar and Novak (1995).

In the limit case of infinitely rigid equipment, A_s is equal to A_p , i.e. to the value in the elastic (for $\mu=1$) or inelastic acceleration response spectrum of the structure at the period T_p . In the limit case of infinitely flexible equipment, the value of A_s is equal to zero. Additionally, it can be concluded from Figures 2.9–2.14 that the damping of the equipment practically has no influence on the ratio A_s/A_{se} .

The shape of floor response spectra is influenced by the hysteretic behaviour of the structure. In the case of the EP model, where the initial stiffness is the same at unloading after yielding and at reloading, the peak values of A_s occur close to the resonance ($T_s \approx T_p$). In the case of the Q_{10} model the peak values of A_s are shifted towards higher periods, due to increasing T_p with increasing plastic deformations.

Figures 2.15–2.20 show the floor response spectra normalized to the peak acceleration of the structure (A_s/A_p). This ratio is mainly influenced by the damping value of the equipment. It can be observed that, in the pre-resonance and resonance regions, the ratio A_s/A_p increases slightly with increasing ductility in the case of the EP model, whereas in the case of the Q_{10} model, in the resonance region, A_s/A_p decreases with increasing ductility.

Figures 2.21–2.23 present a comparison between the floor response spectra obtained for the stiffness degrading Q models (Q_0 and Q_{10}). The results were obtained for soil type B. It can be seen that the floor response spectra A_s obtained for the Q_0 model are lower than the spectra obtained for the Q_{10} model. The reduction is smaller or even disappears in the case of the ratio A_s/A_p , as shown in Figures 2.24–2.26, because the acceleration of the structure A_p is also smaller in the case of zero hardening, as discussed later in Section 3.2.

Figures 2.27 and 2.28 present maximum values of the ratio A_s/A_p , which will be hereinafter referred to as the amplification factor (*AMP*). Note that the peak acceleration of the structure A_p is equal to the value in the floor response spectrum for the zero period of the equipment ($T_s=0$).

$$AMP = \max(A_s / A_p) \quad (2.1)$$

The results obtained for both sets of ground motions indicate that the shape of the response spectrum characterized by the characteristic period of ground motion T_C has only a small influence on the amplification factor, provided that the ratio T_p/T_C is plotted on the x -axis instead of T_p .

It is clear from Figures 2.27 and 2.28 that, for both the EP model and the Q_{10} model of the structure, the main parameter that influences the amplitude of the *AMP* is the damping of the equipment ξ_s . The *AMP* reaches its peak value in the region $T_p/T_C \leq 1$, and then it decreases with the increasing ratio T_p/T_C if the ratio is larger than 1. The study showed that the difference between the *AMP* factors obtained for two different Q models is insignificant, i.e. hardening practically does not influence them.

The influence of ground motion (soil type B versus type D) is negligible, provided that the period T_p is normalized by the characteristic period of the ground motion T_C . In the case of the EP model, the influence of the ductility of the structure (μ) is also small, whereas in the case of the Q model it is moderate. In the case of the EP model, the *AMP* values slightly increase with increasing ductility, whereas in the case of the Q model they decrease (ductility $\mu=1$ corresponds to the elastic case).

Figure 2.29 shows the mean values of the *AMP* factors obtained for the EP model and Q_{10} model for two characteristic cases, i.e. when the ratio T_p/T_C is smaller, and larger than 1, respectively. Mean values were calculated for soil types B and D, and for natural periods of the structure T_p equal to 0.2, 0.3, 0.5, 0.75, 1.0 and 2.0 s. In the case of the EP model, the mean values were computed by taking into account the *AMP* values for ductility factors 1 (elastic structure), 2 and 4, whereas in the case of the Q_{10} model mean values were computed separately for ductility factors 2 and 4. In the case of $T_p/T_C \leq 1$, coefficient of variation (CV), which is defined as the ratio of standard deviation to the mean, amounted to about 0.03–0.05, whereas in the case of $T_p/T_C > 1$, it was in the range from 0.04 to 0.11.

As obvious from the input data described in Section 2.1, in the parametric study the minimum value of the structural period T_p amounted to 0.2 s, whereas the maximum value of the characteristic period of the ground motion T_C amounted to 0.8 s. This means that the previously obtained *AMP* are actually valid in regions $0.25 \leq T_p/T_C \leq 1$ and $T_p/T_C > 1$. This fact initiated additional study on SDOF systems with natural periods lesser than 0.2 s, in order to fill a gap between $T_p/T_C=0$ and $T_p/T_C=0.25$. Even though not important in the case of SDOF structures, such a study is crucial in the case of MDOF structures, since most higher modes lie in this region. In the study, only elastic SDOF systems were considered, with natural periods T_p which amounted to 0.025, 0.035, 0.05, 0.06, 0.075, 0.10, 0.11 and 0.12 s. A set of ground motions which corresponds to the soil type B (see Section 2.1), with the characteristic period T_C equal to 0.5 s, was used as the seismic input. Therefore, the additional *AMP* values were obtained for the ratio T_p/T_C equal to 0.05, 0.07, 0.10, 0.12, 0.15, 0.20, 0.22 and 0.24, and for $\xi_s=1\%$ they amounted to 3.6, 4.9, 9.5, 9.3, 9.5, 10.7, 10.4, 10.4, respectively, whereas for $\xi_s=5\%$ they amounted to 2.2, 2.5, 4.1, 4.2, 4.3, 4.9, 4.8 and 4.5, respectively. The obtained results, which are graphically presented in Section 3.2 (see Figure 3.3), indicate that in the region between $T_p/T_C=0$ and $T_p/T_C=0.25$ the dependence between *AMP* and T_p/T_C is not simple.

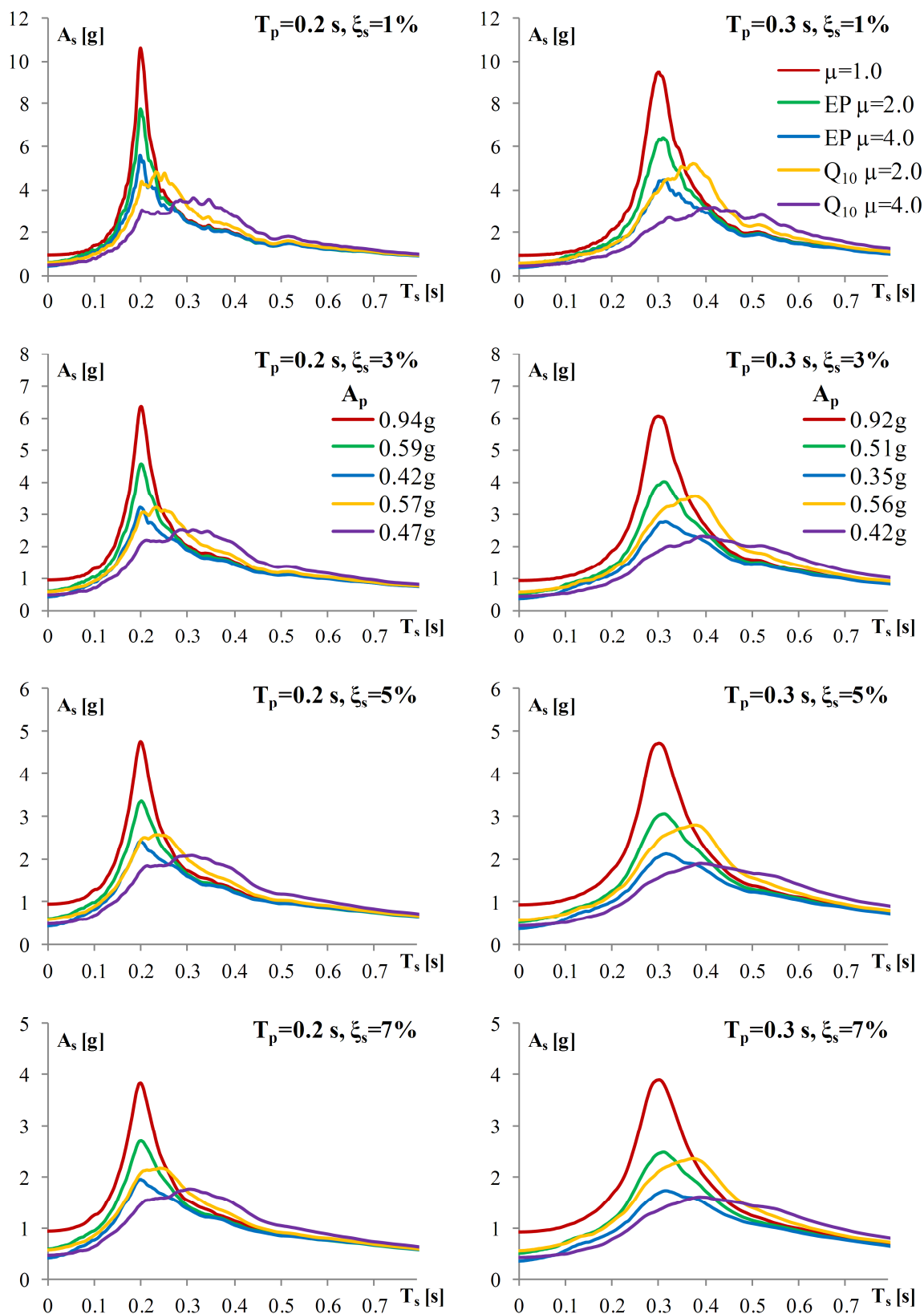


Figure 2.3: Mean values of the floor response spectra (A_s) and peak accelerations (A_p) for the structures with natural periods equal to 0.2 and 0.3 s, 5% damping of the structure and soil type B

Slika 2.3: Povprečne vrednosti etažnih spektrov odziva (A_s) in maksimalnih pospeškov (A_p) za konstrukcije, ki imajo nihajna časa enaka 0.2 in 0.3 s, 5% dušenja konstrukcije in tip tal B

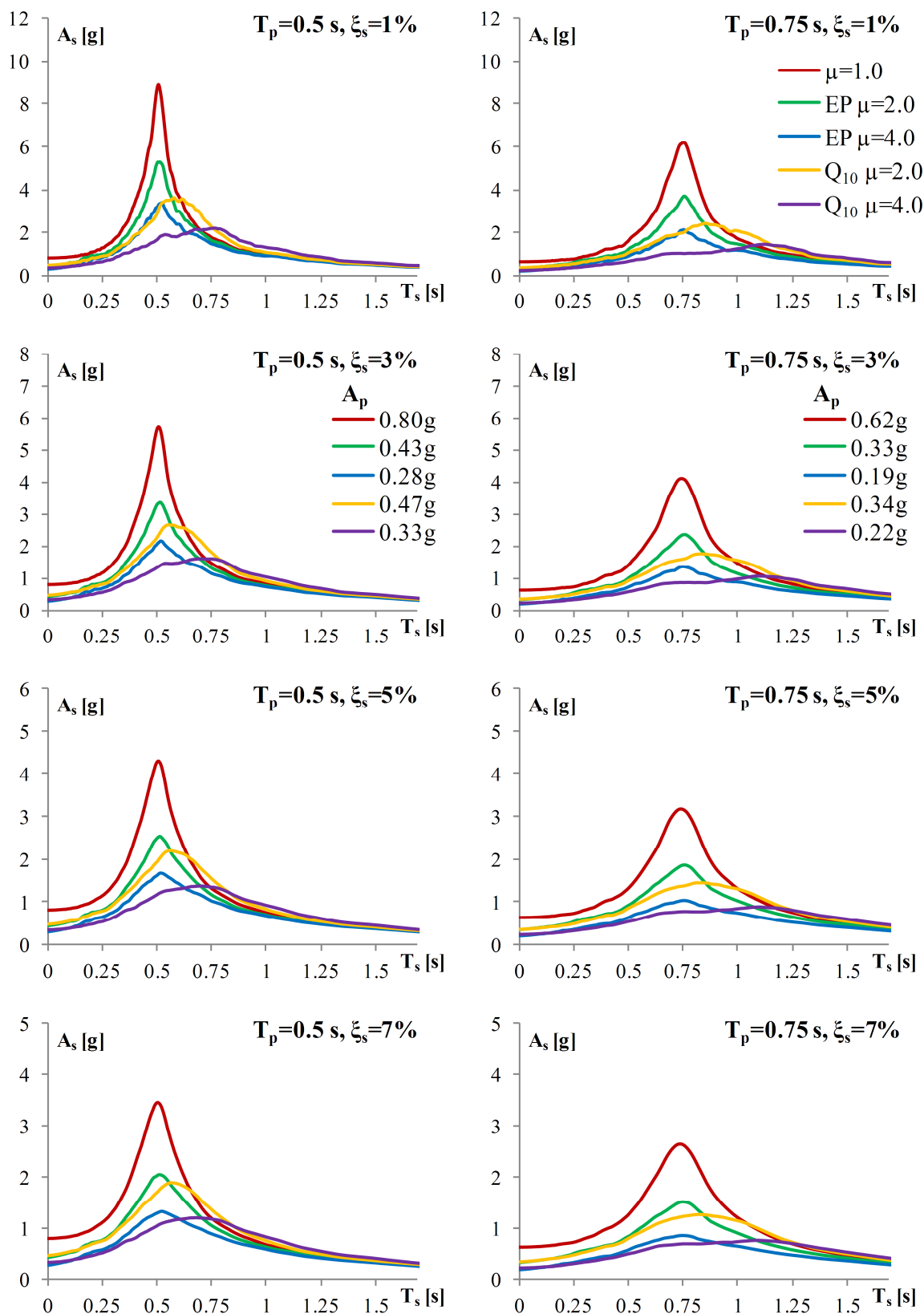


Figure 2.4: Mean values of the floor response spectra (A_s) and peak accelerations (A_p) for the structures with natural periods equal to 0.5 and 0.75 s, 5% damping of the structure and soil type B

Slika 2.4: Povprečne vrednosti etažnih spektrov odziva (A_s) in maksimalnih pospeškov (A_p) za konstrukcije, ki imajo nihajna časa enaka 0.5 in 0.75 s, 5% dušenja konstrukcije in tip tal B

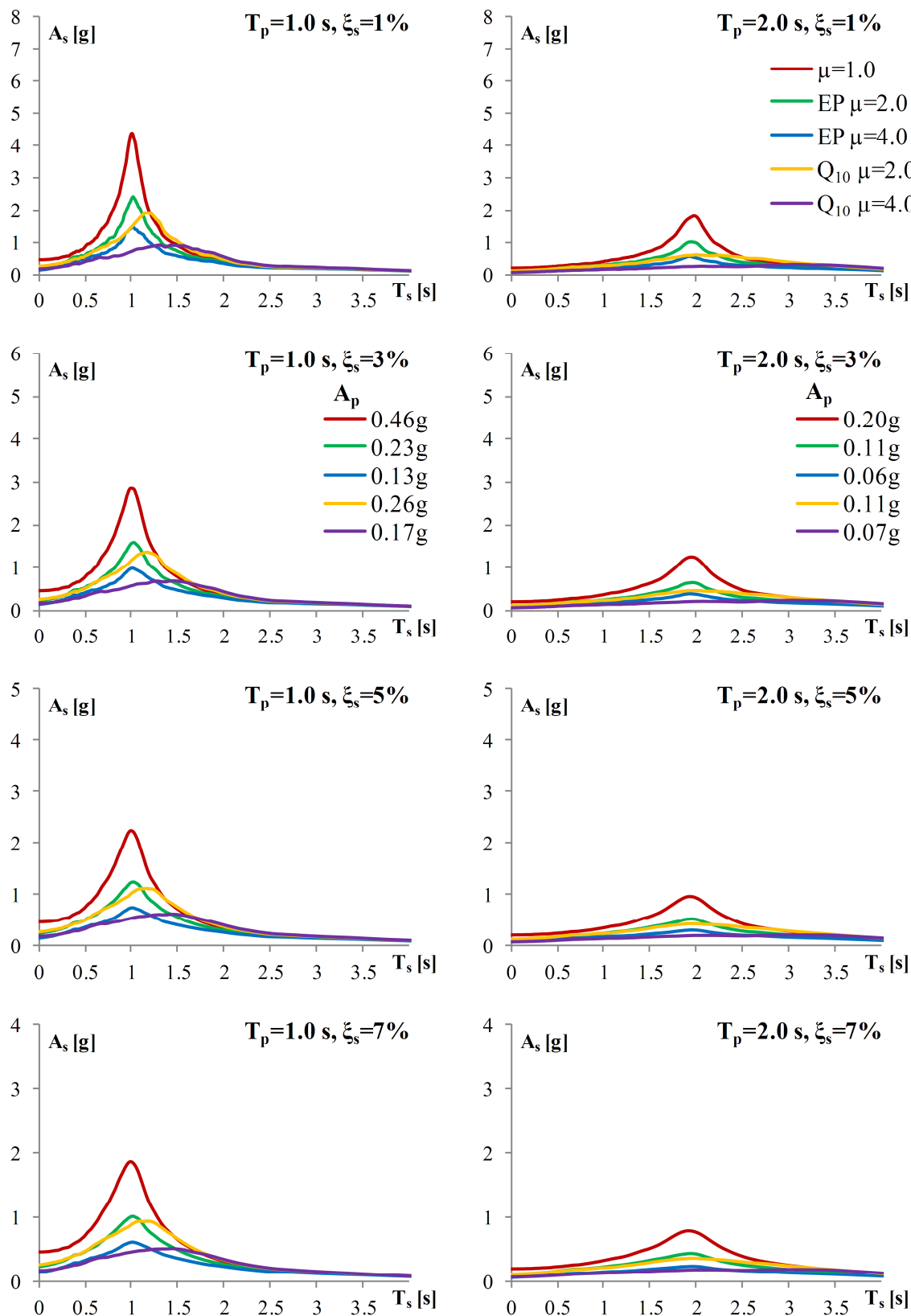


Figure 2.5: Mean values of the floor response spectra (A_s) and peak accelerations (A_p) for the structures with natural periods equal to 1.0 and 2.0 s, 5% damping of the structure and soil type B

Slika 2.5: Povprečne vrednosti etažnih spektrov odziva (A_s) in maksimalnih pospeškov (A_p) za konstrukcije, ki imajo nihajna časa enaka 1.0 in 2.0 s, 5% dušenja konstrukcije in tip tal B

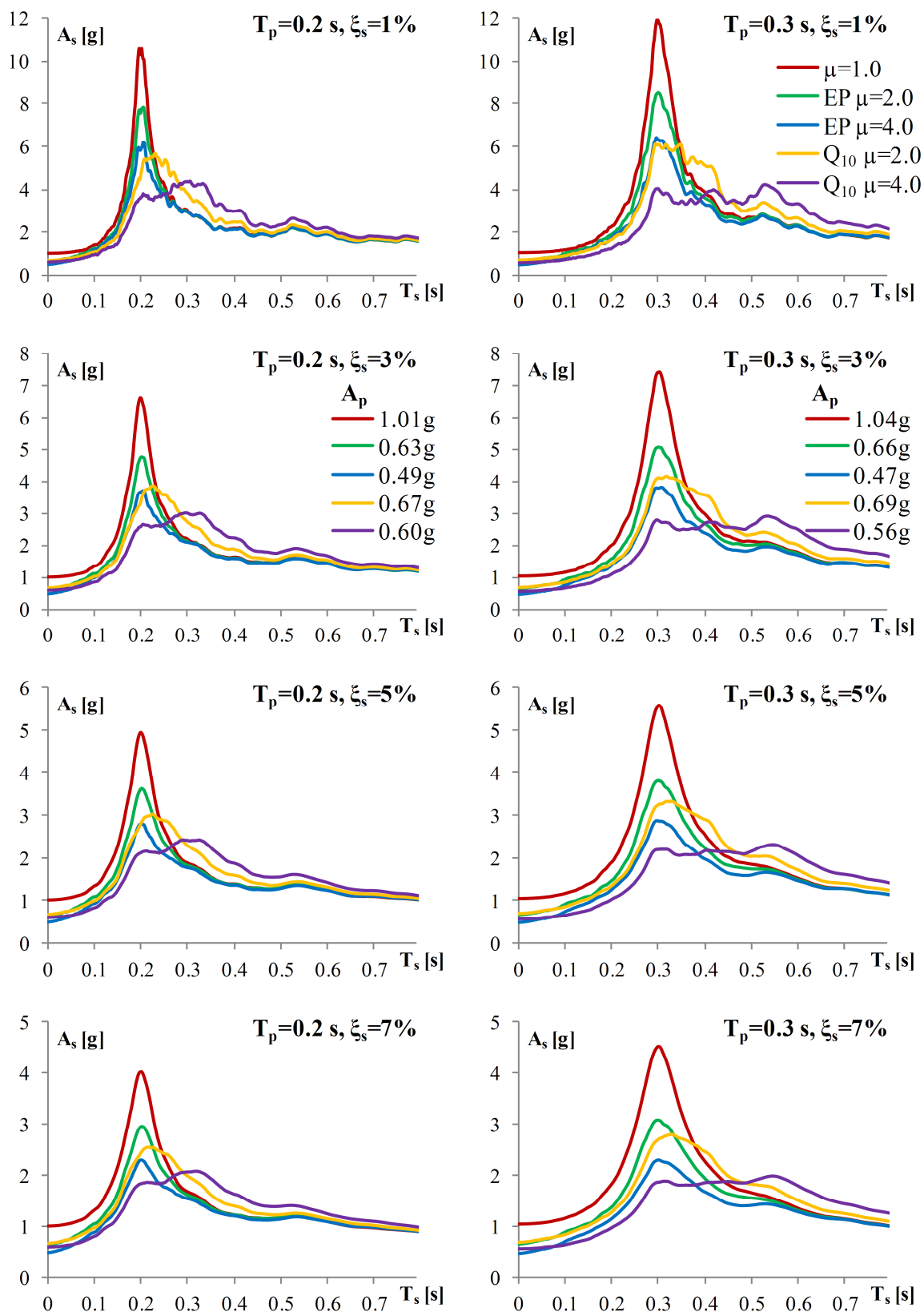


Figure 2.6: Mean values of the floor response spectra (A_s) and peak accelerations (A_p) for the structures with natural periods equal to 0.2 and 0.3 s, 5% damping of the structure and soil type D

Slika 2.6: Povprečne vrednosti etažnih spektrov odziva (A_s) in maksimalnih pospeškov (A_p) za konstrukcije, ki imajo nihajna časa enaka 0.2 in 0.3 s, 5% dušenja konstrukcije in tip tal D

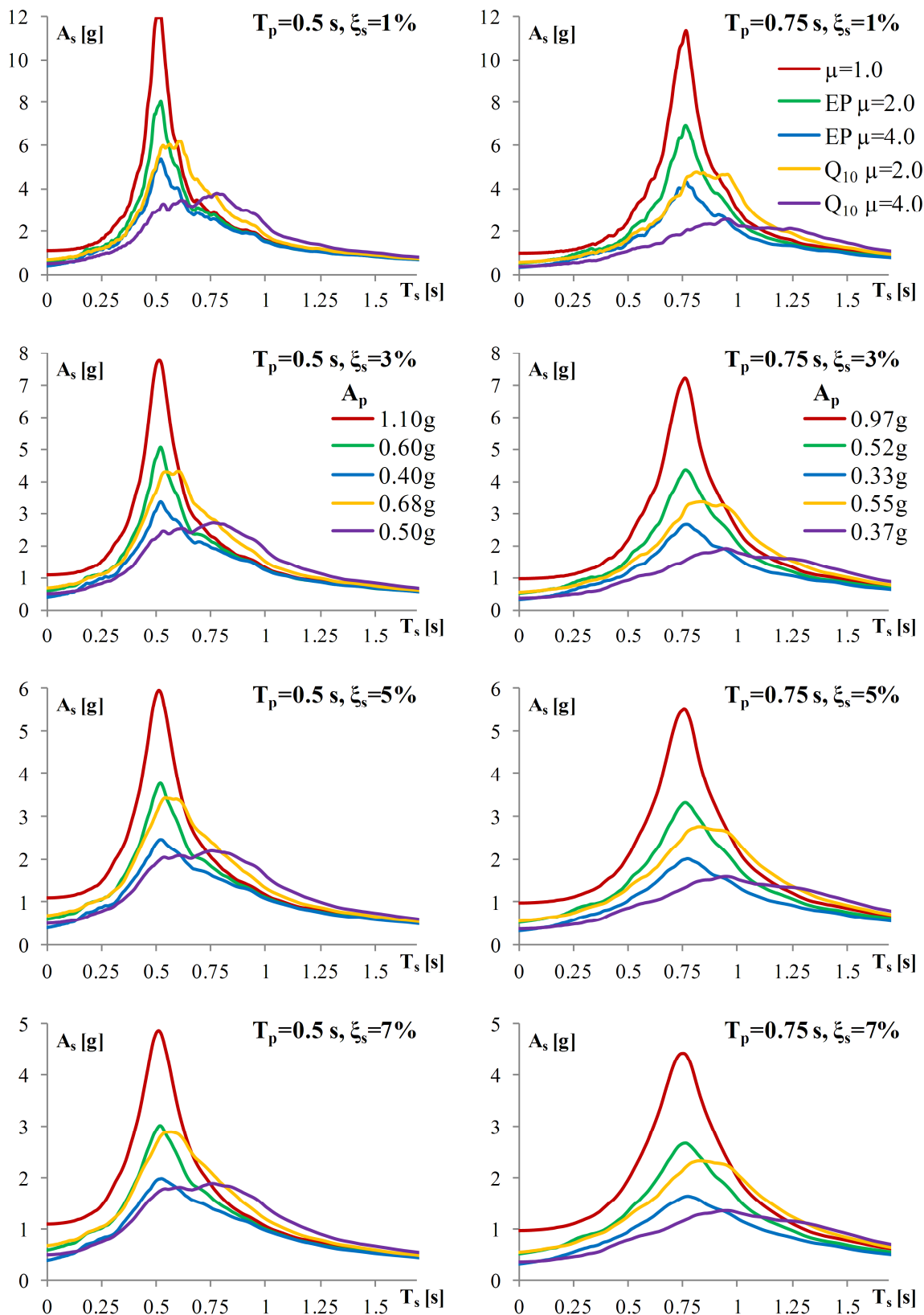


Figure 2.7: Mean values of the floor response spectra (A_s) and peak accelerations (A_p) for the structures with natural periods equal to 0.5 and 0.75 s, 5% damping of the structure and soil type D

Slika 2.7: Povprečne vrednosti etažnih spektrov odziva (A_s) in maksimalnih pospeškov (A_p) za konstrukcije, ki imajo nihajna časa enaka 0.5 in 0.75 s, 5% dušenja konstrukcije in tip tal D

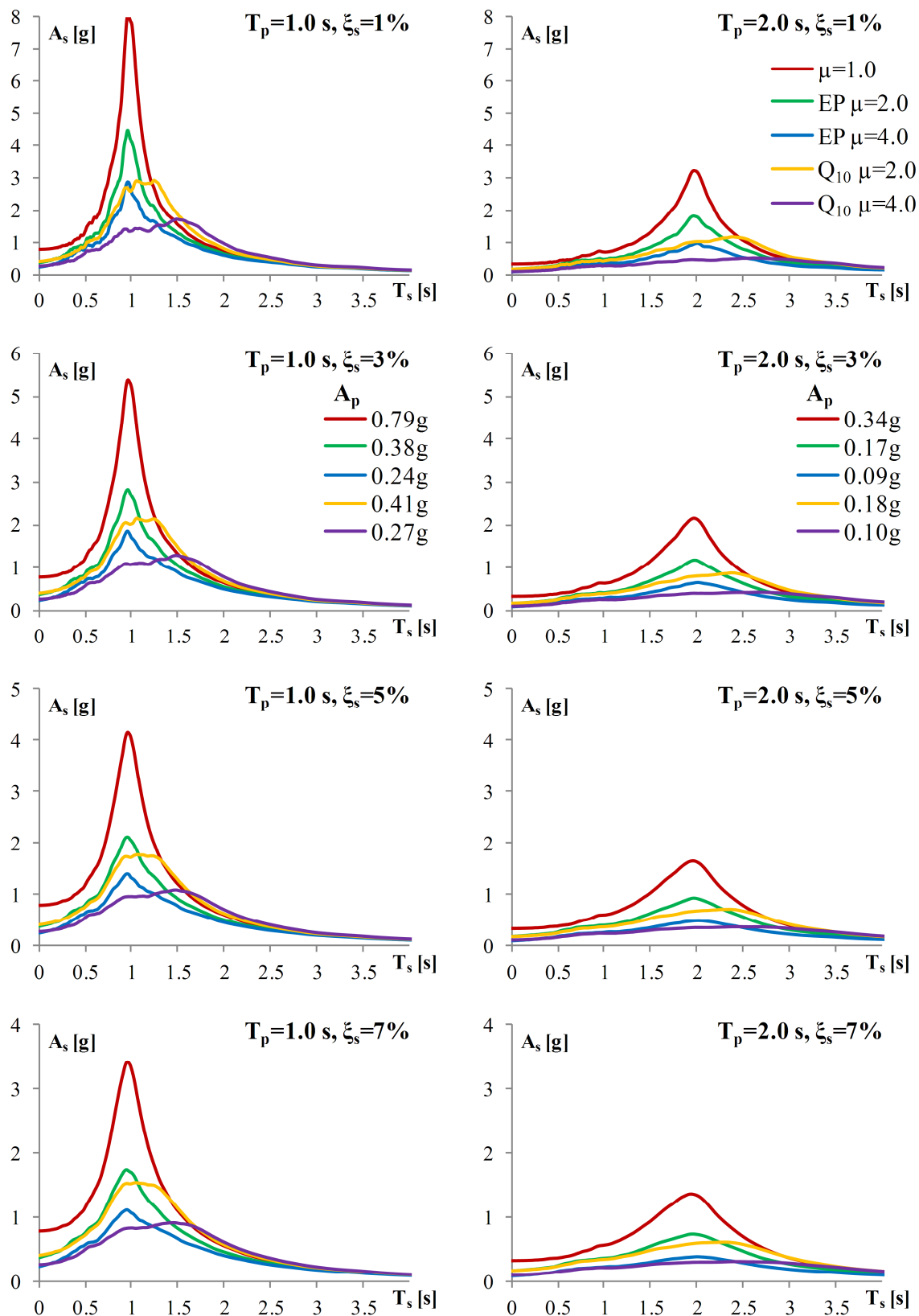


Figure 2.8: Mean values of the floor response spectra (A_s) and peak accelerations (A_p) for the structures with natural periods equal to 1.0 and 2.0 s, 5% damping of the structure and soil type D

Slika 2.8: Povprečne vrednosti etažnih spektrov odziva (A_s) in maksimalnih pospeškov (A_p) za konstrukcije, ki imajo nihajna časa enaka 1.0 in 2.0 s, 5% dušenja konstrukcije in tip tal D

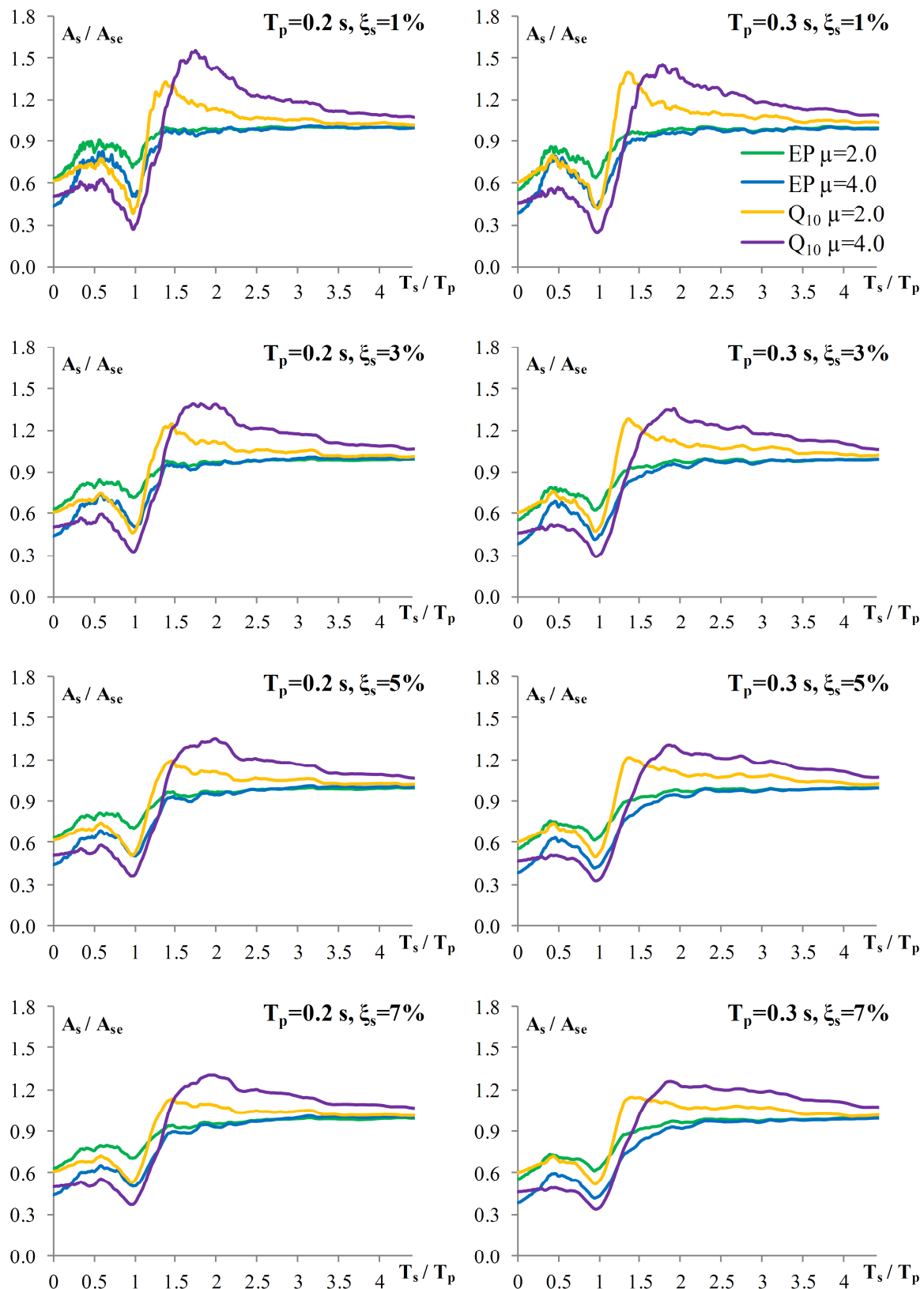


Figure 2.9: The ratio of the floor response spectra of the inelastic and elastic structures with natural periods equal to 0.2 and 0.3 s, 5% damping of the structure and soil type B

Slika 2.9: Razmerje etažnih spektrov odziva neelastičnih in elastičnih konstrukcij, ki imajo nihajna časa 0.2 in 0.3 s, 5% dušenja konstrukcije in tip tal B

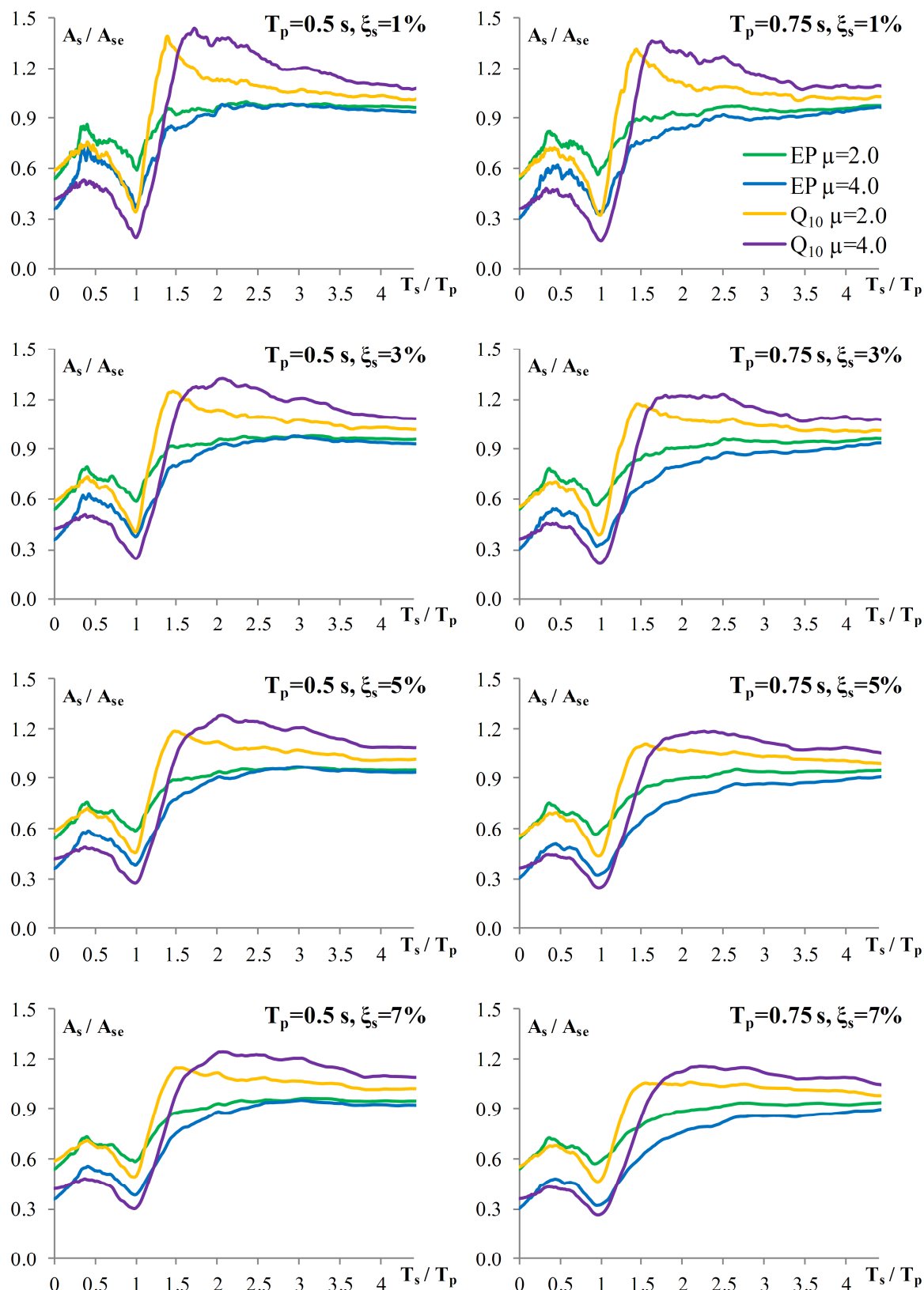


Figure 2.10: The ratio of the floor response spectra of the inelastic and elastic structures with natural periods equal to 0.5 and 0.75 s, 5% damping of the structure and soil type B

Slika 2.10: Razmerje etažnih spektrov odziva neelastičnih in elastičnih konstrukcij, ki imajo nihajna časa 0.5 in 0.75 s, 5% dušenja konstrukcije in tip tal B

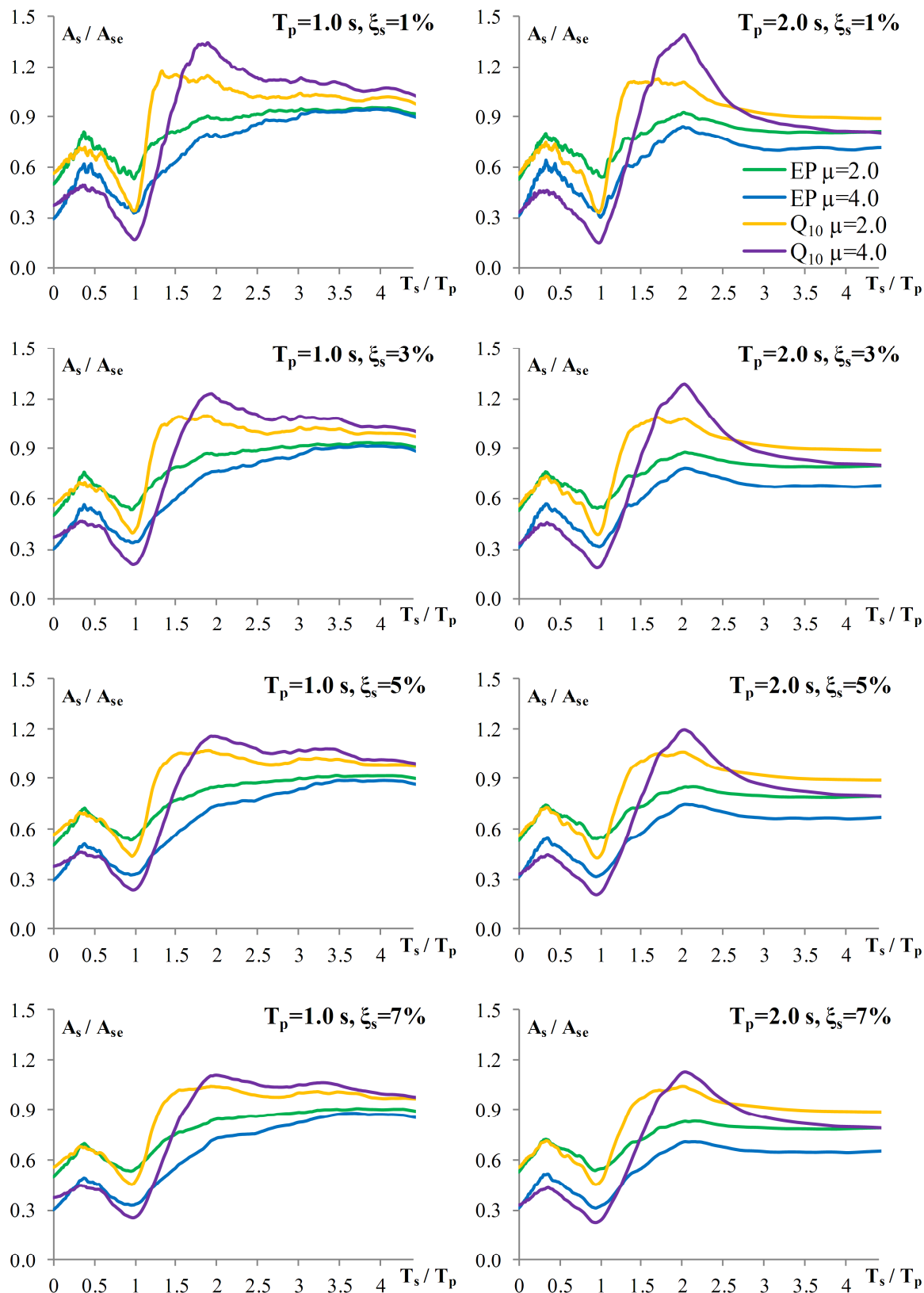


Figure 2.11: The ratio of the floor response spectra of the inelastic and elastic structures with natural periods equal to 1.0 and 2.0 s, 5% damping of the structure and soil type B

Slika 2.11: Razmerje etažnih spektrov odziva neelastičnih in elastičnih konstrukcij, ki imajo nihajna časa 1.0 in 2.0 s, 5% dušenja konstrukcije in tip tal B

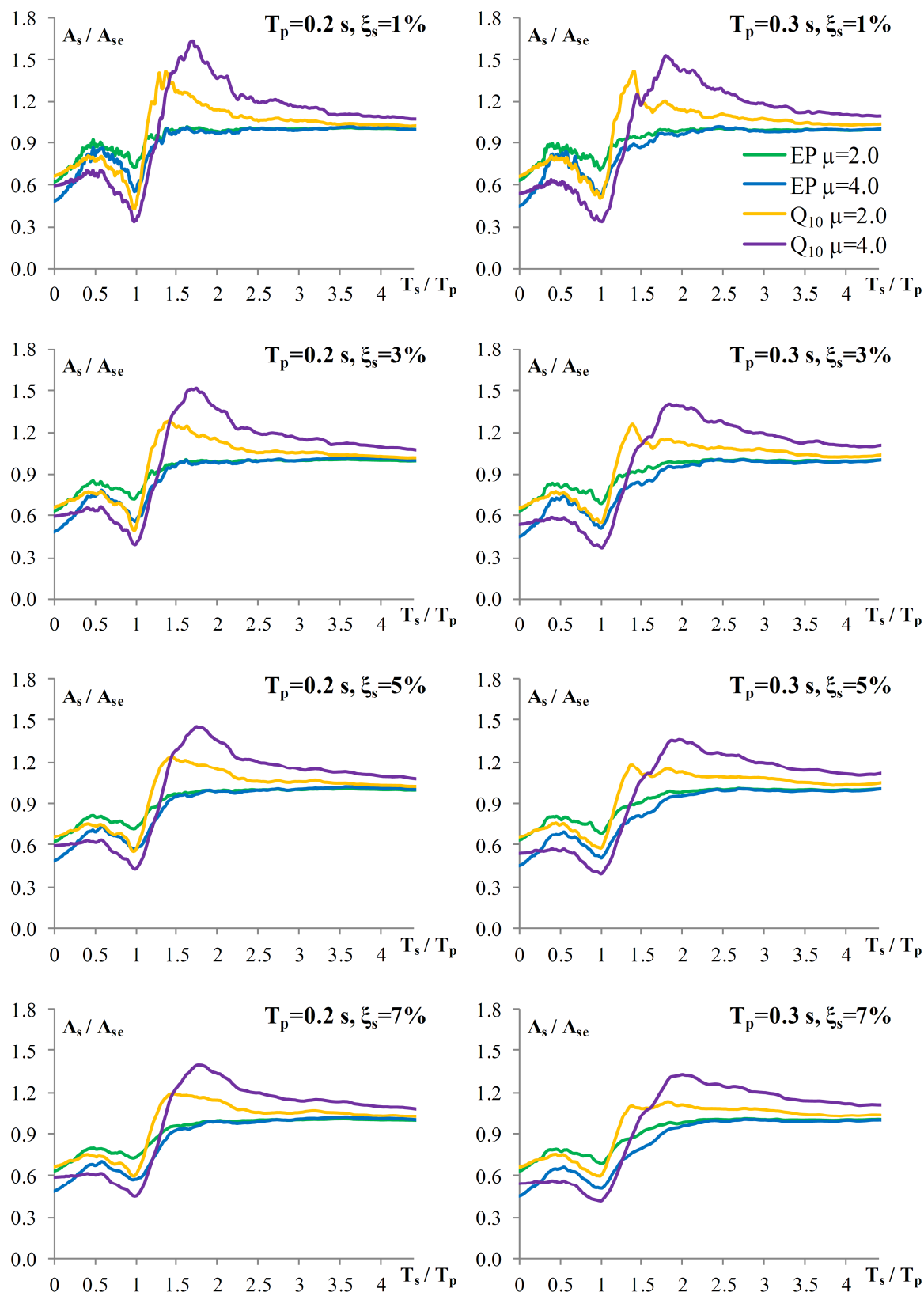


Figure 2.12: The ratio of the floor response spectra of the inelastic and elastic structures with natural periods equal to 0.2 and 0.3 s, 5% damping of the structure and soil type D

Slika 2.12: Razmerje etažnih spektrov odziva neelastičnih in elastičnih konstrukcij, ki imajo nihajna časa 0.2 in 0.3 s, 5% dušenja konstrukcije in tip tal D

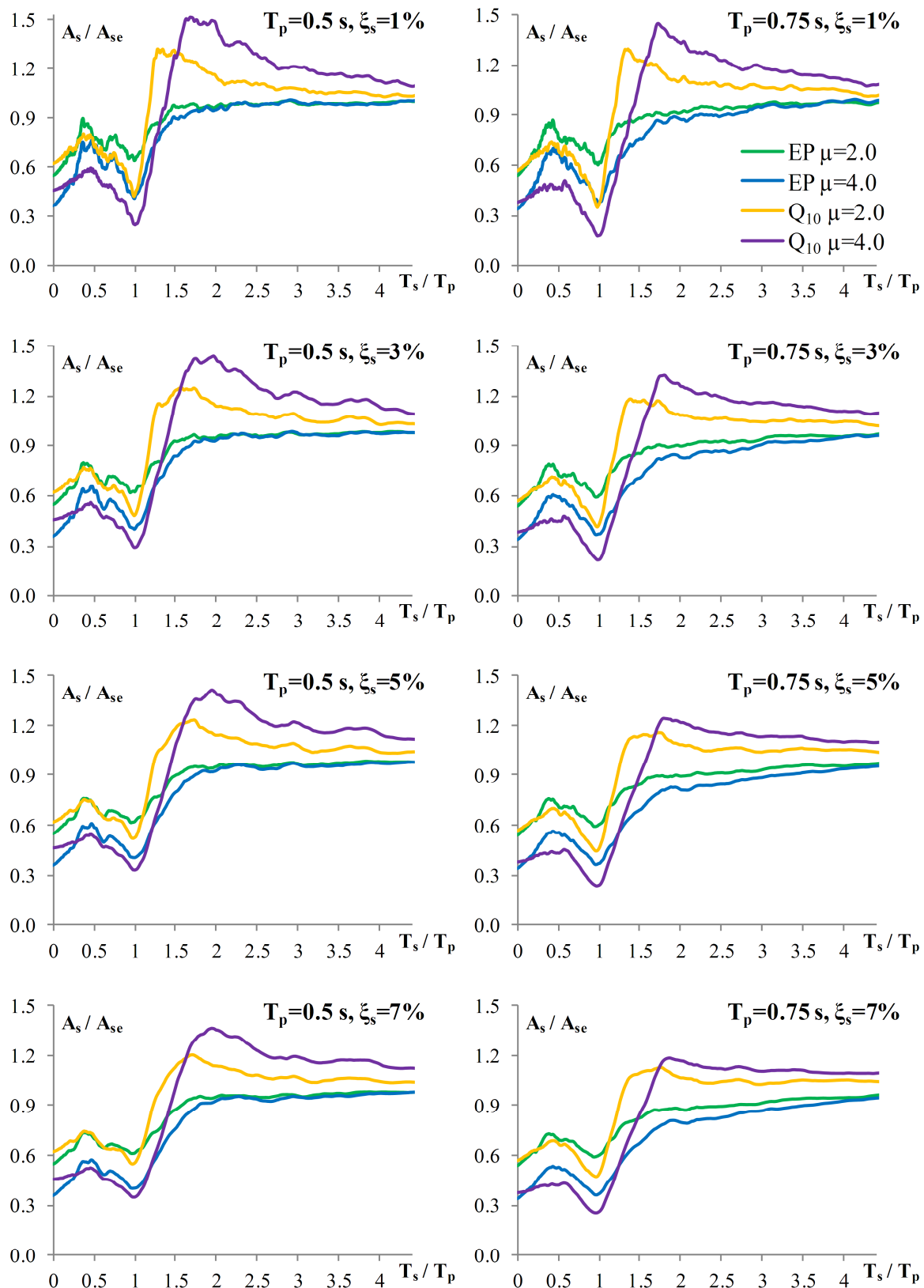


Figure 2.13: The ratio of the floor response spectra of the inelastic and elastic structures with natural periods equal to 0.5 and 0.75 s, 5% damping of the structure and soil type D

Slika 2.13: Razmerje etažnih spektrov odziva neelastičnih in elastičnih konstrukcij, ki imajo nihajna časa 0.5 in 0.75 s, 5% dušenja konstrukcije in tip tal D

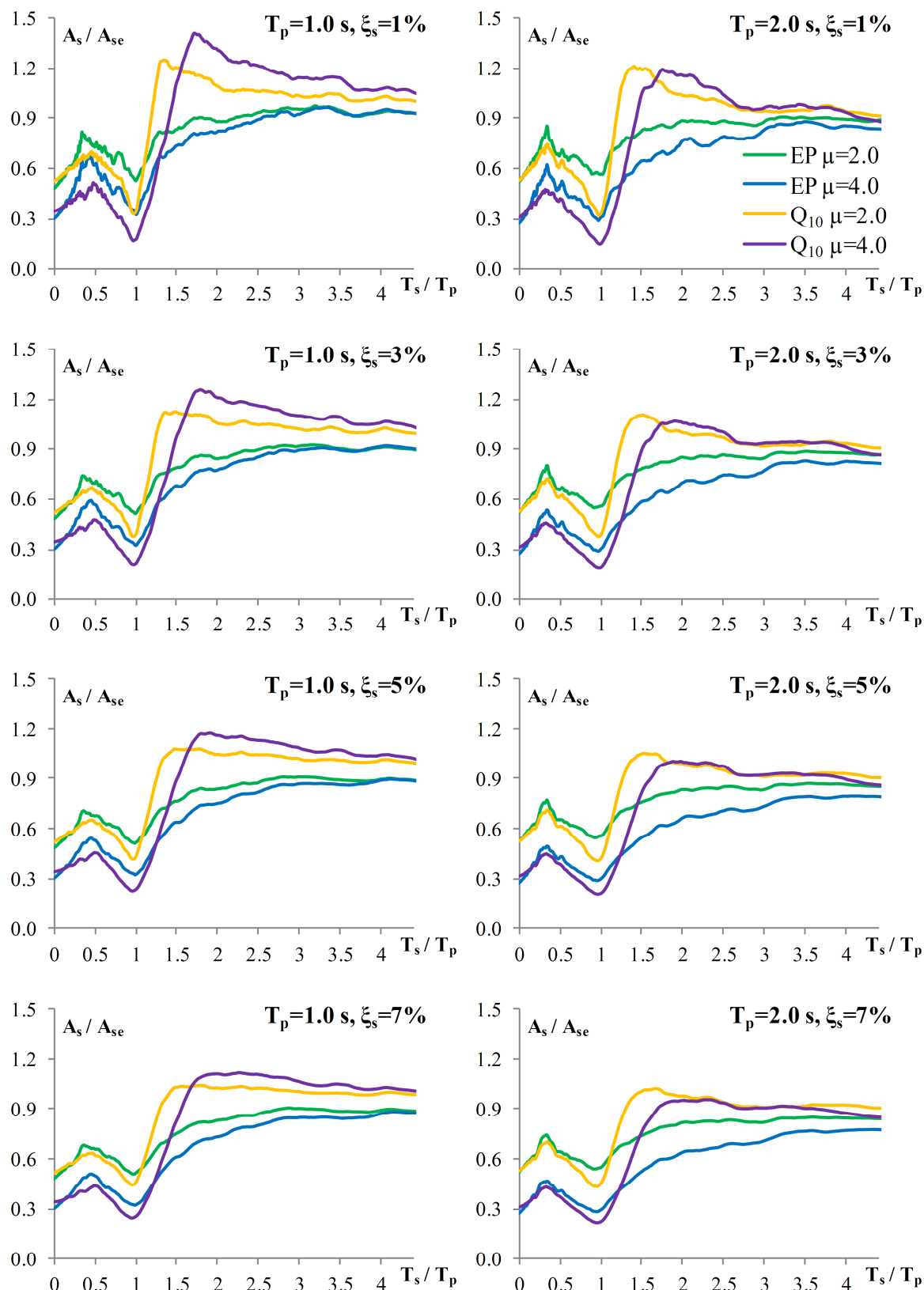


Figure 2.14: The ratio of the floor response spectra of the inelastic and elastic structures with natural periods equal to 1.0 and 2.0 s, 5% damping of the structure and soil type D

Slika 2.14: Razmerje etažnih spektrov odziva neelastičnih in elastičnih konstrukcij, ki imajo nihajna časa 1.0 in 2.0 s, 5% dušenja konstrukcije in tip tal D

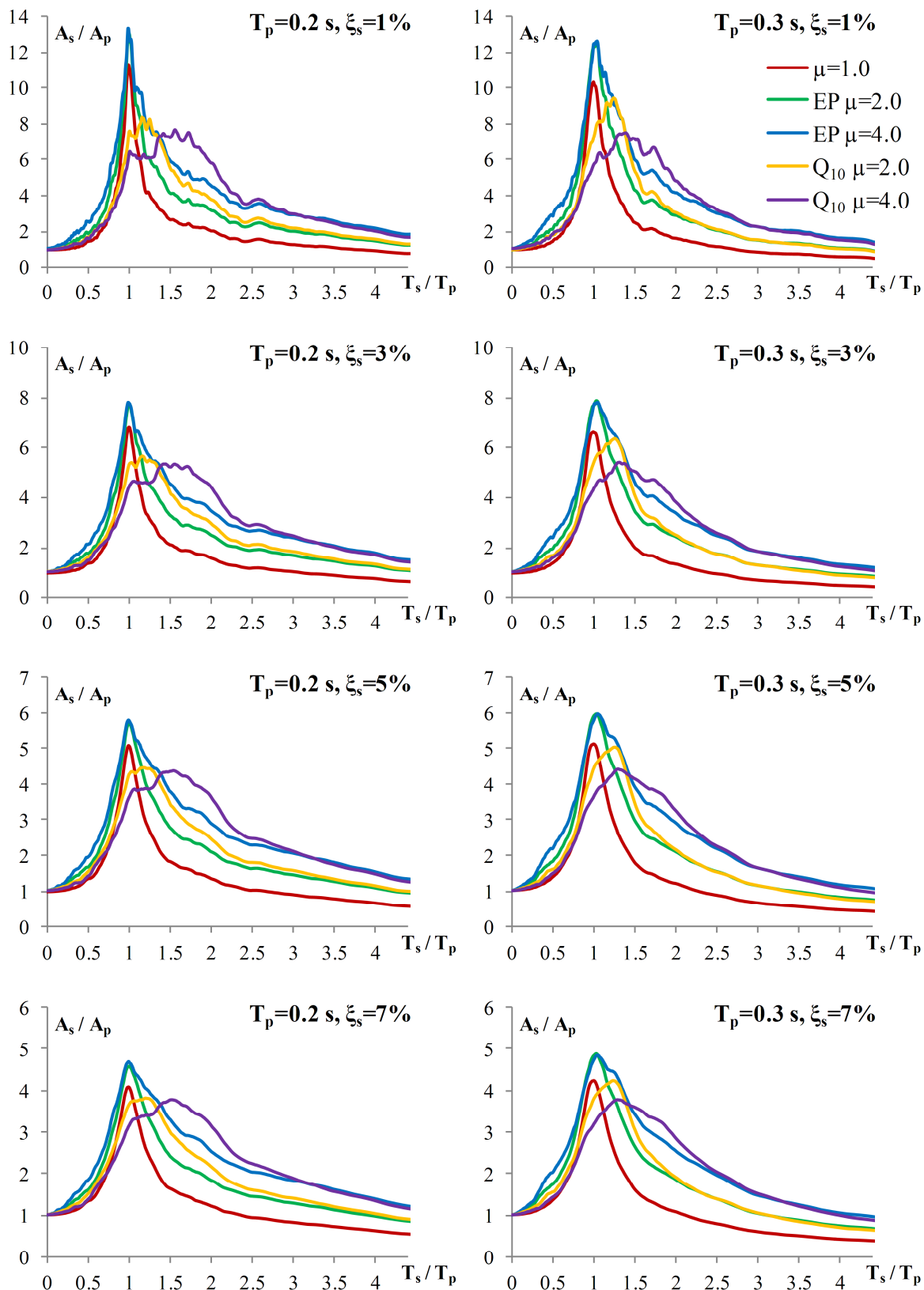


Figure 2.15: Floor response spectra normalized to the peak acceleration of the structures with natural periods equal to 0.2 and 0.3 s, 5% damping of the structure and soil type B

Slika 2.15: Etažni spektri odziva normirani na maksimalni pospešek konstrukcij, ki imajo nihajna časa 0.2 in 0.3 s, 5% dušenja konstrukcije in tip tal B

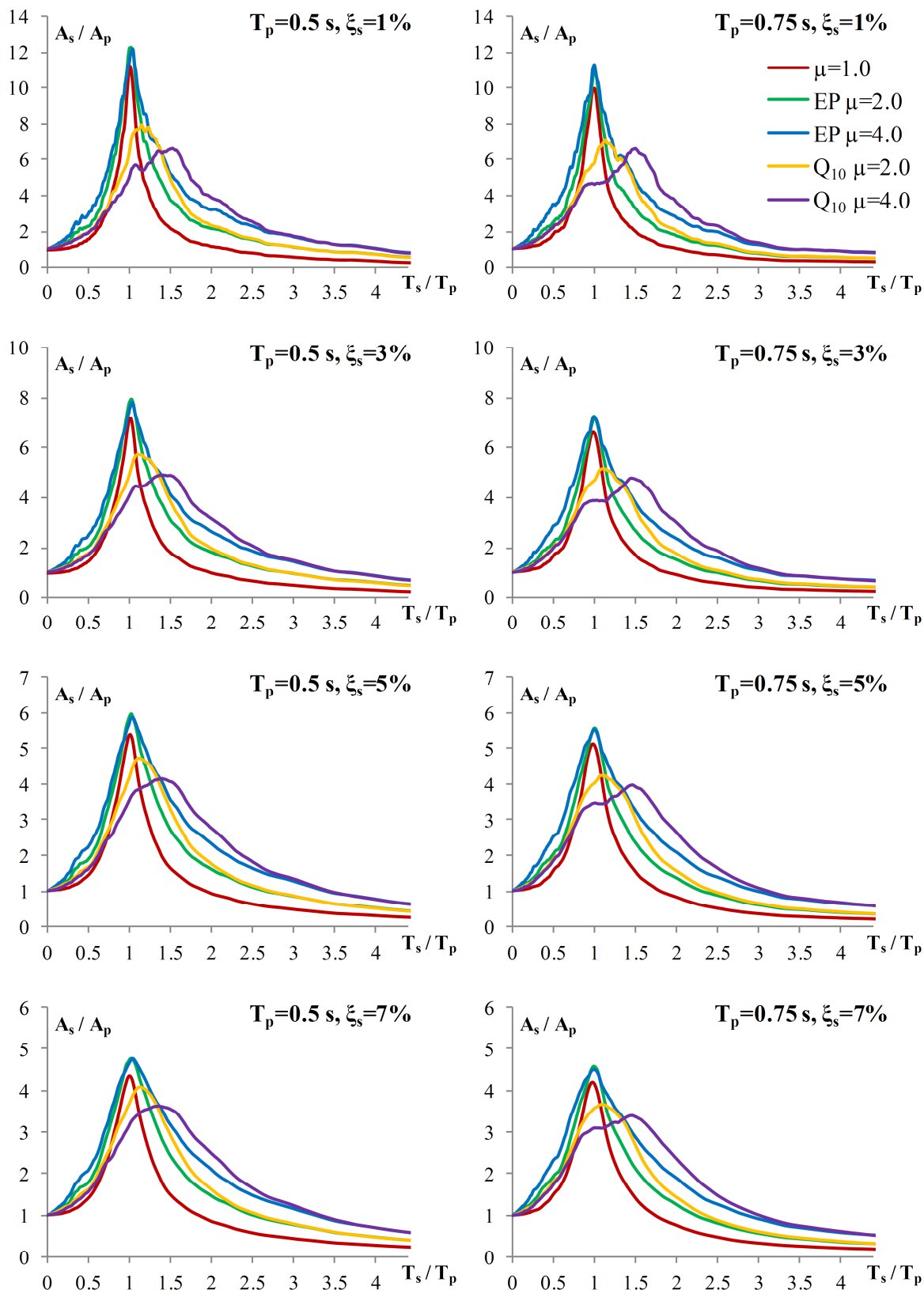


Figure 2.16: Floor response spectra normalized to the peak acceleration of the structures with natural periods equal to 0.5 and 0.75 s, 5% damping of the structure and soil type B

Slika 2.16: Etažni spektri odziva normirani na maksimalni pospešek konstrukcij, ki imajo nihajna časa 0.5 in 0.75 s, 5% dušenja konstrukcije in tip tal B

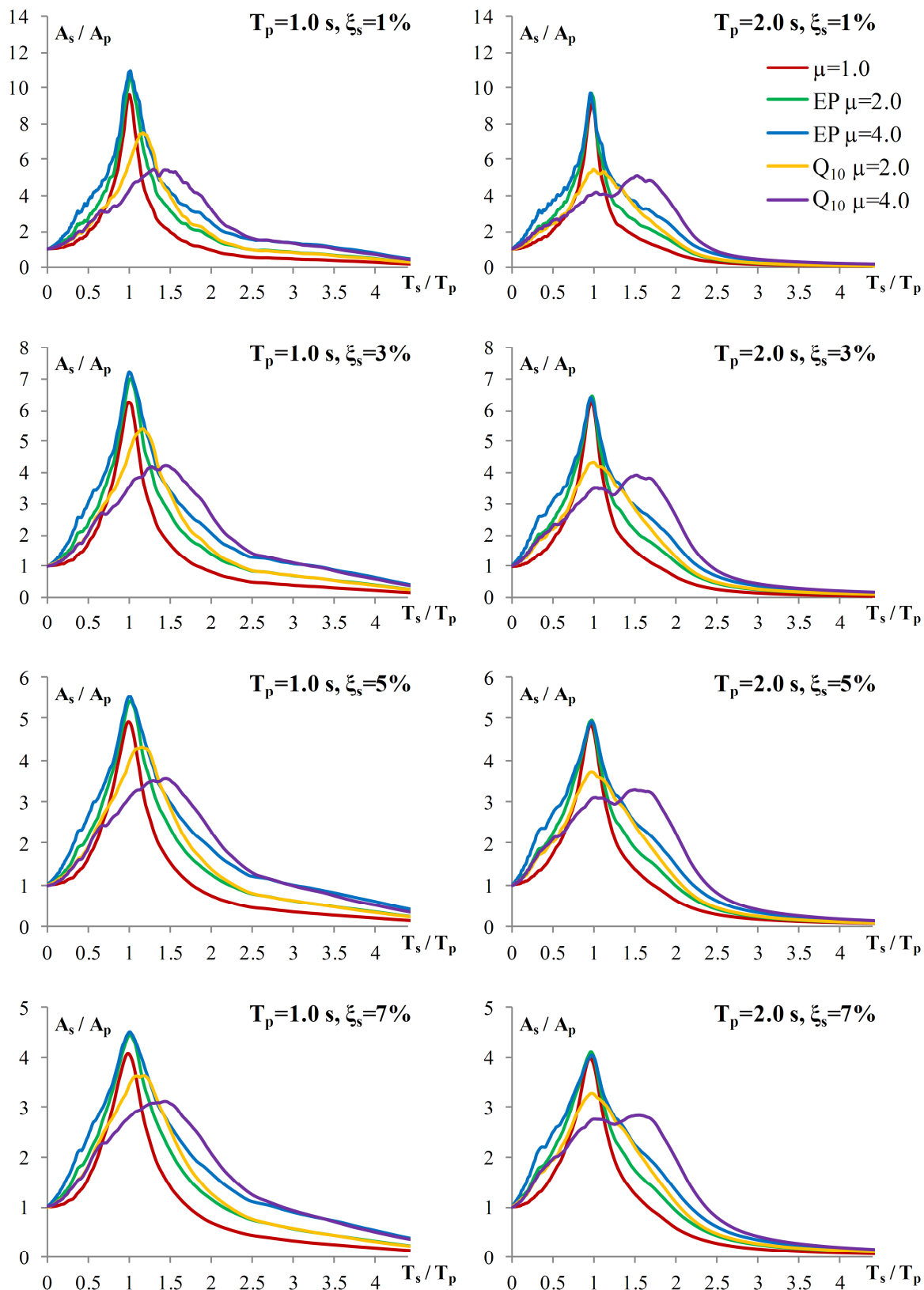


Figure 2.17: Floor response spectra normalized to the peak acceleration of the structures with natural periods equal to 1.0 and 2.0 s, 5% damping of the structure and soil type B

Slika 2.17: Etažni spektri odziva normirani na maksimalni pospešek konstrukcij, ki imajo nihajna časa 1.0 in 2.0 s, 5% dušenja konstrukcije in tip tal B

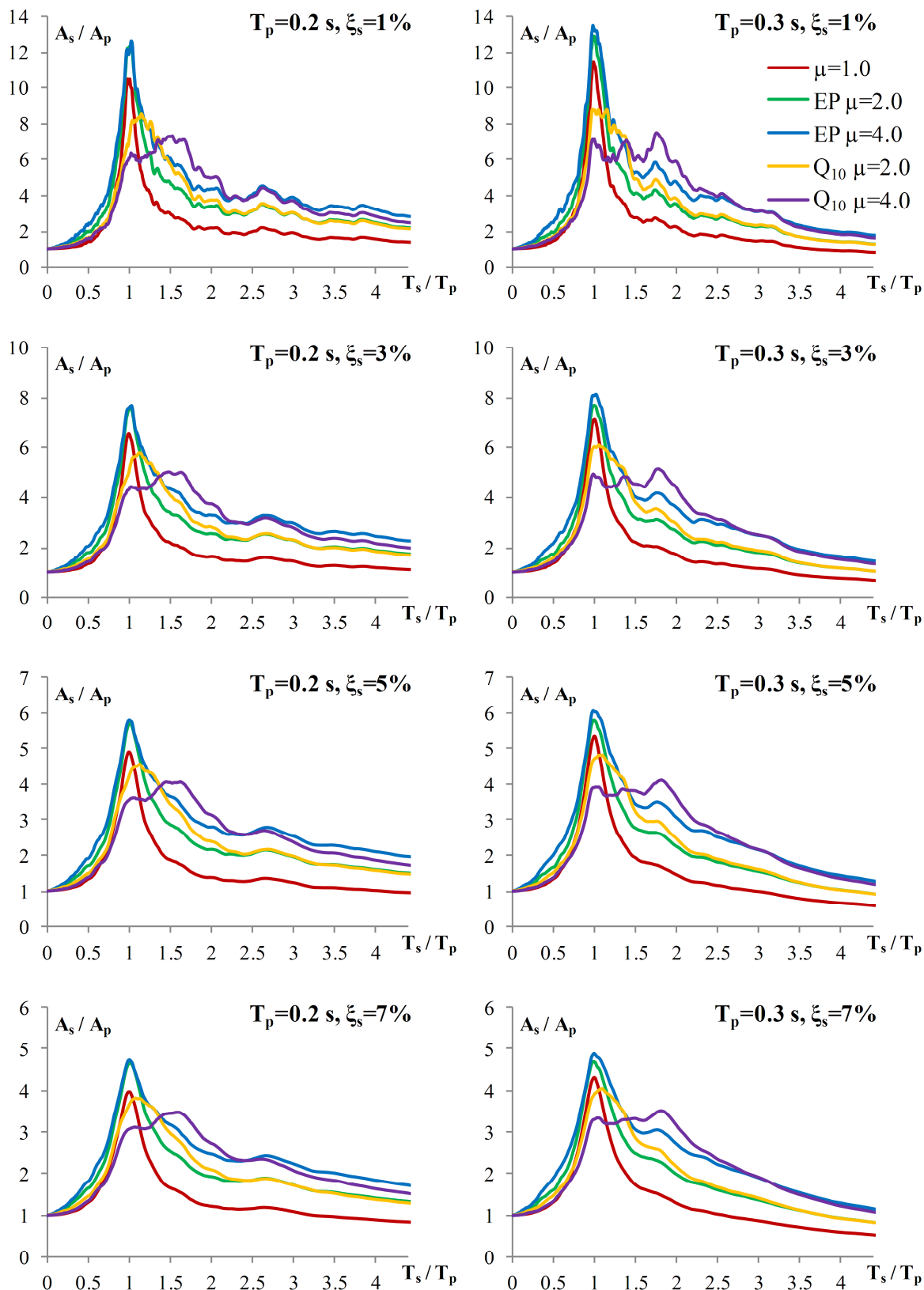


Figure 2.18: Floor response spectra normalized to the peak acceleration of the structures with natural periods equal to 0.2 and 0.3 s, 5% damping of the structure and soil type D

Slika 2.18: Etažni spektri odziva normirani na maksimalni pospešek konstrukcij, ki imajo nihajna časa 0.2 in 0.3 s, 5% dušenja konstrukcije in tip tal D

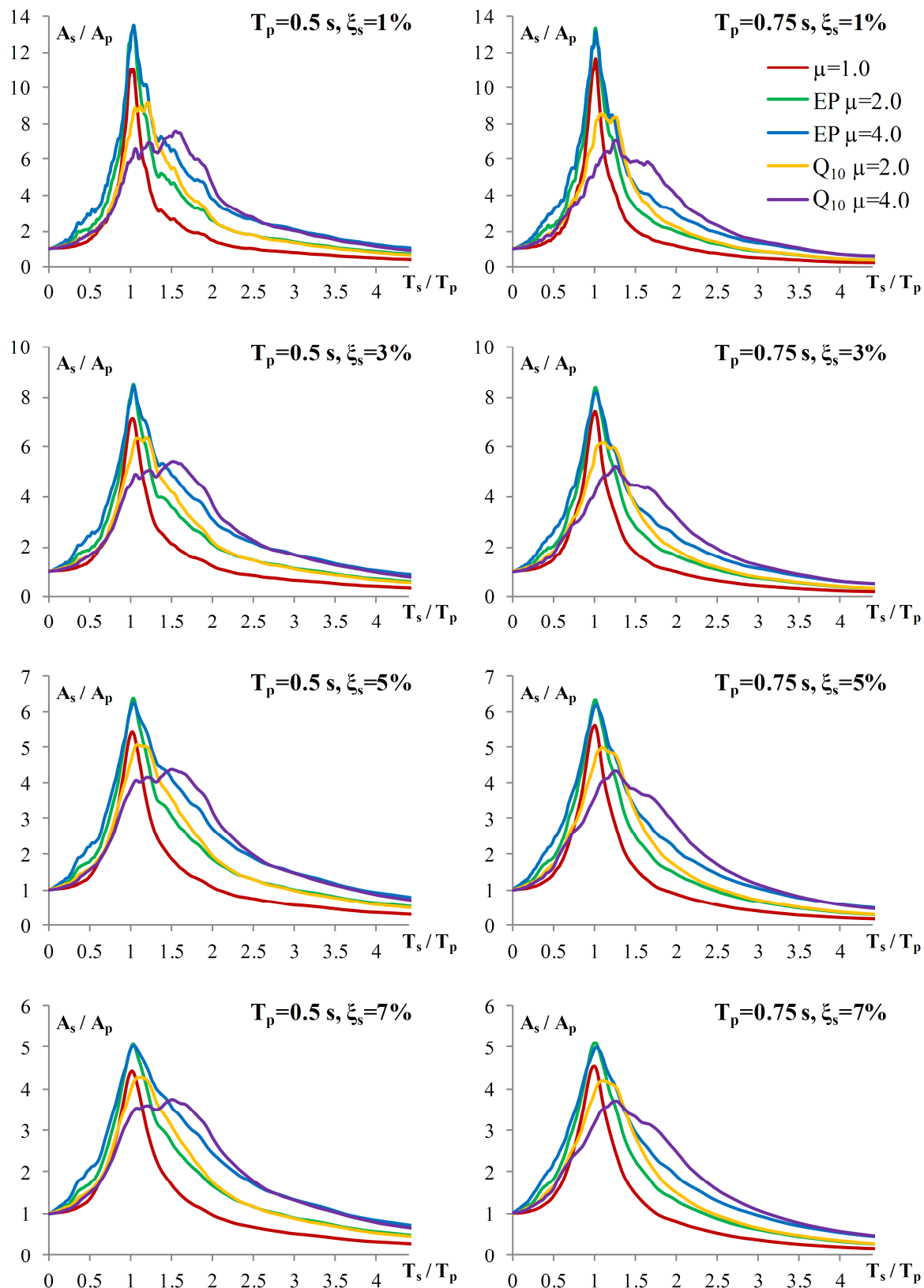


Figure 2.19: Floor response spectra normalized to the peak acceleration of the structures with natural periods equal to 0.5 and 0.75 s, 5% damping of the structure and soil type D

Slika 2.19: Etažni spektri odziva normirani na maksimalni pospešek konstrukcij, ki imajo nihajna časa 0.5 in 0.75 s, 5% dušenja konstrukcije in tip tal D

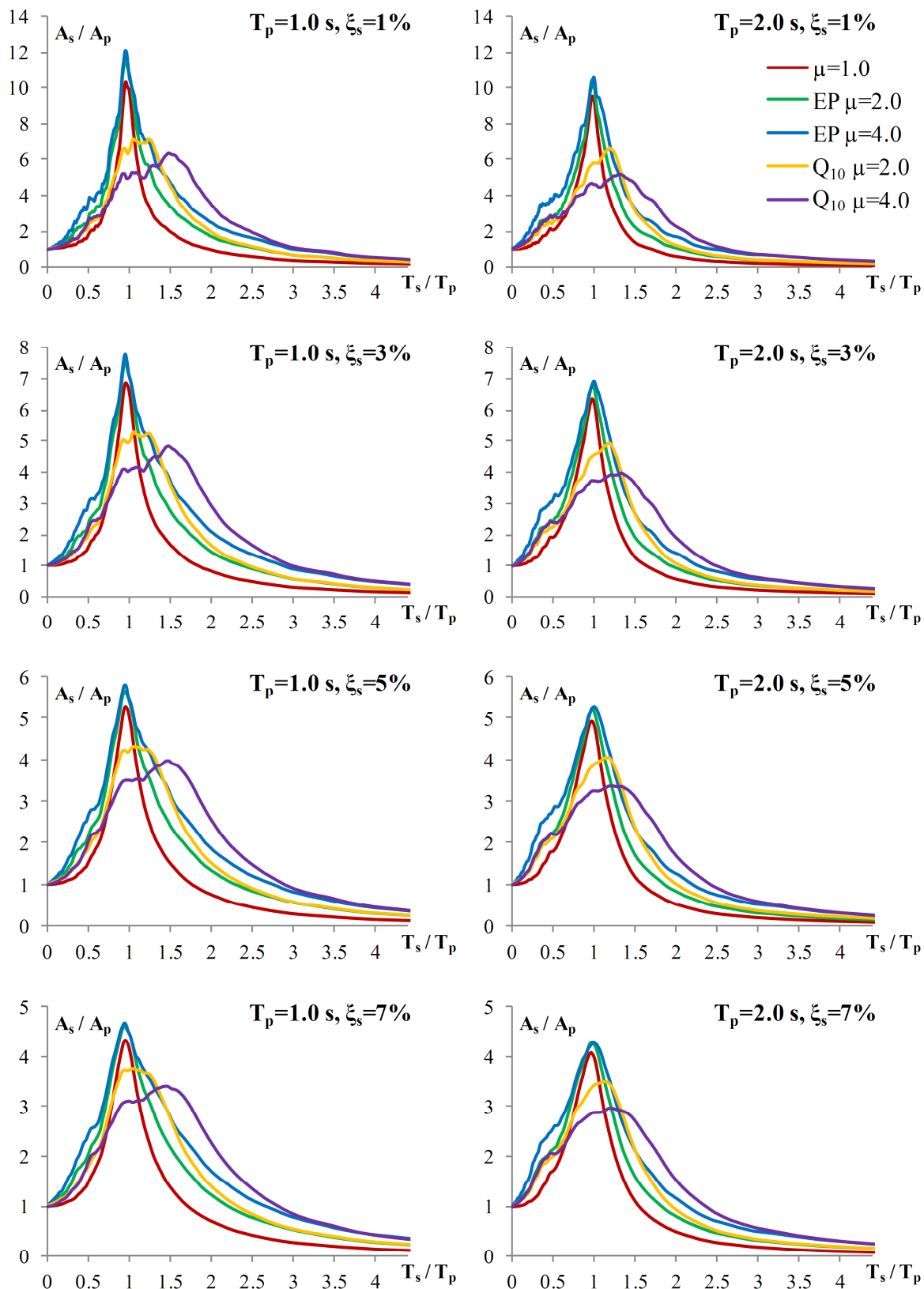


Figure 2.20: Floor response spectra normalized to the peak acceleration of the structures with natural periods equal to 1.0 and 2.0 s, 5% damping of the structure and soil type D

Slika 2.20: Etažni spektri odziva normirani na maksimalni pospešek konstrukcij, ki imajo nihajna časa 1.0 in 2.0 s, 5% dušenja konstrukcije in tip tal D

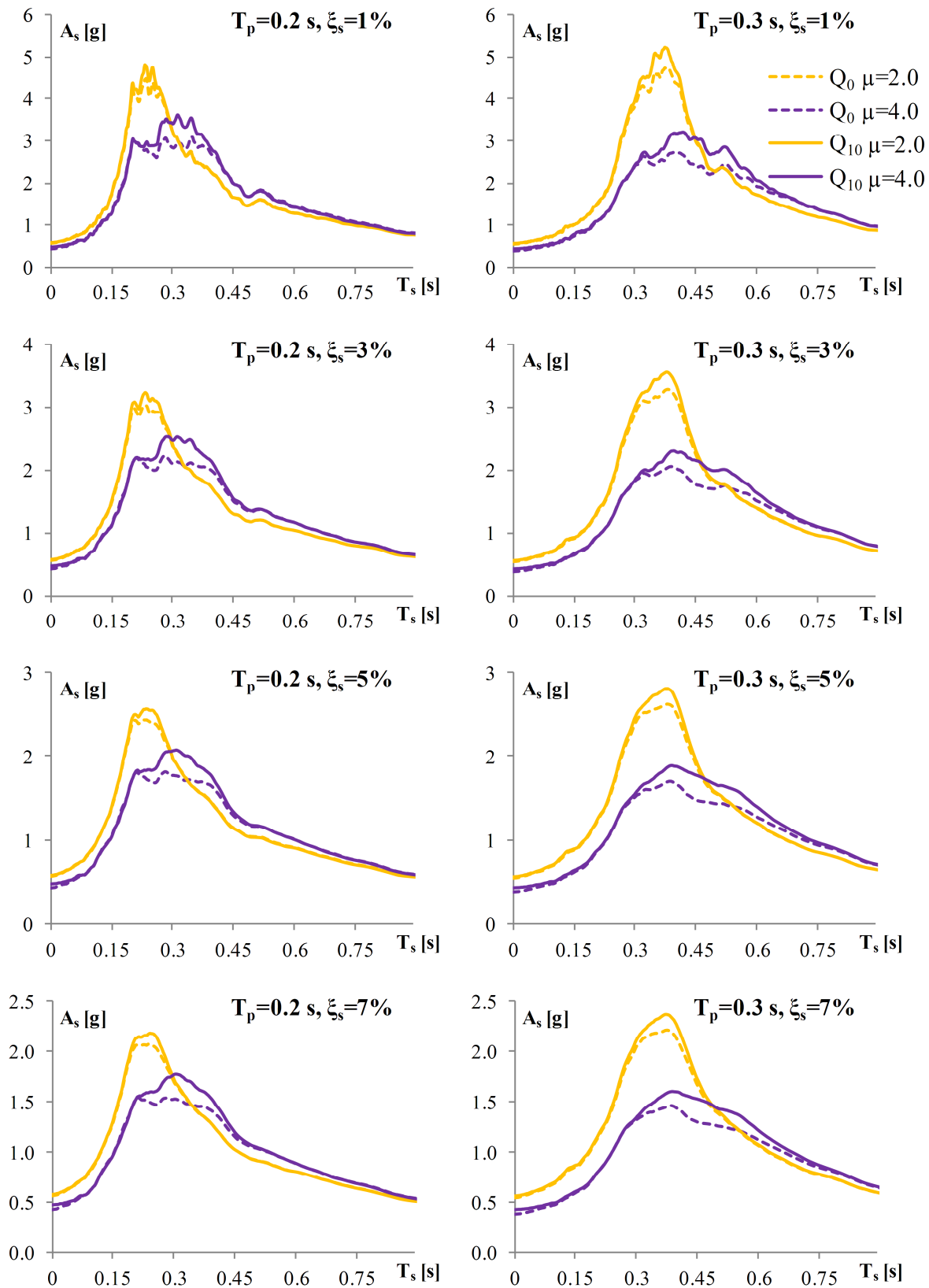


Figure 2.21: A comparison of floor response spectra obtained for different Q models, for the structures with natural periods equal to 0.2 and 0.3 s and 5% damping, soil type B

Slika 2.21: Primerjava etažnih spektrov odziva izračunanih za različna Q modela, za konstrukcije, ki imajo nihajna časa 0.2 in 0.3 s in 5% dušenja, tip tal B

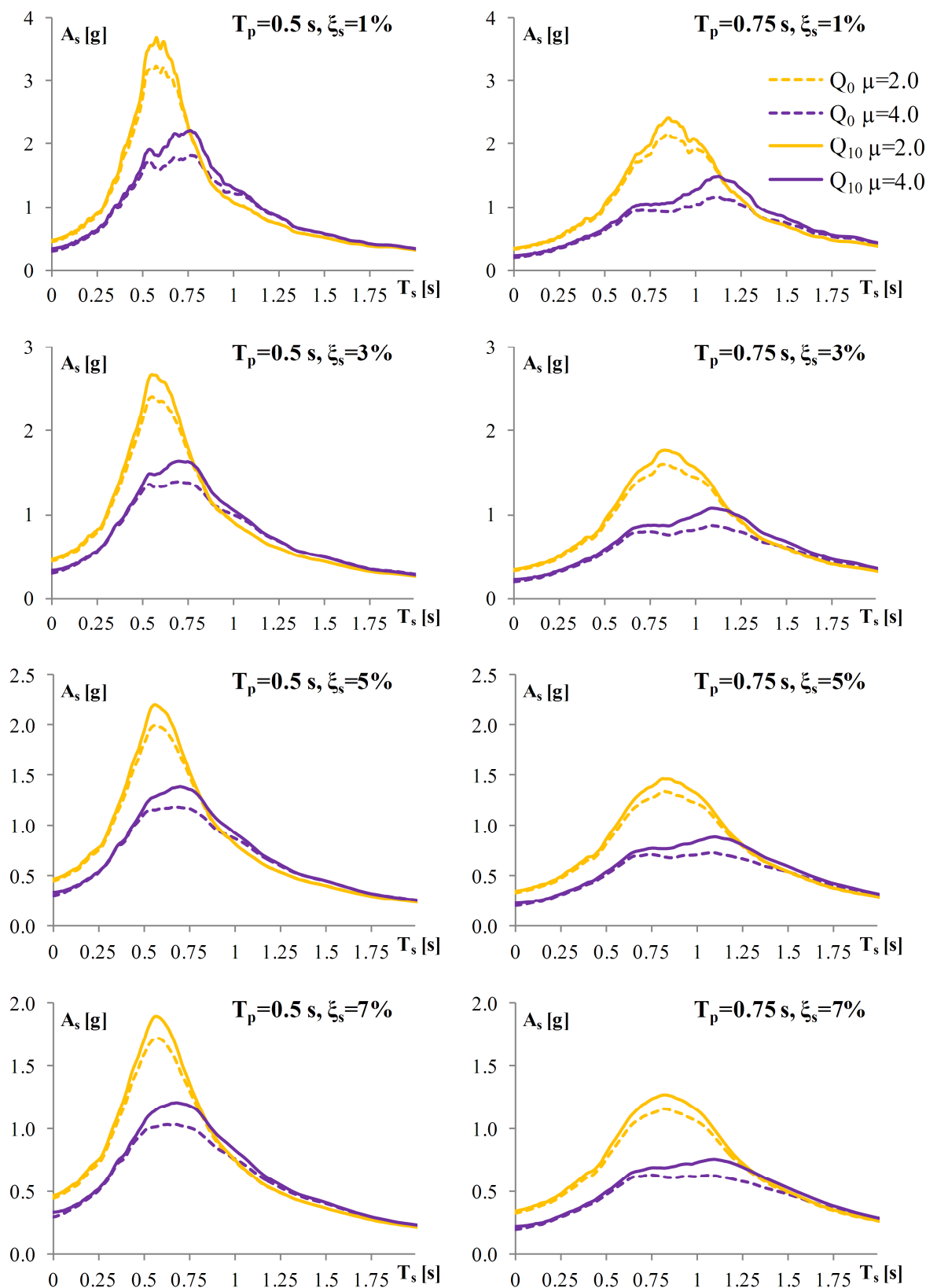


Figure 2.22: A comparison of floor response spectra obtained for different Q models, for the structures with natural periods equal to 0.5 and 0.75 s and 5% damping, soil type B

Slika 2.22: Primerjava etažnih spektrov odziva izračunanih za različna Q modela, za konstrukcije, ki imajo nihajna časa 0.5 in 0.75 s in 5% dušenja, tip tal B

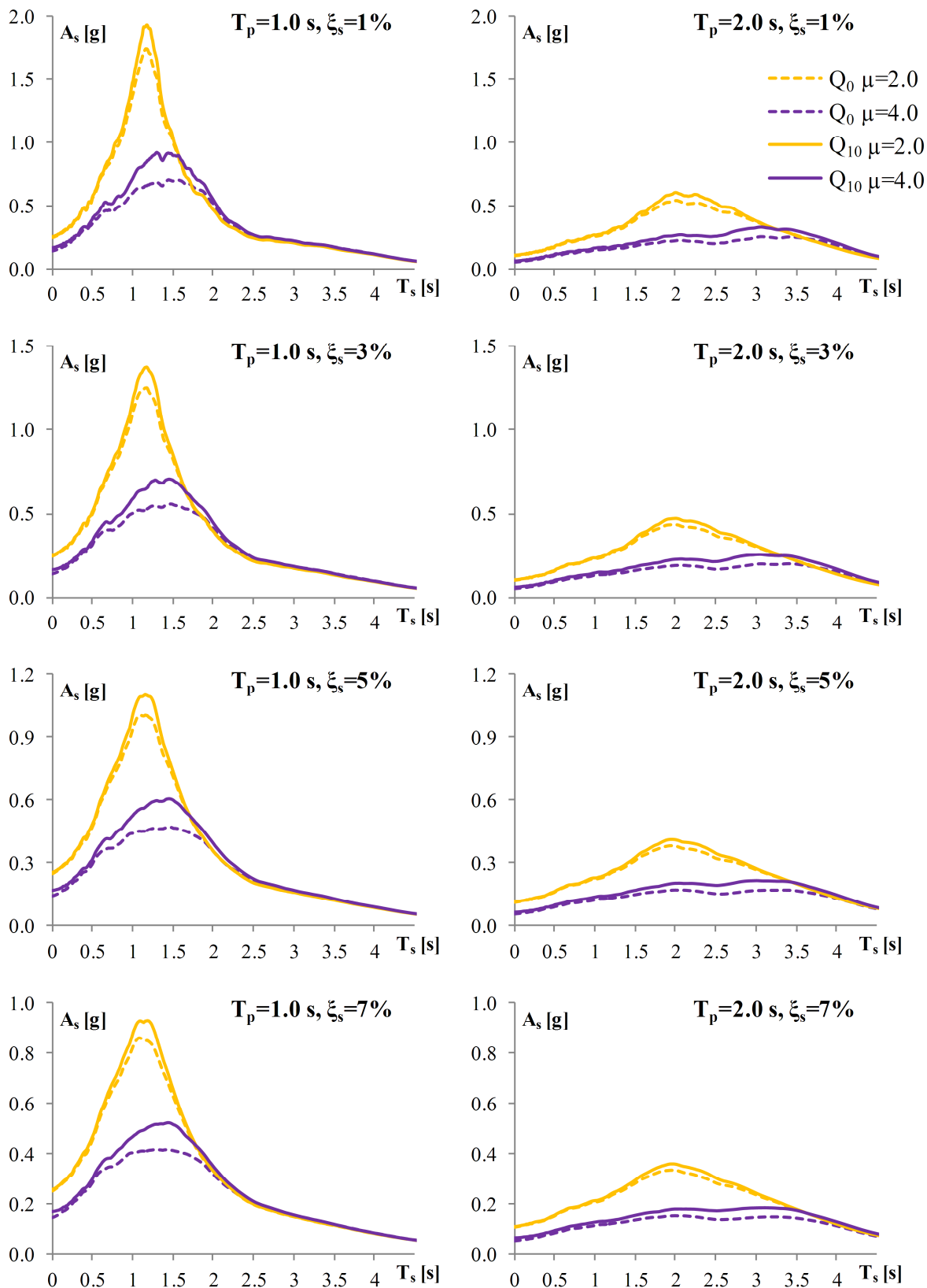


Figure 2.23: A comparison of floor response spectra obtained for different Q models, for the structures with natural periods equal to 1.0 and 2.0 s and 5% damping, soil type B

Slika 2.23: Primerjava etažnih spektrov odziva izračunanih za različna Q modela, za konstrukcije, ki imajo nihajna časa 1.0 in 2.0 s in 5% dušenja, tip tal B

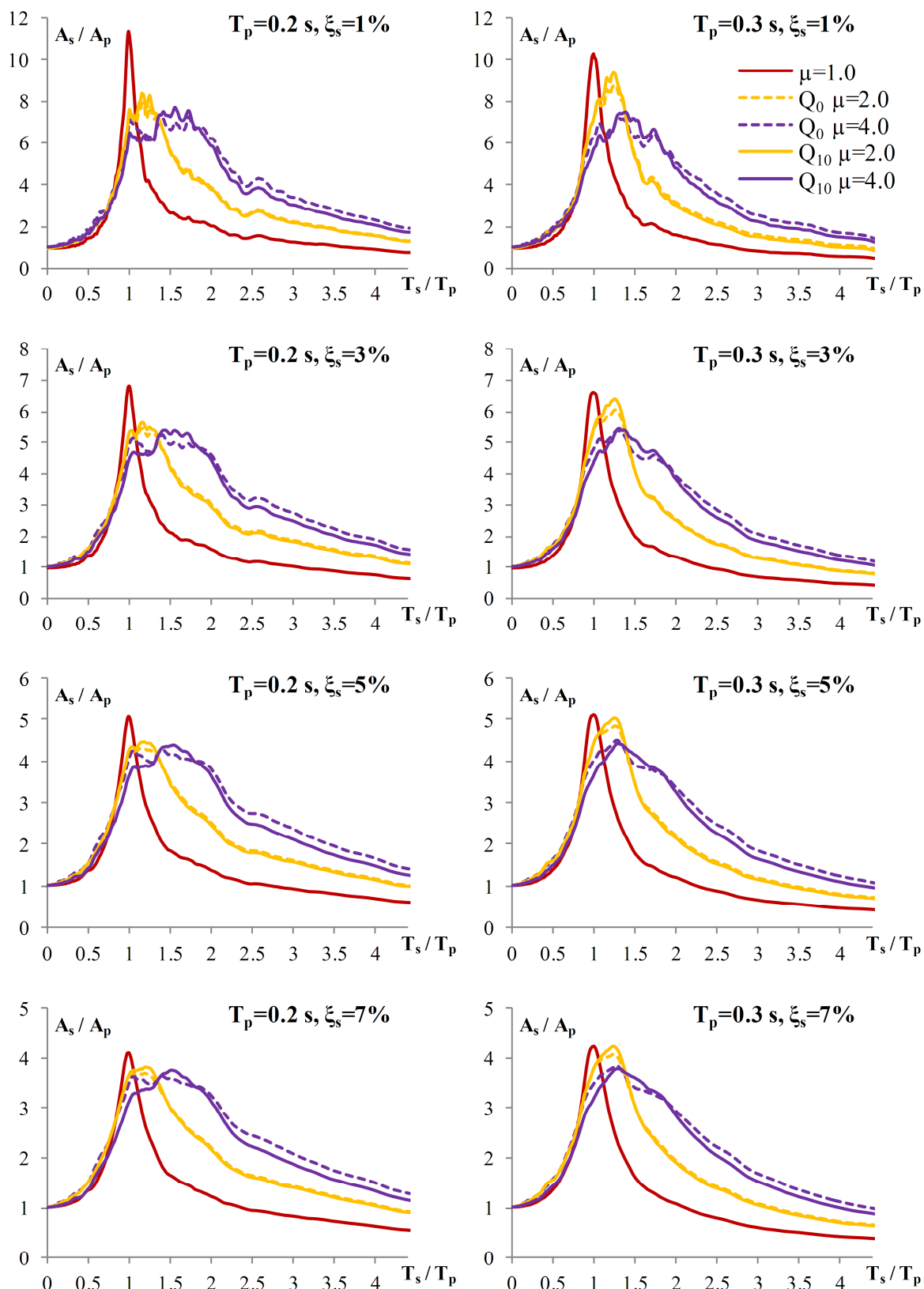


Figure 2.24: A comparison of floor response spectra normalized to the peak acceleration of the structure obtained for different Q models, structures with natural periods equal to 0.2 and 0.3 s and 5% damping, soil type B

Slika 2.24: Primerjava etažnih spektrov odziva normiranih na maksimalni pospešek konstrukcije izračunanih za različna Q modela, za konstrukcije, ki imajo nihajna časa 0.2 in 0.3 s in 5% dušenja, tip tal B

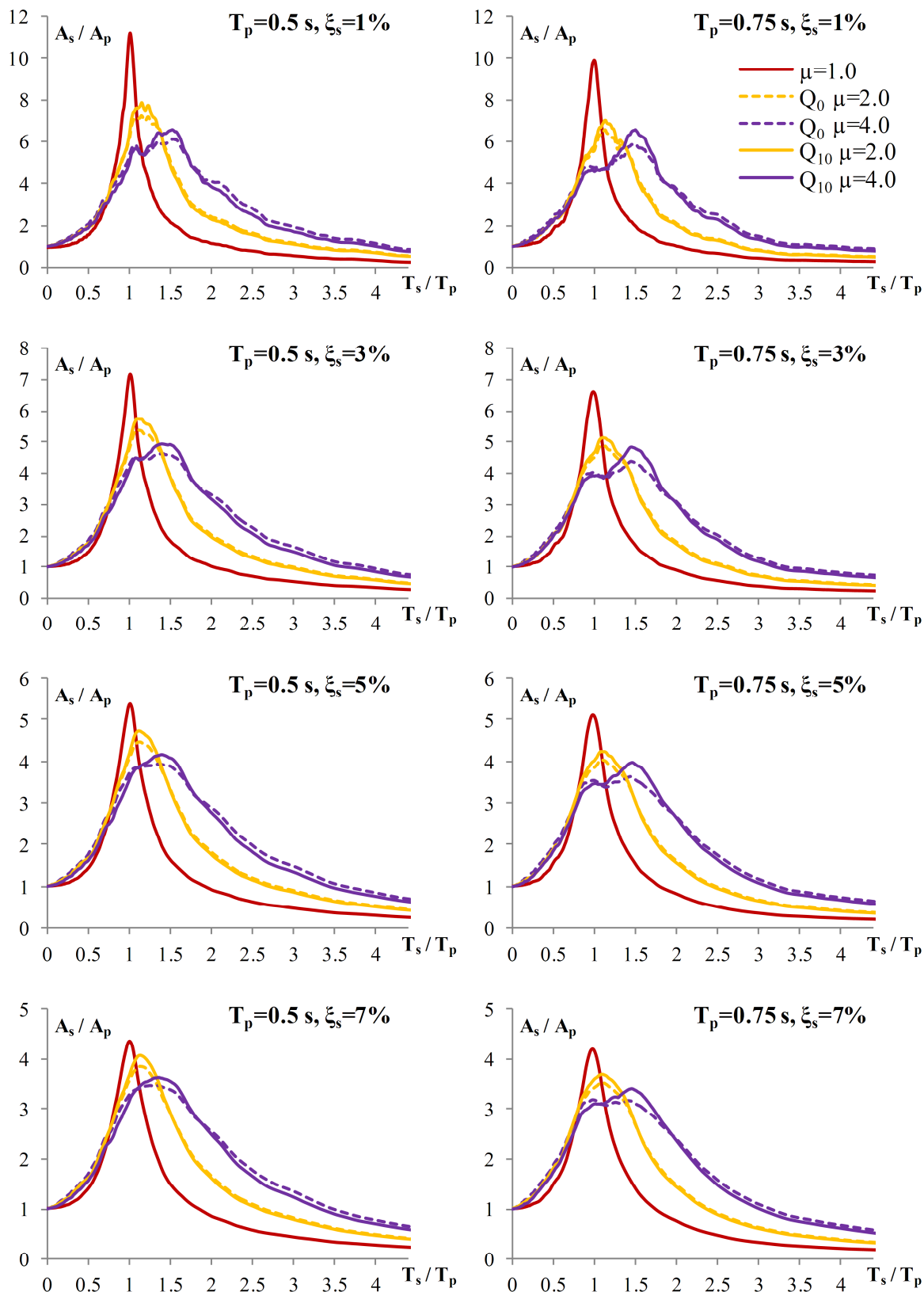


Figure 2.25: A comparison of floor response spectra normalized to the peak acceleration of the structure obtained for different Q models, structures with natural periods equal to 0.5 and 0.75 s and 5% damping, soil type B

Slika 2.25: Primerjava etažnih spektrov odziva normiranih na maksimalni pospešek konstrukcije izračunanih za različna Q modela, za konstrukcije, ki imajo nihajna časa 0.5 in 0.75 s in 5% dušenja, tip tal B

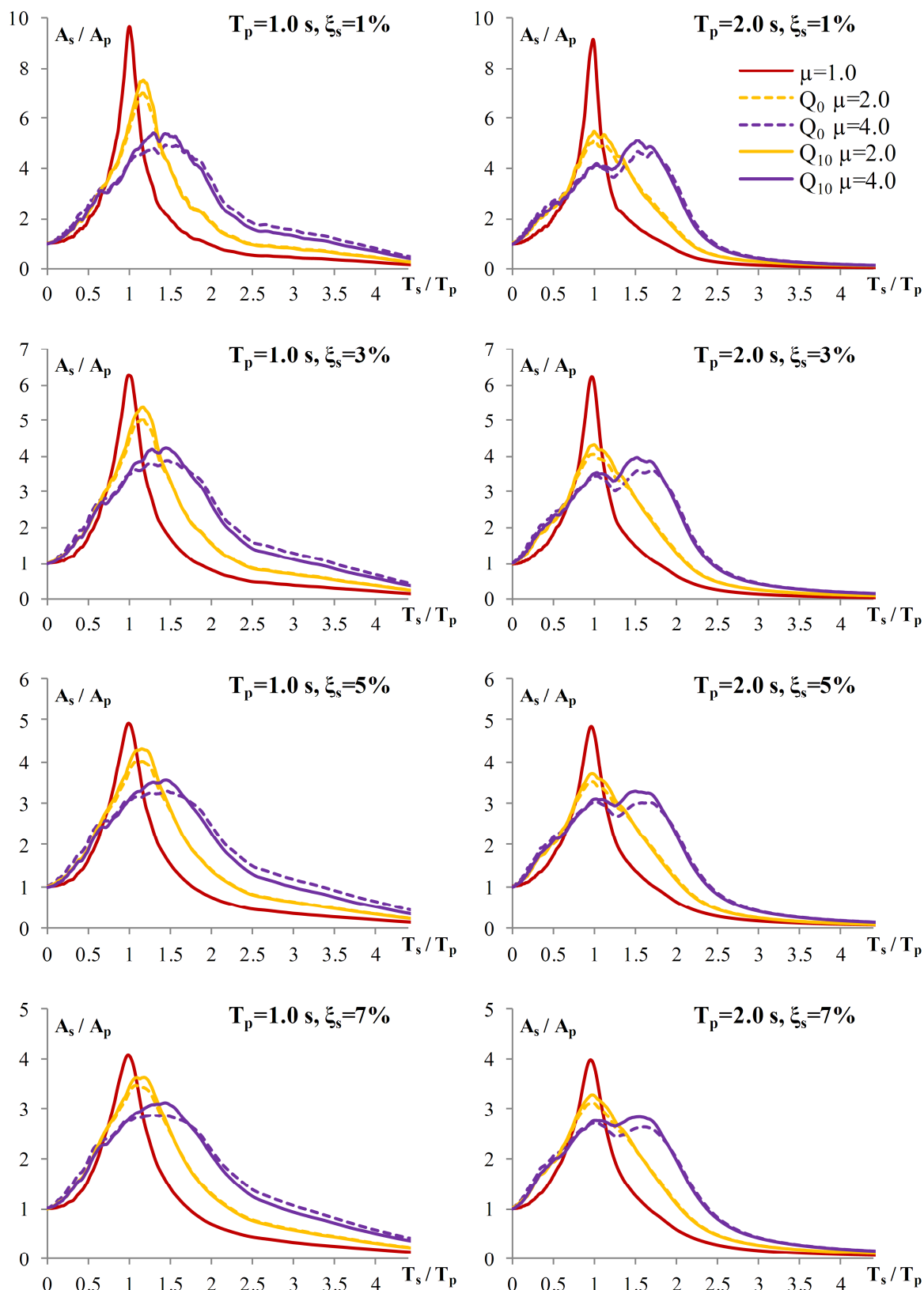


Figure 2.26: A comparison of floor response spectra normalized to the peak acceleration of the structure obtained for different Q models, structures with natural periods equal to 1.0 and 2.0 s and 5% damping, soil type B

Slika 2.26: Primerjava etažnih spektrov odziva normiranih na maksimalni pospešek konstrukcije izračunanih za različna Q modela, za konstrukcije, ki imajo nihajna časa 1.0 in 2.0 s in 5% dušenja, tip tal B

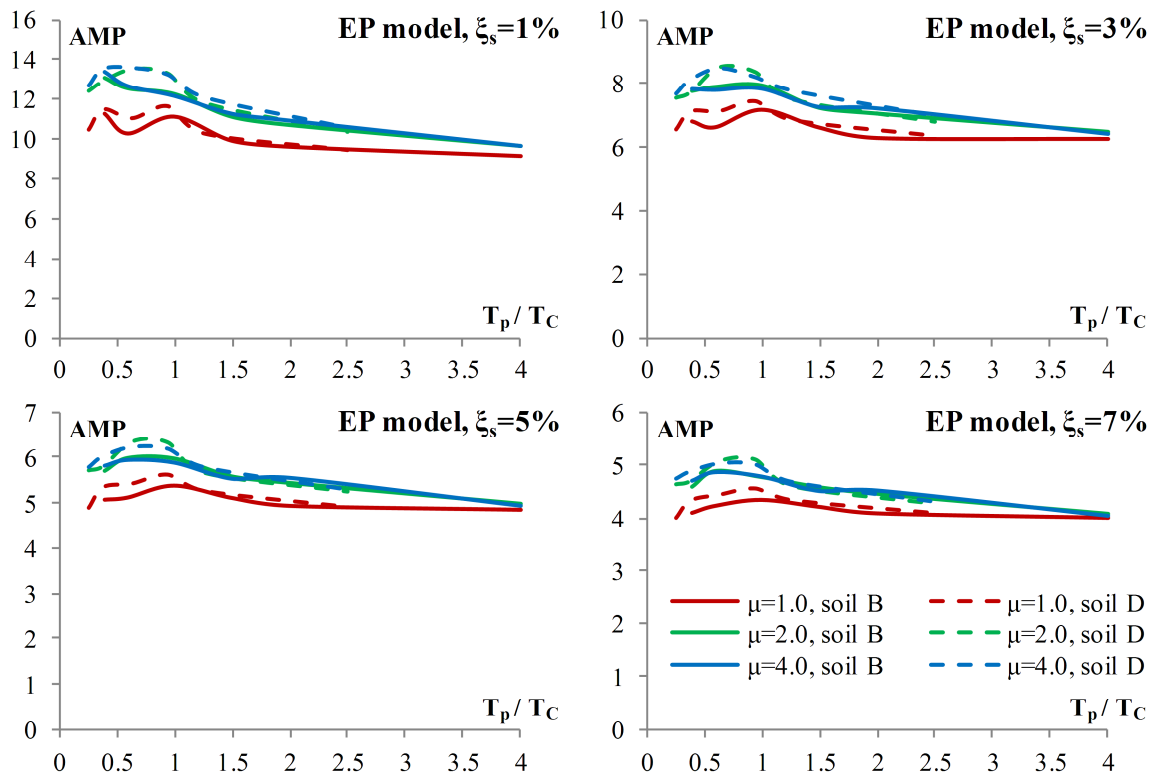
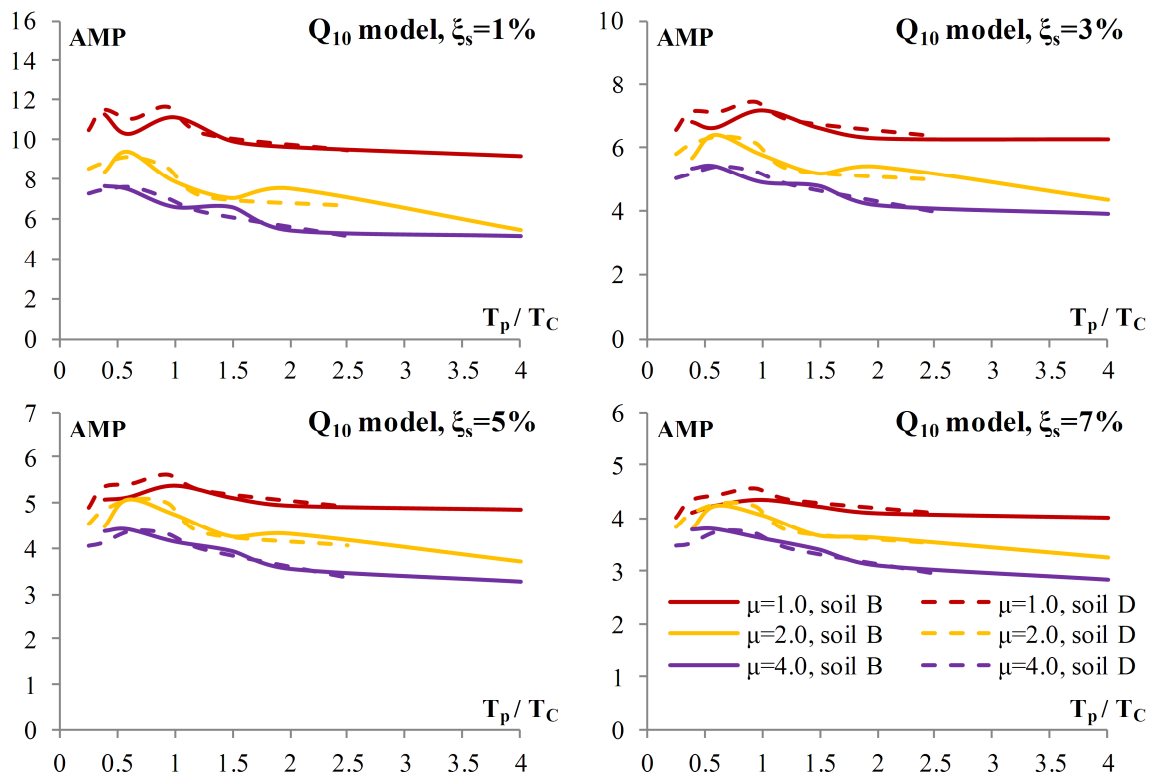


Figure 2.27: The amplification factors (AMP) computed in the parametric study for the EP model of the structure

Slika 2.27: Amplifikacijski faktorji (AMP) izračunani v parametrični študiji za EP model konstrukcije

Figure 2.28: The amplification factors (AMP) computed in the parametric study for the Q_{10} model of the structureSlika 2.28: Amplifikacijski faktorji (AMP) izračunani v parametrični študiji za Q_{10} model konstrukcije

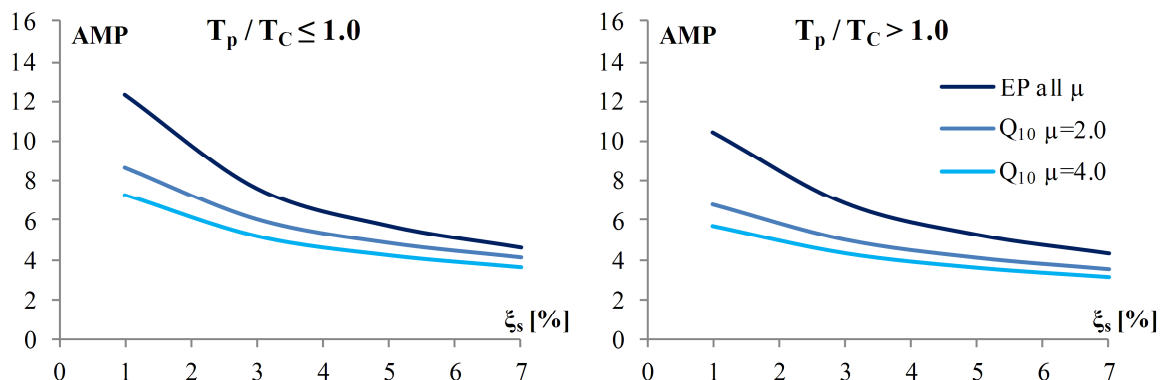


Figure 2.29: The amplification factors (*AMP*) versus the damping of the equipment represented as mean values depending on the ratio T_p/T_C

Slika 2.29: Amplitifikacijski faktorji (*AMP*) v odvisnosti od dušenja opreme predstavljeni kot povprečne vrednosti za različna razmerja T_p/T_C

As mentioned earlier, the *AMP* values slightly increase with an increase in ductility in the case of the EP model (see Figure 2.27). The same phenomenon can also be observed in the studies conducted by Novak and Fajfar (1994) and Oropeza et al. (2010). The cause of this phenomenon should be investigated in detail, which is beyond the scope of this dissertation.

Considering the amount of findings obtained in this chapter, it is convenient to make a brief summary.

- The period range of a floor spectrum can be divided into three regions: the pre-resonance ($T_s/T_p < 0.8$), resonance ($0.8 < T_s/T_p < 1.25$), and post-resonance region ($T_s/T_p > 1.25$).
- In pre-resonance and resonance regions, the behaviour of the equipment is strongly influenced by the behaviour of the primary structure. Both regions are characterized by a significant reduction in A_s due to inelastic structural behaviour.
- The size of the reduction in pre-resonance and resonance regions depends on the ductility demand of the structure. In the post-resonance region the floor response spectrum approaches to the ground motion spectrum as the ratio T_s/T_p decreases. In the post-resonance region, inelastic structural behaviour has a small influence on the floor response spectrum.
- In the limit case of infinitely rigid equipment, A_s is equal to A_p , i.e. to the value in the elastic (for $\mu=1$) or inelastic acceleration response spectrum of the structure at the period T_p . In the limit case of infinitely flexible equipment, the value of A_s is equal to zero.
- The shape of floor response spectra is influenced by the hysteretic behaviour of the structure. In the case of the EP model, the peak values of A_s occur close to the resonance ($T_s \approx T_p$), whereas in the case of the Q_{10} model, the peak values of A_s are shifted towards higher periods.
- The main parameter that influences the amplitude of the *AMP* is the damping of the equipment (ζ_s). The *AMP* reaches its peak value in the region $T_p/T_C \leq 1$, and then it decreases with the increasing ratio T_p/T_C if the ratio is larger than 1. The hardening practically does not influence the *AMP*.
- The influence of ground motion on the *AMP* is negligible, provided that the period T_p is normalized by the characteristic period of the ground motion T_C .
- The obtained results indicate somewhat complicated dependence between the *AMP* and the ratio T_p/T_C in the region between $T_p/T_C=0$ and $T_p/T_C=0.25$.

3 A METHOD FOR DIRECT GENERATION OF FLOOR RESPONSE SPECTRA FOR SINGLE-DEGREE-OF-FREEDOM STRUCTURES

This chapter presents the method for direct generation of floor response spectra for single-degree-of-freedom (SDOF) primary structures, as well as its validation. The development of the method was based on the results obtained and the conclusions made in the parametric study (see Chapter 2), as well as on a very simple method for the direct determination of floor response spectra proposed by Yasui et al. (1993). The idea for the extension of the original method was proposed by Novak and Fajfar (1994).

3.1 Original method

A very simple method for the direct determination of floor response spectra was proposed by Yasui et al. (1993), who derived an equation which is valid in the whole period range. Complete derivation of the method is provided in ANNEX A, whereas it is briefly described in this section.

The derivation was conducted for the case of linear elastic behaviour of both primary structure and equipment (secondary structure), which were modelled as SDOF systems. The equation was derived analytically, by using the Duhamel integral for the response determination. Three responses in terms of absolute acceleration were analysed: the responses of the structure and of the equipment subjected to the ground motion, and the response of the equipment subjected to the absolute acceleration response-history of the structure. The maximum values of the responses were then combined with the SRSS (Square Root of Sum of Squares) combination rule in order to obtain the equation for the floor spectrum generation. The derivation was performed separately for the non-resonant and resonant cases. The two independent equations were then combined together into a single equation for the determination of the floor response spectrum

$$A_{se} = \frac{1}{\sqrt{\left\{1 - (T_p / T_s)^2\right\}^2 + 4(\xi_p + \xi_s)^2 (T_p / T_s)^2}} \sqrt{\left\{(T_p / T_s)^2 S_e(T_p, \xi_p)\right\}^2 + S_e(T_s, \xi_s)^2} \quad (3.1)$$

where A_{se} is a value in the floor acceleration spectrum and S_e is a value in the input elastic acceleration spectrum. $S_e(T_p, \xi_p)$ applies to the elastic primary structure (it was denoted as A_p in the parametric study described in Chapter 2), whereas $S_e(T_s, \xi_s)$ applies to the equipment. The damping values of the structure and equipment are denoted as ξ_p and ξ_s , respectively, whereas T_p and T_s are the natural periods of the structure and equipment, respectively.

Input data for the determination of floor response spectra (which represent absolute accelerations for equipment with a period T_s and damping ξ_s) according to Equation 3.1 are the dynamic properties of the structure and the equipment and the elastic acceleration spectra (for different damping values) representing the ground motion.

The results of conducted analyses indicate that, outside of the resonance region, floor response spectra obtained by the direct method (Equation 3.1) are in good agreement with the "accurate" floor response spectra obtained by response-history analyses (RHA). In the resonance region, however, considerable inaccuracy of the direct method was observed in the study (see Section 3.3).

3.2 Extension and modifications of the original method

In order to make the direct method applicable to the case of inelastic structures, and to improve its accuracy in the resonance region, some changes were made.

To allow the use of the method for inelastic structures, the elastic acceleration spectrum was replaced with an inelastic acceleration spectrum corresponding to the expected ductility demand, as originally proposed by Fajfar and Novak (1994). It should be noted that, in the proposed method, generally, any inelastic acceleration spectrum can be used. Inelastic acceleration spectra are discussed later in this section.

In order to improve the accuracy of the predicted floor response spectra, the spectral values in the resonance region ($T_s \approx T_p$) are determined by means of empirical equations which are based on the results of the parametric study (Chapter 2), rather than on the original equation (Equation 3.1). More details about this procedure are provided later in this section.

Inelastic spectra

Several proposals for inelastic spectra are available in the literature. For practical applications, the most convenient is the application of reduction factors due to ductility R_μ , representing the ratio of elastic and inelastic strength demand (Vidic et al. 1994), i.e. the ratio of the elastic and inelastic pseudo-acceleration spectra, where the inelastic pseudo-acceleration is related to the yield point of the bilinear force-deformation relationship. An early overview of various proposals for the reduction factor R_μ was presented by Miranda and Bertero (1994). The inelastic pseudo-acceleration spectrum, which is used for the analysis and design of the primary structure, can be obtained by reducing the elastic pseudo-acceleration spectrum by means of a reduction factor R_μ . This spectrum can also be used in the process of the determination of floor response spectra, provided that there is no post-yield hardening of the force-deformation curve of the structure. In the case of post-yield hardening, the actual accelerations of the structure increase (compared to the acceleration at the yield point) with an increase in plastic deformation (see Figure 2.2c, and note that the acceleration is proportional to the force). The increase in acceleration due to hardening, normalized by the acceleration at the yield point, depends on the ductility factor μ and can be determined as $\alpha(\mu-1)$, where α is the ratio of the post-yield and elastic stiffness. The following relation applies:

$$A_p(\text{hardening}) / A_p(\text{no hardening}) = 1 + \alpha(\mu - 1) \quad (3.2)$$

where A_p is the maximum acceleration of the primary structure, and α is the ratio of the post-yield and elastic stiffness).

In the validation of the proposed direct method the floor response spectra were first determined by using the "exact" inelastic acceleration spectra, in order to exclude the error introduced by using approximate inelastic spectra. The "exact" inelastic spectra were obtained by nonlinear RHA. The "exact" inelastic spectra for the EP model and for the Q_{10} model are shown in Figure 3.1. However, the use of "exact" inelastic spectra is not feasible in practical applications, so that, in practice, approximate inelastic spectra have to be used. This approximation introduces an additional error in the floor response spectra. The simplified form of the spectra proposed by Vidic et al. (1994) which has been

implemented in Eurocode 8 (2004) was used in this study. Such an inelastic spectrum can be obtained by reducing the elastic acceleration spectrum by a reduction factor R_μ , which is defined as

$$R_\mu = \begin{cases} \frac{T_p}{T_C}(\mu - 1) + 1, & T_p < T_C \\ \mu, & T_p \geq T_C \end{cases} \quad (3.3)$$

where T_p is the natural period of the structure, μ is ductility factor and T_C is the characteristic period of the ground motion (see Section 2.1). The spectra apply for 5% damping of the structure. As a conservative approximation, the spectra for 5% damping can be used also for a lower damping percentage (Vidic et al. 1994).

In the case of zero post-yield stiffness, approximate inelastic acceleration spectra of the structure can be obtained as S_e/R_μ , where S_e is the elastic (pseudo-) acceleration spectrum. If a post-yield stiffness is included in the model, its influence on the absolute acceleration spectrum can be considered by dividing the reduction factor R_μ by $(1 + \alpha(\mu - 1))$ as

$$R_\mu = \frac{R_\mu \text{ (Equation 3.3)}}{1 + \alpha(\mu - 1)} \quad (3.4)$$

A commentary on the application of inelastic pseudo-acceleration spectra, i.e. the reduction factor R_μ , for the seismic design of equipment is presented in ANNEX B.

In Figure 3.1 the "exact" inelastic acceleration spectra obtained from nonlinear RHA are compared with the approximate inelastic acceleration spectra obtained by reducing the target Eurocode 8 (2004) elastic (pseudo-)acceleration spectrum S_e by means of the R_μ factor according to Equation 3.3 in the case of the EP model with zero hardening, and according to Equation 3.4 in the case of the Q_{10} model. The results for soil types B and D and the target ductility demands of 2.0 and 4.0 are shown. The damping of the structure (ζ_p) amounted to 5%. A fair agreement between the "exact" and approximate spectra can be observed, with some exceptions in a very short period range, where the approximate spectral values are quite conservative. Note that the results of the parametric study (see Section 2.3) were shown for cases when the natural periods of the structure amount to 0.2, 0.3, 0.5, 0.75, 1.0 and 2.0 s. The same natural periods will be used later for the validation of the direct method. Since the differences between the "exact" and approximate inelastic acceleration spectra directly influence the accuracy of the proposed direct method, the errors of the approximate inelastic spectra are shown in Tables 3.1 and 3.2, for soil types B and D respectively. A negative value of the error indicates that the approximate spectral value is smaller than the corresponding "exact" value. In Figure 3.2 the "exact" and approximate inelastic spectra obtained for different Q models are compared for considered cases.

Table 3.1: Errors of the approximate spectra in comparison to the "exact" inelastic spectra, soil type B

Preglednica 3.1: Napake približnih spektrov v primerjavi s »točnimi« spektri, tip tal B

Errors [%]		$T_p=0.2$ s	$T_p=0.3$ s	$T_p=0.5$ s	$T_p=0.75$ s	$T_p=1.0$ s	$T_p=2.0$ s
EP model	$\mu=2$	5	6	2	-12	-4	10
	$\mu=4$	-2	-11	-27	-21	-21	-11
Q_{10} model	$\mu=2$	5	7	4	-6	-4	9
	$\mu=4$	-5	-5	-15	-14	-18	9

Table 3.2: Errors of the approximate spectra in comparison to the "exact" inelastic spectra, soil type D

Preglednica 3.2: Napake približnih spektrov v primerjavi s »točnimi« spektri, tip tal D

Errors [%]		$T_p=0.2$ s	$T_p=0.3$ s	$T_p=0.5$ s	$T_p=0.75$ s	$T_p=1.0$ s	$T_p=2.0$ s
EP model	$\mu=2$	24	8	0	-4	3	18
	$\mu=4$	18	2	-10	-18	-17	5
Q_{10} model	$\mu=2$	28	13	-3	0	5	22
	$\mu=4$	22	5	-12	-11	-7	21

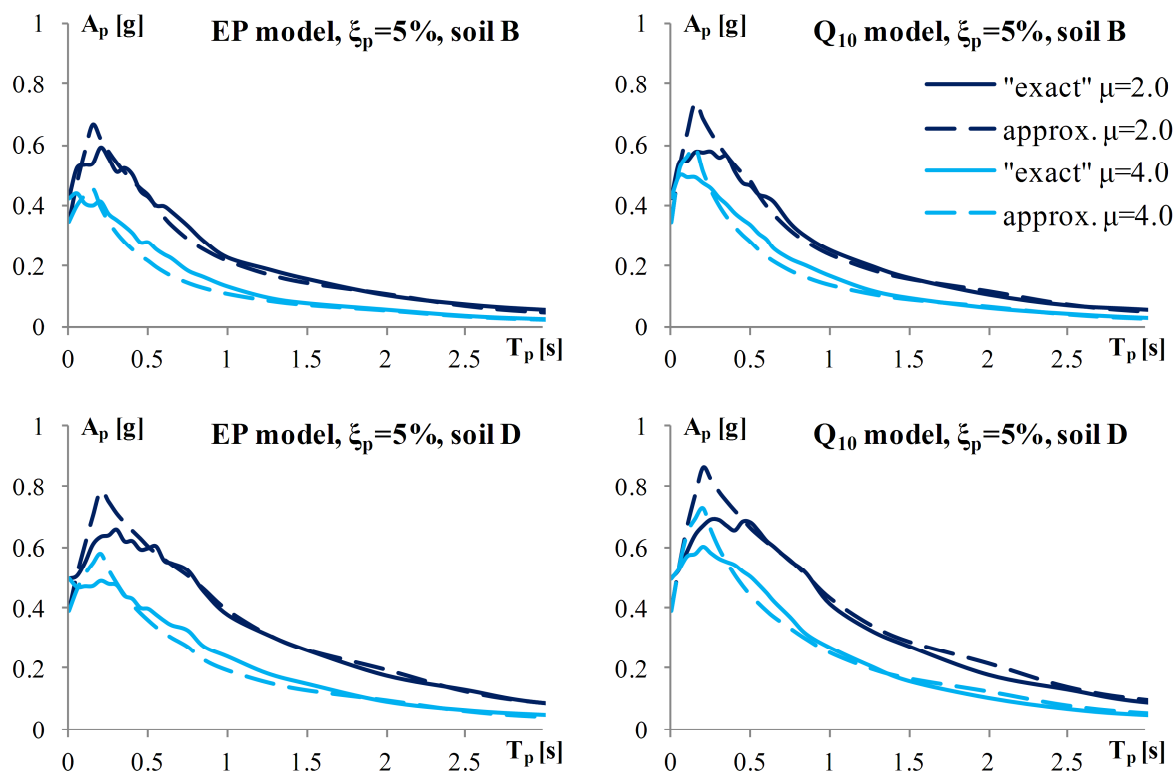


Figure 3.1: "Exact" and approximate inelastic spectra for soil types B and D (5% damping of the structure)

Slika 3.1: »Točni« in približni neelastični spektri za tla tipa B in D (5% dušenja konstrukcije)

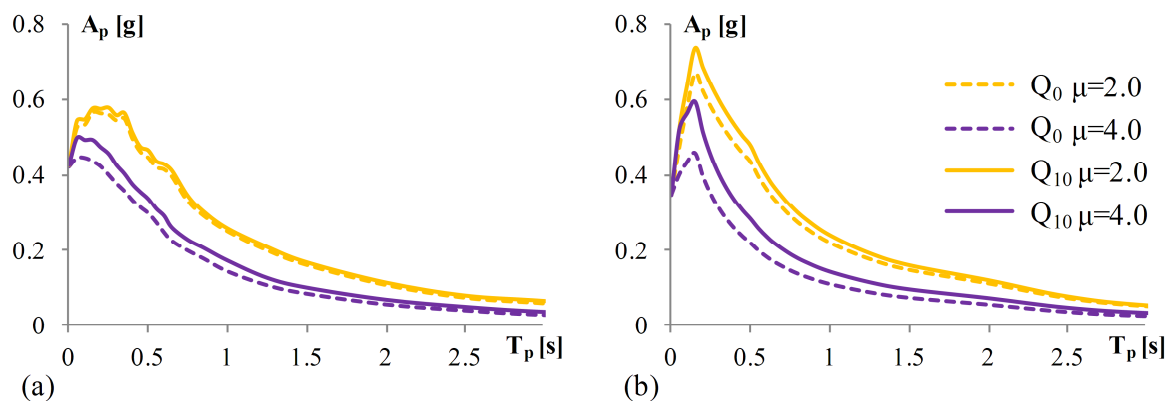


Figure 3.2: A comparison between (a) the "exact" and (b) the approximate inelastic acceleration spectra for the structure (5% damping) obtained for two different Q models, soil type B

Slika 3.2: Primerjava med (a) »točnimi« in (b) približnimi neelastičnimi spektri pospeškov za konstrukcijo (5% dušenja) za dva različna Q modela, tip tal B

Empirical formula for the resonance region

In the resonance region, the formula provided in the original method provides too conservative results even in the case of elastic primary structures (see Section 3.3). The amplification factors which are based on *AMP* values obtained in the parametric study (Figures 2.27–2.29) can be used in order to achieve a more realistic determination of the floor response spectra in the resonance region. In the following text a proposal for amplification factors is made, taking into account the results obtained in the parametric study.

The results of the parametric study suggest that the damping of the equipment has a major influence on the peak values of the floor response spectra. The frequency content of the ground motion (ratio T_p/T_C) and the ductility demand, which is more pronounced in the case of stiffness degrading Q model, have a moderate influence. Based on these observations, the first two influences were taken into account for both the EP and Q model, whereas the influence of ductility was considered only for the Q model.

Additionally, as already mentioned in Section 2.3, it should be noted that in the region between $T_p/T_C=0$ and $T_p/T_C=0.25$ the dependence between *AMP* and T_p/T_C is not simple. In order to simplify things, it was assumed that the dependence is linear, which roughly corresponds to the results obtained in the parametric study. For the starting point ($T_p/T_C=0$), a value of *AMP* was chosen arbitrarily. It arises from the provisions of Eurocode 8 (2004) and it is defined by Equation 3.5

$$AMP(T_p/T_C = 0) = 2.5\eta \quad (3.5)$$

where η denotes damping correction factor, which should be determined according to Equation 3.6 (ζ_s should be entered as a percentage).

$$\eta = \sqrt{10 / (5 + \zeta_s)} \quad (3.6)$$

Equation 3.5 has a theoretical background. If the structure is infinitely stiff ($T_p=0$) then the peak absolute acceleration of its mass is equal to the peak ground acceleration (PGA). This means that the equipment which is situated on such a structure would respond exactly the same as if it would be situated on ground. As a consequence, the response spectrum of the equipment (floor response spectrum) would be equal to the ground response spectrum of the structure.

In Eurocode 8 (2004) a plateau of the constant acceleration range (a range of peak accelerations) is defined as $2.5PGA\eta$, where η is calculated according to Equation 3.6, with the difference of using ζ_p instead of ζ_s . It should be noted that Eurocode 8 (2004) defines the lowest value of η , which amounts to 0.55 and it corresponds to the structural damping equal to 28%. For the calculation of the *AMP*, the values of ζ_s which are appropriate for the considered equipment should be used (for more information about damping values of equipment see e.g. USNRC 1.61 2007).

Therefore, in the case of the EP model of the structure, the *AMP*, which represents the ratio between the peak value of the floor acceleration spectrum and the maximum acceleration of the structure (see Equation 2.1 in Section 2.3), can be approximately determined as (ζ_s should be entered as a percentage)

$$AMP = \begin{cases} \text{linear between AMP from Eq. 3.5 and } AMP(T_p/T_C = 0.20), & 0 \leq T_p/T_C \leq 0.20 \\ 18(1 + \xi_s)^{-0.60}, & 0.20 \leq T_p/T_C \leq 1 \\ 18(1 + \xi_s)^{-0.60} (T_p/T_C)^{-0.20}, & T_p/T_C > 1 \end{cases} \quad (3.7)$$

In the case of the Q model, *AMP* is defined as (ξ_s should be entered as a percentage)

$$AMP = \begin{cases} \text{linear between AMP from Eq. 3.5 and } AMP(T_p/T_C = 0.20), & 0 \leq T_p/T_C \leq 0.20 \\ 18(1 + \xi_s)^{-0.60} (0.6 + 0.4\mu)\mu^{-0.85}, & 0.20 \leq T_p/T_C \leq 1 \\ 18(1 + \xi_s)^{-0.60} (T_p/T_C)^{-0.20} (0.6 + 0.4\mu)\mu^{-0.85}, & T_p/T_C > 1 \end{cases} \quad (3.8)$$

In Equations 3.7 and 3.8 T_p denotes the natural period of the structure, T_C is the characteristic period of the ground motion, ξ_s is the damping of equipment, and μ is the ductility factor.

Note that Equation 3.7 is a special case of Equation 3.8 for ductility $\mu=1$, i.e. for an elastic structure. The proposed amplification factors *AMP* for different values of the ductility demand, and the damping of the equipment equal to 1% and 5%, are presented in Figure 3.3. They are compared with the *AMP* obtained in the parametric study, which are presented in the following manner:

- 1) In the regions $0.25 \leq T_p/T_C \leq 1$ and $T_p/T_C > 1$ the values of the *AMP* presented in Figure 3.3 were determined as mean values for soil types B and D. In the case of the EP model, all analysed ductilities, including the elastic structure, were taken into account when determining the mean values of the *AMP*.
- 2) In the region $0 < T_p/T_C < 0.25$ the values of *AMP* presented in Figure 3.3 were determined from the additional study conducted on elastic SDOF oscillators with very short natural periods, as discussed at the end of the Section 2.3.

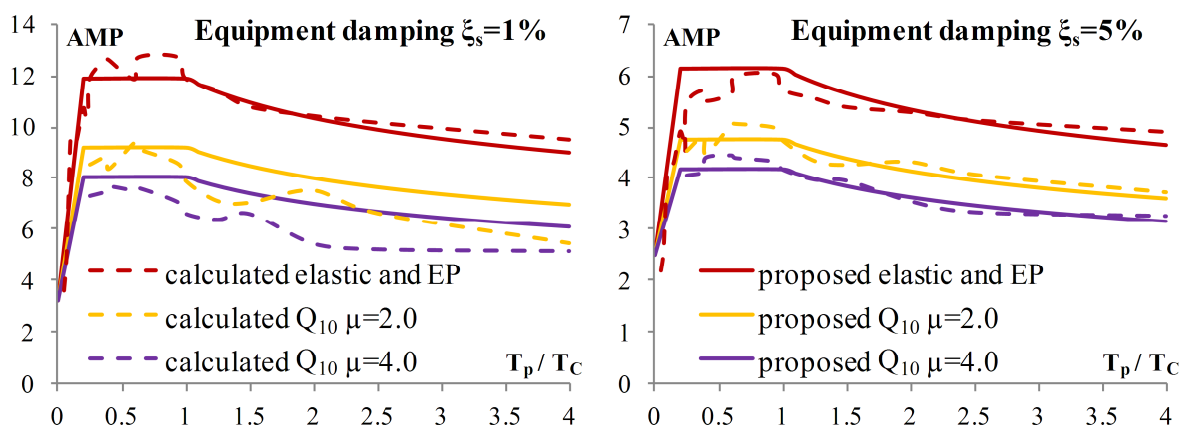


Figure 3.3: Proposed amplification factors and comparison with *AMP* obtained in the parametric study

Slika 3.3: Predlagani faktorji amplifikacije in primerjava z *AMP*, ki so izračunani v parametrični študiji

Simplification in the pre- and post resonance regions

The summand in the denominator in Equation 3.1, which contains the damping coefficients, is important in the resonance region whereas outside of this region it has a negligible effect. In the

proposed approach, Equation 3.1, adapted for inelastic primary structures, is used only outside of the resonance region, whereas in the resonance region the empirical values presented above are applied. For this reason it is possible to delete the summand in the denominator in Equation 3.1, which contains the damping coefficients.

Summary of the proposed method

In the proposed direct method, considering the changes explained above, floor response spectra can be computed for both the EP and Q models as follows:

- 1) In the pre- and post-resonance regions, the spectral values are obtained as

$$A_s = \frac{1}{\left|1 - (T_p/T_s)^2\right|} \sqrt{\left\{ \left(T_p/T_s\right)^2 \frac{S_e(T_p, \zeta_p)}{R_\mu} \right\}^2 + S_e(T_s, \zeta_s)^2} \quad (3.9)$$

where A_s is the value in the floor acceleration spectrum, and S_e is a value in the input elastic acceleration spectrum. $S_e(T_p, \zeta_p)/R_\mu$ applies to the inelastic primary structure, whereas $S_e(T_s, \zeta_s)$ applies to the linear elastic equipment. The damping values of the structure and of the equipment are denoted by ζ_p and ζ_s respectively, whereas T_p and T_s are the natural periods of the structure and the equipment, respectively.

In the case of the stiffness degrading Q model, in the post-resonance region, the ratio T_p/T_s in Equation 3.9 should be replaced by the ratio $T_{p,\mu}/T_s$, where $T_{p,\mu}$ represents the effective natural period of the structure. It depends on the inelastic deformation, which is expressed in terms of ductility. It can be approximately defined by Equation 3.10 proposed by Akiyama (1985). The evaluation of Equation 3.10 is shown in ANNEX C.

$$T_{p,\mu} = T_p \sqrt{\frac{1 + \sqrt{\mu} + \mu}{3}} \quad (3.10)$$

- 2) In the resonance region, the spectral values are limited to the values obtained by Equation 3.11. The amplification factors AMP are defined by Equations 3.7 and 3.8.

$$A_s = AMP \frac{S_e(T_p, \zeta_p)}{R_\mu} \quad (3.11)$$

Note that $S_e(T_p, \zeta_p)/R_\mu$ represents the value in the inelastic acceleration spectrum, i.e. the maximum acceleration of the inelastic primary structure denoted in the parametric study as A_p . R_μ should be determined according to Equation 3.3 in the case of zero post-yield stiffness or according to Equation 3.4 when the influence of hardening needs to be taken into account (i.e. non-zero post-yield stiffness).

Also note that the simplified inelastic spectrum used here can be replaced by any other simplified spectrum available in the literature, or by the "exact" inelastic spectrum (obtained from the nonlinear RHA) also used in Section 3.4.

3.3 Comparison of the original and proposed direct method for elastic structures

In this section, a comparison of the floor response spectra determined from the original direct method proposed by Yasui et al. (1993) and those obtained from the direct method proposed in the previous section is presented (see Figure 3.4) for elastic structures with T_p equal to 0.3 and 1.0 s (soil type B). In both direct approaches the target spectrum of the chosen set of ground motions was used as the seismic input, representing the acceleration of the structure and the equipment. In the resonance region, proposed values of the *AMP* were used in the case of the proposed method. The mean values of floor response spectra determined in the parametric study (described in Section 2.3) are also shown (denoted as RHA). Additionally, broadened mean floor response spectra are plotted (denoted as RHA broadened). Broadening of the peaks of the floor response spectra is a standard procedure, which is intended to take into account the uncertainties related to the determination of the natural periods of the structure. For instance, according to USNRC 1.122 (1978), the frequency region where the spectrum should be broadened is obtained by considering a $\pm 15\%$ variation in the frequencies associated with the spectral peaks. A similar approach (15% broadening of the period) was used for the broadening of spectral peaks in this study. More information on broadening is provided in Section 3.4. The comparison presented in Figure 3.4 shows that the method proposed by Yasui et al. (1993) provides conservative results in the resonance region. In the pre- and post-resonance regions, the results of the original method are in good agreement with the floor response spectra obtained from the RHA.

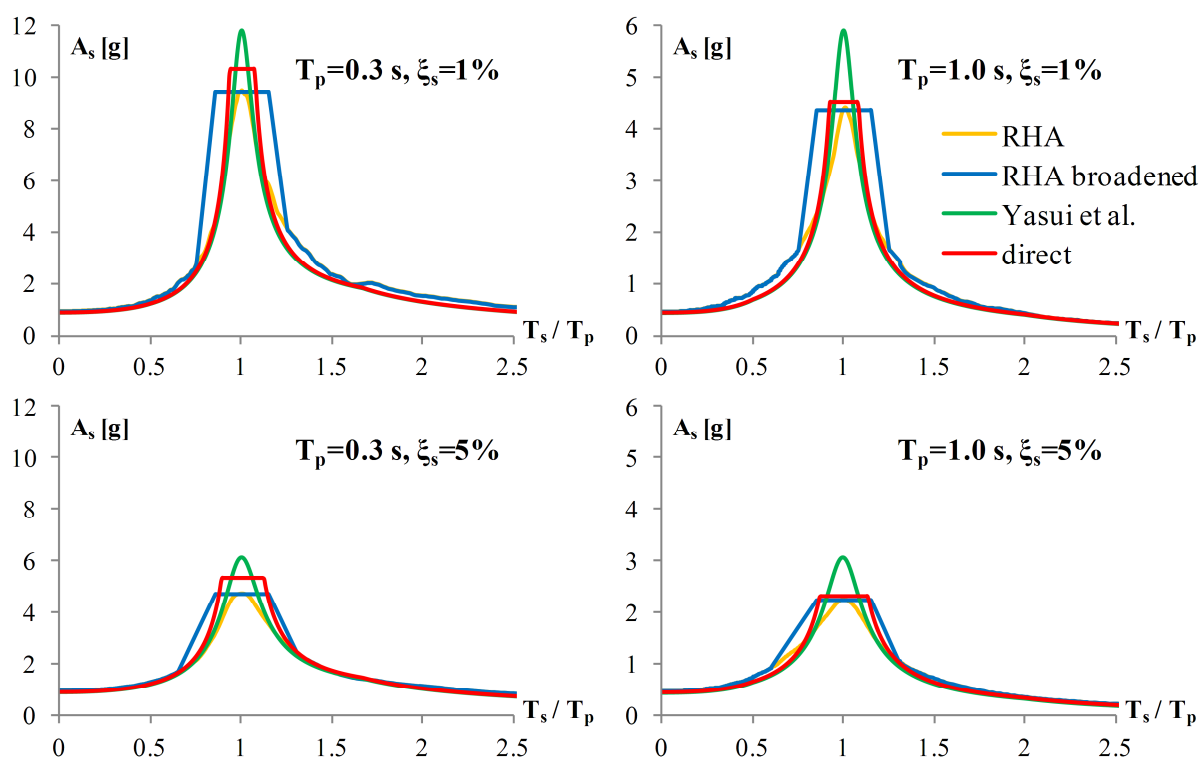


Figure 3.4: A comparison of the floor response spectra for elastic structures for soil type B, 5% damping of the structure

Slika 3.4: Primerjava etažnih spektrov odziva za elastične konstrukcije za tla tipa B, 5% dušenja konstrukcije

The proposed direct method eliminates conservatism in the resonance region, where a fair agreement with the results of the parametric study can be observed. In the pre- and post-resonance regions, the original and proposed methods yield almost the same results.

3.4 Validation of the proposed direct method

The proposed direct method was validated by comparing its results with the floor response spectra obtained in the parametric study (Chapter 2). Selected results shown in this section were obtained for sets of ground records which corresponded to the soil types B and D, for structures with natural periods equal to 0.2, 0.3, 0.5, 0.75, 1.0 and 2.0 s. The EP model and the Q_{10} model were taken into account in the case of soil type D, whereas in the case of soil type B, the Q_0 model was also considered, in addition to the EP and Q_{10} models. Two different values of μ were considered. The damping of the structure amounted to 5%, whereas the damping of the equipment amounted to 1% and 5%.

Figures 3.5–3.19 show the mean (denoted as RHA), mean plus standard deviation (denoted as RHA + σ), and broadened mean (denoted as RHA broadened) values of the floor response spectra obtained in the parametric study (i.e. by using the response-history analysis), as well as the spectra computed from the proposed direct method.

In the direct method, both the "exact" inelastic acceleration spectra (obtained by nonlinear response-history analyses), and the approximate inelastic spectra (obtained by reducing the target Eurocode 8 2004 elastic pseudo-acceleration spectrum by the factor R_{μ}) were used for the structure. In the case of the equipment, the mean elastic spectra of the chosen sets of ground motions were used in the case of the "exact" approach, whereas the target Eurocode 8 (2004) elastic pseudo-acceleration spectra were used in the case of the approximate approach.

By using the "exact" approach, approximations related to the inelastic spectrum and the difference between the mean and target ground motion spectra are eliminated, which allows an evaluation of the basic features of the proposed direct method. On the other hand, by using the approximate approach these approximations are included in the results. In both cases the proposed values of amplification factors AMP were used (Equations 3.7 and 3.8). In Figures 3.5–3.19, the results obtained with the "exact" spectra are denoted as "direct "exact"", whereas those obtained with the approximate spectra are denoted as "direct approx.".

As mentioned above, in the comparison of the floor response spectra, the broadened mean floor response spectra are also shown (RHA broadened). Due to uncertainties related to the determination of the natural period of the structure, the floor response spectra are, in practice, broadened in order to allow moderate shifts (typically $\pm 15\%$) of the frequency or the period of the structure. The existing provisions (e.g. ASCE 4-98 2000) consider structures with linear elastic behaviour. In the case of the EP model of the structure, where peak values of floor response spectra always occur close to the resonance ($T_s \approx T_p$), it is also reasonable to apply the same the $\pm 15\%$ rule. In the case of the Q model, the peaks of floor the spectra are shifted towards higher periods. The size of the shift depends on the ductility demand of the structure, i.e. larger shifts are a consequence of a higher ductility demand. In some cases, though, mean floor response spectra have multiple peaks.

The question is: what kind of peak broadening makes sense in the case of the stiffness degrading Q model? It seems reasonable to assume that both the original and modified natural periods of the structure (T_p and $T_{p,\mu}$, respectively) should be taken into account in the peak broadening procedure. For this reason the plateau of the broadened spectra shown here extends from $T_s/T_p=0.85$ to $T_s/T_{p,\mu}=1.15$. In this way, a quite wide broadened spectrum is obtained, especially in the case of structures with a higher ductility demand.

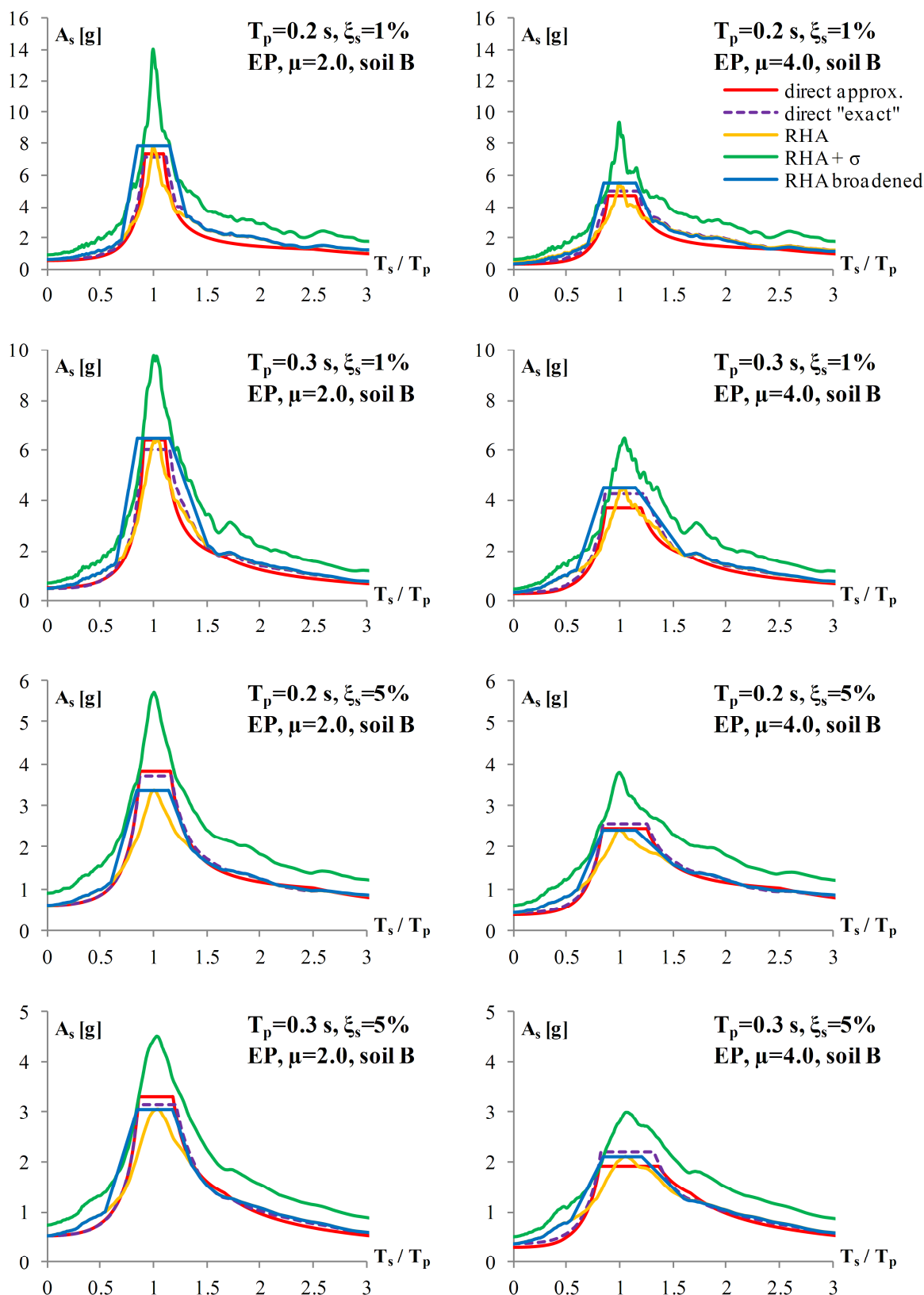


Figure 3.5: Floor response spectra for the EP model of the structure, natural periods equal to 0.2 and 0.3 s, 5% damping of the structure, soil type B

Slika 3.5: Etažni spektri odziva za EP model konstrukcije, nihajni časi enaki 0.2 in 0.3 s, 5% dušenja konstrukcije, tip tal B

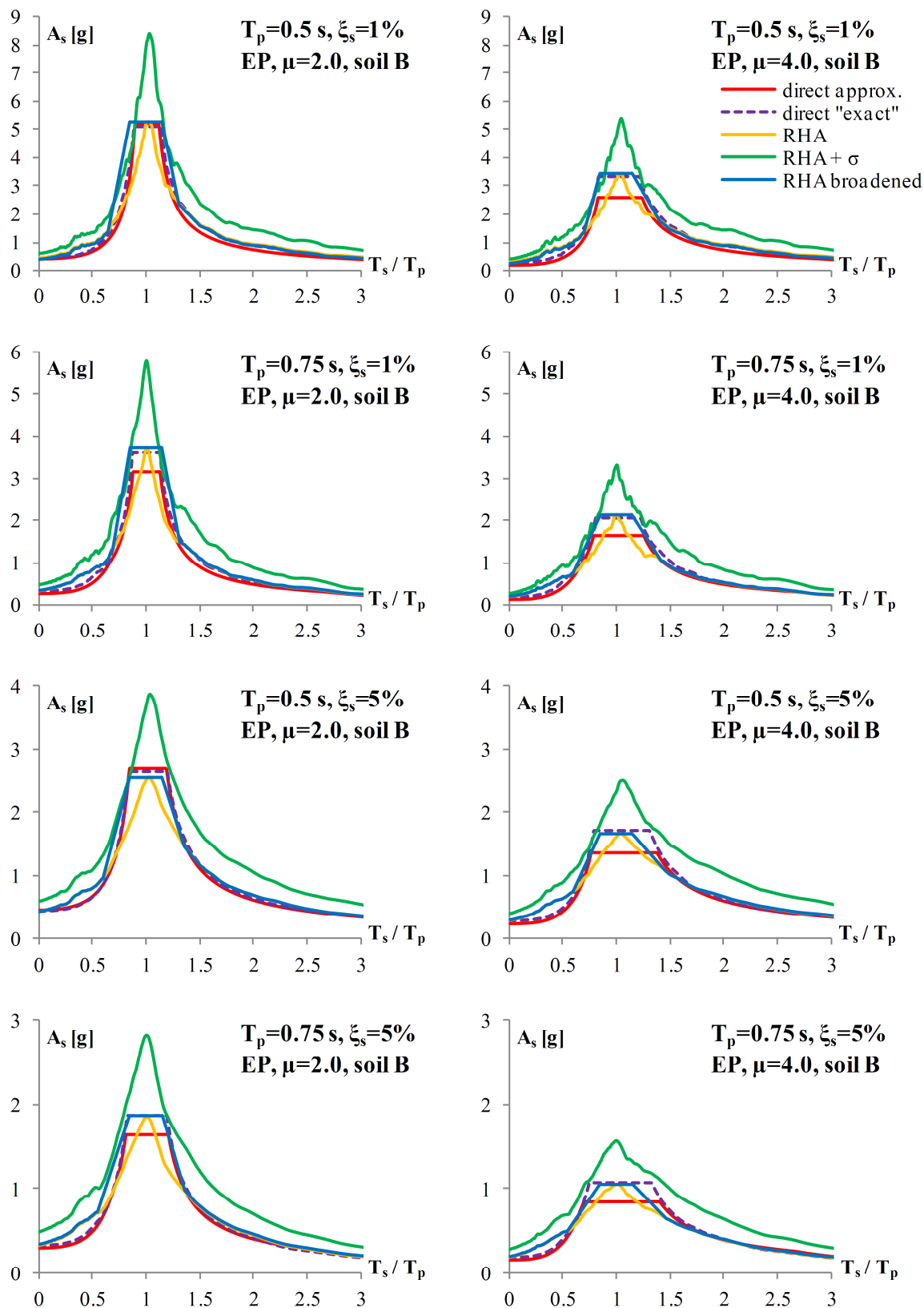


Figure 3.6: Floor response spectra for the EP model of the structure, natural periods equal to 0.5 and 0.75 s, 5% damping of the structure, soil type B

Slika 3.6: Etažni spektri odziva za EP model konstrukcije, nihajni časi enaki 0.5 in 0.75 s, 5% dušenja konstrukcije, tip tal B

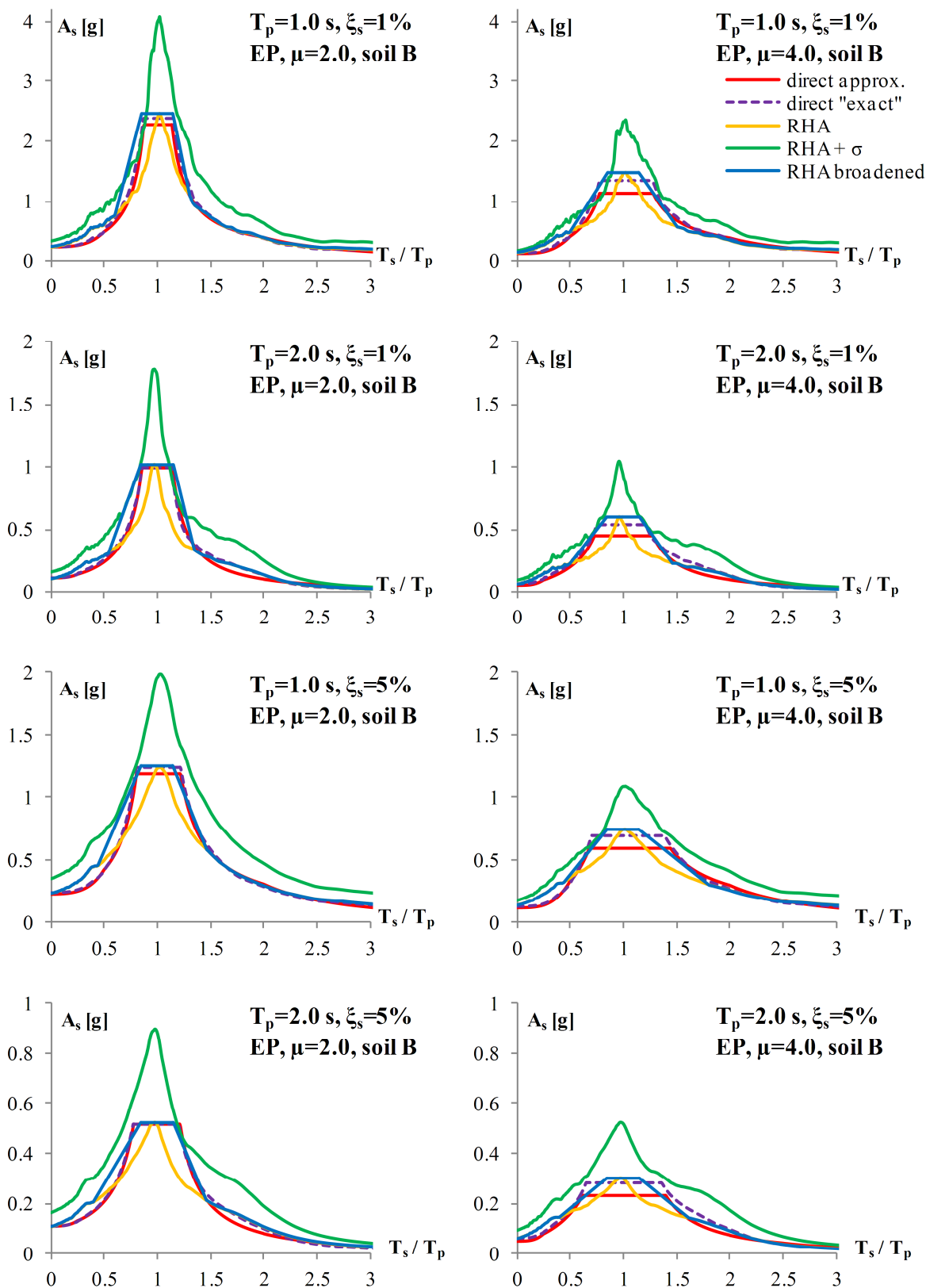


Figure 3.7: Floor response spectra for the EP model of the structure, natural periods equal to 1.0 and 2.0 s, 5% damping of the structure, soil type B

Slika 3.7: Etažni spektri odziva za EP model konstrukcije, nihajni časi enaki 1.0 in 2.0 s, 5% dušenja konstrukcije, tip tal B

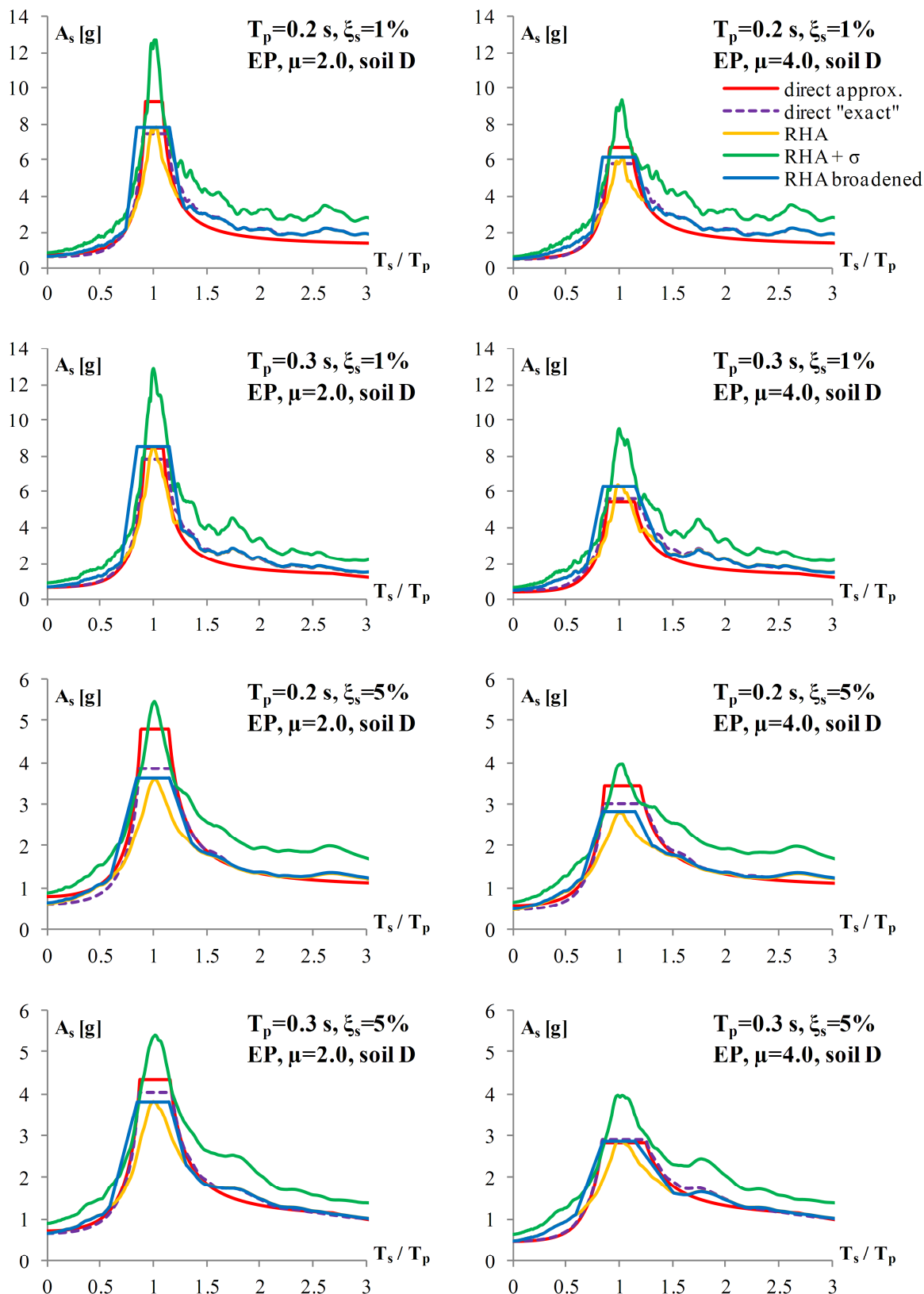


Figure 3.8: Floor response spectra for the EP model of the structure, natural periods equal to 0.2 and 0.3 s, 5% damping of the structure, soil type D

Slika 3.8: Etažni spektri odziva za EP model konstrukcije, nihajni časi enaki 0.2 in 0.3 s, 5% dušenja konstrukcije, tip tal D

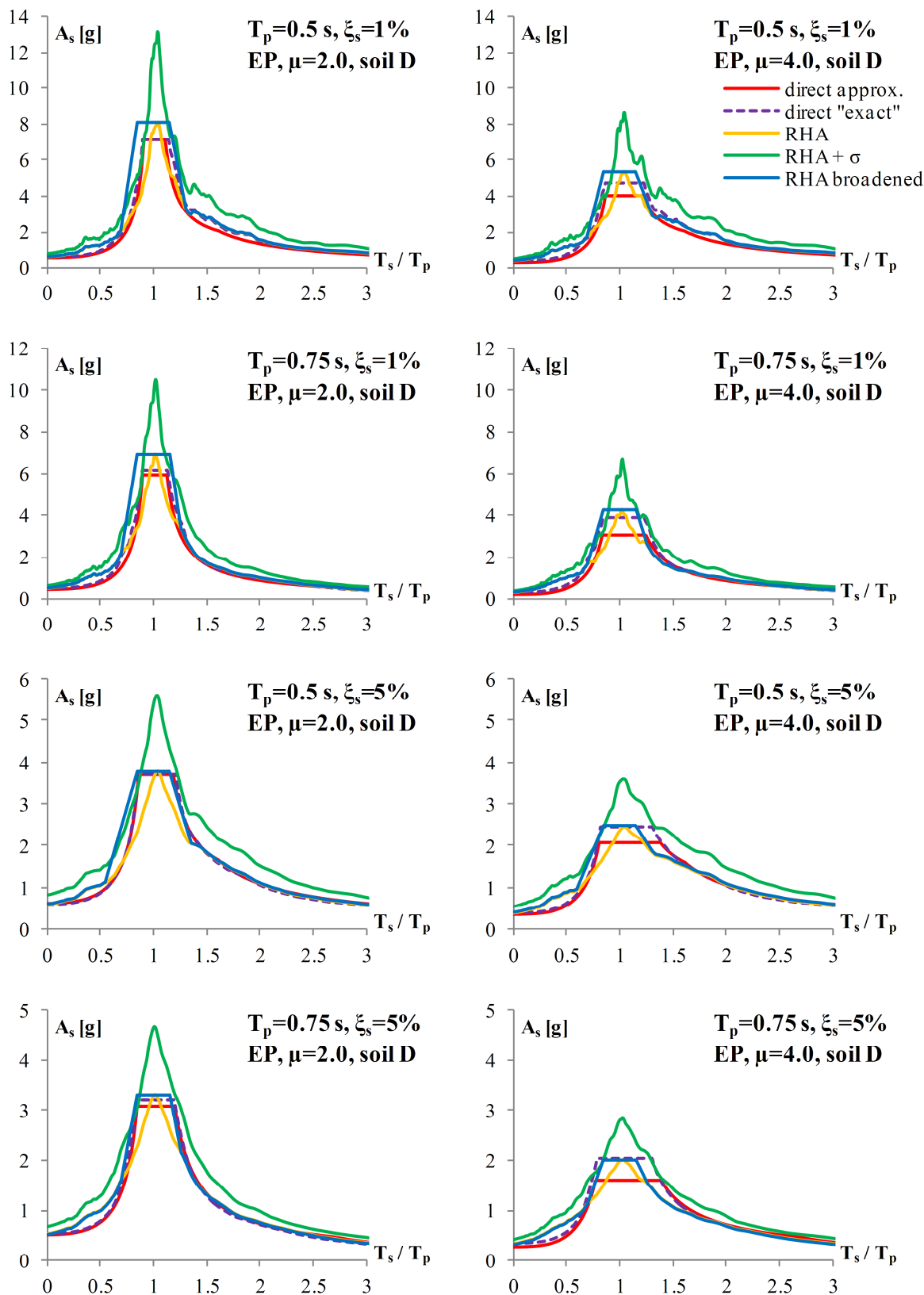


Figure 3.9: Floor response spectra for the EP model of the structure, natural periods equal to 0.5 and 0.75 s, 5% damping of the structure, soil type D

Slika 3.9: Etažni spektri odziva za EP model konstrukcije, nihajni časi enaki 0.5 in 0.75 s, 5% dušenja konstrukcije, tip tal D

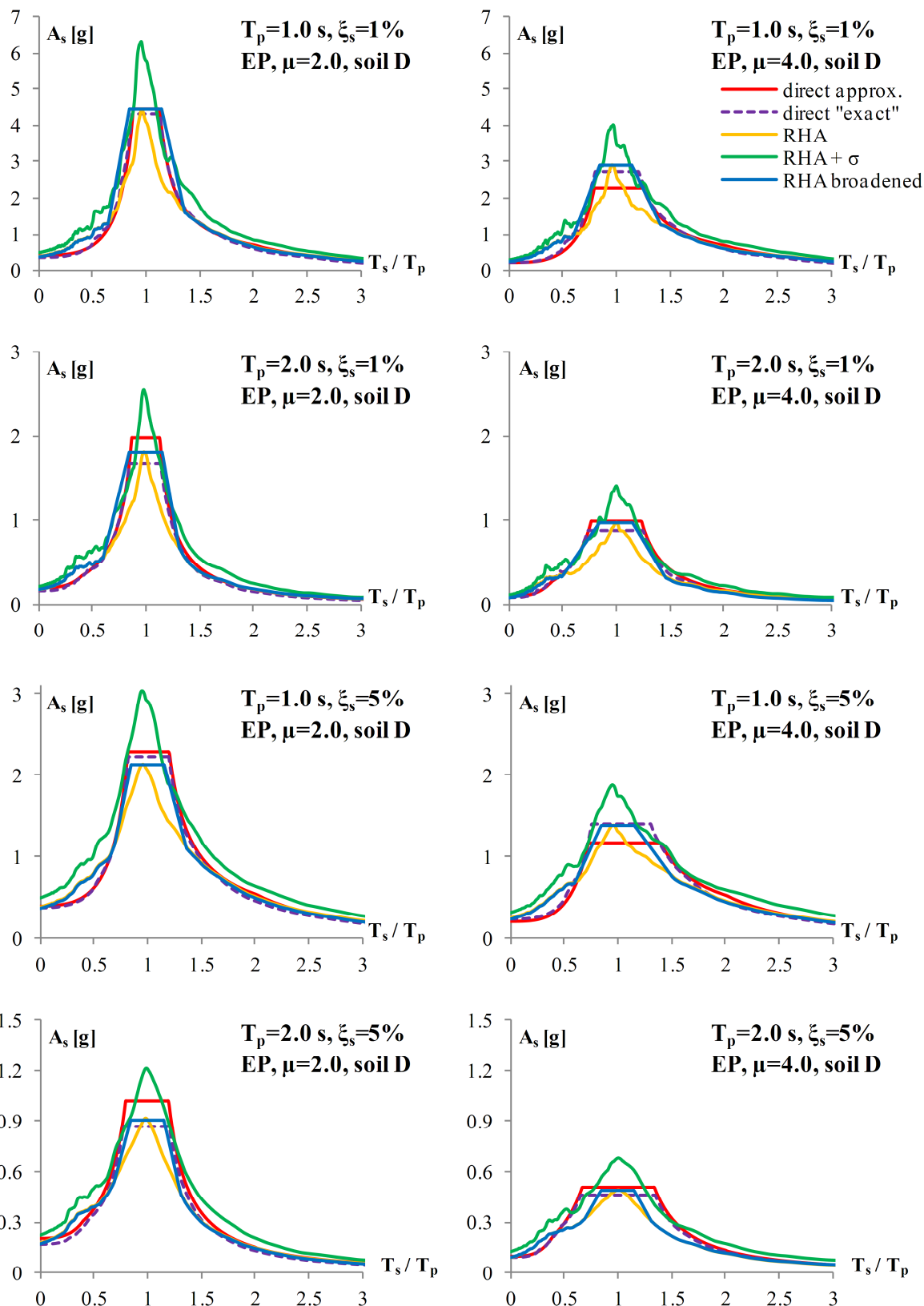


Figure 3.10: Floor response spectra for the EP model of the structure, natural periods equal to 1.0 and 2.0 s, 5% damping of the structure, soil type D

Slika 3.10: Etažni spektri odziva za EP model konstrukcije, nihajni časi enaki 1.0 in 2.0 s, 5% dušenja konstrukcije, tip tal D

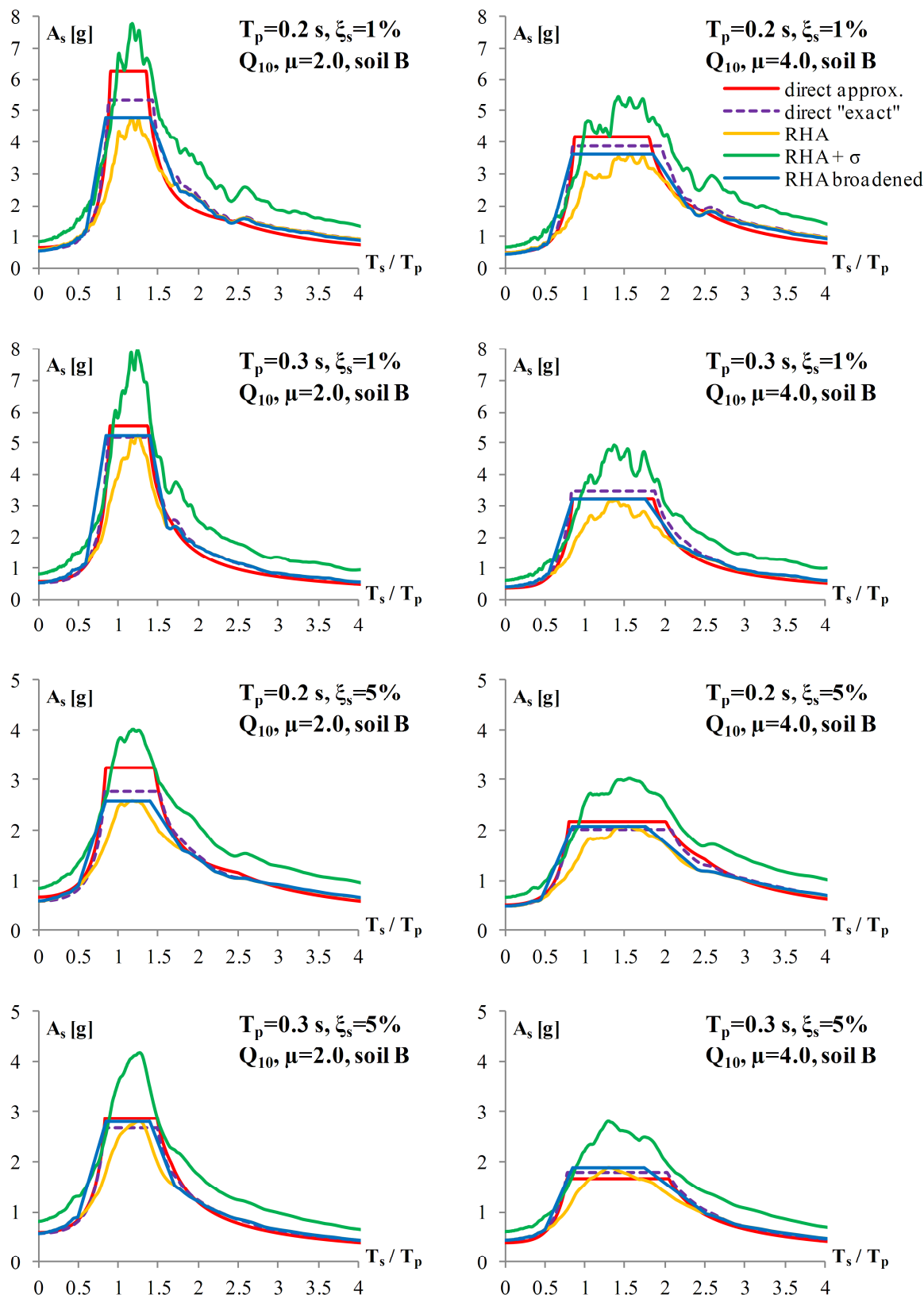


Figure 3.11: Floor response spectra for the Q_{10} model of the structure, natural periods equal to 0.2 and 0.3 s, 5% damping of the structure, soil type B

Slika 3.11: Etažni spektri odziva za Q_{10} model konstrukcije, nihajni časi enaki 0.2 in 0.3 s, 5% dušenja konstrukcije, tip tal B

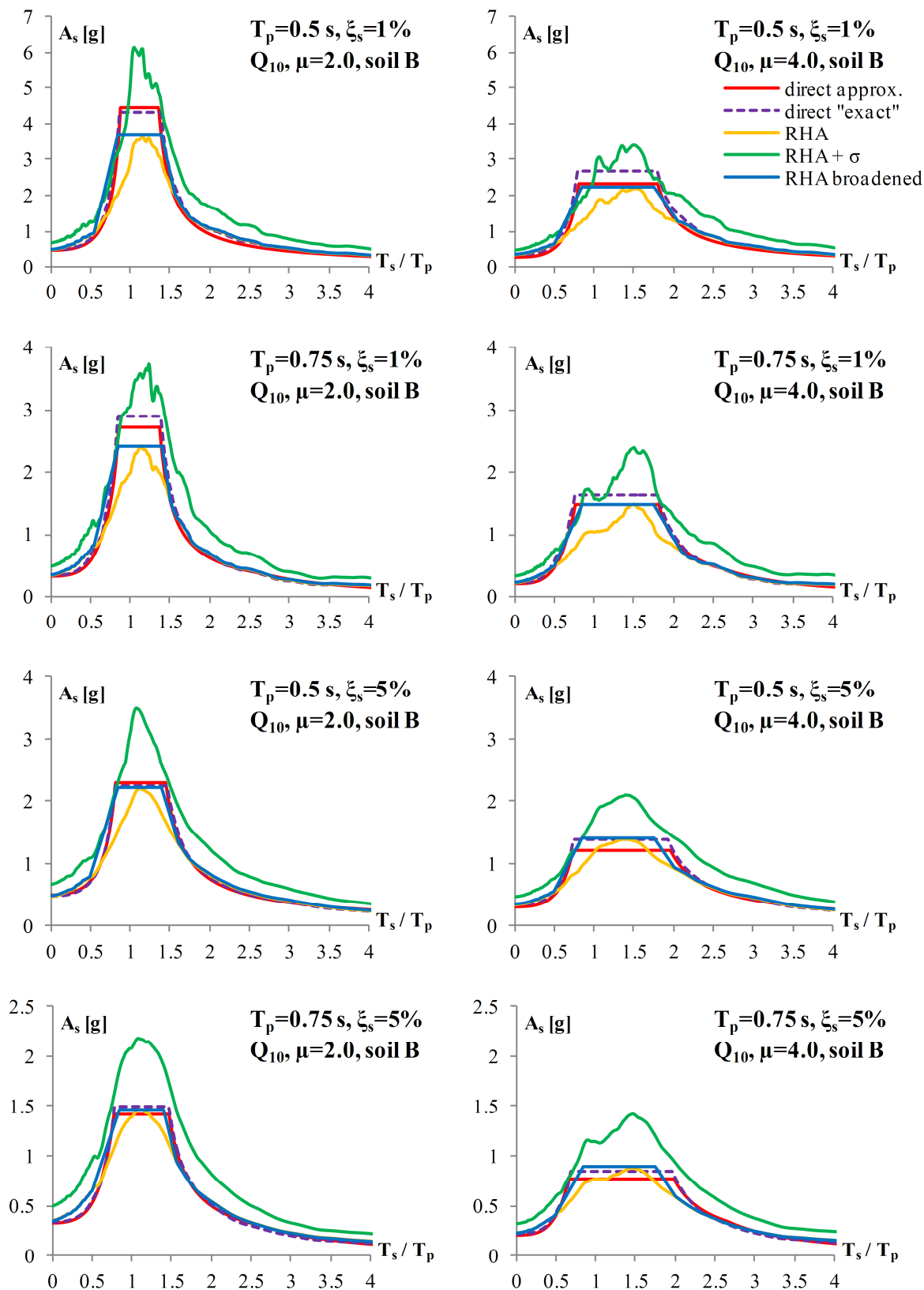


Figure 3.12: Floor response spectra for the Q₁₀ model of the structure, natural periods equal to 0.5 and 0.75 s, 5% damping of the structure, soil type B

Slika 3.12: Etažni spektri odziva za Q₁₀ model konstrukcije, nihajni časi enaki 0.5 in 0.75 s, 5% dušenja konstrukcije, tip tal B

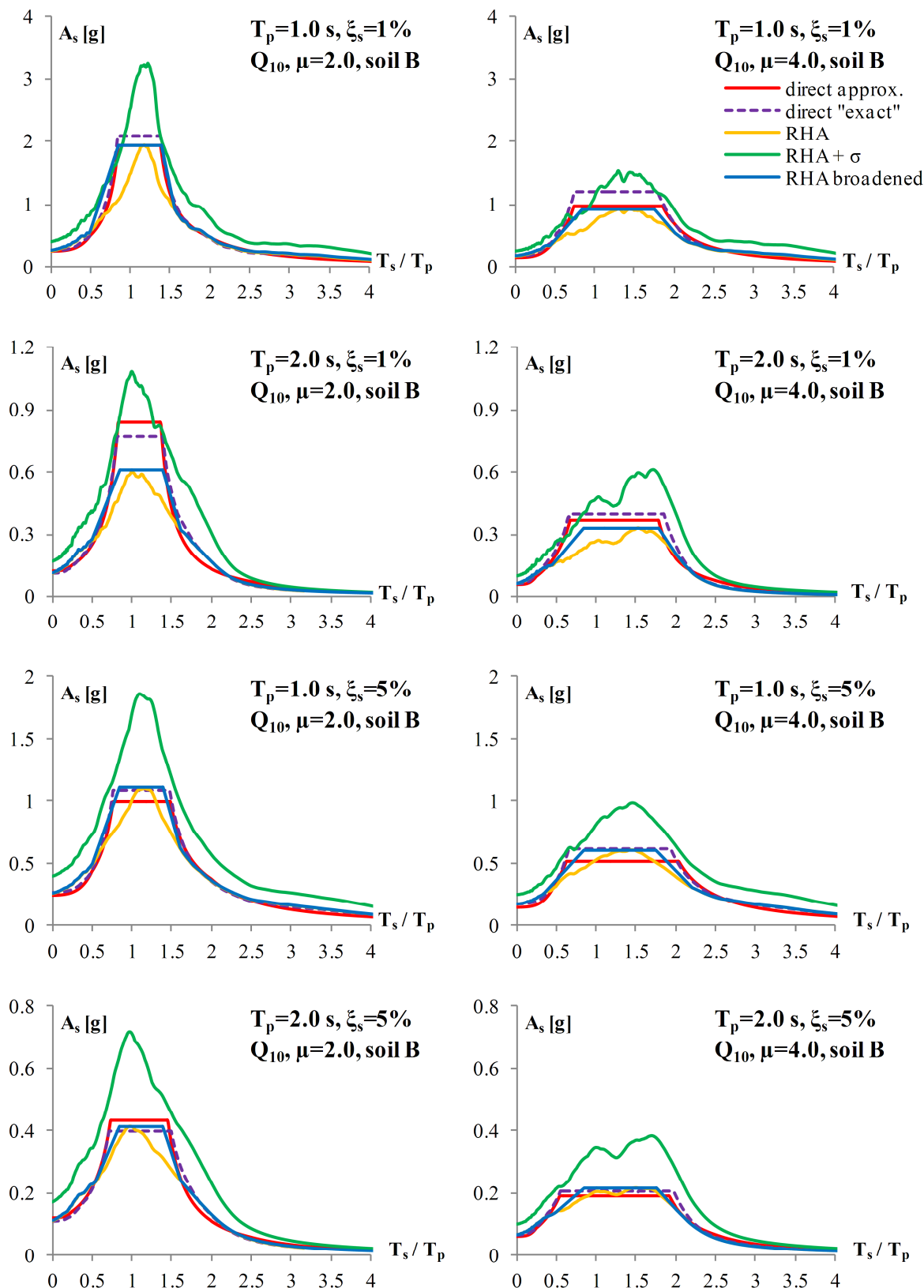


Figure 3.13: Floor response spectra for the Q_{10} model of the structure, natural periods equal to 1.0 and 2.0 s, 5% damping of the structure, soil type B

Slika 3.13: Etažni spektri odziva za Q_{10} model konstrukcije, nihajni časi enaki 1.0 in 2.0 s, 5% dušenja konstrukcije, tip tal B

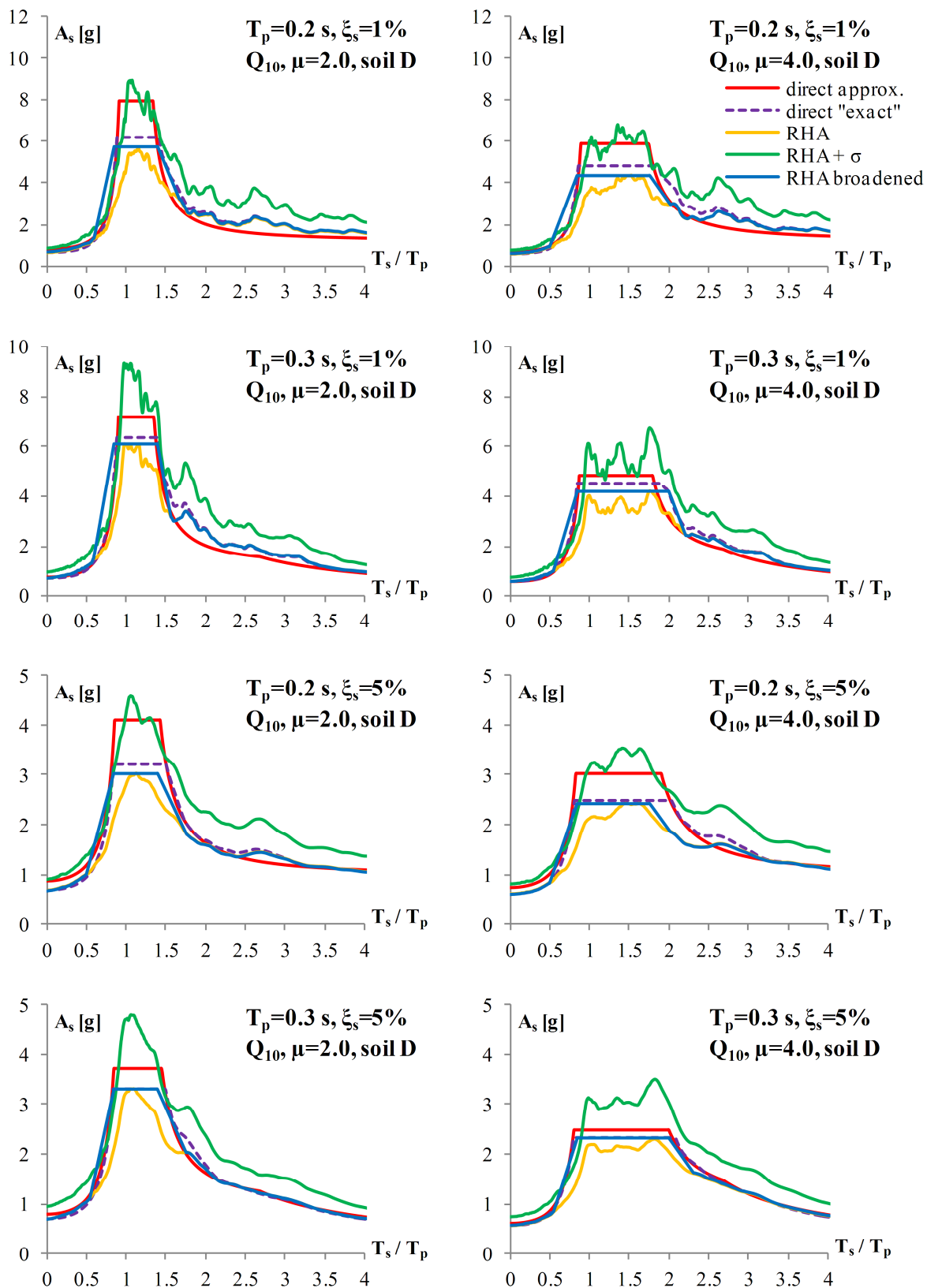


Figure 3.14: Floor response spectra for the Q_{10} model of the structure, natural periods equal to 0.2 and 0.3 s, 5% damping of the structure, soil type D

Slika 3.14: Etažni spektri odziva za Q_{10} model konstrukcije, nihajni časi enaki 0.2 in 0.3 s, 5% dušenja konstrukcije, tip tal D

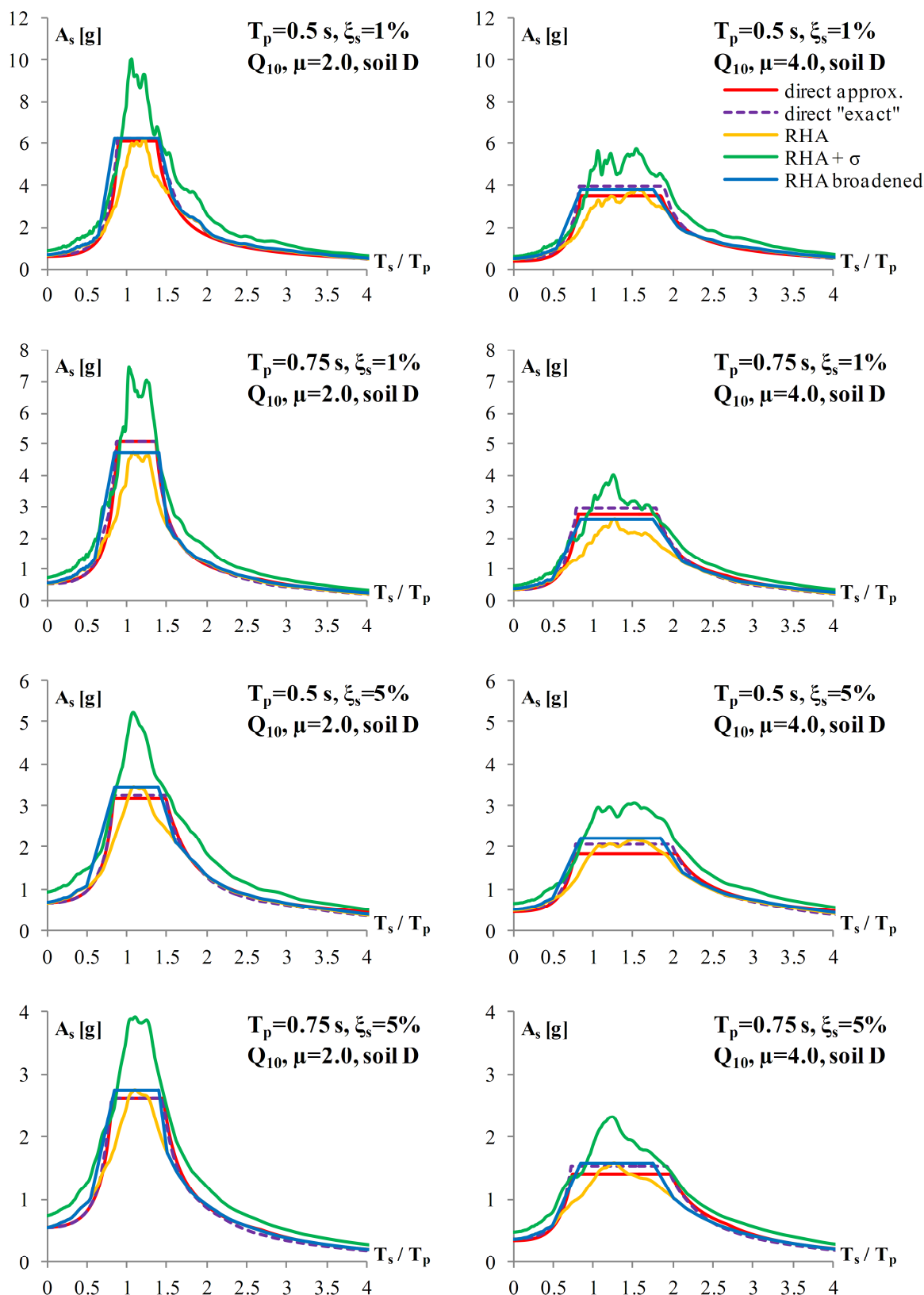


Figure 3.15: Floor response spectra for the Q_{10} model of the structure, natural periods equal to 0.5 and 0.75 s, 5% damping of the structure, soil type D

Slika 3.15: Etažni spektri odziva za Q_{10} model konstrukcije, nihajni časi enaki 0.5 in 0.75 s, 5% dušenja konstrukcije, tip tal D

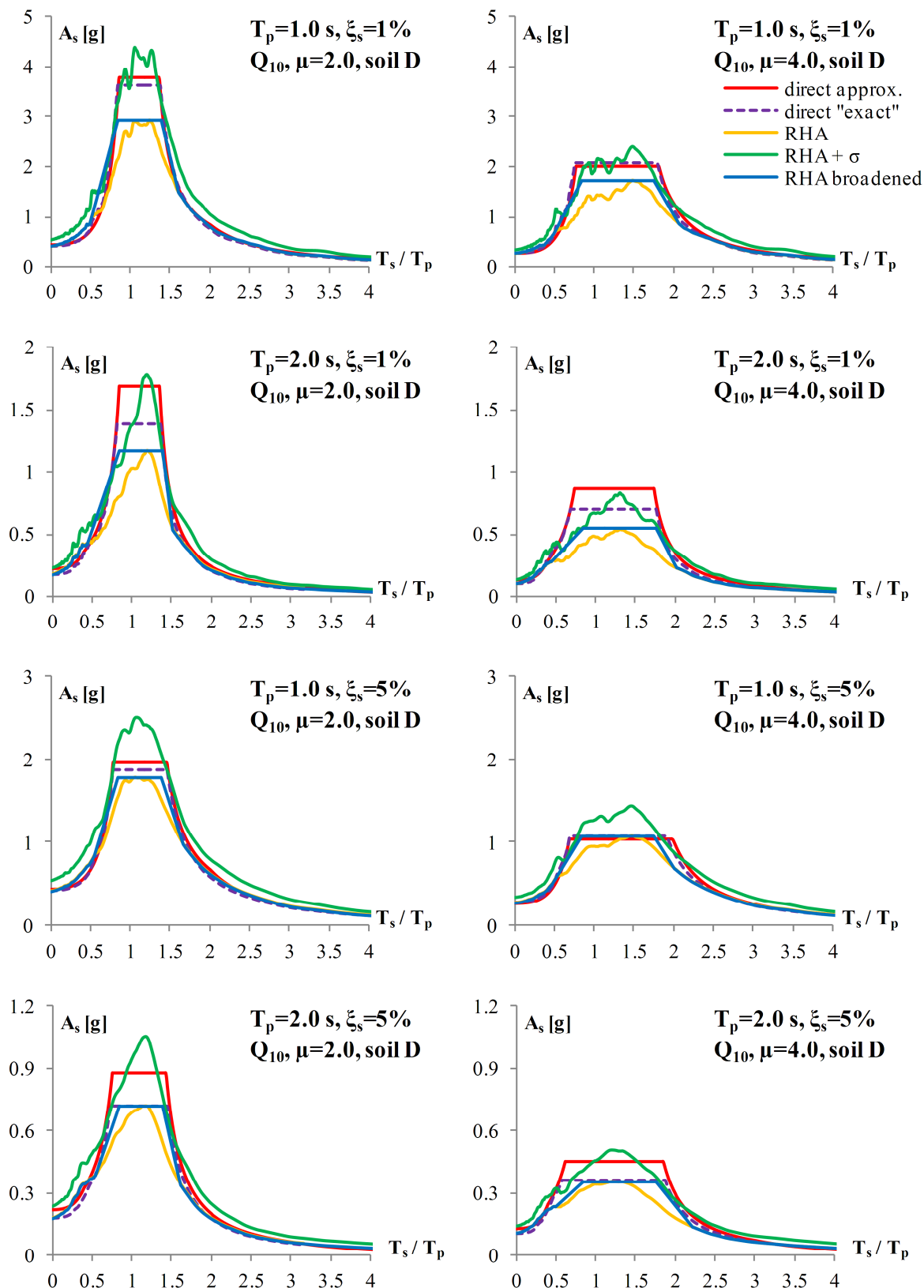


Figure 3.16: Floor response spectra for the Q₁₀ model of the structure, natural periods equal to 1.0 and 2.0 s, 5% damping of the structure, soil type D

Slika 3.16: Etažni spektri odziva za Q₁₀ model konstrukcije, nihajni časi enaki 1.0 in 2.0 s, 5% dušenja konstrukcije, tip tal D

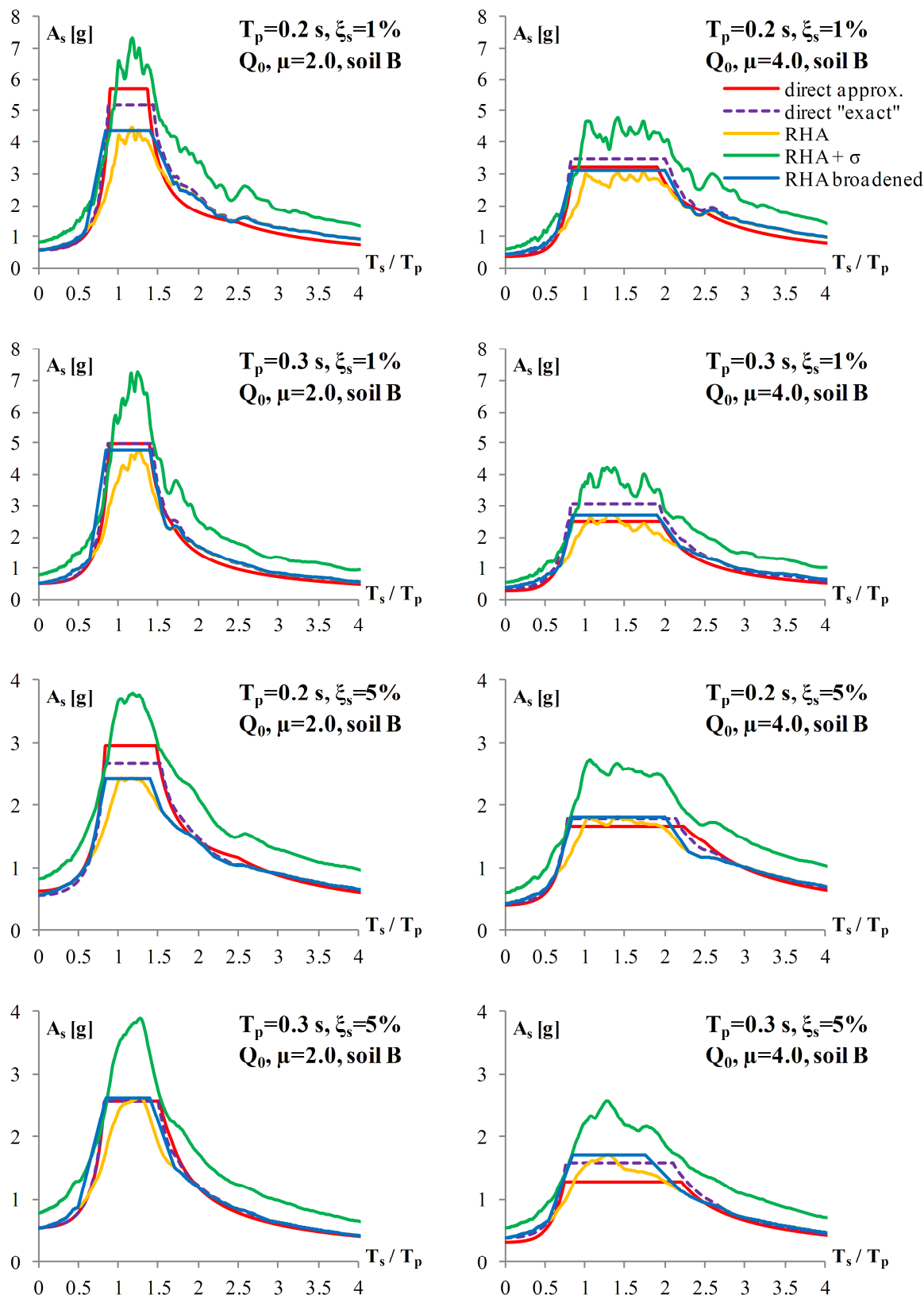


Figure 3.17: Floor response spectra for the Q_0 model of the structure, natural periods equal to 0.2 and 0.3 s, 5% damping of the structure, soil type B

Slika 3.17: Etažni spektri odziva za Q_0 model konstrukcije, nihajni časi enaki 0.2 in 0.3 s, 5% dušenja konstrukcije, tip tal B

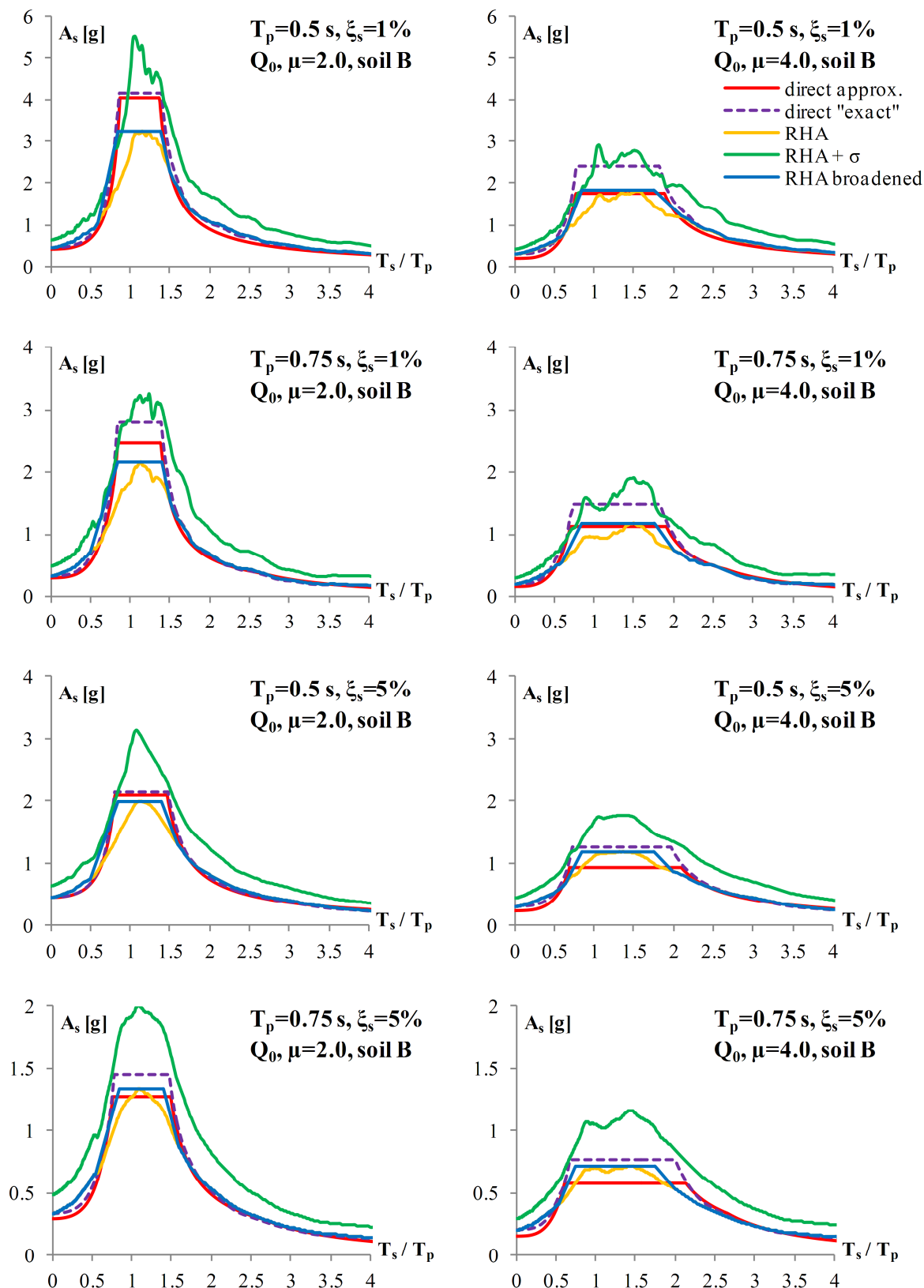


Figure 3.18: Floor response spectra for the Q_0 model of the structure, natural periods equal to 0.5 and 0.75 s, 5% damping of the structure, soil type B

Slika 3.18: Etažni spektri odziva za Q_0 model konstrukcije, nihajni časi enaki 0.5 in 0.75 s, 5% dušenja konstrukcije, tip tal B

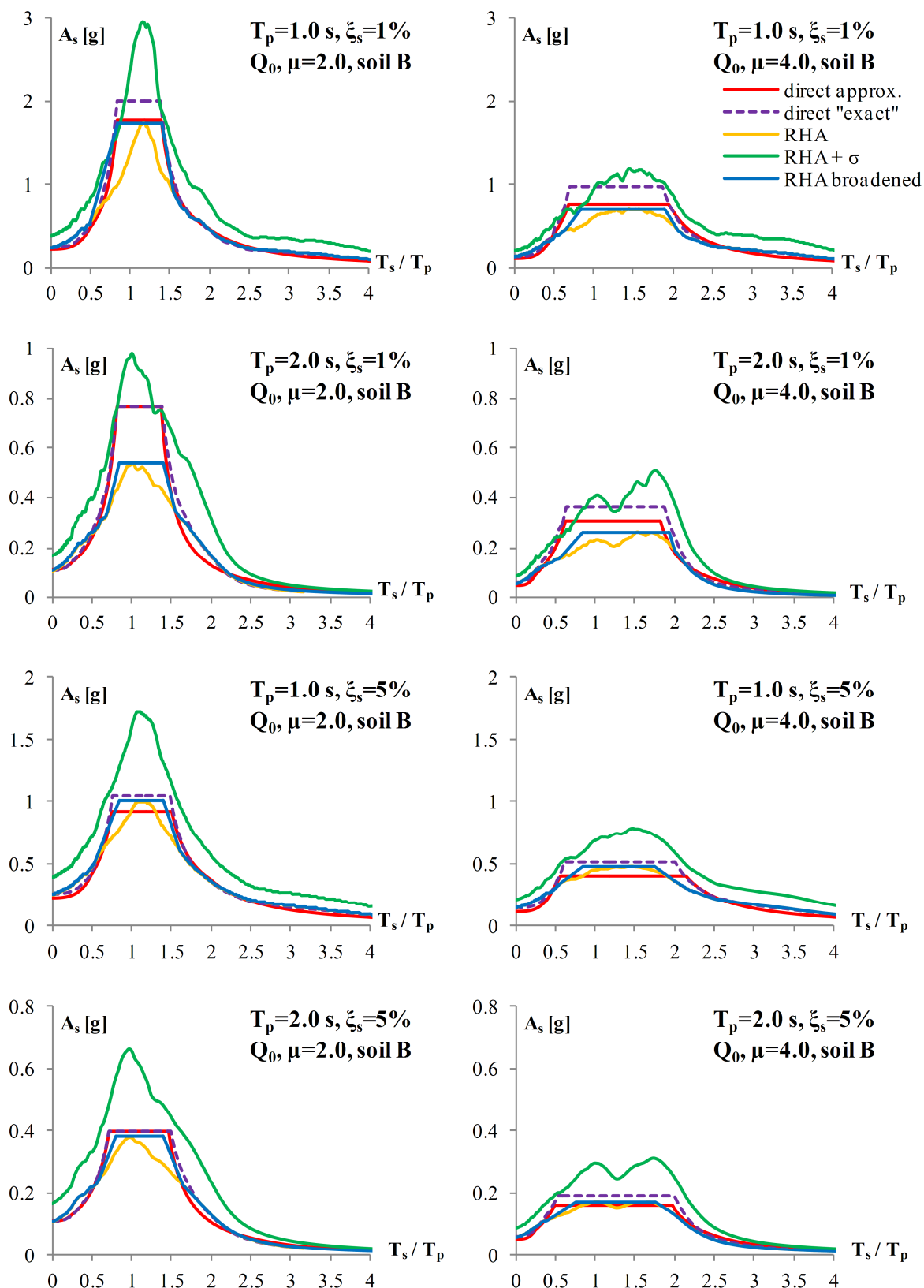


Figure 3.19: Floor response spectra for the Q_0 model of the structure, natural periods equal to 1.0 and 2.0 s, 5% damping of the structure, soil type B

Slika 3.19: Etažni spektri odziva za Q_0 model konstrukcije, nihajni časi enaki 1.0 in 2.0 s, 5% dušenja konstrukcije, tip tal B

It is clear from Figures 3.5–3.19 that the proposed direct method in general provides a fair estimate of the broadened floor acceleration spectra, throughout the whole period range, for all of the analysed hysteretic models, natural periods of the structure, levels of ductility and equipment damping. The differences are due to the simplifications made in the proposed direct method, as well as due to the approximations in the inelastic spectra. The latter source of errors (Tables 3.1 and 3.2) is eliminated if "exact" inelastic spectra are used.

3.5 Comparison of the proposed method with the provisions of Eurocode 8 (2004)

Eurocode 8 (2004) provides guidelines for the design of non-structural elements (equipment). In this section a comparison is made between the results obtained by using the proposed direct method and the Eurocode 8 (2004) provisions. In order to make such comparison possible, the form of Eurocode 8 (2004) basic formula for the design of non-structural elements was slightly modified, using the mass of the element rather than its weight. Horizontal force that should be applied to the non-structural element is now expressed as

$$F_s = \frac{m_s A_s \gamma_s}{q_s} \quad (3.12)$$

where m_s , γ_s , and q_s represent the mass, the importance factor and the behaviour factor of the element, respectively. A_s represents the design acceleration, i.e. the floor response spectrum value, which is calculated as

$$A_s = a_g S \left[\frac{3(1+z/H)}{1+(1-T_s/T_p)^2} - 0.5 \right] \quad (3.13)$$

where a_g is the design ground acceleration on type A ground, S is the soil factor, z is the height of the element above the level of application of the seismic action (foundation or top of a rigid basement), H is the building height measured from the foundation or from the top of a rigid basement, T_s is the fundamental period of the element and T_p is the fundamental period of the structure in the relevant direction. The value of A_s must not be less than $a_g S$ (peak ground acceleration).

It is obvious from Equations 3.12 and 3.13 that inelastic behaviour of the structure, as well as damping of the structure and the equipment, is not taken into account explicitly by Eurocode 8 (2004). On the other hand, the behaviour factor q_s suggests that some inelastic behaviour of non-structural elements is allowed. The ratio z/H takes into account the influence of the vertical position of the element in the structure. For comparison with the proposed direct method, a moderate inelastic behaviour of the primary structure was assumed (the EP and Q₁₀ models with $\mu=2$) and 5% damping for both the primary and secondary structure. Moreover, since the proposed method applies to SDOF systems, $z/H=1$ should be used in Equation 3.13. The ground motion was defined by the Eurocode 8 (2004) type 1 elastic spectrum for soil type B with the peak ground acceleration equal to 0.30g. The natural periods of the primary structure amounted to 0.3, 0.5, 0.75 and 1.0 s. The results are shown in Figure 3.20 and the comparison suggests that the simple Eurocode 8 (2004) equation yields results which are comparable with the average results obtained by the proposed direct method. However, the Eurocode 8 (2004) floor response spectrum depends on the peak ground acceleration, rather than on the maximum acceleration of the primary structure. Therefore, it is obvious that the effect of the natural period of the

primary structure, which was demonstrated through the results of the proposed direct method, is not properly recognized in the Eurocode 8 (2004) provisions.

To summarize: assuming that 5% damping is a reasonable value for the primary structure, the simple Eurocode 8 (2004) formula does not take into account three important influences on the floor response spectra, i.e. the natural period and the level of the inelastic behavior of the primary structure and the damping of the secondary structure. Consequently, it can provide only a very rough idea on the order of magnitude of floor response spectra.

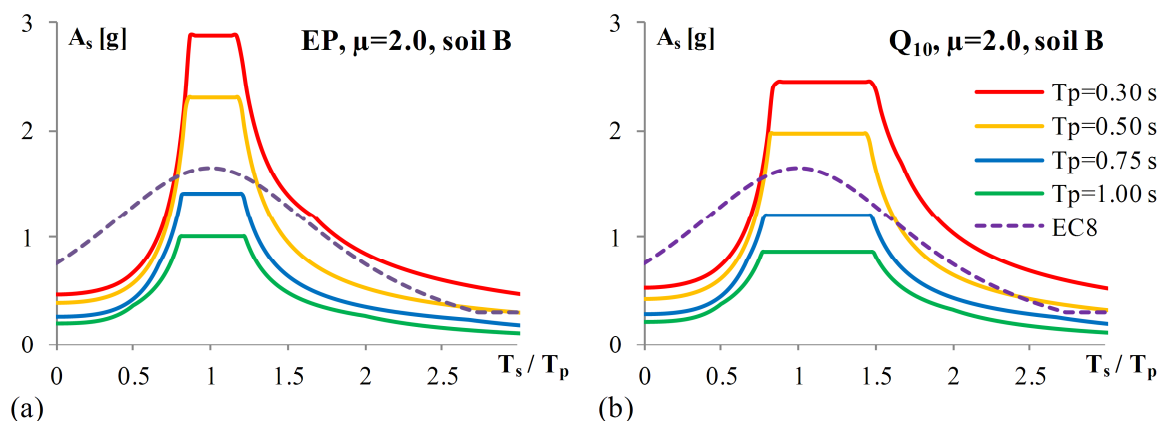


Figure 3.20: Floor response spectra obtained by Eurocode 8 (2004) and the proposed method for (a) EP and (b) Q_{10} models with $\mu=2$, T_p equal to 0.3, 0.5, 0.75 and 1.0 s, type 1 spectrum, soil type B, 5% damping, $a_g S=0.30g$

Slika 3.20: Etažni spektri odziva dobljeni s pomočjo Evrokoda 8 (2004) in predlagane metode za (a) EP in (b) Q_{10} modela z $\mu=2$, T_p enako 0.3, 0.5, 0.75 in 1 s, tip 1 spektra, tip tal B, 5% dušenja, $a_g S=0.30g$

3.6 Comparison of the proposed method with the method proposed by Sullivan et al. (2013)

Sullivan et al. (2013) proposed a direct method which is based on the same assumptions as the direct method proposed in this chapter: inelastic behaviour of the SDOF primary structure, elastic behaviour of the SDOF secondary structure and uncoupled primary-secondary system. Sullivan et al. (2013) have conducted analyses by varying the intensity of the seismic input. In their method, the shape of floor response spectrum is determined by the natural period and inelasticity of the structure, whereas the damping of the equipment determines its magnitude. Equations for the prediction of floor response spectra were proposed and a comparison was made with the method proposed herein. The results of both methods are compared with the "accurate" floor response spectra obtained in the parametric study (see Figures 3.21 and 3.22). In the comparison of the floor response spectra, the broadened mean floor response spectra are also shown. The presented results were obtained for sets of ground records which correspond to soil types B and D, for structures with natural periods equal to 0.3 and 1.0 s. The EP and Q_{10} models were taken into account, and two different values of μ were considered. The damping of the structure amounted to 5%, whereas the damping of the equipment amounted to 1% and 5%.

From Figures 3.21 and 3.22 it can be observed that the method proposed by Sullivan et al. (2013) in all cases provided conservative results in the pre-resonance region, while the results obtained by the direct method proposed herein are more accurate. In the resonance region, for 1% damping of the equipment, the method proposed by Sullivan et al. (2013) again led to slightly conservative results, whereas for 5% damping both methods produced similar results. In the post-resonance region the direct method proposed in this chapter led to more accurate results.

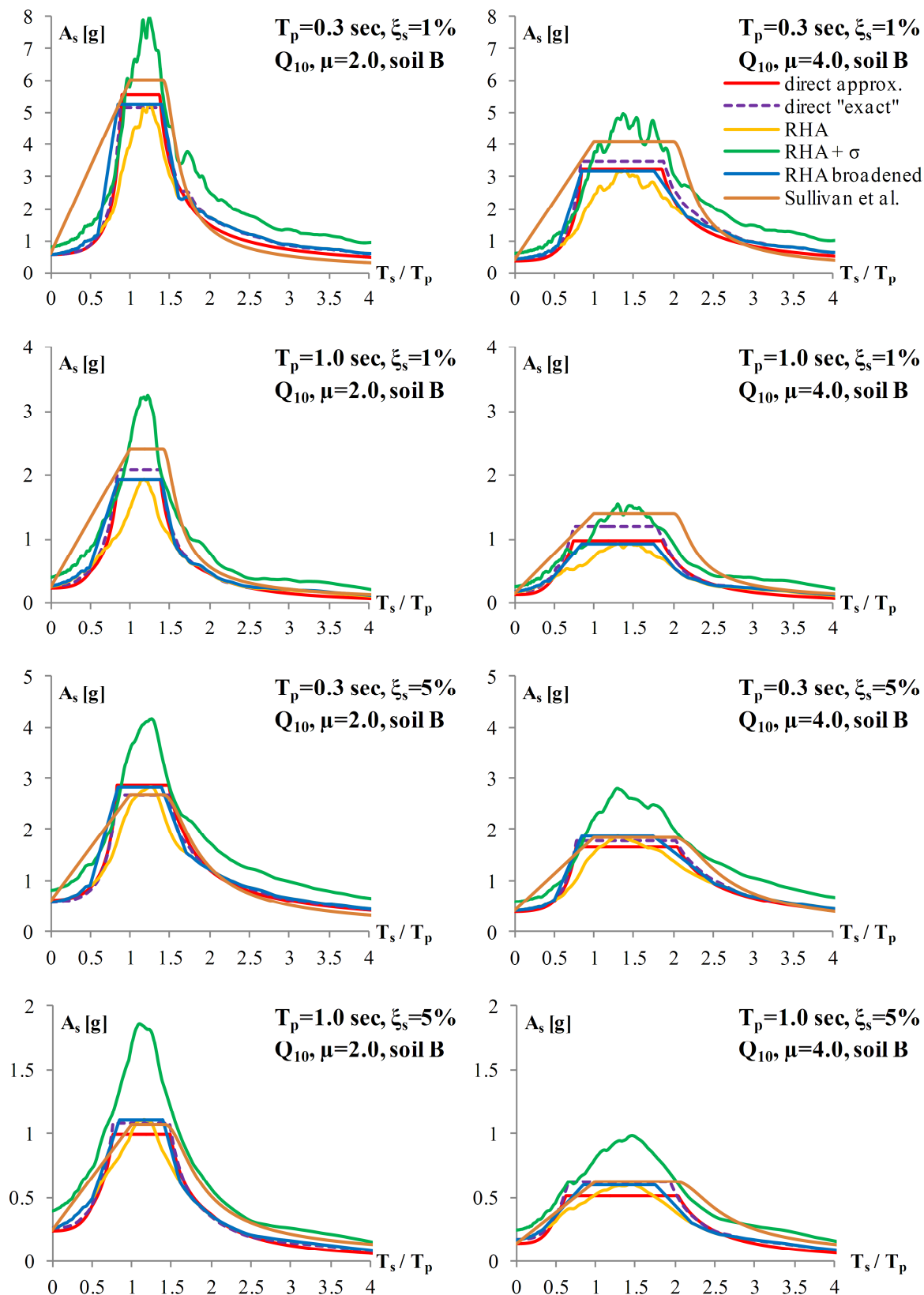


Figure 3.21: Floor response spectra obtained by two direct approaches for the Q_{10} model of the structure, natural periods equal to 0.3 and 1.0 s, 5% damping of the structure, soil type B

Slika 3.21: Etažni spektri odziva dobljeni z dvema direktnima pristopoma za Q_{10} model konstrukcije, nihajni časi enaki 0.3 in 1.0 s, 5% dušenja konstrukcije, tip tal B

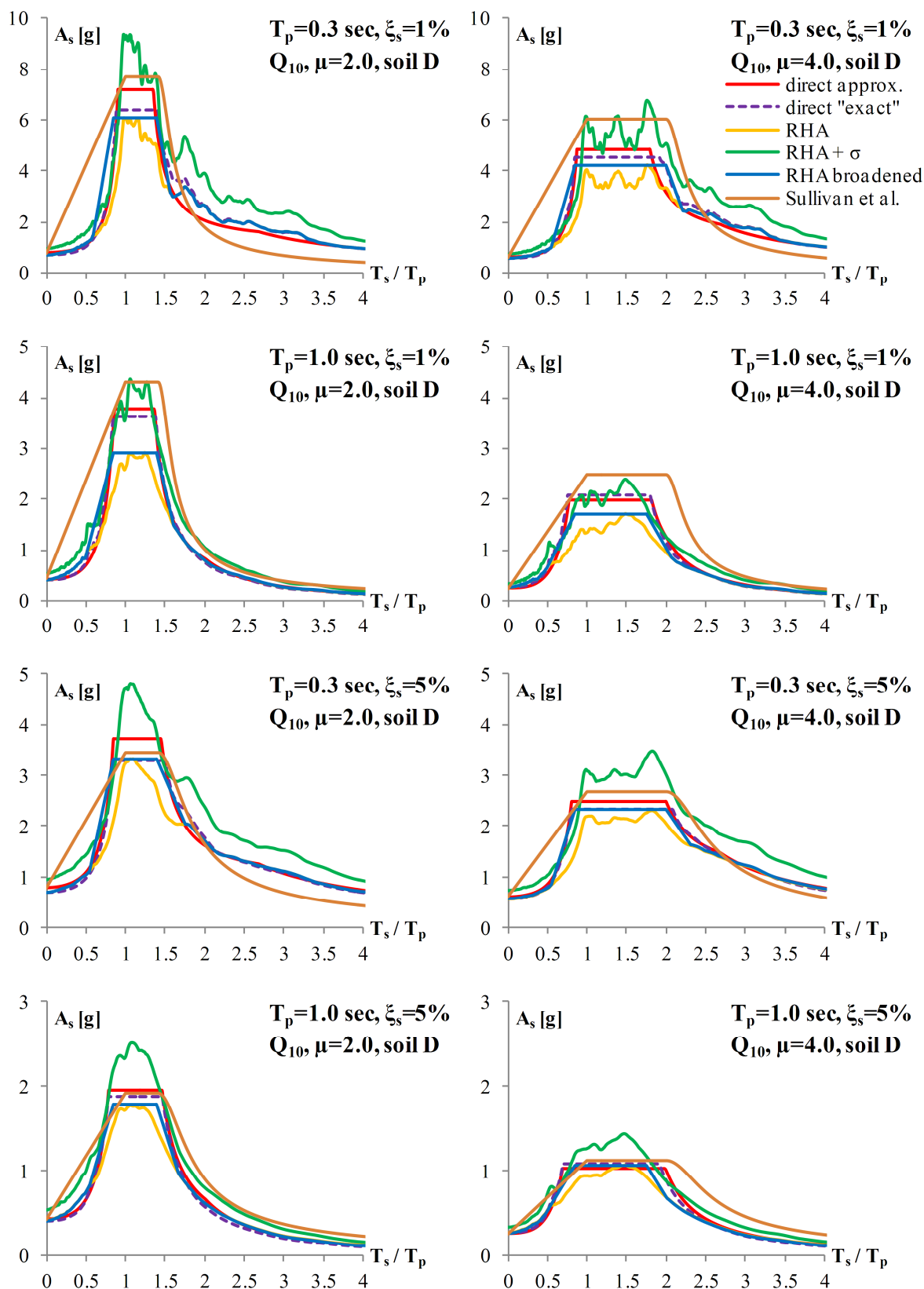


Figure 3.22: Floor response spectra obtained by two direct approaches for the Q_{10} model of the structure, natural periods equal to 0.3 and 1.0 s, 5% damping of the structure, soil type D

Slika 3.22: Etažni spektri odziva dobljeni z dvema direktnima pristopoma za Q_{10} model konstrukcije, nihajni časi enaki 0.3 in 1.0 s, 5% dušenja konstrukcije, tip tal D

3.7 Example of the application of the proposed method

In order to illustrate the application of the proposed direct method, a simple numerical example is provided in this section. Let us consider an RC structure (e.g. a single storey building), which was modelled as a SDOF system with the following characteristics: stiffness $k=1600$ kN/m, mass $m=10$ t, and damping coefficient $\zeta_p=5\%$. The natural period of the structure T_p amounted to 0.5 s. Ground motion was defined by the Eurocode 8 (2004) elastic spectrum (type 1), for soil type B ($T_c=0.5$ s). It was assumed that the peak ground acceleration (PGA) amounted to 0.35g. For $T_p=0.5$ s, the value from the chosen elastic spectrum (S_e) amounted to 0.87g. The structural behaviour was described with the Q_{10} model and the ductility factor amounted to 1.0 (elastic structure) and 2.0. The floor response spectra for equipment damping (ζ_s) equal to 1, 3, 5 and 7% were determined according to Equations 3.9–3.11, using the R_μ factor defined by Equations 3.3 and 3.4 ($R_\mu=1.82$), and amplification factors AMP defined by Equations 3.7 and 3.8. The AMP values are presented in Table 3.3 and the floor response spectra are presented in Figure 3.23.

Table 3.3: The amplification factors AMP used in the numerical example

Preglednica 3.3: Amplifikacijski faktorji AMP uporabljeni v numeričnem primeru

	$\zeta_s=1\%$	$\zeta_s=3\%$	$\zeta_s=5\%$	$\zeta_s=7\%$
$\mu=1$	11.9	7.8	6.1	5.2
$\mu=2$	9.2	6.1	4.8	4.0

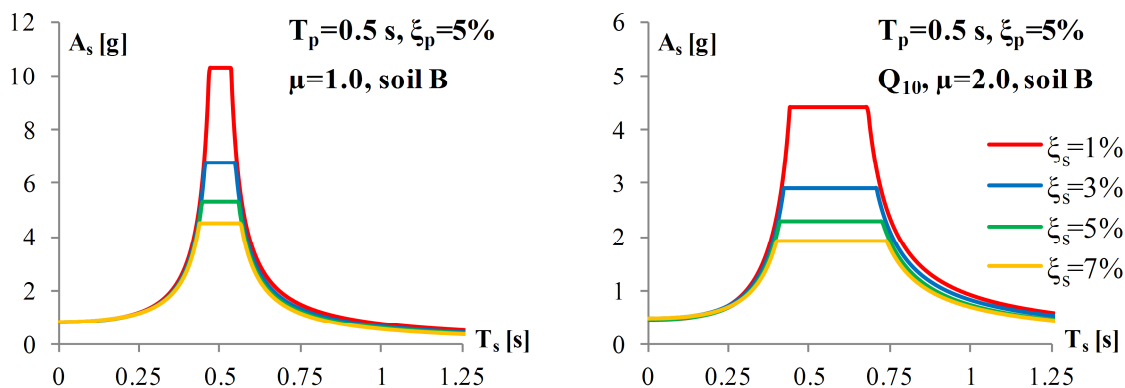


Figure 3.23: Floor response spectra obtained by the proposed direct method for (a) the elastic model and (b) the Q_{10} model of the structure with 5% damping, soil type B (PGA=0.35g)

Slika 3.23: Etažni spektri odziva dobljeni s pomočjo predlagane metode za (a) elastičen model in (b) Q_{10} model konstrukcije s 5% dušenja, tip tal B (PGA=0.35g)

4 PARAMETRIC STUDY OF FLOOR RESPONSE SPECTRA FOR MULTI-DEGREE-OF-FREEDOM STRUCTURES

This chapter presents the results of an extensive parametric study of floor acceleration spectra, taking into account the elastic and inelastic behaviour of the primary structures, and the elastic behaviour of the equipment (secondary structures). Primary structures were modelled as multi-degree-of-freedom (MDOF) systems, whereas a single-degree-of-freedom (SDOF) system represented equipment. In all cases, structures and equipment were treated as uncoupled. In the study, some general characteristics of the floor response spectra in the case of MDOF primary structures were observed.

4.1 Description of seismic input, structural models and structural analysis

In the study a large number of floor response spectra were calculated by using response-history analysis (RHA), as described in Section 1.1. MDOF models were used in the case of elastic and inelastic structures and SDOF model was used for the elastic equipment. Structure-equipment systems were treated as uncoupled. The influences of the type, natural period, hysteretic behaviour and ductility of the structure, as well as the influence of the damping of the equipment were studied.

As the seismic input, a set of 30 ground records, which was used in the case of SDOF primary structures and which corresponded to the soil type B, was used in the study (for more details see Section 2.1). As mentioned in Section 2.1, this set of records has the mean PGA equal to 0.43g and it was chosen so that its mean spectrum matches a target spectrum, which was the type 1 elastic spectrum for soil type B defined by Eurocode 8 (2004), with the PGA equal to 0.35g. The characteristic period of the ground motion (T_C) in the case of soil type B amounts to 0.5 s. The mean and target spectra for 5% damping were fitted between 0.15 and 2.5 s (no value of the mean 5% damping spectrum of the chosen set of ground motions was less than 90% of the corresponding value on the target 5% damping spectrum). For the purpose of this study, the target spectrum was slightly modified. The part of the spectrum between $T=0$ s and $T=T_B=0.15$ s was changed, i.e. it was assumed to be equal to the mean spectrum of the chosen set of ground records (T_B is the lower limit of the constant spectral acceleration branch in Eurocode 8 2004 elastic spectrum). In this way, a complete match between the mean and target spectrum was achieved in the short period range in which most higher modes lie (Figure 4.1). In the period range where natural periods of inelastic modes are anticipated to occur (after 0.15 s), smooth spectrum corresponding to Eurocode 8 (2004) was applied. In this way, the application of the reduction factor R_μ (which should be used in conjunction with smooth spectra) is fully justified.

Several different structures were studied and their properties are presented below. Two types of structures were considered in the study: cantilever walls and frames. In both cases a stiff and a flexible structure was analysed, with the first period of 0.3 and 1.0 s, respectively. The chosen structures cover a wide range of structures which are most common in practice and they represent a starting point for the determination of main properties of floor response spectra in MDOF systems. Inelastic response of the analysed structures was represented by using the same hysteretic models as in the case of SDOF systems (elasto-perfectly plastic and stiffness degrading model, see Chapter 2). It should be noted that in the case of walls, beam-column elements were used, which does not allow an accurate simulation of structural response of walls in the inelastic region. Since the aim of this part of the study was to demonstrate the applicability of the proposed direct method on different structures, it was considered that the chosen simple model was appropriate. The main aspects of structural modelling and analysis are practically the same for all analysed structures and they are described in the following text.

In all cases, planar reinforced concrete structures were considered. The modulus of elasticity of concrete (E_c) amounted to 33 GPa, whereas the modulus of elasticity of steel (E_s) amounted to 200 GPa. The yield strength of reinforcement (f_y) amounted to 500 MPa. According to Eurocode 8 (2004), the stiffness of load bearing elements should be evaluated by taking into account the effects of cracking. The flexural stiffness properties of concrete elements may be taken as 50% of the corresponding stiffness of the uncracked elements. This option was used in the analysis. Shear and torsional deformations were neglected. Structural elements were modelled as beam-column elements and their self-weight was neglected. Therefore, a lumped mass approach was applied in all cases, i.e. lumped masses were assigned to all free nodes.

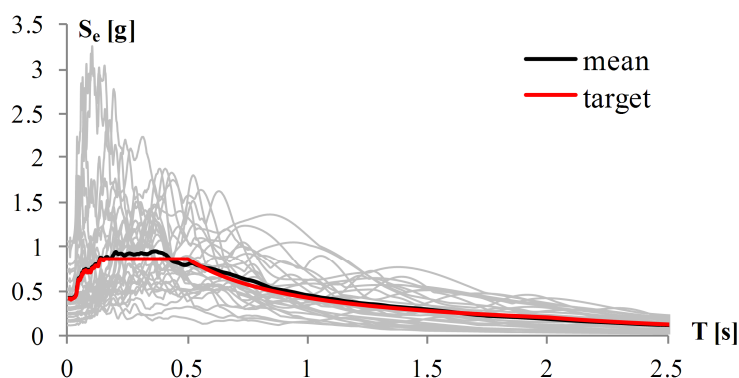


Figure 4.1: Elastic acceleration spectra (5% damping) of individual records, modified target and mean spectrum for soil type B

Slika 4.1: Elastični spektri pospeškov (5% dušenja) posameznih zapisov, modificirani ciljni in povprečni spekter za tla tipa B

In the case of inelastic structures, two different hysteretic models were taken into account: elasto-plastic (EP) and stiffness degrading model with zero hardening (Q_0). Note that the same models were also used in the case of SDOF primary structures (for more details see Section 2.1). Again, structures with strength degradation were not considered in the study. In all cases, Rayleigh damping amounted to 5% with respect to two first modes of the primary structures, whereas "mass-proportional" damping amounted to 1, 3, 5 and 7% in the case of the equipment.

The RHA of the primary structures was conducted by using SAP2000 14.2.4 (for elastic and the EP models) and OpenSees 2.2.2 (for stiffness degrading Q_0 model). In SAP, all structural elements were modelled by using the Frame Element, whereas in OpenSees all structural elements were modelled by using the Elastic Beam Column element (for element details see Mazzoni et al. 2007). A concentrated plasticity approach was used in the case of inelastic structures in all cases. In SAP, plastic hinges were modelled by using the Frame Hinge (Deformation Controlled Moment hinge), whereas in OpenSees Zero-Length element in combination with Hysteretic Material was used (for material details see Mazzoni et al. 2007). In both cases, the behaviour of plastic hinges was represented by moment-rotation relationship. In SAP, only the plastic rotation can be defined since the elastic rotation is determined by the Frame Element containing the plastic hinge. Therefore, the yield moments in hinges are an important part of the input, whereas the yield rotations are not. In OpenSees, both quantities (yield moments and yield rotations) should be defined for each hinge, which means that each hinge has pre-defined stiffness. It is very important to note that infinite rotation capacity was assigned to each plastic hinge, in every analysed structure. This had to be done since the seismic input consisted of ground motions with quite different intensities (for scatter see Figure 4.1) and the prevention of the

structural collapse was crucial, otherwise the results of the study would be useless. In OpenSees, Elastic Beam Column elements were modelled by using the moments of inertia of uncracked sections and, for each plastic hinge, the yield rotation of the uncracked cross section was assumed for the determination of the yield point at the moment-rotation relationship. In this way, when the yield moments in plastic hinges are reached, the effective moment of inertia of the element section approximately equals one half of the moment of inertia of the uncracked section. The same approach was also used by Dolšek and Fajfar (2005). On the other hand, in SAP, the effective moment of inertia of each Frame Element section was achieved by multiplication of the uncracked moment of inertia with the factor equal to 0.5, which produced an exact 50% reduction of the moment of inertia. Consequently, the results of modal analyses conducted in SAP and OpenSees are slightly different.

Newmark integration method was used in the RHA, taking into account coefficients $\gamma=0.5$ and $\beta=0.25$, i.e. acceleration was taken to be a constant within each time step. The size of the time step amounted to 0.001 s in the case of structures whose natural period of the fundamental mode amounted to 0.3 s, and to 0.01 s in the case of structures whose natural period of the fundamental mode amounted to 1.0 s. MATLAB 7.5.0 was used as an input pre-processor and as an output post-processor. Floor response spectra were calculated by using the same code which was used in the case of SDOF primary structures (see Section 2.2). All data obtained in the study were processed in MS Office Excel 2007.

A three-storey cantilever wall with natural period of the fundamental mode equal to 0.3 s (W03)

A three-storey elastic and inelastic cantilever wall was considered in the study. The storey height (with respect to centerline dimensions) amounted to 3 m. Rectangular cross section was assumed and its dimensions (width/length) amounted to 30/300 cm. Lumped mass amounted to 80 t at each storey of the wall. One plastic hinge was assumed at the bottom of the wall.

Wall reinforcement was designed according to Eurocode 2 (2004) and Eurocode 8 (2004). At the bottom of the wall, i.e. in the plastic hinge region, wall reinforcement consisted of two fabric meshes (each placed at the one side of the wall) and longitudinal bars and stirrups in boundary elements. The length of boundary elements amounted to 45 cm. The meshes consisted of 7 mm diameter bars which were spaced at 12.5 cm in both horizontal and vertical directions (a total area of reinforcement amounted to 6.16 cm²/m in each direction). Longitudinal reinforcement of each boundary element consisted of eight 12 mm diameter bars (a total area of longitudinal reinforcement in each boundary element amounted to 9.04 cm²) and it was laterally engaged by two overlapped 6 mm diameter stirrups (outer and inner), whose spacing amounted to 12.5 cm. Reinforcement is presented in Figure 4.2 (note that, when possible, meshes should be anchored into the boundary elements).

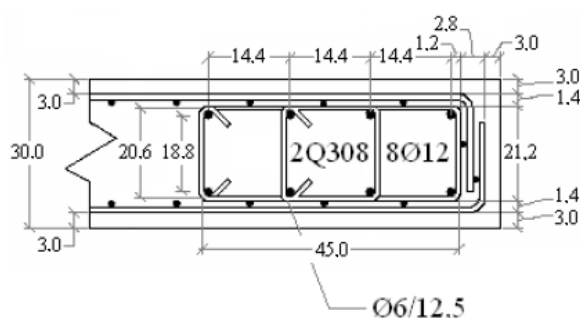


Figure 4.2: Reinforcement at the bottom of the wall W03 (plastic hinge region)

Slika 4.2: Armatura ob vpetju stene W03 (območje plastičnega člena)

The yield moment in the plastic hinge (M_y) was determined from analysis of the wall cross section and it amounted to 4015 kNm. In the analysis, partial factors for materials for ultimate limit state defined in Eurocode 2 (2004) were taken into account, along with the axial load at the wall bottom, which amounted to 2354 kN. The yield rotation (θ_y) in the plastic hinge, used in the case of the Q_0 model (OpenSees) amounted to $5.41 \cdot 10^{-4}$ rad, was determined by using Equation 4.1 (where L_w denotes total height of the wall which amounted to 9 m, whereas I denotes the moment of inertia of the wall cross section in the direction of seismic action and it amounted to 0.675 m^4).

$$\theta_y = \frac{M_y L_w}{3E_c I} \quad (4.1)$$

The natural periods of the structure determined in SAP (elastic and EP models) amounted to 0.30, 0.046 and 0.017 s, respectively, whereas the natural periods of the structure determined in OpenSees (Q_0 model) amounted to 0.31, 0.041 and 0.014 s, respectively. The eigenvectors determined in SAP and OpenSees are presented in columns of matrices Φ_{SAP} and Φ_{OS} in Equations 4.2.

$$\Phi_{SAP} = \begin{bmatrix} +0.156 & +1.000 & +1.000 \\ +0.532 & +1.189 & -0.700 \\ +1.000 & -0.788 & +0.215 \end{bmatrix}, \quad \Phi_{OS} = \begin{bmatrix} +0.250 & +1.000 & +1.000 \\ +0.603 & +0.833 & -0.923 \\ +1.000 & -0.752 & +0.307 \end{bmatrix} \quad (4.2)$$

In the case of SAP, the modal participation factors amounted to 1.29, 0.46 and 0.34, respectively, whereas in the case of OpenSees they amounted to 1.30, 0.48 and 0.20, respectively.

A three-storey cantilever wall with natural period of the fundamental mode equal to 1.0 s (W10)

A three-storey elastic and inelastic cantilever wall was considered in the study. The storey height (with respect to centerline dimensions) amounted to 3 m. Rectangular cross section was assumed and its dimensions (width/length) amounted to 30/150 cm. Lumped mass amounted to 112 t at each storey of the wall. One plastic hinge was assumed at the bottom of the wall. The wall reinforcement was the same as in the case of the wall W03 (for details see Figure 4.2).

The yield moment in the plastic hinge (M_y) was determined from analysis of the wall cross section and it amounted to 1896 kNm. In the analysis, partial factors for materials for ultimate limit state defined in Eurocode 2 (2004) were taken into account, along with the axial load at the wall bottom, which amounted to 3296 kN. The yield rotation (θ_y) in the plastic hinge, used in the case of the Q_0 model (OpenSees) amounted to 0.002 rad, was determined by using Equation 4.1 (L_w amounted to 9 m, whereas I amounted to 0.084 m^4).

The natural periods of the structure determined in SAP (elastic and EP models) amounted to 1.0, 0.153 and 0.057 s, respectively, whereas the natural periods of the structure determined in OpenSees (Q_0 model) amounted to 1.05, 0.136 and 0.046 s, respectively. The eigenvectors determined in SAP and OpenSees are presented in columns of matrices Φ_{SAP} and Φ_{OS} in Equations 4.3.

$$\Phi_{SAP} = \begin{bmatrix} +0.156 & +1.000 & +1.000 \\ +0.532 & +1.188 & -0.699 \\ +1.000 & -0.788 & +0.215 \end{bmatrix}, \quad \Phi_{OS} = \begin{bmatrix} +0.250 & +1.000 & +1.000 \\ +0.603 & +0.833 & -0.923 \\ +1.000 & -0.752 & +0.307 \end{bmatrix} \quad (4.3)$$

In the case of SAP, the modal participation factors amounted to 1.29, 0.46 and 0.34, respectively, whereas in the case of OpenSees they amounted to 1.30, 0.48 and 0.20, respectively.

A three-storey single bay frame with natural period of the fundamental mode equal to 0.3 s (F03)

A three-storey elastic and inelastic single bay frame was considered in the study. The storey height amounted to 3 m, whereas the bay width amounted to 5 m (centerline dimensions were considered). The dimensions of cross sections (width/height) amounted to 50/80 cm in the case of columns and 50/60 cm in the case of beams. Lumped mass amounted to 14 t in each free node, i.e. 28 t at each storey of the frame. Plastic hinges were assumed at the ends of beams and columns. The frame reinforcement is schematically presented in Figure 4.3 and it was chosen arbitrarily. It may correspond to an existing structure built before the implementation of Eurocode 8 (2004).

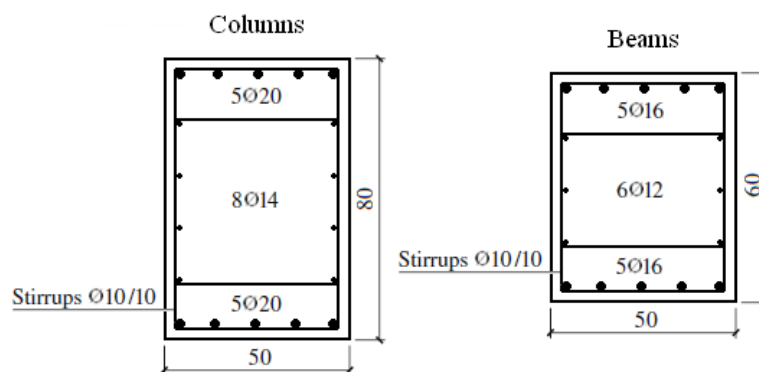


Figure 4.3: Reinforcement of columns and beams in frame F03

Slika 4.3: Armatura stebrov in gred okvirja F03

The yield moments in plastic hinges (M_y) were determined from analysis of the cross sections and they are presented in Table 4.1. In the analysis, partial factors for materials for ultimate limit state defined in Eurocode 2 (2004) were taken into account, along with the corresponding axial loads. The yield rotations (θ_y) in plastic hinges, used in the case of the Q_0 model (OpenSees), were determined by using Equation 4.4 and they are presented in Table 4.1. L denotes total length of the element, which amounted 3 and 5 m in the case of columns and beams, respectively, whereas I denotes the moment of inertia of the element cross section, which amounted to 0.021 and 0.009 m⁴ for columns and beams, respectively.

$$\theta_y = \frac{M_y L}{6E_c I} \quad (4.4)$$

Table 4.1: Axial forces (N), yield moments (M_y) and rotations (θ_y) in plastic hinges (frame F03)

Preglednica 4.1: Osne sile (N), momenti (M_y) in rotacije (θ_y) na meji tečenja v plastičnih členkih (okvir F03)

Elements	N [kN]	M_y [kNm]	θ_y [rad]
Beams	0	225	$6.31 \cdot 10^{-4}$
Columns 1 st floor	412	605	$4.30 \cdot 10^{-4}$
Columns 2 nd floor	275	565	$4.01 \cdot 10^{-4}$
Columns 3 rd floor	137	527	$3.74 \cdot 10^{-4}$

The natural periods of the structure determined in SAP (elastic and EP models) amounted to 0.30, 0.079 and 0.038 s, respectively, whereas the natural periods of the structure determined in OpenSees (Q_0 model) amounted to 0.29, 0.075 and 0.037 s, respectively. The eigenvectors determined in SAP and OpenSees are presented in columns of matrices Φ_{SAP} and Φ_{OS} in Equations 4.5.

$$\Phi_{SAP} = \begin{bmatrix} +0.249 & +1.000 & +1.000 \\ +0.663 & +0.927 & -0.810 \\ +1.000 & -0.864 & +0.288 \end{bmatrix}, \quad \Phi_{OS} = \begin{bmatrix} +0.242 & +1.000 & +1.000 \\ +0.649 & +0.910 & -0.828 \\ +1.000 & -0.833 & +0.295 \end{bmatrix} \quad (4.5)$$

In the case of SAP, the modal participation factors amounted to 1.27, 0.41 and 0.28, respectively, whereas in the case of OpenSees they amounted to 1.28, 0.43 and 0.26, respectively.

A three-storey single bay frame with natural period of the fundamental mode equal to 1.0 s (F10)

A three-storey elastic and inelastic single bay frame was considered in the study. The storey height amounted to 3 m, whereas the bay width amounted to 5 m (centerline dimensions were considered). The dimensions of cross sections (width/height) amounted to 35/35 cm in the case of columns and 35/45 cm in the case of beams. Lumped mass amounted to 23 t in each free node, i.e. 46 t at each storey of the frame. Plastic hinges were assumed at the ends of beams and columns. The frame reinforcement is schematically presented in Figure 4.4 and it was chosen arbitrarily. As it is obvious, flexural stiffness is larger in the case of beams than in the case of columns. In modern seismic design such an approach is not recommended since it can lead to unfavorable plastic mechanisms which can sometimes be hard to predict (e.g. inelasticity occurs in columns at upper storeys). Nevertheless, a great number of structures which were designed and built before modern seismic codes still exist. The main idea was to study floor response spectra in the case of structures which do not meet current design standards.

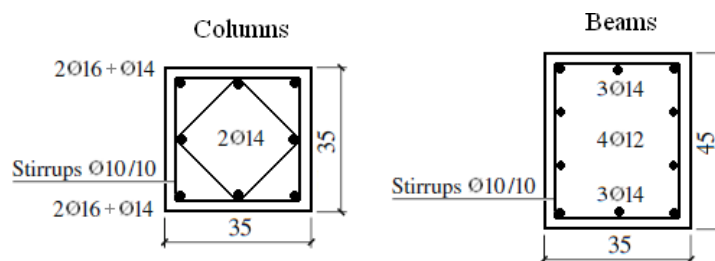


Figure 4.4: Reinforcement of columns and beams in frame F10

Slika 4.4: Armatura stebrov in gred okvirja F10

The yield moments in plastic hinges (M_y) were determined from analysis of the cross sections and they are presented in Table 4.2. In the analysis, partial factors for materials for ultimate limit state defined in Eurocode 2 (2004) were taken into account, along with the corresponding axial loads. The yield rotations (θ_y) in plastic hinges, used in the case of the Q_0 model (OpenSees), were determined by using Equation 4.4 and they are presented in Table 4.2. L denotes total length of the element, which amounted 3 and 5 m in the case of columns and beams, respectively, whereas I denotes the moment of inertia of the element cross section, which amounted to $1.25 \cdot 10^{-3}$ and $2.66 \cdot 10^{-3} \text{ m}^4$ for columns and beams, respectively.

The natural periods of the structure determined in SAP (elastic and EP models) amounted to 1.0, 0.315 and 0.186 s, respectively, whereas the natural periods of the structure determined in OpenSees (Q_0 model) amounted to 0.99, 0.312 and 0.186 s, respectively. The eigenvectors determined in SAP and OpenSees are presented in columns of matrices Φ_{SAP} and Φ_{OS} in Equations 4.6.

Table 4.2: Axial forces (N), yield moments (M_y) and rotations (θ_y) in plastic hinges (frame F10)

Preglednica 4.2: Osne sile (N), momenti (M_y) in rotacije (θ_y) na meji tečenja v plastičnih členkih (okvir F10)

Elements	N [kN]	M_y [kNm]	θ_y [rad]
Beams	0	80	$7.60 \cdot 10^{-4}$
Columns 1 st floor	677	133	$1.60 \cdot 10^{-3}$
Columns 2 nd floor	451	113	$1.40 \cdot 10^{-3}$
Columns 3 rd floor	226	90	$1.10 \cdot 10^{-3}$

$$\Phi_{SAP} = \begin{bmatrix} +0.337 & +1.000 & +1.000 \\ +0.746 & +0.668 & -0.992 \\ +1.000 & -0.835 & +0.404 \end{bmatrix}, \quad \Phi_{OS} = \begin{bmatrix} +0.335 & +1.000 & +1.000 \\ +0.741 & +0.666 & -0.998 \\ +1.000 & -0.829 & +0.404 \end{bmatrix} \quad (4.6)$$

In the case of SAP, the modal participation factors amounted to 1.25, 0.39 and 0.19, respectively, whereas in the case of OpenSees they amounted to 1.25, 0.39 and 0.19, respectively.

For all considered structures the following should be noted: it is obvious that natural periods and mode shapes obtained in SAP are different from the ones obtained in OpenSees. These differences are more pronounced in the case of walls, whereas in the case of frames they can practically be neglected. It is clear that the above described modelling of concentrated plasticity in OpenSees works well in the case of frames with plastic hinges at the ends of beams and columns. On the other hand, in the case of walls with one plastic hinge at the bottom of the wall, such modelling approach may be questionable.

4.2 Results of the study

This section presents the most important results obtained in the parametric study. Some well-known characteristics of floor response spectra have been observed and hereby confirmed. Additionally, several interesting new observations have been made. The results obtained for the elastic, EP and Q_0 models are presented.

The RHA was in all cases conducted by using the seismic input described in Section 4.1. Additionally, in the case of the structures W03, W10 and F10, seismic input was scaled with the scale factor SF . In this way, two different values of ductility (μ) were achieved in the case of inelastic structures.

The exact determination of the achieved ductility is difficult in the case of inelastic MDOF structures. In general, the yield point of the system cannot be determined with certainty. In this study, seismic input consisted of 30 ground motions. In such a case, generally, for each ground motion the structure achieves different ductility. Obviously, the application of a simple and efficient approach for the estimation of the achieved ductility μ was required in the study. For this purpose, the nonlinear pushover-based N2 method was used (for method details see Fajfar 2010 or ANNEX D). The application of pushover analysis is an important part of the N2 method. In this study, in pushover analyses the "first mode" height-wise distribution of lateral loads was assumed, i.e. lateral loads were

determined as the product of the first mode shape component in a considered storey and the storey mass. It should be noted that the results of the N2 method obtained in this section will later be used in Chapters 5 and 6. The natural periods of the primary structure for the mode i and of the equipment are denoted as $T_{p,i}$ and T_s , respectively, whereas the values of floor acceleration spectra are denoted as A_s . The results presented in the following subsections were obtained for structural damping ($\zeta_{p,i}$) equal to 5% with respect to the first and second mode ($\zeta_{p,1}=\zeta_{p,2}=5\%$), whereas the damping of the equipment (ζ_s) amounted to 1 and 5%.

4.2.1 Results obtained for structure W03

A three-storey elastic and inelastic cantilever wall with the natural period of the first mode equal to 0.3 s was considered in the study. The RHA was conducted by using the seismic input described in Section 4.1 and by using the scaled input with the scale factor $SF=0.55$.

In pushover analyses, in the case of the EP model, lateral forces amounted to 12.5, 42.5 and 80.0 kN in the first, second and third storey, respectively, while in the case of the Q_0 model lateral forces amounted to 20.0, 48.3 and 80.0 kN in the first, second and third storey, respectively. In the case of the EP model effective mass m^* and transformation factor Γ amounted to 135.0 t and 1.29, respectively, whereas in the case of the Q_0 model they amounted to 148.3 t and 1.30, respectively.

EP model, input scale factor $SF=0.55$

The pushover analysis was firstly conducted for an arbitrarily chosen target displacement equal to 0.10 m and a pushover curve was obtained and presented in Figure 4.5a (d denotes displacement, whereas F denotes base shear force). Since only one plastic hinge was assumed (at the bottom of the wall), the pushover curve is bilinear. By dividing it with the transformation factor Γ , a pushover curve for the equivalent SDOF system was obtained and presented in Figure 4.5a (d^* denotes displacement, whereas F^* denotes base shear force).

For the equivalent SDOF system, the displacement at the yield point (d_y^*) amounted to 0.70 cm, whereas the corresponding force (F_y^*) amounted to 415.0 kN. The capacity diagram presented in Figure 4.5b was obtained by dividing the forces F^* with the equivalent mass m^* . The acceleration at the yield point (S_{ay}) was determined as F_y^*/m^* and it amounted to 0.31g. The effective period of the equivalent SDOF system (T^*) amounted to 0.30 s.

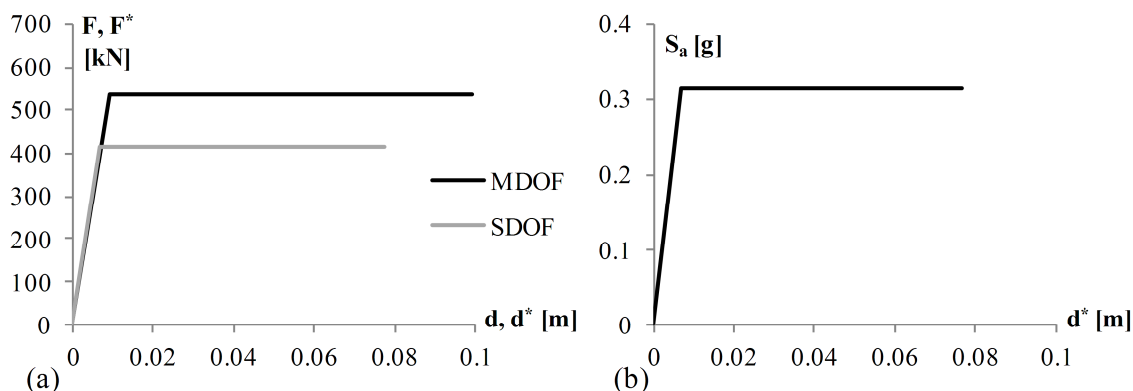


Figure 4.5: (a) Pushover curves for MDOF and SDOF systems and (b) Capacity diagram for the EP model

Slika 4.5: (a) Potisne krivulje za MDOF in SDOF sistema in (b) Diagram kapacitete za EP model

The reduction factor R_μ was determined using the target spectrum (see Figure 4.1) and the SF and it amounted to $SF \cdot S_e(T^*)/S_{ay}=1.54$ ($S_e(T^*)$ amounted to $0.87g$).

Since the effective period T^* is smaller than T_C , the equal displacement rule cannot be applied, i.e. the inelastic displacement demand is not equal to the elastic demand. The displacement demand of the SDOF system (d_t^*) amounted to 1.32 cm, whereas the corresponding ductility demand μ amounted to 1.9 . The target (roof) displacement of the MDOF system (d_t) was determined as the product of Γ and d_t^* and it amounted to 1.70 cm. The corresponding displacements of the first and second storey amounted to 0.41 and 1.01 cm, respectively. Therefore, the components of the inelastic first mode shape amounted to 0.241 , 0.594 and 1.0 in the first, second and third storey, respectively.

EP model, input scale factor $SF=1.0$

The following quantities are the same as in the case of $SF=0.55$: d_y^* , F_y^* , S_{ay} and T^* . The R_μ factor was determined using the target spectrum (see Figure 4.1) and it amounted to $S_e(T^*)/S_{ay}=2.81$ ($S_e(T^*)$ amounted to $0.87g$). d_t^* amounted to 2.78 cm, μ amounted to 4.0 , whereas d_t amounted to 3.59 cm. The displacements of the first and second storey amounted to 1.04 and 2.27 cm, respectively. Finally, the components of the inelastic first mode shape amounted to 0.290 , 0.632 and 1.0 in the first, second and third storey, respectively.

Q_0 model, input scale factor $SF=0.55$

The first pushover analysis was conducted for a target displacement equal to 0.10 m (arbitrarily chosen) and a pushover curve was obtained and presented in Figure 4.6a. The pushover curve is bilinear, since only one plastic hinge was assumed at the bottom of the wall. By dividing the curve with the transformation factor Γ , a pushover curve for the equivalent SDOF system was obtained and presented in Figure 4.6a.

For the equivalent SDOF system, the displacement at the yield point (d_y^*) amounted to 0.72 cm, whereas the corresponding force (F_y^*) amounted to 428.1 kN. The capacity diagram presented in Figure 4.6b was obtained by dividing the forces F^* with the equivalent mass m^* . The acceleration at the yield point (S_{ay}) was determined as F_y^*/m^* and it amounted to $0.29g$. The effective period of the equivalent SDOF system (T^*) amounted to 0.31 s.

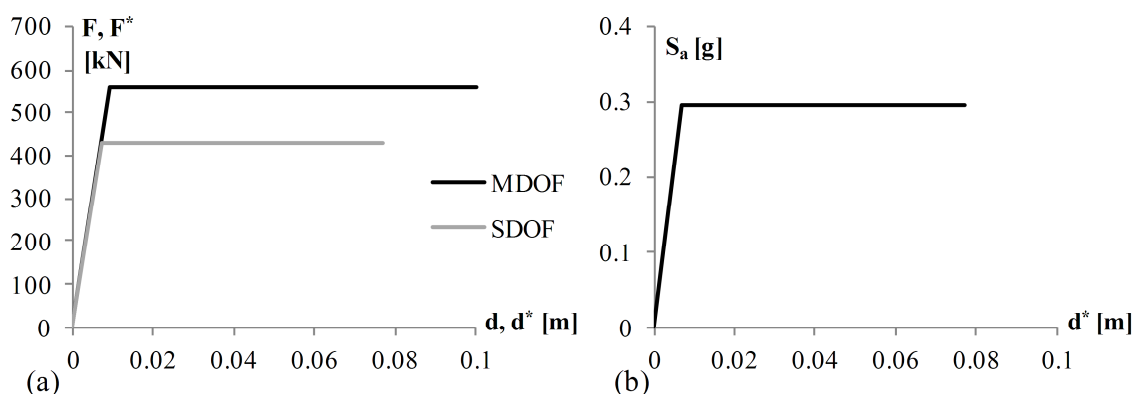


Figure 4.6: (a) Pushover curves for MDOF and SDOF systems and (b) Capacity diagram for the Q_0 model

Slika 4.6: (a) Potisne krivulje za MDOF in SDOF sistema in (b) Diagram kapacitete za Q_0 model

The reduction factor R_μ was determined using the target spectrum (see Figure 4.1) and the SF and it amounted to $SF \cdot S_e(T^*)/S_{ay} = 1.65$ ($S_e(T^*)$ amounted to 0.87g). Since the effective period T^* is smaller than T_C , the equal displacement rule cannot be applied. The displacement demand of the SDOF system (d_t^*) amounted to 1.42 cm, whereas the corresponding ductility demand μ amounted to 2.0. The target (roof) displacement of the MDOF system (d_t) was determined as the product of Γ and d_t^* and it amounted to 1.85 cm. The corresponding displacements of the first and second storey amounted to 0.54 and 1.17 cm, respectively. Therefore, the components of the inelastic first mode shape amounted to 0.292, 0.632 and 1.0 in the first, second and third storey, respectively.

Q₀ model, input scale factor SF=1.0

The following quantities are the same as in the case of $SF=0.55$: d_y^* , F_y^* , S_{ay} and T^* . The R_μ factor was determined using the target spectrum (see Figure 4.1) and it amounted to $S_e(T^*)/S_{ay} = 3.0$ ($S_e(T^*)$ amounted to 0.87g). d_t^* amounted to 2.93 cm, μ amounted to 4.2, whereas d_t amounted to 3.81 cm. The displacements of the first and second storey amounted to 1.19 and 2.48 cm, respectively. Finally, the components of the inelastic first mode shape amounted to 0.312, 0.651 and 1.0 in the first, second and third storey, respectively.

Figures 4.7 and 4.8 show the mean values of the floor response spectra normalized with the mean PGA of the input, which amounted to 0.24g in the case of $SF=0.55$ and to 0.43g in the case of $SF=1.0$. Several interesting observations can be made.

First, let us consider the case of the elastic structure ($\mu=1$). The peak values of floor response spectra occur when the natural period of the equipment is approximately equal to the natural period of the structure in the first and the second mode, i.e. $T_s \approx T_{p,1}$ and $T_s \approx T_{p,2}$. In the first storey, the influence of the second mode is larger than the influence of the first mode. In the second storey, the influence of the first mode becomes more pronounced, whereas in the third storey it is completely dominant. As it is obvious, there is no peak related to the third mode. ASCE 4-98 (2000) and USNRC 1.92 (2006) define a frequency at which spectral acceleration returns to zero period acceleration (f_{ZPA}). In practice it can be assumed that f_{ZPA} amounts to 33 Hz. According to Aziz (2004), the frequency content of real earthquakes is not known above 33 Hz. Therefore, it is reasonable to assume that an earthquake cannot trigger a structure to respond in modes with the frequency above f_{ZPA} . Consequently, the influence of such modes is static, resonance effects do not occur (there is no amplification) so there is no peak in the floor response spectrum. The natural period of the structure in the third mode amounts to $T_{p,3} = 0.017$ s, whereas the frequency of the third mode amounts to 58.8 Hz. This value is larger than f_{ZPA} , which explains why the peak of the floor response spectrum does not exist.

In the case of inelastic structures, the peak values of floor response spectra related to the first mode are smaller than the corresponding peak values obtained for the elastic structure, i.e. they are influenced by structural inelasticity. The size of peak reduction depends on the ductility demand (larger μ produces larger reduction). In the case of the EP model the peak values occur close to the resonance, whereas in the case of the Q₀ model the peak values are shifted towards higher periods. It is clear that the peaks of floor response spectra related to the first mode show the trends which were previously observed in the case of inelastic SDOF structures (see Section 2.3). Peak values of floor response spectra related to the second mode are quite interesting. It can be observed that in the first storey the peak values of the floor response spectra obtained for inelastic structures (for both hysteretic models and all considered ductilities) are larger than the peak values obtained for the elastic structure.

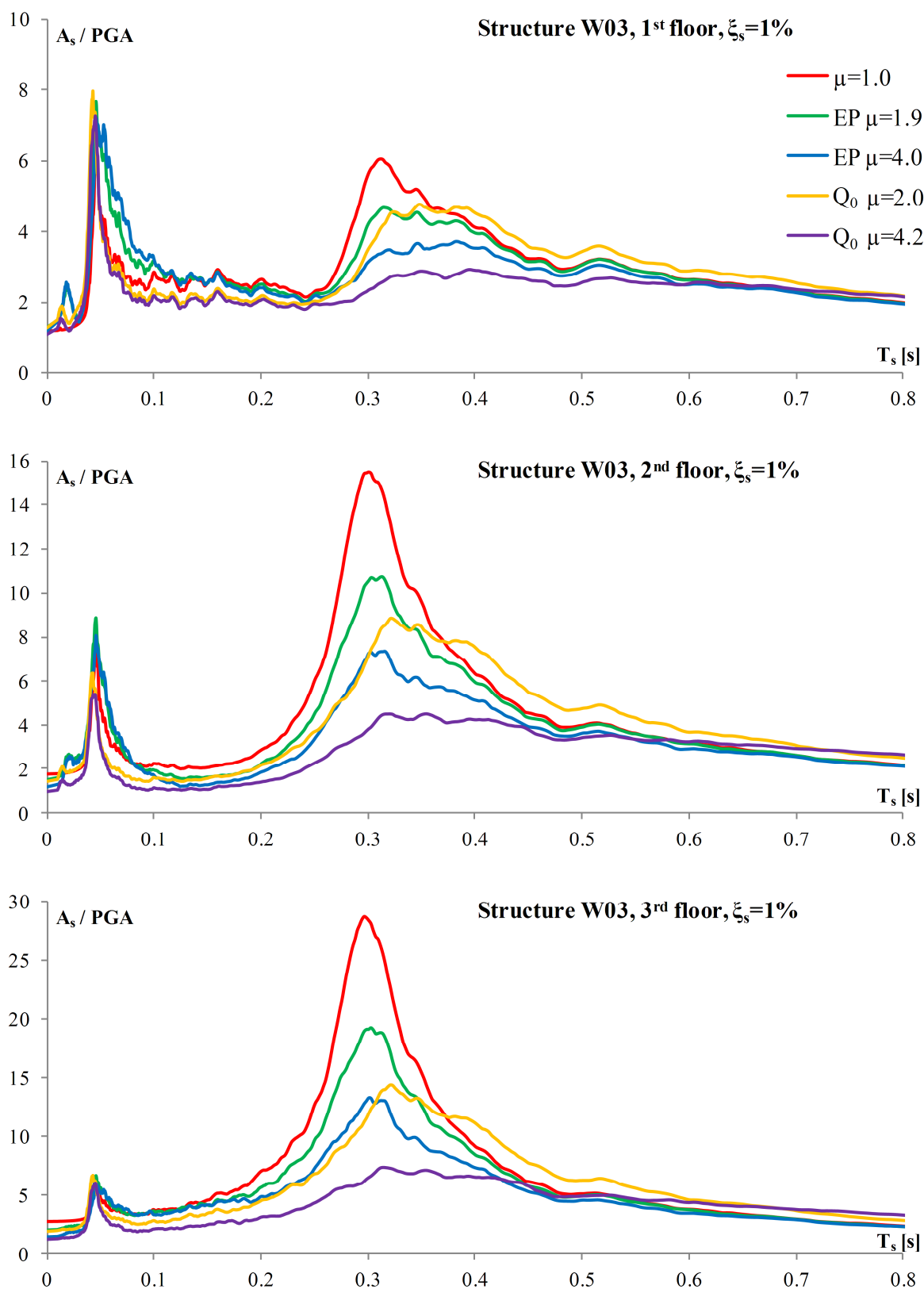


Figure 4.7: Mean values of the floor response spectra normalized with the mean PGA, structure W03 (1% damping of the equipment)

Slika 4.7: Povprečne vrednosti etažnih spektrov odziva normirane s povprečnim PGA, konstrukcija W03 (1% dušenje opreme)

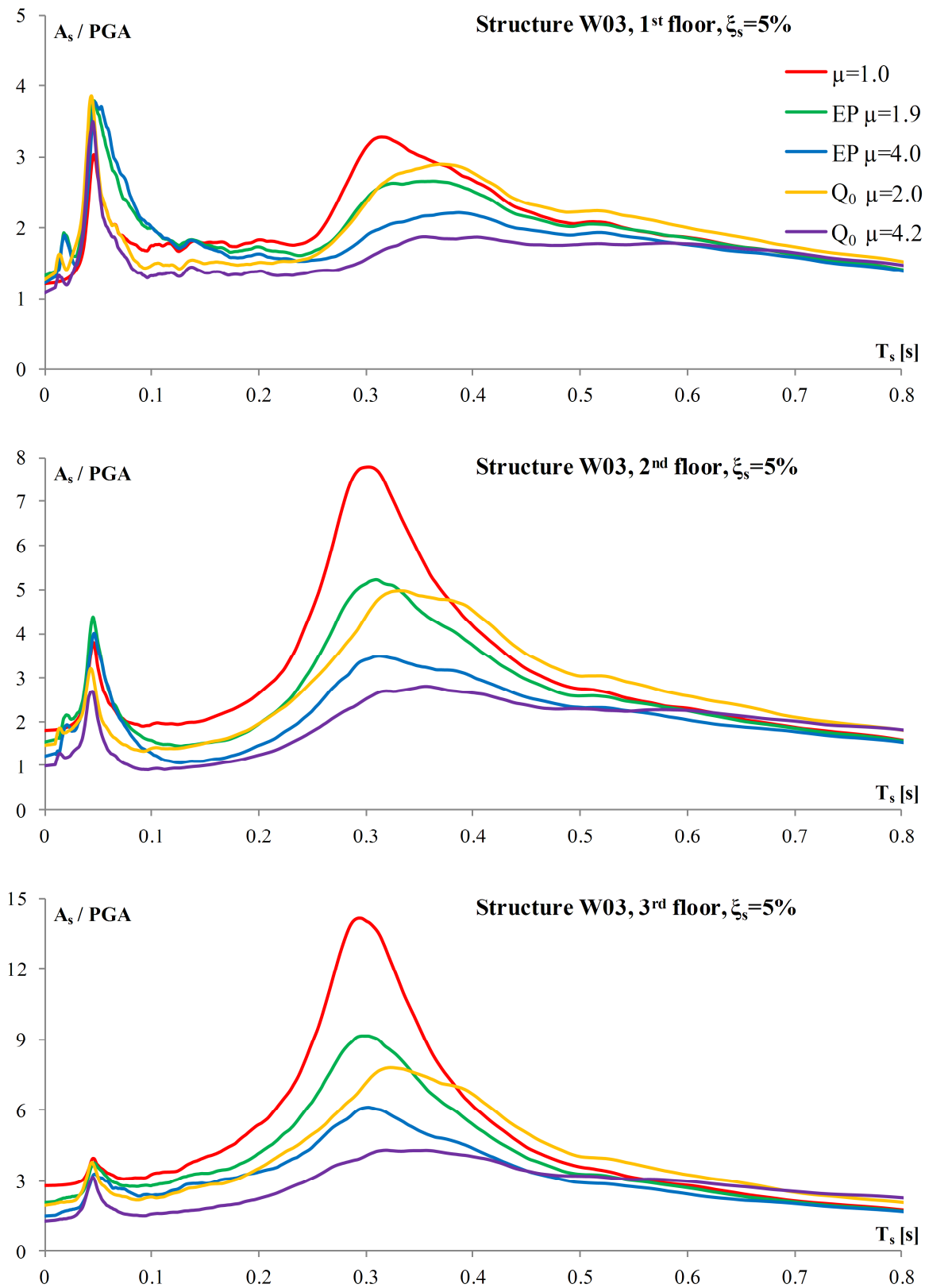


Figure 4.8: Mean values of the floor response spectra normalized with the mean PGA, structure W03 (5% damping of the equipment)

Slika 4.8: Povprečne vrednosti etažnih spektrov odziva normirane s povprečnim PGA, konstrukcija W03 (5% dušenja opreme)

Similar situation can be observed in the second storey in the case of the EP model, while, by contrast, in the case of the Q_0 model, the peak values of the floor response spectra are lower than the ones obtained for the elastic model. In the third storey, for both hysteretic models and all considered ductilities, spectral peaks are close to the peaks obtained for the elastic structure. In the case of the elastic and Q_0 model, in the first storey, the shapes of the resonance regions of floor response spectra related to the second mode are similar. In the first two storeys, small peaks of floor response spectra related to the third mode exist, which is obviously a consequence of structural inelasticity. It should be noted that, due to differences in structural modelling, the results obtained for the Q_0 model are partially comparable.

The phenomena observed in the case of higher modes of inelastic structures (the amplification of the peaks related to the second mode and the existence of the peaks related to the third mode) were also observed in some previous studies. In the study conducted by Sewell et al. (1986) it was observed that in some cases of inelastic structures, floor response spectra values can be greater than the floor response spectra values of the corresponding elastic structures. Similar findings were obtained in the study conducted by Singh et al. (1996), who have concluded that energy from the fundamental mode can be transferred to higher modes. It is obvious that more research on this subject is needed.

4.2.2 Results obtained for structure W10

A three-storey elastic and inelastic cantilever wall with the natural period of the first mode equal to 1.0 s was considered in the study. The RHA was conducted by using the seismic input described in Section 4.1 and by using the scaled input with the scale factor $SF=0.5$.

In pushover analyses, in the case of the EP model, lateral forces amounted to 17.5, 59.5 and 112.0 kN in the first, second and third storey, respectively, while in the case of the Q_0 model lateral forces amounted to 28.0, 67.6 and 112.0 kN in the first, second and third storey, respectively. In the case of the EP model effective mass m^* and transformation factor Γ amounted to 189.0 t and 1.29, respectively, whereas in the case of the Q_0 model they amounted to 207.6 t and 1.30, respectively.

EP model, input scale factor $SF=0.5$

The pushover analysis was firstly conducted for an arbitrarily chosen target displacement equal to 0.10 m and a pushover curve was obtained and presented in Figure 4.9a (d denotes displacement, whereas F denotes base shear force). Since only one plastic hinge was assumed at the bottom of the wall, the pushover curve is bilinear. By dividing it with the transformation factor Γ , a pushover curve for the equivalent SDOF system was obtained and presented in Figure 4.9a (d^* denotes displacement, whereas F^* denotes base shear force).

For the equivalent SDOF system, the displacement at the yield point (d_y^*) amounted to 2.63 cm, whereas the corresponding force (F_y^*) amounted to 196.0 kN. The capacity diagram presented in Figure 4.9b was obtained by dividing the forces F^* with the equivalent mass m^* . The acceleration at the yield point (S_{ay}) was determined as F_y^*/m^* and it amounted to 0.11g. The effective period of the equivalent SDOF system (T^*) amounted to 1.0 s.

The reduction factor R_μ was determined using the target spectrum (see Figure 4.1) and the SF and it amounted to $SF \cdot S_e(T^*)/S_{ay}=2.0$ ($S_e(T^*)$ amounted to 0.44g). Since the effective period T^* is larger than T_C , the equal displacement rule can be applied, i.e. the inelastic displacement demand is equal to the

elastic demand. The displacement demand of the SDOF system (d_t^*) amounted to 5.47 cm, whereas the corresponding ductility demand μ amounted to 2.0. The target (roof) displacement of the MDOF system (d_t) was determined as the product of Γ and d_t^* and it amounted to 7.06 cm. The corresponding displacements of the first and second storey amounted to 1.75 and 4.25 cm, respectively. Therefore, the components of the inelastic first mode shape amounted to 0.248, 0.602 and 1.0 in the first, second and third storey, respectively.

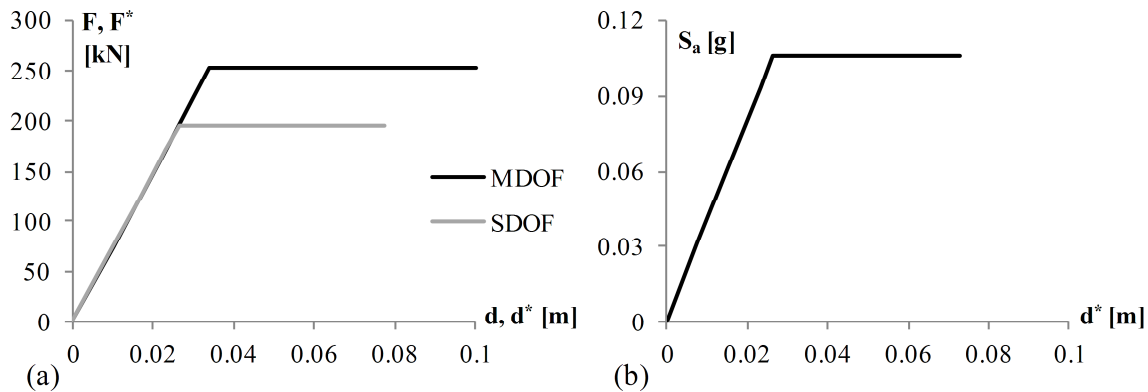


Figure 4.9: (a) Pushover curves for MDOF and SDOF systems and (b) Capacity diagram for the EP model

Slika 4.9: (a) Potisne krivulje za MDOF in SDOF sistema in (b) Diagram kapacitete za EP model

EP model, input scale factor $SF=1.0$

The following quantities are the same as in the case of $SF=0.5$: d_y^* , F_y^* , S_{ay} and T^* . The R_μ factor was determined using the target spectrum (see Figure 4.1) and it amounted to $S_e(T^*)/S_{ay}=4.0$ ($S_e(T^*)$ amounted to 0.44g). d_t^* amounted to 10.93 cm, μ amounted to 4.0, whereas d_t amounted to 14.10 cm. The displacements of the first and second storey amounted to 4.10 and 8.94 cm, respectively. Finally, the components of the inelastic first mode shape amounted to 0.291, 0.634 and 1.0 in the first, second and third storey, respectively.

Q_0 model, input scale factor $SF=0.5$

The first pushover analysis was conducted for a target displacement equal to 0.10 m (arbitrarily chosen) and a pushover curve was obtained and presented in Figure 4.10a. The pushover curve is bilinear, since only one plastic hinge was assumed. By dividing the curve with the transformation factor Γ , a pushover curve for the equivalent SDOF system was obtained and presented in Figure 4.10a.

For the equivalent SDOF system, the displacement at the yield point (d_y^*) amounted to 2.70 cm, whereas the corresponding force (F_y^*) amounted to 202.2 kN. The capacity diagram presented in Figure 4.10b was obtained by dividing the forces F^* with the equivalent mass m^* . The acceleration at the yield point (S_{ay}) was determined as F_y^*/m^* and it amounted to 0.10g. The effective period of the equivalent SDOF system (T^*) amounted to 1.05 s.

The reduction factor R_μ was determined using the target spectrum (see Figure 4.1) and the SF and it amounted to $SF \cdot S_e(T^*)/S_{ay}=2.1$ ($S_e(T^*)$ amounted to 0.41g). Since the effective period T^* is larger than T_C , the equal displacement rule can be applied. The displacement demand of the SDOF system (d_t^*) amounted to 5.62 cm, whereas the corresponding ductility demand μ amounted to 2.1. The target

(roof) displacement of the MDOF system (d_t) was determined as the product of Γ and d_t^* and it amounted to 7.31 cm. The corresponding displacements of the first and second storey amounted to 2.14 and 4.65 cm, respectively. Therefore, the components of the inelastic first mode shape amounted to 0.293, 0.636 and 1.0 in the first, second and third storey, respectively.

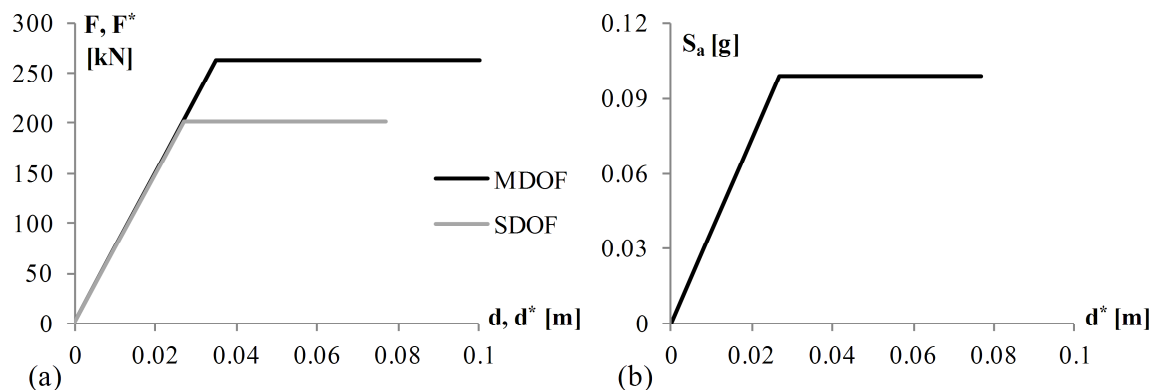


Figure 4.10: (a) Pushover curves for MDOF and SDOF systems and (b) Capacity diagram for the Q_0 model

Slika 4.10: (a) Potisne krivulje za MDOF in SDOF sistema in (b) Diagram kapacitete za Q_0 model

Q_0 model, input scale factor $SF=1.0$

The following quantities are the same as in the case of $SF=0.5$: d_y^* , F_y^* , S_{ay} and T^* . The R_μ factor was determined using the target spectrum (see Figure 4.1) and it amounted to $S_e(T^*)/S_{ay}=4.1$ ($S_e(T^*)$ amounted to 0.41g). d_t^* amounted to 11.23 cm, μ amounted to 4.1, whereas d_t amounted to 14.60 cm. The displacements of the first and second storey amounted to 4.57 and 9.51 cm, respectively. Finally, the components of the inelastic first mode shape amounted to 0.313, 0.651 and 1.0 in the first, second and third storey, respectively.

Figures 4.11 and 4.12 show the mean values of the floor response spectra normalized with the mean PGA values of the input, which amounted to 0.22g in the case of $SF=0.5$ and to 0.43g in the case of $SF=1.0$.

In the case of the elastic structure ($\mu=1$), the peaks of floor response spectra occur when the natural period of the equipment is approximately equal to the natural period of the structure and they are related to all three modes. In the first storey, the influence of higher modes is significantly larger than the influence of the fundamental mode. This is especially pronounced in the case of the second mode, but it can also be observed that the peak related to the third mode exceeds the peak related to first mode. In the second storey the most dominant mode is still the second one, the first mode becomes more pronounced, whereas the influence of the third mode decreases. In the third storey, the first mode is the most pronounced, the influence of the second mode is somewhat smaller, whereas the influence of the third mode diminishes almost completely. From the obtained results it is obvious that the seismic input significantly influences the floor response spectra, i.e. it can be seen that the chosen set of ground motions triggers the structural response in the second mode.

In the case of inelastic structures, the peak values of floor response spectra related to the first mode are smaller than the corresponding peak values obtained for the elastic structure and, as in the case of the structure W03, the size of peak reduction depends on the ductility demand.

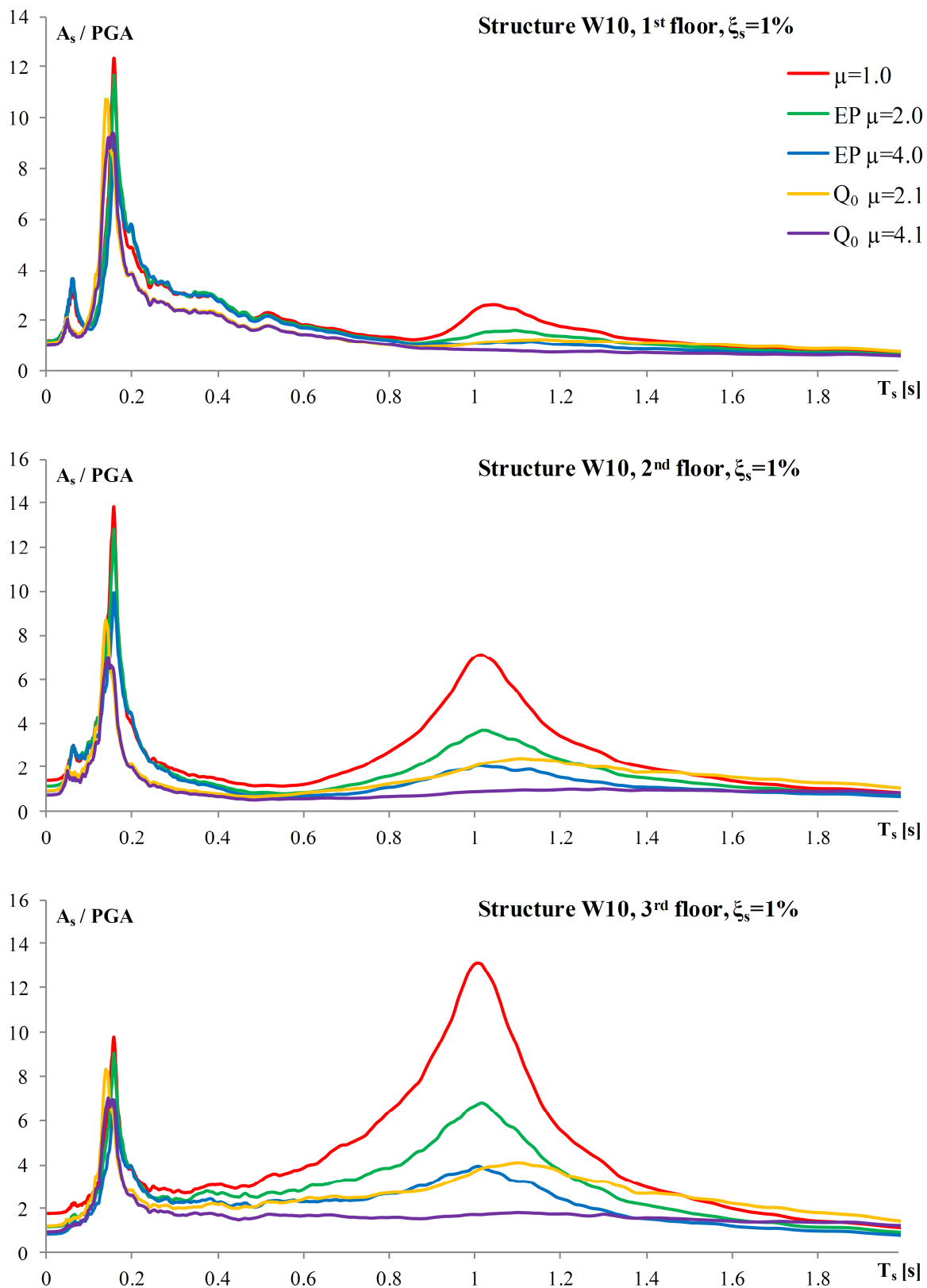


Figure 4.11: Mean values of the floor response spectra normalized with the mean PGA, structure W10 (1% damping of the equipment)

Slika 4.11: Povprečne vrednosti etažnih spektrov odziva normirane s povprečnim PGA, konstrukcija W10 (1% dušenja opreme)

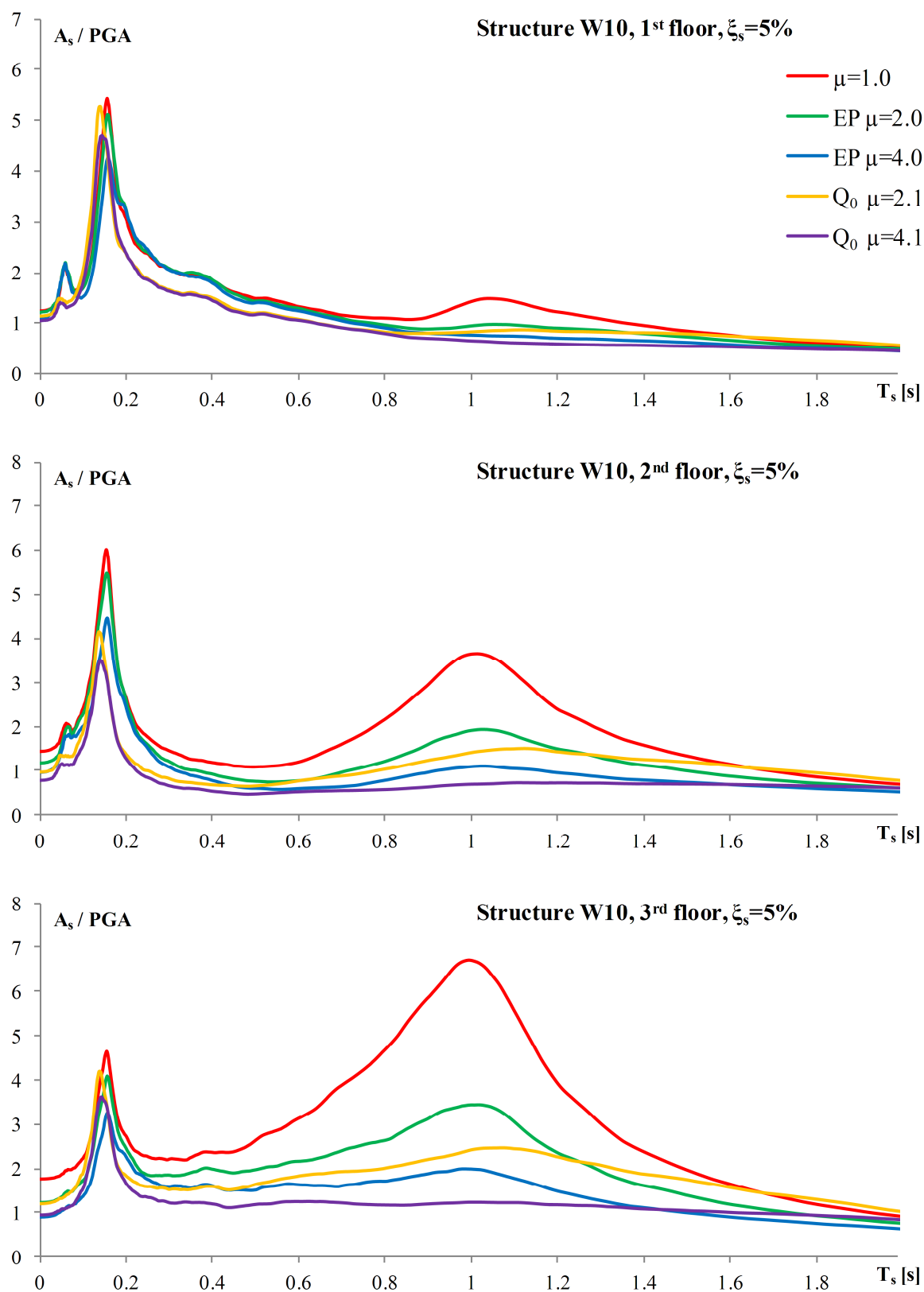


Figure 4.12: Mean values of the floor response spectra normalized with the mean PGA, structure W10 (5% damping of the equipment)

Slika 4.12: Povprečne vrednosti etažnih spektrov odziva normirane s povprečnim PGA, konstrukcija W10 (5% dušenje opreme)

In the case of the EP model the peak values occur close to the resonance, whereas in the case of the Q_0 model the peak values are shifted towards higher periods. Again, it is obvious that the peaks of floor response spectra related to the first mode show the trends which were previously observed in the case of inelastic SDOF structures (see Section 2.3). Peak values of floor response spectra related to the second mode are interesting, since it can be observed that they are reduced in comparison with the peaks obtained for the elastic structure. This applies for both hysteretic models and all considered ductilities. It is also obvious that the size of ductility demand influences the size of the reduction. Therefore, it can be concluded that the inelastic response of the structure is not related only to the fundamental mode, but also to the second mode, in some moderate amount. As for the peaks of the third mode, which are present in the first and in the second storey, it can be observed that in the case of the EP model they are practically equal to the peaks obtained for the elastic structure. In the case of the Q_0 model, they are quite smaller than the peaks obtained for the elastic and the EP model, which is a consequence of different modelling approaches in SAP and OpenSees (as discussed above). For both the second and third mode related peaks, it can be observed that they do not occur at the same value of T_s , which is related to the different natural periods of the structure obtained in SAP and OpenSees.

4.2.3 Results obtained for structure F03

A three-storey elastic and inelastic single bay frame with the natural period of the first mode equal to 0.3 s was considered in the study. The RHA was conducted by using the seismic input described in Section 4.1, i.e. by using the $SF=1.0$.

In pushover analysis, in the case of the EP model, lateral forces amounted to 7.0, 18.6 and 28.0 kN in the first, second and third storey, respectively, while in the case of the Q_0 model lateral forces amounted to 6.8, 18.2 and 28.0 kN in the first, second and third storey, respectively. In the case of the EP model effective mass m^* and transformation factor Γ amounted to 53.5 t and 1.27, respectively, whereas in the case of the Q_0 model they amounted to 53.0 t and 1.28, respectively.

EP model, input scale factor $SF=1.0$

The pushover analysis was firstly conducted for an arbitrarily chosen target displacement equal to 0.10 m and a pushover curve was obtained and presented in Figure 4.13a (d denotes displacement, whereas F denotes base shear force). By dividing it with the transformation factor Γ , a pushover curve for the equivalent SDOF system was obtained and idealized (elasto-perfectly plastic idealization), as shown in Figure 4.13a (d^* denotes displacement, whereas F^* denotes base shear force).

For the equivalent SDOF system, the displacement at the yield point (d_y^*) amounted to 1.33 cm, whereas the corresponding force (F_y^*) amounted to 280.3 kN. The capacity diagram presented in Figure 4.13b was obtained by dividing the forces F^* with the equivalent mass m^* . The acceleration at the yield point (S_{ay}) was determined as F_y^*/m^* and it amounted to 0.53g. The effective period of the equivalent SDOF system (T^*) amounted to 0.32 s.

The reduction factor R_μ was determined using the target spectrum (see Figure 4.1) and it amounted to $S_e(T^*)/S_{ay}=1.64$ ($S_e(T^*)$ amounted to 0.87g). Since the effective period T^* is smaller than T_C , the equal displacement rule cannot be applied. The displacement demand of the SDOF system (d_t^*) amounted to 2.70 cm, whereas the corresponding ductility demand μ amounted to 2.0. The target displacement of the MDOF system (d_t) was determined as the product of Γ and d_t^* and it amounted to 3.43 cm. The corresponding displacements of the first and second storey amounted to 0.84 and 2.17 cm,

respectively. Therefore, the components of the inelastic first mode shape amounted to 0.245, 0.633 and 1.0 in the first, second and third storey, respectively.

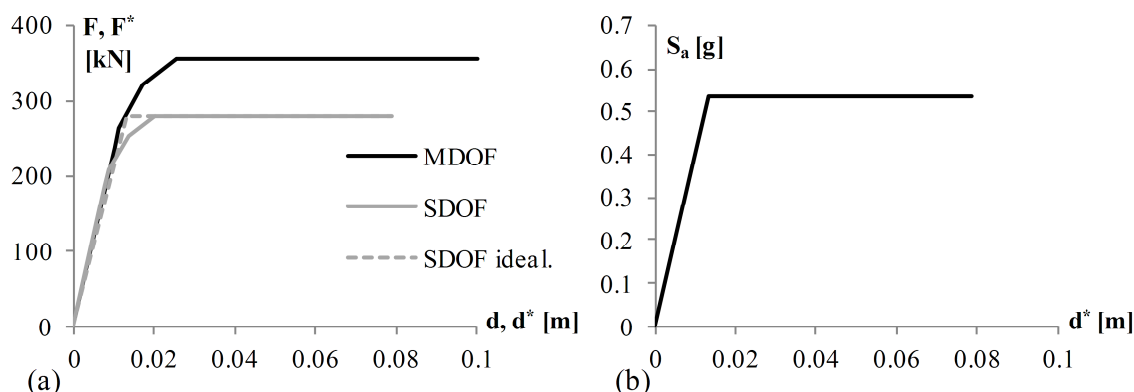


Figure 4.13: (a) Pushover curves for MDOF, SDOF and idealized SDOF system and (b) Capacity diagram for the EP model

Slika 4.13: (a) Potisne krivulje za MDOF, SDOF in idealizirani SDOF sistem in (b) Diagram kapacitete za EP model

Q_0 model, input scale factor $SF=1.0$

The pushover analysis was firstly conducted for an arbitrarily chosen target displacement equal to 0.10 m and a pushover curve was obtained and presented in Figure 4.14a. By dividing it with the transformation factor Γ , a pushover curve for the equivalent SDOF system was obtained and then idealized (elasto-perfectly plastic idealization), as presented in Figure 4.14a.

For the equivalent SDOF system, the displacement at the yield point (d_y^*) amounted to 1.15 cm, whereas the corresponding force (F_y^*) amounted to 277.8 kN. The capacity diagram presented in Figure 4.14b was obtained by dividing the forces F^* with the equivalent mass m^* . The acceleration at the yield point (S_{ay}) was determined as F_y^*/m^* and it amounted to 0.53g. The effective period of the equivalent SDOF system (T^*) amounted to 0.30 s.

The reduction factor R_μ was determined using the target spectrum (see Figure 4.1) and it amounted to $S_e(T^*)/S_{ay}=1.64$ ($S_e(T^*)$ amounted to 0.87g).

Since the effective period T^* is smaller than T_C , the equal displacement rule cannot be applied. The displacement demand of the SDOF system (d_t^*) amounted to 2.39 cm, whereas the corresponding ductility demand μ amounted to 2.1. The target displacement of the MDOF system (d_t) was determined as the product of Γ and d_t^* and it amounted to 3.06 cm. The corresponding displacements of the first and second storey amounted to 0.82 and 1.97 cm, respectively. Therefore, the components of the inelastic first mode shape amounted to 0.268, 0.644 and 1.0 in the first, second and third storey, respectively.

Figures 4.15 and 4.16 show the mean values of the floor response spectra normalized with the mean PGA of the input, which amounted to 0.43g in the case of $SF=1.0$.

In the case of the elastic structure ($\mu=1$), the peaks of floor response spectra, which occur when the natural period of the equipment is approximately equal to the natural period of the structure, are

related to all three modes. In the first storey, the influence of the second mode is slightly smaller than the influence of the fundamental mode, whereas the influence of the third mode is quite small. In the second storey the most dominant mode is the first one, the influence of the second mode significantly decreases, whereas the influence of the third mode diminishes almost completely. In the third storey, the first mode is obviously the most important one, the influence of the second mode is small, whereas the influence of the third mode is not visible.

In the case of inelastic structures, the peak values of floor response spectra related to the first mode are smaller than the corresponding peak values obtained for the elastic structure. In the case of the EP model the peak values occur close to the resonance, whereas in the case of the Q_0 model the peak values are shifted towards higher periods. The peak shift is mostly pronounced in the first storey, it is small in the second storey, whereas in the third storey it practically does not exist. The peaks of floor response spectra related to the first mode show similar trends as in the cases of the structures W03 and W10, as well as in the case of inelastic SDOF structures (see Section 2.3).

In the first storey, peak values of floor response spectra related to the second mode are similar to the peaks obtained for the elastic structure, whereas in the second and in the third storey they are somewhat smaller. In the case of the elastic and EP model, the shapes of the resonance regions of floor response spectra related to the second mode are similar, whereas in the case of the Q_0 model the resonance regions are somewhat wider (the peaks are slightly shifted towards higher periods). In the first storey, in the case of the EP model, the peaks of floor response spectra related to the third mode are slightly larger than the peaks obtained for the elastic structure, whereas the peaks obtained for the Q_0 model are significantly larger. In the second storey, for the EP model, the third mode related peak is quite small and it is practically equal to the one obtained for the elastic structure, while in the case of the Q_0 model significant difference can once again be observed. Finally, in the third storey, the peak related to the third mode can only be observed in the case of the Q_0 model, but its size is practically negligible.

Again, it is obvious that the different modelling approaches in SAP and OpenSees (which were discussed above) may produce certain problems in the comparison of the obtained results. Regardless of that fact, several important trends and characteristics of the floor response spectra may still be recognized.

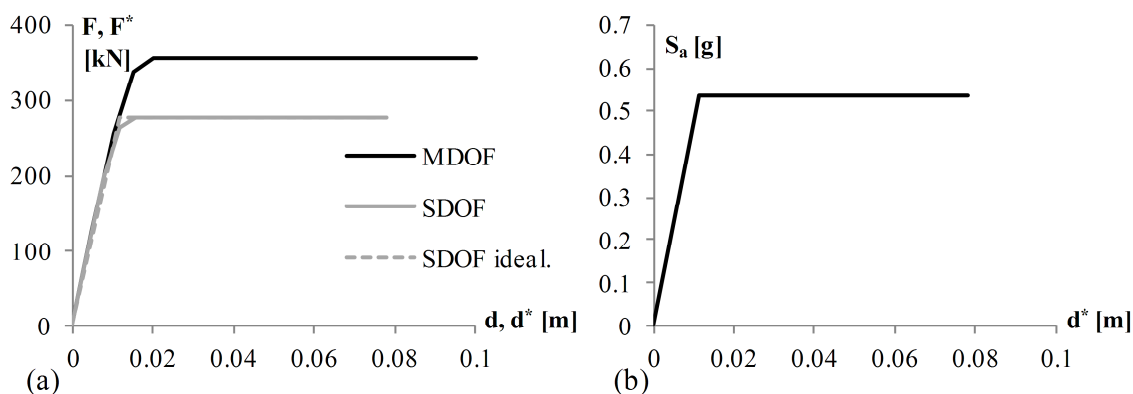


Figure 4.14: (a) Pushover curves for MDOF, SDOF and idealized SDOF system and (b) Capacity diagram for the Q_0 model

Slika 4.14: (a) Potisne krivulje za MDOF, SDOF in idealizirani SDOF sistem in (b) Diagram kapacitete za Q_0 model

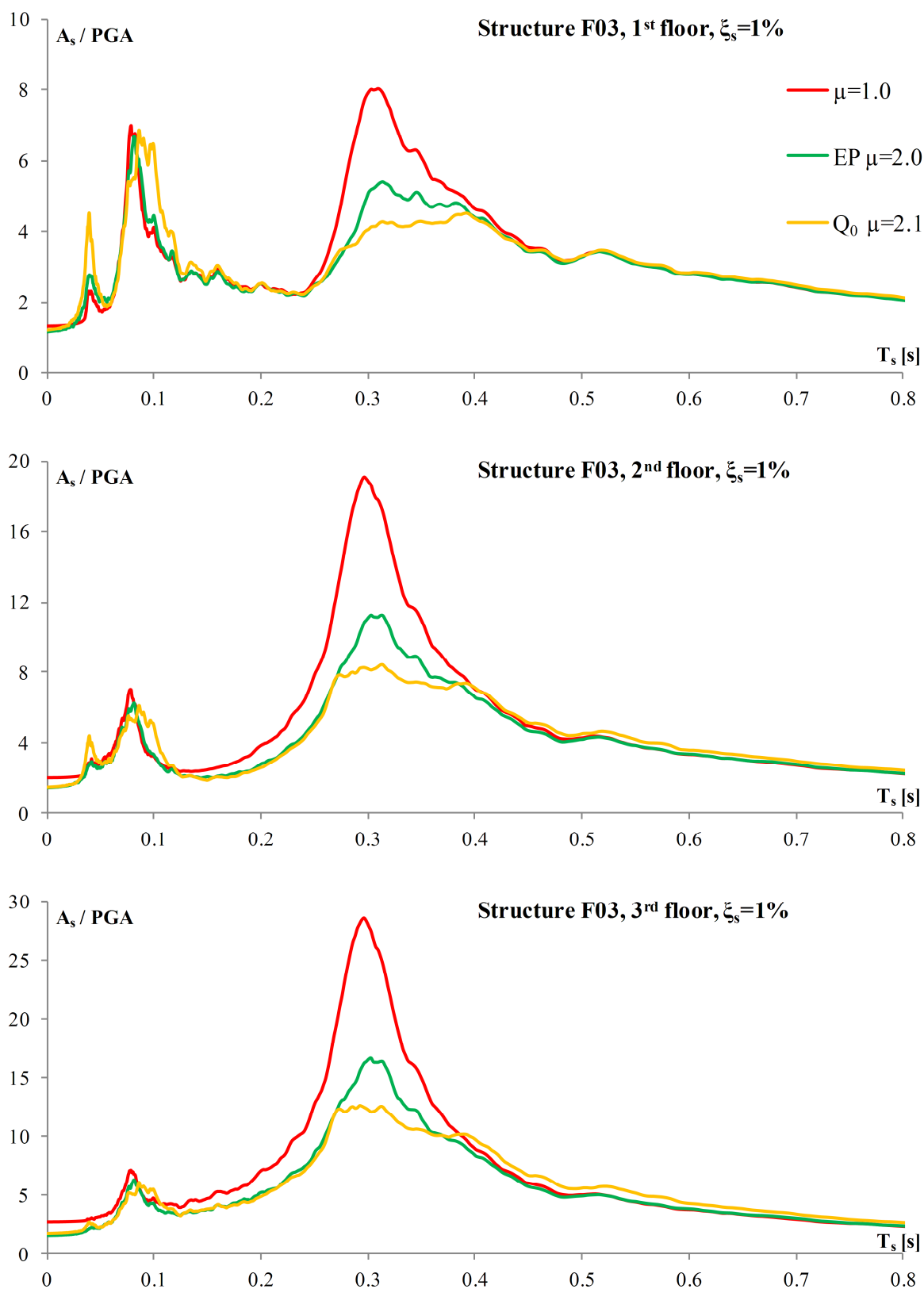


Figure 4.15: Mean values of the floor response spectra normalized with the mean PGA, structure F03 (1% damping of the equipment)

Slika 4.15: Povprečne vrednosti etažnih spektrov odziva normirane s povprečnim PGA, konstrukcija F03 (1% dušenje opreme)

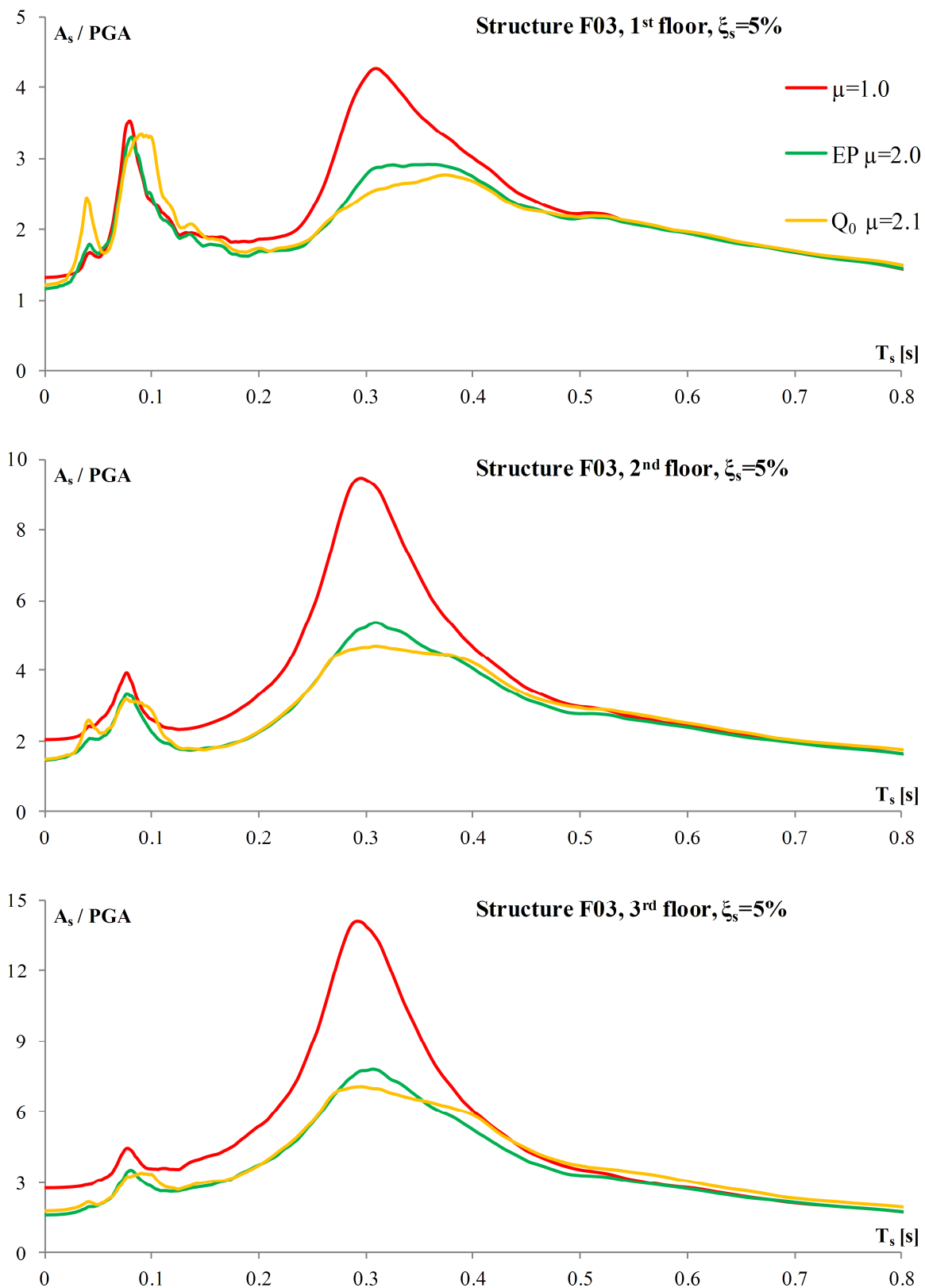


Figure 4.16: Mean values of the floor response spectra normalized with the mean PGA, structure F03 (5% damping of the equipment)

Slika 4.16: Povprečne vrednosti etažnih spektrov odziva normirane s povprečnim PGA, konstrukcija F03 (5% dušenja opreme)

4.2.4 Results obtained for structure F10

A three-storey elastic and inelastic single bay frame with the natural period of the first mode equal to 1.0 s was considered in the study. The RHA was conducted by using the seismic input described in Section 4.1 and by using the scaled input with the scale factor $SF=0.5$.

In pushover analyses, in the case of the EP model, lateral forces amounted to 15.5, 34.3 and 46.0 kN in the first, second and third storey, respectively, while in the case of the Q_0 model lateral forces amounted to 15.4, 34.1 and 46.0 kN in the first, second and third storey, respectively. In the case of the EP model effective mass m^* and transformation factor Γ amounted to 95.8 t and 1.25, respectively, whereas in the case of the Q_0 model they amounted to 95.5 t and 1.25, respectively.

EP model, input scale factor $SF=0.5$

The pushover analysis was firstly conducted for an arbitrarily chosen target displacement equal to 0.10 m and a pushover curve was obtained and presented in Figure 4.17a (d denotes displacement, whereas F denotes base shear force). By dividing it with the transformation factor Γ , a pushover curve for the equivalent SDOF system was obtained and idealized (elasto-perfectly plastic idealization), as shown in Figure 4.17a (d^* denotes displacement, whereas F^* denotes base shear force).

For the equivalent SDOF system, the displacement at the yield point (d_y^*) amounted to 3.09 cm, whereas the corresponding force (F_y^*) amounted to 85.8 kN. The capacity diagram presented in Figure 4.17b was obtained by dividing the forces F^* with the equivalent mass m^* . The acceleration at the yield point (S_{ay}) was determined as F_y^*/m^* and it amounted to 0.09g. The effective period of the equivalent SDOF system (T^*) amounted to 1.17 s.

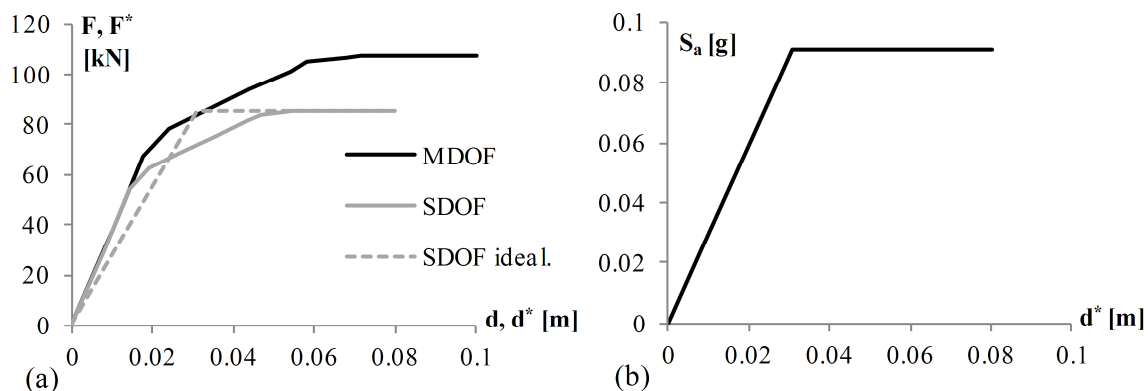


Figure 4.17: (a) Pushover curves for MDOF, SDOF and idealized SDOF system and (b) Capacity diagram for the EP model

Slika 4.17: (a) Potisne krivulje za MDOF, SDOF in idealizirani SDOF sistem in (b) Diagram kapacitete za EP model

The reduction factor R_μ was determined using the target spectrum (see Figure 4.1) and the SF and it amounted to $SF \cdot S_e(T^*)/S_{ay}=2.1$ ($S_e(T^*)$ amounted to 0.37g). Since the effective period T^* is larger than T_C , the equal displacement rule can be applied, i.e. the inelastic displacement demand is equal to the elastic demand. The displacement demand of the SDOF system (d_t^*) amounted to 6.29 cm, whereas the corresponding ductility demand μ amounted to 2.1. The target displacement of the MDOF system (d_t) was determined as the product of Γ and d_t^* and it amounted to 7.86 cm, whereas the corresponding

displacements of the first and second storey amounted to 2.62 and 5.96 cm, respectively. Therefore, the components of the inelastic first mode shape amounted to 0.333, 0.758 and 1.0 in the first, second and third storey, respectively.

EP model, input scale factor $SF=1.0$

The following quantities are the same as in the case of $SF=0.5$: d_y^* , F_y^* , S_{ay} and T^* . The R_μ factor was determined using the target spectrum (see Figure 4.1) and it amounted to $S_e(T^*)/S_{ay}=4.1$ ($S_e(T^*)$ amounted to 0.37g). d_t^* amounted to 12.59 cm, μ amounted to 4.1, whereas d_t amounted to 15.74 cm. The displacements of the first and second storey amounted to 5.25 and 11.22 cm, respectively. Finally, the components of the inelastic first mode shape amounted to 0.334, 0.713 and 1.0 in the first, second and third storey, respectively.

Q_0 model, input scale factor $SF=0.5$

The pushover analysis was firstly conducted for an arbitrarily chosen target displacement equal to 0.10 m and a pushover curve was obtained and presented in Figure 4.18a. By dividing it with the transformation factor Γ , a pushover curve for the equivalent SDOF system was obtained and then idealized (elasto-perfectly plastic idealization), as shown in Figure 4.18a.

For the equivalent SDOF system, the displacement at the yield point (d_y^*) amounted to 2.73 cm, whereas the corresponding force (F_y^*) amounted to 85.7 kN. The capacity diagram presented in Figure 4.18b was obtained by dividing the forces F^* with the equivalent mass m^* . The acceleration at the yield point (S_{ay}) was determined as F_y^*/m^* and it amounted to 0.09g. The effective period of the equivalent SDOF system (T^*) amounted to 1.10 s.

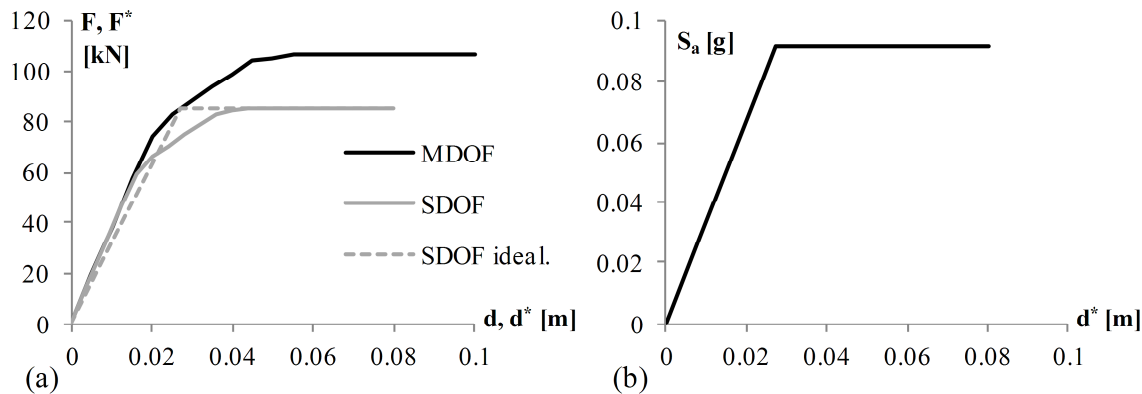


Figure 4.18: (a) Pushover curves for MDOF, SDOF and idealized SDOF system and (b) Capacity diagram for the Q_0 model

Slika 4.18: (a) Potisne krivulje za MDOF, SDOF in idealizirani SDOF sistem in (b) Diagram kapacitete za Q_0 model

The reduction factor R_μ was determined using the target spectrum (see Figure 4.1) and the SF and it amounted to $SF \cdot S_e(T^*)/S_{ay}=2.2$ ($S_e(T^*)$ amounted to 0.40g).

Since the effective period T^* is larger than T_C , the equal displacement rule is applicable. The displacement demand of the SDOF system (d_t^*) amounted to 6.01 cm, whereas the corresponding ductility demand μ amounted to 2.2. The target displacement of the MDOF system (d_t) was

determined as the product of Γ and d_t^* and it amounted to 7.51 cm, whereas the corresponding displacements of the first and second storey amounted to 2.54 and 5.54 cm, respectively. Therefore, the components of the inelastic first mode shape amounted to 0.338, 0.738 and 1.0 in the first, second and third storey, respectively.

Q₀ model, input scale factor SF=1.0

The following quantities are the same as in the case of SF=0.5: d_y^* , F_y^* , S_{ay} and T^* . The R_μ factor was determined using the target spectrum (see Figure 4.1) and it amounted to $S_e(T^*)/S_{ay}=4.4$ ($S_e(T^*)$ amounted to 0.40g). d_t^* amounted to 12.03 cm, μ amounted to 4.4, whereas d_t amounted to 15.04 cm. The displacements of the first and second storey amounted to 5.06 and 10.56 cm, respectively. Finally, the components of the inelastic first mode shape amounted to 0.336, 0.702 and 1.0 in the first, second and third storey, respectively.

Figures 4.19 and 4.20 show the mean values of the floor response spectra normalized with the mean PGA of the input, which amounted to 0.22g in the case of SF=0.5 and to 0.43g in the case of SF=1.0.

In the case of the elastic structure ($\mu=1$), the peak values of floor response spectra occur when the natural period of the equipment is approximately equal to the natural period of the structure and they are related to all three modes. In the first storey, the influence of higher modes is significantly larger than the influence of the fundamental mode, which is especially pronounced in the case of the second mode. The peak related to the third mode is somewhat smaller than the peak related to first mode. In the second storey the peak related to the first mode becomes the most pronounced one, the peak related to the second mode decreases whereas the peak related to the third mode practically remains the same. In the third storey, the first mode remains the most pronounced one, the influence of the second mode is somewhat smaller, whereas the influence of the third mode diminishes almost completely. As in the case of the structure W10, it is obvious from the obtained results that the seismic input significantly influences the floor response spectra. The chosen set of ground motions triggers the structural response in the second mode and the influence of the second mode remains significant even in the top storey of the frame.

In the case of inelastic structures, the peak values of floor response spectra related to the fundamental mode are reduced in comparison with the corresponding peak values obtained for the elastic structure and, as in the case of all previously analysed structures, the size of peak reduction depends on the ductility demand. Like in all other cases, in the case of the EP model the peak values occur close to the resonance, whereas in the case of the Q₀ model the peak values are shifted towards higher periods (which can only be observed for $\mu=2.2$ since there are no peaks in the case of $\mu=4.4$). It can once again be confirmed that the peaks of floor response spectra related to the first mode show the trends which were previously observed in the case of inelastic SDOF structures (see Section 2.3). Peak values of floor response spectra related to the second mode are very interesting, since it can be observed that they are reduced in comparison with the peaks obtained for the elastic structure. This applies for both hysteretic models and all considered ductilities. It is also obvious that the size of the ductility demand influences the size of the reduction. Similar trend was observed in the case of the structure W10, but it is more pronounced here. In the case of the structure W10 (in the case of the Q₀ model) peak values of the second mode are not shifted towards higher periods, whereas in the case of the structure F10 they are. It can actually be observed that the resonance regions and the peaks related to the second mode show similar characteristics to the resonance regions and the peaks related to the fundamental mode, but obviously with smaller ductility demand. This fact raises some interesting questions.

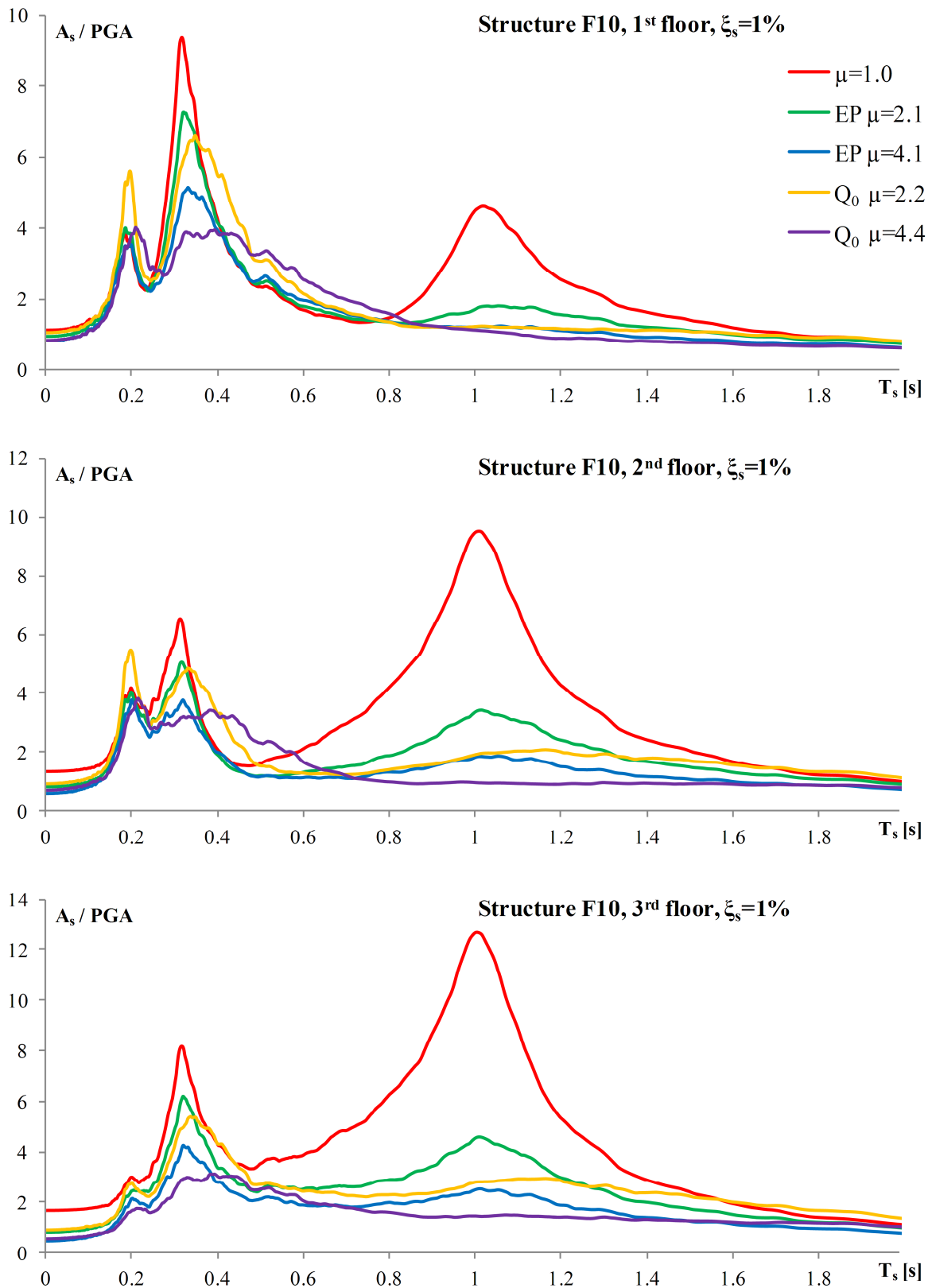


Figure 4.19: Mean values of the floor response spectra normalized with the mean PGA, structure F10 (1% damping of the equipment)

Slika 4.19: Povprečne vrednosti etažnih spektrov odziva normirane s povprečnim PGA, konstrukcija F10 (1% dušenja opreme)

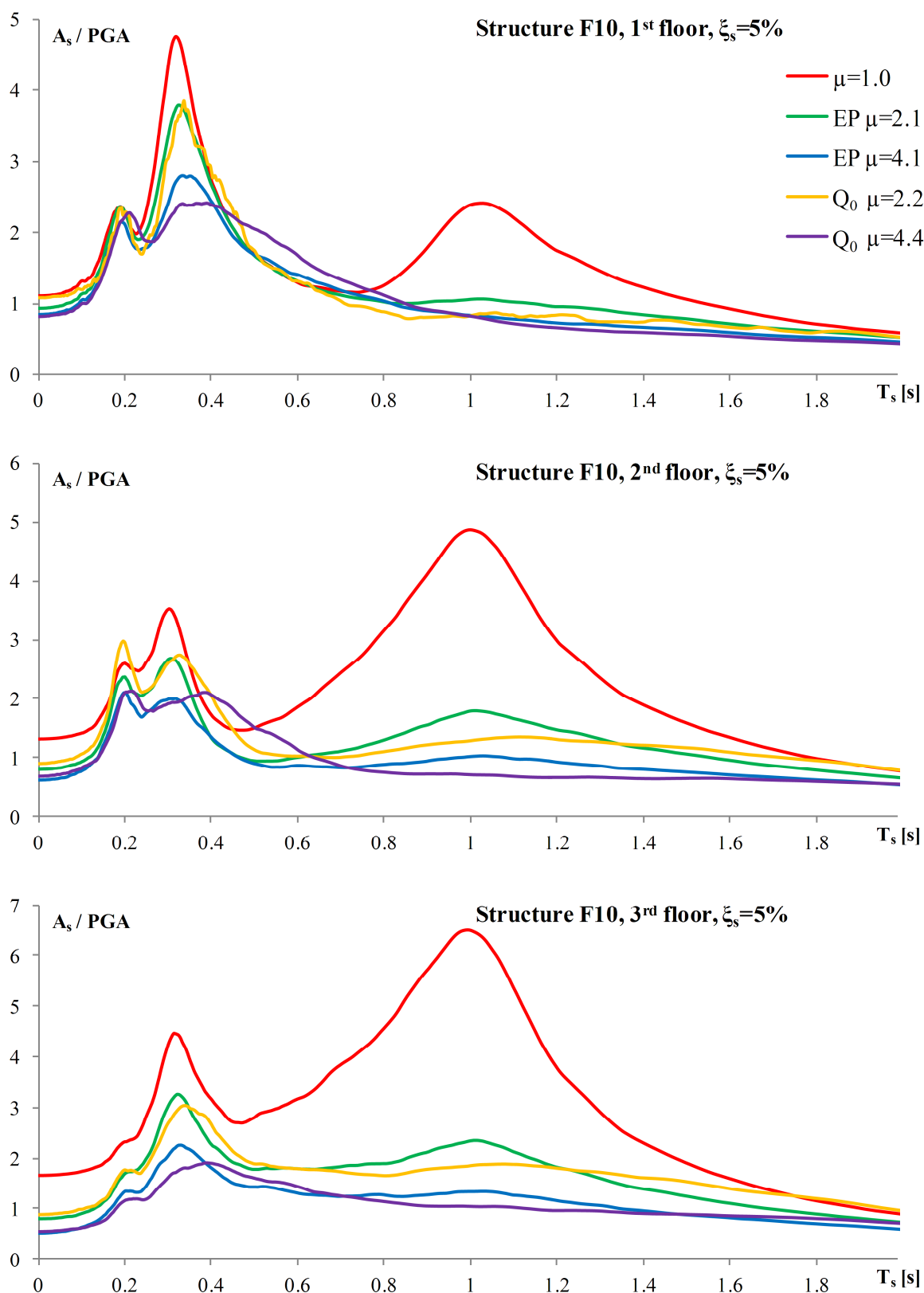


Figure 4.20: Mean values of the floor response spectra normalized with the mean PGA, structure F10 (5% damping of the equipment)

Slika 4.20: Povprečne vrednosti etažnih spektrov odziva normirane s povprečnim PGA, konstrukcija F10 (5% dušenja opreme)

In earthquake engineering, it is often assumed that inelastic behaviour occurs only in the fundamental mode. The results obtained for the structures W10 and F10 suggest inelastic behaviour also in the second mode. It should be noted that both structures are simple planar structures which have only three natural modes. The obtained results imply that in the case of flexible structures with large number of modes inelastic behaviour can perhaps occur in more than several first modes. The question is: how to estimate ductility demand for higher modes? In the case of the structure F10, estimation of the ductility demand for the second mode is presented and explained below. Finally, as for the peaks related to the third mode, it can be observed that in the case of the EP model, in the first storey, they are practically equal to the peaks obtained for the elastic structure. In the second storey they are somewhat smaller, whereas in the third storey they diminish almost completely. In the case of the Q_0 model, in the first and in the second storey, the peaks related to the third mode depend on the ductility demand of the structure, i.e. for the case of $\mu=2.2$ they are larger or practically equal to the peaks obtained for the elastic structure, whereas for the case of $\mu=4.4$ they are smaller or practically equal to the corresponding peaks obtained for the elastic structure. In the third storey, the peaks related to the third mode are negligible.

Estimation of the ductility demand for the second mode

In engineering practice, it is often assumed that inelastic structural behaviour occurs only in the fundamental mode. In some cases though, this assumption cannot be made so it is necessary to determine the seismic demand by taking into account inelasticity related to several modes. Estimation of the seismic demand in such cases may be conducted by using a modal pushover analysis procedure proposed by Chopra and Goel (2002). In the proposed approach, the total seismic demand is determined by combining the seismic demands obtained for modes which were taken into account in the analysis. For each considered mode, the seismic demand is obtained by performing a pushover analysis, in which the distribution of inertia forces obtained for the considered mode is used.

For the purpose of this study, a similar approach was adopted, in the sense of analysing seismic demands in different modes separately. As in the case of the fundamental mode, the N2 method (see Fajfar 2000 or ANNEX D) was used to estimate the seismic demand in the second mode. Namely, in the case of the second mode, eigenvectors obtained in SAP and OpenSees were normalized so that the component of the vector in the third storey amounted to -1.0 . In the case of SAP, the corresponding components in the first and in the second storey amounted to 1.197 and 0.800, respectively, whereas in the case of OpenSees they amounted to 1.207 and 0.804, respectively.

In pushover analyses, in the case of the EP model, lateral forces amounted to 55.1, 36.8 and -46.0 kN in the first, second and third storey, respectively, while in the case of the Q_0 model lateral forces amounted to 55.5, 37.0 and -46.0 kN in the first, second and third storey, respectively. In the case of the EP model effective mass m^* and transformation factor Γ amounted to 45.9 t and 0.32, respectively, whereas in the case of the Q_0 model they amounted to 46.5 t and 0.33, respectively.

For both hysteretic models, in the case when the value of the ductility demand for the fundamental mode is slightly above 2 ($SF=0.5$), the results obtained from the above described approach indicated that the ductility demand for the second mode amounted to 1 (elastic behaviour). The results presented in Figures 4.19 and 4.20 show the opposite trend and it is obvious that the inelastic response actually exists in the second mode. Therefore, the accuracy of the proposed approach is questionable, which will be discussed later. The results obtained for the $SF=1.0$ are presented below.

EP model, input scale factor $SF=1.0$

The pushover analysis was firstly conducted for an arbitrarily chosen target displacement equal to 0.10 m and a pushover curve was obtained and presented in Figure 4.21a (d denotes displacement, whereas F denotes base shear force). It can be seen that the displacement is negative. By dividing forces with the transformation factor Γ and by dividing the displacements with the product of Γ and the component of the second mode vector in the third storey which amounted to -1.0 (for equations see Chopra and Goel 2002), a pushover curve for the equivalent SDOF system was obtained and idealized as elasto-perfectly plastic, as presented in Figure 4.21b (d^* denotes displacement, whereas F^* denotes base shear force).

For the equivalent SDOF system, the displacement at the yield point (d_y^*) amounted to 0.0209 m, whereas the corresponding force (F_y^*) amounted to 352.5 kN. The capacity diagram, which is not presented herein, can be obtained by dividing the forces F^* with the equivalent mass m^* . Nevertheless, the acceleration at the yield point (S_{ay}) of the capacity diagram was determined as F_y^*/m^* and it amounted to 0.78g. The effective period for the second mode of the equivalent SDOF system (T^*) amounted to 0.33 s.

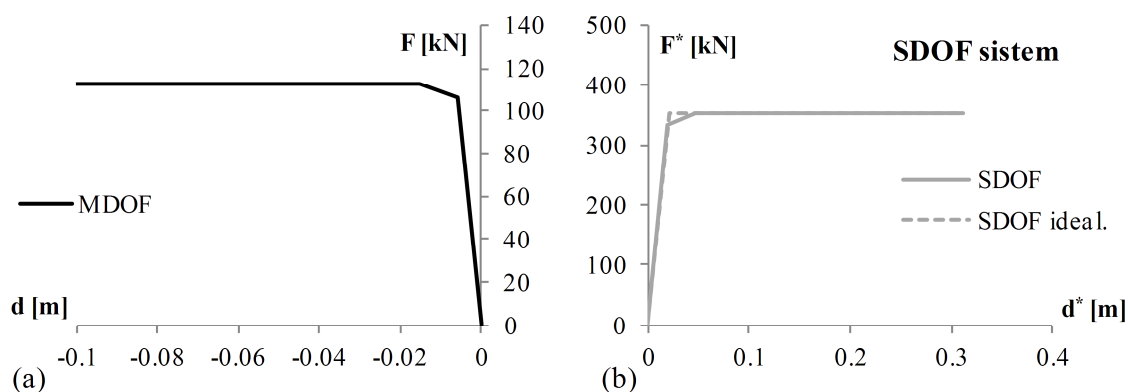


Figure 4.21: Pushover curves for (a) MDOF and (b) SDOF system (the EP model)

Slika 4.21: Potisne krivulje za (a) MDOF in (b) SDOF sistem (EP model)

The reduction factor R_μ was determined using the target spectrum (see Figure 4.1) and it amounted to $S_e(T^*)/S_{ay}=1.12$ ($S_e(T^*)$ amounted to 0.87g). Since the effective period T^* is smaller than T_C , the equal displacement rule cannot be applied. The displacement demand of the SDOF system (d_t^*) amounted to 2.48 cm, whereas the corresponding ductility demand μ amounted to 1.2. The target displacement of the MDOF system (d_t) was determined as the product of $-\Gamma$ and d_t^* and it amounted to -0.79 cm. The corresponding displacements of the first and second storey amounted to 0.70 and 0.41 cm, respectively. Therefore, the components of the inelastic first mode shape amounted to 0.886, 0.519 and -1.0 in the first, second and third storey, respectively.

Q_0 model, input scale factor $SF=1.0$

The procedure which was used in the case of the EP model was repeated in the case of the Q_0 model. The pushover analysis was conducted for an arbitrarily chosen target displacement equal to 0.10 m and a pushover curve was obtained and shown in Figure 4.22a. By dividing forces with the transformation factor Γ and by dividing the displacements with the product of Γ and the component of the second

mode vector in the third storey which amounted to -1.0 , a pushover curve for the equivalent SDOF system was obtained and idealized as elasto-perfectly plastic, as presented in Figure 4.22b.

For the equivalent SDOF system, the displacement at the yield point (d_y^*) amounted to 0.0188 m, whereas the corresponding force (F_y^*) amounted to 347.2 kN. The acceleration at the yield point (S_{ay}) of the capacity diagram was determined as F_y^*/m^* and it amounted to $0.76g$. The effective period for the second mode of the equivalent SDOF system (T^*) amounted to 0.32 s.

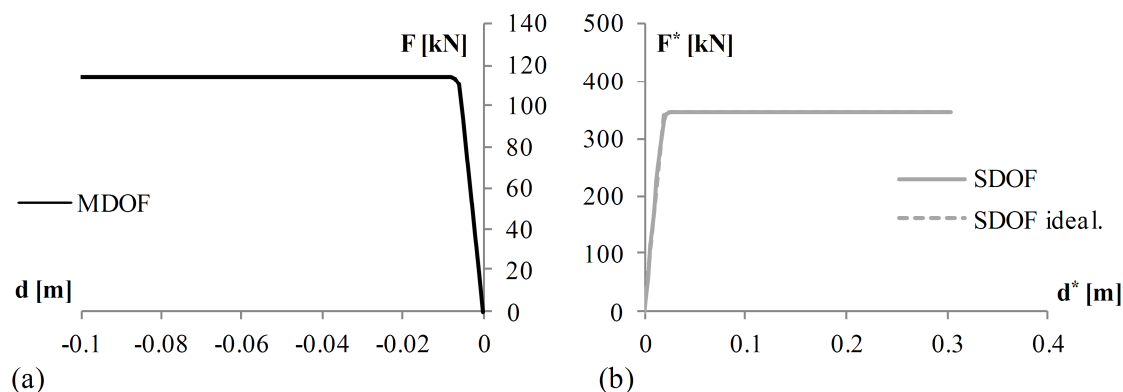


Figure 4.22: Pushover curves for (a) MDOF and (b) SDOF system (the Q_0 model)

Slika 4.22: Potisne krivulje za (a) MDOF in (b) SDOF sistem (Q_0 model)

The reduction factor R_μ was determined using the target spectrum (see Figure 4.1) and it amounted to $S_e(T^*)/S_{ay}=1.14$ ($S_e(T^*)$ amounted to $0.87g$). Since the effective period T^* is smaller than T_C , the equal displacement rule cannot be applied. The displacement demand of the SDOF system (d_i^*) amounted to 2.37 cm, whereas the corresponding ductility demand μ amounted to 1.2 . The target displacement of the MDOF system (d_i) was determined as the product of $-I$ and d_i^* and it amounted to -0.78 cm. The corresponding displacements of the first and second storey amounted to 0.73 and 0.44 cm, respectively. Therefore, the components of the inelastic first mode shape amounted to 0.936 , 0.564 and -1.0 in the first, second and third storey, respectively.

Note that, for both hysteretic models, achieved ductilities for the second mode were obtained for the case when the value of the ductility demand for the fundamental mode is slightly above 4. The estimated ductility demand in the case of the second mode is slightly larger than 1 for both hysteretic models, which implies almost elastic structural behaviour. Such estimation is not in compliance with the results presented in Figures 4.19 and 4.20, which imply that the ductility demands are significantly larger. Unfortunately, it can be seen that the proposed approach produces underestimated ductility demands.

An additional check of the above presented approach was conducted by analysing the ductility demand in the second mode of the structure W10. Namely, as mentioned above, in the case of the structure W10 peaks related to the second mode are also somewhat lower than the peaks obtained for the elastic structure. The main idea for this additional check lies in the difference between structural systems of the F10 and W10. The analysis was conducted for the EP model and the ductility demand of the fundamental mode which amounted to 4.0 ($SF=1.0$). As expected, the obtained results indicated elastic structural behaviour of the structure W10 in the second mode. For the considered cases, it can be concluded that the type of structural system has no influence on the results which were obtained from the proposed approach.

4.2.5 Influence of individual modes on floor response spectra

The influence of individual modes on floor response spectra was examined by taking into account elastic structures W03 and W10. In both cases, the approach described in the following text was applied.

A generalized SDOF system concept was used for the determination of absolute accelerations in every mode and at each storey of the structure (for details see Chopra 2012). Since both structures have three natural modes, three generalized SDOF systems were used in both cases and they were represented by simple oscillators. The natural period of each oscillator was equal to the natural period of the structure in the considered mode. In the case of oscillators which represented the first and second mode, a "mass-proportional" damping amounted to 5%, whereas in the case of oscillators which represented the third mode the "mass-proportional" damping amounted to 12% for both the W03 and the W10. The damping values for the third mode were determined by using Equation 4.7 (see Chopra 2012). Note that $\omega_{p,3}$ denotes the natural circular frequency of the third mode. Additionally, note that a_0 and a_1 (respectively) denote the mass and stiffness coefficients of the Rayleigh damping model, which were determined under the assumption that damping in the first ($\zeta_{p,1}$) and the second ($\zeta_{p,2}$) mode amounts to 5%.

$$\xi_{p,3} = \frac{a_0}{2\omega_{p,3}} + \frac{a_1\omega_{p,3}}{2} \quad (4.7)$$

Two ground motions were considered as the seismic input: Kalamata with the PGA equal to 0.30g and Ionian with the PGA equal to 0.25g (for more details see Table 2.1). The RHA was conducted by using the Newmark integration method, taking into account coefficients $\gamma=0.5$ and $\beta=0.25$ (a constant acceleration within each time step). The size of the time step amounted to 0.001 s in all cases.

Figures 4.23–4.26 present absolute floor accelerations (A) obtained for individual modes. Note that only the parts of the response in which the peak values occur are shown.

In the case of the structure W03 and Kalamata, it is obvious that significant absolute accelerations due to the second and third mode occur in the first storey. The peaks related to higher modes occur practically at the same time and it is obvious that they are very close to the peak of the first mode. Moreover, all modes are almost in-phase within the part of the time interval where the peak values occur. In the second storey, absolute acceleration due to the first mode is the most pronounced one. Also, absolute accelerations due to the second and third modes are now mutually out-of-phase. In the third storey, absolute acceleration due to the first mode is the most significant one. In the case of Ionian, similar trends can be observed. Nevertheless, it should be noted that in the first storey absolute accelerations due to the second and third mode show interesting matching, i.e. the responses are very similar. It is obvious that in the first storey, for both ground motions, absolute accelerations due to all modes are practically in-phase. This is of great importance since it brings up a question of suitable combination rule, which will be discussed later.

In the case of the structure W10 and Kalamata, in the first storey, absolute acceleration due to the second mode is the most pronounced one. A significant influence of the third mode can also be observed. It is obvious that the frequency content of Kalamata triggers the structural response in higher modes, which was previously discussed in Subsection 4.2.2.

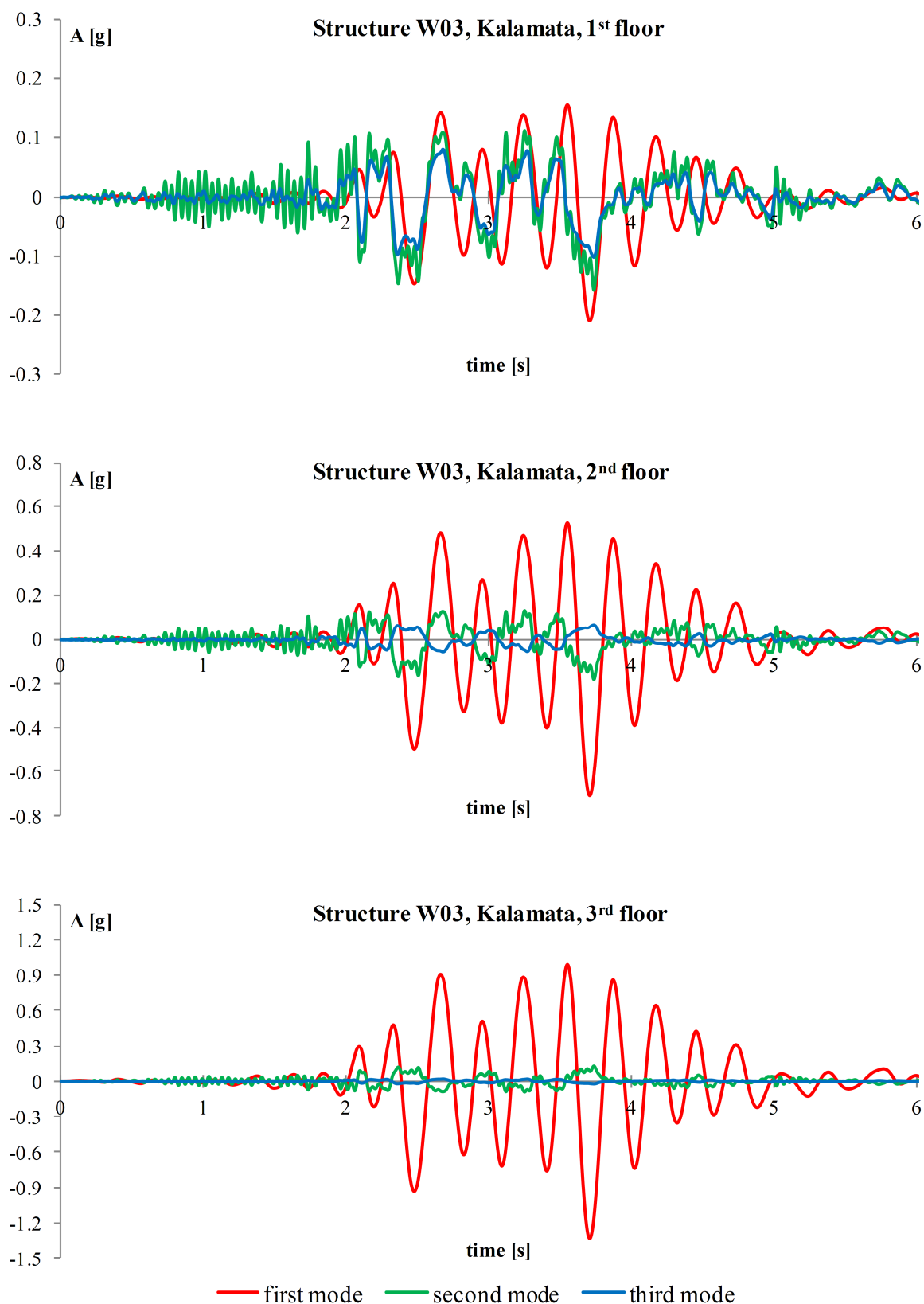


Figure 4.23: Absolute floor accelerations obtained for individual modes in the case of structure W03 and Kalamata earthquake

Slika 4.23: Absolutni etažni pospeški dobljeni za posamezne oblike v primeru konstrukcije W03 in Kalamata potresa

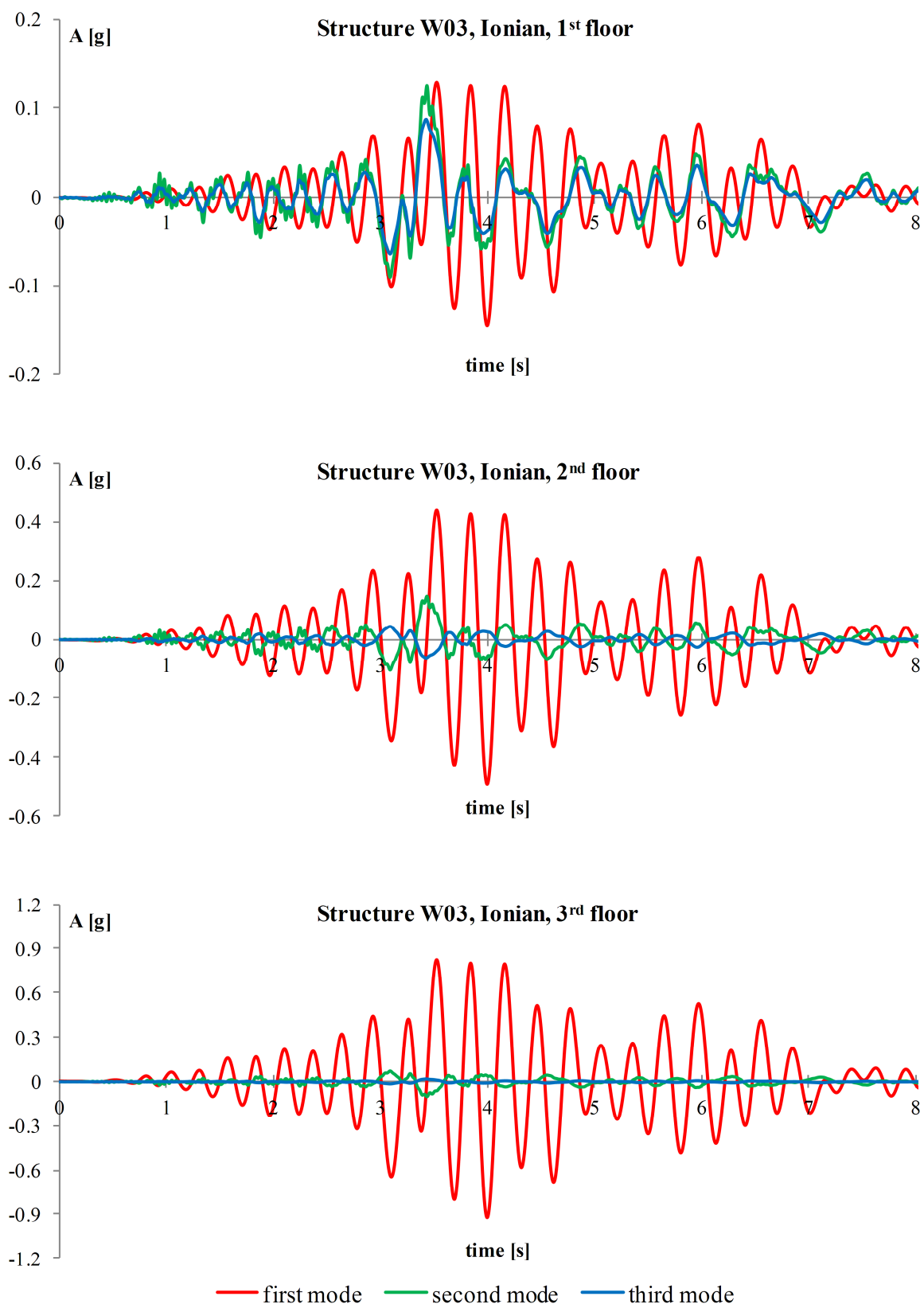


Figure 4.24: Absolute floor accelerations obtained for individual modes in the case of structure W03 and Ionian earthquake

Slika 4.24: Absolutni etažni pospeški dobljeni za posamezne oblike v primeru konstrukcije W03 in Ionian potresa

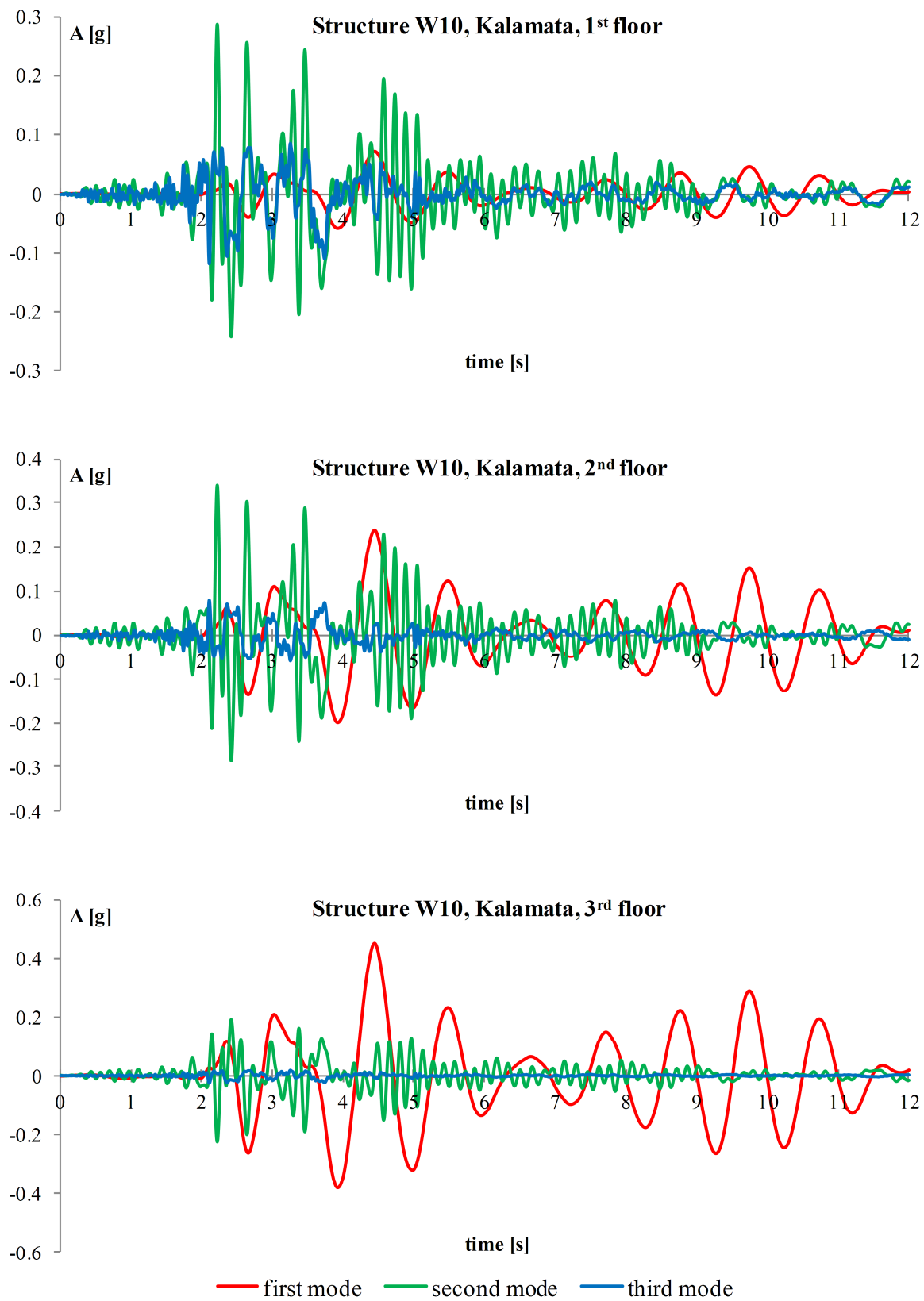


Figure 4.25: Absolute floor accelerations obtained for individual modes in the case of structure W10 and Kalamata earthquake

Slika 4.25: Absolutni etažni pospeški dobljeni za posamezne oblike v primeru konstrukcije W10 in Kalamata potresa

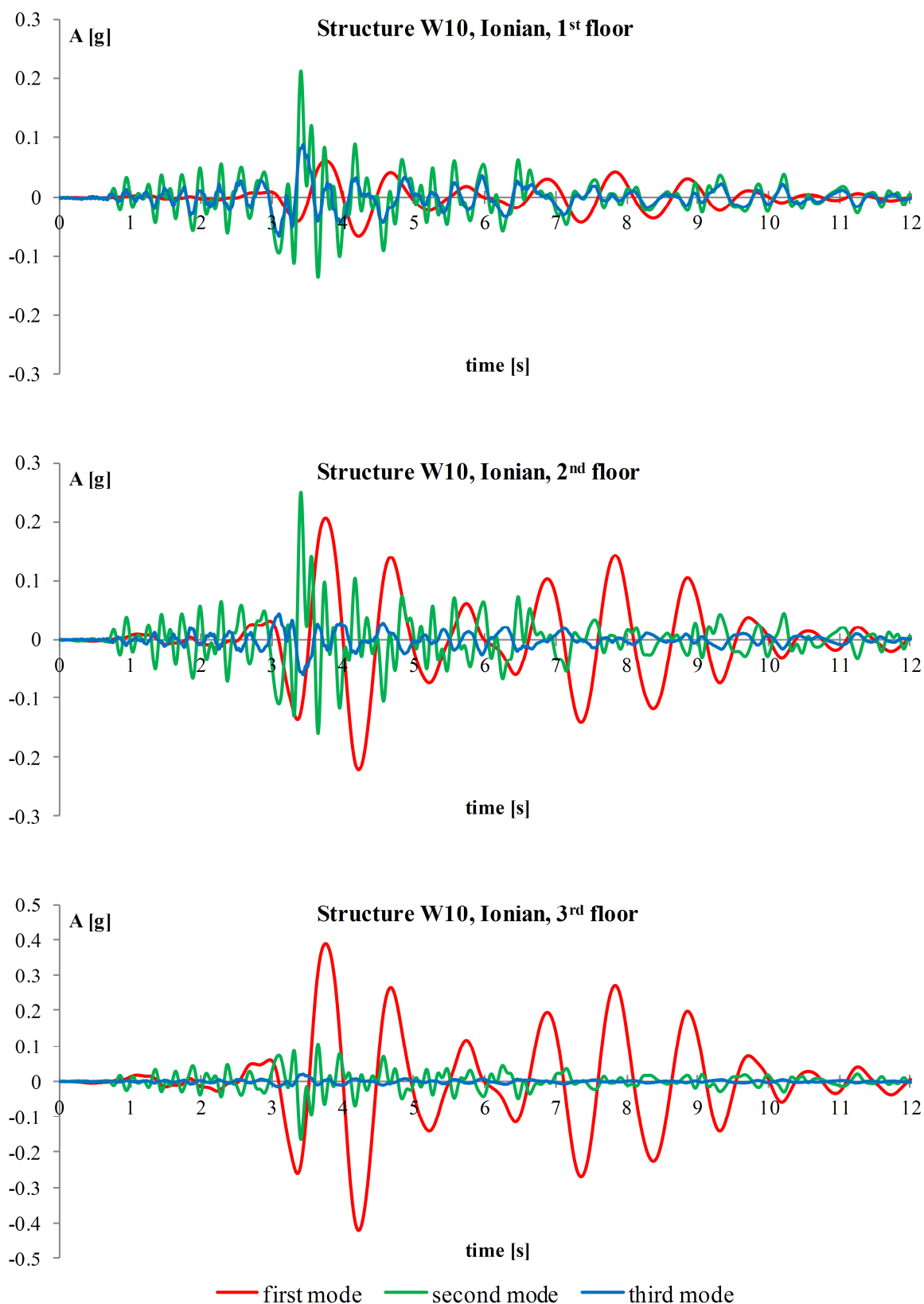


Figure 4.26: Absolute floor accelerations obtained for individual modes in the case of structure W10 and Ionian earthquake

Slika 4.26: Absolutni etažni pospeški dobljeni za posamezne oblike v primeru konstrukcije W10 in Ionian potresa

In the second storey, absolute acceleration due to the second mode slightly increases, the influence of the third mode slightly decreases whereas the influence of the first mode becomes more pronounced. In the third storey, absolute acceleration due to the first mode is the most pronounced one, the influence of the second mode is fairly small, whereas the third mode becomes practically irrelevant. From the results obtained for Ionian, similar conclusions can be made as in the case of Kalamata.

Figures 4.27–4.30 show: floor response spectra determined by using absolute accelerations obtained from the response of MDOF structures (denoted as MDOF), floor response spectra determined by using absolute accelerations obtained for individual modes (denoted as "first mode", "second mode" and "third mode"), elastic spectra of the considered ground motions (denoted as Kalamata and Ionian), floor response spectra obtained by SRSS combination of the floor response spectra of individual modes (denoted as SRSS) and floor response spectra obtained by algebraic summation of the floor response spectra of individual modes (denoted as ALGSUM). All presented spectra were normalized with the corresponding PGA. In all cases, the damping of the equipment amounted to 5%.

For all considered cases it can be seen that for natural periods of the equipment which are significantly larger than the natural period of the fundamental mode of the structure ($T_s \gg T_{p,1}$), MDOF floor response spectra become equal to the elastic spectra of the considered ground motions, which was also observed in the case of SDOF primary structures. This phenomenon is more obvious in the case of the structure W03 since the drawing scale of the x -axis represents values of T_s which are notably larger than $T_{p,1}=0.3$ s.

In the case of the structure W03 and both considered ground motions, it can be observed that the shape of floor response spectra obtained for the second and third mode generally matches the shape of the ground motion spectra, which is most evident in the first storey. Apart from the difference in magnitude which arises from the different modal contributions, an additional difference is the peak in the spectra related to the second mode, which occurs when the natural period of the second mode approximately equals the natural period of the equipment ($T_{p,2} \approx T_s$). In the first storey and outside of the resonance region, it can be seen that the floor response spectrum related to the first mode has a similar magnitude to the spectra related to higher modes. In the second storey, the floor response spectrum related to the first mode becomes the most dominant one and it is quite close to the MDOF spectrum. This is even more pronounced in the third storey.

A similar conclusion regarding higher modes can be drawn in the case of the structure W10, again for both considered ground motions. The only difference is the peak in the spectra related to the third mode, which in this case exists and it is located near the natural period of the third mode of the structure ($T_{p,3}$). Even though in higher storeys the floor response spectrum related to the first mode becomes the most pronounced one in the most of the period range, in the case of Kalamata it can be observed that the floor response spectra related to the second mode have notable influence. Obviously, Kalamata triggers significant structural response in the second mode. In the case of Ionian a similar situation can be observed, but the influence of the second mode is fairly smaller.

The main idea for showing the SRSS and ALGSUM spectra came as a need to clarify several issues. The floor response spectra can be determined for individual modes. The problem is: how to combine them in order to determine the MDOF spectra? The choice of a suitable combination rule is a question which needs to be resolved, since the floor response spectra obtained for individual modes are always positive, which arises from the definition of the spectrum. As for the well-known SRSS rule, this fact is irrelevant, since the minus sign is lost anyway. On the other hand, it is clear that the algebraic

summation rule would be in this case practically equal to the absolute summation rule, since there are no negative values in the floor response spectra. This problem was overcome by using the finding discovered during the development of the method for direct determination of floor response spectra for inelastic MDOF structures (presented in Chapter 6). Namely, it was discovered that the sign of the floor response spectrum of an individual mode in a considered storey is controlled by the product of a modal participation factor and the corresponding component of the mode shape.

For both considered structures, normalization of eigenvectors produced positive modal participation factors in all cases, which means that the sign of the floor response spectrum of individual mode is controlled by the sign of the mode shape component. Moreover, eigenvectors were in all cases normalized so that in the first storey all components are positive, in the second storey a component of the third mode is negative, whereas in the third storey a component of the second mode is negative (see Equations 4.2 and 4.3). Therefore, in the ALGSUM combination procedure the following was assumed: in the case of the first mode, floor response spectra are positive at all storeys, in the case of the second mode they are positive in the first and in the second storey, whereas in the case of the third mode they are positive in the first and in the third storey.

By analysing Figures 4.27–4.30 several important observations can be made. For all considered cases, in the first storey, it is obvious that shortly after the peak related to the fundamental mode ALGSUM produced floor response spectra which perfectly match the MDOF spectra. This fact is of great importance and it represents one of the foundations for the development of the method for the direct determination of floor response spectra for inelastic MDOF structures, which is presented in Chapter 6. In the period range between $T_s=0$ and T_s which approximately equals the natural period related to the fundamental mode ($T_s \approx T_{p,1}$), the ALGSUM produced conservative results. In the case of the SRSS combination rule, it can be seen that, in the first storey, in the most of the period range it produced quite poor results in the case of the structure W03, whereas in the case of the W10 the results are somewhat better, especially in the period range between $T_s=0$ and T_s which is approximately equal to the natural period related to the second mode ($T_s \approx T_{p,2}$). From the presented results, it is obvious that in the period range between $T_s=0$ and $T_s \approx T_{p,1}$ a fairly good estimation of the MDOF spectra is somewhere between the ALGSUM and the SRSS combination rules. Several modal combination rules which enable the production of such results exist in the literature, and they are discussed in detail in ANNEX F and Chapter 5.

In the second and in the third storey, the ALGSUM again produced perfect results in the period range after $T_{p,1}$, for all considered cases. In the period range between $T_s=0$ and $T_s \approx T_{p,1}$ the results obtained for the W03 are quite good, whereas in the case of the W10 they are quite poor, i.e. in the second storey they are very conservative, while in the third storey they are non-conservative or even negative, which is not possible. The SRSS produced very good results in the whole period range in the case of the W03, whereas in the case of the W10 it produced somewhat poorer results, i.e. in the second storey between the peaks related to the first and second mode, the obtained results are conservative, while in the same period range, in the third storey, they are slightly non-conservative.

To summarize: it is obvious that finding an appropriate modal combination rule which should be used for combination of the floor response spectra obtained for individual modes is not straightforward. A proposal for combination of individual floor response spectra is presented in Chapter 6. The proposal is based on the application of different modal combination rules in the period range before and after the resonance region related to the fundamental mode.

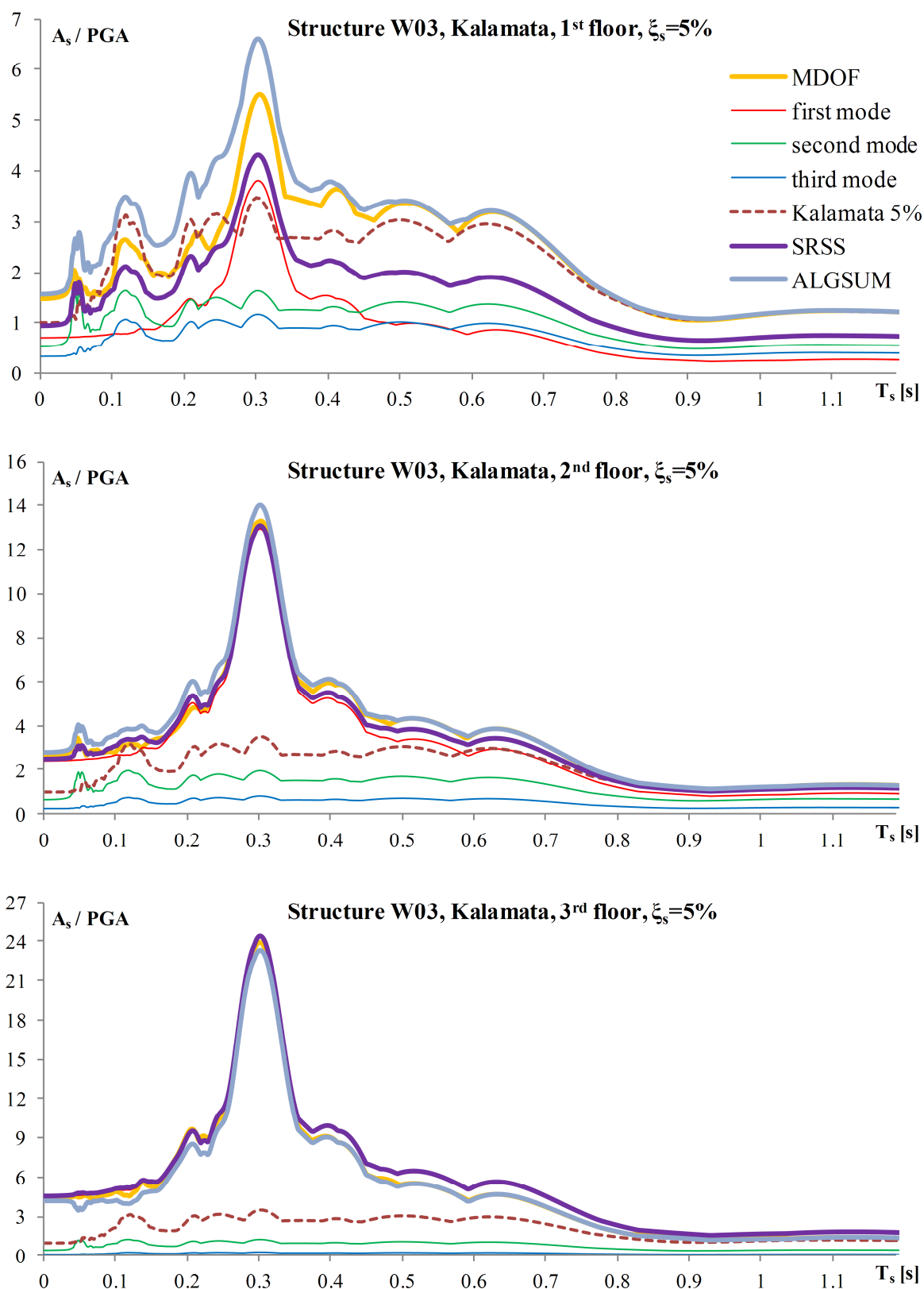


Figure 4.27: Kalamata elastic spectrum and floor response spectra obtained for MDOF structure, individual modes and by using SRSS and ALGSUM combination rules (structure W03)

Slika 4.27: Kalamata elastični spekter in etažni spektri odziva dobljeni za MDOF konstrukcijo, posamezne oblike in z uporabo SRSS in ALGSUM kombinacijskih pravil (konstrukcija W03)

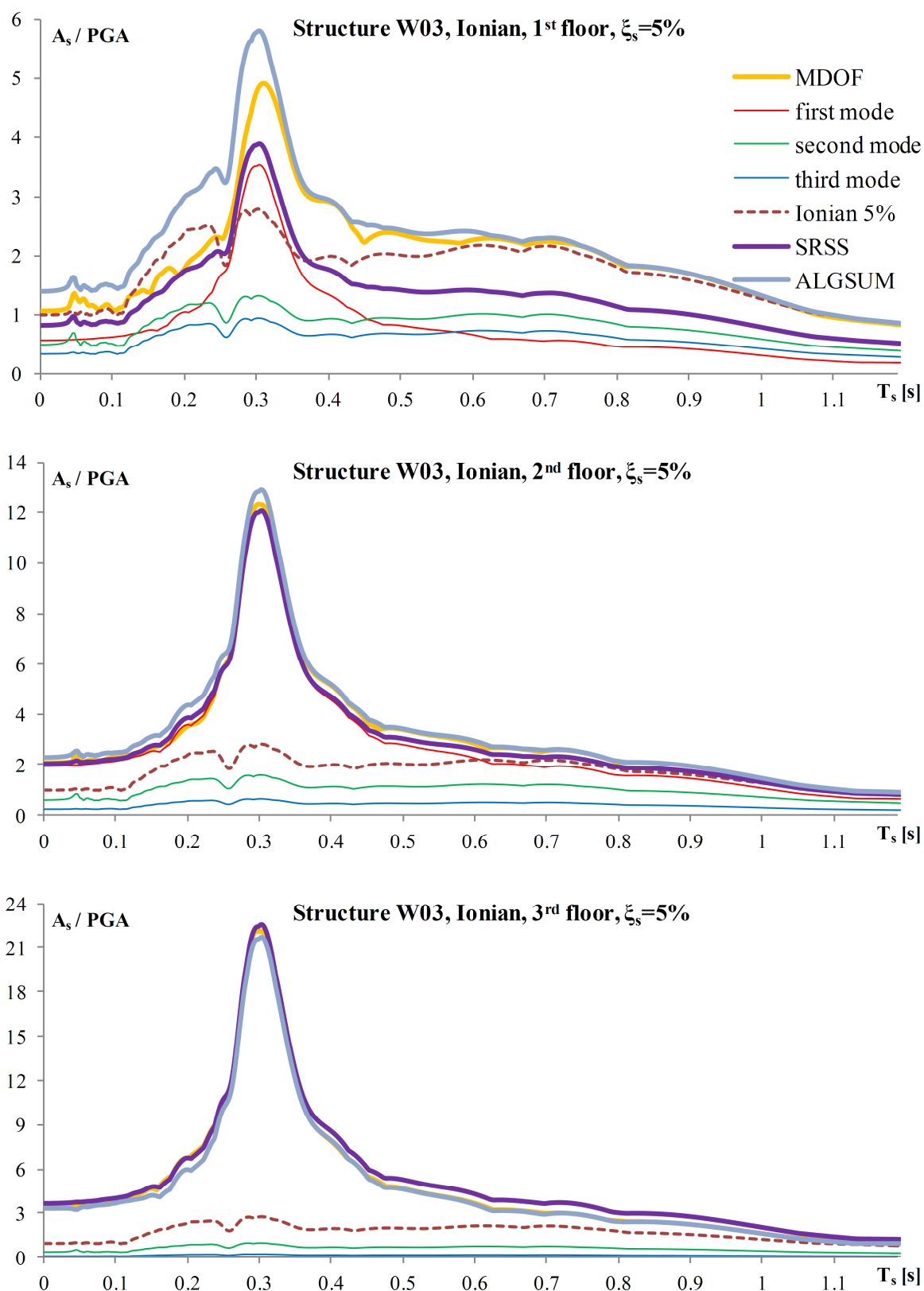


Figure 4.28: Ionian elastic spectrum and floor response spectra obtained for MDOF structure, individual modes and by using SRSS and ALGSUM combination rules (structure W03)

Slika 4.28: Ionian elastični spekter in etažni spektri odziva dobljeni za MDOF konstrukcijo, posamezne oblike in z uporabo SRSS in ALGSUM kombinacijskih pravil (konstrukcija W03)

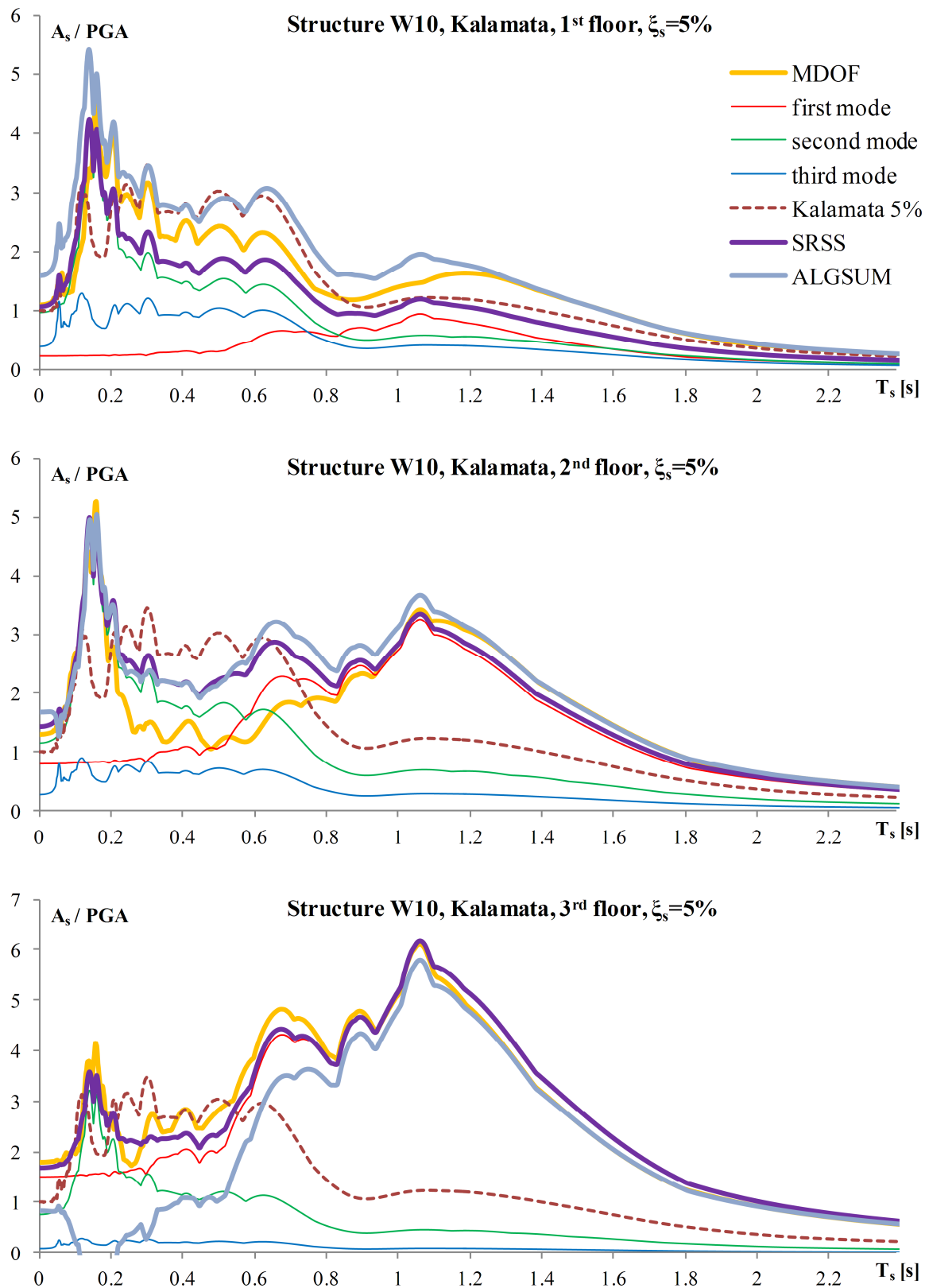


Figure 4.29: Kalamata elastic spectrum and floor response spectra obtained for MDOF structure, individual modes and by using SRSS and ALGSUM combination rules (structure W10)

Slika 4.29: Kalamata elastični spekter in etažni spektri odziva dobljeni za MDOF konstrukcijo, posamezne oblike in z uporabo SRSS in ALGSUM kombinacijskih pravil (konstrukcija W10)

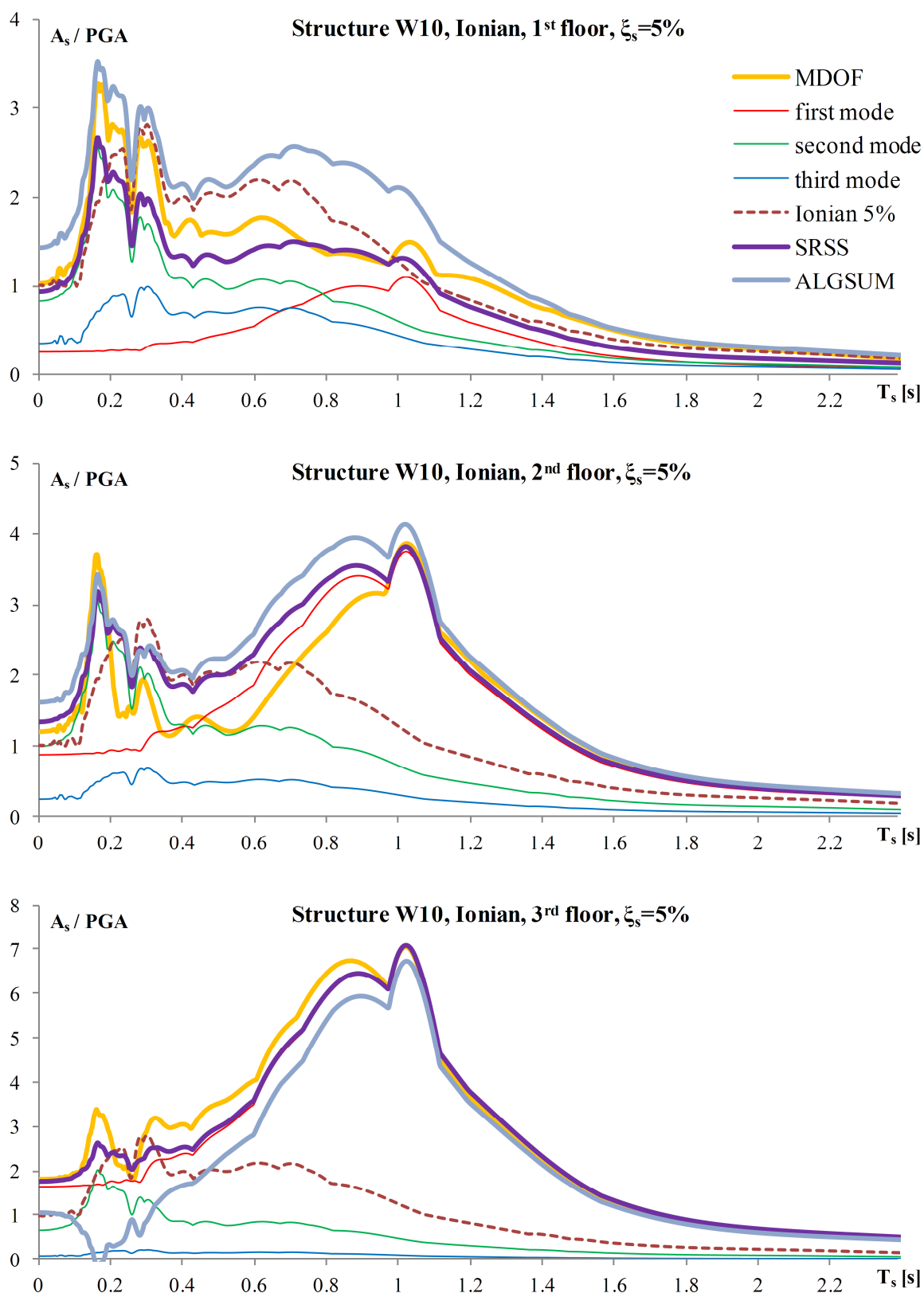


Figure 4.30: Ionian elastic spectrum and floor response spectra obtained for MDOF structure, individual modes and by using SRSS and ALGSUM combination rules (structure W10)

Slika 4.30: Ionian elastični spekter in etažni spektri odziva dobljeni za MDOF konstrukcijo, posamezne oblike in z uporabo SRSS in ALGSUM kombinacijskih pravil (konstrukcija W10)

Considering the amount of findings obtained in this chapter, it is convenient to make a brief summary.

Elastic MDOF structures

- The effects of higher modes turned out to be significant for both stiff (W03 and F03) and flexible (W10 and F10) structures, especially in lower storeys. It was observed that there were practically no peaks related to the modes with very high frequencies, i.e. above f_{ZPA} .
- It was observed that the floor response spectra approach to the ground motion spectra after $T_s/T_{p,i}=1$, as the ratio T_s/T_p decreases. By conducting modal RHAs on the structures W03 and W10 for two ground motions, absolute accelerations were determined for individual modes and they were used as an input for calculation of corresponding floor response spectra (for individual modes). It was observed that in the period range in which the natural periods of the equipment are larger than the natural period of the fundamental mode of the structure ($T_s > T_{p,i}$), the application of the algebraic summation rule (ALGSUM) on the individual floor response spectra produced floor response spectra which perfectly matched the floor response spectra obtained for MDOF structures.

Inelastic MDOF structures

- The applied seismic input was scaled in order to achieve different values of ductility (μ) and the nonlinear pushover-based N2 method was used for the determination of the achieved ductility by assuming the "first mode" height-wise distribution of lateral loads. For all considered cases, apart from the determination of the achieved ductility for inelastic modes, the corresponding components of inelastic mode shapes were also determined by the N2 method. It is very important to note that these results were later used in the validation of the proposed procedure for the direct determination of peak floor accelerations and for the validation of the direct method proposed for MDOF structures.
- The peak values of floor response spectra related to the fundamental mode are smaller than the corresponding peak values obtained for elastic structures. In the case of the EP model, the peaks occur close to the resonance, whereas in the case of the Q model, the peaks are shifted towards higher periods. Generally, the peak values of floor response spectra related to the fundamental mode show trends which were observed in the case of inelastic SDOF structures.
- In the case of the inelastic stiff structures (W03 and F03), it was observed that the peak values related to higher modes can be larger than the corresponding peak values obtained for elastic structures. An even more interesting observation is the existence of peaks related to the modes with frequency above f_{ZPA} .
- In the case of the inelastic flexible structures (W10 and F10), in certain cases, the peak values of floor response spectra related to the second mode are reduced in comparison with the peak values obtained for elastic structures. In such cases, it was observed that the resonance regions and peaks related to the second mode show similar trends to the resonance regions and peaks related to the fundamental mode, but with a notably smaller ductility. Therefore, the obtained results imply that in the case of flexible structures with a large number of modes, inelastic behaviour may influence several modes. In the case of the wall W10, with one plastic hinge at the bottom, it is obvious that the reduction of the spectral peaks cannot be connected with the inelastic behaviour related to the second mode. In the results obtained for the frame F10, for certain ground motions, it was observed that yielding can occur in columns at upper storeys, which clearly indicates that the inelastic behaviour is related to the second mode.

5 PEAK FLOOR ACCELERATIONS IN MULTI-DEGREE-OF-FREEDOM STRUCTURES

Peak floor acceleration (PFA) represents one of the most important parameters in the seismic design of the equipment. In this chapter a discussion of PFAs in elastic and inelastic multi-degree-of-freedom (MDOF) primary structures is presented. In addition, PFAs obtained from the parametric study of floor response spectra for MDOF structures (Chapter 4) are presented and compared with PFAs obtained directly from the proposed approach.

5.1 Introduction

In the seismic design of acceleration-sensitive equipment, PFA represents an unavoidable parameter which is, in majority of cases, the most important one. The PFA also represents a significant part in the floor response spectrum approach. Namely, it is a starting point of the floor response spectrum, i.e. the spectral value determined for infinitely rigid equipment.

When a structure is analysed by using the response-history analysis (RHA), the determination of PFAs is quite straightforward. In the case of modal response spectrum analysis, PFAs are determined for every considered mode by using some of the standard procedures (see e.g. Chopra 2012). Such determined PFAs should be combined with an appropriate modal combination rule in order to determine the total PFAs. The most common modal combination rules used in earthquake engineering are the SRSS and CQC rules, which generally produce good results for most response quantities (e.g. displacements and inter-storey drifts). Unfortunately, the results obtained from the SRSS and CQC rules are not satisfactory in the case of absolute accelerations, especially when the stiff MDOF structures are considered. The main reason for this is the fact that higher mode effects are more pronounced in the case of absolute accelerations than in the case of some other quantities (e.g. displacements). Therefore, in the case when modal analysis is used for the determination of PFAs, modal combination rules which are more appropriate than the SRSS and CQC rules should be applied.

USNRC 1.92 (2006) proposes several methods which are simple, easy to use and appropriate for modal combination of absolute floor accelerations obtained for individual modes. Nevertheless, it should be noted that they can be applied for modal combination of any response quantity. Before becoming a part of USNRC 1.92 (2006), these methods were examined and evaluated (see NUREG/CR-6645 1999). The combination methods which should be considered are the methods defined by Gupta and Lindley-Yow, coupled with the Missing Mass method. The application of these methods is fairly simple. Namely, modes with frequencies below f_{ZPA} (discussed in Subsection 4.2.1) are considered in a modal solution and Gupta's or Lindley-Yow method should be applied to them. The contribution of modes with frequencies above f_{ZPA} should be taken into account through an additional – substituting mode by using the Missing Mass method. The influence of this substituting mode on the system's response is calculated by performing a static analysis. Finally, the total response is obtained by combining the results from the modal solution (Gupta or Lindley-Yow) and from the Missing Mass method. A detailed overview of the USNRC 1.92 (2006) modal combination methods is presented in ANNEX F.

The direct determination of PFAs in elastic and inelastic MDOF structures, based on the above described modal combination approach, is presented in the following text. Nevertheless, it should be noted that such an approach, even though quite simple, may not always produce sufficiently accurate PFAs, primarily since absolute accelerations show great sensitivity when it comes to higher mode effects. It should be noted that a significant number of researchers have made an effort to develop

simplified approaches which may provide "more accurate" estimation of PFAs in elastic (see e.g. Miranda and Taghavi 2005, Singh et al. 2006, Kumari and Gupta 2007, Pozzi and Der Kiureghian 2012 and Moschen et al. 2014) and inelastic structures (see e.g. Rodriguez et al. 2002, Chaudhuri and Hutchinson 2011, Wieser et al. 2013 and Moschen et al. 2013). Up to this moment, none of these approaches has been widely accepted in practice. In addition, the seismic design of equipment is governed by different design codes, in which acceleration demands are also taken into account in terms of the PFA. An interesting simultaneous evaluation of several design codes was conducted by Pinkawa et al. (2014), who have concluded that an improvement of existing codes is needed in order to achieve more rational and reliable seismic design of equipment.

5.2 Estimation of peak floor accelerations in elastic and inelastic MDOF structures

In the case of MDOF structures analysed by using a modal response spectrum analysis, the PFA value for the mode i at the floor j (PFA_{ij}) can be obtained from Equation 5.1

$$PFA_{ij} = \Gamma_i \phi_{ij} \frac{S_e(T_{p,i}, \zeta_{p,i})}{R_\mu} \quad (5.1)$$

where S_e denotes a value in the input elastic acceleration spectrum, $T_{p,i}$ and $\zeta_{p,i}$ denote natural period and damping of the structure for the mode i , respectively, R_μ represents a reduction factor due to ductility (which was discussed in detail in Section 3.2), Γ_i represents modal participation factor for the mode i , whereas ϕ_{ij} is the value of the mode shape component for the mode i at the floor j .

It is important to note that in the case of elastic MDOF structures, R_μ amounts to 1.0 for all modes and that the values of $T_{p,i}$, Γ_i , and ϕ_{ij} determined in elastic modal analysis can be used.

In the case of inelastic MDOF structures, for modes in which structural response is nonlinear, the above mentioned quantities should be assumed. For the purpose of this study, the nonlinear pushover-based N2 method was used (see Fajfar 2000 or ANNEX D), as described in Section 4.2. The N2 method is a part of Eurocode 8 (2004) and it has been widely accepted in practice. Of course, any other appropriate approach/method can be used. When the N2 method is used for inelastic modes, it is important to underline that $S_e(T_{p,i}, \zeta_{p,i})$ should be replaced by $S_e(T_{p,i}^*)$, where $T_{p,i}^*$ denotes the effective natural period of the equivalent SDOF system (T^* in the N2 method, for details see ANNEX D), and that the values of ϕ_{ij} are determined from the inelastic deformed shape.

Equation 5.1 should be applied for modes with frequencies below f_{ZPA} (i.e. for the first n modes) and Gupta's or Lindley-Yow method should be used for the modal combination of the obtained PFAs. This can be simply described by Equation 5.2 (for more details on the application of Gupta's and Lindley-Yow method see ANNEX F).

$$Gupta \text{ or } Lindley\text{-}Yow(PFA_{ij}) \Big|_{i=1}^n \Rightarrow \begin{cases} PFA_{rigid,j}, & \text{Equation F.3 in Appendix F} \\ PFA_{periodic,j}, & \text{Equations F.4 in Appendix F} \end{cases} \quad (5.2)$$

In the case of modes with frequencies above f_{ZPA} , PFAs should be determined by using the Missing Mass method, which can be conducted by using Equation 5.3, whose general form is presented in ANNEX F (note that ZPA denotes zero period acceleration).

$$PFA_{mm,j} = \left\{ 1 - \sum_{i=1}^n \Gamma_i \phi_{ij} \right\} ZPA \quad (5.3)$$

Finally, the peak floor acceleration at the floor j is obtained from Equation 5.4.

$$PFA_j = \sqrt{\left(PFA_{rigid,j} + PFA_{mm,j} \right)^2 + \left(PFA_{periodic,j} \right)^2} \quad (5.4)$$

In the case of elastic structures, the accuracy of the above presented procedure depends on the accuracy of seismic input and on the accuracy of the approach used for the combination of the PFAs obtained for individual modes. In the case of inelastic structures, the accuracy of the estimated PFAs also depends on the accuracy of the method/approach used for the determination of the PFAs related to inelastic modes. Also, it should be noted that the modal superposition approach is fully justified in the case of elastic structures, whereas in the case of inelastic structures, it represents an approximation.

5.2.1 Results obtained for elastic MDOF structures

The validation of the proposed procedure for direct determination of PFAs was firstly conducted in the case of elastic MDOF structures, by using Gupta's method coupled with the Missing Mass method. All structures which were considered in the parametric study described in Chapter 4 (W03, W10, F03 and F10) were also considered in this subsection (Gupta's coefficients used in the combination process are presented in ANNEX F). Such obtained PFAs were compared with the mean PFAs obtained in the parametric study, as well as with the PFAs obtained by using the SRSS rule.

In all considered cases, as in the case of the RHA analysis (Chapter 4), Rayleigh damping amounted to 5% with respect to two first modes ($\zeta_{p,1} = \zeta_{p,2} = 5\%$). Equation 4.7 from Subsection 4.2.5 was used for the determination of damping values related to the third mode ($\zeta_{p,3}$). It amounted to 12% in the case of the structure W10 (already determined in Subsection 4.2.5), 9% in the case of the structure F03 and 7% in the case of the structure F10. In the case of the structure W03, the frequency of the third mode is larger than f_{ZPA} so the damping value of the third mode is irrelevant, i.e. the Missing Mass method was applied.

Seismic input was the mean elastic spectrum of the chosen set of ground motions which corresponds to the soil type B, and which was described in Sections 2.1 and 4.1. By using such "exact" input, approximations related to the difference between the mean and target ground motion spectra were eliminated, which provided a proper evaluation of the combination approach based on Gupta's and Missing Mass method, as well as the SRSS rule. It should be noted that spectral accelerations for the first two modes were obtained directly from the mean elastic input spectrum (which was calculated for 5% damping). In the case of the third mode, spectral accelerations were determined by taking into account damping values obtained for the third mode. Namely, the third mode of each structure was represented through an elastic SDOF oscillator with the corresponding natural period and damping. The RHA of each oscillator was conducted by using the set of ground motions which corresponds to the soil type B (for details see Section 2.1). Thus, spectral accelerations for the third mode of the structures W10, F03 and F10 were determined as the mean values of accelerations determined from the considered seismic input. Also note that the ZPA used in the Missing Mass method for the structure W03 is equal to the mean PGA of the input, which amounted to 0.43g.

The PFAs obtained from the proposed procedure (denoted as "direct (Gupta)") were compared with the mean PFAs obtained from the RHA (denoted as RHA) and from the SRSS rule (denoted as "direct (SRSS)"), as presented in Figure 5.1. All PFAs were normalized with the mean PGA of the applied input.

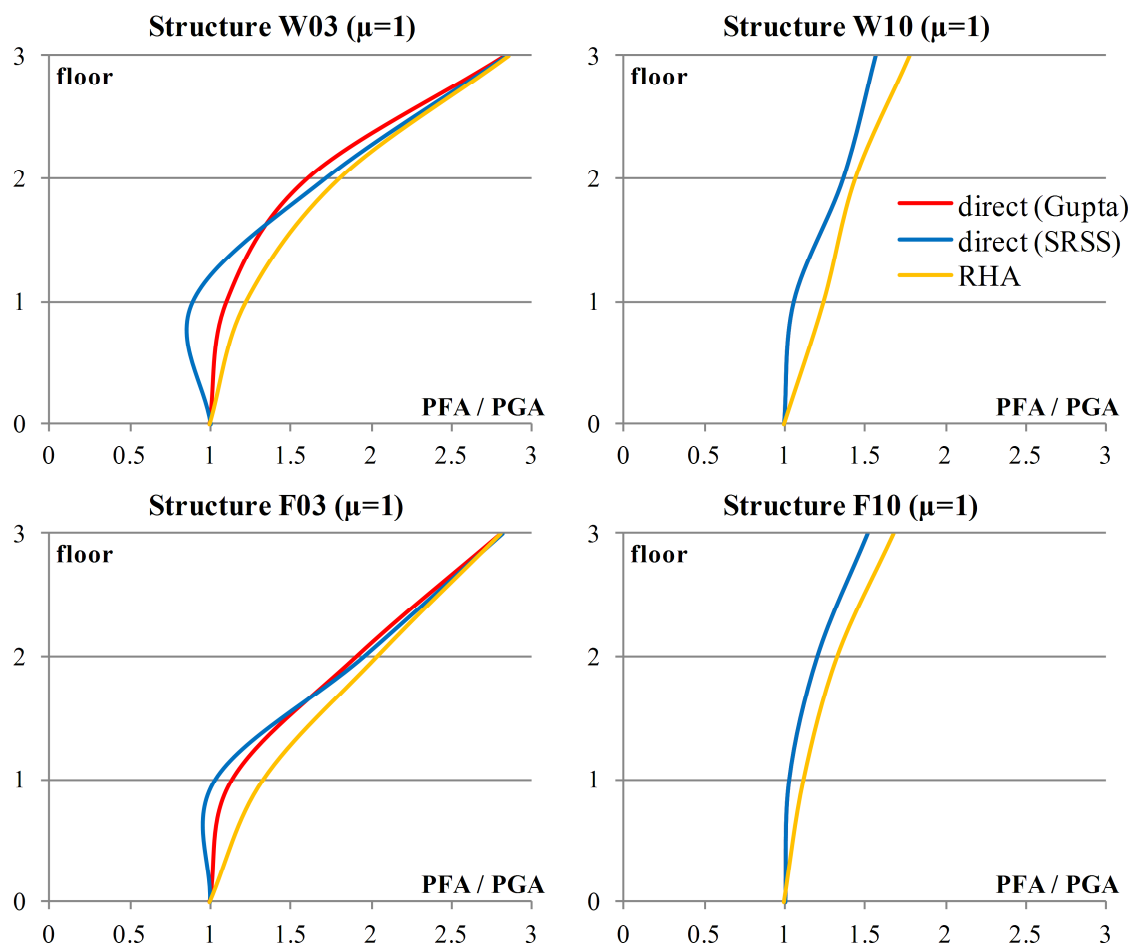


Figure 5.1: Peak floor accelerations of the elastic structures W03, W10, F03 and F10 normalized with the mean PGA, obtained directly (by using the "exact" input) and from the RHA

Slika 5.1: Maksimalni etažni pospeški elastičnih konstrukcij W03, W10, F03 in F10 normirani s povprečnim PGA, dobljeni direktno (ob uporabi »točnega« inputa) in iz RHA

From Figure 5.1, in the case of the structures W03 and F03, it can be observed that in the first storey both direct approaches led to non-conservative results and that Gupta's method is significantly more accurate than the SRSS rule, especially in the case of the structure W03. In the second storey, the SRSS rule produced slightly better results, which are still somewhat non-conservative in comparison with the results obtained from the RHA. In the third storey, both direct approaches produced practically the same results, which are in good agreement with the RHA results. In the case of the structures W10 and F10, there is no difference in the results obtained by using Gupta's method and the SRSS rule, which is a consequence of the fact that for structures with longer natural periods Gupta's method tends to become equivalent to the SRSS rule. This fact is important since it implies that Gupta's method is more general than the SRSS rule and that it should therefore be used instead of it, in all cases.

It is obvious that for all considered structures PFAs obtained directly are in all cases non-conservative in comparison with the mean PFAs obtained from the RHA, which implies that Gupta's method does not provide sufficiently accurate modal combination of accelerations. On the other hand, for the time being, there is no adequate alternative, since the method is simple and therefore quite appropriate for application. Nevertheless, it is clear that more research is needed on the subject of modal combination of absolute accelerations, which are obviously more sensitive than other quantities (e.g. displacements or inter-storey drifts).

In addition, the validation of the proposed procedure for direct determination of PFAs was also conducted by using the modified Eurocode 8 (2004) target spectrum, described in Section 4.1. Such approximate input incorporates approximations related to the difference between the mean and target ground motion spectra for natural periods larger than $T_B=0.15$ s (T_B is the lower limit of the constant spectral acceleration branch in Eurocode 8 2004 elastic spectrum). In the case of the structures W03 and F03, only the natural period of the first mode is larger than T_B (input approximation is related to the first mode), in the case of the structure W10, natural periods of the first two modes are larger than T_B (input approximation is related to the first and to the second mode), whereas in the case of the structure F10, all natural periods are above T_B (input approximation is related to all modes). For the direct determination of PFAs only Gupta's method was applied. The PFAs obtained directly by using the approximate input are presented in Figure 5.2 (denoted as "direct approx.") and they are compared with the mean PFAs obtained from the RHA (denoted as RHA). Also, the direct PFAs obtained by using Gupta's method and "exact" input (previously presented in Figure 5.1) are presented in Figure 5.2 (denoted as "direct "exact"") in order to point out the differences in the results obtained when using the "exact" and approximate input.

It can be observed from Figure 5.2 that in the case of the structures W03 and F03, in the first storey, there is practically no difference in the direct PFAs obtained by using different seismic inputs. This arises from the fact that in the first storey, the influence of the first mode, to which the input approximation is related to, is significantly smaller than the influence of the second and third mode (for which there is no input approximation). The increasing differences between the "direct approx." and "direct "exact" results observed in the second and third storey imply that the influence of the first mode increases along the height of the structures. From the results presented in Figure 5.2, it can also be seen that in the case of the structures W10 and F10 there is no significant difference between the direct PFAs obtained by using different seismic inputs, even though for these structures more input approximations are present than in the case of the structures W03 and F03. Apparently, the input approximations related to different modes have different signs so they tend to annul each other.

5.2.2 Results obtained for inelastic MDOF structures

The validation of the proposed procedure for direct determination of PFAs was also conducted in the case of inelastic MDOF structures, in the same manner as in the case of elastic MDOF structures (presented in the previous subsection), by using the modified Eurocode 8 (2004) target spectrum (described in Section 4.1) as seismic input. Thus, all approximations are now present in the direct determination of PFAs: seismic input, modal combination (Gupta's method was used, for combination coefficients see ANNEX F) and the nonlinear N2 method. It should be noted that for all considered structures, inelastic structural behaviour was considered only in the fundamental mode and that quantities used in Equation 5.1, which are related to the inelastic fundamental mode ($T_{p,1}^*$, $S_e(T_{p,1}^*)$, R_μ , $\Gamma_I(I)$ and ϕ_{Ij}), were determined in Section 4.2 by using the N2 method.

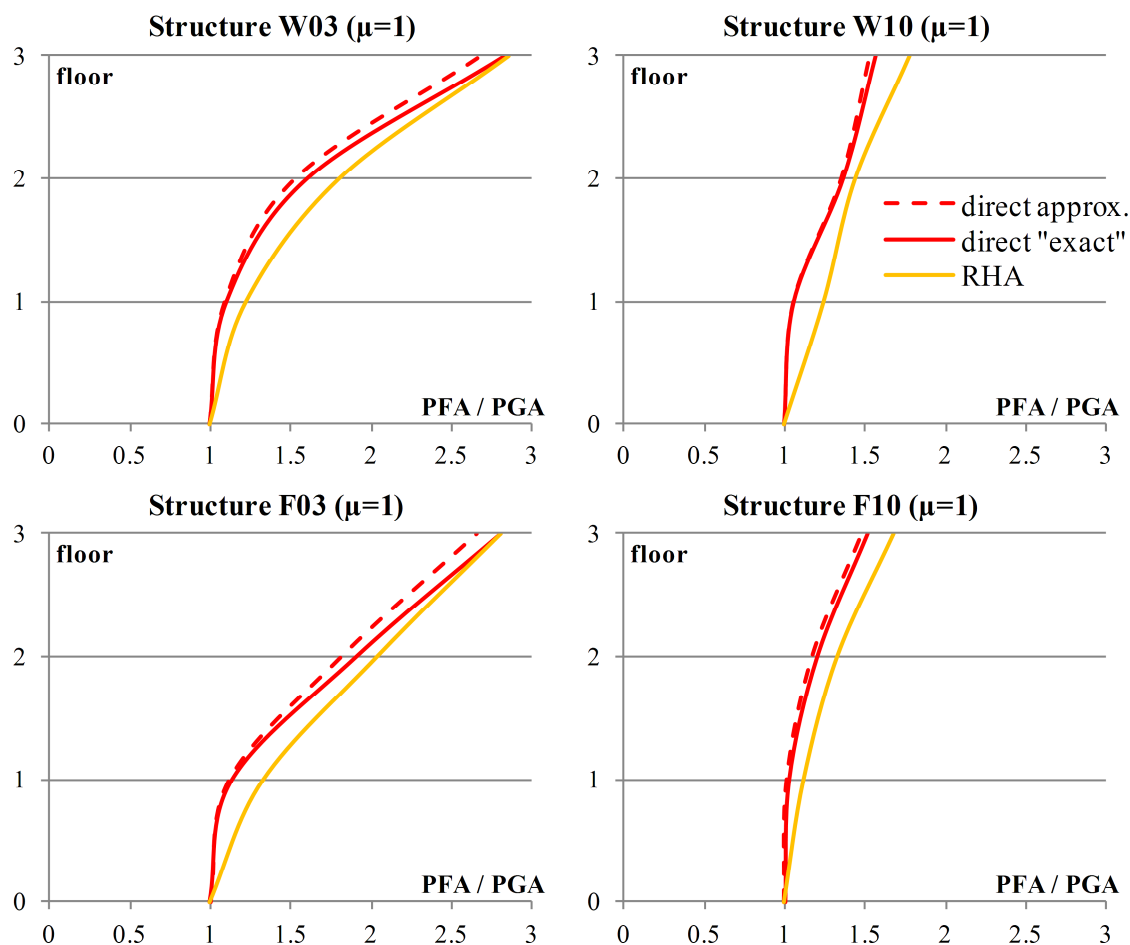


Figure 5.2: Peak floor accelerations of the elastic structures W03, W10, F03 and F10 normalized with the mean PGA, obtained directly (by using the approximate and "exact" input) and from the RHA

Slika 5.2: Maksimalni etažni pospeški elastičnih konstrukcij W03, W10, F03 in F10 normirani s povprečnim PGA, dobljeni direktno (ob uporabi približnega in »točnega« inputa) in iz RHA

The PFAs obtained from the proposed procedure (denoted as "direct") were compared with the mean PFAs obtained from the RHA (denoted as RHA), the mean PFAs plus standard deviation (denoted as $RHA + \sigma$), and the mean PFAs minus standard deviation (denoted as $RHA - \sigma$), as presented in Figures 5.3–5.6. Note that all PFAs were normalized with the PGA of the input.

In the case of the structure W03, the direct PFAs presented in Figure 5.3 are significantly lower than the PFAs obtained from the RHA. In several cases they are almost equal or even lower than the $RHA - \sigma$ results, which is quite unfavorable. Nevertheless, such conservatism was expected since it existed even in the case of the elastic W03 structure (see "direct approx" results in Figure 5.2). Obviously, structural inelasticity led to an additional deviation of the direct results. It is interesting that, for both hysteretic models and for all analysed ductilities, the shape of the height-wise distribution of the direct PFAs is very similar to the distribution of the PFAs obtained from the RHA.

From the results presented in Figure 5.4, obtained for the structure W10, it can be seen that the proposed direct approach produces satisfying agreement between the direct PFAs and the PFAs obtained from the RHA. The obtained results are somewhat better in the case of the Q_0 model. Interestingly, in several cases, PFAs obtained from the RHA are lower than the PGA.

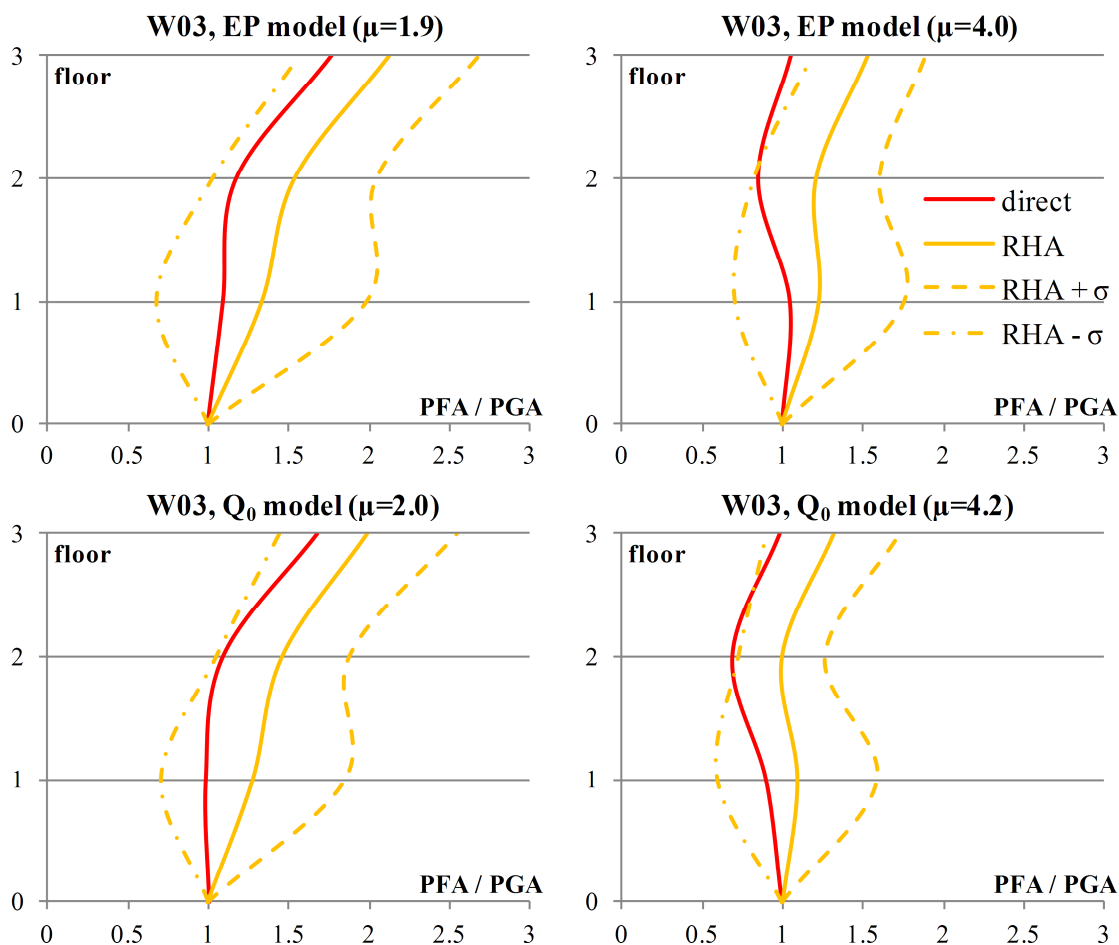


Figure 5.3: Peak floor accelerations of the inelastic structure W03 normalized with the PGA, obtained directly and from the RHA

Slika 5.3: Maksimalni etažni pospeški neelastične konstrukcije W03 normirani s PGA, dobljeni direktno in iz RHA

As in the case of the structure W03, the direct PFAs obtained in the case of the structure F03 are non-conservative comparing to the PFAs obtained from the RHA, which is mainly pronounced in the first and in the second storey, as shown in Figure 5.5. In the third storey, the estimation of PFAs is significantly better. The accuracy of the proposed direct approach is similar for both hysteretic models. The shape of the height-wise distribution of the PFAs obtained from the RHA is almost linear, which is quite interesting since it resembles the results obtained for elastic structures (see e.g. Figure 5.1).

In the case of the structure F10, from the results presented in Figure 5.6, it can be observed that the PFAs obtained from the proposed direct approach are in a fairly good agreement with the PFAs obtained from the RHA, especially in the case of higher ductilities. For all considered cases, the deviations from the RHA results are not substantial. In all cases except one (first storey of the Q_0 model, $\mu=2.2$), the PFAs obtained from the RHA are lower than the PGA (a similar phenomenon was also observed in the case of the structure W10).

From all results presented in Figures 5.3–5.6, it is obvious that in the case of inelastic structures, the proposed approach for the direct determination of PFAs generally produces slightly better results in the case of more flexible structures (W10 and F10).

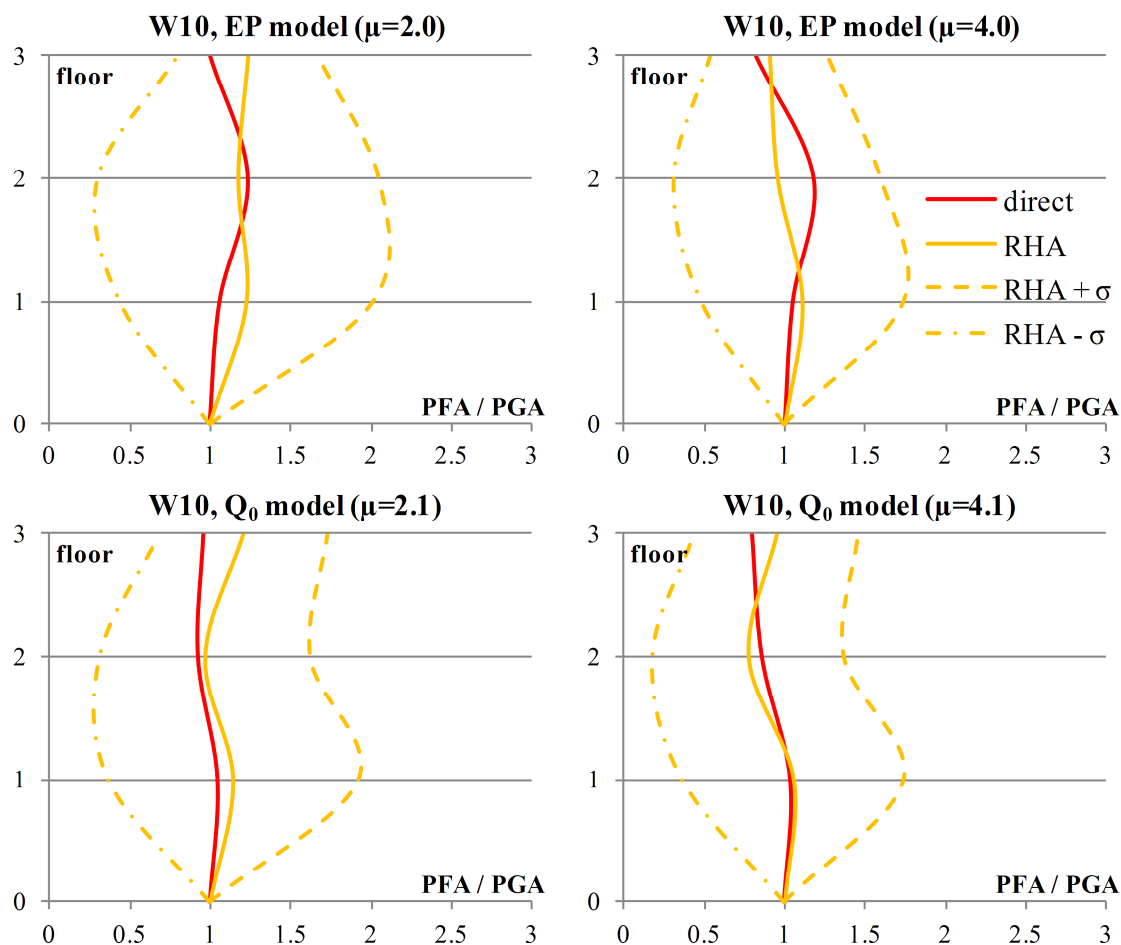


Figure 5.4: Peak floor accelerations of the inelastic structure W10 normalized with the PGA, obtained directly and from the RHA

Slika 5.4: Maksimalni etažni pospeški neelastične konstrukcije W10 normirani s PGA, dobljeni direktno in iz RHA

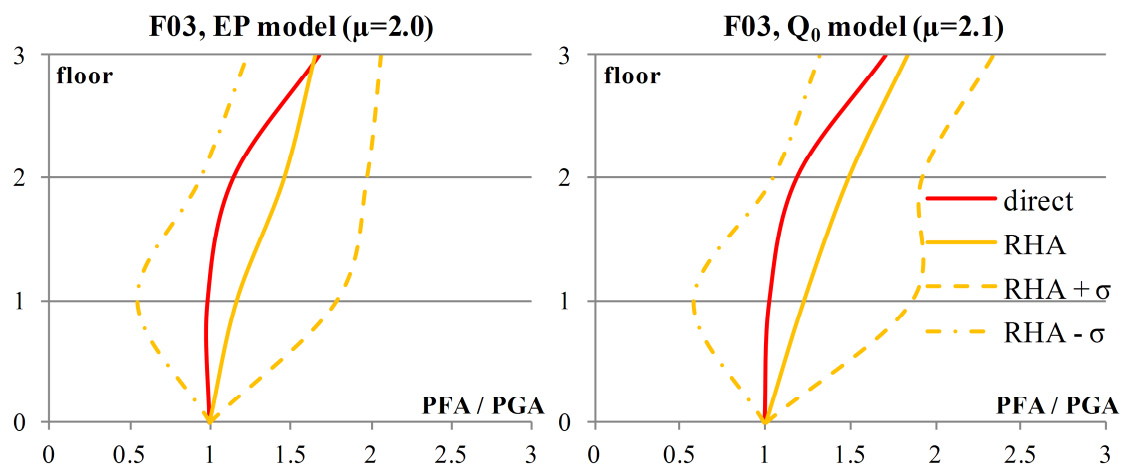


Figure 5.5: Peak floor accelerations of the inelastic structure F03 normalized with the PGA, obtained directly and from the RHA

Slika 5.5: Maksimalni etažni pospeški neelastične konstrukcije F03 normirani s PGA, dobljeni direktno in iz RHA

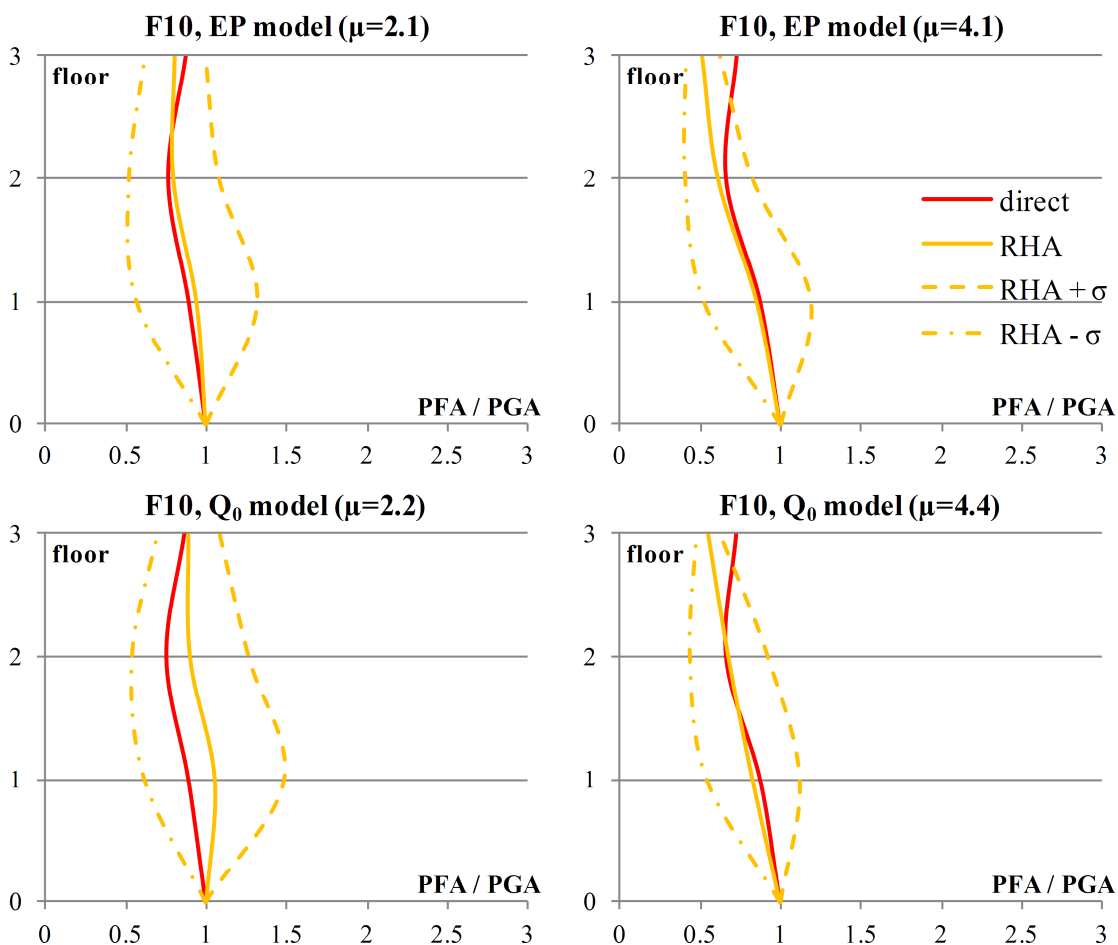


Figure 5.6: Peak floor accelerations of the inelastic structure F10 normalized with the PGA, obtained directly and from the RHA

Slika 5.6: Maksimalni etažni pospeški neelastične konstrukcije F10 normirani s PGA, dobljeni direktno in iz RHA

6 A METHOD FOR DIRECT GENERATION OF FLOOR RESPONSE SPECTRA FOR MULTI-DEGREE-OF-FREEDOM STRUCTURES

In this chapter a method for direct generation of floor response spectra for multi-degree-of-freedom (MDOF) primary structures is presented. The method is based on the previously developed method for SDOF structures (Chapter 3). The results obtained by the proposed method are compared with the results obtained in the parametric study of floor response spectra for MDOF structures (Chapter 4), which provides a proper evaluation of the method's accuracy.

6.1 Formulation of the direct method

6.1.1 Direct floor response spectra for individual modes

Modes with frequency below f_{ZPA}

The direct method proposed for inelastic SDOF structures (presented in Chapter 3) can be expanded to the case of inelastic MDOF structures in order to obtain the direct floor response spectra for individual modes.

- 1) In the pre- and post-resonance regions, floor response spectra values for the mode i at the floor j ($A_{s,ij}$) can be obtained from Equation 6.1 (which was derived in ANNEX E) as

$$A_{s,ij} = \frac{\Gamma_i \phi_{ij}}{\left| 1 - (T_{p,i}/T_s)^2 \right|} \sqrt{\left\{ (T_{p,i}/T_s)^2 \frac{S_e(T_{p,i}, \xi_{p,i})}{R_\mu} \right\}^2 + S_e(T_s, \xi_s)^2} \quad (6.1)$$

where $T_{p,i}$ and T_s denote natural periods of the structure for the mode i and of the equipment, respectively, $\xi_{p,i}$ and ξ_s denote damping coefficients of the structure for the mode i and of the equipment, respectively, S_e is a value in the input elastic acceleration spectrum, R_μ is a reduction factor due to ductility μ (discussed in Section 3.2), Γ_i represents modal participation factor for the mode i , whereas ϕ_{ij} is the value of the mode shape component for the mode i at the floor j .

In the case of infinitely rigid equipment ($T_s=0$), Equation 6.1 becomes equal to Equation 5.1, i.e. the floor response spectrum value $A_{s,ij}$ is equal to the peak floor acceleration for the mode i at the floor j (PFA_{ij}).

In the case of the EP model, in the post-resonance region, the ratio $T_{p,i}/T_s$ in Equation 6.1 should be replaced by the ratio $T_{p,i}^*/T_s$ (the determination of $T_{p,i}^*$ is discussed below). In the case of the stiffness degrading Q model, also in the post-resonance region, the ratio $T_{p,i}/T_s$ in Equation 6.1 should be replaced by the ratio $T_{p,i,\mu}/T_s$, where $T_{p,i,\mu}$ represents the effective natural period of the structure. It depends on the inelastic deformation expressed in terms of ductility μ and it can be approximately determined from Equation 6.2.

$$T_{p,i,\mu} = T_{p,i}^* \sqrt{\frac{1 + \sqrt{\mu + \mu}}{3}} \quad (6.2)$$

- 2) In the resonance regions, the spectral values $A_{s,ij}$ should be limited to the values obtained from Equation 6.3. The amplification factors AMP_i are defined by Equations 6.4 and 6.5.

$$A_{s,ij} = AMP_i \Gamma_i \phi_{ij} \frac{S_e(T_{p,i}, \xi_{p,i})}{R_\mu} \quad (6.3)$$

Note that in the case of elastic MDOF structures, R_μ amounts to 1.0 for all modes and that the values of $T_{p,i}$, Γ_i , and ϕ_{ij} determined in elastic modal analysis are used in Equations 6.1 and 6.3.

As previously discussed in Section 5.2, in the case of inelastic MDOF structures, for modes in which structural response is nonlinear, the above mentioned quantities can be determined by the N2 method (for details see Fajfar 2000 or ANNEX D), as described in Section 4.2. Again, any other suitable approach/method is applicable. When the N2 method is used for inelastic modes, it is important to underline that $S_e(T_{p,i}, \xi_{p,i})$ should be replaced by $S_e(T_{p,i}^*)$, where $T_{p,i}^*$ denotes the effective natural period of the equivalent SDOF system (i.e. T^* in the N2 method, for details see ANNEX D), and that the values of ϕ_{ij} are determined from the inelastic deformed shape.

In the case of the EP model, AMP_i can be determined as (ξ_s should be entered as a percentage)

$$AMP_i = \left\{ \begin{array}{ll} 2.5\sqrt{10/(5+\xi_s)}, & T_{p,i}/T_C = 0 \\ \text{linear between } AMP_i(T_{p,i}/T_C = 0) \text{ and } AMP_i(T_{p,i}/T_C = 0.20), & 0 < T_{p,i}/T_C < 0.20 \\ 18(1+\xi_s)^{-0.60}, & 0.20 \leq T_{p,i}/T_C \leq 1 \\ 18(1+\xi_s)^{-0.60} (T_{p,i}/T_C)^{-0.20}, & T_{p,i}/T_C > 1 \end{array} \right\} \quad (6.4)$$

In the case of the Q model, AMP_i can be determined as (ξ_s should be entered as a percentage)

$$AMP_i = \left\{ \begin{array}{ll} 2.5\sqrt{10/(5+\xi_s)}, & T_{p,i}/T_C = 0 \\ \text{linear between } AMP_i(T_{p,i}/T_C = 0) \text{ and } AMP_i(T_{p,i}/T_C = 0.20), & 0 < T_{p,i}/T_C < 0.20 \\ 18(1+\xi_s)^{-0.60} (0.6+0.4\mu)\mu^{-0.85}, & 0.20 \leq T_{p,i}/T_C \leq 1 \\ 18(1+\xi_s)^{-0.60} (T_{p,i}/T_C)^{-0.20} (0.6+0.4\mu)\mu^{-0.85}, & T_{p,i}/T_C > 1 \end{array} \right\} \quad (6.5)$$

In Equations 6.4 and 6.5 T_C denotes the characteristic period of the ground motion.

Finally, the following should be noted. Structural inelasticity is often related only to the fundamental mode. In the proposed direct method structural inelasticity can be taken into account also in higher modes. In such cases, the corresponding values of R_μ and μ determined for these modes should be taken into account in the application of the direct method. Whether a considered higher mode is inelastic or not is a question that cannot be answered with certainty. It depends on many parameters such as: natural periods of the structure, characteristic period of the seismic input (T_C), amount of the ductility present in the fundamental mode, etc. Unfortunately, it is still not possible to propose a rational and reliable approach which would lead to an answer regarding this subject. Nevertheless, by taking into account the results obtained in the dissertation, it is reasonable to assume that inelastic

structural behaviour will be present in the second mode if the natural period of the fundamental mode ($T_{p,1}$) is larger than T_C and the ductility demand (μ) in the fundamental mode is high.

Modes with frequency above f_{ZPA}

All modes with frequency above f_{ZPA} are taken into account through a single, substituting mode. The direct floor response spectrum for this mode is determined from Equation F.12 shown in ANNEX F.

6.1.2 Combination of direct floor response spectra obtained for individual modes

In the proposed direct method for MDOF structures, floor response spectra are determined for each mode separately. In order to determine the resulting direct floor response spectra, a combination of the direct floor response spectra calculated for individual modes is needed. The modal superposition approach is fully justified in the case of elastic structures, whereas in the case of inelastic structures it represents an approximation. In the study, it was discovered that the SRSS rule produces rather poor results when it is applied for the combination of floor response spectra. Combination methods which are considered appropriate for the purpose of floor response spectra are the methods defined by Gupta and Lindley-Yow, coupled with the Missing Mass method (as proposed in USNRC 1.92 2006). These methods were already discussed and applied in Chapter 5 and explained in detail in ANNEX F. Unfortunately, neither of these methods works well in the whole period range, which is discussed below.

In the case of longer natural periods of the equipment T_s , a floor response spectrum is controlled by the ground motion spectrum. This can be observed in the results of the response-history analysis (RHA) conducted on SDOF structures (see Section 2.3). The same phenomenon can also be observed in the case of MDOF structures, as discussed in Subsection 4.2.5. It has a theoretical background and it can be easily explained. Let us first consider a SDOF structure and Equation 3.9 in Section 3.2. If T_s becomes large, the ratio T_p/T_s approaches to zero. At $T_p/T_s=0$ Equation 6.6 applies

$$A_s = S_e(T_s, \xi_s) \quad (6.6)$$

where A_s is the value in the floor acceleration spectrum for SDOF structure and S_e is a value in the input elastic acceleration spectrum.

Similarly, for the mode i and the floor j of a MDOF structure, by taking into account a large value of T_s in Equation 6.1, the ratio $T_{p,i}/T_s$ approaches to zero and, in the limit case, Equation 6.7 applies.

$$A_{s,ij} = \Gamma_i \phi_{ij} S_e(T_s, \xi_s) \quad (6.7)$$

From Equation 6.7 it is obvious that the value of $A_{s,ij}$ can be either positive or negative. This fact was previously mentioned in Subsection 4.2.5, in which the algebraic summation rule (ALGSUM) was used for the combination of floor response spectra obtained for individual modes for considered elastic structures. In Subsection 4.2.5 it was shown that the application of the ALGSUM rule in the period range shortly after the resonance related to the fundamental mode ($T_s > T_{p,1}$) produced a perfect match between the combined floor response spectra and the floor response spectra obtained by considering MDOF structures (see Figures 4.27–4.30). This fact was of great importance for the development of the direct method presented in this chapter, and an attempt to explain it is made in the following text.

If the total number of modes of an elastic MDOF structure is denoted by N , the following relationship can be obtained (derivation is presented in ANNEX G):

$$\sum_{i=1}^N \Gamma_i \phi_{ij} = 1 \quad (6.8)$$

Equation 6.8 implies that if the algebraic summation rule is applied at each floor of an elastic MDOF structure and all modes are taken into account, for large values of T_s , a floor response spectrum becomes equal to the ground motion spectrum (which was presented through the results in Subsection 4.2.5, see Figures 4.27–4.30). For the floor j this can be written as:

$$A_{s,j} = S_e(T_s, \xi_s) \sum_{i=1}^N \Gamma_i \phi_{ij} = S_e(T_s, \xi_s) \quad (6.9)$$

The application of the algebraic summation rule (ALGSUM) was an assumption, which led to the relationship defined by Equation 6.9, and the results obtained in the parametric study of floor response spectra (Subsection 4.2.5) confirm this assumption. It should be noted that the ALGSUM, even though rarely used in the response spectrum analysis, is applied in the RHA. Obviously, when it comes to floor response spectra and flexible equipment, the application of the ALGSUM is justified.

The conducted analyses indicated that the combination methods proposed by USNRC 1.92 (2006) should be applied in the period range of the floor response spectrum where the ratios $T_{p,i}/T_s$ do not approach zero (i.e. where acceleration of the structure has a significant influence on the floor response spectrum) and that the ALGSUM should be applied in the period range where the ratios $T_{p,i}/T_s$ approach zero (i.e. where the floor response spectrum is controlled by the ground motion spectrum).

The peak of the floor response spectrum which is related to the fundamental mode of the structure is the one which is the "closest" to the large values of T_s . Therefore, in the case of the fundamental mode, the influence of structural acceleration on the floor response spectrum is present for significantly larger values of T_s in comparison with the influence of structural accelerations produced by higher modes, which disappears shortly after the resonance region of the considered higher mode (i.e. after $T_{p,i} \approx T_s$). In other words, in the case of higher modes, the ratio $T_{p,i}/T_s$ soon approaches zero (usually long before the peak related to the first mode is reached) and Equation 6.7 becomes valid.

Based on the above discussion, it is proposed to conduct the following steps in order to obtain the resulting direct floor response spectrum:

- 1) In the period range between $T_s=0$ and the end of the resonance plateau of the direct floor response spectrum related to the fundamental mode, combine the direct floor response spectra calculated for individual modes by using one of the USNRC 1.92 (2006) methods, as shown in Figure 6.1.
- 2) In the period range after the resonance related to the fundamental mode (i.e. after $T_s/T_{p,i}=1$), combine the direct floor response spectra calculated for individual modes from the formula for the post-resonance region by using the ALGSUM rule, as shown in Figure 6.1.
- 3) Combined spectra from steps 1 (USNRC) and 2 (ALGSUM) should be linked. If they intersect (see Figure 6.1a), then the linking point is determined by the intersection. If there is no intersection, the plateau obtained in step 1 should be extended towards the larger periods of

equipment in order to obtain an intersection with the floor response spectrum determined in step 2 (see Figure 6.1b).

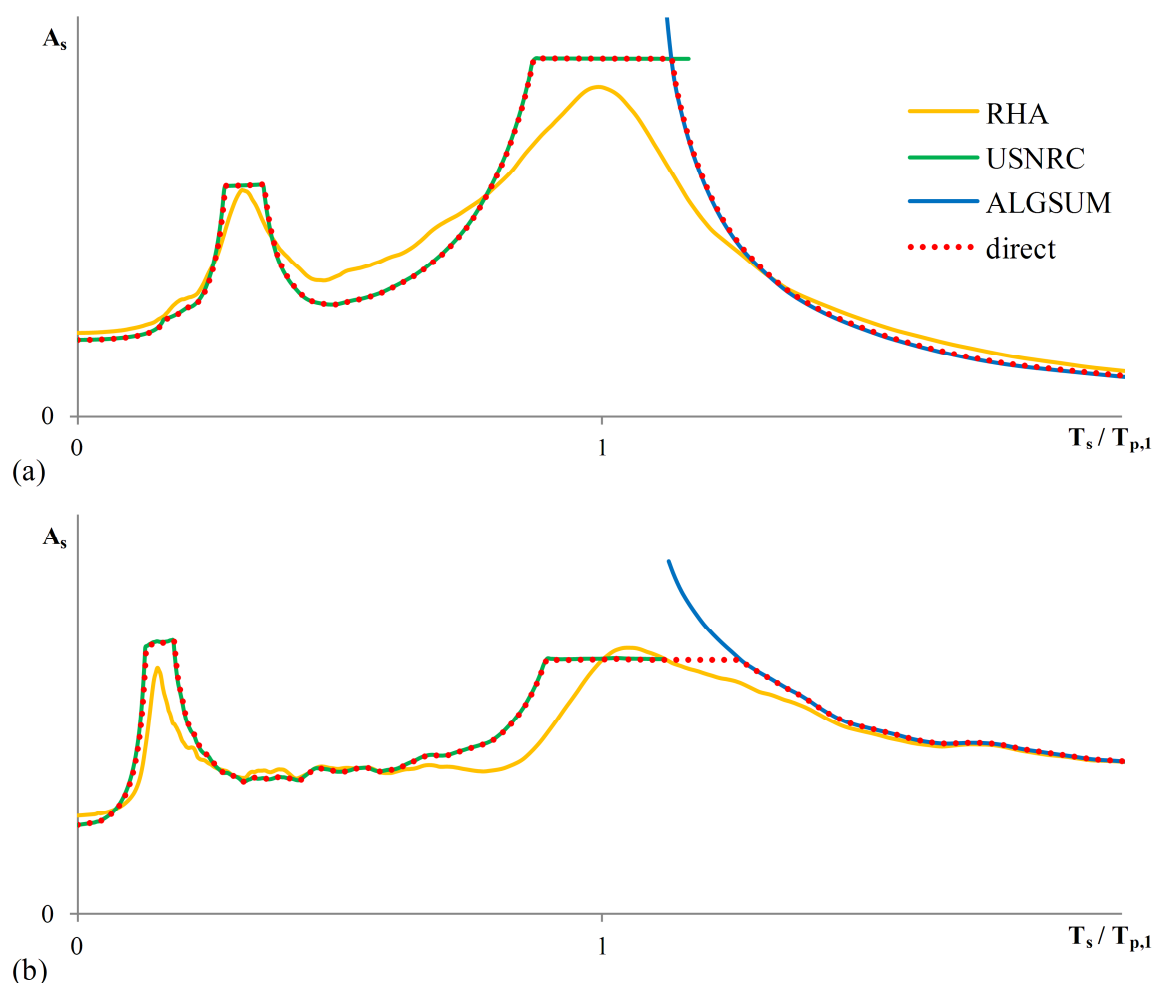


Figure 6.1: Linking of floor response spectra obtained by USNRC 1.92 (2006) methods and the ALGSUM rule

Slika 6.1: Povezava etažnih spektrov odziva dobljenih z USNRC 1.92 (2006) metodo in ALGSUM pravila

6.2 Validation of the proposed method – elastic structures

The validation of the proposed direct method for MDOF structures was firstly conducted by taking into account elastic MDOF structures, and the results obtained from the direct method were compared with the results obtained in the parametric study (see Chapter 4). All MDOF structures which were considered in the parametric study (W03, W10, F03 and F10) were also considered in this section.

In the direct method, as in the case of the RHA analyses (Chapter 4), Rayleigh damping amounted to 5% with respect to two first modes ($\zeta_{p,1}=\zeta_{p,2}=5\%$), whereas "mass-proportional" damping amounted to 1 and 5% in the case of the equipment (ζ_s). In the validation of the direct method, Gupta's combination method coupled with the Missing Mass method was used (see USNRC 1.92 2006 and ANNEX F). Since the damping value is needed for each considered mode with the frequency below f_{ZPA} , Equation 4.7 from Subsection 4.2.5 was used for the determination of the damping values related to the third mode ($\zeta_{p,3}$). It amounted to 12% in the case of W10 (already determined in Section 4.2.5), 9% in the case of F03 and 7% in the case of F10 (already determined in Subsection 5.2.1). In the case of the

structure W03, the frequency of the third mode is larger than f_{ZPA} , so the damping value of the third mode is not important, i.e. the Missing Mass method was applied.

Seismic input for the direct method was the mean elastic spectrum of the chosen set of ground motions which corresponds to the soil type B (see Sections 2.1 and 4.1). By using such input, approximations related to the difference between the mean and target ground motion spectra were eliminated, which allowed a proper evaluation of the proposed direct method. It should be noted that spectral accelerations for the first two modes were obtained directly from the mean elastic input spectrum (which was calculated for 5% damping). The determination of spectral accelerations which correspond to the third mode (for which the damping values are different than 5%) was described in Subsection 5.2.1. Also note that Equation F.12 from ANNEX F was used in the Missing Mass method in the case of the structure W03.

Figures 6.2–6.9 show the mean (denoted as RHA) and the mean plus standard deviation (denoted as $RHA + \sigma$) values of the floor response spectra obtained in the parametric study (i.e. by using the RHA), as well as the spectra computed by the proposed direct method (denoted as "direct"). As discussed in Sections 3.3 and 3.4, due to uncertainties related to the determination of the natural periods of the structure, the RHA spectra should be broadened in the resonance regions (see USNRC 1.122 1978 and ASCE 4-98 2000). In this section the broadening procedure was applied only in the case of the structure W03 (denoted as "RHA broadened" in Figures 6.2 and 6.3). Even though in the case of other structures broadening of spectral peaks was omitted, it should be noted that it would produce the results similar to the ones obtained for the structure W03. All spectra presented in Figures 6.2–6.9 were normalized with the mean PGA of the input, which amounted to 0.43g.

Generally, it can be observed that for all considered elastic structures, at all storeys and in the whole period range, the proposed direct method produced floor response spectra which are in good agreement with the floor response spectra obtained from the RHA. This agreement suggests that the proposed method is able to closely predict the approximate floor response spectra in the case of elastic MDOF primary structures.

6.3 Validation of the proposed method – inelastic structures

The validation of the proposed direct method for MDOF structures was also conducted in the case of inelastic MDOF structures, in the same manner as in the case of elastic MDOF structures presented in the previous section. The only difference was the input, which in this case was the modified Eurocode 8 (2004) target spectrum (described in Section 4.1). It should be noted that for all considered structures, inelastic behaviour was considered only in the fundamental mode and that quantities used in Equations 6.1–6.3 and 6.5, which are related to the inelastic fundamental mode, were determined in Section 4.2 by using the N2 method ($T_{p,1}^*$, $S_e(T_{p,1}^*)$, R_μ , μ , Γ_1 (Γ) and ϕ_{1j}).

Figures 6.10–6.37 show the mean (denoted as RHA) and the mean plus standard deviation (denoted as $RHA + \sigma$) values of the floor response spectra obtained in the parametric study (i.e. by using the RHA), as well as the spectra computed by the proposed direct method (denoted as "direct"). All spectra presented in Figures 6.10–6.37 were normalized with the PGA of the input.

In the case of the structure W03 (Figures 6.10–6.17), it is obvious that the direct method produced good results in the resonance region related to the fundamental mode, as well as in the post-resonance region where the ALGSUM rule was applied. In the resonance region related to the second mode, the

results obtained from the proposed method are non-conservative, which is mainly a consequence of the fact that an amplification of the second mode occurred, as discussed in Section 4.2.1, as well as of the significant scatter related to the seismic input, which is discussed in ANNEX H. In the period range between the resonance regions related to the first and second mode, the proposed direct method generally produced sufficiently accurate results.

From the results obtained for the structure W10 (Figures 6.18–6.25), it is obvious that the proposed direct method generally produced fairly good results in the whole period range. It should be noted that in the resonance region related to the second mode, for both hysteretic models and higher ductility demand μ (which amounted to 4.0 in the case of the EP model and to 4.1 in the case of the Q_0 model), the proposed method provided slightly conservative plateaus. This arises from the fact that some moderate amount of structural inelasticity exists in the second mode, as discussed in Section 4.2.2.

From Figures 6.26–6.29, which present the results obtained for the structure F03, it can be seen that the proposed direct method produced very good results in the case of the EP model, almost in the whole period range. Some slight deviations can be observed in the case of very stiff equipment in the second storey, where the results obtained from the direct method are somewhat non-conservative. In the case of the Q_0 model, the direct method provided good results in the resonance region related to the fundamental mode, as well as in the post-resonance region (where the ALGSUM rule is applied). In the resonance region related to the second mode, the results obtained from the proposed method slightly deviate from the results obtained from the RHA, mainly due to the fact that spectral peaks in the RHA results are slightly shifted towards higher periods, as mentioned in Section 4.2.3.

In the case of the structure F10 (Figures 6.30–6.37), it can be seen that in the case of the EP model and the lower ductility demand ($\mu=2.1$), the proposed direct method produced fair results in the whole period range with somewhat conservative plateaus related to the first and second mode. In the case of the EP model and the higher ductility demand ($\mu=4.1$), the obtained results are quite accurate in the resonance regions related to the first and third mode at all storeys, whereas the plateaus related to the second mode are very conservative, again at all storeys. In the case of the Q_0 model, the accuracy of the method varies, i.e. it depends on the period range, storey of the structure, and damping of the equipment. The accuracy is not satisfactory mostly in the resonance region related to the second mode. A detailed check of the RHA results has shown that the response of the structure F10 in the second mode is inelastic in the case of some ground motions. Therefore, the assumption used in the proposed direct method, that the response in higher modes is elastic, yields conservative results. Further research is needed in order to improve the accuracy of the results of the direct method in the cases when inelasticity occurs in higher modes. Some attempts have been made to take into account the reduction of accelerations due to inelastic behaviour in higher modes (see Section 4.2.4), but the results have not improved much. There is also a danger that the approach would become too complex for practical application. Thus, it seems to be reasonable that, for the time being, the assumption of elastic behaviour in higher modes is used.

From the obtained results it can be observed that, in general, satisfactory accuracy of the direct floor response spectra can be achieved. It should be underlined that in the case of inelastic structures various input parameters influence structural response, which makes its accurate prediction very hard. Among these parameters, seismic input represents an important part. The seismic input used in this study consisted of ground motions with quite different intensities. A brief analysis of scatter related to the seismic input and floor response spectra is presented in ANNEX H.

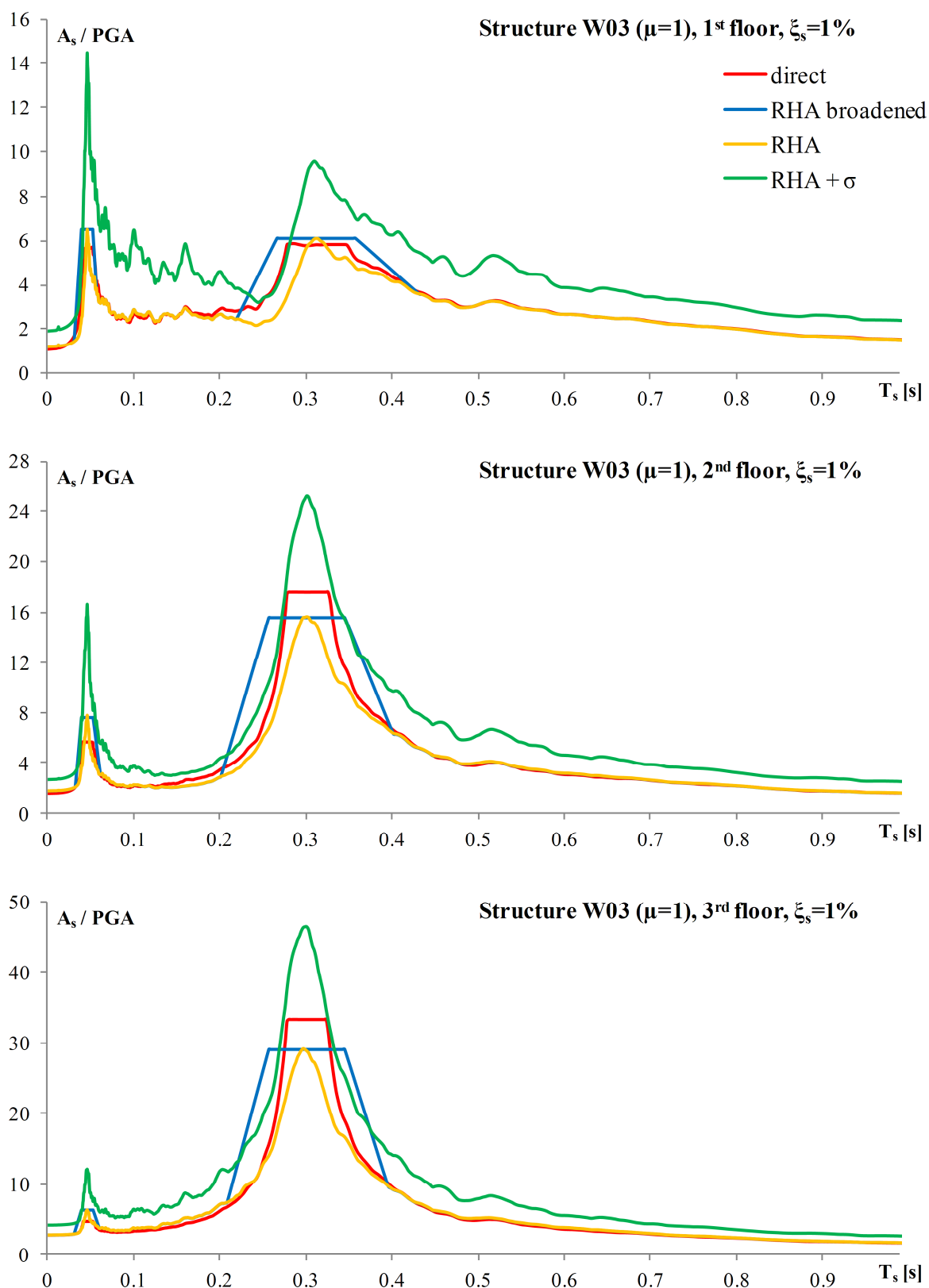


Figure 6.2: Floor response spectra for the elastic model of the structure W03 normalized with the mean PGA of the input, for 1% damping of the equipment

Slika 6.2: Etažni spektri odziva za elastičen model konstrukcije W03 normirani s povprečnim PGA inputa, za 1% dušenja opreme

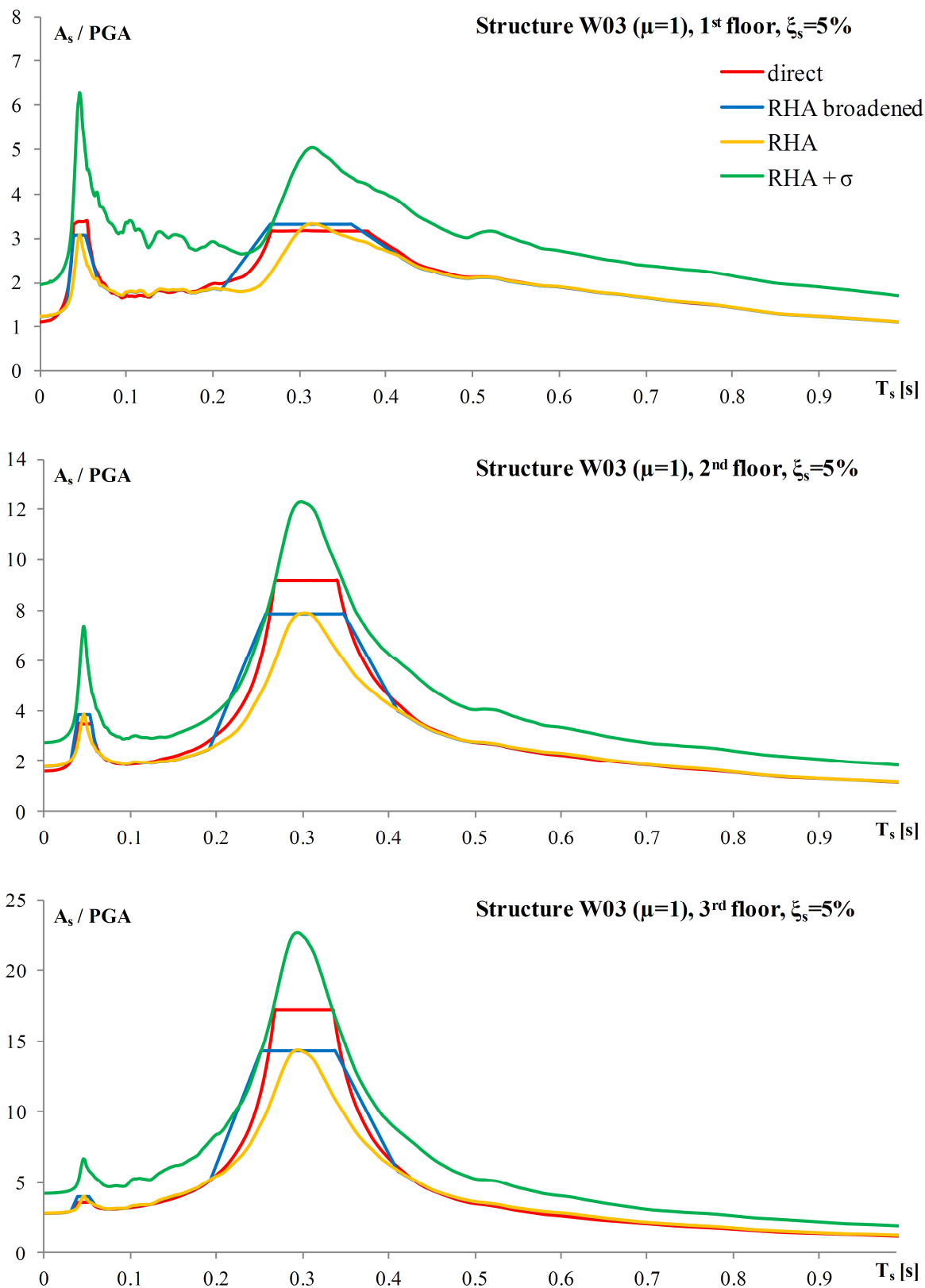


Figure 6.3: Floor response spectra for the elastic model of the structure W03 normalized with the mean PGA of the input, for 5% damping of the equipment

Slika 6.3: Etažni spektri odziva za elastičen model konstrukcije W03 normirani s povprečnim PGA inputa, za 5% dušenja opreme

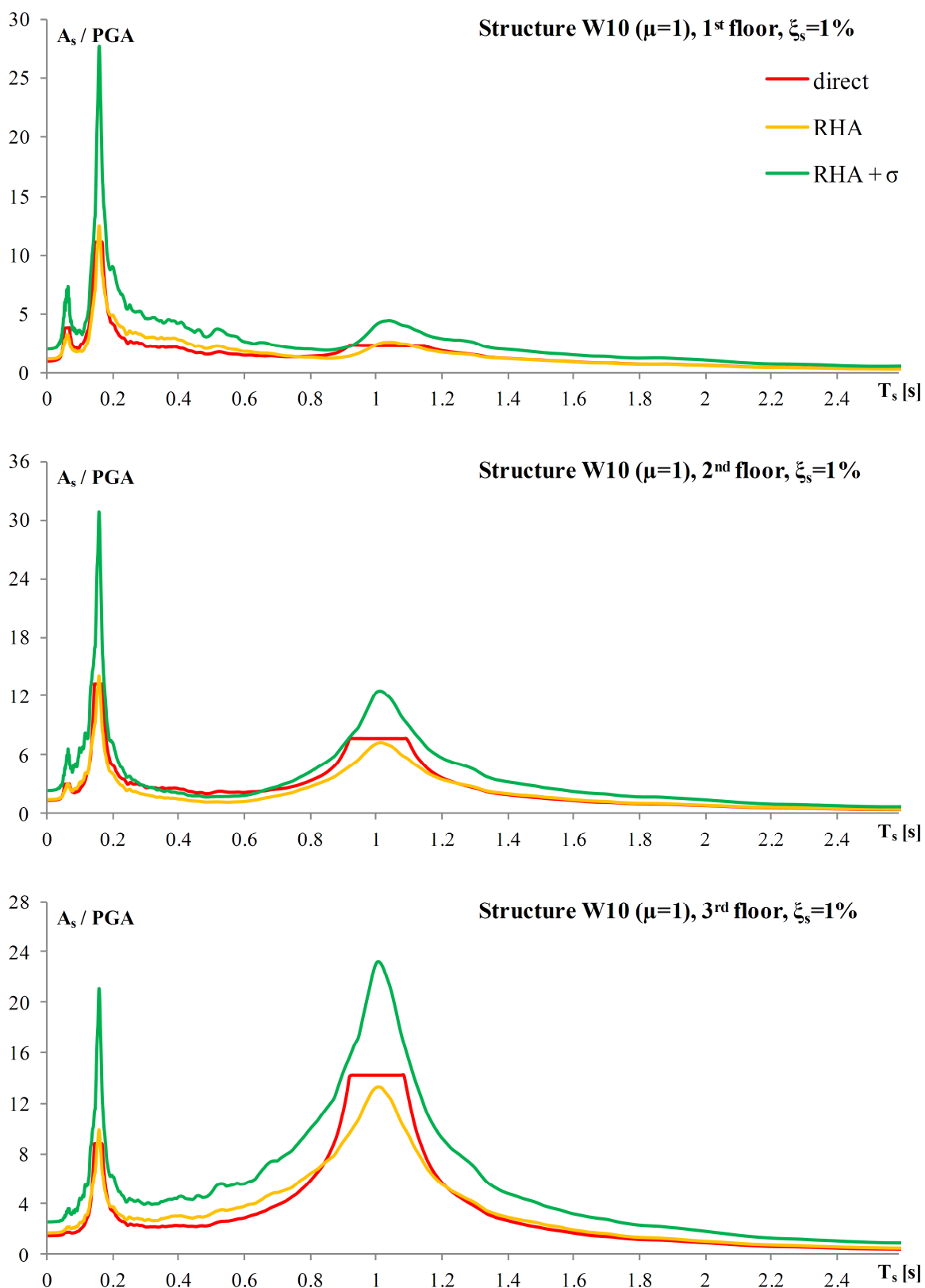


Figure 6.4: Floor response spectra for the elastic model of the structure W10 normalized with the mean PGA of the input, for 1% damping of the equipment

Slika 6.4: Etažni spektri odziva za elastičen model konstrukcije W10 normirani s povprečnim PGA inputa, za 1% dušenja opreme

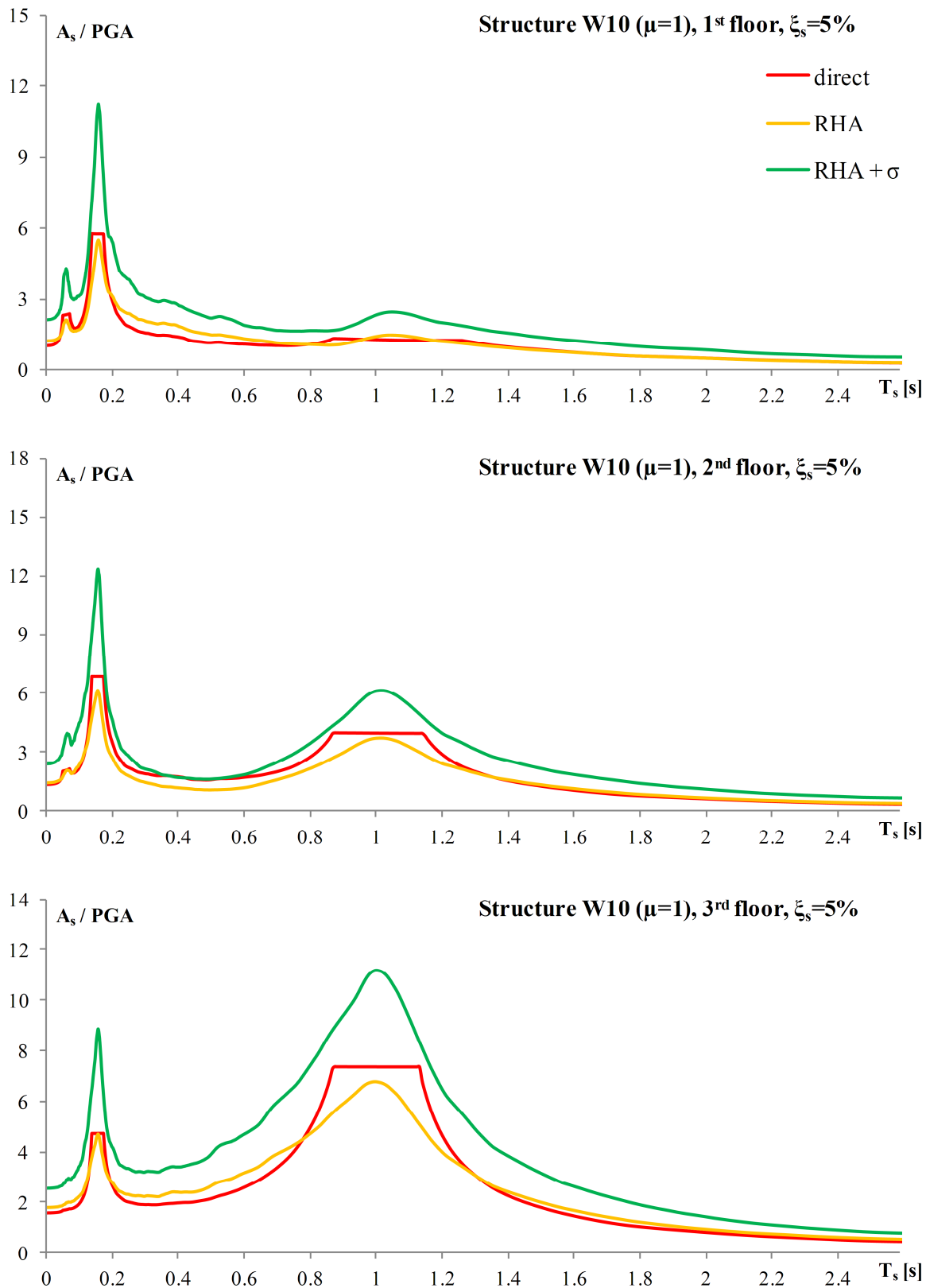


Figure 6.5: Floor response spectra for the elastic model of the structure W10 normalized with the mean PGA of the input, for 5% damping of the equipment

Slika 6.5: Etažni spektri odziva za elastičen model konstrukcije W10 normirani s povprečnim PGA inputa, za 5% dušenja opreme

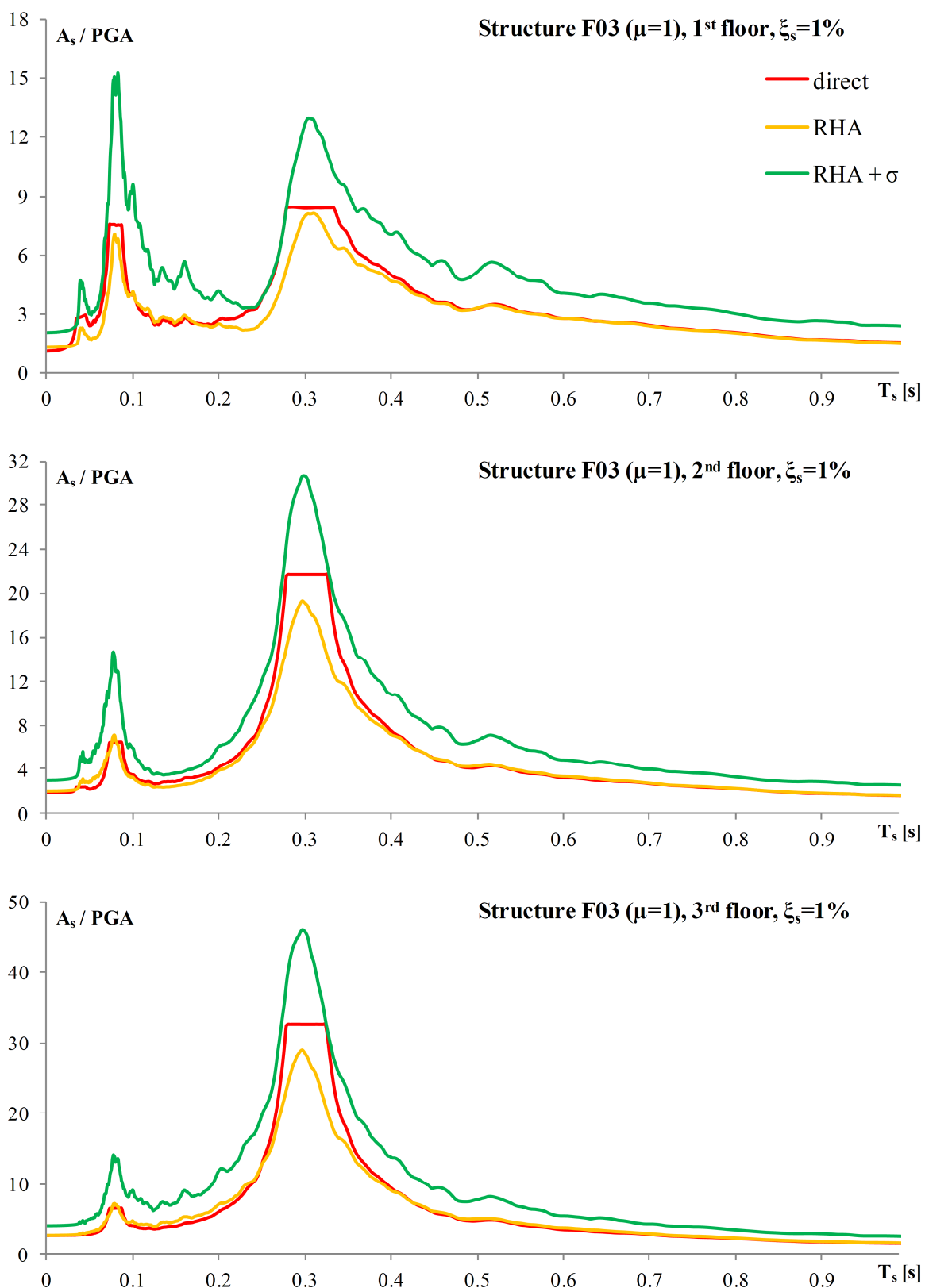


Figure 6.6: Floor response spectra for the elastic model of the structure F03 normalized with the mean PGA of the input, for 1% damping of the equipment

Slika 6.6: Etažni spektri odziva za elastičen model konstrukcije F03 normirani s povprečnim PGA inputa, za 1% dušenja opreme

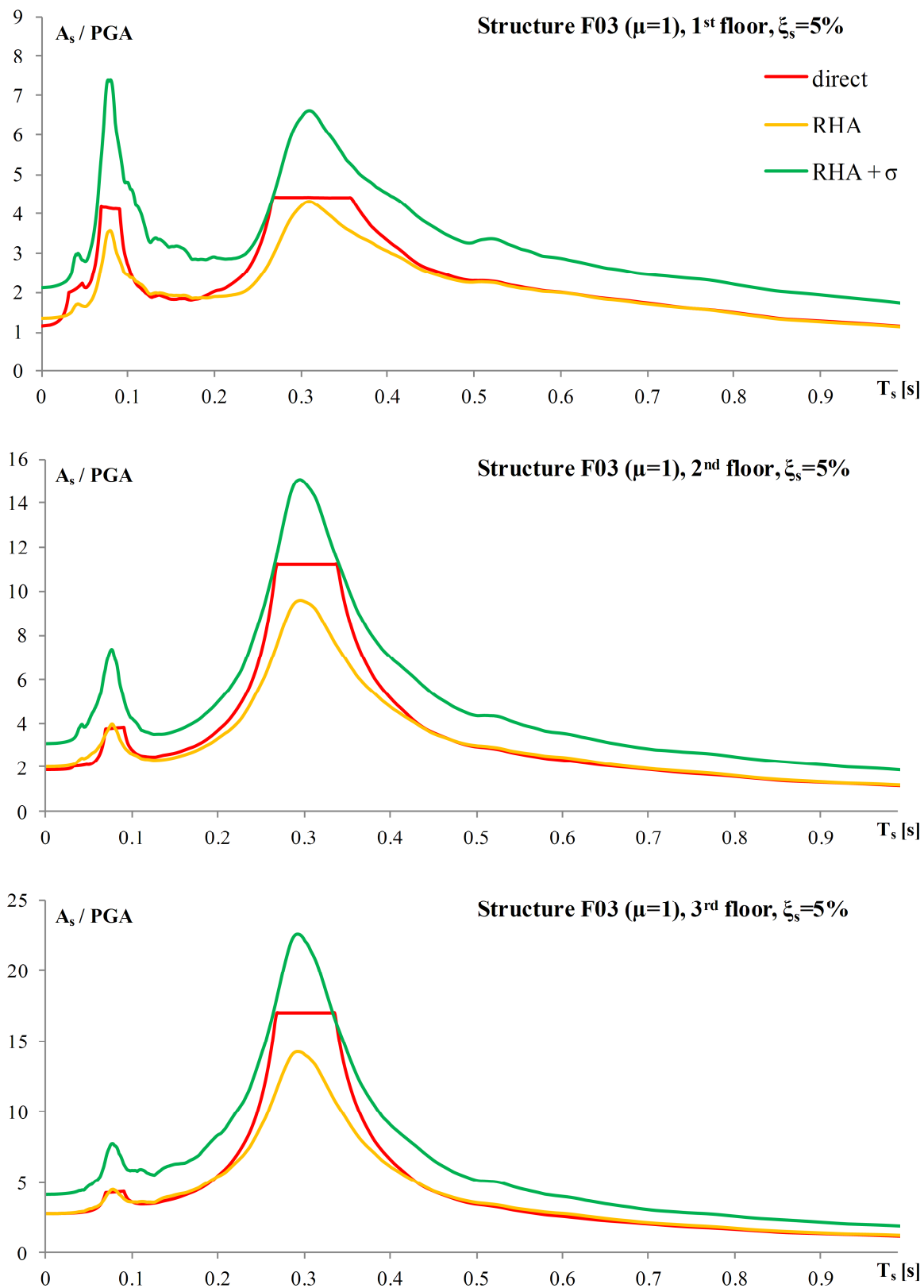


Figure 6.7: Floor response spectra for the elastic model of the structure F03 normalized with the mean PGA of the input, for 5% damping of the equipment

Slika 6.7: Etažni spektri odziva za elastičen model konstrukcije F03 normirani s povprečnim PGA inputa, za 5% dušenja opreme

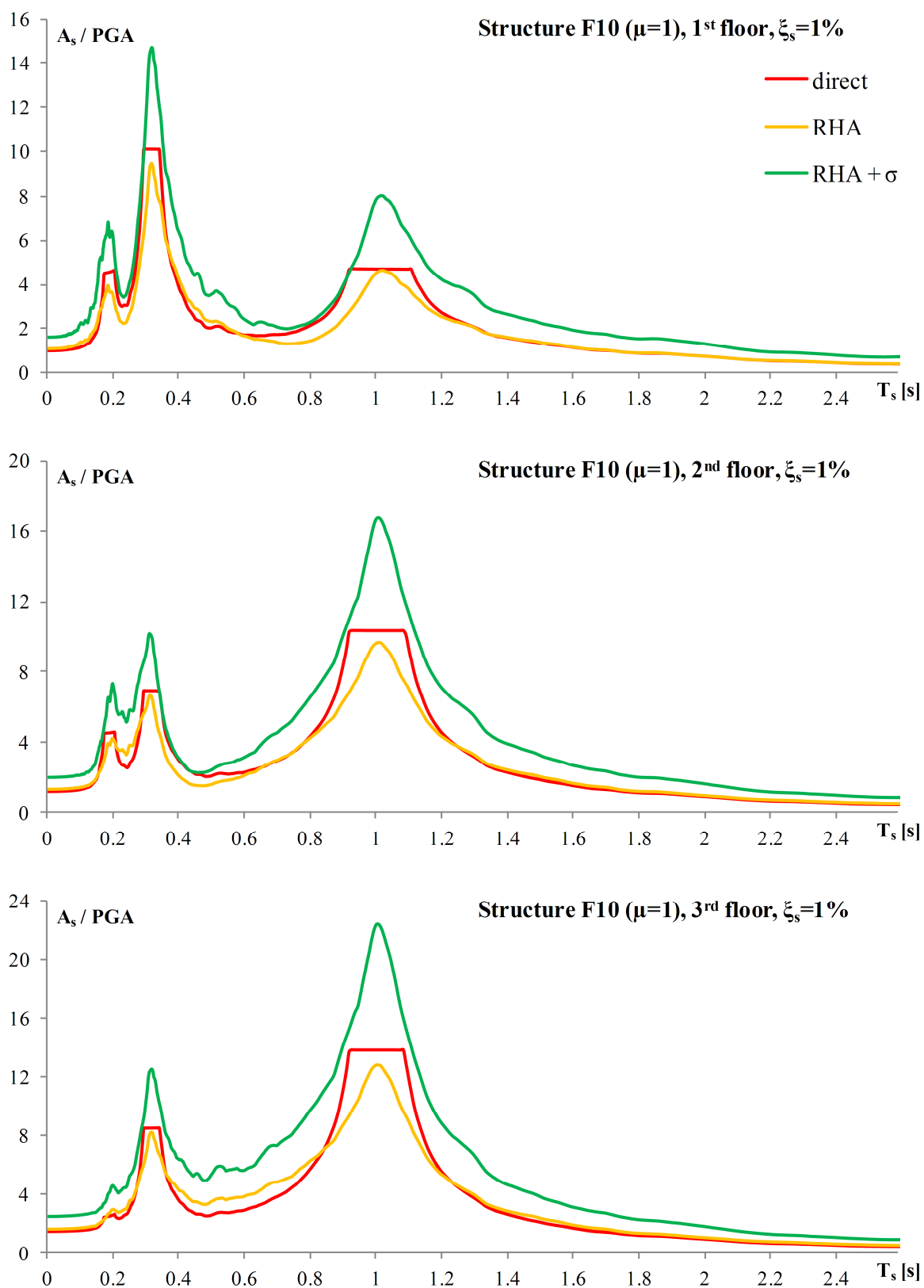


Figure 6.8: Floor response spectra for the elastic model of the structure F10 normalized with the mean PGA of the input, for 1% damping of the equipment

Slika 6.8: Etažni spektri odziva za elastičen model konstrukcije F10 normirani s povprečnim PGA inputa, za 1% dušenja opreme

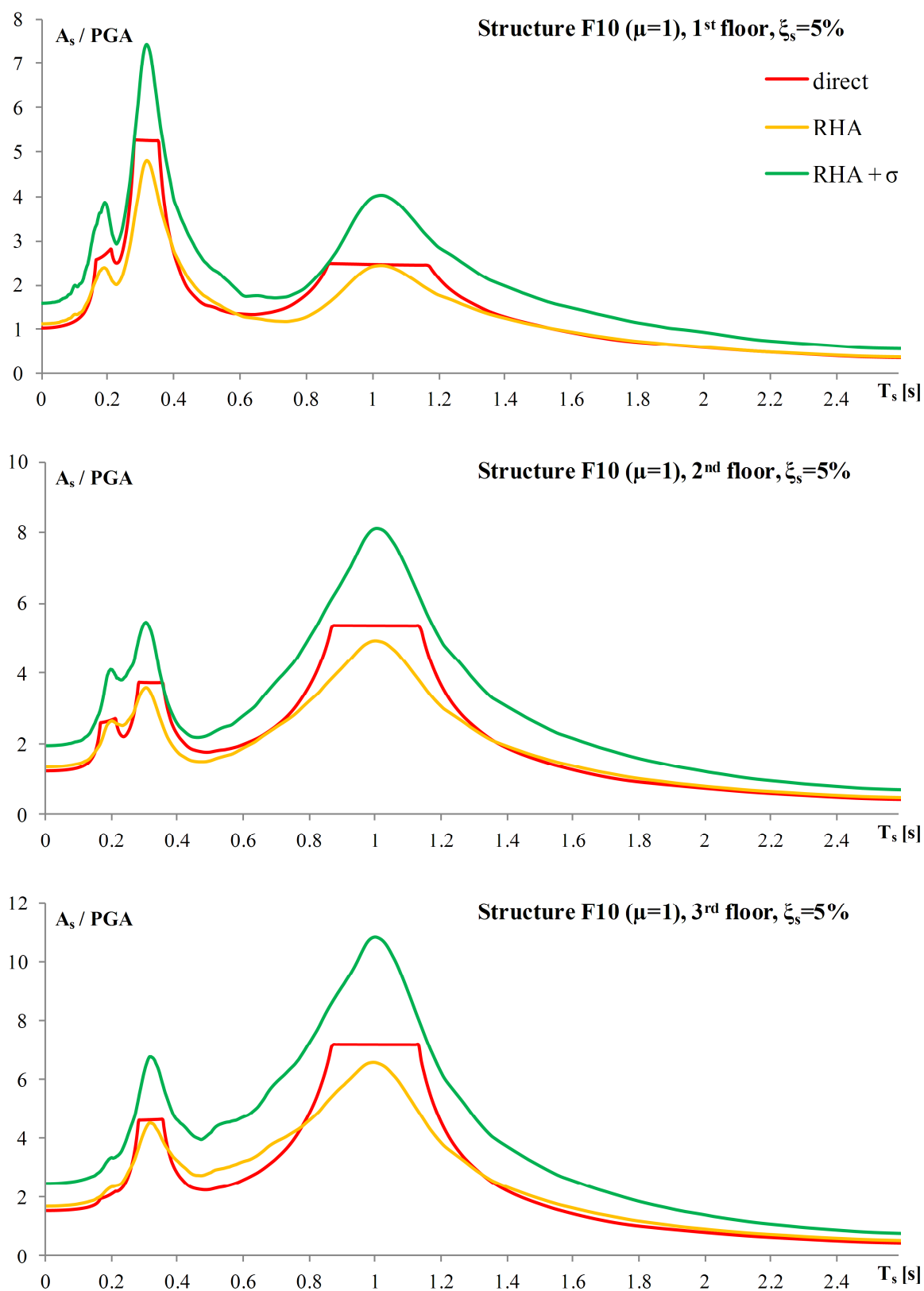


Figure 6.9: Floor response spectra for the elastic model of the structure F10 normalized with the mean PGA of the input, for 5% damping of the equipment

Slika 6.9: Etažni spektri odziva za elastičen model konstrukcije F10 normirani s povprečnim PGA inputa, za 5% dušenja opreme

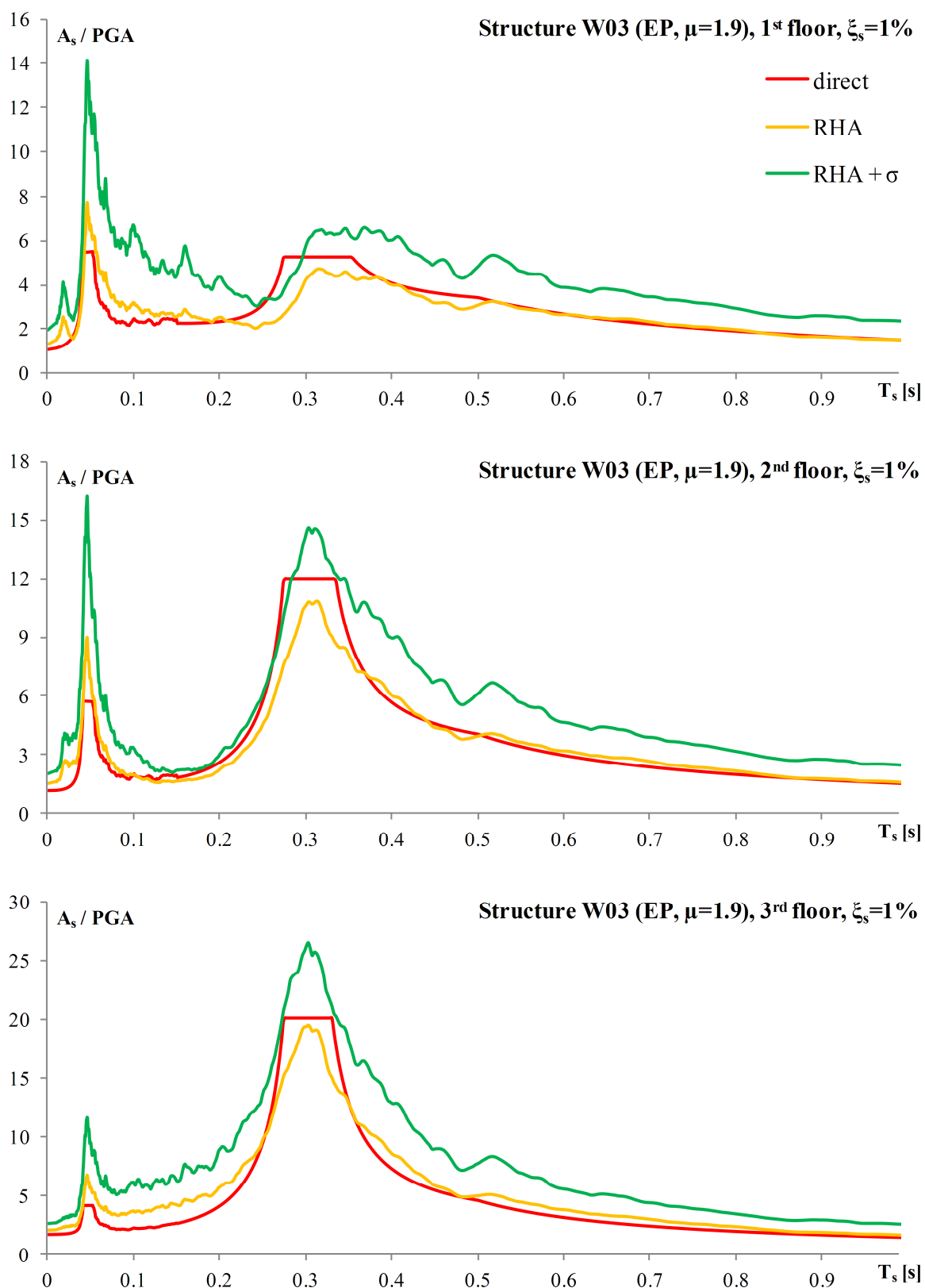


Figure 6.10: Floor response spectra for the EP model of the structure W03 (ductility $\mu=1.9$) normalized with the PGA of the input, for 1% damping of the equipment

Slika 6.10: Etažni spektri odziva za EP model konstrukcije W03 (ductility $\mu=1.9$) normirani s PGA inputa, za 1% dušenja opreme

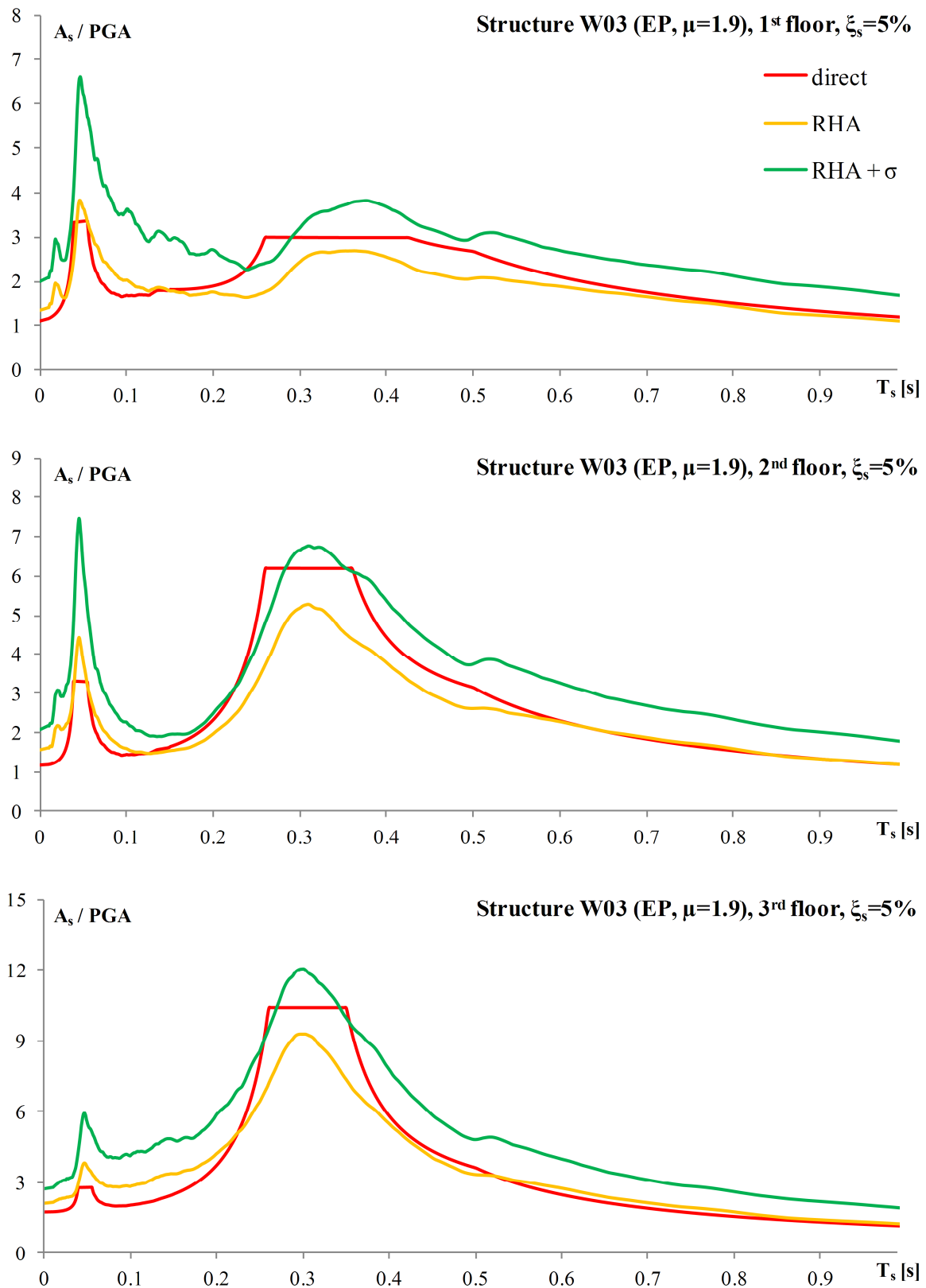


Figure 6.11: Floor response spectra for the EP model of the structure W03 (ductility $\mu=1.9$) normalized with the PGA of the input, for 5% damping of the equipment

Slika 6.11: Etažni spektri odziva za EP model konstrukcije W03 (ductility $\mu=1.9$) normirani s PGA inputa, za 5% dušenja opreme

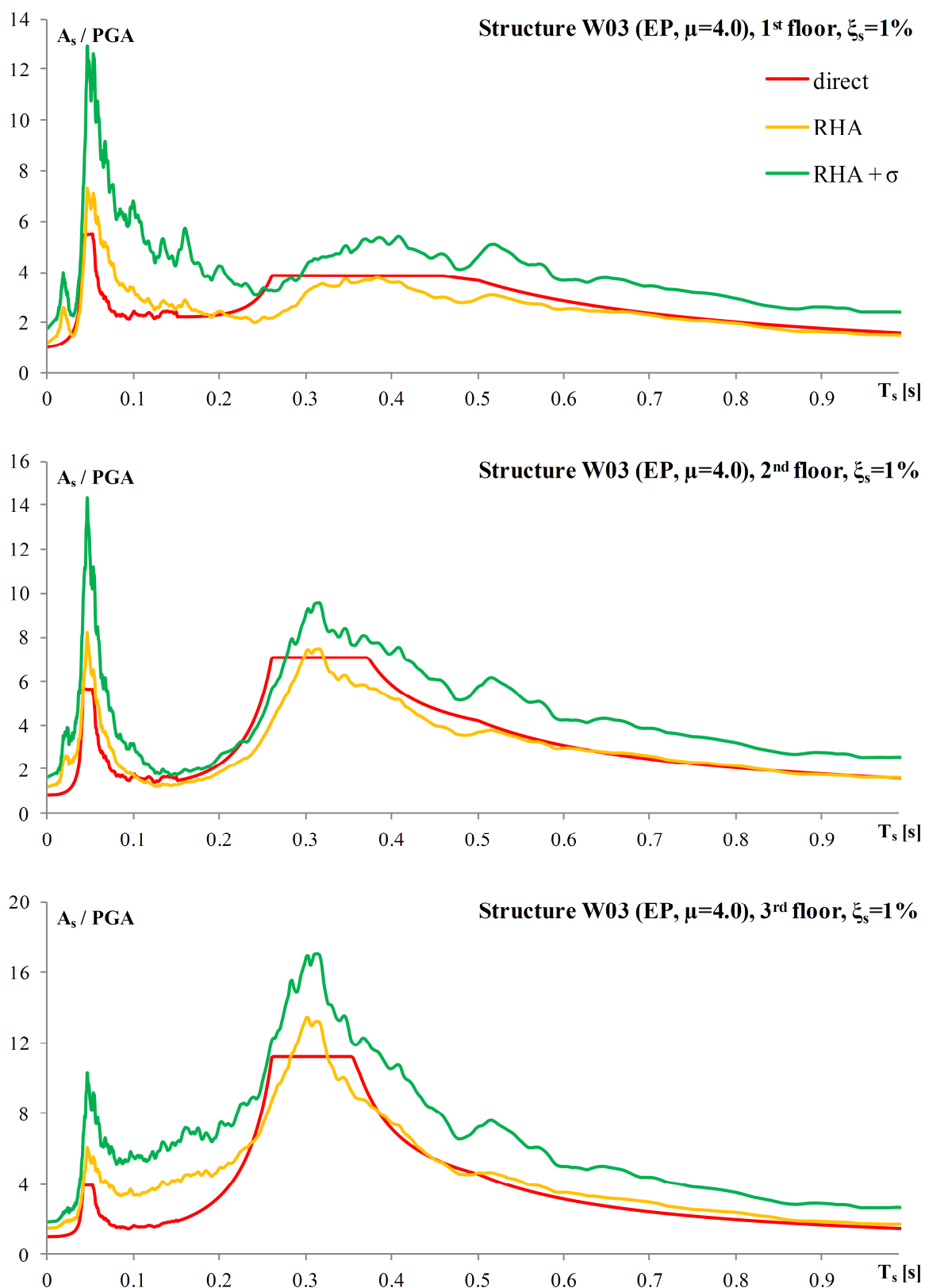


Figure 6.12: Floor response spectra for the EP model of the structure W03 (ductility $\mu=4.0$) normalized with the PGA of the input, for 1% damping of the equipment

Slika 6.12: Etažni spektri odziva za EP model konstrukcije W03 (ductility $\mu=4.0$) normirani s PGA inputa, za 1% dušenja opreme

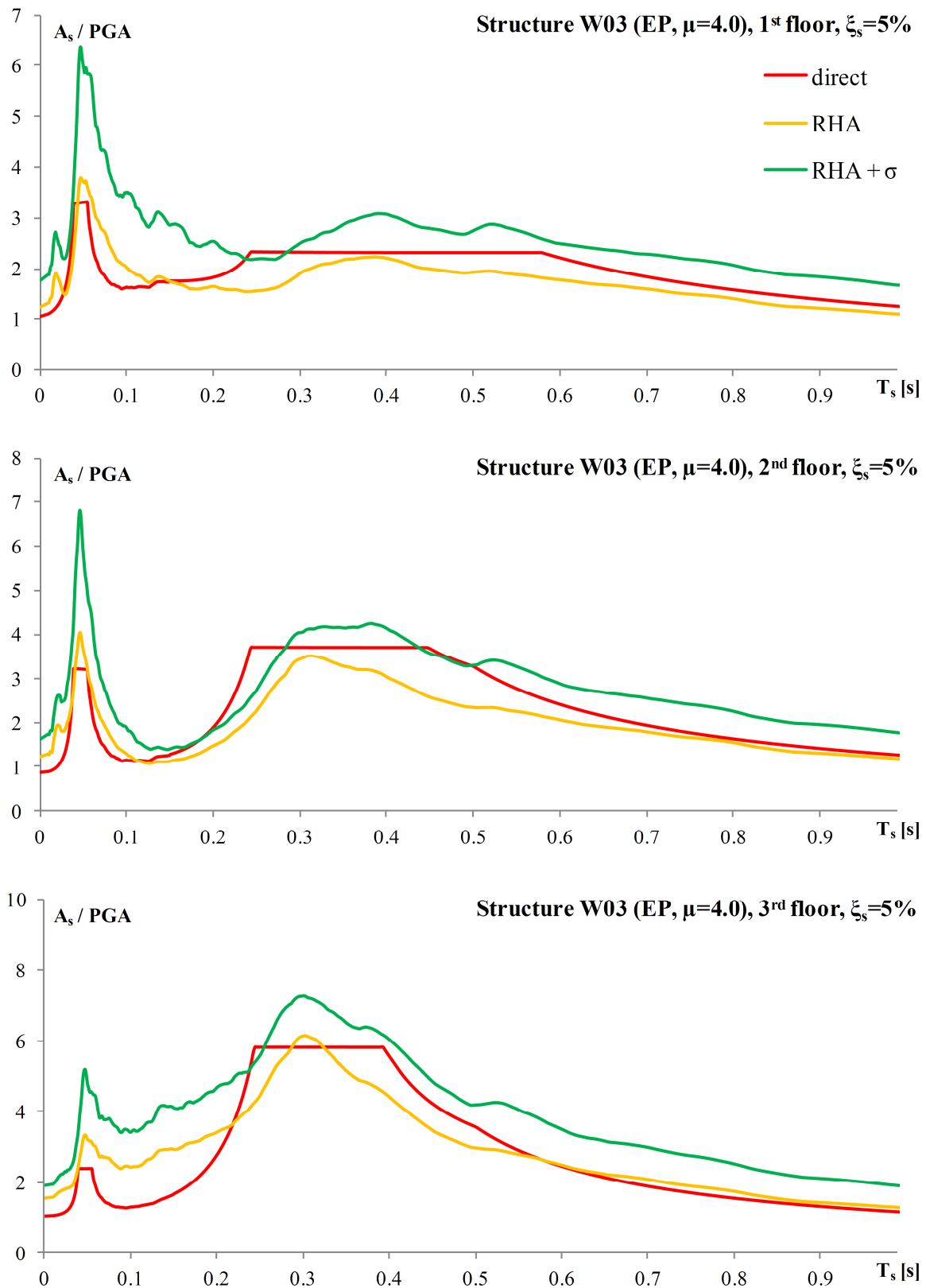


Figure 6.13: Floor response spectra for the EP model of the structure W03 (ductility $\mu=4.0$) normalized with the PGA of the input, for 5% damping of the equipment

Slika 6.13: Etažni spektri odziva za EP model konstrukcije W03 (ductility $\mu=4.0$) normirani s PGA inputa, za 5% dušenja opreme

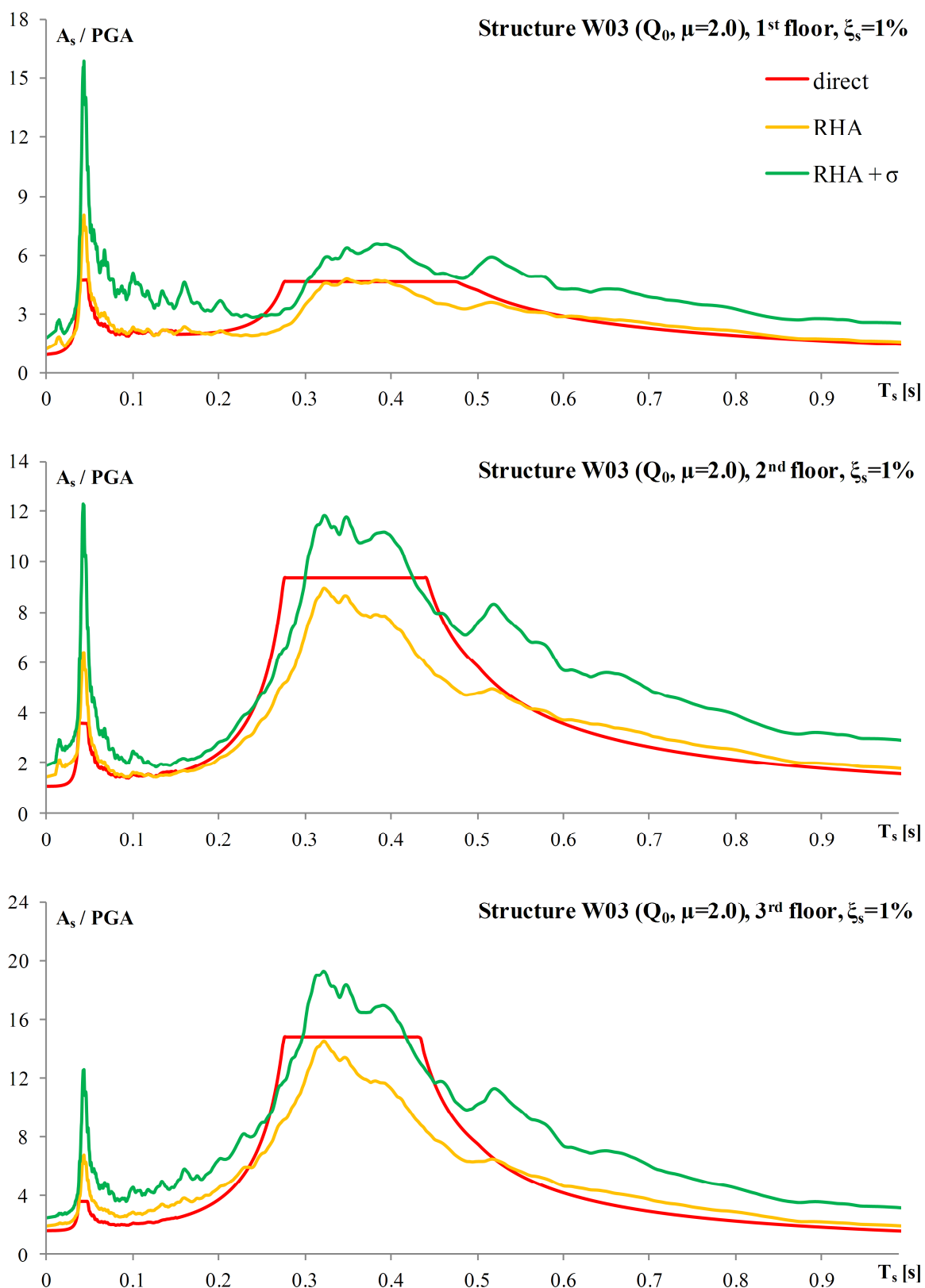


Figure 6.14: Floor response spectra for the Q_0 model of the structure W03 (ductility $\mu=2.0$) normalized with the PGA of the input, for 1% damping of the equipment

Slika 6.14: Etažni spektri odziva za Q_0 model konstrukcije W03 (ductility $\mu=2.0$) normirani s PGA inputa, za 1% dušenja opreme

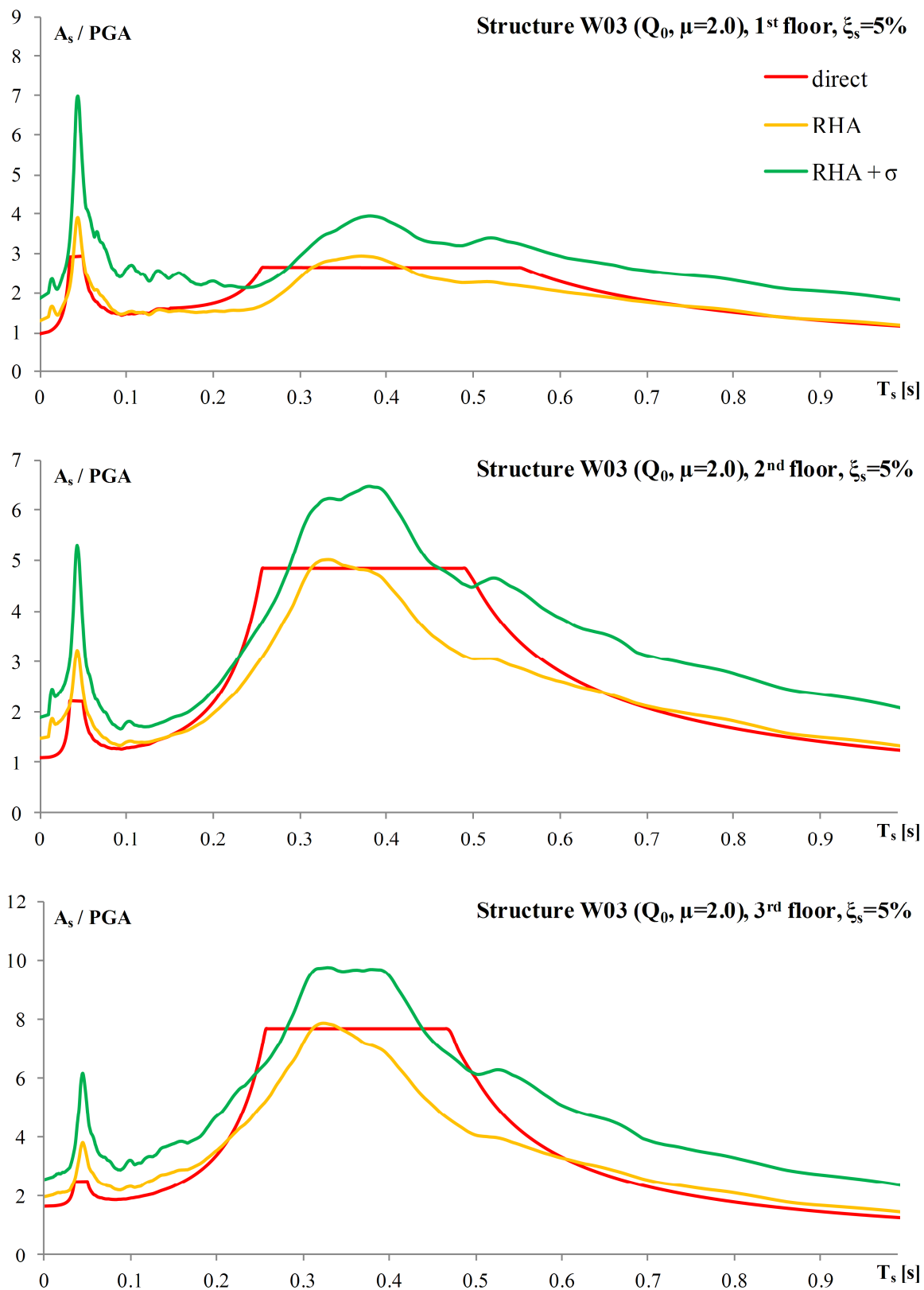


Figure 6.15: Floor response spectra for the Q_0 model of the structure W03 (ductility $\mu=2.0$) normalized with the PGA of the input, for 5% damping of the equipment

Slika 6.15: Etažni spektri odziva za Q_0 model konstrukcije W03 (ductility $\mu=2.0$) normirani s PGA inputa, za 5% dušenja opreme

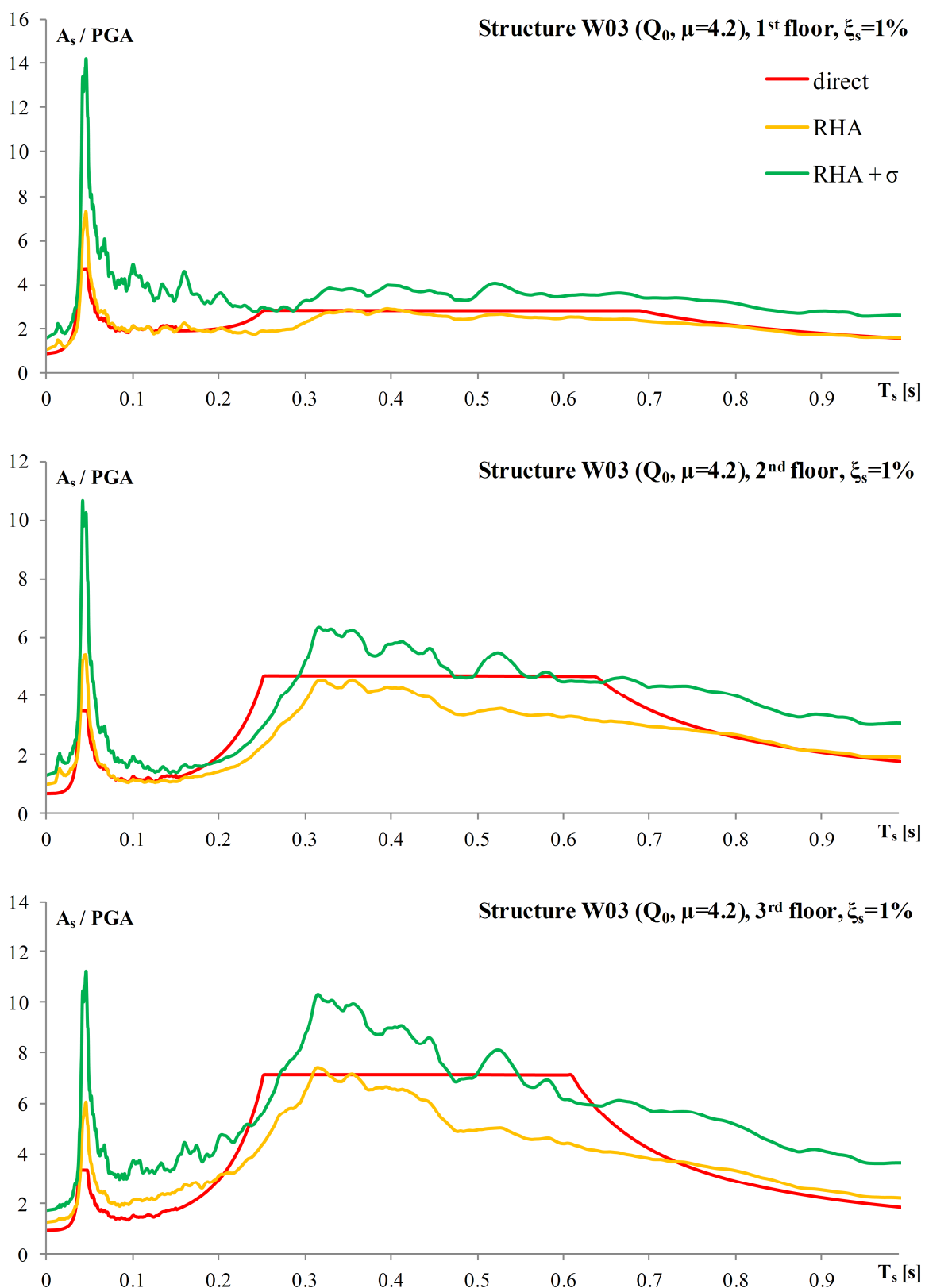


Figure 6.16: Floor response spectra for the Q_0 model of the structure W03 (ductility $\mu=4.2$) normalized with the PGA of the input, for 1% damping of the equipment

Slika 6.16: Etažni spektri odziva za Q_0 model konstrukcije W03 (ductility $\mu=4.2$) normirani s PGA inputa, za 1% dušenja opreme

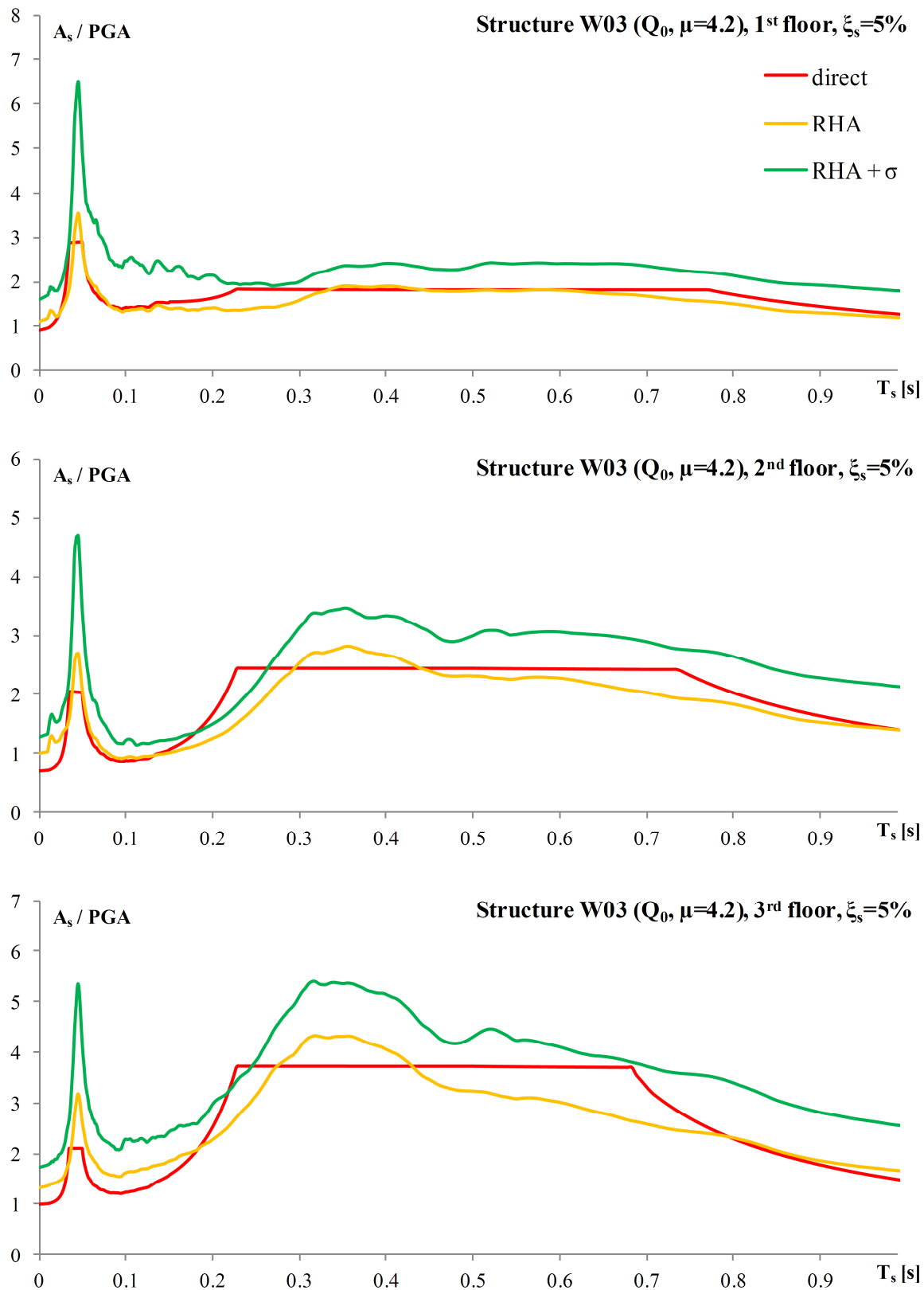


Figure 6.17: Floor response spectra for the Q_0 model of the structure W03 (ductility $\mu=4.2$) normalized with the PGA of the input, for 5% damping of the equipment

Slika 6.17: Etažni spektri odziva za Q_0 model konstrukcije W03 (ductility $\mu=4.2$) normirani s PGA inputa, za 5% dušenja opreme

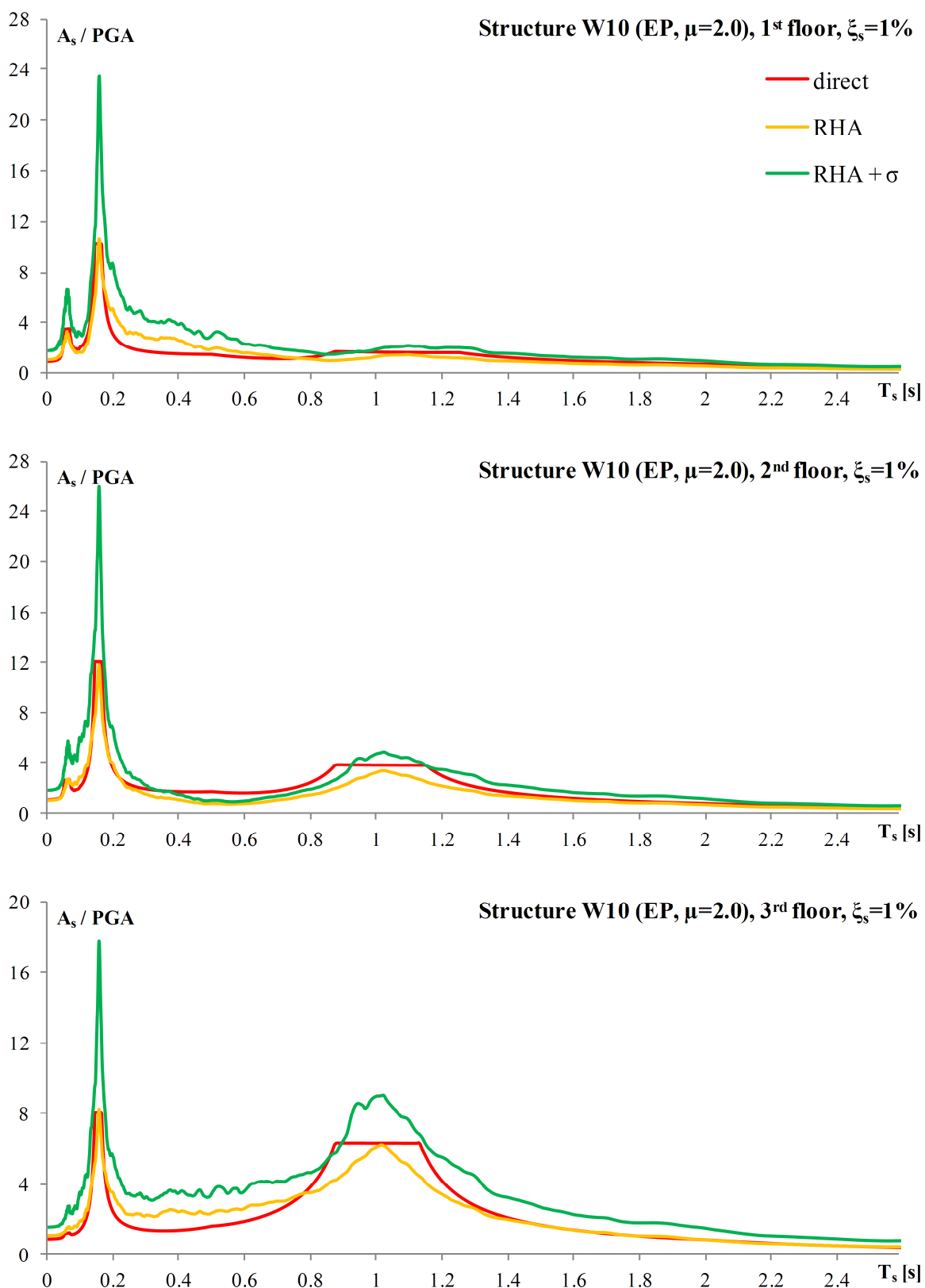


Figure 6.18: Floor response spectra for the EP model of the structure W10 (ductility $\mu=2.0$) normalized with the PGA of the input, for 1% damping of the equipment

Slika 6.18: Etažni spektri odziva za EP model konstrukcije W10 (ductility $\mu=2.0$) normirani s PGA inputa, za 1% dušenja opreme

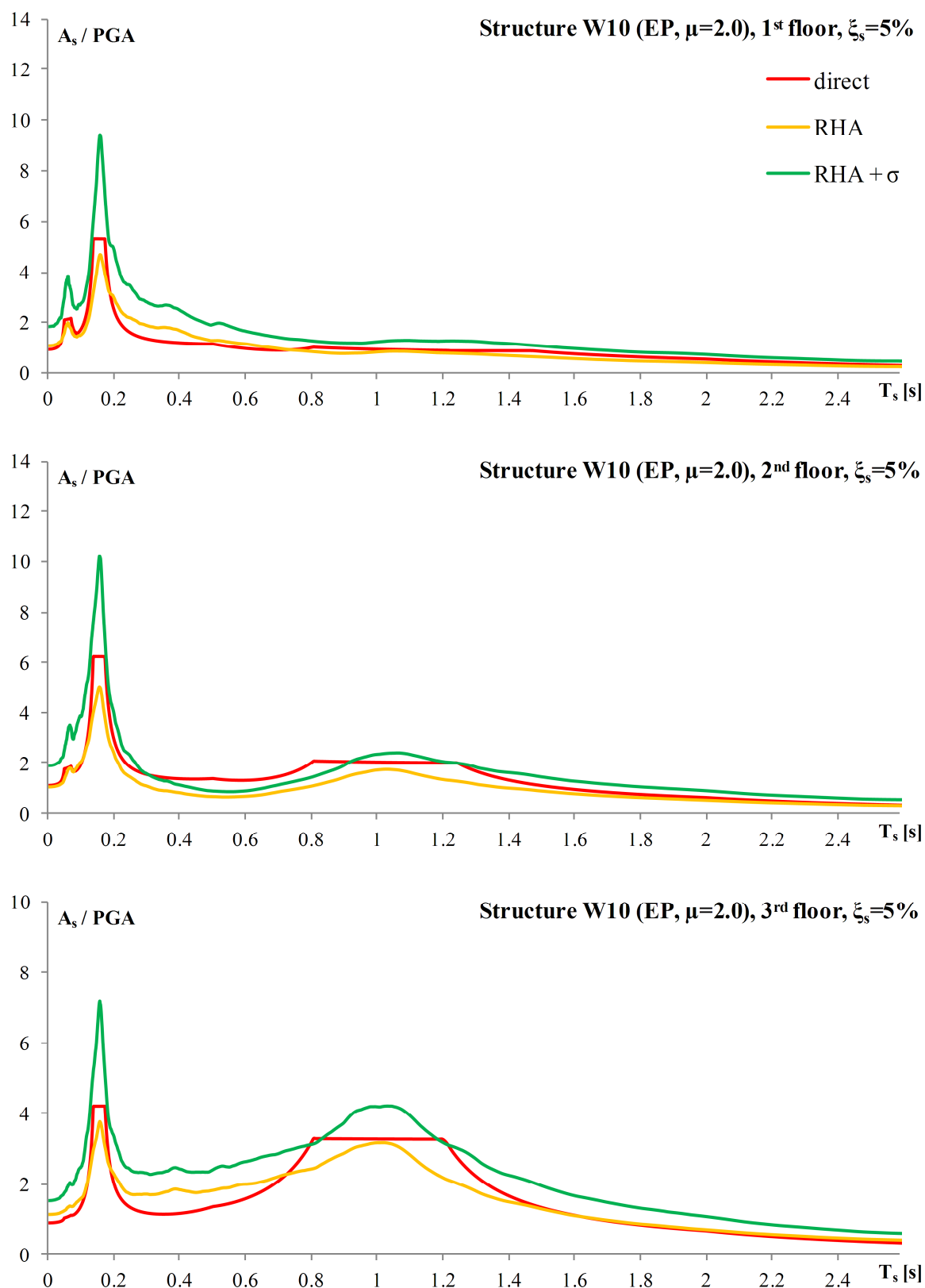


Figure 6.19: Floor response spectra for the EP model of the structure W10 (ductility $\mu=2.0$) normalized with the PGA of the input, for 5% damping of the equipment

Slika 6.19: Etažni spektri odziva za EP model konstrukcije W10 (ductility $\mu=2.0$) normirani s PGA inputa, za 5% dušenja opreme

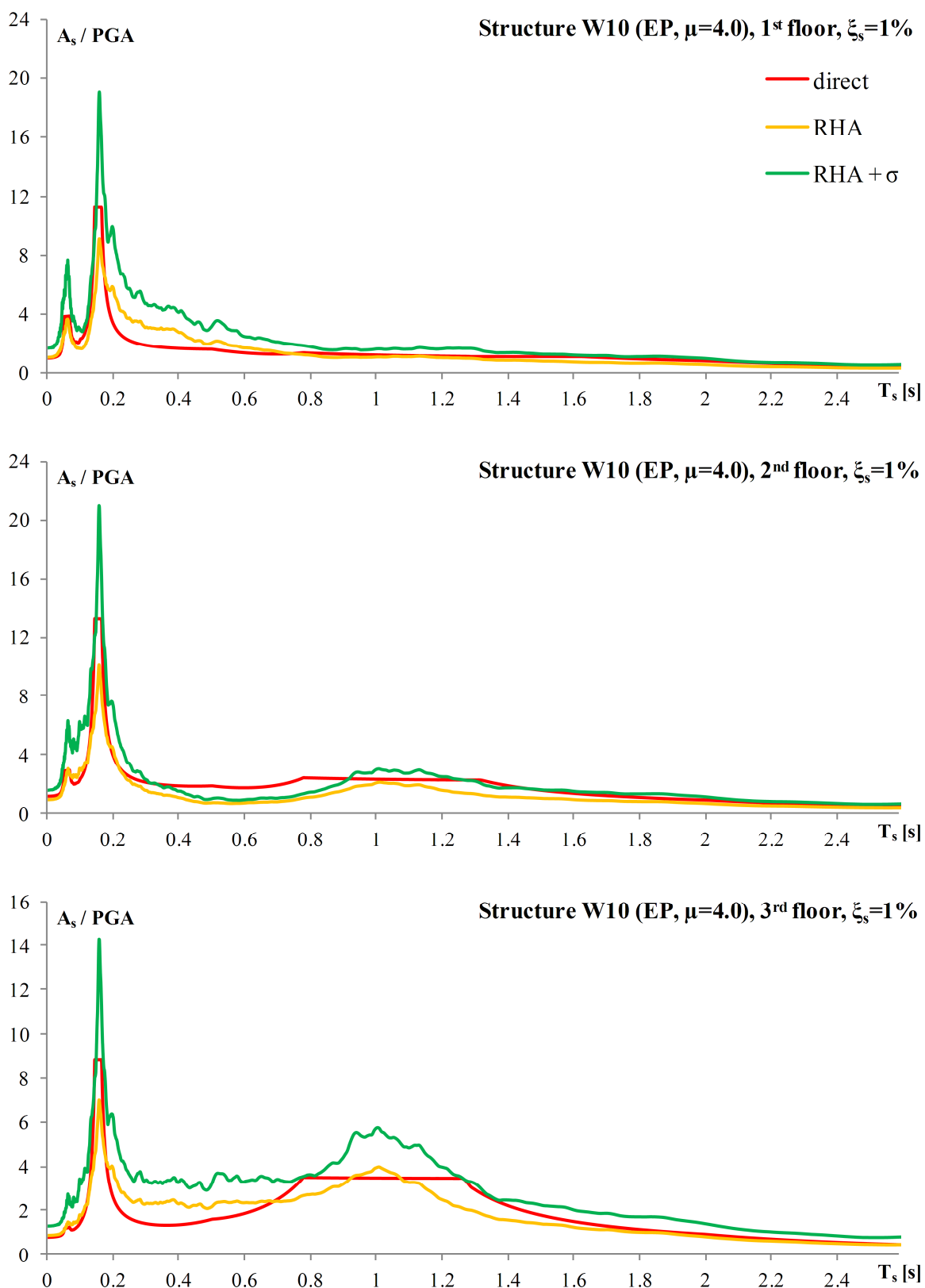


Figure 6.20: Floor response spectra for the EP model of the structure W10 (ductility $\mu=4.0$) normalized with the PGA of the input, for 1% damping of the equipment

Slika 6.20: Etažni spektri odziva za EP model konstrukcije W10 (ductility $\mu=4.0$) normirani s PGA inputa, za 1% dušenja opreme

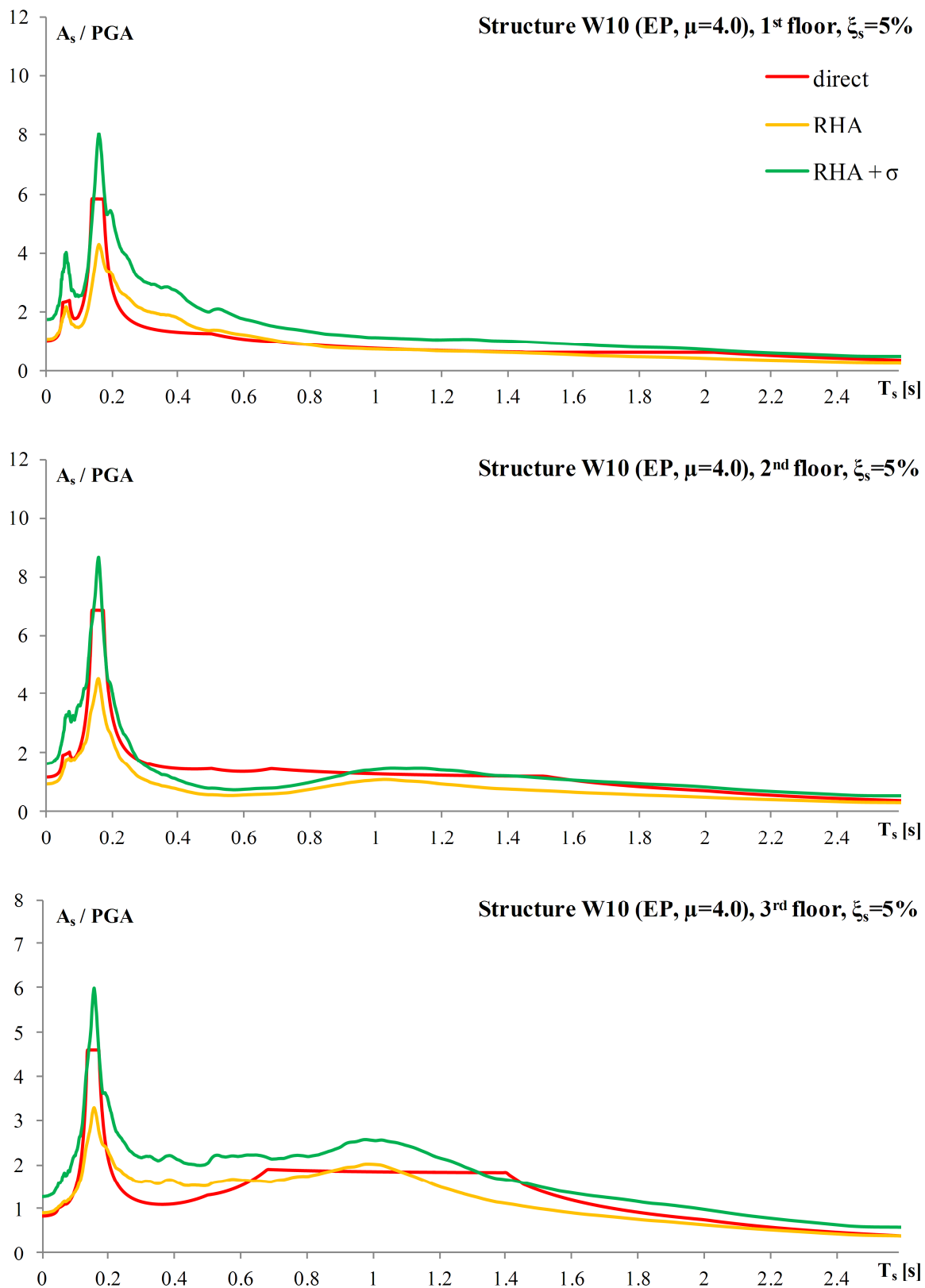


Figure 6.21: Floor response spectra for the EP model of the structure W10 (ductility $\mu=4.0$) normalized with the PGA of the input, for 5% damping of the equipment

Slika 6.21: Etažni spektri odziva za EP model konstrukcije W10 (ductility $\mu=4.0$) normirani s PGA inputa, za 5% dušenja opreme

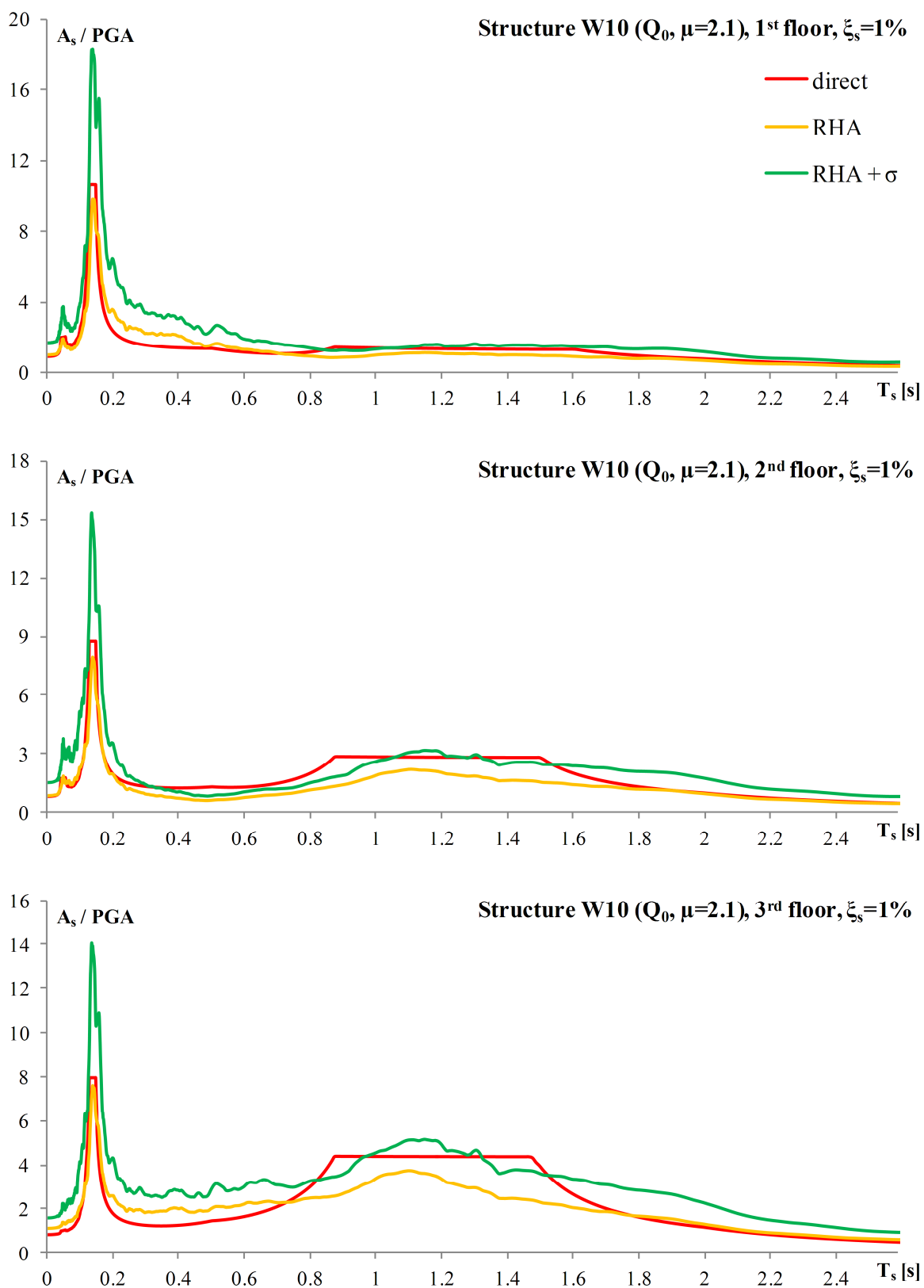


Figure 6.22: Floor response spectra for the Q_0 model of the structure W10 (ductility $\mu=2.1$) normalized with the PGA of the input, for 1% damping of the equipment

Slika 6.22: Etažni spektri odziva za Q_0 model konstrukcije W10 (ductility $\mu=2.1$) normirani s PGA inputa, za 1% dušenja opreme

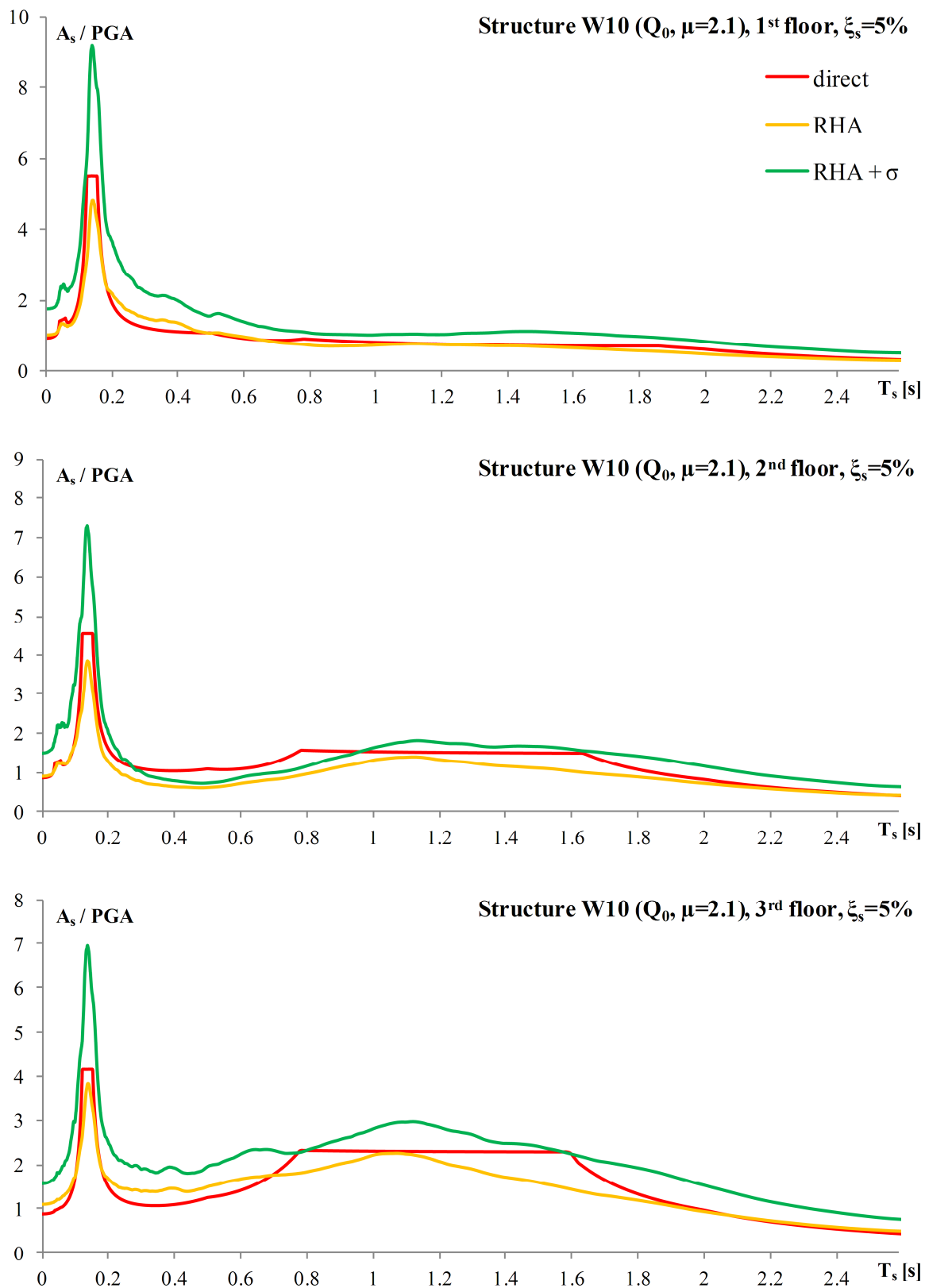


Figure 6.23: Floor response spectra for the Q_0 model of the structure W10 (ductility $\mu=2.1$) normalized with the PGA of the input, for 5% damping of the equipment

Slika 6.23: Etažni spektri odziva za Q_0 model konstrukcije W10 (ductility $\mu=2.1$) normirani s PGA inputa, za 5% dušenja opreme

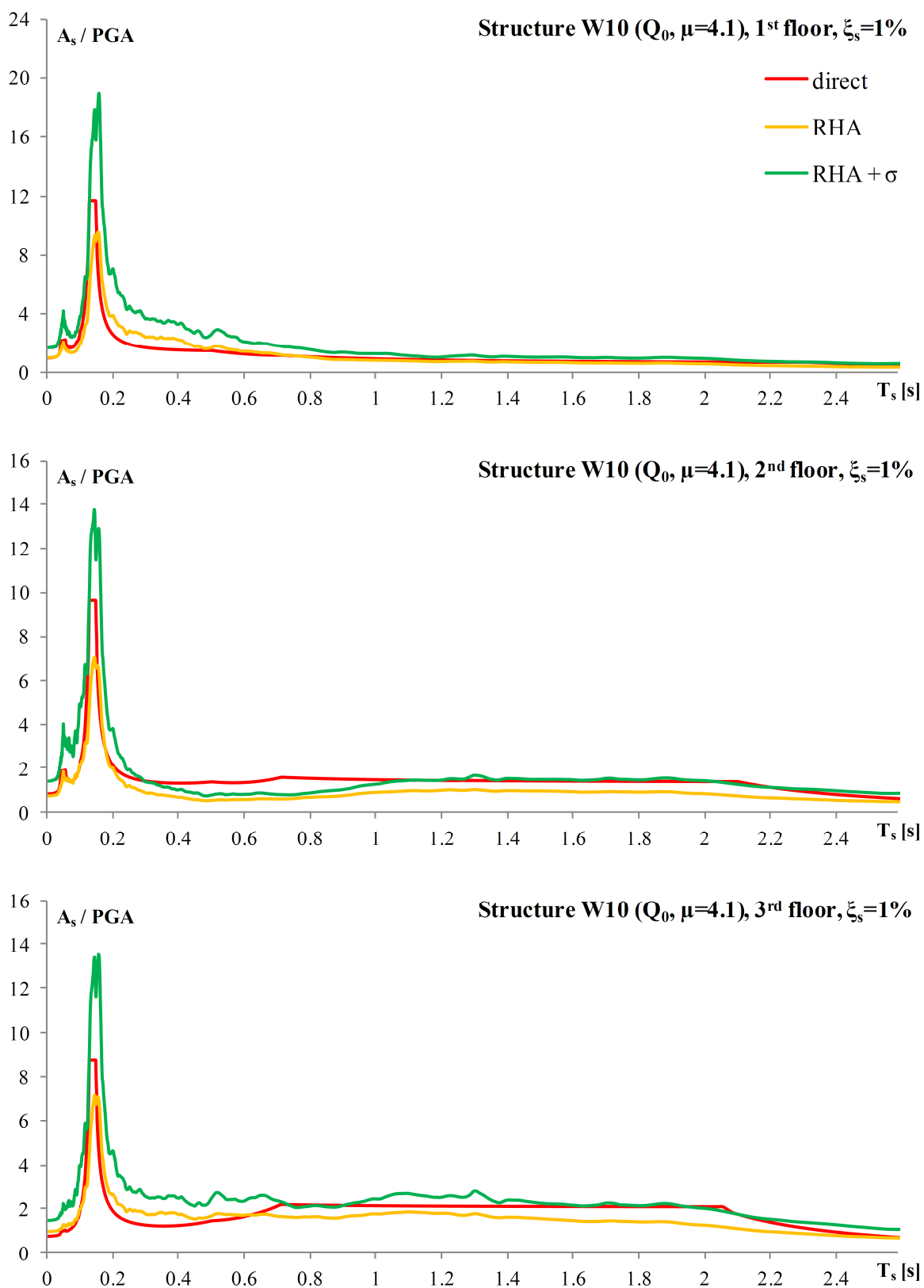


Figure 6.24: Floor response spectra for the Q_0 model of the structure W10 (ductility $\mu=4.1$) normalized with the PGA of the input, for 1% damping of the equipment

Slika 6.24: Etažni spektri odziva za Q_0 model konstrukcije W10 (ductility $\mu=4.1$) normirani s PGA inputa, za 1% dušenja opreme

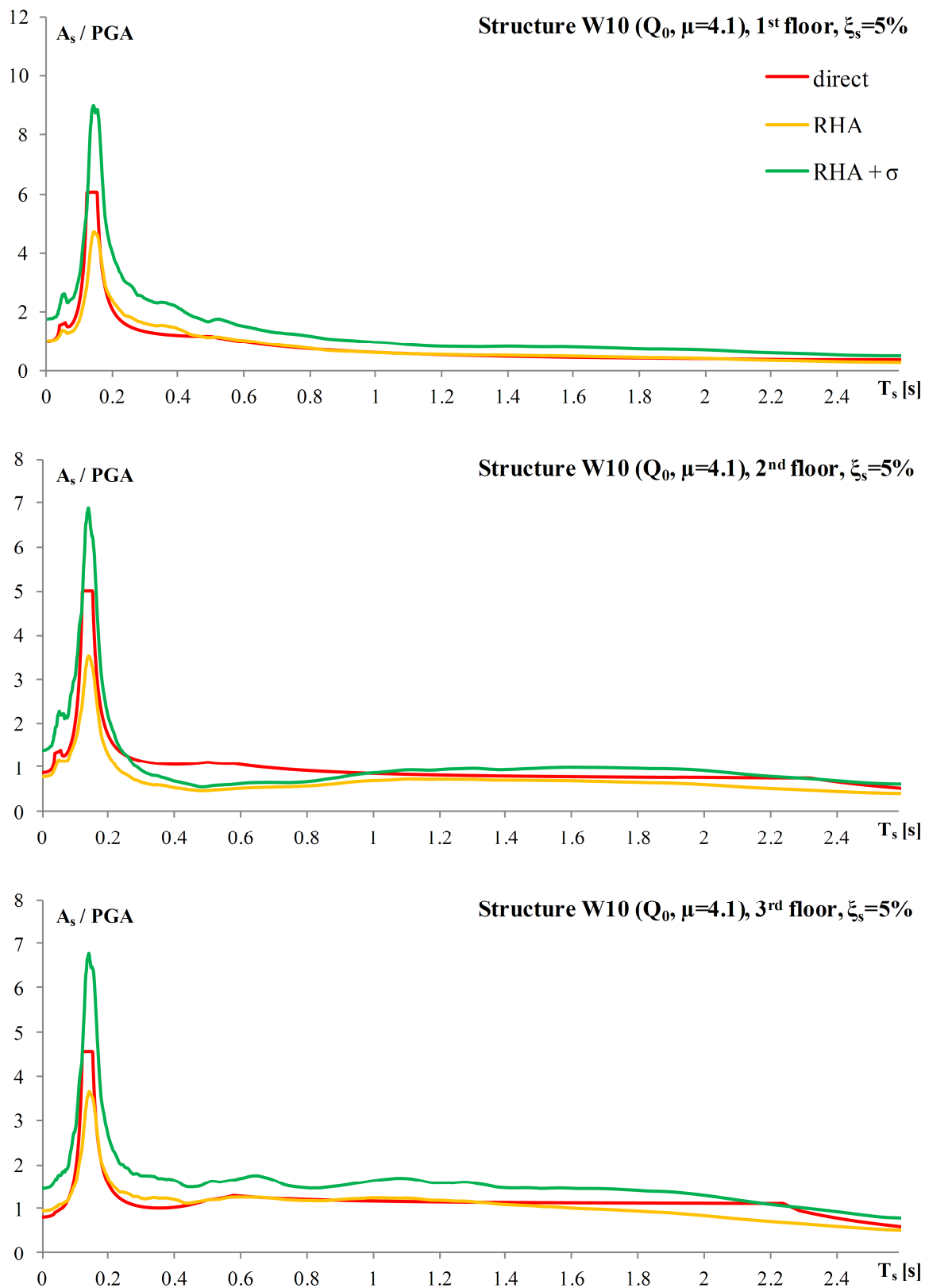


Figure 6.25: Floor response spectra for the Q_0 model of the structure W10 (ductility $\mu=4.1$) normalized with the PGA of the input, for 5% damping of the equipment

Slika 6.25: Etažni spektri odziva za Q_0 model konstrukcije W10 (ductility $\mu=4.1$) normirani s PGA inputa, za 5% dušenja opreme

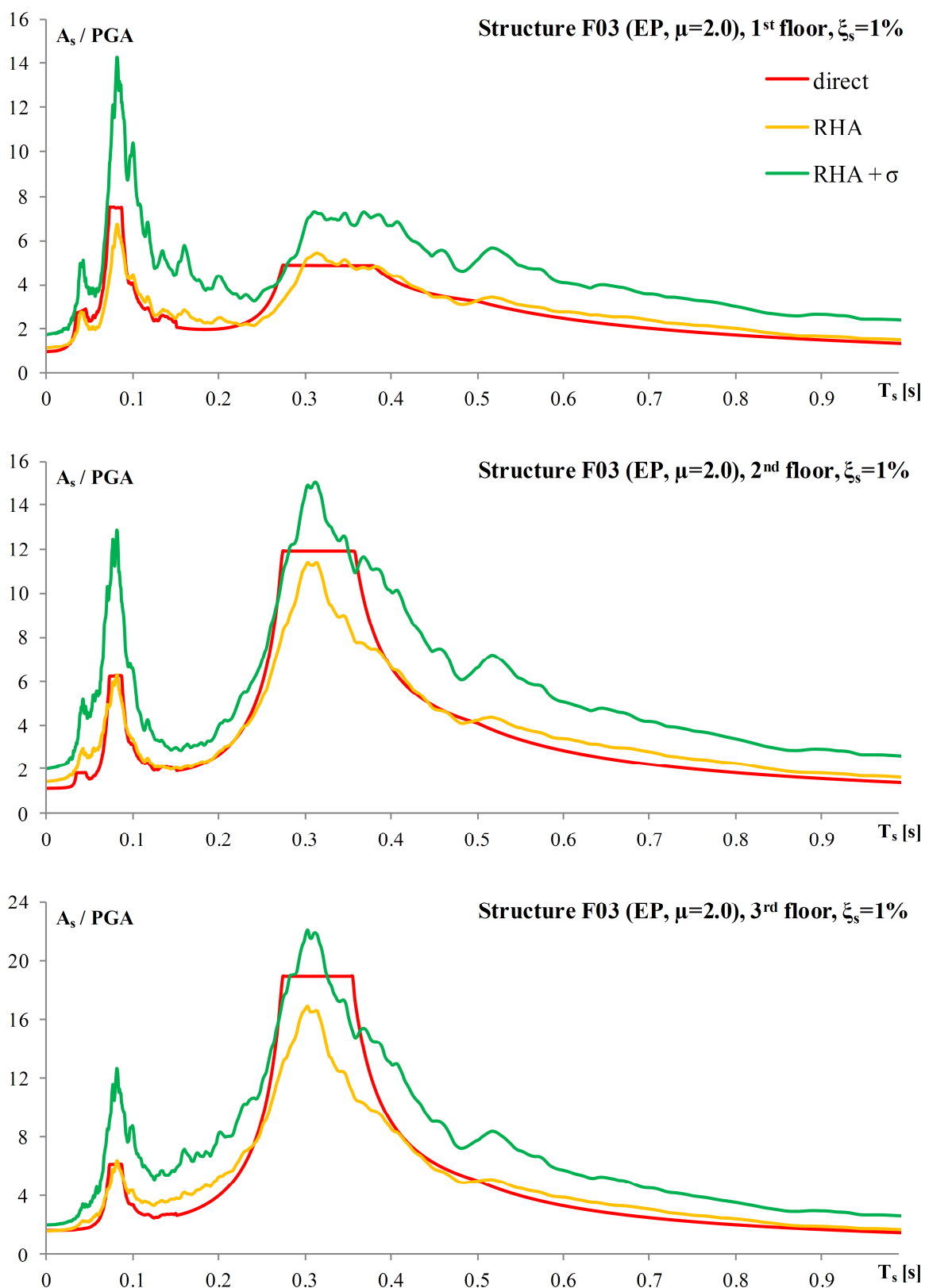


Figure 6.26: Floor response spectra for the EP model of the structure F03 (ductility $\mu=2.0$) normalized with the PGA of the input, for 1% damping of the equipment

Slika 6.26: Etažni spektri odziva za EP model konstrukcije F03 (ductility $\mu=2.0$) normirani s PGA inputa, za 1% dušenja opreme

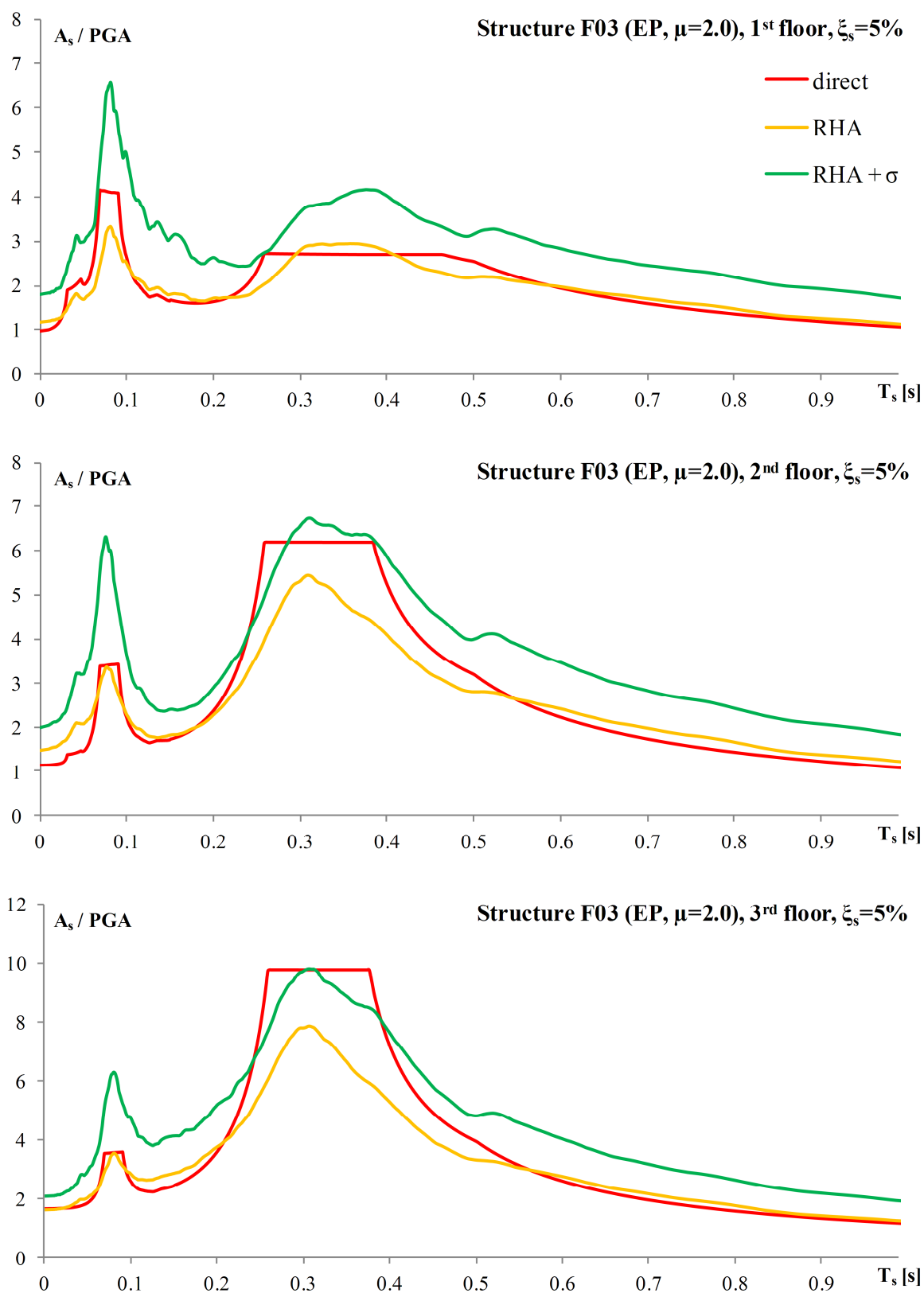


Figure 6.27: Floor response spectra for the EP model of the structure F03 (ductility $\mu=2.0$) normalized with the PGA of the input, for 5% damping of the equipment

Slika 6.27: Etažni spektri odziva za EP model konstrukcije F03 (ductility $\mu=2.0$) normirani s PGA inputa, za 5% dušenja opreme

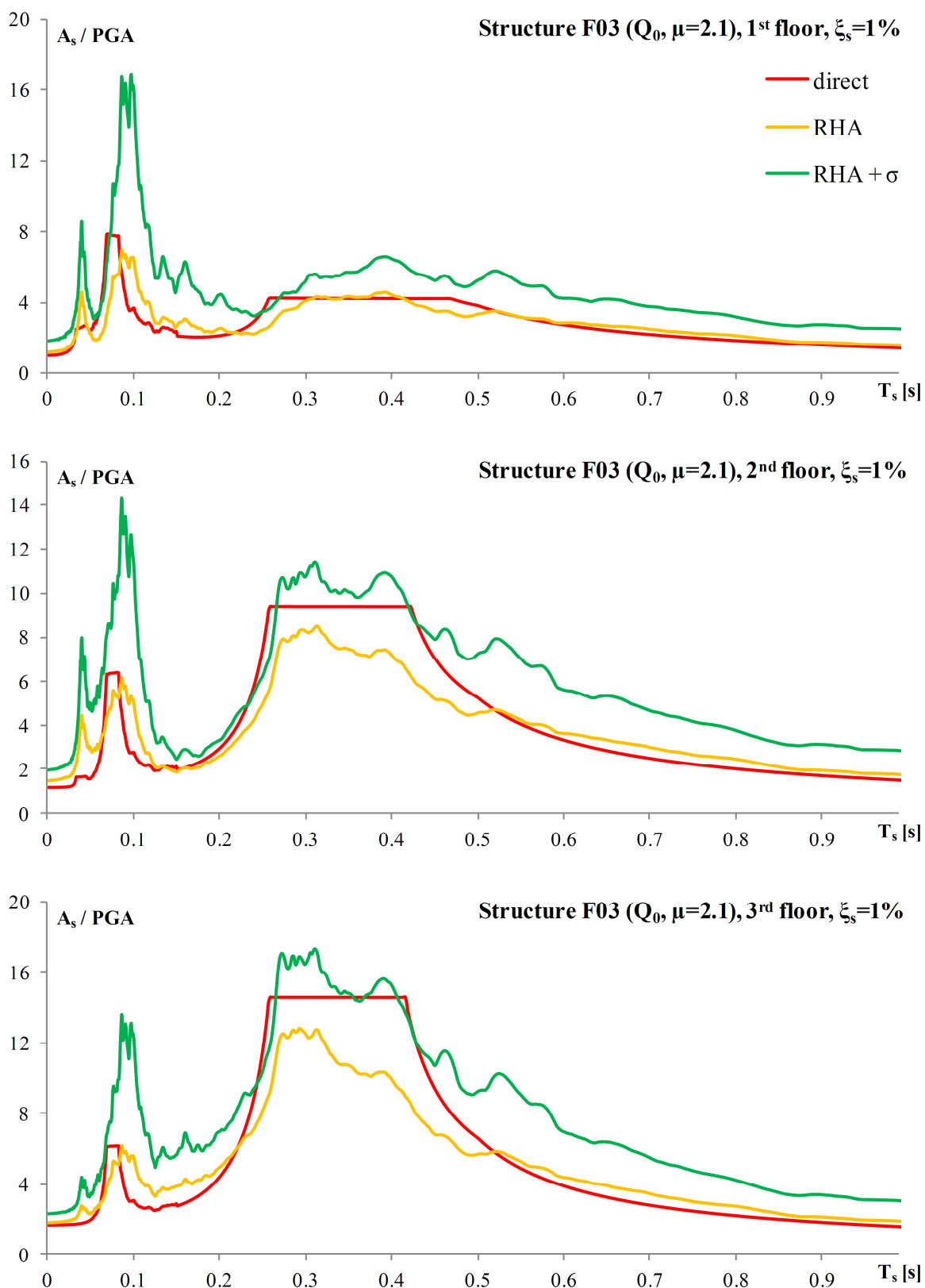


Figure 6.28: Floor response spectra for the Q_0 model of the structure F03 (ductility $\mu=2.1$) normalized with the PGA of the input, for 1% damping of the equipment

Slika 6.28: Etažni spektri odziva za Q_0 model konstrukcije F03 (ductility $\mu=2.1$) normirani s PGA inputa, za 1% dušenja opreme

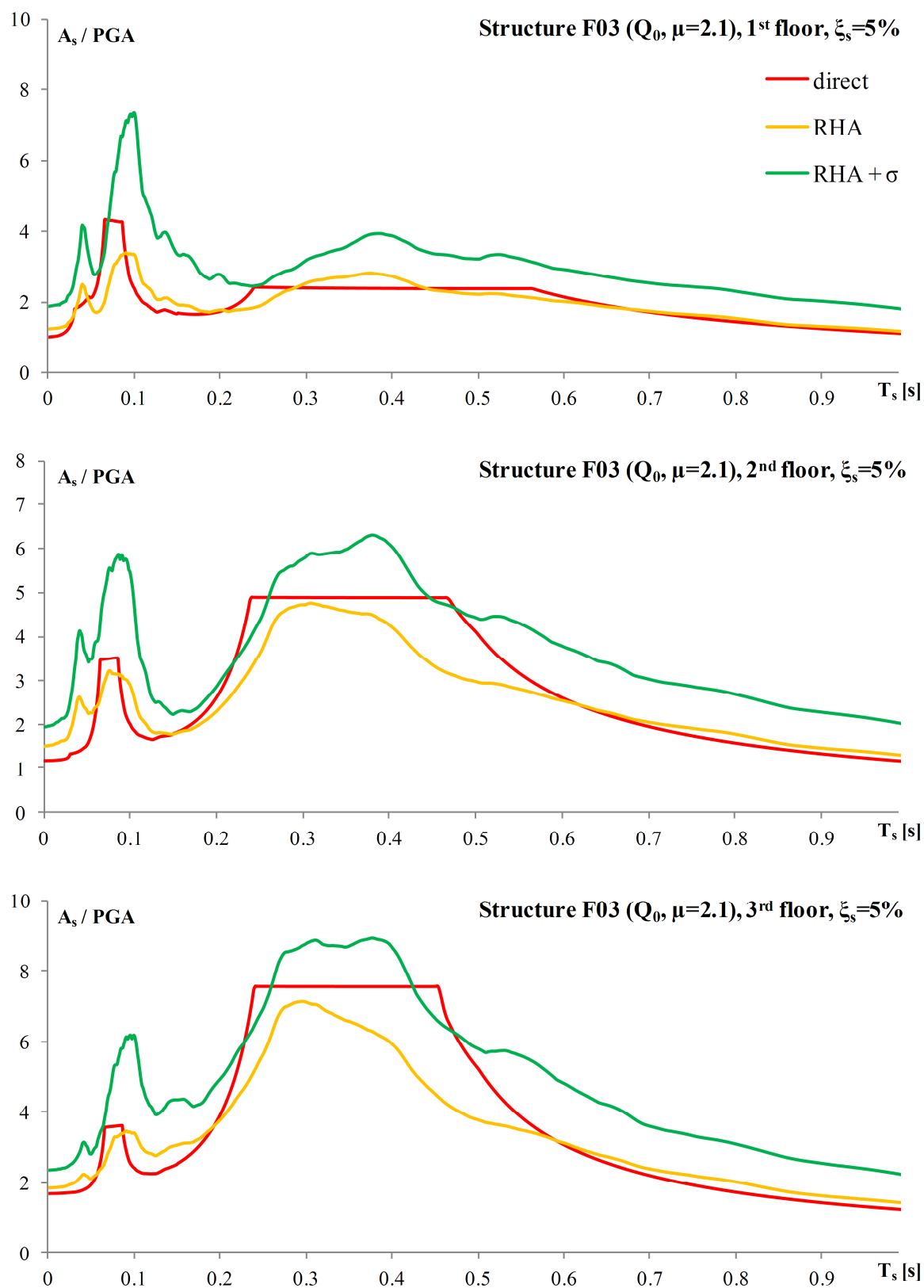


Figure 6.29: Floor response spectra for the Q_0 model of the structure F03 (ductility $\mu=2.1$) normalized with the PGA of the input, for 5% damping of the equipment

Slika 6.29: Etažni spektri odziva za Q_0 model konstrukcije F03 (ductility $\mu=2.1$) normirani s PGA inputa, za 5% dušenja opreme

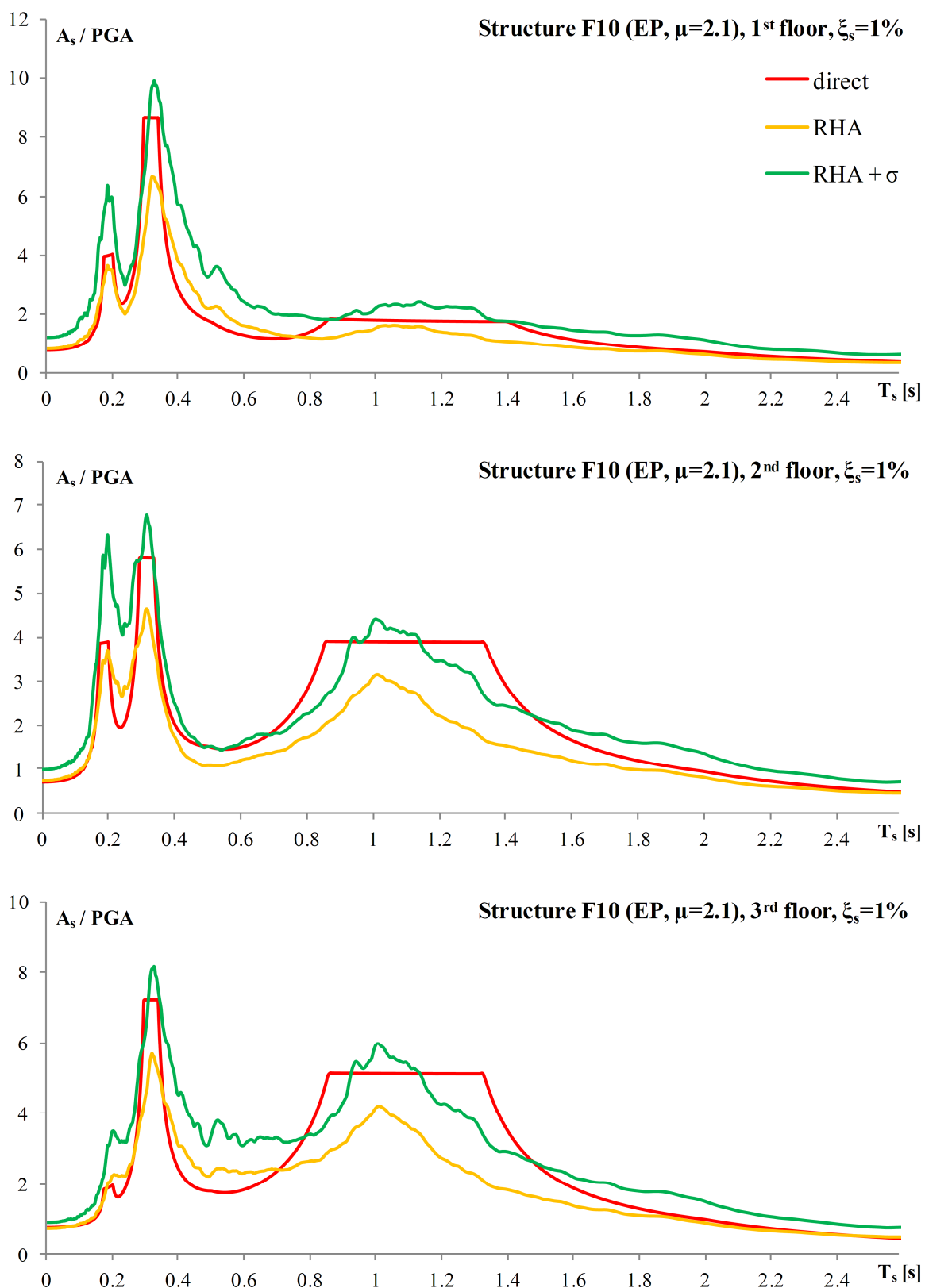


Figure 6.30: Floor response spectra for the EP model of the structure F10 (ductility $\mu=2.1$) normalized with the PGA of the input, for 1% damping of the equipment

Slika 6.30: Etažni spektri odziva za EP model konstrukcije F10 (ductility $\mu=2.1$) normirani s PGA inputa, za 1% dušenja opreme

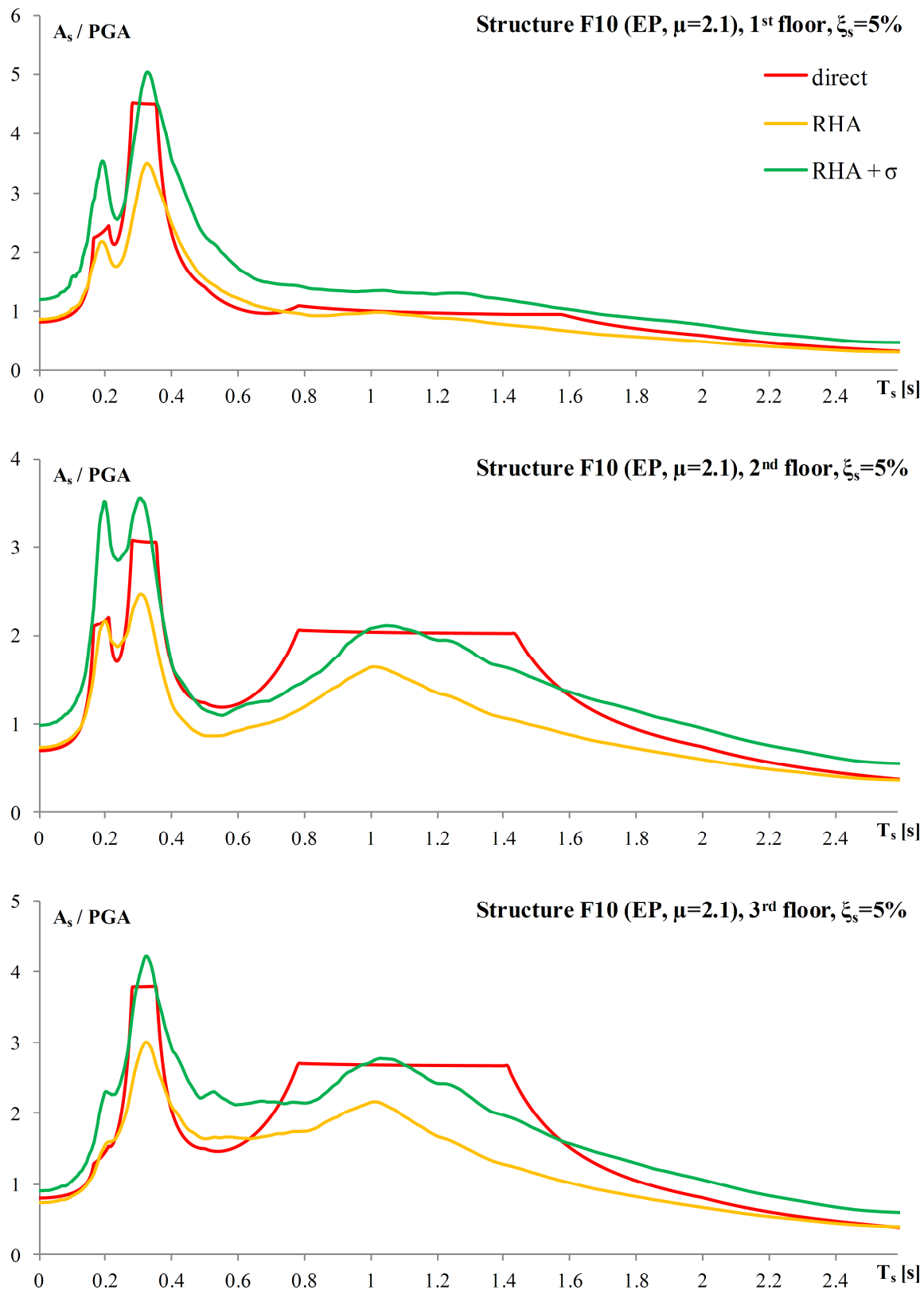


Figure 6.31: Floor response spectra for the EP model of the structure F10 (ductility $\mu=2.1$) normalized with the PGA of the input, for 5% damping of the equipment

Slika 6.31: Etažni spektri odziva za EP model konstrukcije F10 (ductility $\mu=2.1$) normirani s PGA inputa, za 5% dušenja opreme

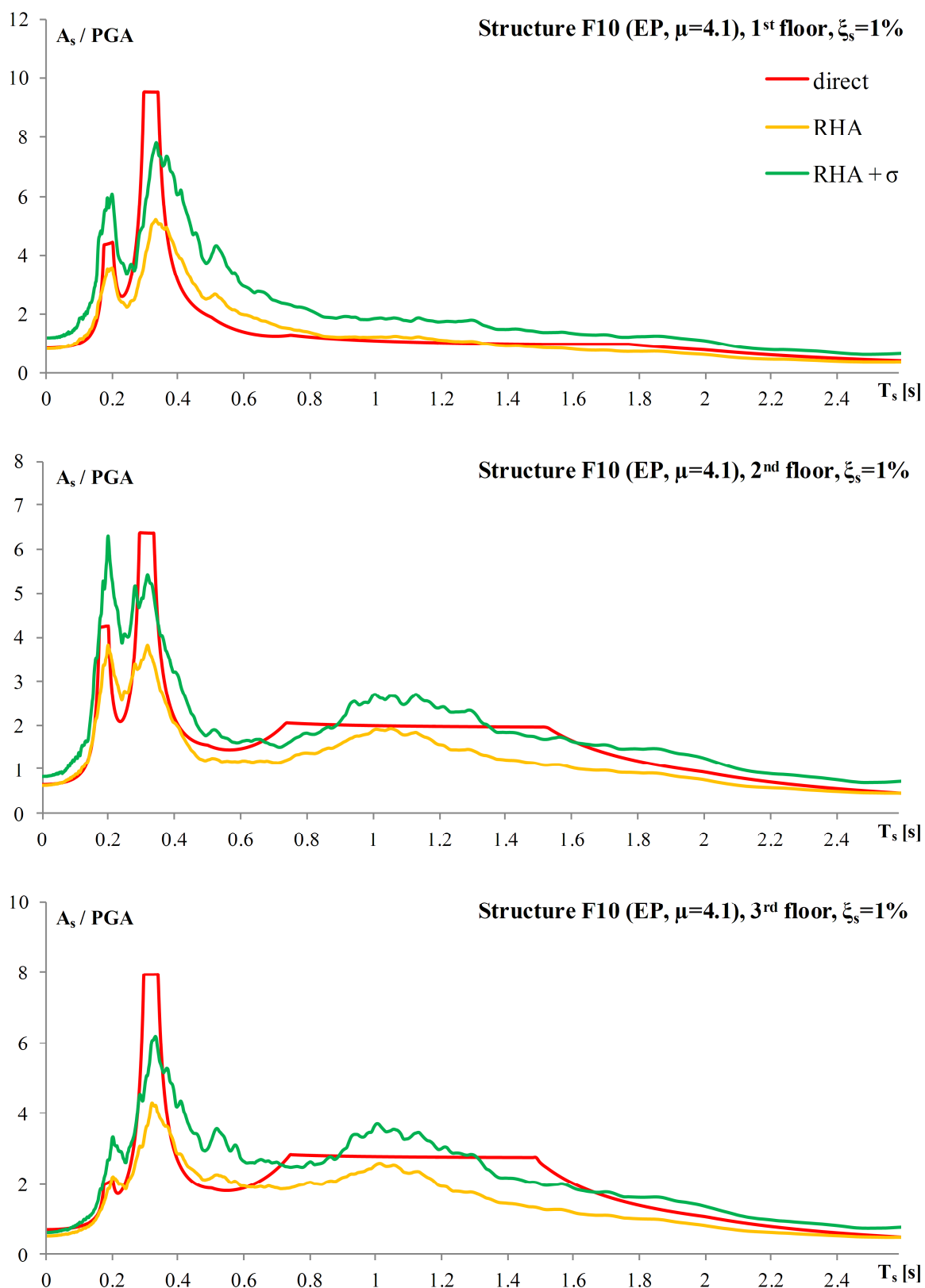


Figure 6.32: Floor response spectra for the EP model of the structure F10 (ductility $\mu=4.1$) normalized with the PGA of the input, for 1% damping of the equipment

Slika 6.32: Etažni spektri odziva za EP model konstrukcije F10 (ductility $\mu=4.1$) normirani s PGA inputa, za 1% dušenja opreme

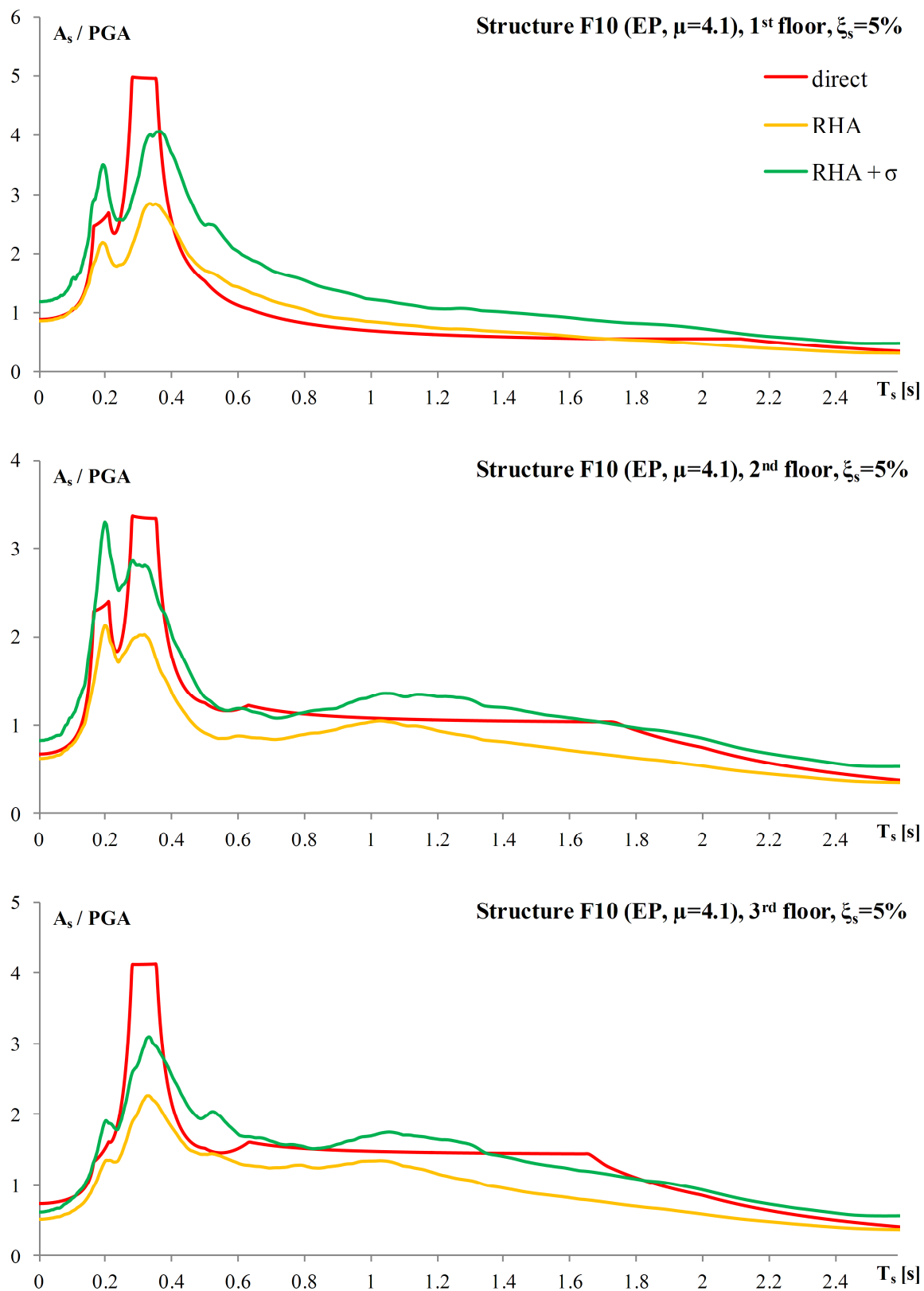


Figure 6.33: Floor response spectra for the EP model of the structure F10 (ductility $\mu=4.1$) normalized with the PGA of the input, for 5% damping of the equipment

Slika 6.33: Etažni spektri odziva za EP model konstrukcije F10 (ductility $\mu=4.1$) normirani s PGA inputa, za 5% dušenja opreme

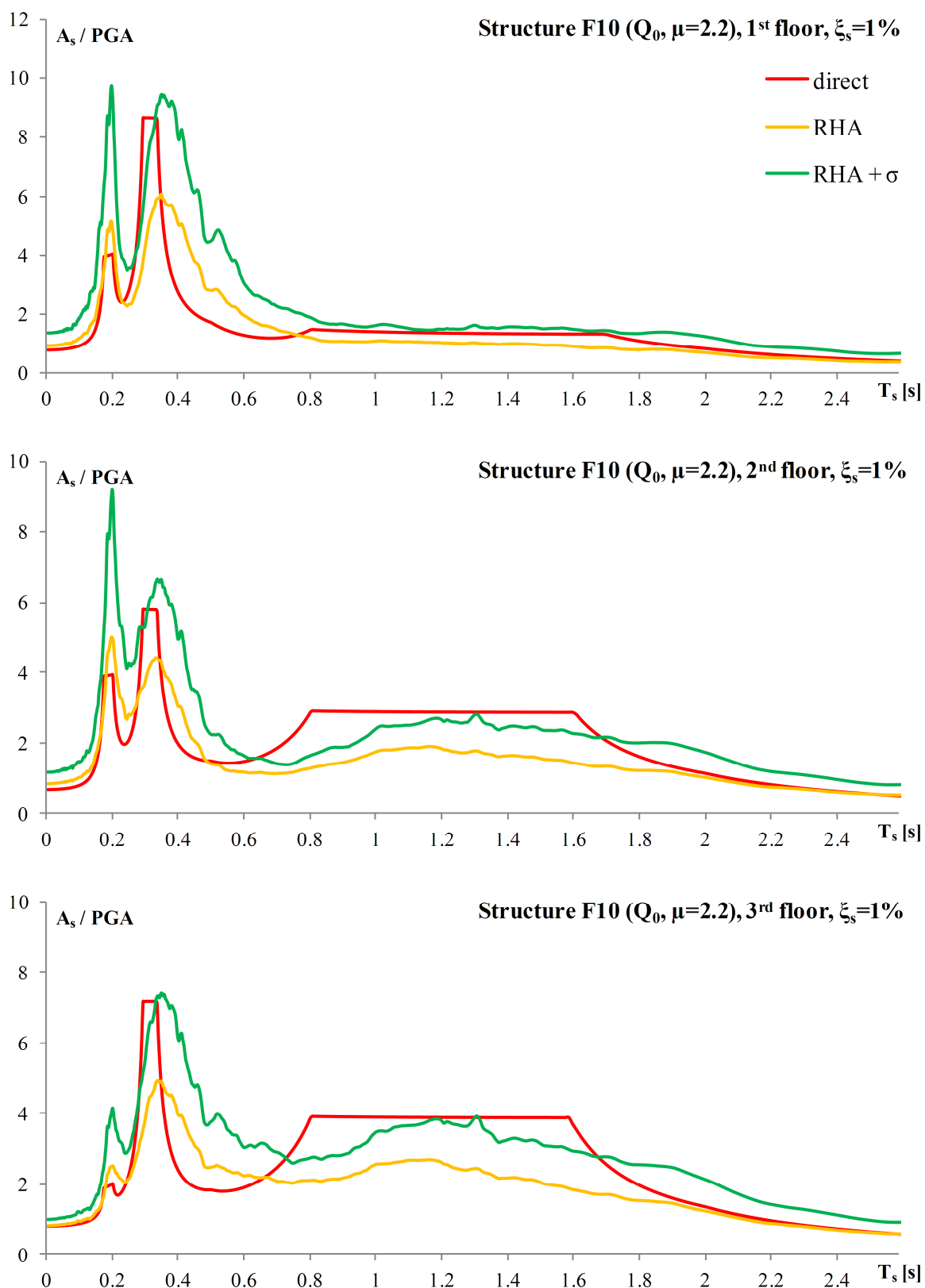


Figure 6.34: Floor response spectra for the Q_0 model of the structure F10 (ductility $\mu=2.2$) normalized with the PGA of the input, for 1% damping of the equipment

Slika 6.34: Etažni spektri odziva za Q_0 model konstrukcije F10 (ductility $\mu=2.2$) normirani s PGA inputa, za 1% dušenja opreme

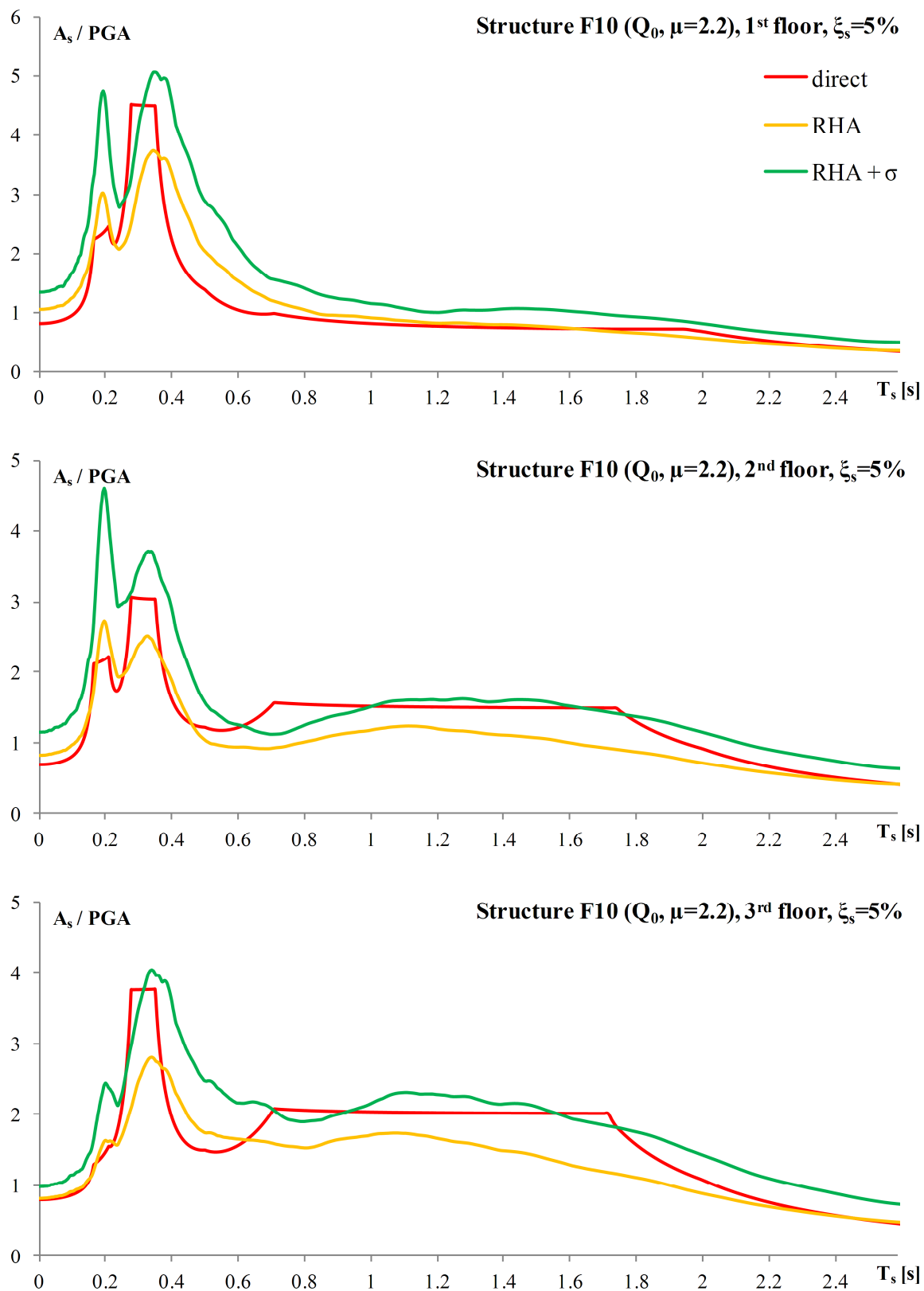


Figure 6.35: Floor response spectra for the Q_0 model of the structure F10 (ductility $\mu=2.2$) normalized with the PGA of the input, for 5% damping of the equipment

Slika 6.35: Etažni spektri odziva za Q_0 model konstrukcije F10 (ductility $\mu=2.2$) normirani s PGA inputa, za 5% dušenja opreme

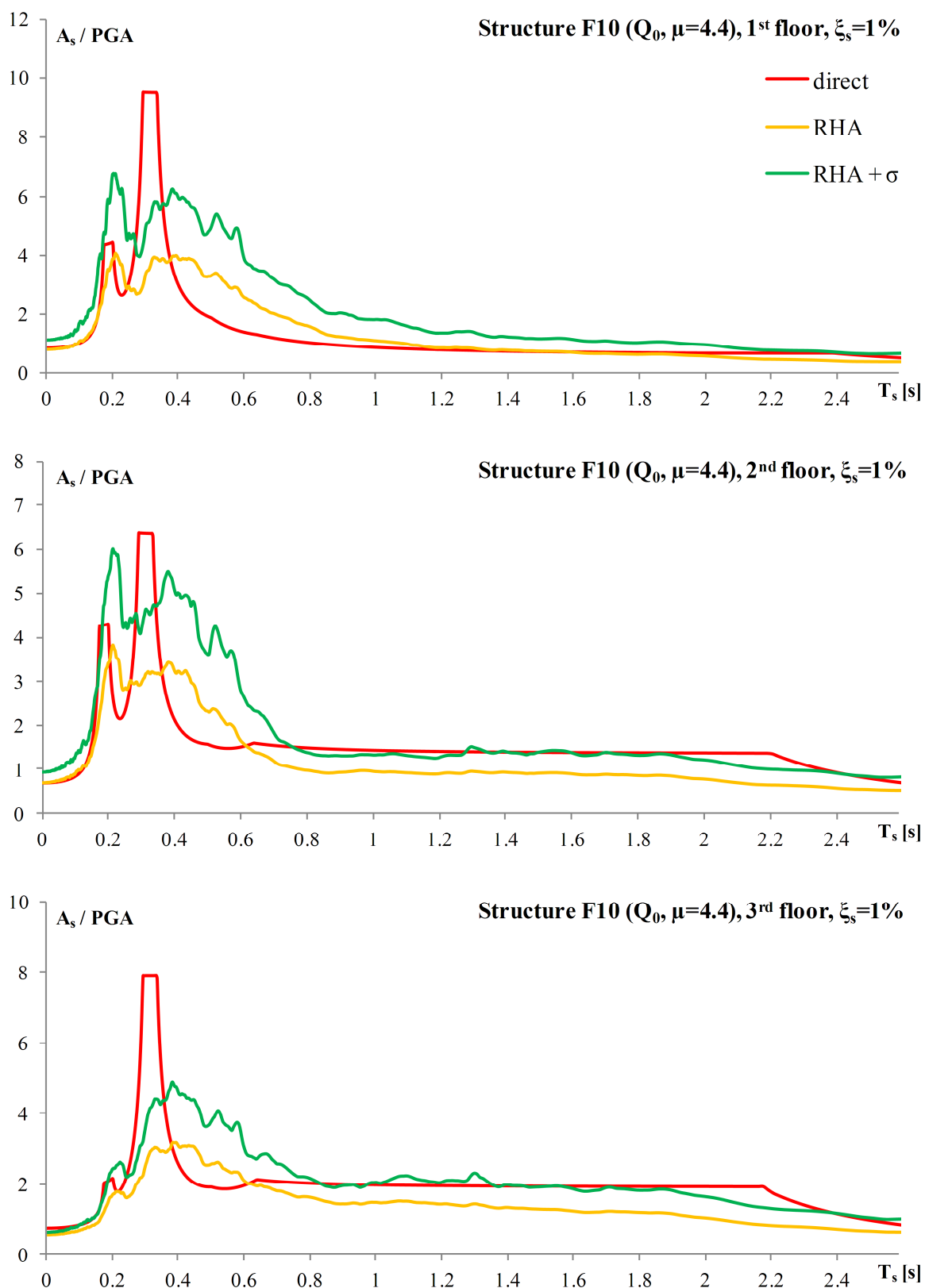


Figure 6.36: Floor response spectra for the Q_0 model of the structure F10 (ductility $\mu=4.4$) normalized with the PGA of the input, for 1% damping of the equipment

Slika 6.36: Etažni spektri odziva za Q_0 model konstrukcije F10 (ductility $\mu=4.4$) normirani s PGA inputa, za 1% dušenja opreme

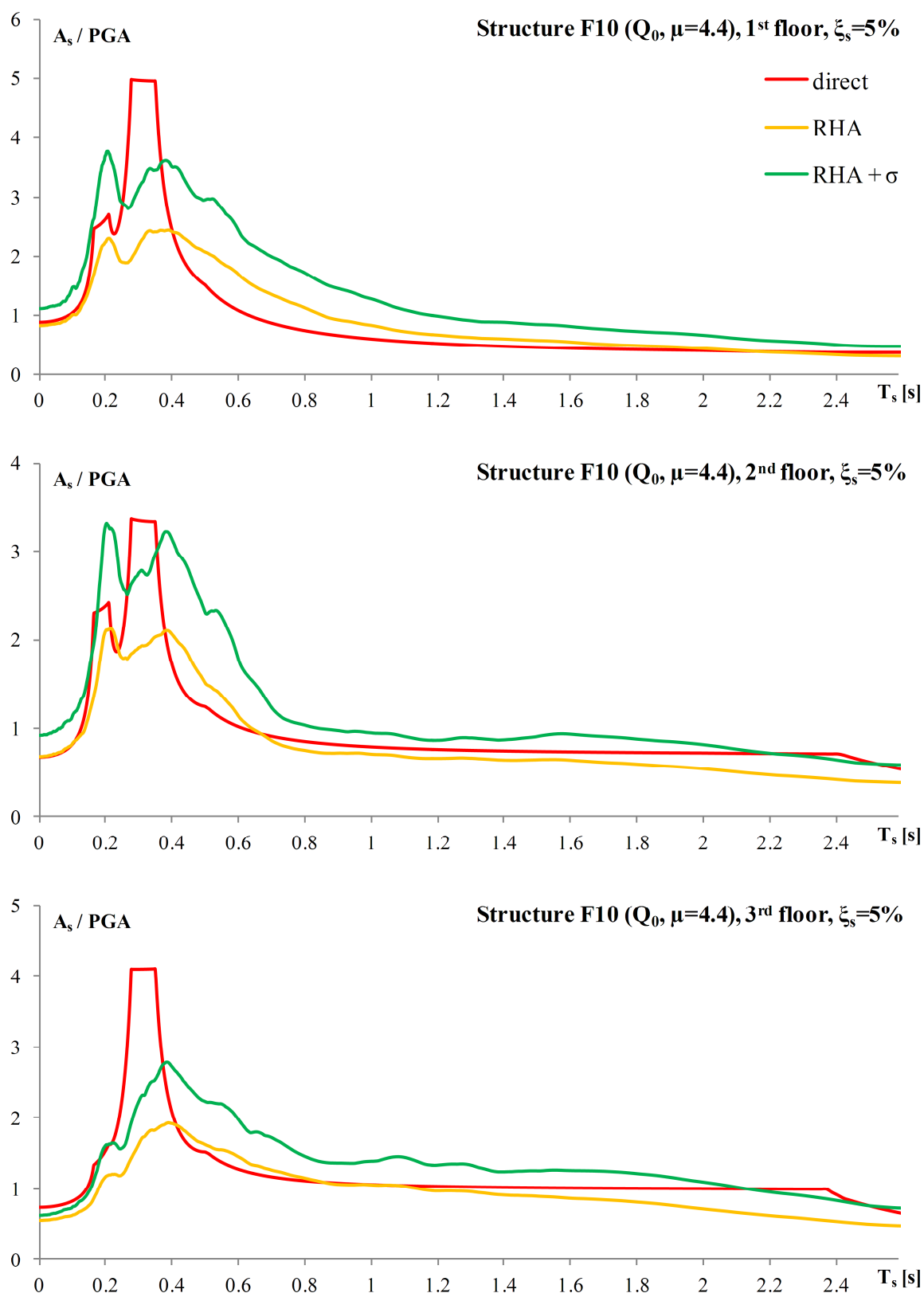


Figure 6.37: Floor response spectra for the Q_0 model of the structure F10 (ductility $\mu=4.4$) normalized with the PGA of the input, for 5% damping of the equipment

Slika 6.37: Etažni spektri odziva za Q_0 model konstrukcije F10 (ductility $\mu=4.4$) normirani s PGA inputa, za 5% dušenja opreme

Reasonable accuracy of the results obtained by the proposed direct method suggests that the method may represent a useful tool in the stage of conceptual design, as well as for checking of the results obtained from more elaborate (RHA) analyses. The method can also be used as a basis for simplified code procedures.

7 A STEP-BY-STEP OVERVIEW OF THE METHOD FOR DIRECT GENERATION OF FLOOR RESPONSE SPECTRA FOR MDOF STRUCTURES

In this chapter a step-by-step overview of the method for direct generation of floor response spectra for MDOF structures is presented, along with a numerical example of the application of the method.

7.1 Main steps in the application of the direct method

1) Determination of direct floor response spectra for individual modes

Modes with frequencies below f_{ZPA}

All modes with frequencies below f_{ZPA} are taken into account as described below.

- a. In the pre- and post-resonance regions, floor response spectra values for the mode i at the floor j ($A_{s,ij}$) are obtained from Equation 6.1.

$$A_{s,ij} = \frac{\Gamma_i \phi_{ij}}{|1 - (T_{p,i}/T_s)^2|} \sqrt{\left\{ \left(T_{p,i}/T_s \right)^2 \frac{S_e(T_{p,i}, \xi_{p,i})}{R_\mu} \right\}^2 + S_e(T_s, \xi_s)^2} \quad (6.1)$$

In the case of inelastic structures, for inelastic modes, the following modifications of Equation 6.1 should be taken into account in the post-resonance region:

- In the case of the EP model, the ratio $T_{p,i}/T_s$ should be replaced by the ratio $T_{p,i}^*/T_s$, where $T_{p,i}^*$ is the effective natural period of the equivalent SDOF system (denoted as T^* in the N2 method).
- In the case of the stiffness degrading Q model, the ratio $T_{p,i}/T_s$ should be replaced by the ratio $T_{p,i,\mu}/T_s$, where $T_{p,i,\mu}$ is determined from Equation 6.2.

$$T_{p,i,\mu} = T_{p,i}^* \sqrt{\frac{1 + \sqrt{\mu + \mu}}{3}} \quad (6.2)$$

Note that in the case of infinitely rigid equipment ($T_s=0$) Equation 6.1 becomes equal to Equation 5.1, i.e. the floor response spectrum value $A_{s,ij}$ is equal to the peak floor acceleration for the mode i at the floor j (PFA_{ij}).

- b. In the resonance regions, the spectral values $A_{s,ij}$ are limited to the values obtained from Equation 6.3. The amplification factors AMP_i used in Equation 6.3 are determined from Equations 6.4 (for the EP model) and 6.5 (for the Q model).

$$A_{s,ij} = AMP_i \Gamma_i \phi_{ij} \frac{S_e(T_{p,i}, \xi_{p,i})}{R_\mu} \quad (6.3)$$

Note that in the case of elastic structures, R_μ amounts to 1.0 for all modes and that the values of $T_{p,i}$, Γ_i , and ϕ_{ij} determined in elastic modal analysis are used in steps **1a** and **1b**.

In the case of inelastic structures, for modes in which structural response is nonlinear, the above mentioned quantities are determined by the N2 method. When the N2 method is used for inelastic modes, it is important to underline that $S_e(T_{p,i}, \xi_{p,i})$ should be replaced by $S_e(T_{p,i}^*)$ and that the values of ϕ_{ij} are determined from the inelastic deformed shape.

$$AMP_i = \left\{ \begin{array}{ll} 2.5\sqrt{10/(5+\xi_s)}, & T_{p,i}/T_C = 0 \\ \text{linear between } AMP_i(T_{p,i}/T_C = 0) \text{ and } AMP_i(T_{p,i}/T_C = 0.20), & 0 < T_{p,i}/T_C < 0.20 \\ 18(1+\xi_s)^{-0.60}, & 0.20 \leq T_{p,i}/T_C \leq 1 \\ 18(1+\xi_s)^{-0.60} (T_{p,i}/T_C)^{-0.20}, & T_{p,i}/T_C > 1 \end{array} \right\} \quad (6.4)$$

$$AMP_i = \left\{ \begin{array}{ll} 2.5\sqrt{10/(5+\xi_s)}, & T_{p,i}/T_C = 0 \\ \text{linear between } AMP_i(T_{p,i}/T_C = 0) \text{ and } AMP_i(T_{p,i}/T_C = 0.20), & 0 < T_{p,i}/T_C < 0.20 \\ 18(1+\xi_s)^{-0.60} (0.6+0.4\mu)\mu^{-0.85}, & 0.20 \leq T_{p,i}/T_C \leq 1 \\ 18(1+\xi_s)^{-0.60} (T_{p,i}/T_C)^{-0.20} (0.6+0.4\mu)\mu^{-0.85}, & T_{p,i}/T_C > 1 \end{array} \right\} \quad (6.5)$$

Modes with frequencies above f_{ZPA}

All modes with frequencies above f_{ZPA} are taken into account through a single, substituting mode. The direct floor response spectrum for this mode is determined from Equation F.12 presented in ANNEX F.

2) Combination of direct floor response spectra obtained for individual modes

- a. In the period range between $T_s=0$ and the end of the resonance plateau of the direct floor response spectrum related to the fundamental mode, combine the direct floor response spectra calculated for individual modes by using one of the USNRC 1.92 (2006) methods (Gupta's or Lindley-Yow method, coupled with the Missing Mass method), as shown in Figure 6.1.
- b. In the period range after the resonance related to the fundamental mode (i.e. after $T_s/T_{p,i}=1$), combine the direct floor response spectra calculated for individual modes from the formula for the post-resonance region by using the algebraic summation rule (ALGSUM), as shown in Figure 6.1.
- c. Combined spectra from steps **a** and **b** should be linked. If they intersect (see Figure 6.1a), the linking point is determined by the intersection. If there is no intersection, the plateau obtained in step **a** should be extended towards the larger periods of equipment in order to obtain an intersection with the floor response spectrum determined in step **b** (see Figure 6.1b).

It should be noted that the modal superposition approach, which is used in the direct method, is fully justified in the case of elastic structures, whereas in the case of inelastic structures it represents an approximation.

7.2 Numerical example of the application of the direct method

For the purpose of a numerical example presented in this section, let us consider the three-storey frame F03, previously described in Section 4.1.

For convenience, the main properties of the frame F03 are repeated herein. The storey height amounts to 3 m, whereas the bay width amounts to 5 m (with respect to centerline dimensions). The dimensions of cross sections (width/height) amount to 50/80 cm in the case of columns and 50/60 cm in the case of beams. Lumped mass amounts to 14 t in each free node, i.e. 28 t at each storey of the frame. Plastic hinges are assumed at the ends of beams and columns. Reinforcement is presented in Figure 4.3 (Section 4.1). The modulus of elasticity of concrete (E_c) amounts to 33 GPa, the modulus of elasticity of steel (E_s) amounts to 200 GPa, whereas the yield strength of reinforcement (f_y) amounts to 500 MPa. Axial forces in beams and columns and yield moments and rotations in plastic hinges are presented in Table 4.1. Inelastic structural behaviour is represented by using the Q_0 model. It is assumed that structural damping in all three modes ($\zeta_{p,1}$, $\zeta_{p,2}$ and $\zeta_{p,3}$) amounts to 5%.

Task: Equipment will be installed at each storey of the considered structure. Nevertheless, at this stage of the design, the properties of the equipment are unknown. Therefore, the determination of peak floor accelerations (PFAs) and floor response spectra in the whole period range is needed, by taking into account equipment damping ζ_s equal to 5%. Seismic input is defined by the Eurocode 8 (2004) target spectrum for soil type B, described in Section 2.1 (see Figure 2.1a), and it has the characteristic period of ground motion T_C equal to 0.5 s. PGA of the input amounts to 0.35g. Both elastic and inelastic structural behaviour should be considered. It is assumed that structural inelasticity will occur only in the fundamental mode.

7.2.1 Modal analysis

Modal analysis was conducted in OpenSees, with respect to the effective moment of inertia of each Elastic Beam Column element. The effective moment of inertia amounted to approximately 50% of the uncracked moment of inertia, which was achieved by the approach proposed by Došek and Fajfar (2005), as discussed in Section 4.1. The natural periods of the frame F03 amounted to $T_{p,1}=0.29$ s, $T_{p,2}=0.075$ s and $T_{p,3}=0.037$ s, whereas the eigenvectors are presented below. The modal participation factors amounted to $\Gamma_1=1.28$, $\Gamma_2=0.43$ and $\Gamma_3=0.26$.

$$\phi_1 = \begin{Bmatrix} +0.242 \\ +0.649 \\ +1.000 \end{Bmatrix}, \quad \phi_2 = \begin{Bmatrix} +1.000 \\ +0.910 \\ -0.833 \end{Bmatrix}, \quad \phi_3 = \begin{Bmatrix} +1.000 \\ -0.828 \\ +0.295 \end{Bmatrix}$$

7.2.2 Application of the N2 method on the fundamental mode

Lateral loads are determined as the product of the first mode shape component in a considered storey and the storey mass as

$$\mathbf{P} = \mathbf{M}\phi_1 = \begin{bmatrix} 28 & 0 & 0 \\ 0 & 28 & 0 \\ 0 & 0 & 28 \end{bmatrix} \begin{Bmatrix} +0.242 \\ +0.649 \\ +1.000 \end{Bmatrix} = \begin{Bmatrix} 6.8 \\ 18.2 \\ 28.0 \end{Bmatrix}$$

where \mathbf{P} denotes the vector of lateral loads and \mathbf{M} denotes the mass matrix.

After the pushover analysis is performed up to an arbitrarily chosen roof displacement equal to 0.10 m, a relationship between the base shear force (F) and the top (roof) displacement (d) is determined (see Figure 4.14a in Subsection 4.2.3).

Effective mass m^* and transformation factor Γ (which is equal to modal participation factor Γ_1) are determined as

$$m^* = \phi_1^T \mathbf{M} \mathbf{I} = 53.0 \text{ t}, \quad \Gamma = \frac{m^*}{\phi_1^T \mathbf{M} \phi_1} = 1.28$$

where \mathbf{I} denotes unity vector.

In order to obtain the quantities of an equivalent SDOF system, the quantities obtained for MDOF system are divided with the transformation factor Γ . Therefore, the base shear force and the displacement of the equivalent SDOF system (F^* and d^*) are obtained as

$$F^* = \frac{F}{\Gamma}, \quad d^* = \frac{d}{\Gamma}$$

The obtained F^*-d^* relationship is presented in Figure 4.14a (Subsection 4.2.3) and it is idealized as elasto-perfectly plastic (for procedure details see ANNEX B in Eurocode 8 2004). The determination of the yield force which represents the ultimate strength of the equivalent SDOF system (F_y^*) and the corresponding yield displacement (d_y^*) is straightforward. The values of F_y^* and d_y^* amount to 277.8 kN and 1.15 cm, respectively.

The effective natural period of the equivalent SDOF system is determined as

$$T^* = 2\pi \sqrt{\frac{m^* d_y^*}{F_y^*}} = 0.30 \text{ s}$$

The acceleration S_a is obtained by dividing the F^* with the effective mass m^* . The plot of S_a versus the displacement d^* represents a capacity diagram which is presented in Figure 4.14b (Subsection 4.2.3). The acceleration S_{ay} is the one that corresponds to the yield force F_y^* and is determined as

$$S_{ay} = \frac{F_y^*}{m^*} = \frac{277.8}{9.81 \cdot 53} = 0.53g$$

The reduction factor R_μ is determined as

$$R_\mu = \frac{S_e(T^*)}{S_{ay}} = \frac{0.87g}{0.53g} = 1.64$$

Since $T^* < T_C$, the equal displacement rule is not applicable. The displacement demand is determined as

$$d_t^* = \frac{\left(\frac{T^*}{2\pi}\right)^2 S_e(T^*)}{R_\mu} \left(1 + (R_\mu - 1) \frac{T_C}{T^*}\right) = 2.39 \text{ cm}$$

The corresponding ductility demand μ is obtained as

$$\mu = 1 + (R_\mu - 1) \frac{T_C}{T^*} = 2.1$$

The target displacement ($d_3=d_t$) is determined as shown below and pushover analysis is performed up to it.

$$d_3 = d_t = \Gamma d_t^* = 3.06 \text{ cm}$$

The corresponding displacements of the first and second storey amount to $d_1=1.04$ cm and $d_2=2.27$ cm, respectively. The vector of inelastic first mode shape (ϕ_1^{inel}) is determined as

$$\phi_1^{inel} = \begin{Bmatrix} d_1 / d_3 \\ d_2 / d_3 \\ d_3 / d_3 \end{Bmatrix} = \begin{Bmatrix} +0.268 \\ +0.644 \\ +1.000 \end{Bmatrix}$$

It should be noted that, when needed, the N2 method can also be applied for inelastic higher modes.

7.2.3 Determination of PFAs and floor response spectra for individual modes

Elastic fundamental mode

The value in an input elastic acceleration spectrum (S_e) at $T_{p,1}=0.29$ s for $\zeta_{p,1}=5\%$ amounts to 0.87g. Amplification factor AMP_1 amounts to 6.14 (Equation 6.4) for equipment damping ζ_s equal to 5%.

Peak floor accelerations are determined from Equation 5.1 as:

$$\begin{Bmatrix} PFA_{11} \\ PFA_{12} \\ PFA_{13} \end{Bmatrix} = \Gamma_1 \phi_1 S_e(T_{p,1}, \zeta_{p,1}) = 1.28 \begin{Bmatrix} +0.242 \\ +0.649 \\ +1.000 \end{Bmatrix} 0.87\text{g} = \begin{Bmatrix} +0.27 \\ +0.72 \\ +1.11 \end{Bmatrix} \text{g}$$

Floor response spectra are determined as:

1st floor

- The pre- and post-resonance regions (Equation 6.1):

$$A_{s,11} = \frac{0.31}{|1 - (0.29/T_s)^2|} \sqrt{\left\{0.87\text{g} \left(0.29/T_s\right)^2\right\}^2 + S_e(T_s, \zeta_s)^2}$$

- The resonance region (Equation 6.3):

$$A_{s,11} = 1.65g$$

2nd floor

- The pre- and post-resonance regions (Equation 6.1):

$$A_{s,12} = \frac{0.83}{\left|1 - (0.29/T_s)^2\right|} \sqrt{\left\{0.87g(0.29/T_s)^2\right\}^2 + S_e(T_s, \xi_s)^2}$$

- The resonance region (Equation 6.3):

$$A_{s,12} = 4.44g$$

3rd floor

- The pre- and post-resonance regions (Equation 6.1):

$$A_{s,13} = \frac{1.28}{\left|1 - (0.29/T_s)^2\right|} \sqrt{\left\{0.87g(0.29/T_s)^2\right\}^2 + S_e(T_s, \xi_s)^2}$$

- The resonance region (Equation 6.3):

$$A_{s,13} = 6.84g$$

Inelastic fundamental mode

The value in an input inelastic acceleration spectrum (S_e/R_μ) at $T_{p,1}^* = 0.29$ s (for $\xi_{p,1} = 5\%$) amounts to 0.53g (see Section 7.2.2). Amplification factor AMP_I amounts to 4.71 (Equation 6.5) for equipment damping ξ_s equal to 5%.

Peak floor accelerations are determined from Equation 5.1 as:

$$\begin{Bmatrix} PFA_{11} \\ PFA_{12} \\ PFA_{13} \end{Bmatrix} = \Gamma_I \phi^{inel} \frac{S_e(T_{p,1}^*)}{R_\mu} = 1.28 \begin{Bmatrix} +0.268 \\ +0.644 \\ +1.000 \end{Bmatrix} 0.53g = \begin{Bmatrix} +0.18 \\ +0.44 \\ +0.68 \end{Bmatrix} g$$

Floor response spectra are determined as:

1st floor

- The pre-resonance region (Equation 6.1):

$$A_{s,11} = \frac{0.34}{|1 - (0.29/T_s)^2|} \sqrt{\left\{0.53g(0.29/T_s)^2\right\}^2 + S_e(T_s, \xi_s)^2}$$

- The post-resonance region (Equations 6.1 and 6.2):

$$A_{s,11} = \frac{0.34}{|1 - (0.37/T_s)^2|} \sqrt{\left\{0.53g(0.37/T_s)^2\right\}^2 + S_e(T_s, \xi_s)^2}$$

- The resonance region (Equation 6.3):

$$A_{s,11} = 0.86g$$

2nd floor

- The pre-resonance region (Equation 6.1):

$$A_{s,12} = \frac{0.82}{|1 - (0.29/T_s)^2|} \sqrt{\left\{0.53g(0.29/T_s)^2\right\}^2 + S_e(T_s, \xi_s)^2}$$

- The post-resonance region (Equations 6.1 and 6.2):

$$A_{s,12} = \frac{0.82}{|1 - (0.37/T_s)^2|} \sqrt{\left\{0.53g(0.37/T_s)^2\right\}^2 + S_e(T_s, \xi_s)^2}$$

- The resonance region (Equation 6.3):

$$A_{s,12} = 2.06g$$

3rd floor

- The pre-resonance region (Equation 6.1):

$$A_{s,13} = \frac{1.28}{|1 - (0.29/T_s)^2|} \sqrt{\left\{0.53g(0.29/T_s)^2\right\}^2 + S_e(T_s, \xi_s)^2}$$

- The post-resonance region (Equations 6.1 and 6.2):

$$A_{s,13} = \frac{1.28}{|1 - (0.37/T_s)^2|} \sqrt{\left\{0.53g(0.37/T_s)^2\right\}^2 + S_e(T_s, \xi_s)^2}$$

- The resonance region (Equation 6.3):

$$A_{s,13} = 3.20g$$

Second mode

The value in an input elastic acceleration spectrum (S_e) at $T_{p,2}=0.075$ s for $\xi_{p,2}=5\%$ amounts to $0.61g$. Amplification factor AMP_2 amounts to 5.23 (Equation 6.4) for equipment damping ξ_s equal to 5% .

Peak floor accelerations are determined from Equation 5.1 as:

$$\begin{Bmatrix} PFA_{21} \\ PFA_{22} \\ PFA_{23} \end{Bmatrix} = \Gamma_2 \phi S_e(T_{p,2}, \xi_{p,2}) = 0.43 \begin{Bmatrix} +1.000 \\ +0.910 \\ -0.833 \end{Bmatrix} 0.61g = \begin{Bmatrix} +0.26 \\ +0.24 \\ -0.22 \end{Bmatrix} g$$

Floor response spectra are determined as:

1st floor

- The pre- and post-resonance regions (Equation 6.1):

$$A_{s,21} = \frac{0.43}{|1 - (0.075/T_s)^2|} \sqrt{\left\{0.61g(0.075/T_s)^2\right\}^2 + S_e(T_s, \xi_s)^2}$$

- The resonance region (Equation 6.3):

$$A_{s,21} = 1.37g$$

2nd floor

- The pre- and post-resonance regions (Equation 6.1):

$$A_{s,22} = \frac{0.39}{|1 - (0.075/T_s)^2|} \sqrt{\left\{0.61g(0.075/T_s)^2\right\}^2 + S_e(T_s, \xi_s)^2}$$

- The resonance region (Equation 6.3):

$$A_{s,22} = 1.25g$$

3rd floor

- The pre- and post-resonance regions (Equation 6.1):

$$A_{s,23} = \frac{-0.36}{|1 - (0.075/T_s)^2|} \sqrt{\left\{0.61g(0.075/T_s)^2\right\}^2 + S_e(T_s, \xi_s)^2}$$

- The resonance region (Equation 6.3):

$$A_{s,23} = -1.14g$$

Third mode

The value in an input elastic acceleration spectrum (S_e) at $T_{p,3}=0.037$ s for $\zeta_{p,3}=5\%$ amounts to 0.48g. Amplification factor AMP_3 amounts to 3.85 (Equation 6.4) for equipment damping ζ_s equal to 5%.

Peak floor accelerations are determined from Equation 5.1 as:

$$\begin{Bmatrix} PFA_{31} \\ PFA_{32} \\ PFA_{33} \end{Bmatrix} = \Gamma_{33} \phi S_e(T_{p,3}, \zeta_{p,3}) = 0.26 \begin{Bmatrix} +1.000 \\ -0.828 \\ +0.295 \end{Bmatrix} 0.48g = \begin{Bmatrix} +0.12 \\ -0.10 \\ +0.04 \end{Bmatrix} g$$

Floor response spectra are determined as:

1st floor

- The pre- and post-resonance regions (Equation 6.1):

$$A_{s,31} = \frac{0.26}{|1 - (0.037/T_s)^2|} \sqrt{\{0.48g(0.037/T_s)^2\}^2 + S_e(T_s, \zeta_s)^2}$$

- The resonance region (Equation 6.3):

$$A_{s,31} = 0.48g$$

2nd floor

- The pre- and post-resonance regions (Equation 6.1):

$$A_{s,32} = \frac{-0.22}{|1 - (0.037/T_s)^2|} \sqrt{\{0.48g(0.037/T_s)^2\}^2 + S_e(T_s, \zeta_s)^2}$$

- The resonance region (Equation 6.3):

$$A_{s,32} = -0.40g$$

3rd floor

- The pre- and post-resonance regions (Equation 6.1):

$$A_{s,33} = \frac{0.08}{|1 - (0.037/T_s)^2|} \sqrt{\left\{0.48g(0.037/T_s)^2\right\}^2 + S_e(T_s, \xi_s)^2}$$

- The resonance region (Equation 6.3):

$$A_{s,33} = 0.14g$$

7.2.4 Combination of PFAs and floor response spectra obtained for individual modes

Gupta's method is used for the combination of PFAs and floor response spectra obtained for individual modes. Combination coefficients are presented in ANNEX F, but for convenience their determination is repeated herein.

Gupta's coefficients for modal combination are determined from frequencies f_1 and f_2 (for more details see ANNEX F).

By taking into account the seismic input (Eurocode 8 2004 target spectrum described in Section 2.1), the frequency f_1 is determined as shown below (T_B is the lower limit of the period of the constant spectral acceleration branch and it amounts to 0.15 s).

$$f_1 = \frac{1}{T_B} = 6.67 \text{ Hz}$$

By taking into account $f_{ZPA}=33 \text{ Hz}$, the frequency f_2 is determined as

$$f_2 = \frac{f_1 + 2f_{ZPA}}{3} = 24.22 \text{ Hz}$$

The rigid response coefficients α_i for the first (α_1), second (α_2) and third mode (α_3) are determined from Equations F.8 (ANNEX F). The periodic coefficients are determined as $(1-\alpha_i^2)^{0.5}$. The results are presented in Table 7.1.

Table 7.1: Gupta's coefficients for modal combination (elastic and Q_0 structure F03)

Preglednica 7.1: Guptini koeficienti za modalno kombinacijo (elastična in Q_0 konstrukcija F03)

mode	$T_{p,i}$ [s]	f_i [Hz]	α_i	$(1-\alpha_i^2)^{0.5}$
1	0.29	3.45	0	1
2	0.075	13.33	0.54	0.84
3	0.037	27.03	1	0

The resulting PFAs are determined as:

1st floor

$$PFA_{rigid,1} = 0.54PFA_{21} + PFA_{31}$$

$$PFA_{periodic,1} = \sqrt{(PFA_{11})^2 + (0.84PFA_{21})^2}$$

$$PFA_1 = \sqrt{(PFA_{rigid,1})^2 + (PFA_{periodic,1})^2}$$

2nd floor

$$PFA_{rigid,2} = 0.54PFA_{22} + PFA_{32}$$

$$PFA_{periodic,2} = \sqrt{(PFA_{12})^2 + (0.84PFA_{22})^2}$$

$$PFA_2 = \sqrt{(PFA_{rigid,2})^2 + (PFA_{periodic,2})^2}$$

3rd floor

$$PFA_{rigid,3} = 0.54PFA_{23} + PFA_{33}$$

$$PFA_{periodic,3} = \sqrt{(PFA_{13})^2 + (0.84PFA_{23})^2}$$

$$PFA_3 = \sqrt{(PFA_{rigid,3})^2 + (PFA_{periodic,3})^2}$$

The resulting direct floor response spectra, presented in Figure 7.1, are determined as:

1st floor

- The period range between $T_s=0$ and the end of the resonance plateau of the direct floor response spectrum related to the fundamental mode:

$$A_{s,rigid,1} = 0.54A_{s,21} + A_{s,31}$$

$$A_{s,periodic,1} = \sqrt{(A_{s,11})^2 + (0.84A_{s,21})^2}$$

$$A_{s,1} = \sqrt{(A_{s,rigid,1})^2 + (A_{s,periodic,1})^2}$$

- The period range after the resonance related to the fundamental mode (i.e. after $T_s/T_{p,1}=1$):

$$A_{s,1} = A_{s,11} + A_{s,21} + A_{s,31}$$

The spectra obtained for both period ranges are linked by applying the procedure described in step 2c in Section 7.1.

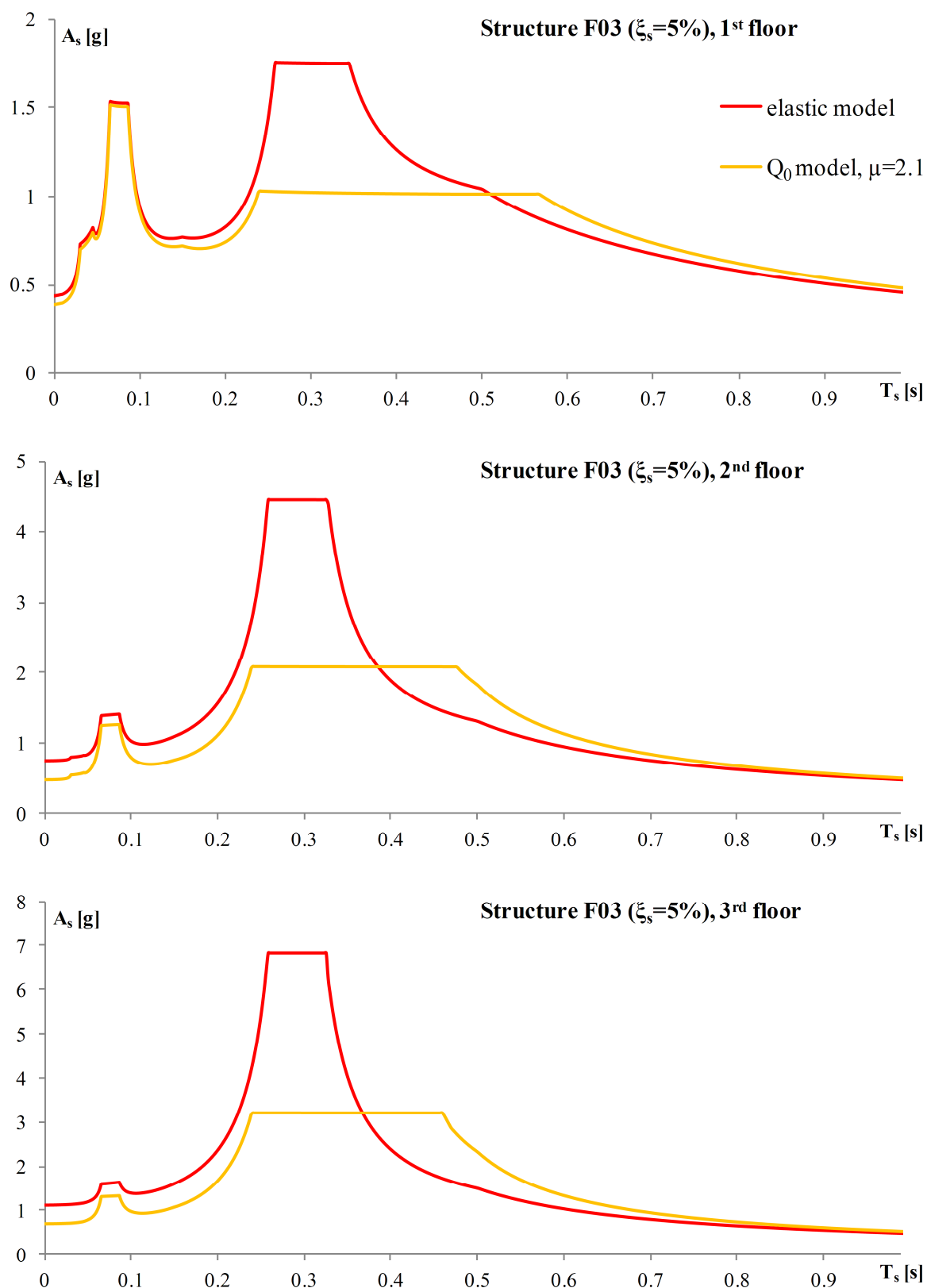


Figure 7.1: Floor response spectra for elastic and Q_0 model (ductility $\mu=2.1$) of the structure F03, for 5% damping of the equipment

Slika 7.1: Etažni spektri odziva za elastičen in Q_0 model (duktilnost $\mu=2.1$) konstrukcije F03, za 5% dušenja opreme

2nd floor

- The period range between $T_s=0$ and the end of the resonance plateau of the direct floor response spectrum related to the fundamental mode:

$$A_{s,rigid,2} = 0.54A_{s,22} + A_{s,32}$$

$$A_{s,periodic,2} = \sqrt{(A_{s,12})^2 + (0.84A_{s,22})^2}$$

$$A_{s,2} = \sqrt{(A_{s,rigid,2})^2 + (A_{s,periodic,2})^2}$$

- The period range after the resonance related to the fundamental mode (i.e. after $T_s/T_{p,1}=1$):

$$A_{s,2} = A_{s,12} + A_{s,22} + A_{s,32}$$

The spectra obtained for both period ranges are linked by applying the procedure described in step **2c** in Section 7.1.

3rd floor

- The period range between $T_s=0$ and the end of the resonance plateau of the direct floor response spectrum related to the fundamental mode:

$$A_{s,rigid,3} = 0.54A_{s,23} + A_{s,33}$$

$$A_{s,periodic,3} = \sqrt{(A_{s,13})^2 + (0.84A_{s,23})^2}$$

$$A_{s,3} = \sqrt{(A_{s,rigid,3})^2 + (A_{s,periodic,3})^2}$$

- The period range after the resonance related to the fundamental mode (i.e. after $T_s/T_{p,1}=1$):

$$A_{s,3} = A_{s,13} + A_{s,23} + A_{s,33}$$

The spectra obtained for both period ranges are linked by applying the procedure described in step **2c** in Section 7.1.

8 CONCLUSIONS

In the dissertation extensive parametric studies of floor response spectra were conducted on SDOF and MDOF primary structures. Both elastic and inelastic primary structures were taken into account. In all cases equipment was represented through a linear elastic SDOF oscillator. A structure-equipment system was always treated as uncoupled. A great number of floor response spectra were calculated by using the response-history analysis (RHA) and various influences on floor response spectra were examined: the type, natural period, hysteretic behaviour, and ductility of the structure, as well as the damping of the equipment. In the case of SDOF primary structures the influence of the ground motion characteristics was also investigated.

Based on the results obtained in the parametric study conducted on SDOF primary structures, a simple method for determination of floor response spectra directly from the design response spectrum was proposed. A preliminary version of the direct method was presented in two conference papers (Vukobratović and Fajfar 2012, 2013), whereas the final version was published in a scientific journal (Vukobratović and Fajfar 2015). The research continued with studying elastic and inelastic MDOF models of the primary structure. As the result, the method for direct determination of floor response spectra was extended to MDOF structures.

8.1 Main findings

The results obtained in the parametric study conducted on SDOF primary structures confirmed some well-known characteristics of the floor response spectra (in terms of absolute accelerations) and led to several new findings, as discussed in the following text.

The period range of a floor response spectrum can be roughly divided into three regions, depending on the ratio between the natural period of the equipment (T_s) and the natural period of the structure (T_p): the pre-resonance ($T_s/T_p < 0.8$), resonance ($0.8 < T_s/T_p < 1.25$), and post-resonance region ($T_s/T_p > 1.25$).

It was shown that in the pre-resonance and resonance regions, the behaviour of the equipment is strongly influenced by the behaviour of the primary structure. Both regions are characterized by a significant reduction in floor response spectra due to inelastic structural behaviour. The size of the reduction depends on the size of ductility demand μ . In the post-resonance region, the floor response spectrum is controlled by the ground motion spectrum, i.e. the floor response spectrum approaches to the ground motion spectrum as the ratio T_s/T_p decreases. In the limit case of infinitely rigid equipment ($T_s=0$), the floor response spectrum value (A_s) is equal to the acceleration of the structure (A_p), i.e. to the value in the elastic (for $\mu=1$) or inelastic acceleration response spectrum of the structure at the period T_p . In the limit case of infinitely flexible equipment, the value of the floor response spectrum is equal to zero.

The shape of floor response spectra is influenced by the hysteretic behaviour of the structure. In the case of the elasto-plastic (EP) model, the peak values of floor response spectra occur close to the resonance ($T_s \approx T_p$). In the case of the stiffness degrading (Q) model the peak values of floor response spectra are shifted towards higher periods, due to increasing T_p with increasing plastic deformations.

In the study, the maximum value of the ratio A_s/A_p was defined as an amplification factor *AMP*. Note that the peak acceleration of the structure A_p is equal to the value in the floor response spectrum for the zero period of the equipment ($T_s=0$). For both the EP model and the Q model of the primary structure,

the main parameter that influences the amplitude of the *AMP* is the damping of the equipment ζ_s . In the case of the EP model, the influence of the ductility of the structure (μ) on the *AMP* is small, whereas in the case of the Q model it is moderate. In the case of the EP model, the *AMP* values slightly increase with increasing ductility, whereas in the case of the Q model they decrease. The results obtained for both sets of considered ground motions indicate that the shape of the response spectrum characterized by the characteristic period of ground motion T_C has only a small influence on the *AMP*, provided that the ratio T_p/T_C is plotted on the x -axis instead of T_p . The *AMP* reaches its peak value in the region $0.20 \leq T_p/T_C \leq 1$. In the region $0 \leq T_p/T_C < 0.20$ the obtained results indicate that the decrease of the ratio T_p/T_C leads to the decrease of the *AMP*. In the limit case when $T_p/T_C = 0$ the value of the *AMP* can be assessed by using existing design provisions. The *AMP* decreases with the increasing ratio T_p/T_C if the ratio is larger than 1. Additionally, the study also showed that moderate hardening after yield point in the Q model practically does not influence the *AMP*.

Based on the results obtained and conclusions made in the parametric study, a method for direct generation of floor response spectra from ground motion spectrum was developed. The development was based on a very simple direct method proposed by Yasui et al. (1993), which was limited to elastic primary structures, as well as on the idea for its extension into nonlinear range, which was first proposed by Novak and Fajfar (1994). In order to make the original direct method applicable for inelastic SDOF structures and to improve its accuracy in the resonance region, some changes were introduced: the elastic acceleration spectrum was replaced with an inelastic acceleration spectrum corresponding to the expected ductility demand, and the spectral values in the resonance region ($T_s \approx T_p$) were determined by means of empirical equations which are based on the results of the parametric study (*AMP*).

For the case of elastic SDOF structures, some of the results obtained by using the proposed direct method were compared with the results of the original method proposed by Yasui et al. (1993), as well as with the results obtained in the parametric study, i.e. the results of the RHA. It was shown that the results of the proposed direct method are more accurate than the results obtained from the original method proposed by Yasui et al. (1993). In order to validate the proposed direct method for the case of inelastic SDOF structures, the obtained results were compared with the results obtained from the RHA and a good agreement was observed.

The results of the direct method were also compared with the results obtained from the direct method proposed by Sullivan et al. (2013). It was shown that the direct method proposed herein provides more accurate prediction of floor response spectra than the method proposed by Sullivan et al. (2013). Also, the provisions of Eurocode 8 (2004), which consider the design of non-structural elements, were examined. It was concluded that the simple Eurocode 8 (2004) formula does not take into account three important influences on floor response spectra: the natural period of the primary structure (in terms of its influence on structural accelerations), the level of the inelastic behavior of the primary structure, and the damping of the equipment (secondary structure).

In the parametric study conducted on MDOF primary structures, four simple three-storey planar reinforced concrete structures were considered. Structural elements were modelled as beam-column elements, their self-weight was neglected and a lumped mass approach was applied. The RHA was conducted by using SAP2000 14.2.4 (for the elastic and EP models) and OpenSees 2.2.2 (for stiffness degrading Q model without hardening). A concentrated plasticity approach was used in the case of inelastic structures. For both hysteretic models, the behaviour of plastic hinges was represented by moment-rotation relationship. Infinite rotation capacity was assigned to each plastic hinge in every

analysed structure, which had to be done since the seismic input consisted of ground motions with quite different intensities and the prevention of the structural collapse was crucial, otherwise statistics would have been invalidated. According to the provisions of Eurocode 8 (2004), the effects of cracking should be considered (i.e. the flexural stiffness properties of concrete elements may be taken as 50% of the corresponding stiffness of uncracked elements). In OpenSees, Elastic Beam Column elements were modelled by using the moments of inertia of uncracked sections and, for each plastic hinge, the yield rotation of the uncracked cross section was assumed for the determination of the yield point at the moment-rotation relationship. In this way, when the yield moments in plastic hinges are reached, the effective moment of inertia of the element section approximately equals one half of the moment of inertia of the uncracked section. On the other hand, in SAP, the effective moment of inertia of each Frame Element section was achieved by multiplication of the uncracked moment of inertia with the factor equal to 0.5, which produced an exact 50% reduction of the moment of inertia. As a consequence, the results of modal analyses conducted in SAP and OpenSees were somewhat different, especially in the case of considered wall structures. This led to certain problems in comparing of the results of the parametric study.

In the case of elastic MDOF structures it was observed that the peak values of floor response spectra occur when the natural period of the equipment is approximately equal to one of the natural periods of the structure, as it was observed in the case of SDOF structures. The effects of higher modes turned out to be significant for both stiff and flexible structures, especially in lower storeys. In stiff structures this was a consequence of the in-phase response of individual modes. In flexible structures structural response in higher modes was a consequence of the nature of the applied seismic input, which led to structural response in higher modes. It was also observed that there were practically no peaks related to the modes with very high frequencies, i.e. with frequencies above the frequency at which spectral acceleration practically returns to zero period acceleration (f_{ZPA}). Therefore, it can be concluded that the influence of such modes is static and that resonance effects do not occur, i.e. there is no amplification. Finally, it was observed that the floor response spectra approach to the ground motion spectra after $T_s/T_{p,1}=1$, as the ratio T_s/T_p decreases ($T_{p,1}$ denotes the natural period of the fundamental mode).

The above mentioned higher mode effects initiated an investigation of the influence of individual modes on floor response spectra, which was conducted on two elastic structures (one stiff and one flexible). Two ground motions were considered as seismic input. First, modal response-history analysis of each structure was conducted and absolute accelerations were examined. In the case of the stiff structure significant absolute accelerations due to higher modes occurred in the first storey. For both considered ground motions, peaks related to higher modes occurred practically at the same time and they were very close to the peak of the first mode. Moreover, all modes were almost in-phase within the part of the time interval where the peak values occurred. This fact confirmed the above mentioned fact regarding the higher modes. In the case of the flexible structure significant absolute accelerations due to higher modes were also observed in the first storey, again for both considered ground motions. The main reason for this is the frequency content of the applied ground motions, as already mentioned above.

Absolute floor accelerations determined for individual modes of the considered structures were used as input for the calculation of the corresponding (individual) floor response spectra. It was observed that in the period range in which the natural periods of the equipment are larger than the natural period of the fundamental mode of the structure ($T_s > T_{p,1}$), the application of the algebraic summation rule (ALGSUM) on the floor response spectra obtained for individual modes produced floor response

spectra which perfectly matched the floor response spectra obtained for MDOF structures. This fact is of great importance and it represented one of the foundations for the development of the method for the direct determination of floor response spectra for inelastic MDOF structures, as discussed below.

In the case of inelastic MDOF structures, the seismic input was scaled in order to achieve different values of ductility (μ). The exact determination of the ductility demand is difficult since the yield point of the system cannot be determined with certainty. The nonlinear pushover-based N2 method was used for this purpose. In the study, in pushover analyses the "first mode" height-wise distribution of lateral loads was assumed, i.e. lateral loads were determined as the product of the first mode shape component in a considered storey and the storey mass. For all considered cases, apart from determination of the ductility demand for inelastic modes, the corresponding components of inelastic mode shapes were also determined from the N2 method. It is very important to note that these results were used later in the validation of the proposed procedure for direct determination of peak floor accelerations and for the validation of the direct method proposed for MDOF structures. Note that, as an approximation, the superposition of results obtained for different modes was used, as usual in simplified pushover-based nonlinear procedures.

In the case of inelastic structures, the peak values of floor response spectra related to the first mode are smaller than the corresponding peak values obtained for elastic structures. In the case of the EP model the peak values occur close to the resonance, whereas in the case of the Q model the peak values are shifted towards higher periods. It can be concluded that peaks of floor response spectra related to the first mode show trends which were previously observed in the case of inelastic SDOF structures.

Several interesting observations were made regarding floor response spectra peaks related to higher modes, in both stiff and flexible structures, as discussed below.

In the case of stiff structures it was observed that the peak values (related to higher modes) obtained for inelastic structures can be larger than the corresponding peak values obtained for elastic structures, i.e. an amplification of peak values can occur. An even more interesting observation is existence of peaks related to the modes with frequency above f_{ZPA} . Both observed phenomena confirm the findings of previous studies conducted by Sewell et al. (1986) and Singh et al. (1996). More research on this subject is needed.

In the case of flexible structures, in certain cases, peak values of floor response spectra related to the second mode are reduced in comparison with the peak values obtained for elastic structures. In such cases, it was observed that the resonance regions and peaks related to the second mode show similar characteristics as the resonance regions and peaks related to the fundamental mode, but with a notably smaller ductility. This fact raised some interesting questions. In earthquake engineering, it is often assumed that inelastic behaviour occurs only in the fundamental mode. The obtained results suggested inelastic behaviour also in the second mode. It should be noted that considered structures were simple planar structures which have only three natural modes. Therefore, the obtained results imply that in the case of flexible structures with large number of modes inelastic behaviour can perhaps occur in several first modes. If the assumption of inelastic behaviour related only to the fundamental mode cannot be made, it is necessary to determine the seismic demand by taking into account several modes. The estimation of the seismic demand in such cases can be conducted by the N2 method, in the same manner as proposed in a procedure developed by Chopra and Goel (2002). For the purpose of this study, a similar approach was adopted, in the sense of analysing seismic demands in different modes separately. As in the case of the fundamental mode, the N2 method was used to estimate the seismic

demand in the second mode. The results of the applied approach produced somewhat underestimated ductility demands. Further research on this problem is needed.

The results of the parametric study conducted on MDOF primary structures provided a basis for the study of perhaps one of the most important parameters in the seismic design of acceleration-sensitive equipment: peak floor acceleration (PFA). The PFA also represents significant part in the floor response spectrum approach. The determination of PFAs is quite straightforward when a structure is analysed by using the response-history analysis. In engineering practice, modal response spectrum analysis is usually applied. In such a case, PFAs are determined for each considered mode by using one of the standard procedures. The determined PFAs should be combined with a suitable modal combination rule in order to determine the total PFAs. In the study it was concluded that the most common modal combination rules used in earthquake engineering (SRSS and CQC), which generally produce good results for most response quantities (e.g. displacements and inter-storey drifts), are sometimes not satisfactory in the case of absolute accelerations, especially when stiff MDOF structures are considered. The main reason for this is the fact that higher mode effects are more pronounced in the case of absolute accelerations than in the case of most other quantities (e.g. displacements).

Several methods for modal combination proposed by USNRC 1.92 (2006) turned out to be appropriate for application in the case of absolute floor accelerations obtained for individual modes. The combination methods which are considered as appropriate are the methods defined by Gupta and Lindley-Yow, coupled with the Missing Mass method.

A procedure for the direct determination of PFAs in elastic MDOF structures, based on the modal response spectrum analysis and the above mentioned modal combination methods, was proposed. In the case of inelastic structures, the procedure was coupled with the N2 method. The proposed procedure is fairly simple. However, it should be noted that, in some cases of inelastic structures, it may not always produce sufficiently accurate PFAs, primarily due to fact that absolute accelerations show great sensitivity to higher mode effects.

Finally, based on the results of parametric study and on the direct method previously developed for SDOF structures, a method for direct generation of floor response spectra for MDOF structures was developed. In the proposed method, in the case of inelastic structures, absolute floor accelerations are determined from the N2 method (as discussed above). Floor response spectra are determined for each mode separately. In order to determine the resulting direct floor response spectra a combination of the direct floor response spectra calculated for individual modes should be conducted. In the period range of the floor response spectrum between $T_s=0$ and a value of T_s which is located shortly after the peak related to the fundamental mode, i.e. $T_s/T_{p,1}=1$, the combination methods proposed by USNRC 1.92 (2006) should be used (Gupta or Lindley-Yow method, coupled with the Missing Mass method). In the rest of the period range (flexible equipment), the ALGSUM rule should be applied.

In the case of considered elastic MDOF structures, at all storeys and in the whole period range, the proposed direct method produced floor response spectra which were in good agreement with the floor response spectra obtained from the RHA. In the case of inelastic structures the obtained results were, generally, less accurate. The largest deviation from the results of RHA was observed in the case of flexible frame, where the inelastic behaviour in the second mode was evident. However, considering all uncertainties involved in the problem, the results obtained by the proposed direct method can, in the majority of cases, be characterized as satisfactory. The proposed direct method represents a useful

tool in the stage of conceptual design, as well as for checking of the results obtained from more elaborate analyses. Also, the method can be used as a basis for simplified code procedures.

8.2 Original contributions

The analyses and studies conducted in the dissertation led to various findings and proposals which represent significant scientific contributions in the field related to seismic design and assessment of acceleration-sensitive non-structural components (equipment). The findings mostly confirm and expand the observations made by other researchers. Based on these findings an original practice-oriented method for direct determination of floor acceleration spectra was developed and verified. The proposed method can be used for both elastic and inelastic primary structures modelled as SDOF or MDOF systems. The results related to SDOF of structures have been already published in the journal with the second largest impact factor (in 2013) in the field of earthquake engineering. More details on the main contributions of the dissertation are described below.

- The identification of the most important parameters which influence floor acceleration spectra in SDOF primary structures.

A large number of floor acceleration spectra, which were determined from response-history analysis by varying several input parameters, enabled an investigation of the effects which inelastic structural behaviour of the SDOF primary structure has on the response of the equipment. The main characteristics of floor acceleration spectra were recognized in the whole period range and a clear distinction between the pre-resonance, resonance and post-resonance regions was made. The ratio of the peak value of the floor acceleration spectrum and the peak acceleration of the structure was recognized as an important parameter and it was named as an amplification factor (*AMP*).

- A proposal of a simple practice-oriented method for direct generation of floor response spectra from ground motion spectra for SDOF primary inelastic structures.

Based on the idea of Novak and Fajfar (1994), a method for direct generation of floor response spectra in elastic SDOF structures proposed by Yasui et al. (1993) was improved and extended on inelastic SDOF structures. Outside of the resonance region the proposed direct method has a theoretical background because its development was based on the principles of structural dynamics. In the resonance region, empirical values of the *AMP* obtained in the parametric study were used as a basis for the definition of relatively simple equations which describe the dependence between the *AMP* and the parameters which influence them.

- The identification of several important parameters which influence floor acceleration spectra in MDOF primary structures.

By conducting response-history analyses for four simple planar structures some quite significant findings regarding the floor response spectra in MDOF primary structures were obtained. As in the case of SDOF structures, main characteristics of floor acceleration spectra were recognized in the whole period range. A clear distinction between period ranges before and after the peak related to the fundamental mode was made. It was observed that the floor response spectra approach the ground motion spectra after reaching the peak related to the fundamental mode. Important effects of higher modes on absolute accelerations and floor

response spectra were recognized, in both elastic and inelastic structures. In the case of stiff structures it was observed that, in some cases, floor response spectra peaks obtained for inelastic structures can be larger than the peaks obtained for corresponding elastic structures. Moreover, an interesting existence of peaks related to modes with frequencies above f_{ZPA} was also observed in inelastic structures. Both observations are important since they confirm findings obtained by Sewell et al. (1986) and Singh et al. (1996). In the case of flexible structures it was observed that inelastic structural behaviour can also occur in higher modes. In such cases, resonance regions related to the second mode showed similar characteristics to the resonance regions related to the fundamental mode, but with a notably smaller ductility.

- The evaluation of modal combination rules

It was observed that the application of the SRSS combination rule on absolute accelerations does not always produce satisfactory results and it was shown that modal combination methods proposed by USNRC 1.92 (2006) lead to better estimation of the total response. It should be noted that the SRSS rule is a special case of the methods proposed by USNRC 1.92 (2006).

- A proposal of a procedure for direct determination of peak floor accelerations (PFAs) in MDOF primary structures.

Based on the N2 method and modal combination methods proposed by USNRC 1.92 (2006), a procedure for the direct determination of PFAs in elastic and inelastic MDOF structures was proposed. It should be noted that the modal superposition, which is fully applicable in the case of elastic structures, is an approximation in the case of inelastic structures.

- The development of a practice-oriented method for direct generation of floor response spectra from ground motion spectra for MDOF primary structures.

A method for direct generation of floor response spectra for MDOF structures was developed by expanding the developed method for SDOF primary structures. Important parts of the method are: the modal superposition (which is an approximation in the case of inelastic structures), modal combination methods which are different in different period ranges of the equipment (methods proposed by USNRC 1.92 2006 and algebraic summation rule), and the N2 method. The proposed direct method represents a useful tool in the stage of conceptual design, as well as for checking of the results obtained from more elaborate analyses. It can also be used as a basis for simplified code procedures. In the case of flexible structures with inelastic response in higher modes the results obtained by the proposed method are less accurate and there seems to be still some room for improvements.

8.3 Suggestions for further research

In the past, not enough research has been devoted to seismic issues related to non-structural elements and content of the buildings. Thus, there is a great need for more research in this area. Determination of seismic demand for acceleration-sensitive equipment is a field which badly needs further studies, especially in relation to the development of simplified methods which could improve the seismic design and assessment of equipment in practice. A partial list of problems to be studied is listed below.

The parametric studies, including those in this dissertation, are usually performed on relatively simple elastic and inelastic MDOF primary structures. Even though the obtained results provide a very good insight in the basic characteristics of floor acceleration spectra, it is considered that more parametric studies should be performed on more specific and complex structures. Special attention should be paid to effects of higher modes in both stiff and flexible inelastic structures.

During the development and validation of the direct approaches for determination of peak floor accelerations and floor acceleration spectra, it was discovered that, generally, most existing modal combination rules may not provide sufficiently accurate results when applied on absolute accelerations, primarily due to the fact that absolute accelerations are very sensitive to higher mode effects. Therefore, the development of an improved modal combination rule may lead to significant improvements in engineering practice.

In the case of inelastic MDOF primary structures, especially stiff ones, the proposed direct approach for determination of peak floor accelerations generally produced somewhat underestimated results. Therefore, some improvements of the proposed procedure may be considered, perhaps in the sense of introducing correction factors.

Further research is needed for taking into account inelastic response in higher modes of MDOF primary structures in a more accurate way.

The proposed direct method for determination of floor response spectra has theoretical background outside the resonance region, i.e. it is based on the principles of structural dynamics. In the resonance region, the values of the *AMP* obtained in the parametric study conducted on SDOF systems were used as a basis for the definition of the *AMP*. Since the aforementioned parametric study was conducted for selected natural periods of SDOF systems, two sets of ground motions, three hysteretic models and three target ductility demands, it is recommendable to conduct additional parametric studies in which more input parameters would be taken into account, e.g.: very short natural periods of the SDOF systems, ground motions of different type (primarily near fault ground motions), hysteretic rules in which strength degradations is taken into account.

The floor response spectra concept is based on uncoupled (separate) analysis of the structure-equipment system which may lead to conservative results. This is most obvious in cases when the mass of equipment is not negligible in comparison to the mass of the primary structure. In such cases more accurate estimation of floor response spectra could be achieved if coupling effects are taken into account. It is anticipated that coupling can be considered implicitly in the proposed direct method and, therefore, a study on this subject should be conducted.

Finally, in the proposed direct method inelastic behaviour is considered only in the primary structure. As a possibility for an extension of the proposed direct method, inelastic structural behaviour of the equipment should also be considered.

POVZETEK

Uvod

Izkušnje kažejo, da je med potresi oprema v stavbah lahko izpostavljena velikim pospeškom. Primerna odpornost opreme med potresom je velikega pomena v industrijskih stavbah, kot so na primer nuklearne elektrarne, so za potresno projektiranje in evaluacijo različne opreme običajno uporabljeni etažni spektri odziva.

Za drugo polovico 20. stoletja je značilna masovna gradnja velikega števila nuklearnih elektrarn. Potresna analiza opreme (sekundarnih sistemov) je bila v takšnih konstrukcijah neizogibna. V tem času je veliko raziskovalcev posvetilo precej truda razvoju racionalnih metod za potresno analizo in potresno projektiranje sekundarnih sistemov. Razvoj teh metod je bil potreben za zagotavljanje zadostne varnosti kritične opreme v industrijskih stavbah med potresom. Natančna analiza sekundarnih sistemov je lahko precej komplicirana. Predlagane so bile različne metode za analizo. Nekatere so temeljile na empiričnih podatkih, druge pa so uporabljale principe dinamike konstrukcij. Dejstvo, da imata primarna in sekundarna konstrukcija lahko zelo različne dinamične karakteristike, in da jih projektirajo različne ekipe v različnih časih, sta povzročala veliko težav raziskovalcem. Zaradi tega razvoj primerno zanesljive in relativno enostavne metode za potresno analizo sekundarnih sistemov predstavlja velik izziv v potresnem inženirstvu.

V zadnjih treh desetletjih gradnja novih nuklearnih elektrarn ni tako pogosta. Je pa treba vse konstrukcije, ki so bile zgrajene v preteklosti, ponovno oceniti. Predpisi so se pomembno spremenili od časa, ko so bile te konstrukcije projektirane in zgrajene.

Tema doktorske disertacije

Primarna in sekundarna konstrukcija predstavljata celoto. Da bi zajeli vse medsebojne vplive, je v principu treba obe konstrukciji analizirati kot povezan sistem. Takšen sistem nima klasičnih nihajnih oblik in (najbolj pogosto) ni klasično dušen, zaradi česar je analiza zelo komplicirana. Čeprav analiza povezanega sistema pripelje do bolj natančnih rezultatov, ni praktična in tudi ni upravičena za vsakdanjo prakso.

Etažni spektri pospeškov so običajno uporabljeni za potresno projektiranje in oceno opreme, ki je občutljiva na pospeške. Koncept etažnih spektrov odziva temelji na nepovezani analizi konstrukcije in opreme, kar pomeni, da je njihova interakcija zanemarjena (slika 1.1). Koncept je upravičen v primerih, ko je masa opreme značilno manjša od mase konstrukcije, na primer vsaj stokrat. Če ta pogoj ni izpolnjen, so etažni spektri odziva običajno konservativni (npr. slika 3.1-2 v ASCE 4-98 2000, Adam in Furtmüller 2008, Adam in sod. 2013, Pinkawa in sod. 2014).

V disertaciji je predpostavljeno, da je masa opreme značilno manjša od mase konstrukcije, kar pomeni, da se lahko uporabijo etažni spektri odziva. Glavni koraki za izračun etažnih spektrov odziva (»classical approach« na sliki 1.1) so:

- 1) Časovna analiza odziva primarne konstrukcije ob uporabi skupine akceleroграмov.
- 2) Določitev odziva etaže v smislu časovnega odziva absolutnega etažnega pospeška.
- 3) Izračun etažnega spektra pospeškov, ki ustreza absolutnim pospeškom določenim v koraku (2).

Da bi se izognili dolgim numeričnim analizam, je veliko raziskovalcev predlagalo metode, ki omogočajo določitev etažnih spektrov odziva direktno iz projektnega spektra tal («direct approach» na sliki 1.1). Poleg projektnega spektra tal, so vhodni podatki tudi dinamične karakteristike primarne in sekundarne konstrukcije. Zaradi svoje enostavnosti se takšne metode pogosto uporabljajo v praksi. Razvoj zgodnjih metodah temelji na predpostavki, da primarna in sekundarna konstrukcija med potresom ostaneta v linearno elastičnem območju. Celó v primerih konstrukcij izrednega pomena, kot so nuklearne elektrarne, pa je upravičeno dovoliti zmerno količino neelastičnega obnašanja med potresom. To dejstvo je pomembno, ker zanemarjenje vpliva neelastičnosti konstrukcije lahko pripelje do nerealnih rezultatov za etažne pospeške.

Če je upoštevano neelastično obnašanje konstrukcije in/ali opreme, je mogoče doseči pomembne redukcije maksimalnih vrednosti etažnih spektrov odziva. Le malo raziskovalcev se je ukvarjalo z izpeljavo poenostavljenih metod, ki upoštevajo neelastično obnašanje konstrukcije v analizi, in pomanjkanje takšnih metod je očitno. Tiste metode, ki obstajajo, pa so večinoma precej zapletene in nepraktične za širšo uporabo, ali pa nimajo zadostne natančnosti. Zaradi tega ugotavljamo, da za prakso uporabna direktna metoda, ki upošteva nelinearno obnašanje primarne konstrukcije, še vedno manjka.

Ob zavedanju pomembnosti vpliva, ki ga ima neelastično obnašanje konstrukcije na odziv sekundarnih sistemov, sta kot glavna cilja disertacije izbrana analiza tega vpliva in razvoj metode uporabne za prakso, ki upošteva neelastično obnašanje primarne konstrukcije. Analize so narejene na nepovezanih sistemih konstrukcija-oprema. Neelastično obnašanje je predpostavljeno le v primarni konstrukciji, oprema pa ostaja v linearno elastičnem območju. Torej, glavni cilji disertacije so:

- raziskava učinkov, ki jih ima neelastično obnašanje konstrukcij z eno prostostno stopnjo (SDOF) in konstrukcij z več prostostnimi stopnjami (MDOF) na odziv opreme (sekundarnih konstrukcij) za različne modele histerez, in primerjava novih ugotovitev s obstoječimi, in
- razvoj nove enostavne za prakso uporabne metode za direktno določanje etažnih spektrov odziva, ki upošteva neelastičnost konstrukcije.

Kratek pregled literature

Razvoj metod za določanje etažnih spektrov odziva se je začel v zgodnjih 1970-ih. Zelo natančen pregled prvih metod je dal Villaverde (1997). Vse metode, ki so omenjene v tem pregledu, temeljijo na predpostavki o elastičnem obnašanju konstrukcije in opreme. Celó v primerih izredno pomembnih konstrukcij, kot so nuklearne elektrarne, je upravičeno dovoliti zmerno neelastično obnašanja med močnimi potresi. Zgodnje raziskave tega fenomena je naredil Kelly (1978). Lin in Mahin (1985) sta natančno raziskala učinke neelastičnih deformacij, različnih modelov histerez in velikosti dušenja opreme, ob upoštevanju SDOF sistema za konstrukcijo in opremo. Sewell in sod. (1986) so naredili obsežno študijo etažnih spektrov odziva v MDOF sistemih ob upoštevanju različnih parametrov. Yasui in sod. (1993) so predlagali enostavno metodo za direktno določanje etažnih spektrov odziva v elastičnih SDOF konstrukcijah. Ta metoda predstavlja zelo pomemben del disertacije in je detajlno obravnavana v poglavju 3 in v PRILOGI A. Novak in Fajfar (1994) sta naredila parametrično študijo, ki je temeljila na nepovezani analizi SDOF konstrukcije in SDOF opreme. V študiji so raziskani učinki različnih parametrov na etažne spektre pospeškov. Razširjena študija je objavljena v Fajfar in Novak (1995). Singh in sod. (1996) so v svoji študiji dobili zelo zanimive rezultate. Namreč, pokazali so, da so v nekaterih primerih v območju visokih frekvenc etažni spektri odziva v neelastičnih konstrukcijah lahko večji od etažnih spektrov odziva elastičnih konstrukcij. Rodriguez in sod. (2002) so pokazali, da

neelastično obnašanje konstrukcije reducira maksimalne etažne pospeške in predlagali so enostavno proceduro za določitev projektnih etažnih horizontalnih sil. Medina in sod. (2006) so raziskali etažne spektre odziva za primer lahke opreme, ki se nahaja v okvirnih konstrukcijah, in ugotovili da so najbolj pomembni parametri, ki vplivajo na obliko in velikost etažnega spektra odziva: nihajni čas konstrukcije, lokacija opreme v konstrukciji in dušenje opreme. Oropeza in sod. (2010) so raziskali odziv nekonstrukcijskih komponent v primeru nepovezanega sistema in neelastičnega obnašanja konstrukcije. Predstavili so tudi predlog za modifikacijo aktualnih predpisov. Maniatakis in sod. (2013) so ugotovili, da so efekti višjih nihajnih oblik v armiranobetonskih okvirjih pomembni, celo v primerih ravninskih konstrukcij. Moschen in sod. (2013) so predlagali metodologijo za oceno maksimalnih etažnih pospeškov v neelastičnih MDOF konstrukcijah. Sullivan in sod. (2013) so naredili študijo etažnih spektrov pospeškov v SDOF konstrukcijah, ki imajo elastično in neelastično obnašanje. Predstavili so tudi empirični pristop za direktno določanje etažnih spektrov odziva, v katerem nihajni čas in neelastičnost konstrukcije definirata obliko etažnega spektra odziva in kjer dušenje definira njegovo magnitudo. Calvi in Sullivan (2014) sta razširila prejšnjo študijo na MDOF sisteme in sta predlagala metodo za direktno določanje etažnih spektrov odziva v elastičnih konstrukcijah. Pinkawa in sod. (2014) so naredili oceno določb nekaterih predpisov in zaključili, da obstoječa določila niso ustrezna za projektiranje opreme.

Parametrična študija etažnih spektrov odziva v elastičnih in neelastičnih SDOF konstrukcijah

V poglavju 2 so prikazani rezultati obsežne parametrične študije etažnih spektrov odziva, ki so dobljeni za SDOF konstrukcije. Upoštevano je bilo elastično in neelastično konstrukcijsko obnašanje, medtem ko je oprema v vseh primerih obravnavana kot linearno elastičen SDOF sistem. Sistem konstrukcija-oprema je bil analiziran kot nepovezan. V parametrični študiji je bilo izračunano veliko število etažnih spektrov pospeškov. Raziskani so bili vplivi različnih faktorjev na etažne spektre odziva: nihajni čas, histerezno obnašanje in duktilnost konstrukcije, in tudi dušenje opreme. Raziskan je bil tudi vpliv značilnosti vhodnih akceleroگرامov. V analizi sta bili uporabljeni dve različni skupini, vsaka s po 30 akceleroگرامi.

Izbira akceleroگرامov za vsako skupino je narejena tako, da njen povprečni spekter pospeškov ustreza ciljnemu spektru, ki ga je predstavljal elastičen spekter (tip 1) po Evrokodu 8 (2004) za tip tal B in tip tal D. Maksimalni pospešek tla (PGA, ki je enak $a_g S$), uporabljen pri ciljnih spektrih, je znašal 0,35g in 0,39g za tla B in D. Povprečni maksimalni pospešek tal (PGA) za izbrane skupine akceleroگرامov je znašal 0,43g in 0,50 g za tla B in D. Značilna perioda potresa T_C za tla B in D znaša 0,5 in 0,8 s. Ujemanje med ciljnim in povprečnim spektrom (za 5% dušenja) je zagotovljeno v območju 0,15 in 2,5 s, kar je v skladu z določbami Evrokoda 8 (2004).

Razlike v PGA pri nizkih periodah niso pomembne, saj obravnavani nihajni časi (opisani spodaj) niso v tem območju. Podatki o potresih so predstavljeni v preglednicah 2.1 in 2.2, ciljni in povprečni spektri za tla B in D pa na sliki 2.1.

SDOF oscilatorji, ki predstavljajo konstrukcijo, so imeli nihajne čase 0,2, 0,3, 0,5, 0,75, 1,0 in 2,0 s. Uporabljeni so bili trije različni histerezni modeli: elasto-plastičen (EP) in modela s padajočo togostjo (Q), brez utrditve (Q_0) in z 10% utrditve (Q_{10}). V primeru Q modela (Q-Hyst model v Saaidi in Sozen 1979) je koeficient zmanjšanja togosti ob razbremenjevanju znašal 0,5. Tipična histerezna obnašanja so pokazana na sliki 2.2. Predpostavljen je konstanten faktor duktilnosti μ , ki je znašal 1,5, 2,0 in 4,0. Dušenje, ki je proporcionalno masi, je znašalo 5% v primeru konstrukcije, in 1, 3, 5 in 7% v primeru opreme.

Pokazani so rezultati parametrične študije, ki so dobljeni za elastične, EP in Q_{10} modele. Etažni spektri odziva, ki so pokazani na slikah 2.3–2.8, predstavljajo povprečne vrednosti, medtem ko rezultati na slikah 2.9–2.14 predstavljajo razmerja etažnih spektrov odziva izračunanih za neelastične (A_s) in ustrezne elastične konstrukcije (A_{se}). Ugotovljeno je, da se območje period etažnega spektra odziva približno lahko razdeli na tri območja, odvisno od razmerja nihajnega časa opreme (T_s) in nihajnega časa konstrukcije (T_p): predresonančno ($0,8 < T_s/T_p < 1,25$), resonančno in poresonančno območje ($T_s/T_p > 1,25$).

Iz slik 2.3–2.8 je razvidno, da je v predresonančnem in resonančnem območju obnašanje opreme odvisno od obnašanja konstrukcije. V obeh območjih so opažene značilne redukcije v etažnih spektrih odziva v primerih, ko je obnašanje konstrukcije neelastično. Velikost redukcij je odvisna od velikosti duktilnosti μ , kar je pomembno dejstvo. V poresonančnem območju se etažni spekter odziva z zmanjševanjem razmerja T_s/T_p , približuje spektru tal kar je tudi zelo pomembno dejstvo. V mejnem primeru neskončno toge opreme ($T_s=0$) je vrednost etažnega spektra odziva (A_s) enaka pospešku konstrukcije (A_p), oziroma vrednosti v elastičnem ali neelastičnem spektru pospeškov za konstrukcijo pri periodi T_p . V primeru neskončno podajne opreme je vrednost etažnega spektra odziva enaka nič. Dodatno je iz slik 2.9–2.14 razvidno, da dušenje opreme praktično ne vpliva na razmerje A_s/A_{se} .

Oblika etažnega spektra odziva je odvisna od histereznega obnašanja konstrukcije. V primeru EP modela se maksimalne vrednosti etažnih spektrov odziva pojavljajo blizu resonance ($T_s \approx T_p$). V primeru Q modela so maksimalne vrednosti etažnih spektrov odziva premaknjene proti daljšim nihajnim časom zaradi povečanja T_p s povečanjem plastičnih deformacij.

Na slikah 2.15–2.20 so pokazani etažni spektri odziva normirani na pospešek konstrukcije A_p . Na to razmerje ima največji vpliv dušenje opreme.

Slike 2.21–2.23 kažejo primerjavo med etažnimi spektri odziva za Q model z utrditvijo in brez nje (Q_{10} in Q_0). Ti rezultati so dobljeni za tla B. Iz njih je razvidno, da so etažni spektri odziva, ki so izračunani za Q_0 model, nižji od tistih, ki so izračunani za Q_{10} model. Ta redukcija je manjša, ali je celo ni, če se gleda razmerje A_s/A_p , prikazano na slikah 2.24–2.26, ker je tudi pospešek konstrukcije A_p manjši v primeru modela Q_0 .

V študiji je bila maksimalna vrednost razmerja A_s/A_p definirana kot faktor amplifikacije *AMP*. Treba se je zavedati, da je maksimalni pospešek konstrukcije A_p enak vrednosti v etažnem spektru odziva za periodo opreme, ki je enaka nič ($T_s=0$). Za oba histerezna modela, EP in Q, je glavni parameter, ki vpliva na amplitudo *AMP*, dušenje opreme ζ_s (sliki 2.27 in 2.28). V primeru EP modela je vpliv duktilnosti konstrukcije (μ) na *AMP* majhen, v primeru Q modela pa je zmeren. V primeru EP modela se vrednosti *AMP* nekoliko povečujejo z večanjem duktilnosti, v primeru Q modela pa se manjšajo. Rezultati, dobljeni za obe skupini akcelorogramov, kažejo, da oblika spektra, ki je opisana z značilnostno periodo potresa T_C , zelo malo vpliva na *AMP*, če je na x -osi prikazano razmerje T_p/T_C namesto periode T_p .

AMP doseže svojo maksimalno vrednost v območju $0,20 \leq T_p/T_C \leq 1$. V območju $0 \leq T_p/T_C < 0,20$ dobljeni rezultati kažejo, da manjšanje razmerja T_p/T_C povzroča manjšanje *AMP*. *AMP* se tudi manjša s povečanjem razmerja T_p/T_C , če je to razmerje večje od 1. Dodatno je študija tudi pokazala, da utrditev praktično ne vpliva na *AMP*. Odvisnost *AMP* od dušenja opreme ζ_s in razmerja T_p/T_C je prikazana na sliki 2.29.

Direktna metoda za določanje etažnih spektrov odziva v elastičnih in neelastičnih SDOF konstrukcijah

V poglavju 3, ob upoštevanju parametrične študije in metode za direktno določanje etažnih spektrov odziva, ki so jo predlagali Yasui in sod. (1993), razvita direktna metoda za določanje etažnih spektrov odziva, ki je uporabna za neelastične SDOF konstrukcije. Idejo za razširitev metode, ki so jo za elastične konstrukcije predlagali Yasui in sod. (1993), sta dala Novak in Fajfar (1994).

Yasui in sod. (1993) so izpeljali enačbo (enačba 3.1, str. 44), ki je veljavna v celotnem območju nihajnih časov in ta izpeljava je predstavljena v PRILOGI A. Iz opravljenih analiz je ugotovljeno, da predlagana enačba daje dobre rezultate izven resonančnega območja, medtem ko v resonančnem območju pripelje do zelo konservativnih rezultatov. Razširitev metode na neelastične SDOF konstrukcije in popravek natančnosti v resonančnem območju sta bila dve pomembni nalogi, opravljeni v okviru disertacije. Prva je bila rešena z uporabo neelastičnega namesto elastičnega spektra za konstrukcijo, druga pa z definicijo empiričnih vrednosti *AMP*, ki temeljijo na rezultatih parametrične študije.

V literaturi so predlagani različni neelastični spektri. Za konstrukcijo najbolj pogosto temeljijo na redukcijskem faktorju R_{μ} , ki predstavlja razmerje elastičnih in neelastičnih zahtev. V disertaciji vsi uporabljeni neelastični spektri temeljijo na postopku, ki so ga razvili Vidic in sod. (1994), in v katerem je neelastičen spekter določen kot reducirani elastični spekter s R_{μ} faktorjem. Ugotovljeno je bilo, da je ta pristop uporaben za etažne spektre odziva v primerih, ko ni utrditve. V primerih, ko obstaja utrditev, so pospeški konstrukcije nekaj večji (enačba 3.2, str. 45). R_{μ} faktor, ki so ga predlagali Vidic in sod. (1994) je tudi implementiran v Evrokod 8 (2004) in se lahko določi iz enačbe 3.3, str. 46. Če je pa treba v analizi upoštevati utrditev, se lahko R_{μ} faktor določi iz enačbe 3.4, str. 46. Na sliki 3.1 so primerjani »točni« neelastični spektri, ki so dobljeni iz analize časovnega odziva, in približni neelastični spektri, ki so dobljeni iz R_{μ} faktorja. Napake približnih neelastičnih spektrov so pokazane v preglednicah 3.1 in 3.2. Dodatno je primerjava »točnih« in približnih neelastičnih spektrov, dobljenih za različna Q modela, prikazana na sliki 3.2.

V resonančnem območju so rezultati parametrične študije uporabljeni za definicijo empiričnih enačb za določitev *AMP*. V primeru $T_p/T_C=0$ je *AMP* definiran z enačbami 3.5 in 3.6, str. 48. Ta definicija je v skladu z določbami Evrokoda 8 (2004). Za določitev *AMP* v celotnem območju razmerj T_p/T_C sta predlagani enačbi 3.7 in 3.8 (str. 49) za EP in Q model. Predlagani *AMP* so na sliki 3.3 primerjani z *AMP*, ki so dobljeni iz parametrične študije.

V predlagani direktni metodi za določanje etažnih spektrov odziva v neelastičnih SDOF konstrukcijah se v preresonančnem in poresonančnem območju vrednosti etažnega spektra odziva lahko določijo z enačbo 3.9, v resonančnem območju pa z enačbo 3.11 (obe enačbi ste prikazani na str. 50). Če je Q model uporabljen v analizi, je treba upoštevati podaljšani nihajni čas konstrukcije (Akiyama 1985, PRILOGA C), ki se lahko določi z enačbo 3.10, str. 50.

Za nekatere primere elastičnih konstrukcij so rezultati metode, ki je predlagana v disertaciji, primerjani z rezultati originalne metode, ki so jo predlagali Yasui in sod. (1993). Ob primerjavi so pokazani tudi rezultati iz parametrične študije, oziroma »točni« etažni spektri odziva. Rezultati primerjave, ki so pokazani na sliki 3.4, kažejo, da v resonančnem območju metoda, ki je predlagana v disertaciji, daje značilno boljšo oceno vrednosti etažnih spektrov odziva kot jo daje originalna metoda. Izven resonančnega območja metodi dajeta skoraj enake rezultate. Rezultati direktne metode, ki je

predlagana v disertaciji, so primerjani tudi z rezultati parametrične študije, opravljene na neelastičnih konstrukcijah (slike 3.5–3.19). Primerjava je narejena za veliko primerov in ugotovljeno je, da predlagana metoda zagotavlja dobro oceno etažnih spektrov odziva, oziroma da se njeni rezultati dobro ujemajo z rezultati, ki so dobljeni iz časovne analize odziva. Nekateri rezultati predlagane direktne metode, ki so dobljeni za neelastične konstrukcije, so tudi primerjani z rezultati metode, ki so jo predlagali Sullivan in sod. (2013). Pokazano je, da predlagana metoda daje večinoma boljše rezultate (slike 3.21 in 3.22). Raziskana so bila tudi določila Evrokoda 8 (2004), ki se nanašajo na projektiranje opreme. Ugotovljeno je, da je ta določila potrebno modificirati, saj ne zagotavljajo zadostne natančnosti (slika 3.20). Nazadnje je predstavljen enostaven primer uporabe predlagane direktne metode (preglednica 3.3 in slika 3.23).

Parametrična študija etažnih spektrov odziva v elastičnih in neelastičnih MDOF konstrukcijah

V poglavju 4 so predstavljeni rezultati obsežne parametrične študije etažnih spektrov odziva v MDOF konstrukcijah, ob upoštevanju elastičnega in neelastičnega konstrukcijskega obnašanja. V vseh primerih je predpostavljeno elastično obnašanje opreme. Predpostavljeno je, da konstrukcija in oprema nista povezana. Raziskani so vplivi tipa, nihajnega časa, histereznega obnašanja in duktilnosti konstrukcije, ter vpliv dušenja opreme. Uporabljena je skupina akceleroگرامov, ki se nanaša na tla B (preglednica 2.1, slika 4.1).

V parametrični študiji so obravnavane štiri enostavne ravninske armiranobetonske konstrukcije. Modul elastičnosti betona (E_c) znaša 33 GPa. Modul elastičnosti jekla (E_s) znaša 200 GPa, meja tečenja jekla (f_y) pa 500 MPa. Elementi konstrukcij so modelirani kot linijski, njihova lastna teža je zanemarljiva in uporabljen je pristop s koncentriranimi masami. Časovna analiza odziva je narejena ob uporabi programa SAP2000 14.2.4 (za elastičen in EP model) in OpenSees 2.2.2 (za Q model brez utrditve). V primeru neelastičnih konstrukcij je uporabljen pristop s koncentrirano plastičnostjo. Za oba histerezna modela je obnašanje plastičnih členkov določeno z zvezo moment-rotacija. V vsakem plastičnem členu je predpostavljena neskončna kapaciteta rotacije. To je potrebno, ker so uporabljeni akceleroگرامi precej različnih jakosti. V študiji je opaženo, da obstajajo težave pri uporabi modelov s koncentrirano plastičnostjo v OpenSees-u. Togostna matrika konstrukcije je sestavljena iz togosti linijskih elementov in iz togosti plastičnih členkov. Poskus, da se ta problem odpravi v elastičnem območju, je bil narejen tako, da je bila upoštevana nična rotacija v točki tečenja (v odnosu moment-rotacija), vendar je to pripeljalo do velikih numeričnih težav. Zaradi tega je bil uporabljen približen pristop, ki sta ga predlagala Dolšek in Fajfar (2005), kar pa je privedlo do nekompatibilnosti rezultatov dobljenih s SAP 2000, zlasti v primeru sten. To je povzročalo določene probleme v primerjavi rezultatov parametrične študije.

Obravnavane so bile štiri trietažne konstrukcije (višina etaž je enaka v vseh primerih in znaša 3 m).

Stena W03:

Dimenzije prereza stene so 30/300 cm. Masa v vsaki etaži znaša 80 t. Armatura stene je projektirana v skladu z določbami Evrokoda 2 (2004) in Evrokoda 8 (2004), in je pokazana na sliki 4.2. Trije nihajni časi iz SAP-a (elastičen in EP model) znašajo 0,30, 0,046 in 0,017 s, nihajni časi iz OpenSees-a (Q_0 model) pa znašajo 0,31, 0,041 in 0,014 s. Nihajne oblike iz SAP-a in OpenSees-a so pokazane v enačbah 4.2, str. 76. Plastični členek je predpostavljen ob vpetju stene. Moment na meji tečenja znaša 4015 kNm za osno silo 2354 kN. Za potrebe modeliranja v OpenSees-u je izračunana rotacija na meji tečenja, ki znaša $5,41 \cdot 10^{-4}$ rad (enačba 4.1, str. 76). Modalni faktorji participacije določeni v SAP-u

znašajo 1,29, 0,46 in 0,34, modalni faktorji participacije določeni v OpenSees-u pa znašajo 1,30, 0,48 in 0,20.

Stena W10:

Dimenzije prereza stene so 30/150 cm. Masa v vsaki etaži znaša 112 t. Armatura stene je enaka kot v primeru stene W03, in pokazana je na sliki 4.2. Nihajni časi iz SAP-a (elastičen in EP model) znašajo 1,0, 0,153 in 0,057 s, nihajni časi iz OpenSees-a (Q_0 model) pa znašajo 1,05, 0,136 in 0,046 s. Nihajne oblike iz SAP-a in OpenSees-a so pokazane v enačbah 4.3, str. 76. Plastični členek je predpostavljen ob vpetju stene. Moment na meji tečenja znaša 1896 kNm za osno silo 3296 kN. Za potrebe modeliranja v OpenSees-u je izračunana rotacija na meji tečenja, ki znaša 0,002 rad (enačba 4.1, str. 76). Modalni faktorji participacije določeni v SAP-u znašajo 1,29, 0,46 in 0,34, modalni faktorji participacije določeni v OpenSees-u pa znašajo 1,30, 0,48 in 0,20.

Okvir F03:

V okviru z enim poljem F03 je razpon gred 5 m. Dimenzije stebrov in gred znašajo 50/80 in 50/60 cm. Masa v vsakem vozlišču znaša 14 t, oziroma masa v vsaki etaži znaša 28 t. Armatura stebrov in gred je prikazana na sliki 4.3. Nihajni časi iz SAP-a (elastičen in EP model) znašajo 0,30, 0,079 in 0,038 s, nihajni časi iz OpenSees-a (Q_0 model) pa znašajo 0,29, 0,075 in 0,037 s. Nihajne oblike iz SAP-a in OpenSees-a so pokazane v enačbah 4.5, str. 78. Plastični členki so predpostavljeni na koncih stebrov in gred. Osne sile, momenti in rotacije na meji tečenja so izračunani iz enačbe 4.4 (str. 77) in prikazani v preglednici 4.1. Modalni faktorji participacije, določeni v SAP-u, znašajo 1,27, 0,41 in 0,28, modalni faktorji participacije določeni v OpenSees-u pa znašajo 1,28, 0,43 in 0,26.

Okvir F10:

V okviru z enim poljem F10 je razpon gred 5 m. Dimenzije stebrov in gred znašajo 35/35 in 35/45 cm. Masa v vsakem vozlišču znaša 23 t, oziroma masa v vsaki etaži znaša 46 t. Armatura stebrov in gred je prikazana na sliki 4.4. Nihajni časi iz SAP-a (elastičen in EP model) znašajo 1,0, 0,315 in 0,186 s, nihajni časi iz OpenSees-a (Q_0 model) pa znašajo 0,99, 0,312 in 0,186 s. Nihajne oblike iz SAP-a in OpenSees-a so prikazane v enačbah 4.6, str. 79. Plastični členki so predpostavljeni na koncih stebrov in gred. Osne sile, momenti in rotacije na meji tečenja so izračunani iz enačbe 4.4 (str. 77) in prikazani v preglednici 4.2. Modalni faktorji participacije določeni v SAP-u znašajo 1,25, 0,39 in 0,19, modalni faktorji participacije določeni v OpenSees-u pa znašajo 1,25, 0,39 in 0,19.

Za vse obravnavane primere očitno velja, da se nihajni časi in oblike dobljeni s SAP-om in OpenSees-om nekoliko razlikujejo. Razlike so pomembne pri stenah, pri okvirjih so pa zanemarljive. Jasno je, da zgoraj opisan pristop v modeliranju daje dobre rezultate pri okvirjih, pri stenah pa je vprašljiv.

Za potrebe analize elastičnih konstrukcij je uporabljen originalen (neskaliran) potresni input. Iz dobljenih rezultatih (slike 4.7, 4.8, 4.11, 4.12, 4.15, 4.16, 4.19 in 4.20) je očitno, da se maksimalne vrednosti etažnih spektrov odziva pojavijo, ko je nihajni čas opreme približno enak enemu od nihajnih časov konstrukcije. Vplivi višjih nihajnih oblik so se izkazali kot pomembni, zlasti v spodnjih etažah. V togih konstrukcijah (W03 in F03) je to posledica dejstva, da je nihanje v posameznih oblikah v fazi med seboj. V podajnih konstrukcijah (W10 in F10) je odziv v višjih oblikah posledica narave uporabljenega inputa. Dodatno je opaženo, da v etažnih spektrih odziva praktično ni špic v povezavi z nihajnimi oblikami, ki imajo zelo visoke frekvence, oziroma frekvence nad frekvenco f_{ZPA} , pri kateri je spektralni pospešek praktično enak maksimalnemu pospešku tal. Zaradi tega se lahko zaključi, da je vpliv takšnih nihajnih oblik statičen in da se resonančni efekti ne javljajo, oziroma ni amplifikacije.

Opaženo je tudi, da se etažni spektri odziva bližajo spektru tal po špici prve oblike ($T_s/T_{p,1}=1$) z manjšanjem razmerja $T_s/T_{p,1}$ ($T_{p,1}$ označuje nihajni čas prve oblike).

Zgoraj omenjeni vplivi višjih nihajnih oblik so vzpodbudili raziskavo vpliva posameznih oblik na etažne spektre odziva, kar je narejeno za dve elastični konstrukciji (W03 in W10). Za input sta uporabljena dva akcelerograma. Najprej je bila narejena časovna analiza odziva za posamezne oblike za vsako konstrukcijo. Analizirani so bili absolutni pospeški (slike 4.23–4.26). V primeru konstrukcije W03 (slike 4.23 in 4.24) so v prvi etaži prisotni pomembni absolutni pospeški zaradi višjih oblik. Za oba potresa sta se špici, ki sta povezani z drugo in tretjo obliko, pojavili praktično istočasno in sta (časovno) blizu špice, ki je povezana s prvo nihajno obliko. Poleg tega so vse nihajne oblike praktično v fazi med seboj v delu intervala, v katerem so pospeški maksimalni. V primeru konstrukcije W10 so pomembni absolutni pospeški, ki so povezani z višimi nihajnimi oblikami, opaženi v prvi etaži, spet za oba potresa. Glavni razlog za to je frekvenčna sestava uporabljenih akcelerogramov.

Absolutni pospeški, ki so določeni za posamezne oblike, so bili uporabljeni kot vhodni podatek za določanje ustreznih (posameznih) etažnih spektrov odziva. Opaženo je bilo, da v območju nihajnih časov opreme, večjih od nihajnega časa prve oblike ($T_s > T_{p,1}$), uporaba algebraične vsote (ALGSUM) za etažne spektre odziva, dobljene za posamezne oblike, vodi do etažnih spektrov odziva, ki se idealno ujemajo s spektri, dobljenimi za MDOF konstrukcije. To dejstvo je velikega pomena in predstavlja enega od temeljev pri razvoju metode za direktno določanje etažnih spektrov odziva v elastičnih in neelastičnih MDOF konstrukcijah.

Za analizo neelastičnih konstrukcij je bil poleg originalnega inputa uporabljen tudi skaliran input za primere konstrukcij W03, W10 in F10, kar je omogočilo doseganje različnih vrednosti duktilnosti. Uporabljena sta bila EP in Q_0 model histereznega obnašanja.

Določitev vrednosti dosežene duktilnosti v analizi neelastičnih MDOF konstrukcij ni enostavna. V parametrični študiji je uporabljena skupina sestavljena od 30 akcelerogramov, za vsak akcelerogram pa je dosežena različna vrednost duktilnosti konstrukcije. Zato je bil uporabljen poenostavljen pristop za določitev dosežene duktilnosti. Uporabljena je bila N2 metoda, ki temelji na potisni analizi (Fajfar 2000 in PRILOGA D). V potisnih analizah je bila predpostavljena razporeditev obtežbe, ki ustreza prvi nihajni obliki. Treba je poudarjati, da rezultati, dobljeni z N2 metodo, niso uporabljeni le za določitev duktilnosti. N2 metoda namreč predstavlja pomemben del direktnega pristopa, ki je pokazan v poglavjih 5 in 6.

Rezultati N2 metode (slike 4.5, 4.6, 4.9, 4.10, 4.13, 4.14, 4.17, 4.18, 4.21 in 4.22) tu ne bodo detajlno opisani zaradi obsežnosti, ker gre za standarden postopek.

Etažne spektre odziva smo računali za naslednje primere neelastičnih konstrukcij:

- Stena W03: EP model ($\mu=1,9$ in $\mu=4,0$) in Q model ($\mu=2,0$ in $\mu=4,2$).
- Stena W10: EP model ($\mu=2,0$ in $\mu=4,0$) in Q model ($\mu=2,1$ in $\mu=4,1$).
- Okvir F03: EP model ($\mu=2,0$) in Q model ($\mu=2,1$).
- Okvir F10: EP model ($\mu=2,1$ in $\mu=4,1$) in Q model ($\mu=2,2$ in $\mu=4,4$).

Rezultati študije (slike 4.7, 4.8, 4.11, 4.12, 4.15, 4.16, 4.19 in 4.20) kažejo da so v spektrih neelastičnih konstrukcij špice zaradi prve oblike nižje od ustreznih špic, dobljenih za elastične konstrukcije. V primeru EP modela se te špice pojavljajo blizu resonance elastične konstrukcije,

medtem ko so v primeru Q modela špice premaknjene proti daljšim nihajnim časom. Špice kažejo trende, ki so podobni trendom, ki so bili opaženi pri neelastičnih SDOF konstrukcijah.

Nekaj zanimivosti je opaženih pri spektralnih špicah, ki se nanašajo na višje nihajne oblike. To velja za toge (W03 in F03) in podajne (W10 in F10) konstrukcije.

V primeru togih konstrukcij so špice, dobljene za neelastične konstrukcije, lahko višje od ustreznih špic, dobljenih za elastične konstrukcije. Še bolj zanimiva ugotovitev je obstoj spektralnih špic, ki se nanašajo na nihajne oblike s frekvenco večjo od f_{ZPA} . Obe ugotovitvi potrdijo rezultate prejšnjih študij, ki so jih opravili Sewell in sod. (1986) in Singh in sod. (1996).

V primeru podajnih konstrukcij so v posameznih primerih špice etažnih spektrov odziva, ki so povezane z drugo nihajno obliko, reducirane v primerjavi s špicami, ki se pojavijo v elastičnih konstrukcijah. V takšnih primerih je opaženo, da imajo špice podobne lastnosti kot maksimalne vrednosti, ki so povezane s prvo obliko, vendar z značilno manjšo duktilnostjo. Glede na to, da je v potresnem inženirstvu pogosto predpostavljeno, da se neelastičnost pojavi le v prvi obliki, so navedena opažanja pripeljala do nekaj zanimivih vprašanj. Dobljeni rezultati kažejo, da se neelastičnost lahko pojavi tudi v višjih oblikah. Če se to lahko zgodi v primerih enostavnih konstrukcij, ki so bile predmet študije, potem je jasno, da je realno pričakovati, da do tega lahko pride tudi v konstrukcijah, ki imajo pomembno večje število nihajnih oblik. Če ni možno predpostaviti, da je neelastično obnašanje vezano le za prvo obliko, potem je treba pravilno oceniti potresne zahteve tudi v višjih neelastičnih oblikah. Chopra in Goel (2002) sta predlagala modalno potisno analizo, ki zagotavlja oceno zahtev v posameznih oblikah. V disertaciji je bil uporabljen podoben postopek, le da je bila uporabljena N2 metoda. Rezultati, dobljeni za konstrukcijo F10 (sliki 4.21 in 4.22), kažejo da je takšen pristop nekoliko podcenil duktilnost.

Direktno določanje etažnih pospeškov v elastičnih in neelastičnih MDOF konstrukcijah

Rezultati parametrične študije, opravljene na MDOF konstrukcijah, predstavljajo med drugim osnovo za analizo enega od najbolj pomembnih parametrov za potresno projektiranje opreme občutljive na pospeške: maksimalnega pospeška etaže (PFA). Analiza je predstavljena v poglavju 5. Predlagan je tudi postopek za direktno določanje maksimalnih etažnih pospeškov, ki temelji na N2 metodi.

Določitev PFA je v primeru časovne analize odziva zamudna, vendar konceptualno enostavna. V inženirski praksi je najbolj pogosto uporabljena modalna spektralna analiza, v kateri so PFA določeni za posamezne oblike na podlagi standardnega pristopa (npr. Chopra 2012). Tako določene PFA je treba kombinirati z ustreznim kombinacijskim pravilom, da bi določili celotni PFA. V študiji je bilo ugotovljeno, da najbolj pogosto uporabljana kombinacijska pravila (SRSS in CQC), ki ponavadi zagotavljajo dovolj točne rezultate za večino količin (npr. pomikov), niso dovolj natančna v primeru absolutnih pospeškov v spodnjih etažah, zlasti v primerih togih MDOF konstrukcij. Glavni razlog za to je dejstvo je velika občutljivost absolutnih pospeškov na vplive višjih oblik. Pokazalo se je, da so v takšnih primerih bolj primerne metode za modalno kombinacijo, ki so navedene v USNRC 1.92 (2006). Treba je poudariti, da so te metode uporabne za katerokoli količino. Ustrezne kombinacijske metode so tiste, ki so jih predlagali Gupta in Lindley-Yow in ki so povezane z metodo manjkajoče mase (Missing Mass). Preden so postale sestavni del USNRC 1.92 (2006), so bile omenjene metode raziskane in preverjene v NUREG/CR-6645 (1999). Uporaba omenjenih metod je enostavna. Nihajne oblike s frekvencami nižjimi od f_{ZPA} , so zajete v modalni rešitvi in za njih je treba uporabiti Guptino ali Lindley-Yow metodo. Vpliv nihajnih oblik s frekvencami, višjimi od f_{ZPA} , je treba upoštevati z

uporabo ene same dodatne oblike, ki je določena z metodo manjkajoče mase. Vpliv te oblike na odziv sistema je določen s statično analizo. Končno je celotni odziv dobljen s kombinacijo rezultatov modalne analize in metode z manjkajočo maso. Pregled kombinacijskih metod iz USNRC 1.92 (2006) je predstavljen v PRILOGI F.

Predlog postopka za direktno določanje PFA v elastičnih in neelastičnih konstrukcijah, ki temelji na kombinacijskih pravilih, omenjenih zgoraj, je predstavljen v nadaljevanju. Treba je poudariti, da predlagani postopek ne zagotavlja rezultatov zadostne natančnosti v vseh primerih. Razlog je predvsem velika občutljivost absolutnih pospeškov na vpliv višjih nihajnih oblik. Nekateri raziskovalci so se potrudili razviti poenostavljene postopke za določanje »bolj natančnih« PFA v elastičnih (npr. Miranda in Taghavi 2005, Singh in sod. 2006, Kumari in Gupta 2007, Pozzi in Der Kiureghian 2012 in Moschen in sod. 2014) in neelastičnih (npr. Rodriguez in sod. 2002, Chaudhuri in Hutchinson 2011, Wieser in sod. 2013 in Moschen in sod. 2013) konstrukcijah. Do tega trenutka, noben od omenjenih postopkov še ni bil široko sprejet v praksi. Tudi potresno projektiranje opreme, obravnavano v različnih predpisih, običajno temelji na PFA. Pinkawa in sod. (2014) so naredili zanimivo primerjalno študijo določb nekaj predpisov in ugotovili, da je potrebno izboljšanje aktualnih predpisov.

Vrednosti PFA v konstrukciji se lahko določijo z uporabo enačbe 5.1 (str. 116). V primeru neelastičnih konstrukcij je zelo pomemben del predlaganega postopka uporaba N2 metode, kar je detajlno opisano v poglavju 5. Uporaba kombinacijskih metod iz USNRC 1.92 (2006) v primeru PFA je predstavljena v enačbah 5.2 (str. 116), 5.3 in 5.4 (str. 117). Treba je poudariti da je pri neelastičnih konstrukcijah uporaba modalne superpozicije približek.

Natančnost predlaganega postopka je najprej ocenjena za primere elastičnih konstrukcij, ki so obravnavane v parametrični študiji. Rezultati predlaganega postopka so primerjani z rezultati PFA, dobljenimi iz parametrične študije in, dodatno, z rezultati dobljenimi ob uporabi SRSS pravila (slika 5.1). Ugotovljeno je, da v primeru togih konstrukcij (W03 in F03) postopek ne zagotavlja prav dobrih rezultatov v prvi etaži. V primeru podajnih konstrukcij (W10 in F10) so rezultati, dobljeni z Guptino metodo praktično enaki rezultatom, ki so dobljeni iz SRSS pravila zaradi dejstva, da Guptina metoda pri podajnih konstrukcijah prehaja v SRSS pravilo. V primeru elastičnih konstrukcij je v predlaganem postopku uporabljen tudi približen input spekter (slika 4.1). To je narejeno predvsem zaradi tega, ker je ta input uporabljen tudi za neelastične konstrukcije in je bilo pomembno videti, kakšna odstopanja se pojavijo že pri elastičnih konstrukcijah (pričakovati je, da so odstopanja pri neelastičnih konstrukcijah precej večja). Treba je poudariti da je približen input takšen, da za nihajne oblike z nihajnim časom manjšim od 0,15 s ni razlike med spektralnimi vrednostmi, torej da sta ciljni in točni spekter popolnoma enaka. To npr. pomeni, da za konstrukcije W03 in F03 razlika med točnim in približnim inputom obstaja le ob prvi obliki. Rezultati, predstavljeni na sliki 5.2, so pokazali, da se odstopanja večajo po višini konstrukcij, oziroma z večanjem vpliva prve oblike, za katero je pri vseh obravnavanih konstrukcijah obstajala razlika med točnim in približnim inputom (za oblike z nihajnimi časi manjšim od 0,15 s ni razlike med točnim in približnim inputom).

Primerjava direktnih PFA, dobljenih s predlaganim postopkom, je narejena tudi za neelastične konstrukcije in rezultati so pokazani na slikah 5.3–5.6. Iz rezultatov je razvidno, da predlagani postopek daje bolj natančne rezultate v primeru podajnih konstrukcij (W10 in F10). V primeru togih konstrukcij (W03 in F03) so rezultati načeloma nekonservativni, v nekaterih primerih pa celo padejo pod vrednost točnega PFA, zmanjšane za standardno devijacijo.

Direktna metoda za določanje etažnih spektrov odziva v elastičnih in neelastičnih MDOF konstrukcijah

V poglavju 6 je razvita in preverjena metoda za direktno določanje etažnih spektrov pospeškov v neelastičnih MDOF konstrukcijah. Metoda izhaja iz direktne metode, razvite za SDOF konstrukcije in iz rezultatov parametrične študije, opravljene na MDOF konstrukcijah.

V predlagani metodi so etažni spektri odziva določeni za posamezne oblike in so nato kombinirani. Ta postopek je v primeru neelastičnih konstrukcij seveda približek.

Prvi korak predlagane metode predstavlja izračun etažnega spektra odziva za posamezno obliko. Izven resonančnega območja se to naredi za vsako etažo z uporabo enačbe 6.1 (str. 124). V resonančnem območju se spektralne vrednosti določijo z enačbo 6.3 (str. 125), ob uporabi enačb za izračun *AMP* (enačba 6.4 za EP model in enačba 6.5 za Q model, str. 125). Pri Q modelih je treba upoštevati podaljšanje osnovnega nihajnega časa konstrukcije, oziroma enačbo 6.2 (str. 124). Pomemben del direktne metode je N2 metoda in njeni rezultati predstavljajo količine, ki so uporabljene v omenjenih enačbah. V poglavju 6 so podani natančni komentarji, ki se nanašajo na posamezne količine in uporabo rezultatov iz N2 metode. Dodatno je v PRILOGI D prikazan način določanja etažnih pospeškov iz etažnih pomikov.

Drugi korak predstavlja kombinacija direktnih spektrov, določenih za posamezne oblike. Postopek je opisan in analiziran v poglavju 6. Poudariti je treba naslednje: v prvem delu območja period opreme (med $T_s=0$ in vrednostjo T_s , ki se nahaja kmalu po špicu v spektru, ki izhaja iz prve oblike) je treba uporabiti eno od metod, predlaganih v USNRC 1.92 (2006). V preostanku območja period opreme (podajna oprema) je treba uporabiti algebraično vsoto (ALGSUM). Upravičenost njena uporabe je dokazana z enačbami 6.6–6.9 (str. 126 in 127). V poglavju 6 so podana tudi navodila za povezovanje spektrov dobljenih ob uporabi različnih kombinacijskih pravil (USNRC in ALGSUM). Grafični opis povezave je prikazan na sliki 6.1.

Predlagana direktna metoda je najprej preverjena za primere elastičnih konstrukcij W03, W10, F03 in F10. Uporabljen je točen input, s čemer so eliminirane napake, ki izhajajo iz razlik ciljnega spektra in povprečnega spektra izbranih akceleroگرامov (slika 4.1). V direktni metodi je uporabljena Guptina metoda kombinacije, ki je bila povezana z metodo manjkajoče mase. Glede na nihajne čase konstrukcij je bila metoda manjkajoče mase uporabljena edino v primeru konstrukcije W03. Rezultati primerjave so pokazani na slikah 6.2–6.9. Rezultati kažejo, da za vse obravnavane primere konstrukcij, v vseh etažah in v celotnem območju period opreme predlagana direktna metoda vodi do rezultatov, ki se zelo dobro ujemajo z rezultati, dobljenimi s časovno analizo odziva.

Pri preverjanju predlagane direktne metode za neelastične konstrukcije (slike 6.10–6.37) je bil uporabljen približen input (ki je že omenjen pri direktnem določanju PFA). Razlog za to je uporaba redukcijskih faktorjev, ki se praviloma uporabljajo le za gladke spektre. V omenjenih enačbah metode so za neelastične oblike uporabljene vrednosti, določene z N2 metodo. Dobljeni rezultati so primerjani z rezultati, dobljenimi s časovno analizo odziva. V večini primerov se vidi solidno ujemanje. V nekaterih primerih, predvsem pri Q modelih, pa je natančnost predlagane metode nekoliko slabša. Ne glede na to lahko, ob upoštevanju vseh negotovosti, povezanih z določanjem etažnih spektrov odziva za neelastične konstrukcije, zaključimo, da v veliki večini primerov predlagana metoda daje dobro oceno etažnih spektrov odziva v neelastičnih konstrukcijah.

Prispevki doktorske disertacije

Analize in študije, opravljene v disertaciji, so pripeljale do različnih ugotovitev in predlogov, ki predstavljajo pomembne znanstvene prispevke na področju potresnega inženirstva v povezavi s projektiranjem in z ocenjevanjem opreme. Ugotovitve v glavnem potrjujejo in razširjajo opažanja drugih raziskovalcev. Na podlagi teh opažanj, je bila razvita in verificirana originalna in za prakso uporabna metoda za direktno določanje etažnih spektrov pospeškov. Predlagana metoda je uporabna za elastične in neelastične konstrukcije, modelirane kot SDOF in/ali MDOF sistem. Glavni prispevki disertacije so:

- Identifikacije najbolj pomembnih parametrov, ki vplivajo na etažne spektre pospeškov v SDOF konstrukcijah.

Veliko število etažnih spektrov pospeškov, ki so bili določeni s časovno analizo odziva ob spreminjanju nekaj vhodnih parametrov, je omogočilo raziskavo vpliva, ki ga ima neelastično obnašanje SDOF primarne konstrukcije na odziv opreme. Glavne lastnosti etažnih spektrov odziva so bile ugotovljene v celotnem območju period opreme in narejena je bila jasna ločitev predresonančnega, resonančnega in poresonančnega območja. Razmerje maksimalne vrednosti etažnega spektra odziva in pospeška konstrukcije je definirano kot faktor amplifikacije *AMP*.

- Predlog metode za direktno določanje etažnih spektrov pospeškov za neelastične SDOF primarne konstrukcije.

Novak in Fajar (1994) sta prikazala idejo za izboljšanje in razširitev metode, ki so jo predlagali Yasui in sod. (1993). Ta ideja je uporabljena in realizirana v disertaciji. Razvita je metoda za direktno določanje etažnih spektrov pospeškov v neelastičnih SDOF primarnih konstrukcij. Direktni spektri dobljeni iz predlagane metoda izven resonančnega območja imajo teoretično osnovo. V resonančnem območju vrednosti etažnih spektrov odziva temeljijo na empiričnih faktorjih amplifikacije, ki so predlagani na podlagi rezultatov parametrične študije.

- Identifikacije nekaj pomembnih parametrov, ki vplivajo na etažne spektre pospeškov v MDOF konstrukcijah.

Študija etažnih spektrov odziva, dobljenih s časovno analizo odziva za štiri enostavne ravninske konstrukcije je omogočila identifikacijo nekaj zelo pomembnih karakteristik etažnih spektrov pospeškov v MDOF konstrukcijah. Narejena je jasna ločitev med območji period opreme v pred- in poresonančnem območju, ki izhaja iz prve nihajne oblike. Opaženo je bilo, da se etažni spektri pospeškov približujejo spektrom tal po resonanci prve oblike. Raziskani so bili vplivi višjih nihajnih oblik. Ugotovljeno je bilo, da imajo lahko zelo pomemben vpliv na absolutne pospeške in etažne spektre pospeškov v elastičnih in neelastičnih konstrukcijah. V primeru togih konstrukcij je bilo ugotovljeno, da so v posameznih primerih špice etažnih spektrov odziva, dobljene za neelastične konstrukcije, lahko višje od špic, dobljenih za elastične konstrukcije. Še bolj zanimivo je, da obstajajo tudi špice, ki izhajajo iz oblik z zelo visokimi frekvencami (nad f_{ZPA}). Obe ugotovitvi sta bile že opaženi (Sewell in sod. 1986 in Singh in sod. 1996). V primeru podajnih konstrukcij je bilo opaženo, da neelastično obnašanje lahko obstaja tudi v višjih oblikah. V takšnih primerih imajo resonančna območja, ki pripadajo drugi obliki, podobne trende, kot so se pokazali v resonančnih območjih, ki so povezana s

prvo obliko. Predlagan je postopek za oceno zahtev v neelastičnih višjih oblikah, ki temelji na N2 metodi in modalni potisni analizi, ki sta jo predlagala Chopra in Goel (2002).

- Predlog postopka za direktno določanje maksimalnih etažnih pospeškov (PFA) v MDOF primarnih konstrukcijah.

Opaženo je bilo, da uporaba SRSS kombinacijskega pravila za absolutne pospeške ne zagotavlja rezultatov zadostne natančnosti v spodnjem delu konstrukcije. Zaradi tega so bile uporabljene metode za modalno kombinacijo, ki so opisane v USNRC 1.92 (2006). Na ta način so bili dobljeni bolj natančni rezultati za PFA v elastičnih in neelastičnih MDOF primarnih konstrukcijah. V neelastičnih konstrukcijah je bila za določanje pospeškov uporabljena N2 metoda.

- Predlog metode za direktno določanje etažnih spektrov pospeškov za neelastične MDOF primarne konstrukcije.

Metoda za direktno določanje etažnih spektrov pospeškov za MDOF konstrukcije je razvita z razširitvijo metode, razvite za SDOF primarne konstrukcije. Pomembni deli metode so: modalna superpozicija (ki je aproksimacija v primeru neelastičnih konstrukcij), različne metode modalne kombinacije v različnem območjem period opreme (metode predlagane v USNRC 1.92 2006 in algebraična vsota), in N2 metoda. Predlagana direktna metoda je koristno orodje v fazi idejnega prjektiranja, in tudi za kontrolo rezultatov dobljenih iz bolj natančnih analiz. Metoda se lahko uporabi kot osnova za poenostavljene procedure v predpisih.

Predlogi nadaljnjih raziskav

Število raziskav, ki so bile v preteklosti posvečene problemom potresne analize nekonstrukcijskih elementov in vsebine stavb, ni zadostno. Določitev potresnih zahtev za opremo, ki je občutljiva na pospeške, je področje, ki nujno potrebuje nadaljne raziskave, zlasti v zvezi z razvojem poenostavljenih metod, ki lahko izboljšajo potresno projektiranje in oceno opreme v praksi. Delni seznam problemov, ki jih je treba raziskati, je omenjen spodaj.

Parametrične študije, vključno s tistimi v tej disertaciji, so običajno narejene za razmeroma enostavne elastične in neelastične MDOF primarne konstrukcije. Čeprav dobljeni rezultati omogočajo zelo dober pregled glavnih karakteristik etažnih spektrov pospeškov, je treba narediti več parametričnih študij na bolj specifičnih in kompliciranih konstrukcijah. Posebno pozornost je treba posvetiti vplivu višjih nihajnih oblik.

Med razvojem in validacijo direktnih pristopov za določanje maksimalnih etažnih pospeškov in etažnih spektrov pospeškov je bilo ugotovljeno, da, na splošno, večina obstoječih pravil za modalno kombinacijo ne zagotavlja dovolj natančnih rezultatov v primeru absolutnih pospeškov, saj so absolutni pospeški zelo občutljivi na vplive višjih nihajnih oblik. Zaradi tega lahko razvoj pravila za modalno kombinacijo, ki je bolj ustrezno za uporabo v primeru absolutnih pospeškov, pripelje do pomembnega napredka v inženirski praksi.

V primeru neelastičnih MDOF konstrukcij, zlasti togih, daje predlagani direktni pristop za določanje maksimalnih etažnih pospeškov na splošno nekoliko nekonservativne rezultate. Zaradi tega bo v

prihodnosti treba upoštevati določena izboljšanja predlagane procedure, morda v smislu uvedbe korekcijskih faktorjev.

Predlagana direktna metoda za določanje etažnih spektrov odziva ima teoretično ozadje izven resonančnega območja, saj temelji na principih dinamike konstrukcij. V resonančnem območju so kot osnova za definicijo *AMP*, uporabljenih v predlagani direktni metodi, uporabljene vrednosti *AMP*, dobljene v parametrični študiji narejeni na SDOF sistemih. Parametrična študija bila narejena za izbrane nihajne čase SDOF sistemov, dve skupini akcelerogramov, tri histerezne modele in tri vrednosti ciljne duktilnosti. Priporočljivo je narediti dodatne parametrične študije, v katerih bi analizirali še več vhodnih parametrov, npr. zelo kratki nihajni časi SDOF sistemov, akcelerogrami različnih karakteristik (predvsem »near fault« akcelerogrami), histerezna pravila, v katerih je upoštevano padanje nosilnosti.

Koncept etažnih spektrov odziva temelji na nepovezani analizi sistema konstrukcija-oprema, kar lahko pripelje do konservativnih rezultatov. To dejstvo je najbolj očitno v primerih, ko masa opreme ni zanemarljiva v primerjavi z maso konstrukcije. V takšnih primerih je mogoče dobiti bolj natančno oceno etažnih spektrov odziva, če se na nek način upoštevajo vplivi povezanosti konstrukcije in opreme. Pričakujemo, da je to povezanost možno upoštevati implicitno v predlagani direktni metodi, vendar je treba za to narediti ustrezno študijo.

V predlagani direktni metodi je neelastičnost upoštevana le v primarni konstrukciji. Kot možnost za razširitev predlagane direktne metode je treba upoštevati tudi neelastično obnašanje opreme.

REFERENCES

- Adam, C., Fotiu, P. A. 2000. Dynamic analysis of inelastic primary-secondary systems. *Eng. Struct.* 22, 1: 58–71.
doi:10.1016/S0141-0296(98)00073-X
- Adam, C., Furtmüller, T. 2008. Response of Nonstructural Components in Ductile Load-bearing Structures Subjected to Ordinary Ground Motions. In: *Proceedings of the 14th World Conference on Earthquake Engineering*, Beijing, China, 12–17 October 2008. Beijing, China, Chinese Association of Earthquake Engineering, International Association for Earthquake Engineering: Paper no 05-01-0327.
- Adam, C., Furtmüller, T., Moschen, L. 2013. Floor Response Spectra for Moderately Heavy Nonstructural Elements Attached to Ductile Frame Structures. *Comput. Meth. Earthq. Eng.* 2: 69–89.
doi:10.1007/978-94-007-6573-3_4
- Akiyama, H. 1985. *Earthquake-Resistant Limit-State Design for Buildings*. University of Tokyo Press, Tokyo.
- ASCE 4-98 2000. *Seismic Analysis of Safety-Related Nuclear Structures and Commentary*. American Society of Civil Engineers, Reston, VA, USA.
- Aziz, T. S. 2004. Design earthquake ground motions for nuclear power plants. In: *Proceedings of the 13th World Conference on Earthquake Engineering*, Vancouver, B.C., Canada, 1–6 August 2004. Vancouver, Canada, Canadian Association for Earthquake Engineering, International Association for Earthquake Engineering: Paper no 934.
- Baker, J. W. 2007. Quantitative Classification of Near-Fault Ground Motions Using Wavelet Analysis. *Bull. Seismol. Soc. Am.* 97, 5: 1486–1501.
doi:10.1785/0120060255
- Calvi, P. M., Sullivan, T. J.. 2014. Estimating floor spectra in multiple degree of freedom systems. *Earthq. Struct.* 7, 1: 17–38.
doi:10.12989/eas.2014.7.1.017
- Chaudhuri, S. R., Hutchinson, T. 2011. Effect of Nonlinearity of Frame Buildings on Peak Horizontal Floor Acceleration. *J. Earthq. Eng.* 15, 1: 124–142.
doi:10.1080/13632461003668046
- Chaudhuri, S. R., Villaverde, R. 2008. Effect of Building Nonlinearity on Seismic Response of Nonstructural Components: A Parametric Study. *ASCE J. Struct. Eng.* 134, 4: 661–670.
doi:10.1061/(ASCE)0733-9445(2008)134:4(661)
- Chopra, A. K. 2012. *Dynamics of Structures: Theory and Applications to Earthquake Engineering*, 4th Edition. Prentice Hall, Englewood Cliffs, New Jersey.
- Chopra, A. K., Goel, R. K. 2002. A modal pushover analysis procedure for estimating seismic demands for buildings. *Earth. Eng. Struct. Dyn.* 31, 3: 561–582.
doi:10.1002/eqe.144

- Dolšek, M., Fajfar, P. 2005. Post Test Analyses of the SPEAR Test Building. University of Ljubljana. <http://www.ikpir.com/projects/spear/PostTestModel.pdf> (Obtained on 17.12.2014.)
- EN 1992-1:2004. Eurocode 2 – Design of concrete structures. Part 1-1: General rules and rules for buildings. European Committee for Standardization (CEN), Brussels.
- EN 1998-1:2004. Eurocode 8 – Design of structures for earthquake resistance. Part 1: General rules, seismic actions and rules for buildings. European Committee for Standardization (CEN), Brussels.
- Fajfar, P. 2000. A Nonlinear Analysis Method for Performance Based Seismic Design. *Earthq. Spectra*. 16, 3: 573–592.
doi:10.1193/1.1586128
- Fajfar, P., Novak, D. 1995. Floor response spectra for inelastic structures. In: Transactions of the 13th International Conference on Structural Mechanics in Reactor Technology (SMiRT 13), Porto Alegre, Brazil, 13–18 August 1995. Porto Alegre, Brazil, International Association for Structural Mechanics in Reactor Technology, Universidade Federal do Rio Grande do Sul: Paper K044/1, p. 259–264.
- George, Z., Gupta, A. K. 1995. Closed-form equations for response of secondary systems. In: Transactions of the 13th International Conference on Structural Mechanics in Reactor Technology (SMiRT 13), Porto Alegre, Brazil, 13–18 August 1995. Porto Alegre, Brazil, International Association for Structural Mechanics in Reactor Technology, Universidade Federal do Rio Grande do Sul: Paper K076/1, p. 453–458.
- Gupta, A. K., Jaw, J. W. 1986. A new instructure response spectrum (IRS) method for multiply connected secondary systems with coupling effects. *Nucl. Eng. Des.* 96, 1: 63–80.
doi:10.1016/0029-5493(86)90162-7
- Iervolino, I., Galasso, C., Cosenza, E. 2010. REXEL: computer aided record selection for code-based seismic structural analysis. *Bull. Earthq. Eng.* 8, 2: 339–362.
doi:10.1007/s10518-009-9146-1
- Igusa, T. 1990. Response Characteristics of Inelastic 2-DOF Primary-Secondary System. *ASCE J. Eng. Mech.* 116, 5:1160–1174.
doi:10.1061/(ASCE)0733-9399(1990)116:5(1160)
- Igusa, T., Der Kiureghian, A. 1985. Generation of floor response spectra including oscillator-structure interaction. *Earth. Eng. Struct. Dyn.* 13, 5: 661–676.
doi:10.1002/eqe.4290130508
- Jayaram, N., Lin, T., Baker, J. W. 2011. A Computationally Efficient Ground-Motion Selection Algorithm for Matching a Target Response Spectrum Mean and Variance. *Earthq. Spectra*. 27, 3: 797–815.
doi:10.1193/1.3608002
- Kelly, T. E. 1978. Floor Response of Yielding Structures. *Bull. N. Z. Natl. Soc. Earth. Eng.* 11, 4: 255–272.

Kreslin, M., Fajfar, P. 2012. The extended N2 method considering higher mode effects in both plan and elevation. *Bull. Earthq. Eng.* 10, 2: 695–715.

doi:10.1007/s10518-011-9319-6

Kumari, R., Gupta, V. K. 2007. A Modal Combination Rule for Peak Floor Accelerations in Multistoried Buildings. *ISET J. Earthq. Tech.* 44, 1: 213–231. Paper no 483.

Lin, J., Mahin, S. A. 1985. Seismic Response of Light Subsystems on Inelastic Structures. *ASCE J. Struct. Eng.* 111, 2: 400–417.

doi:10.1061/(ASCE)0733-9445(1985)111:2(400)

Maniatakis, C. A., Psycharis, I. N., Spyarakos, C. C. 2013. Effect of higher modes on the seismic response and design of moment-resisting RC frame structures. *Eng. Struct.* 56: 417–430.

doi:10.1016/j.engstruct.2013.05.021

Mazzoni, S., McKenna, F., Scott, M. H., Fenves, G. L. 2007. *OpenSees Command Language Manual*. Pacific Earthquake Engineering Research (PEER) Center, University of California, Berkeley, CA, USA.

Medina, R. A., Sankaranarayanan, R., Kingston, K. M. 2006. Floor response spectra for light components mounted on regular moment-resisting frame structures. *Eng. Struct.* 28, 14: 1927–1940.

doi:10.1016/j.engstruct.2006.03.022

Miranda, E., Bertero, V. 1994. Evaluation of Strength Reduction Factors for Earthquake-Resistant Design. *Earthq. Spectra* 10, 2: 357–379.

doi:10.1193/1.1585778

Miranda, E., Taghavi, S. 2005. Approximate Floor Acceleration Demands in Multistory Buildings. I: Formulation. *ASCE J. Struct. Eng.* 131, 2: 203–211.

doi:10.1061/(ASCE)0733-9445(2005)131:2(203)

Moschen, L., Vamvatsikos, D., Adam, C. 2013. Towards a static pushover approximation of peak floor accelerations. In: *Proceedings of the Vienna Congress on Recent Advances in Earthquake Engineering and Structural Dynamics (VEESD 2013)*, Vienna, Austria, 28–30 August 2013. Vienna, Austria, Austrian Association for Earthquake Engineering and Structural Dynamics (OGE), Vienna University of Technology: Paper no 94.

Moschen, L., Vamvatsikos, D., Adam, C. 2014. A Modified Response Spectrum Method for Estimating Peak Floor Acceleration Demands in Elastic Regular Frame Structures. In: *Proceedings of the Second European Conference on Earthquake Engineering and Seismology*, Istanbul, Turkey, 25–29 August 2014. Istanbul, Turkey, Republic of Turkey Prime Ministry, Disaster and Emergent Management Presidency, Turkish Earthquake Foundation Earthquake Engineering Committee: Paper no 349.

Novak, D., Fajfar, P. 1994. Nelinearni etažni spektri odziva za racionalno aseizmično projektiranje opreme. In: *Zbornik 16. zborovanja gradbenih konstruktorjev Slovenije (in Slovenian)*, Bled, Slovenia, 8–9 September 1994. Ljubljana, Slovenia, Društvo gradbenih konstruktorjev: p. 95–102.

NUREG/CR-6645 1999. Reevaluation of Regulatory Guidance on Modal Response Combination Methods for Seismic Response Spectrum Analysis. U.S. Nuclear Regulatory Commission, Washington, D.C., USA.

Oropeza, M., Favez, P., Lestuzzi, P. 2010. Seismic response of nonstructural components in case of nonlinear structures based on floor response spectra method. *Bull. Earthq. Eng.* 8, 2: 387–400.
doi:10.1007/s10518-009-9139-0

Peters, K. A., Schmitz, D., Wagner, U. 1977. Determination of Floor Response Spectra on the Basis of the Response Spectrum Method. *Nucl. Eng. Des.* 44, 2: 255–262.
doi:10.1016/0029-5493(77)90032-2

Pinkawa, M., Hoffmeister, B., Feldmann, M. 2014. A critical review of current approaches on the determination of seismic force demands on nonstructural components. In: *Proceedings of the 9th International Conference on Structural Dynamics*, Porto, Portugal, 30 June – 2 July 2014. Porto, Portugal, European Association for Structural Dynamics, Faculty of Engineering of the University of Porto (FEUP).

Politopoulos, I. 2010. Floor Spectra of Nonlinear MDOF Structures. *J. Earthq. Eng.* 14, 5: 726–742.
doi:10.1080/13632460903427826

Politopoulos, I., Feau, C. 2007. Some aspects of floor spectra of 1DOF nonlinear primary structures. *Earthq. Eng. Struct. Dyn.* 36, 8: 975–993.
doi:10.1002/eqe.664

Pozzi, M., Der Kiureghian, A. 2012. Response Spectrum Analysis for Floor Acceleration. In: *Proceedings of the 15th World Conference on Earthquake Engineering*, Lisbon, Portugal, 24–28 September 2012. Lisbon, Portugal, Portuguese Society for Earthquake Engineering, International Association for Earthquake Engineering: Paper no 5578.

Rodriguez, M. E., Restrepo, J. I., Carr, A. J. 2002. Earthquake-induced floor horizontal accelerations in buildings. *Earthq. Eng. Struct. Dyn.* 31, 3: 693–718.
doi:10.1002/eqe.149

Saiidi, M., Sozen, M. A. 1979. Simple and complex models for nonlinear seismic response of reinforced concrete structures. *Civil Engineering Studies, Structural Research Series No. 465*. University of Illinois, Urbana, IL.

Sankaranarayanan, R., Medina, R. A. 2007. Acceleration response modification factors for nonstructural components attached to inelastic moment-resisting frame structures. *Earthq. Eng. Struct. Dyn.* 36, 14: 2189–2210.
doi:10.1002/eqe.724

Sewell, R. T., Cornell, C. A., Toro, G. R., McGuire, R. K. 1986. A study of factors influencing floor response spectra in nonlinear multi-degree-of-freedom-structures, Report No. 82. The John A. Blume Earthquake Engineering Center, Stanford University, Stanford, CA, USA.

Shooshtari, M., Saatcioglu, M., Naumoski, N., Foo, S. 2010. Floor response spectra for seismic design of operational and functional components of concrete buildings in Canada. *Can. J. Civ. Eng.* 37, 12: 1590–1599.

doi:10.1139/L10-094

Singh, M. P., Sharma, A.M. 1983. An alternative procedure for direct generation of seismic floor spectra. In: *Transactions of the 7th International Conference on Structural Mechanics in Reactor Technology (SMiRT 7)*, Chicago, IL, USA, 22–26 August 1983. Chicago, IL, USA, The Commission of the European Communities, Argonne National Laboratory: Paper K6/10, p. 437–444.

Singh, M. P., Chang, T-S., Suárez, L. E. 1996. Floor response spectrum amplification due to yielding of supporting structure. In: *Proceedings of the 11th World Conference on Earthquake Engineering*, Acapulco, Mexico, 23–28 June 1996. Oxford, England, Elsevier Science Ltd: Paper no 1444.

Singh, M. P., Moreschi, L. M., Suárez, L. E., Matheu, E. E. 2006. Seismic Design Forces. I: Rigid Nonstructural Components. *ASCE J. Struct. Eng.* 132, 10: 1524–1532.

doi:10.1061/(ASCE)0733-9445(2006)132:10(1524)

Singh, M. P., Moreschi, L. M., Suárez, L. E., Matheu, E. E. 2006. Seismic Design Forces. II: Flexible Nonstructural Components. *ASCE J. Struct. Eng.* 132, 10: 1533–1542.

doi:10.1061/(ASCE)0733-9445(2006)132:10(1533)

Suarez, L. E., Singh, M. P. 1987. Floor response spectra with structure–equipment interaction effects by a mode synthesis approach. *Earth. Eng. Struct. Dyn.* 15, 2: 141–158.

doi:10.1002/eqe.4290150202

Sullivan, T. J., Calvi, P. M., Nascimbene, R. 2013. Towards improved floor spectra estimates for seismic design. *Earthq. Struct.* 4, 1: 109–132.

doi:10.12989/eas.2013.4.1.109

Taghavi, S., Miranda, E. 2005. Approximate Floor Acceleration Demands in Multistory Buildings. II: Applications. *ASCE J. Struct. Eng.* 131, 2: 212–220.

doi:10.1061/(ASCE)0733-9445(2005)131:2(212)

USNRC Regulatory Guide 1.122 1978. Development of floor design response spectra for seismic design of floor-supported equipment or components, Revision 1. U.S. Nuclear Regulatory Commission, Washington, D.C., USA.

USNRC Regulatory Guide 1.92 2006. Combining modal responses and spatial components in seismic response analysis. U.S. Nuclear Regulatory Commission, Washington, D.C., USA.

USNRC Regulatory Guide 1.61 2007. Damping values for seismic design of nuclear power plants. U.S. Nuclear Regulatory Commission, Washington, D.C., USA.

Vanmarcke, E. H. 1977. A Simple Procedure for Predicting Amplified Response Spectra and Equipment Response. In: *Proceedings of the 6th World Conference on Earthquake Engineering*, New Delhi, India, 10–14 January 1977. New Delhi, India, Indian Society of Earthquake Technology: Volume 3, 3323–3327.

Vidic, T. 1988. Določanje etažnih spektrov odziva. In: Zbornik 10. zborovanja gradbenih konstruktorjev Slovenije (in Slovenian), Bled, Slovenia, 14–16 September 1988. Ljubljana, Slovenia, Društvo gradbenih konstruktorjev: p. 173–180.

Vidic, T., Fajfar, P., Fischinger, M. 1994. Consistent inelastic design spectra: strength and displacement. *Earth. Eng. Struct. Dyn.* 23, 5: 507–521.
doi:10.1002/eqe.4290230504

Villaverde, R. 1987. Simplified approach for the seismic analysis of equipment attached to elastoplastic structures. *Nucl. Eng. Des.* 103, 3: 267–279.
doi:10.1016/0029-5493(87)90310-4

Villaverde, R. 1991. Approximate formulas to calculate the seismic response of light attachments to buildings. *Nucl. Eng. Des.* 128, 3: 349–368.
doi:10.1016/0029-5493(91)90172-E

Villaverde, R. 1997. Seismic Design of Secondary Structures: State of the Art. *ASCE J. Struct. Eng.* 123, 8: 1011–1019.
doi:10.1061/(ASCE)0733-9445(1997)123:8(1011)

Villaverde, R. 2006. Simple method to estimate the seismic nonlinear response of nonstructural components in buildings. *Eng. Struct.* 28, 8: 1209–1221.
doi:10.1016/j.engstruct.2005.11.016

Vukobratović, V., Fajfar, P. 2012. A method for direct determination of inelastic floor response spectra. In: Proceedings of the 15th World Conference on Earthquake Engineering, Lisbon, Portugal, 24–28 September 2012. Lisbon, Portugal, Portuguese Society for Earthquake Engineering, International Association for Earthquake Engineering: Paper no 727.

Vukobratović, V., Fajfar, P. 2013. A method for direct generation of floor acceleration spectra for inelastic structures. In: Transactions of the 22nd International Conference on Structural Mechanics in Reactor Technology (SMiRT 22), San Francisco, CA, USA, 18–23 August 2013. San Francisco, CA, USA, International Association for Structural Mechanics in Reactor Technology: Paper no 215.

Vukobratović, V., Fajfar, P. 2015. A method for the direct determination of approximate floor response spectra for SDOF inelastic structures. *Bull. Earthq. Eng.* 13, 5: 1405–1424.
doi:10.1007/s10518-014-9667-0

Wieser, J., Pekcan, G., Zaghi, A. E., Itani, A., Maragakis, M. 2013. Floor Accelerations in Yielding Special Moment Resisting Frame Structures. *Earthq. Spectra.* 29, 3: 987–1002. doi:10.1193/1.4000167

Uma, S. R., Zhao, J. X., King, A. B. 2010. Seismic actions on acceleration sensitive non-structural components in ductile frames. *Bull. N. Z. Soc. Earthq. Eng.* 43, 2: 110–125.

Yasui, Y., Yoshihara, J., Takeda, T., Miyamoto, A. 1993. Direct generation method for floor response spectra. In: Transactions of the 12th International Conference on Structural Mechanics in Reactor Technology (SMiRT 12), Stuttgart, Germany, 15–20 August 1993. Amsterdam, Holland, Elsevier Science Publishers B.V.: Paper K13/4, p. 367–372.

**ANNEX A: DERIVATION OF THE DIRECT METHOD PROPOSED BY YASUI ET AL.
 (1993)**

Yasui et al. (1993) proposed a method for determination of floor response spectra directly from ground motion spectrum. The method is valid in the whole period range. The derivation was conducted for the case of the linear elastic behaviour of a primary structure and equipment, which were modelled as SDOF systems. The interaction between the structure and the equipment was not taken into account (uncoupled system). The equation for direct determination of floor response spectra was derived analytically, by using the Duhamel integral for the response determination. It should be noted that the derivation conducted by Yasui et al. (1993) was not presented in their paper in detail. Therefore, the derivation presented herein was conducted independently in order to confirm the accuracy of the equations derived by Yasui et al. (1993).

If a SDOF structure is exposed to ground acceleration $\ddot{u}_g(t)$, then its response in terms of displacement, velocity and acceleration can be expressed by Equations A.1–A.3, respectively, where ω represents natural circular frequency and ξ represents damping coefficient.

$$u(t) = -\frac{1}{\omega} \int_0^t \ddot{u}_g(\tau) \exp\{-\xi\omega(t-\tau)\} \sin \omega(t-\tau) d\tau \quad (\text{A.1})$$

$$\begin{aligned} \dot{u}(t) = & \xi \int_0^t \ddot{u}_g(\tau) \exp\{-\xi\omega(t-\tau)\} \sin \omega(t-\tau) d\tau - \\ & - \int_0^t \ddot{u}_g(\tau) \exp\{-\xi\omega(t-\tau)\} \cos \omega(t-\tau) d\tau \end{aligned} \quad (\text{A.2})$$

$$\begin{aligned} \ddot{u}(t) = & \omega(1-\xi^2) \int_0^t \ddot{u}_g(\tau) \exp\{-\xi\omega(t-\tau)\} \sin \omega(t-\tau) d\tau + \\ & + 2\xi\omega \int_0^t \ddot{u}_g(\tau) \exp\{-\xi\omega(t-\tau)\} \cos \omega(t-\tau) d\tau \end{aligned} \quad (\text{A.3})$$

In the derivation process, the absolute acceleration of the mass of the primary structure exposed to $\ddot{u}_g(t)$ is denoted as $\ddot{u}_p(t)$. The absolute acceleration of the mass of the equipment exposed to $\ddot{u}_p(t)$ is denoted as $\ddot{u}_s(t)$. Additionally, the absolute acceleration of the mass of the equipment exposed directly to $\ddot{u}_g(t)$ is denoted as $\ddot{u}_{sg}(t)$.

Since damping coefficient is rather small, Equation A.3 can be significantly simplified and $\ddot{u}_p(t)$, $\ddot{u}_s(t)$ and $\ddot{u}_{sg}(t)$ can be expressed as

$$\ddot{u}_p(t) = \omega_p \int_0^t \ddot{u}_g(\tau) \exp\{-\xi_p \omega_p(t-\tau)\} \sin \omega_p(t-\tau) d\tau \quad (\text{A.4})$$

$$\ddot{u}_s(t) = \omega_s \int_0^t \ddot{u}_p(\tau) \exp\{-\xi_s \omega_s(t-\tau)\} \sin \omega_s(t-\tau) d\tau \quad (\text{A.5})$$

$$\ddot{u}_{sg}(t) = \omega_s \int_0^t \ddot{u}_g(\tau) \exp\{-\xi_s \omega_s(t-\tau)\} \sin \omega_s(t-\tau) d\tau \quad (\text{A.6})$$

where ω_p and ω_s denote natural circular frequencies of the structure and equipment, respectively, whereas ξ_p and ξ_s denote damping coefficients of the structure and equipment, respectively.

The derivation of the equation for direct determination of floor response spectra was conducted separately for non-resonant ($\omega_p \neq \omega_s$) and resonant cases ($\omega_p = \omega_s$).

Non-resonant case ($\omega_p \neq \omega_s$)

In order to simplify the derivation of the equation for a non-resonant case, it was assumed that damping coefficients for the structure (ξ_p) and equipment (ξ_s) amounted to 0%. By using such an assumption and Equations A.4–A.6, Equations A.7–A.9 were obtained.

$$\ddot{u}_p(t) = \omega_p \int_0^t \ddot{u}_g(\tau) \sin \omega_p(t - \tau) d\tau \quad (\text{A.7})$$

$$\ddot{u}_s(t) = \omega_s \int_0^t \ddot{u}_p(\tau) \sin \omega_s(t - \tau) d\tau \quad (\text{A.8})$$

$$\ddot{u}_{sg}(t) = \omega_s \int_0^t \ddot{u}_g(\tau) \sin \omega_s(t - \tau) d\tau \quad (\text{A.9})$$

Throughout the derivation process, integration by parts was frequently used, and it can be generally described by Equation A.10.

$$\int_a^b u dv = uv \Big|_a^b - \int_a^b v du \quad (\text{A.10})$$

By applying integration by parts on Equation A.8, the following relationships were obtained:

$$\begin{aligned} u = \ddot{u}_p(\tau) &\rightarrow & du &= \frac{d}{d\tau} \ddot{u}_p(\tau) d\tau \\ dv = \sin \omega_s(t - \tau) d\tau &\rightarrow & v &= \int_0^t \sin \omega_s(t - \tau) d\tau = \frac{\cos \omega_s(t - \tau)}{\omega_s} \end{aligned} \quad (\text{A.11})$$

$$\begin{aligned} \ddot{u}_s(t) &= \omega_s \left\{ \ddot{u}_p(\tau) \frac{\cos \omega_s(t - \tau)}{\omega_s} \Big|_{\tau=0}^{\tau=t} - \int_0^t \frac{\cos \omega_s(t - \tau)}{\omega_s} \frac{d}{d\tau} \ddot{u}_p(\tau) d\tau \right\} = \\ &= \left(\ddot{u}_p(t) - \underbrace{\ddot{u}_p(0) \cos \omega_s t}_0 \right) - \int_0^t \frac{d}{d\tau} \ddot{u}_p(\tau) \cos \omega_s(t - \tau) d\tau = \\ &= \ddot{u}_p(t) - \int_0^t \frac{d}{d\tau} \ddot{u}_p(\tau) \cos \omega_s(t - \tau) d\tau \end{aligned} \quad (\text{A.12})$$

The relationship defined by Equation A.13 was used throughout the derivation process.

$$\frac{d}{dt} \int_{\alpha(t)}^{\beta(t)} f(x, t) dx = \int_{\alpha(t)}^{\beta(t)} \frac{\partial}{\partial t} f(x, t) dx + f(\beta(t), t) \beta'(t) - f(\alpha(t), t) \alpha'(t) \quad (\text{A.13})$$

By using τ instead of x in Equation A.13, the following relationship was obtained:

$$\frac{d}{dt} \int_0^t f(\tau, t) d\tau = \int_0^t \frac{\partial}{\partial t} f(\tau, t) d\tau + f(\tau, t) \Big|_{\tau=t} \quad (\text{A.14})$$

which led to

$$\begin{aligned} \frac{d}{d\tau} \ddot{u}_p(\tau) &= \frac{d}{d\tau} \omega_p \int_0^\tau \underbrace{\ddot{u}_g(\zeta) \sin \omega_p(\tau - \zeta)}_{f(\zeta, \tau)} d\zeta = \\ &= \omega_p \left[\int_0^\tau \frac{\partial}{\partial \tau} \ddot{u}_g(\zeta) \sin \omega_p(\tau - \zeta) d\zeta + \underbrace{f(\tau, \tau)}_0 \right] = \\ &= \omega_p^2 \int_0^\tau \ddot{u}_g(\zeta) \cos \omega_p(\tau - \zeta) d\zeta \end{aligned} \quad (\text{A.15})$$

Equation A.12 was transformed into Equation A.16, which was subjected to integration by parts.

$$\ddot{u}_s(t) = \ddot{u}_p(t) - \int_0^t \underbrace{\omega_p^2 \int_0^\tau \ddot{u}_g(\zeta) \cos \omega_p(\tau - \zeta) d\zeta}_u \underbrace{\cos \omega_s(t - \tau)}_v d\tau \quad (\text{A.16})$$

$$\begin{aligned} du &= \left\{ \omega_p^2 \int_0^\tau -\ddot{u}_g(\zeta) \omega_p \sin \omega_p(\tau - \zeta) d\zeta + \omega_p^2 \underbrace{f(\tau, \tau)}_{\ddot{u}_g(\tau)} \right\} d\tau = \\ &= \left\{ -\omega_p^3 \int_0^\tau \ddot{u}_g(\zeta) \sin \omega_p(\tau - \zeta) d\zeta + \omega_p^2 \ddot{u}_g(\tau) \right\} d\tau, \quad v = -\frac{\sin \omega_s(t - \tau)}{\omega_s} \end{aligned} \quad (\text{A.17})$$

$$\ddot{u}_s(t) = \ddot{u}_p(t) + \underbrace{\frac{\sin \omega_s(t - \tau)}{\omega_s} \omega_p^2 \int_0^\tau \ddot{u}_g(\zeta) \cos \omega_p(\tau - \zeta) d\zeta}_{0} \Big|_{\tau=0}^{\tau=t} - \quad (\text{A.18})$$

$$- \int_0^t \frac{\sin \omega_s(t - \tau)}{\omega_s} \left(-\omega_p^3 \int_0^\tau \ddot{u}_g(\zeta) \sin \omega_p(\tau - \zeta) d\zeta + \omega_p^2 \ddot{u}_g(\tau) \right) d\tau$$

$$\ddot{u}_s(t) = \ddot{u}_p(t) + \frac{\omega_p^2}{\omega_s} \int_0^t \underbrace{\omega_p \int_0^\tau \ddot{u}_g(\zeta) \sin \omega_p(\tau - \zeta) d\zeta}_{\ddot{u}_p(\tau)} \sin \omega_s(t - \tau) d\tau - \quad (\text{A.19})$$

$$- \frac{\omega_p^2}{\omega_s} \int_0^t \ddot{u}_g(\tau) \sin \omega_s(t - \tau) d\tau$$

$$\ddot{u}_s(t) = \ddot{u}_p(t) + \left(\frac{\omega_p}{\omega_s} \right)^2 \underbrace{\omega_s \int_0^t \ddot{u}_p(\tau) \sin \omega_s(t - \tau) d\tau}_{\ddot{u}_s(t)} - \quad (\text{A.20})$$

$$- \left(\frac{\omega_p}{\omega_s} \right)^2 \underbrace{\omega_s \int_0^t \ddot{u}_g(\tau) \sin \omega_s(t - \tau) d\tau}_{\ddot{u}_{sg}(t)} = \ddot{u}_p(t) + \left(\frac{\omega_p}{\omega_s} \right)^2 \ddot{u}_s(t) - \left(\frac{\omega_p}{\omega_s} \right)^2 \ddot{u}_{sg}(t)$$

Finally, the absolute acceleration of the mass of the equipment was expressed by Equation A.21 as

$$\ddot{u}_s(t) = \frac{1}{\left(\frac{\omega_s}{\omega_p}\right)^2 - 1} \left\{ \left(\frac{\omega_s}{\omega_p}\right)^2 \ddot{u}_p(t) - \ddot{u}_{sg}(t) \right\} \quad (\text{A.21})$$

If elastic response acceleration spectra of $\ddot{u}_g(t)$, denoted as $S_e(\omega, \zeta)$, are used to describe maximum values of $\ddot{u}_p(t)$ and $\ddot{u}_{sg}(t)$ and the SRSS rule is used to combine these maximums, then the values of floor acceleration spectra (A_{se}) can be determined from Equation A.22 (ζ_p and ζ_s denote damping coefficients for the structure and equipment, respectively).

$$A_{se} = \frac{1}{\left|\left(\frac{\omega_s}{\omega_p}\right)^2 - 1\right|} \sqrt{\left\{ \left(\frac{\omega_s}{\omega_p}\right)^2 S_e(\omega_p, \zeta_p) \right\}^2 + S_e(\omega_s, \zeta_s)^2} \quad (\text{A.22})$$

Resonant case ($\omega_p = \omega_s$)

In the case of resonance ($\omega_p = \omega_s$), Equation A.22 diverges, so separate derivation is necessary. It was assumed that non-zero damping coefficients apply for the structure ($\zeta_p \neq 0$) and equipment ($\zeta_s \neq 0$).

The relationships defined by Equations A.23 and A.24 were used permanently throughout the derivation process, whereas the condition of equal natural circular frequencies of the structure and equipment ($\omega_p = \omega_s$) was used at the end of it.

$$\begin{aligned} & \int \exp\{-\xi_s \omega_s (t - \tau)\} \sin \omega_s (t - \tau) d\tau \approx \\ & \approx \frac{1}{\omega_s} \left\{ \xi_s \sin \omega_s (t - \tau) + \cos \omega_s (t - \tau) \right\} \exp\{-\xi_s \omega_s (t - \tau)\} \end{aligned} \quad (\text{A.23})$$

$$\begin{aligned} & \int \exp\{-\xi_s \omega_s (t - \tau)\} \cos \omega_s (t - \tau) d\tau \approx \\ & \approx \frac{1}{\omega_s} \left\{ -\sin \omega_s (t - \tau) + \xi_s \cos \omega_s (t - \tau) \right\} \exp\{-\xi_s \omega_s (t - \tau)\} \end{aligned} \quad (\text{A.24})$$

When integration by parts was applied on Equation A.5, the relationships defined by Equations A.25–A.31 were obtained:

$$\begin{aligned} du &= \frac{d}{d\tau} \ddot{u}_p(\tau) d\tau \\ v &= \int \exp\{-\xi_s \omega_s (t - \tau)\} \sin \omega_s (t - \tau) d\tau \approx \\ & \approx \frac{1}{\omega_s} \left\{ \xi_s \sin \omega_s (t - \tau) + \cos \omega_s (t - \tau) \right\} \exp\{-\xi_s \omega_s (t - \tau)\} \end{aligned} \quad (\text{A.25})$$

$$\begin{aligned} \ddot{u}_s(t) &= \omega_s \ddot{u}_p(\tau) \frac{1}{\omega_s} \left\{ \xi_s \sin \omega_s(t-\tau) + \cos \omega_s(t-\tau) \right\} \exp\{-\xi_s \omega_s(t-\tau)\} \Bigg|_{\tau=0}^{\tau=t} - \\ &- \omega_s \frac{\xi_s}{\omega_s} \int_0^t \frac{d}{d\tau} \ddot{u}_p(\tau) \exp\{-\xi_s \omega_s(t-\tau)\} \sin \omega_s(t-\tau) d\tau - \\ &- \omega_s \frac{1}{\omega_s} \int_0^t \frac{d}{d\tau} \ddot{u}_p(\tau) \exp\{-\xi_s \omega_s(t-\tau)\} \cos \omega_s(t-\tau) d\tau \end{aligned} \quad (\text{A.26})$$

$$\begin{aligned} \ddot{u}_s(t) &= \ddot{u}_p(t) - \xi_s \int_0^t \frac{d}{d\tau} \ddot{u}_p(\tau) \exp\{-\xi_s \omega_s(t-\tau)\} \sin \omega_s(t-\tau) d\tau - \\ &- \int_0^t \frac{d}{d\tau} \ddot{u}_p(\tau) \exp\{-\xi_s \omega_s(t-\tau)\} \cos \omega_s(t-\tau) d\tau \end{aligned} \quad (\text{A.27})$$

$$\begin{aligned} \frac{d}{d\tau} \ddot{u}_p(\tau) &= \frac{d}{d\tau} \omega_p \int_0^\tau \underbrace{\ddot{u}_g(\zeta) \exp\{-\xi_p \omega_p(\tau-\zeta)\} \sin \omega_p(\tau-\zeta)}_{f(\zeta, \tau)} d\zeta = \\ &= \omega_p \left[\int_0^\tau \frac{\partial}{\partial \tau} \ddot{u}_g(\zeta) \exp\{-\xi_p \omega_p(\tau-\zeta)\} \sin \omega_p(\tau-\zeta) d\zeta + \underbrace{f(\tau, \tau)}_0 \right] \end{aligned} \quad (\text{A.28})$$

$$\begin{aligned} \frac{d}{d\tau} \ddot{u}_p(\tau) &= \omega_p \int_0^\tau \ddot{u}_g(\zeta) (-\xi_p \omega_p) \exp\{-\xi_p \omega_p(\tau-\zeta)\} \sin \omega_p(\tau-\zeta) d\zeta + \\ &+ \omega_p \int_0^\tau \ddot{u}_g(\zeta) \omega_p \exp\{-\xi_p \omega_p(\tau-\zeta)\} \cos \omega_p(\tau-\zeta) d\zeta \end{aligned} \quad (\text{A.29})$$

$$\begin{aligned} \frac{d}{d\tau} \ddot{u}_p(\tau) &= \omega_p^2 \int_0^\tau \ddot{u}_g(\zeta) \exp\{-\xi_p \omega_p(\tau-\zeta)\} \cos \omega_p(\tau-\zeta) d\zeta - \\ &- \xi_p \omega_p^2 \int_0^\tau \ddot{u}_g(\zeta) \exp\{-\xi_p \omega_p(\tau-\zeta)\} \sin \omega_p(\tau-\zeta) d\zeta \end{aligned} \quad (\text{A.30})$$

$$\begin{aligned} \ddot{u}_s(t) &= \ddot{u}_p(t) - \xi_s \int_0^t \omega_p^2 \int_0^\tau \ddot{u}_g(\zeta) \exp\{-\xi_p \omega_p(\tau-\zeta)\} \cos \omega_p(\tau-\zeta) d\zeta \cdot \\ &\cdot \exp\{-\xi_s \omega_s(t-\tau)\} \sin \omega_s(t-\tau) d\tau + \\ &+ \xi_s \int_0^t \xi_p \omega_p^2 \int_0^\tau \ddot{u}_g(\zeta) \exp\{-\xi_p \omega_p(\tau-\zeta)\} \sin \omega_p(\tau-\zeta) d\zeta \cdot \\ &\cdot \exp\{-\xi_s \omega_s(t-\tau)\} \sin \omega_s(t-\tau) d\tau - \\ &- \int_0^t \omega_p^2 \int_0^\tau \ddot{u}_g(\zeta) \exp\{-\xi_p \omega_p(\tau-\zeta)\} \cos \omega_p(\tau-\zeta) d\zeta \cdot \\ &\cdot \exp\{-\xi_s \omega_s(t-\tau)\} \cos \omega_s(t-\tau) d\tau + \\ &+ \int_0^t \xi_p \omega_p^2 \int_0^\tau \ddot{u}_g(\zeta) \exp\{-\xi_p \omega_p(\tau-\zeta)\} \sin \omega_p(\tau-\zeta) d\zeta \cdot \\ &\cdot \exp\{-\xi_s \omega_s(t-\tau)\} \cos \omega_s(t-\tau) d\tau \end{aligned} \quad (\text{A.31})$$

Equation A.31 is quite complicated and its parts were analysed separately. It was rewritten as

$$\ddot{u}_s(t) = \ddot{u}_p(t) - \xi_s A + \xi_s B - C + D \quad (\text{A.32})$$

$$\begin{aligned}
A &= \int_0^t \omega_p^2 \int_0^\tau \ddot{u}_g(\zeta) \exp\{-\xi_p \omega_p (\tau - \zeta)\} \cos \omega_p (\tau - \zeta) d\zeta \cdot \\
&\cdot \exp\{-\xi_s \omega_s (t - \tau)\} \sin \omega_s (t - \tau) d\tau \\
B &= \int_0^t \xi_p \omega_p^2 \int_0^\tau \ddot{u}_g(\zeta) \exp\{-\xi_p \omega_p (\tau - \zeta)\} \sin \omega_p (\tau - \zeta) d\zeta \cdot \\
&\cdot \exp\{-\xi_s \omega_s (t - \tau)\} \sin \omega_s (t - \tau) d\tau \\
C &= \int_0^t \omega_p^2 \int_0^\tau \ddot{u}_g(\zeta) \exp\{-\xi_p \omega_p (\tau - \zeta)\} \cos \omega_p (\tau - \zeta) d\zeta \cdot \\
&\cdot \exp\{-\xi_s \omega_s (t - \tau)\} \cos \omega_s (t - \tau) d\tau \\
D &= \int_0^t \xi_p \omega_p^2 \int_0^\tau \ddot{u}_g(\zeta) \exp\{-\xi_p \omega_p (\tau - \zeta)\} \sin \omega_p (\tau - \zeta) d\zeta \cdot \\
&\cdot \exp\{-\xi_s \omega_s (t - \tau)\} \cos \omega_s (t - \tau) d\tau
\end{aligned} \tag{A.33}$$

It should be noted that $\xi_s B$ can be neglected in Equation A.32 since damping of the structure (ξ_p) exists in B , i.e. it is obvious that $\xi_s \xi_p$ is practically equal to zero. The following relationship was obtained:

$$\ddot{u}_s(t) = \ddot{u}_p(t) - \xi_s A - C + D \tag{A.34}$$

Integration by parts was first applied on the part A of Equation A.34 and the following relationships were obtained:

$$\begin{aligned}
dv &= \exp\{-\xi_s \omega_s (t - \tau)\} \sin \omega_s (t - \tau) d\tau \\
v &= \int \exp\{-\xi_s \omega_s (t - \tau)\} \sin \omega_s (t - \tau) d\tau \approx \\
&\approx \frac{1}{\omega_s} \{ \xi_s \sin \omega_s (t - \tau) + \cos \omega_s (t - \tau) \} \exp\{-\xi_s \omega_s (t - \tau)\}
\end{aligned} \tag{A.35}$$

$$\begin{aligned}
u &= \omega_p^2 \int_0^\tau \underbrace{\ddot{u}_g(\zeta) \exp\{-\xi_p \omega_p (\tau - \zeta)\} \cos \omega_p (\tau - \zeta) d\zeta}_{f(\zeta, \tau)} \\
du &= \omega_p^2 \left\{ \int_0^\tau \frac{\partial}{\partial \tau} \ddot{u}_g(\zeta) \exp\{-\xi_p \omega_p (\tau - \zeta)\} \cos \omega_p (\tau - \zeta) d\zeta + \underbrace{f(\tau, \tau)}_{\ddot{u}_g(\tau)} \right\} d\tau = \\
&= -\xi_p \omega_p^3 \int_0^\tau \ddot{u}_g(\zeta) \exp\{-\xi_p \omega_p (\tau - \zeta)\} \cos \omega_p (\tau - \zeta) d\zeta d\tau - \\
&- \omega_p^3 \int_0^\tau \ddot{u}_g(\zeta) \exp\{-\xi_p \omega_p (\tau - \zeta)\} \sin \omega_p (\tau - \zeta) d\zeta d\tau + \omega_p^2 \ddot{u}_g(\tau) d\tau
\end{aligned} \tag{A.36}$$

$$\begin{aligned}
uv \Big|_{\tau=0}^{\tau=t} &= \omega_p^2 \int_0^\tau \ddot{u}_g(\zeta) \exp\{-\xi_p \omega_p (\tau - \zeta)\} \cos \omega_p (\tau - \zeta) d\zeta \cdot \\
&\cdot \frac{1}{\omega_s} \{ \xi_s \sin \omega_s (t - \tau) + \cos \omega_s (t - \tau) \} \exp\{-\xi_s \omega_s (t - \tau)\} \Big|_{\tau=0}^{\tau=t} \begin{pmatrix} \tau = t \\ \zeta = \tau \end{pmatrix}
\end{aligned} \tag{A.37}$$

$$uv \Big|_{\tau=0}^{\tau=t} = \frac{\omega_p^2}{\omega_s} \int_0^t \underbrace{\ddot{u}_g(\tau) \exp\{-\xi_p \omega_p (t - \tau)\} \cos \omega_p (t - \tau) d\tau}_{=-\ddot{u}_p(t)} = -\frac{\omega_p^2}{\omega_s} \ddot{u}_p(t) \tag{A.38}$$

$$\begin{aligned}
 -\int_0^t v du &= \frac{\omega_p^2}{\omega_s} \int_0^t \underbrace{\omega_p \int_0^\tau \ddot{u}_g(\zeta) \exp\{-\xi_p \omega_p (\tau - \zeta)\} \sin \omega_p (\tau - \zeta) d\zeta}_{\ddot{u}_p(\tau)} \cdot \\
 &\cdot \exp\{-\xi_s \omega_s (t - \tau)\} \cos \omega_s (t - \tau) d\tau - \\
 &-\frac{\omega_p^2}{\omega_s} \int_0^t \ddot{u}_g(\tau) \exp\{-\xi_s \omega_s (t - \tau)\} \cos \omega_s (t - \tau) d\tau
 \end{aligned} \tag{A.39}$$

Note that all parts of Equation A.39 which were multiplied by damping coefficient of the structure and/or equipment were intentionally left out since A was multiplied by damping of the equipment (ξ_s) in Equation A.34, i.e. these parts are practically equal to zero in Equation A.34.

$$\begin{aligned}
 -\int_0^t v du &= \frac{\omega_p^2}{\omega_s} \int_0^t \ddot{u}_p(\tau) \exp\{-\xi_s \omega_s (t - \tau)\} \cos \omega_s (t - \tau) d\tau - \\
 &-\frac{\omega_p^2}{\omega_s} \int_0^t \ddot{u}_g(\tau) \exp\{-\xi_s \omega_s (t - \tau)\} \cos \omega_s (t - \tau) d\tau
 \end{aligned} \tag{A.40}$$

$$-\int_0^t v du = -\frac{\omega_p^2}{\omega_s} \dot{u}_s(t) + \frac{\omega_p^2}{\omega_s} \dot{u}_{sg}(t) \tag{A.41}$$

$$A = uv \Big|_{\tau=0}^{\tau=t} - \int_0^t v du = -\frac{\omega_p^2}{\omega_s} \dot{u}_p(t) - \frac{\omega_p^2}{\omega_s} \dot{u}_s(t) + \frac{\omega_p^2}{\omega_s} \dot{u}_{sg}(t) \tag{A.42}$$

The following relationship between velocity and acceleration was applied in Equation A.42:

$$\omega \dot{u}(t) \approx \ddot{u}(t) \tag{A.43}$$

$$A = -\frac{\omega_p}{\omega_s} \ddot{u}_p(t) - \left(\frac{\omega_p}{\omega_s}\right)^2 \ddot{u}_s(t) + \left(\frac{\omega_p}{\omega_s}\right)^2 \ddot{u}_{sg}(t) \tag{A.44}$$

Integration by parts was applied on the part C of Equation A.34 and the following was obtained:

$$\begin{aligned}
 dv &= \exp\{-\xi_s \omega_s (t - \tau)\} \cos \omega_s (t - \tau) d\tau \\
 v &= \int \exp\{-\xi_s \omega_s (t - \tau)\} \cos \omega_s (t - \tau) d\tau \approx \\
 &\approx \frac{1}{\omega_s} \{-\sin \omega_s (t - \tau) + \xi_s \cos \omega_s (t - \tau)\} \exp\{-\xi_s \omega_s (t - \tau)\}
 \end{aligned} \tag{A.45}$$

$$\begin{aligned}
 u &= \omega_p^2 \int_0^\tau \ddot{u}_g(\zeta) \exp\{-\xi_p \omega_p (\tau - \zeta)\} \cos \omega_p (\tau - \zeta) d\zeta \\
 du &= -\xi_p \omega_p^3 \int_0^\tau \ddot{u}_g(\zeta) \exp\{-\xi_p \omega_p (\tau - \zeta)\} \cos \omega_p (\tau - \zeta) d\zeta d\tau - \\
 &-\omega_p^3 \int_0^\tau \ddot{u}_g(\zeta) \exp\{-\xi_p \omega_p (\tau - \zeta)\} \sin \omega_p (\tau - \zeta) d\zeta d\tau + \omega_p^2 \ddot{u}_g(\tau) d\tau
 \end{aligned} \tag{A.46}$$

$$uv|_{\tau=0}^{\tau=t} = \omega_p^2 \int_0^{\tau} \ddot{u}_g(\zeta) \exp\{-\xi_p \omega_p(\tau - \zeta)\} \cos \omega_p(\tau - \zeta) d\zeta \cdot \frac{1}{\omega_s} \left\{ -\sin \omega_s(t - \tau) + \xi_s \cos \omega_s(t - \tau) \right\} \exp\{-\xi_s \omega_s(t - \tau)\} \Bigg|_{\tau=0}^{\tau=t} \begin{pmatrix} \tau = t \\ \zeta = \tau \end{pmatrix} \quad (\text{A.47})$$

$$uv|_{\tau=0}^{\tau=t} = -\xi_s \frac{\omega_p^2}{\omega_s} \dot{u}_p(t) = -\xi_s \frac{\omega_p}{\omega_s} \ddot{u}_p(t) \quad (\text{A.48})$$

$$\begin{aligned} -\int_0^t v du &= -\xi_p \frac{\omega_p^3}{\omega_s} \int_0^t \int_0^{\tau} \ddot{u}_g(\zeta) \exp\{-\xi_p \omega_p(\tau - \zeta)\} \cos \omega_p(\tau - \zeta) d\zeta \cdot \\ &\cdot \exp\{-\xi_s \omega_s(t - \tau)\} \sin \omega_s(t - \tau) d\tau - \\ &- \frac{\omega_p^2}{\omega_s} \int_0^t \underbrace{\omega_p \int_0^{\tau} \ddot{u}_g(\zeta) \exp\{-\xi_p \omega_p(\tau - \zeta)\} \sin \omega_p(\tau - \zeta) d\zeta}_{\ddot{u}_p(\tau)} \cdot \\ &\cdot \exp\{-\xi_s \omega_s(t - \tau)\} \sin \omega_s(t - \tau) d\tau + \\ &+ \left(\frac{\omega_p}{\omega_s} \right)^2 \underbrace{\omega_s \int_0^t \ddot{u}_g(\tau) \exp\{-\xi_s \omega_s(t - \tau)\} \sin \omega_s(t - \tau) d\tau}_{\ddot{u}_{sg}(t)} + \\ &+ \xi_s \frac{\omega_p^2}{\omega_s} \int_0^t \underbrace{\omega_p \int_0^{\tau} \ddot{u}_g(\zeta) \exp\{-\xi_p \omega_p(\tau - \zeta)\} \sin \omega_p(\tau - \zeta) d\zeta}_{\ddot{u}_p(\tau)} \cdot \\ &\cdot \exp\{-\xi_s \omega_s(t - \tau)\} \cos \omega_s(t - \tau) d\tau - \\ &- \xi_s \frac{\omega_p^2}{\omega_s} \int_0^t \underbrace{\ddot{u}_g(\tau) \exp\{-\xi_s \omega_s(t - \tau)\} \cos \omega_s(t - \tau) d\tau}_{-\ddot{u}_{sg}(t)} \end{aligned} \quad (\text{A.49})$$

Note that the part of Equation A.49 which was multiplied by damping coefficients of the structure and equipment was intentionally left out since it is practically equal to zero.

$$\begin{aligned} -\int_0^t v du &= -\xi_p \frac{\omega_p^3}{\omega_s} \int_0^t \int_0^{\tau} \ddot{u}_g(\zeta) \exp\{-\xi_p \omega_p(\tau - \zeta)\} \cos \omega_p(\tau - \zeta) d\zeta \cdot \\ &\cdot \exp\{-\xi_s \omega_s(t - \tau)\} \sin \omega_s(t - \tau) d\tau - \\ &- \left(\frac{\omega_p}{\omega_s} \right)^2 \underbrace{\omega_s \int_0^t \ddot{u}_p(\tau) \exp\{-\xi_s \omega_s(t - \tau)\} \sin \omega_s(t - \tau) d\tau}_{\ddot{u}_s(t)} \\ &+ \left(\frac{\omega_p}{\omega_s} \right)^2 \ddot{u}_{sg}(t) + \xi_s \frac{\omega_p^2}{\omega_s} \underbrace{\int_0^t \ddot{u}_p(\tau) \exp\{-\xi_s \omega_s(t - \tau)\} \cos \omega_s(t - \tau) d\tau}_{-\ddot{u}_s(t)} + \\ &+ \xi_s \frac{\omega_p^2}{\omega_s} \dot{u}_{sg}(t) \end{aligned} \quad (\text{A.50})$$

$$\begin{aligned}
 -\int_0^t v du &= -\xi_p \frac{\omega_p^3}{\omega_s} \int_0^t \int_0^\tau \ddot{u}_g(\zeta) \exp\{-\xi_p \omega_p (\tau - \zeta)\} \cos \omega_p (\tau - \zeta) d\zeta \cdot \\
 &\cdot \exp\{-\xi_s \omega_s (t - \tau)\} \sin \omega_s (t - \tau) d\tau - \left(\frac{\omega_p}{\omega_s}\right)^2 \ddot{u}_s(t) + \left(\frac{\omega_p}{\omega_s}\right)^2 \ddot{u}_{sg}(t) - \\
 &- \xi_s \left(\frac{\omega_p}{\omega_s}\right)^2 \ddot{u}_s(t) + \xi_s \left(\frac{\omega_p}{\omega_s}\right)^2 \ddot{u}_{sg}(t)
 \end{aligned} \tag{A.51}$$

Now the part *C* of Equation A.34 can be expressed as

$$\begin{aligned}
 C &= -\xi_s \frac{\omega_p}{\omega_s} \ddot{u}_p(t) - \xi_p \frac{\omega_p^3}{\omega_s} \int_0^t \int_0^\tau \ddot{u}_g(\zeta) \exp\{-\xi_p \omega_p (\tau - \zeta)\} \cos \omega_p (\tau - \zeta) d\zeta \cdot \\
 &\cdot \exp\{-\xi_s \omega_s (t - \tau)\} \sin \omega_s (t - \tau) d\tau - \left(\frac{\omega_p}{\omega_s}\right)^2 \ddot{u}_s(t) + \left(\frac{\omega_p}{\omega_s}\right)^2 \ddot{u}_{sg}(t) - \\
 &- \xi_s \left(\frac{\omega_p}{\omega_s}\right)^2 \ddot{u}_s(t) + \xi_s \left(\frac{\omega_p}{\omega_s}\right)^2 \ddot{u}_{sg}(t)
 \end{aligned} \tag{A.52}$$

Integration by parts was applied on the part *D* of Equation A.34 and the following relationships were obtained:

$$\begin{aligned}
 dv &= \exp\{-\xi_s \omega_s (t - \tau)\} \cos \omega_s (t - \tau) d\tau \\
 v &= \int \exp\{-\xi_s \omega_s (t - \tau)\} \cos \omega_s (t - \tau) d\tau \approx \\
 &\approx \frac{1}{\omega_s} \{-\sin \omega_s (t - \tau) + \xi_s \cos \omega_s (t - \tau)\} \exp\{-\xi_s \omega_s (t - \tau)\}
 \end{aligned} \tag{A.53}$$

$$\begin{aligned}
 u &= \xi_p \omega_p^2 \int_0^\tau \ddot{u}_g(\zeta) \exp\{-\xi_p \omega_p (\tau - \zeta)\} \sin \omega_p (\tau - \zeta) d\zeta \\
 du &= -\xi_p^2 \omega_p^3 \int_0^\tau \ddot{u}_g(\zeta) \exp\{-\xi_p \omega_p (\tau - \zeta)\} \sin \omega_p (\tau - \zeta) d\zeta d\tau + \\
 &+ \xi_p \omega_p^3 \int_0^\tau \ddot{u}_g(\zeta) \exp\{-\xi_p \omega_p (\tau - \zeta)\} \cos \omega_p (\tau - \zeta) d\zeta d\tau
 \end{aligned} \tag{A.54}$$

$$\begin{aligned}
 uv \Big|_{\tau=0}^{\tau=t} &= \xi_p \omega_p^2 \int_0^\tau \ddot{u}_g(\zeta) \exp\{-\xi_p \omega_p (\tau - \zeta)\} \sin \omega_p (\tau - \zeta) d\zeta \cdot \\
 &\cdot \frac{1}{\omega_s} \{-\sin \omega_s (t - \tau) + \xi_s \cos \omega_s (t - \tau)\} \exp\{-\xi_s \omega_s (t - \tau)\} \Big|_{\tau=0}^{\tau=t} \begin{pmatrix} \tau = t \\ \zeta = \tau \end{pmatrix} \\
 uv \Big|_{\tau=0}^{\tau=t} &\approx 0
 \end{aligned} \tag{A.55}$$

$$\begin{aligned}
 -\int_0^t v du &= \xi_p \frac{\omega_p^3}{\omega_s} \int_0^t \int_0^\tau \ddot{u}_g(\zeta) \exp\{-\xi_p \omega_p (\tau - \zeta)\} \cos \omega_p (\tau - \zeta) d\zeta \cdot \\
 &\cdot \exp\{-\xi_s \omega_s (t - \tau)\} \sin \omega_s (t - \tau) d\tau
 \end{aligned} \tag{A.56}$$

Note that the parts of Equation A.56 which were multiplied by two or more damping values were intentionally left out since these parts are practically equal to zero.

Finally, the part D of Equation A.34 can be expressed as

$$D = \xi_p \frac{\omega_p^3}{\omega_s} \int_0^t \int_0^\tau \ddot{u}_g(\zeta) \exp\{-\xi_p \omega_p (\tau - \zeta)\} \cos \omega_p (\tau - \zeta) d\zeta \cdot \exp\{-\xi_s \omega_s (t - \tau)\} \sin \omega_s (t - \tau) d\tau \quad (\text{A.57})$$

When A , C and D were inserted in Equation A.34, the following relationship was obtained:

$$\begin{aligned} \ddot{u}_s(t) = & \ddot{u}_p(t) + \xi_s \frac{\omega_p}{\omega_s} \ddot{u}_p(t) + \xi_s \left(\frac{\omega_p}{\omega_s}\right)^2 \ddot{u}_s(t) - \xi_s \left(\frac{\omega_p}{\omega_s}\right)^2 \ddot{u}_{sg}(t) + \\ & + \xi_s \frac{\omega_p}{\omega_s} \ddot{u}_p(t) + \xi_p \frac{\omega_p^3}{\omega_s} \int_0^t \int_0^\tau \ddot{u}_g(\zeta) \exp\{-\xi_p \omega_p (\tau - \zeta)\} \cos \omega_p (\tau - \zeta) d\zeta \cdot \\ & \cdot \exp\{-\xi_s \omega_s (t - \tau)\} \sin \omega_s (t - \tau) d\tau + \left(\frac{\omega_p}{\omega_s}\right)^2 \ddot{u}_s(t) - \left(\frac{\omega_p}{\omega_s}\right)^2 \ddot{u}_{sg}(t) + \end{aligned} \quad (\text{A.58})$$

$$\begin{aligned} & + \xi_s \left(\frac{\omega_p}{\omega_s}\right)^2 \ddot{u}_s(t) - \xi_s \left(\frac{\omega_p}{\omega_s}\right)^2 \ddot{u}_{sg}(t) + \\ & + \xi_p \frac{\omega_p^3}{\omega_s} \int_0^t \int_0^\tau \ddot{u}_g(\zeta) \exp\{-\xi_p \omega_p (\tau - \zeta)\} \cos \omega_p (\tau - \zeta) d\zeta \cdot \\ & \cdot \exp\{-\xi_s \omega_s (t - \tau)\} \sin \omega_s (t - \tau) d\tau \end{aligned}$$

$$\begin{aligned} \ddot{u}_s(t) = & \ddot{u}_p(t) \left\{ 1 + 2\xi_s \frac{\omega_p}{\omega_s} \right\} + \left(\frac{\omega_p}{\omega_s}\right)^2 \{1 + 2\xi_s\} \{ \ddot{u}_s(t) - \ddot{u}_{sg}(t) \} + \\ & + 2\xi_p \frac{\omega_p}{\omega_s} \int_0^t \omega_p^2 \int_0^\tau \ddot{u}_g(\zeta) \exp\{-\xi_p \omega_p (\tau - \zeta)\} \cos \omega_p (\tau - \zeta) d\zeta \cdot \end{aligned} \quad (\text{A.59})$$

$$\cdot \exp\{-\xi_s \omega_s (t - \tau)\} \sin \omega_s (t - \tau) d\tau$$

$$\ddot{u}_s(t) = \ddot{u}_p(t) \left\{ 1 + 2\xi_s \frac{\omega_p}{\omega_s} \right\} + \left(\frac{\omega_p}{\omega_s}\right)^2 \{1 + 2\xi_s\} \{ \ddot{u}_s(t) - \ddot{u}_{sg}(t) \} + 2\xi_p \frac{\omega_p}{\omega_s} A \quad (\text{A.60})$$

$$\begin{aligned} \ddot{u}_s(t) = & \ddot{u}_p(t) \left\{ 1 + 2\xi_s \frac{\omega_p}{\omega_s} \right\} + \left(\frac{\omega_p}{\omega_s}\right)^2 \{1 + 2\xi_s\} \{ \ddot{u}_s(t) - \ddot{u}_{sg}(t) \} - \\ & - 2\xi_p \left(\frac{\omega_p}{\omega_s}\right)^2 \ddot{u}_p(t) - 2\xi_p \left(\frac{\omega_p}{\omega_s}\right)^3 \ddot{u}_s(t) + 2\xi_p \left(\frac{\omega_p}{\omega_s}\right)^3 \ddot{u}_{sg}(t) \end{aligned} \quad (\text{A.61})$$

$$\begin{aligned} \ddot{u}_s(t) = & \ddot{u}_p(t) \left\{ 1 + 2\xi_s \frac{\omega_p}{\omega_s} - 2\xi_p \left(\frac{\omega_p}{\omega_s} \right)^2 \right\} + \\ & + \ddot{u}_s(t) \left(\frac{\omega_p}{\omega_s} \right)^2 \left\{ 1 + 2\xi_s - 2\xi_p \frac{\omega_p}{\omega_s} \right\} - \ddot{u}_{sg}(t) \left(\frac{\omega_p}{\omega_s} \right)^2 \left\{ 1 + 2\xi_s - 2\xi_p \frac{\omega_p}{\omega_s} \right\} \end{aligned} \quad (\text{A.62})$$

The condition of equal natural circular frequencies of the structure and equipment ($\omega_p = \omega_s$) was applied, so the following expression was obtained:

$$\ddot{u}_s(t) = \ddot{u}_p(t) \underbrace{\left\{ 1 + 2(\xi_s - \xi_p) \right\}}_{\approx 1} + \ddot{u}_s(t) \left\{ 1 + 2(\xi_s - \xi_p) \right\} - \ddot{u}_{sg}(t) \underbrace{\left\{ 1 + 2(\xi_s - \xi_p) \right\}}_{\approx 1} \quad (\text{A.63})$$

$$2(\xi_p - \xi_s) \ddot{u}_s(t) \approx \ddot{u}_p(t) - \ddot{u}_{sg}(t) \quad (\text{A.64})$$

Finally, the maximum absolute acceleration of the mass of the equipment can be expressed by Equation A.65.

$$2(\xi_p + \xi_s) \ddot{u}_s(t) \Big|_{\max} = \left\{ \ddot{u}_p(t) - \ddot{u}_{sg}(t) \right\} \Big|_{\max} \quad (\text{A.65})$$

Equation A.65 can be expressed in the same manner as Equation A.22, i.e. by using elastic response acceleration spectra of $\ddot{u}_g(t)$:

$$A_{se} = \frac{1}{2(\xi_p + \xi_s)} \sqrt{S_e(\omega_p, \xi_p)^2 + S_e(\omega_s, \xi_s)^2} \quad (\text{A.66})$$

In order to obtain an equation which can be used for the direct determination of floor acceleration spectra in the whole period range, Equations A.22 and A.66 were linked together as:

$$A_{se} = \frac{1}{\sqrt{\left\{ 1 - \left(\frac{\omega_s}{\omega_p} \right)^2 \right\}^2 + 4(\xi_p + \xi_s)^2 \left(\frac{\omega_s}{\omega_p} \right)^2}} \sqrt{\left\{ \left(\frac{\omega_s}{\omega_p} \right)^2 S_e(\omega_p, \xi_p) \right\}^2 + S_e(\omega_s, \xi_s)^2} \quad (\text{A.67})$$

If natural periods of the structure (T_p) and equipment (T_s) are used instead of the natural circular frequencies ω_p and ω_s , Equation A.67 can be expressed as:

$$A_{se} = \frac{1}{\sqrt{\left\{ 1 - \left(\frac{T_p}{T_s} \right)^2 \right\}^2 + 4(\xi_p + \xi_s)^2 \left(\frac{T_p}{T_s} \right)^2}} \sqrt{\left\{ \left(\frac{T_p}{T_s} \right)^2 S_e(T_p, \xi_p) \right\}^2 + S_e(T_s, \xi_s)^2} \quad (\text{A.68})$$

which concludes the derivation process.

ANNEX B: APPLICATION OF THE REDUCTION FACTOR R_μ IN THE SEISMIC DESIGN OF EQUIPMENT

In the seismic design of primary structures, the application of inelastic pseudo-acceleration spectra is widely adopted. For the design purposes, inelastic pseudo-acceleration spectra are obtained by reducing elastic pseudo-acceleration spectra with the reduction factor R_μ , which represents the ratio of elastic and inelastic strength demand (Vidic et al. 1994). Numerous researchers have investigated the relationship between elastic and inelastic acceleration spectra and proposed various definitions of the reduction factor R_μ , which is also often called strength reduction factor, since it represents the ratio of elastic and inelastic strength demands. A list of the most important propositions made by different authors was provided by Miranda and Bertero (1994).

In the methods for direct generation of floor response spectra proposed in the dissertation, R_μ proposed by Vidic et al. (1994) is used. This R_μ was defined on a basis of pseudo-acceleration spectra. One of the most common assumptions in earthquake engineering is that the pseudo-acceleration is practically equal to the absolute acceleration. It will be shown that, generally, this assumption is valid only in the case of linear elastic primary structures, while in the case of inelastic structures, significant differences occur, especially in the case of structures with higher ductility demand.

First, the accuracy of the reduction factor R_μ proposed by Vidic et al. (1994) was investigated. Analyses were conducted for two different sets of ground motions (described in Section 2.1). "Mass-proportional" damping of the SDOF structure amounted to 5%. The constant target ductility factor μ was assumed throughout the whole period range and it amounted to 1.0 (linear elastic structure), 1.5, 2.0 and 4.0. The EP and Q₁₀ hysteretic models were taken into account. Mean values of elastic and inelastic pseudo-acceleration spectra for each set of ground motions were calculated by using the aforementioned hysteretic models and target ductility factors. Reduction factors R_μ were calculated as the ratio of elastic and inelastic pseudo-acceleration spectra and the results are presented in Figure B.1.

It can be observed from Figure B.1 that the R_μ proposed by Vidic et al. (1994) is in good agreement with the "exact" reduction factor for both sets of ground motions, both hysteretic models and all target ductility factors μ , and therefore, this study confirms its accuracy.

Second, mean values of elastic and inelastic absolute acceleration spectra were calculated by using all of the aforementioned input data. The "exact" reduction factor R_μ was calculated as the ratio of elastic and inelastic absolute acceleration spectra and again compared with the R_μ proposed by Vidic et al. (1994). The results are presented in Figure B.2.

It is obvious from Figure B.2 that the "exact" reduction factors R_μ are in good agreement with R_μ proposed by Vidic et al. (1994), for both sets of ground records and both hysteretic models, but only in cases of low target ductility factors μ . It can also be observed from Figures B.1 and B.2 that the "exact" reduction factors R_μ obtained from the absolute acceleration spectra are in all cases smaller than those obtained from the pseudo-acceleration spectra. This means that the values of absolute acceleration spectra are larger than the values of pseudo-acceleration spectra. The conducted analyses indicated that the differences between spectral values increase with an increase in the ductility demand of the structure, whereas in the case of a linear elastic structure these differences practically do not exist. In order to identify the causes that lead to differences between inelastic absolute and pseudo-acceleration spectra, additional analyses were conducted, whereby some of the structural properties were modified.

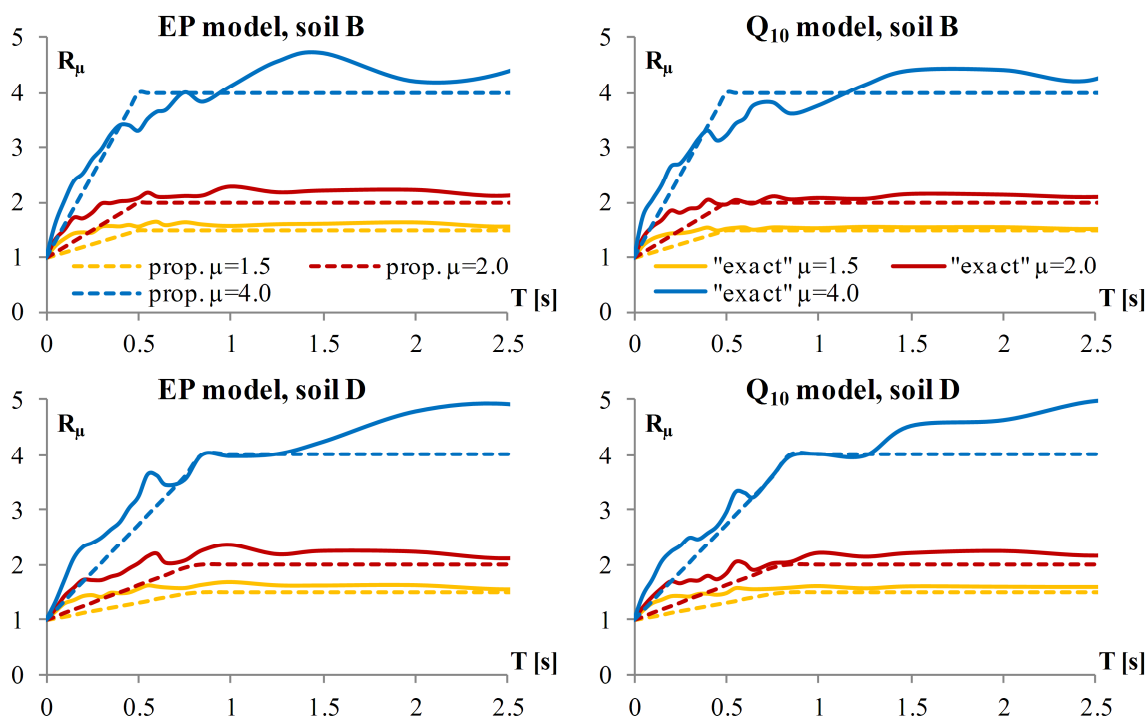


Figure B.1: Proposed simplified and "exact" reduction factors R_μ calculated from pseudo-acceleration spectra (5% damping of the structure)

Slika B.1: Predlagani približni in »točni« redukcijski faktorji R_μ izračunani iz spektrov pseudo-pospeškov (5% dušenja konstrukcije)

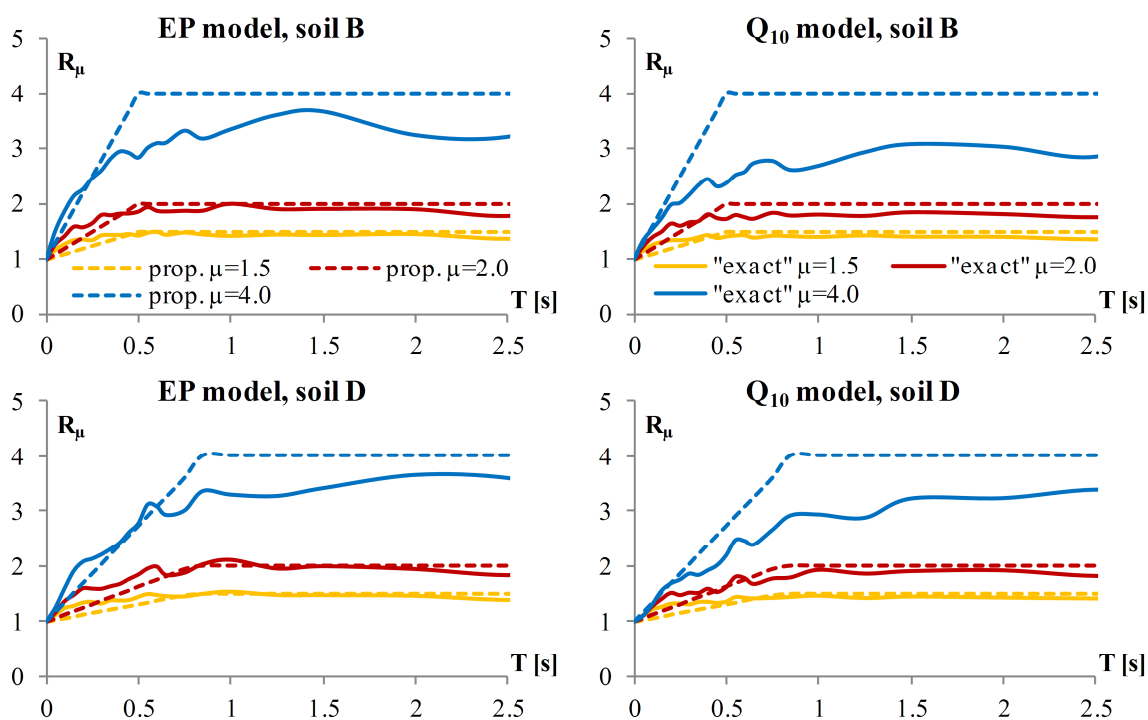


Figure B.2: Proposed simplified and "exact" reduction factors R_μ calculated from absolute acceleration spectra (5% damping of the structure)

Slika B.2: Predlagani približni in »točni« redukcijski faktorji R_μ izračunani iz spektrov absolutnih pospeškov (5% dušenja konstrukcije)

The first structural property that was modified was the damping of the structure, and it was taken to be equal to 0%. It is well-known that damping forces tend to produce unrealistic results in the case of inelastic structures, especially in those with high ductility demand. By using several ground motions as input, structures with different natural periods and different ductility demands were analysed and absolute and pseudo-accelerations were calculated. The results of the analyses showed that the differences between absolute and pseudo-accelerations did no longer exist in the case of the EP model, whereas in the case of the Q_{10} model that was not the case. By keeping the zero damping of the structure, the Q hysteretic model was modified so that the hardening was not taken into account (Q_0 model). Analyses were conducted again and the obtained results showed that the differences between absolute and pseudo-accelerations vanished. Therefore, the following can be concluded:

- 1) In the case of inelastic structures, absolute and pseudo-accelerations cannot be treated as equal.
- 2) An increase in the ductility demand increases the differences between absolute and pseudo-accelerations.
- 3) The above mentioned differences are caused by damping forces and by the hysteretic behaviour of the structure (hardening turned out to be an important cause).

Up to this point a "mass-proportional" damping model was used in all cases. In order to investigate the influence of damping forces, two additional damping models were used: damping proportional to secant stiffness and damping proportional to current stiffness. Due to simplicity, only the EP model of the structure was analysed. Structural response was analysed in terms of inertial, damping and resisting forces. In structures, inertial forces are associated with absolute accelerations, while resisting forces are associated with pseudo-accelerations. Damping force represents the difference between inertial and resisting forces. This difference is especially obvious when inelastic structural behaviour occurs. Again, several ground motions were applied as input and structures with different natural periods and different ductility demands were analysed.

The influence of damping forces was most significant in the case of the "mass-proportional" damping model, i.e. the differences between inertial and resisting forces were the largest. Damping proportional to secant stiffness gave somewhat smaller influence of damping forces, i.e. smaller differences between inertial and resisting forces. In the case when damping was proportional to current stiffness, inertial and resisting forces were almost equal, which means that damping forces practically did not influence the response in the inelastic region.

Since resisting forces in structures are associated with pseudo-accelerations, it is fully justified to use pseudo-acceleration spectra and corresponding R_{μ} factors for seismic design of both elastic and inelastic primary structures. On the other hand, equipment is exposed to absolute accelerations of the primary structure. The results presented above clearly show that in the case of inelastic primary structures, absolute and pseudo-accelerations cannot be treated as equal. Differences between them increase with an increase in the ductility demand. This implies that the application of an inelastic spectrum obtained by reducing the elastic acceleration spectrum by a reduction factor R_{μ} may sometimes produce slightly non-conservative results in the seismic design of equipment. The main reason for this is the fact that the reduction factors R_{μ} provided in the literature are based on pseudo-accelerations. Unfortunately, as far as the author of this dissertation knows, there are no proposals for the calculation of inelastic absolute acceleration spectra, nor there are any discussions regarding the relationship between inelastic absolute and pseudo-accelerations.

ANNEX C: EVALUATION OF THE EQUATION FOR DETERMINATION OF THE EFFECTIVE NATURAL PERIOD OF THE STRUCTURE PROPOSED BY AKIYAMA (1985)

In the case of inelastic SDOF structures whose behaviour is represented by stiffness degrading (Q) models, natural periods are longer in comparison to the corresponding elastic systems. Therefore, the effective natural period ($T_{p,\mu}$) should replace the "elastic" natural period (T_p) in analysis.

A simple proposal for approximate determination of the effective natural period ($T_{p,\mu}$) was made by Akiyama (1985). $T_{p,\mu}$ can be expressed by Equation C.1, which was obtained with a slight change of the form of the equation originally proposed by Akiyama (1985). Note that μ denotes ductility factor in Equation C.1.

$$T_{p,\mu} = T_p \sqrt{\frac{1 + \sqrt{\mu} + \mu}{3}} \quad (\text{C.1})$$

The accuracy of Equation C.1 was investigated by using some of the results obtained in the parametric study of floor response spectra conducted on SDOF primary structures (Chapter 2). Namely, the values of $T_{p,\mu}$ obtained from Equation C.1 were compared with the "accurate" $T_{p,\mu}$ determined from the position of floor response spectra peaks obtained in the parametric study. The selected results shown herein were obtained for set of ground records which corresponds to soil type B (see Section 2.1), for structures with natural periods equal to 0.2, 0.3, 0.5, 0.75, 1.0 and 2.0 s. The Q model with 10% hardening (Q_{10}) was taken into account, and three different values of μ were considered (1.5, 2.0 and 4.0). The damping of the structure amounted to 5%, whereas the damping of the equipment (ζ_s) amounted to 1% and 5%.

The errors of the approximate $T_{p,\mu}$ obtained from Equation C.1 are shown in Tables C.1 and C.2, for the damping of the equipment equal to 1% and 5% respectively. A negative error indicates that the approximate $T_{p,\mu}$ is smaller than the corresponding "accurate" $T_{p,\mu}$ obtained in the parametric study.

Table C.1: The errors of the approximate $T_{p,\mu}$ in comparison to the "accurate" $T_{p,\mu}$, 1% damping of the equipment

Preglednica C.1: Napake približnih $T_{p,\mu}$ v primerjavi s »točnimi« $T_{p,\mu}$, 1% dušenja opreme

Errors [%]	$T_p=0.2$ s	$T_p=0.3$ s	$T_p=0.5$ s	$T_p=0.75$ s	$T_p=1.0$ s	$T_p=2.0$ s
$\mu=1.5$	7	-3	6	5	1	11
$\mu=2.0$	5	-2	5	7	4	22
$\mu=4.0$	-2	9	-1	1	18	0

Table C.2: The errors of the approximate $T_{p,\mu}$ in comparison to the "accurate" $T_{p,\mu}$, 5% damping of the equipment

Preglednica C.2: Napake približnih $T_{p,\mu}$ v primerjavi s »točnimi« $T_{p,\mu}$, 5% dušenja opreme

Errors [%]	$T_p=0.2$ s	$T_p=0.3$ s	$T_p=0.5$ s	$T_p=0.75$ s	$T_p=1.0$ s	$T_p=2.0$ s
$\mu=1.5$	10	2	3	5	4	13
$\mu=2.0$	4	-3	9	12	5	25
$\mu=4.0$	0	17	9	5	7	3

It can be concluded from Tables C.1 and C.2 that Equation C.1 generally provides a good estimate of the effective natural period $T_{p,\mu}$. Larger deviations can be observed in the case of the structure whose natural period amounts to 2.0 s.

ANNEX D: OVERVIEW OF THE N2 METHOD

This annex presents an overview of the nonlinear pushover-based N2 method, which was developed at the University of Ljubljana by Prof. Fajfar and his associates (for method details see Fajfar 2000). Being relatively simple, it represents a powerful tool for the performance based design. It has been widely accepted in practice and it was also integrated in Eurocode 8 (2004). Nevertheless, like all approximate methods, the N2 method has several limitations. It is applicable in the case of structures for which the influence of higher modes is small. Approximate inelastic spectra are used in the method, but there is no limitation on the type of inelastic spectra which should be applied. The assumption of time-independent deformed shape in the pushover analysis represents an important approximation, which may produce certain problems in the case of structures where higher mode effects are significant. The problem of higher mode effects can be overcome by using the extended N2 method proposed by Kreslin and Fajfar (2012). The method takes into account higher mode effects both in plan and in elevation, and it is based on the assumption of elastic structural behaviour in the case of higher modes, i.e. the contribution of higher modes can be determined by using the elastic modal analysis. The main steps of the standard N2 method used in the dissertation are presented below. An approach for the determination of floor accelerations from the obtained floor displacements is also proposed.

A mathematical model of the structure should be established. It should be represented with a planar MDOF system used in standard elastic analysis, and complemented with the nonlinear force-deformation relationships for structural elements, which are most commonly beam-column elements with plastic hinges at both ends (concentrated plasticity approach). Seismic input should be defined and it is represented through the elastic pseudo-acceleration spectrum S_e , through which the structural damping is taken into account. Performing a pushover analysis represents the next step in the application of the method. It is common to assume the "first mode" height-wise distribution of lateral loads. For this purpose, the vector of the first mode from the elastic modal analysis (ϕ_1) should be normalized so that its component in the top storey amounts to 1.0. Lateral loads should be determined as the product of the first mode shape component in a considered storey and the storey mass as

$$\mathbf{P} = \mathbf{M}\phi_1 \quad (\text{D.1})$$

where \mathbf{P} denotes the vector of lateral loads and \mathbf{M} denotes a mass matrix. After the pushover analysis is performed, a relationship between the base shear (F) and the top displacement (d) is determined.

Effective mass m^* and transformation factor Γ can be determined from Equations D.2 (\mathbf{I} denotes unity vector).

$$m^* = \phi_1^T \mathbf{M} \mathbf{I}, \quad \Gamma = \frac{m^*}{\phi_1^T \mathbf{M} \phi_1} \quad (\text{D.2})$$

In order to obtain the quantities of an equivalent SDOF system, the quantities obtained for MDOF system should be divided with the transformation factor Γ . Therefore, the base shear force and the displacement of the equivalent SDOF system (F^* and d^*) are obtained from Equations D.3.

$$F^* = \frac{F}{\Gamma}, \quad d^* = \frac{d}{\Gamma} \quad (\text{D.3})$$

The obtained F^*-d^* relationship should be idealized as elasto-perfectly plastic (see Figure D.1 taken from Eurocode 8 2004). The yield force, which represents the ultimate strength of the idealized system, is denoted as F_y^* , whereas the corresponding yield displacement is denoted as d_y^* . Both quantities should be determined so that the areas under the actual and idealized force–deformation curves are equal.

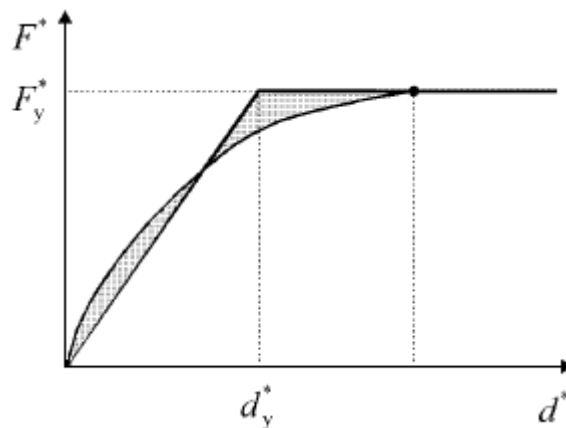


Figure D.1: The determination of the idealized force–displacement relationship

Slika D.1: Določitev idealizirane zveze sila–pomik

The effective natural period of the equivalent SDOF system can be determined from Equation D.4.

$$T^* = 2\pi \sqrt{\frac{m^* d_y^*}{F_y^*}} \quad (\text{D.4})$$

If the idealized force F^* is divided with the effective mass m^* , the acceleration S_a is obtained. The plot of S_a versus the idealized displacement d^* represents a capacity diagram, in which the acceleration S_{ay} is the one that corresponds to the yield force F_y^* . The determination of the reduction factor R_μ represents the next step which can be conducted by using Equation D.5.

$$R_\mu = \frac{S_e(T^*)}{S_{ay}} \quad (\text{D.5})$$

In the case when the effective period T^* is larger than the characteristic period of the ground motion T_C , equal displacement rule can be applied (inelastic displacement demand is equal to elastic demand). By contrast, when $T^* < T_C$, equal displacement rule is not applicable. The displacement demand can be determined according to Equations D.6 (S_{de} is a value in the elastic displacement spectrum).

$$d_t^* = \frac{S_{de}(T^*)}{R_\mu} \left(1 + (R_\mu - 1) \frac{T_C}{T^*} \right) = \frac{\left(\frac{T^*}{2\pi} \right)^2 S_e(T^*)}{R_\mu} \left(1 + (R_\mu - 1) \frac{T_C}{T^*} \right), \quad T^* < T_C \quad (\text{D.6})$$

$$d_t^* = S_{de}(T^*) = \left(\frac{T^*}{2\pi} \right)^2 S_e(T^*), \quad T^* \geq T_C$$

The corresponding ductility demand μ can be obtained from Equations D.7.

$$\begin{aligned} \mu &= 1 + (R_\mu - 1) \frac{T_C}{T^*}, & T^* < T_C \\ \mu &= R_\mu, & T^* \geq T_C \end{aligned} \quad (\text{D.7})$$

The target displacement in the top storey of the MDOF system (d_t) can be determined from Equation D.8 and pushover analysis should be performed up to it.

$$d_t = \Gamma d_t^* \quad (\text{D.8})$$

Storey displacements d_j (j denotes a storey) are determined once the pushover analysis is conducted and the floor accelerations a_j can be determined from Equation D.9.

$$a_j = \left(\frac{2\pi}{T^*} \right)^2 \frac{d_j}{\mu} \quad (\text{D.9})$$

Equation D.9 is based on Equations D.10 and D.11 (a denotes absolute acceleration and d denotes displacement), which are valid for SDOF systems represented with a bilinear force–displacement relationship (see Equations 2 and 3 in Fajfar 2000).

$$a = \frac{S_e(T^*)}{R_\mu} \quad (\text{D.10})$$

$$d = \frac{\mu}{R_\mu} \left(\frac{T^*}{2\pi} \right)^2 S_e(T^*) = \mu \left(\frac{T^*}{2\pi} \right)^2 a \quad (\text{D.11})$$

Storey accelerations can also be determined by using the inelastic first mode shape vector ϕ_i^{inel} . The component of the vector at each storey is obtained as the ratio of floor and roof displacements, obtained from the pushover analysis conducted up to the target displacement d_t . The acceleration in the floor j can be determined from Equation D.12. Such an approach is used in the proposed procedure for the direct determination of peak floor accelerations and floor response spectra in inelastic MDOF structures.

$$a_j = \Gamma \phi_{i,j}^{inel} \frac{S_e(T^*)}{R_\mu} \quad (\text{D.12})$$

ANNEX E: FORMULA FOR DIRECT GENERATION OF FLOOR RESPONSE SPECTRA OUTSIDE THE RESONANCE REGION FOR MDOF STRUCTURES

The derivation presented herein is similar to the one presented in ANNEX A. It was conducted under the assumption of the linear elastic behaviour of the MDOF primary structure and SDOF equipment. The interaction between the structure and equipment was neglected, i.e. uncoupled analysis was taken into account, and the Duhamel integral for the response determination was used (for equations see A.1–A.3 in ANNEX A).

The absolute acceleration of the mass of the primary structure for the mode i at the floor j exposed to $\ddot{u}_g(t)$ is denoted as $\ddot{u}_{p,ij}(t)$. The absolute acceleration of the mass of the equipment exposed to $\ddot{u}_{p,ij}(t)$ is denoted as $\ddot{u}_{s,ij}(t)$. Additionally, the absolute acceleration of the mass of the equipment exposed directly to $\ddot{u}_g(t)$ is denoted as $\ddot{u}_{sg}(t)$.

Analogous to the case of elastic SDOF primary structures considered in ANNEX A, $\ddot{u}_{p,ij}(t)$, $\ddot{u}_{s,ij}(t)$ and $\ddot{u}_{sg}(t)$ can be expressed as

$$\ddot{u}_{p,ij}(t) = \Gamma_i \phi_{ij} \omega_{p,i} \int_0^t \ddot{u}_g(\tau) \exp\{-\zeta_{p,i} \omega_{p,i} (t-\tau)\} \sin \omega_{p,i} (t-\tau) d\tau \quad (\text{E.1})$$

$$\ddot{u}_{s,ij}(t) = \omega_s \int_0^t \ddot{u}_{p,ij}(\tau) \exp\{-\zeta_s \omega_s (t-\tau)\} \sin \omega_s (t-\tau) d\tau \quad (\text{E.2})$$

$$\ddot{u}_{sg}(t) = \omega_s \int_0^t \ddot{u}_g(\tau) \exp\{-\zeta_s \omega_s (t-\tau)\} \sin \omega_s (t-\tau) d\tau \quad (\text{E.3})$$

where $\omega_{p,i}$ and ω_s denote natural circular frequencies of the structure for the mode i and equipment, respectively, $\zeta_{p,i}$ and ζ_s denote the damping of the structure for the mode i and equipment, respectively, Γ_i is modal participation factor for the mode i , ϕ_{ij} is a value of eigenvector for the mode i at the floor j .

The derivation of the equation for the direct determination of floor response spectra was conducted for non-resonant cases ($\omega_{p,i} \neq \omega_s$), as shown below. Due to simplicity, zero damping was assumed for the structure and equipment, i.e. $\zeta_{p,i} = \zeta_s = 0\%$. By using this assumption and Equations E.1–E.3, Equations E.4–E.6 were obtained.

$$\ddot{u}_{p,ij}(t) = \Gamma_i \phi_{ij} \omega_{p,i} \int_0^t \ddot{u}_g(\tau) \sin \omega_{p,i} (t-\tau) d\tau \quad (\text{E.4})$$

$$\ddot{u}_{s,ij}(t) = \omega_s \int_0^t \ddot{u}_{p,ij}(\tau) \sin \omega_s (t-\tau) d\tau \quad (\text{E.5})$$

$$\ddot{u}_{sg}(t) = \omega_s \int_0^t \ddot{u}_g(\tau) \sin \omega_s (t-\tau) d\tau \quad (\text{E.6})$$

By applying integration by parts on Equation E.5, Equation E.7 was obtained.

$$\ddot{u}_{s,ij}(t) = \ddot{u}_{p,ij}(t) - \int_0^t \frac{d}{d\tau} \ddot{u}_{p,ij}(\tau) \cos \omega_s (t-\tau) d\tau \quad (\text{E.7})$$

By using the relationship defined by Equation A.13 in the same manner as in ANNEX A, Equation E.8 was obtained.

$$\frac{d}{d\tau} \ddot{u}_{p,ij}(\tau) = \Gamma_i \phi_{ij} \omega_{p,i}^2 \int_0^\tau \ddot{u}_g(\zeta) \cos \omega_{p,i}(\tau - \zeta) d\zeta \quad (\text{E.8})$$

Equation E.7 was transformed into Equation E.9, which was subjected to integration by parts.

$$\ddot{u}_{s,ij}(t) = \ddot{u}_{p,ij}(t) - \Gamma_i \phi_{ij} \int_0^t \underbrace{\omega_{p,i}^2 \int_0^\tau \ddot{u}_g(\zeta) \cos \omega_{p,i}(\tau - \zeta) d\zeta}_u \underbrace{\cos \omega_s(t - \tau)}_{dv} d\tau \quad (\text{E.9})$$

$$\begin{aligned} du &= \left\{ \omega_{p,i}^2 \int_0^\tau -\ddot{u}_g(\zeta) \omega_{p,i} \sin \omega_{p,i}(\tau - \zeta) d\zeta + \omega_{p,i}^2 \frac{f(\tau, \tau)}{\ddot{u}_g(\tau)} \right\} d\tau = \\ &= \left\{ -\omega_{p,i}^3 \int_0^\tau \ddot{u}_g(\zeta) \sin \omega_{p,i}(\tau - \zeta) d\zeta + \omega_{p,i}^2 \ddot{u}_g(\tau) \right\} d\tau, \quad v = -\frac{\sin \omega_s(t - \tau)}{\omega_s} \end{aligned} \quad (\text{E.10})$$

$$\ddot{u}_{s,ij}(t) = \ddot{u}_{p,ij}(t) + \Gamma_i \phi_{ij} \underbrace{\frac{\sin \omega_s(t - \tau)}{\omega_s} \omega_{p,i}^2 \int_0^\tau \ddot{u}_g(\zeta) \cos \omega_{p,i}(\tau - \zeta) d\zeta}_{\Big|_{\tau=0}^{\tau=t}} - \quad (\text{E.11})$$

$$- \Gamma_i \phi_{ij} \int_0^t \frac{\sin \omega_s(t - \tau)}{\omega_s} \left(-\omega_{p,i}^3 \int_0^\tau \ddot{u}_g(\zeta) \sin \omega_{p,i}(\tau - \zeta) d\zeta + \omega_{p,i}^2 \ddot{u}_g(\tau) \right) d\tau$$

$$\ddot{u}_{s,ij}(t) = \ddot{u}_{p,ij}(t) + \frac{\omega_{p,i}^2}{\omega_s} \int_0^t \underbrace{\Gamma_i \phi_{ij} \omega_{p,i} \int_0^\tau \ddot{u}_g(\zeta) \sin \omega_{p,i}(\tau - \zeta) d\zeta}_{\ddot{u}_{p,ij}(\tau)} \sin \omega_s(t - \tau) d\tau - \quad (\text{E.12})$$

$$- \Gamma_i \phi_{ij} \frac{\omega_{p,i}^2}{\omega_s} \int_0^t \ddot{u}_g(\tau) \sin \omega_s(t - \tau) d\tau$$

$$\ddot{u}_{s,ij}(t) = \ddot{u}_{p,ij}(t) + \left(\frac{\omega_{p,i}}{\omega_s} \right)^2 \underbrace{\omega_s \int_0^t \ddot{u}_{p,ij}(\tau) \sin \omega_s(t - \tau) d\tau}_{\ddot{u}_{s,ij}(t)} - \quad (\text{E.13})$$

$$- \Gamma_i \phi_{ij} \left(\frac{\omega_{p,i}}{\omega_s} \right)^2 \underbrace{\omega_s \int_0^t \ddot{u}_g(\tau) \sin \omega_s(t - \tau) d\tau}_{\ddot{u}_{sg}(t)} = \ddot{u}_{p,ij}(t) + \left(\frac{\omega_{p,i}}{\omega_s} \right)^2 \ddot{u}_{s,ij}(t) - \Gamma_i \phi_{ij} \left(\frac{\omega_{p,i}}{\omega_s} \right)^2 \ddot{u}_{sg}(t)$$

Finally, the absolute acceleration of the mass of the equipment can be expressed by Equation E.14.

$$\ddot{u}_{s,ij}(t) = \frac{1}{\left(\frac{\omega_s}{\omega_{p,i}} \right)^2 - 1} \left\{ \left(\frac{\omega_s}{\omega_{p,i}} \right)^2 \ddot{u}_{p,ij}(t) - \Gamma_i \phi_{ij} \ddot{u}_{sg}(t) \right\} \quad (\text{E.14})$$

It can be observed that Equation E.14 is analogous to Equation A.21 from ANNEX A. The only difference is the presence of the product $\Gamma_i \phi_{ij}$, which is visible in the case of the acceleration of the equipment, whereas in the case of the acceleration of the structure it is contained within the $\ddot{u}_{p,ij}(t)$ (see Equation E.1).

If elastic response acceleration spectra of $\ddot{u}_g(t)$, denoted as $S_e(\omega, \xi)$, are used to describe maximum values of $\ddot{u}_{p,ij}(t)$ and $\ddot{u}_{sg}(t)$, then the maximum accelerations of the structure and equipment for the mode i and the storey j can be determined as $\Gamma_i \phi_{ij} S_e(\omega_{p,i}, \xi_{p,i})$ and $\Gamma_i \phi_{ij} S_e(\omega_s, \xi_s)$, respectively.

If the SRSS rule is used to combine these maximums, floor acceleration spectrum values outside the resonance region for the mode i at the floor j ($A_{se,ij}$) can be determined by Equation E.15.

$$A_{se,ij} = \frac{\Gamma_i \phi_{ij}}{\left| \left(\frac{\omega_s}{\omega_{p,i}} \right)^2 - 1 \right|} \sqrt{\left\{ \left(\frac{\omega_s}{\omega_{p,i}} \right)^2 S_e(\omega_{p,i}, \xi_{p,i}) \right\}^2 + S_e(\omega_s, \xi_s)^2} \quad (\text{E.15})$$

It is obvious from Equation E.15 that the floor response spectra values for individual modes may be positive or negative, which depends on the sign of the product $\Gamma_i \phi_{ij}$. This may seem strange since by definition any spectrum should be positive. On the other hand, floor response spectra obtained for individual modes do not have any physical meaning, which justifies the negative sign.

Finally, in the case of inelastic MDOF primary structures, the direct determination of floor response spectra ($A_{s,ij}$) outside the resonance region can be conducted by using the same approach as in the case of inelastic SDOF primary structures, i.e. by using the R_μ factor (Equations E.16).

$$A_{s,ij} = \frac{\Gamma_i \phi_{ij}}{\left| \left(\frac{\omega_s}{\omega_{p,i}} \right)^2 - 1 \right|} \sqrt{\left\{ \left(\frac{\omega_s}{\omega_{p,i}} \right)^2 \frac{S_e(\omega_{p,i}, \xi_{p,i})}{R_\mu} \right\}^2 + S_e(\omega_s, \xi_s)^2} \quad (\text{E.16})$$

If natural periods of the structure ($T_{p,i}$) and equipment (T_s) are used rather than natural circular frequencies $\omega_{p,i}$ and ω_s , Equation E.16 can be expressed as

$$A_{s,ij} = \frac{\Gamma_i \phi_{ij}}{\left| \left(\frac{T_{p,i}}{T_s} \right)^2 - 1 \right|} \sqrt{\left\{ \left(\frac{T_{p,i}}{T_s} \right)^2 \frac{S_e(T_{p,i}, \xi_{p,i})}{R_\mu} \right\}^2 + S_e(T_s, \xi_s)^2} \quad (\text{E.17})$$

which concludes the derivation process.

ANNEX F: OVERVIEW OF MODAL COMBINATION RULES PROPOSED BY USNRC 1.92 (2006)

USNRC 1.92 (2006) proposes methods which are considered acceptable for combining modal responses and spatial components in seismic analysis of nuclear power plant structures, systems and components. All proposed methods were previously examined and evaluated in an extensive study which is presented in NUREG/CR-6645 (1999). Combination methods which are presented in this annex are Gupta's method, Lindley-Yow method and the Missing Mass method.

In the methods defined by Gupta and Lindley-Yow, modal responses are divided into rigid (in-phase) and periodic (out-of-phase) components. If R_i denotes the response in the mode i , then rigid (Rr_i) and periodic (Rp_i) components of the response are obtained from Equations F.1 and F.2 as

$$Rr_i = R_i \alpha_i \quad (\text{F.1})$$

$$Rp_i = R_i \sqrt{1 - \alpha_i^2} \quad (\text{F.2})$$

where α_i denotes the rigid response coefficient, which varies from 0 (for completely periodic modes) to 1 (for completely rigid modes). The definition of α_i is different in Gupta's and Lindley-Yow method, which will be discussed below.

All rigid components of modal responses (Rr_i) should be combined by using the algebraic summation rule (ALGSUM) in order to obtain a total rigid component (Equation F.3), whereas all periodic components of modal responses (Rp_i) should be combined by using the CQC rule (or the SRSS rule in cases when modes are sufficiently separated) in order to obtain a total periodic component (Equations F.4). Note that in both cases n denotes a number of considered modes in the combination of responses and that ε_{ij} denotes the modal correlation coefficient for modes i and j in the CQC combination rule.

$$Rr = \sum_{i=1}^n Rr_i \quad (\text{F.3})$$

$$Rp = \sqrt{\sum_{i=1}^n \sum_{j=1}^n \varepsilon_{ij} Rp_i Rp_j} \quad (\text{CQC}), \quad Rp = \sqrt{\sum_{i=1}^n Rp_i^2} \quad (\text{SRSS}) \quad (\text{F.4})$$

The total response (R) is obtained by combining the total rigid (Rr) and the total periodic component (Rp) by using the SRSS rule (Equation F.5).

$$R = \sqrt{Rr^2 + Rp^2} \quad (\text{F.5})$$

In nuclear power plants, which are stiff structures, a significant number of modes may have frequencies above the frequency at which the spectral acceleration returns to zero period acceleration (f_{ZPA}). In practice, it is commonly assumed that f_{ZPA} amounts to 33 Hz, i.e. it is considered that it is not likely that any earthquake will trigger a structure to respond in modes with the frequency above 33 Hz (see e.g. Aziz 2004). In such cases, provided that only modes with frequencies below f_{ZPA} are included in the analysis, the mass associated with modes with frequencies above f_{ZPA} is missing. By ignoring

this mass, it is likely that an underestimate of seismic demands will occur, so therefore it should be taken into account.

The Missing Mass method represents an approach which takes into account the contribution of the mass related to the modes which were not considered in the modal solution (i.e. the modes with frequencies above f_{ZPA}). In the Missing Mass method the influence of such modes is taken into account through an additional – substituting mode and the response of the system is calculated by performing a static analysis (the details of the Missing Mass method are presented below). The contribution of the missing mass represents the response which is completely rigid (in-phase) and, as such, it should be taken into account along with the rigid components of modal responses Rr_i (e.g. from Gupta's or Lindley-Yow method). This practically means that when modes with frequencies above f_{ZPA} are taken into account through the Missing Mass method, Equation F.6 should be used instead of Equation F.3, i.e. the total rigid (Rr) response is obtained as

$$Rr = \sum_{i=1}^n Rr_i + R_{mm} \quad (F.6)$$

where R_{mm} denotes the response obtained from the Missing Mass method.

Finally, the total response (R) is again obtained by using Equation F.5.

Method proposed by Lindley-Yow

In this method the rigid response coefficient α_i should be determined according to Equation F.7

$$\alpha_i = \frac{ZPA}{S_{ai}} \quad (F.7)$$

where ZPA is the zero period acceleration and S_{ai} is the spectral acceleration for the mode i .

As mentioned above, values of α_i vary between 0 and 1. From Equation F.7 it is obvious that $\alpha_i=1$ when $S_{ai}=ZPA$, whereas the minimum value of α_i is reached when the peak spectral acceleration occurs. For example, in the Eurocode 8 (2004) elastic acceleration spectrum, peak value occurs at the spectral period equal to T_B , which is the lower limit of the constant spectral acceleration branch. After the spectral period exceeds T_C , which is the upper limit of the constant spectral acceleration branch, α_i begins to increase and it would exceed 1 for $S_{ai}<ZPA$. According to USNRC 1.92 (2006), this limitation of Lindley-Yow method can be overcome by setting α_i to 0 for all modes with natural periods larger than T_C . Based on the conclusions made in this study, α_i should be set to 0 for all modes with natural periods larger than T_B , i.e. at the beginning of the constant spectral acceleration branch, which practically means that all modes with natural periods larger than T_B are completely periodic (out-of-phase). The choice of using T_B instead of T_C arises from the fact that Lindley-Yow method has the identical form as Gupta's method (described below) in which, according to USNRC 1.92 (2006), T_B is used.

Maybe there is a reason why USNRC 1.92 (2006) proposes different boundaries for Lindley-Yow and Gupta's method, but there is also a possibility that a slight inconsistency is present in the provisions.

In order to determine Lindley-Yow coefficients for modal combination, let us consider the elastic primary structures W03, W10, F03 and F10 described in Section 4.1, as well as the mean elastic spectrum of the chosen set of ground motions which corresponds to the soil type B (described in Sections 2.1 and 4.1). The ZPA of the applied elastic spectrum amounts to 0.43g. $T_{p,i}$ denotes the natural period of the structure for the mode i . The obtained results are presented in Tables F.1–F.4.

Table F.1: Lindley-Yow coefficients for modal combination in the case of the elastic structure W03

Preglednica F.1: Lindley-Yow koeficienti za modalno kombinacijo v primeru elastične konstrukcije W03

mode	$T_{p,i}$ [s]	S_{ai} [g]	α_i	$(1-\alpha_i^2)^{0.5}$
1	0.30	0.92	0	1
2	0.046	0.64	0.67	0.74
3	0.017	0.43	1	0

Table F.2: Lindley-Yow coefficients for modal combination in the case of the elastic structure W10

Preglednica F.2: Lindley-Yow koeficienti za modalno kombinacijo v primeru elastične konstrukcije W10

mode	$T_{p,i}$ [s]	S_{ai} [g]	α_i	$(1-\alpha_i^2)^{0.5}$
1	1.0	0.45	0	1
2	0.153	0.86	0	1
3	0.057	0.57	0.75	0.66

Table F.3: Lindley-Yow coefficients for modal combination in the case of the elastic structure F03

Preglednica F.3: Lindley-Yow koeficienti za modalno kombinacijo v primeru elastične konstrukcije F03

mode	$T_{p,i}$ [s]	S_{ai} [g]	α_i	$(1-\alpha_i^2)^{0.5}$
1	0.30	0.92	0	1
2	0.079	0.72	0.60	0.80
3	0.038	0.51	0.84	0.54

Table F.4: Lindley-Yow coefficients for modal combination in the case of the elastic structure F10

Preglednica F.4: Lindley-Yow koeficienti za modalno kombinacijo v primeru elastične konstrukcije F10

mode	$T_{p,i}$ [s]	S_{ai} [g]	α_i	$(1-\alpha_i^2)^{0.5}$
1	1.0	0.45	0	1
2	0.315	0.92	0	1
3	0.186	0.81	0.53	0.85

Method proposed by Gupta

In this method the rigid response coefficient α_i should be determined according to Equation F.8

$$\alpha_i = \begin{cases} 0, & f_i \leq f_1 \\ \frac{\ln(f_i / f_1)}{\ln(f_2 / f_1)}, & f_1 \leq f_i \leq f_2 \\ 1, & f_i \geq f_2 \end{cases} \quad (\text{F.8})$$

where f_i denotes a frequency of the mode i , whereas f_1 and f_2 are discussed below.

According to USNRC 1.92 (2006), in the case of single-peaked (unbroadened) spectra, the frequency f_I can be determined according to Equation F.9

$$f_I = \frac{S_{a\max}}{2\pi S_{v\max}} \quad (\text{F.9})$$

where $S_{a\max}$ and $S_{v\max}$ denote maximum values of spectral acceleration and velocity, respectively. If broadened spectra are used, according to USNRC 1.92 (2006), f_I can be taken equal to a frequency at which constant spectral acceleration branch begins. For example, in the case of the Eurocode 8 (2004) elastic acceleration spectrum, f_I should be equal to $1/T_B$.

USNRC 1.92 (2006) defines f_2 as the frequency equal to f_r , which is the lowest frequency at which the responses of SDOF oscillators become completely correlated with the input motion. Such a definition of f_2 is applicable to all types of response spectra. Nevertheless, it should be noted that the determination of f_2 is not straightforward and that results of Gupta's method are sensitive to the value of f_2 used. In order to determine the frequency f_2 , Equation F.10 can be used (NUREG/CR-6645 1999).

$$f_2 = \frac{f_I + 2f_{ZPA}}{3} \quad (\text{F.10})$$

It should be noted that Gupta's method is slightly superior to Lindley-Yow method, since it has no limitation regarding modes with natural periods larger than T_B .

In order to determine Gupta's coefficients for modal combination, the elastic structures W03, W10, F03 and F10 (described in Section 4.1) were considered. The mean elastic spectrum of the chosen set of ground motions which corresponds to the soil type B has multiple peaks (see Sections 2.1 and 4.1), which led to a question of choice of f_I . In order to simplify things, f_I was determined by taking into account the target Eurocode 8 (2004) elastic spectrum for the soil type B (described in Section 4.1). The value of T_B which corresponds to the target spectrum amounts to 0.15 s. Therefore, f_I amounted to $1/T_B=6.67$ Hz, whereas f_2 amounted to 24.22 Hz (from Equation F.10, by taking into account $f_{ZPA}=33$ Hz). The obtained results are presented in Tables F.5–F.8. Note that the values presented in Tables F.5–F.8 are also applicable in the case of inelastic structures when the EP model is used.

Table F.5: Gupta's coefficients for modal combination in the case of the elastic and EP structure W03

Preglednica F.5: Gupta's koeficienti za modalno kombinacijo v primeru elastične in EP konstrukcije W03

mode	$T_{p,i}$ [s]	f_i [Hz]	α_i	$(1-\alpha_i^2)^{0.5}$
1	0.30	3.33	0	1
2	0.046	21.74	0.92	0.39
3	0.017	58.82	1	0

Table F.6: Gupta's coefficients for modal combination in the case of the elastic and EP structure W10

Preglednica F.6: Gupta's koeficienti za modalno kombinacijo v primeru elastične in EP konstrukcije W10

mode	$T_{p,i}$ [s]	f_i [Hz]	α_i	$(1-\alpha_i^2)^{0.5}$
1	1.0	1.0	0	1
2	0.153	6.54	0	1
3	0.057	17.54	0.75	0.66

Table F.7: Gupta's coefficients for modal combination in the case of the elastic and EP structure F03

Preglednica F.7: Guptini koeficienti za modalno kombinacijo v primeru elastične in EP konstrukcije F03

mode	$T_{p,i}$ [s]	f_i [Hz]	α_i	$(1-\alpha_i^2)^{0.5}$
1	0.30	3.33	0	1
2	0.079	12.66	0.50	0.87
3	0.038	26.32	1	0

Table F.8: Gupta's coefficients for modal combination in the case of the elastic and EP structure F10

Preglednica F.8: Guptini koeficienti za modalno kombinacijo v primeru elastične in EP konstrukcije F10

mode	$T_{p,i}$ [s]	f_i [Hz]	α_i	$(1-\alpha_i^2)^{0.5}$
1	1.0	1.0	0	1
2	0.315	3.17	0	1
3	0.186	5.38	0	1

Gupta's coefficients were also determined for the Q_0 model (Tables F.9–F.12), since for the considered structures, the results of modal analyses conducted in SAP and OpenSees were different.

Table F.9: Gupta's coefficients for modal combination in the case of the Q_0 structure W03

Preglednica F.9: Guptini koeficienti za modalno kombinacijo v primeru Q_0 konstrukcije W03

mode	$T_{p,i}$ [s]	f_i [Hz]	α_i	$(1-\alpha_i^2)^{0.5}$
1	0.31	3.23	0	1
2	0.041	24.39	1	0
3	0.014	71.43	1	0

Table F.10: Gupta's coefficients for modal combination in the case of the Q_0 structure W10

Preglednica F.10: Guptini koeficienti za modalno kombinacijo v primeru Q_0 konstrukcije W10

mode	$T_{p,i}$ [s]	f_i [Hz]	α_i	$(1-\alpha_i^2)^{0.5}$
1	1.05	0.95	0	1
2	0.136	7.35	0.10	0.99
3	0.046	21.74	0.92	0.39

Table F.11: Gupta's coefficients for modal combination in the case of the Q_0 structure F03

Preglednica F.11: Guptini koeficienti za modalno kombinacijo v primeru Q_0 konstrukcije F03

mode	$T_{p,i}$ [s]	f_i [Hz]	α_i	$(1-\alpha_i^2)^{0.5}$
1	0.29	3.45	0	1
2	0.075	13.33	0.54	0.84
3	0.037	27.03	1	0

Table F.12: Gupta's coefficients for modal combination in the case of the Q_0 structure F10

Preglednica F.12: Guptini koeficienti za modalno kombinacijo v primeru Q_0 konstrukcije F10

mode	$T_{p,i}$ [s]	f_i [Hz]	α_i	$(1-\alpha_i^2)^{0.5}$
1	0.99	1.01	0	1
2	0.312	3.21	0	1
3	0.186	5.38	0	1

Note that in the case of the structure W03, the frequency of the third mode amounts to 58.82 Hz (elastic and EP models) and 71.43 Hz (Q₀ model), which is larger than $f_{ZPA}=33$ Hz. It is obvious from Tables F.1, F.5 and F.9 that both Lindley-Yow and Gupta's method can include the in-phase contribution of the third mode. However, according to NUREG/CR-6645 (1999), it is more practical to apply these methods only for modes with frequencies below f_{ZPA} , and to combine them with the Missing Mass method in order to take into account the contribution of modes with frequencies above f_{ZPA} . This is particularly meaningful in the case of structures with a great number of DOFs.

Missing Mass method

The contribution of the mass related to the modes which are omitted from the modal solution (modes with frequencies above f_{ZPA}) should not be neglected. In the Missing Mass method, the influence of such modes is taken into account through an additional – substituting mode and the response of the system is calculated by performing a static analysis. As discussed above, the response obtained from the Missing Mass method is completely in-phase with the time-varying seismic input. This fact, even though irrelevant in the response spectrum analysis where only peak response is obtained, implies that the zero period acceleration (ZPA) is used for the determination of the missing mass loading. Therefore, the vector of pseudo-static forces which should be applied to the structure (\mathbf{P}) can be determined from Equation F.11 as

$$\mathbf{P} = \mathbf{M} \left\{ \mathbf{U}_b - \sum_{i=1}^n \Gamma_i \boldsymbol{\phi}_i \right\} ZPA \quad (\text{F.11})$$

where \mathbf{M} denotes a mass matrix, \mathbf{U}_b denotes the influence vector (i.e. the displacement vector of the structure when the support undergoes a unit displacement in the direction of earthquake motion), n denotes the number of modes which were taken into account in the modal solution (i.e. modes with frequencies below f_{ZPA}), Γ_i represents modal participation factor for the mode i , whereas $\boldsymbol{\phi}_i$ represents the eigenvector of the mode i .

It should be noted that Equation F.11 was taken from ASCE 4-98 (2000) which also proposes the Missing Mass method.

Static analysis of the structure subjected to the forces determined from Equation F.11 (\mathbf{P}) will produce maximum responses associated with higher modes (R_{nm}), which should be combined with the quantities determined from the modal solution (see Equation F.6).

For the purpose of floor response spectra, the situation is somewhat different. Namely, the response which is important is the peak acceleration of equipment which is attached to the structure. Therefore, by taking into account a planar structure (for which all members of the vector \mathbf{U}_b are equal to 1), floor response spectra values associated with higher modes, i.e. with the missing mass, at the floor j ($A_{s,mmj}$) can be obtained from Equation F.12

$$A_{s,mmj} = \left\{ 1 - \sum_{i=1}^n \Gamma_i \phi_{ij} \right\} S_e(T_s, \zeta_s) \quad (\text{F.12})$$

where S_e is a value in the input elastic acceleration spectrum for the equipment with natural period T_s and damping coefficient ζ_s .

In ANNEX G it was shown that in the case of elastic structures, the relationship defined by Equation F.13 is valid (note that N denotes the total number of modes).

$$\sum_{i=1}^N \Gamma_i \phi_{ij} = 1 \quad (\text{F.13})$$

From Equations F.11–F.13 it is clear that all modes which were omitted from the modal solution (modes with frequencies above f_{ZPA}) are automatically taken into account in the Missing Mass method.

In order to conclude this annex, the main steps of the application of the above described USNRC 1.92 (2006) methods are summarized below.

- 1) Modal responses should be determined only for modes with frequencies below f_{ZPA} .
- 2) Lindley-Yow or Gupta's method should be applied to the responses determined in step (1).
- 3) The Missing Mass method should be applied in order to obtain the response related to the modes with frequencies above f_{ZPA} .
- 4) The total response should be determined by combining the results from steps (2) and (3).

ANNEX G: DERIVATION OF EQUATION G.1

The main objective of this annex is to present the derivation of Equation G.1.

$$\sum_{i=1}^N \Gamma_i \phi_i = \mathbf{I} \quad (\text{G.1})$$

In Equation G.1 N denotes the total number of modes, Γ_i represents modal participation factor for the mode i , ϕ_i is the vector of the mode i obtained from elastic modal analysis and \mathbf{I} denotes unity vector.

Modal participation factor can be expressed by Equation G.2 (notation taken from Chopra 2012)

$$\Gamma_i = \frac{L_i}{M_i}, \quad L_i = \phi_i^T \mathbf{M} \mathbf{I}, \quad M_i = \phi_i^T \mathbf{M} \phi_i \quad (\text{G.2})$$

where \mathbf{M} denotes a mass matrix.

Multiplying of Equation G.1 with $\mathbf{I}^T \mathbf{M}$ from the left leads to Equation G.3.

$$\sum_{i=1}^N \Gamma_i \underbrace{\mathbf{I}^T \mathbf{M} \phi_i}_{L_i} = \underbrace{\mathbf{I}^T \mathbf{M} \mathbf{I}}_{\text{total mass}} \quad (\text{G.3})$$

The product $\Gamma_i L_i$ represents the effective modal mass for the mode i (M_i^*), as presented by Equation G.4.

$$\Gamma_i L_i = \frac{L_i^2}{M_i} = M_i^* \quad (\text{G.4})$$

The sum of the effective modal masses for all modes is equal to the total mass of the structure, as shown by Equation G.5 (for derivation see Chopra 2012). Note that j denotes a floor, whereas m denotes a mass situated at the floor.

$$\sum_{i=1}^N M_i^* = \sum_{j=1}^N m_j = \text{total mass} \quad (\text{G.5})$$

Equations G.3 and G.5 confirm the accuracy of the relationship assumed by Equation G.1.

ANNEX H: A BRIEF ANALYSIS OF SCATTER RELATED TO THE SEISMIC INPUT AND FLOOR RESPONSE SPECTRA

All results in seismic analyses are uncertain. In this annex some quantitative information is provided about the dispersion of the results due to the randomness of ground motions.

The seismic input used in the dissertation consists of ground motions with quite different intensities (see Figure 2.1 in Section 2.1). In the case of SDOF and MDOF primary structures, a set of ground motions which corresponds to the soil type B was used in the study (for details see Section 2.1). Elastic acceleration spectra of individual records obtained for 5% damping are presented in Figure H.1a (gray lines), along with their mean (denoted as "mean"), mean plus standard deviation (denoted as "mean + σ "), mean minus standard deviation (denoted as "mean - σ "), median (denoted as "median"), 15th percentile (denoted as "15th percentile"), and 85th percentile (denoted as "85th percentile") values. In Figure H.1b, the coefficient of variation CV, which is defined as the ratio of standard deviation to the mean, is presented.

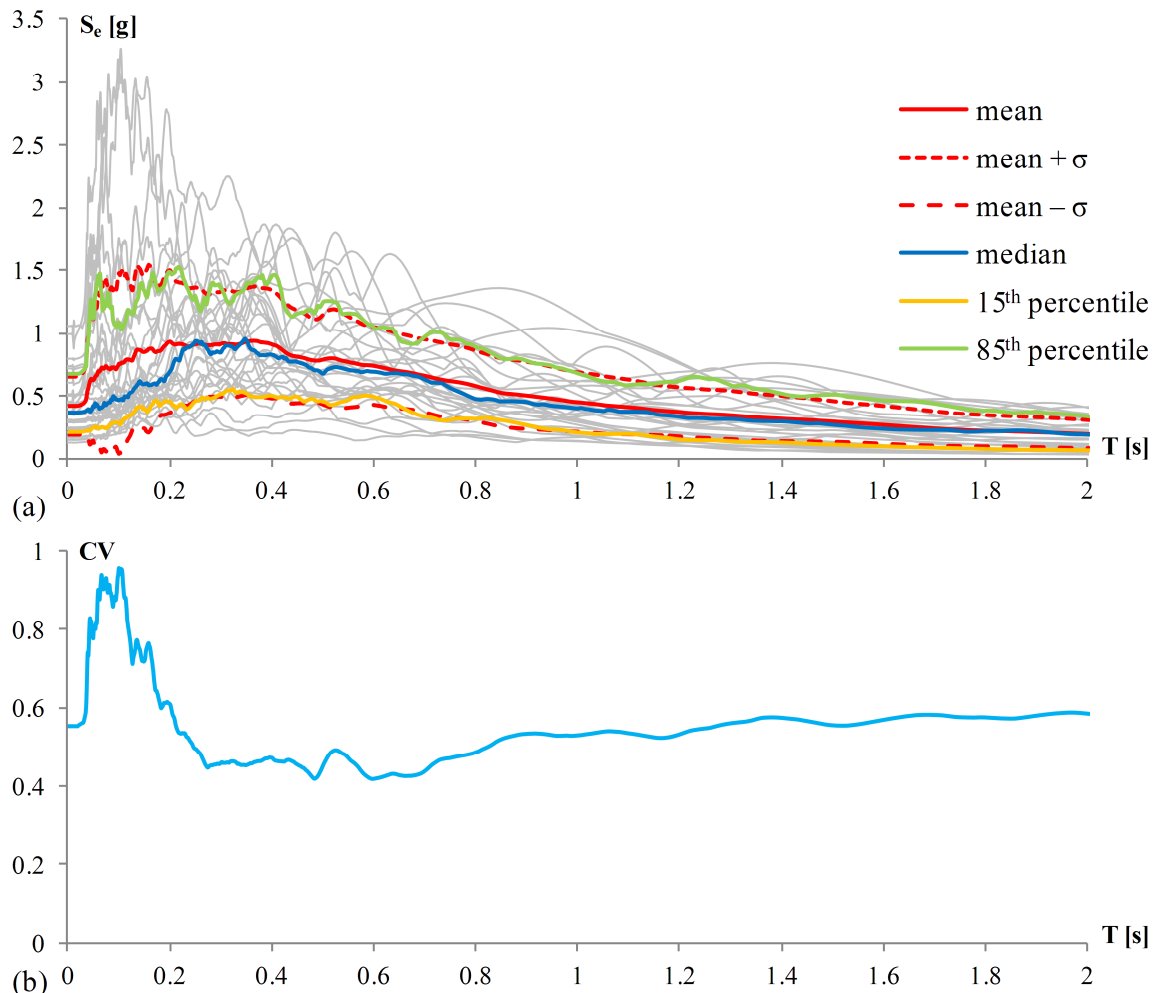


Figure H.1: (a) Elastic acceleration spectra (5% damping) of individual records for soil type B, mean values, mean plus standard deviation values and mean minus standard deviation values; (b) coefficient of variation (CV)

Slika H.1: (a) Elastični spektri pospeškov (5% dušenja) posameznih zapisov za tip tal B, povprečne vrednosti, povprečne vrednosti plus standardna devijacija in povprečne vrednosti minus standardna devijacija; (b) koeficient variacije (CV)

In Figure H.1, a significant scatter can be observed, especially in the range of very short periods. Roughly, the largest values of the CV are situated between $T=0.05$ s and $T=0.20$ s, i.e. in the period range where higher modes of the analysed stiff structures (W03 and F03) lie. The peak value of the CV almost reaches unity. It should also be noted that in the rest of the period range the CV amounts to approximately 0.5, which is a quite large value. In the very short period range, the mean spectral values are also notably larger than the median values, indicating that the distribution is not normal.

In Figures H.2 and H.3 several examples of floor response spectra in inelastic SDOF and MDOF structures are shown. The mean (denoted as "mean"), mean plus standard deviation (denoted as "mean + σ "), mean minus standard deviation (denoted as "mean - σ "), median (denoted as "median"), 15th percentile (denoted as "15th percentile"), and 85th percentile (denoted as "85th percentile") values of floor response spectra obtained from the response-history analyses, as well as the direct floor response spectra obtained from the proposed method (denoted as "direct"), are shown. Figure H.2 shows the results obtained for inelastic SDOF primary structures with natural periods (T_p) equal to 0.3 and 1.0 s (EP and Q_0 model were considered, with target ductility μ which amounted to 2). Figure H.3 shows the results obtained for the first storey of inelastic MDOF primary structures: wall W03 (EP model, $\mu=1.9$), wall W10 (Q_0 model, $\mu=2.1$), frame F03 (EP model, $\mu=2.0$) and frame F10 (Q_0 model, $\mu=2.2$). In all considered cases the damping of the equipment (ζ_s) amounted to 5%.

It is obvious from Figure H.2 that in the case of SDOF structures, there is a good agreement between the mean and median values of floor response spectra, even though the median values are slightly lower, which is most pronounced in the resonance region. The obtained results suggest almost normal (Gaussian) distribution. Also, a good agreement can be observed between the "mean - σ " and "15th percentile" values, as well as between the "mean + σ " and "85th percentile" values.

The results obtained for MDOF primary structures, presented in Figure H.3, suggest that the largest differences between the mean and median values of floor response spectra occur in the very short period range (i.e. between $T=0.05$ s and $T=0.20$ s). This indicates that the distribution is not normal (Gaussian). In the case of the structures W10 and F03, the peak values of floor response spectra related to the second and third mode are significantly lower in the case of the median than in the case of the mean results. In the case of the structure W03, the peak related to the second mode is somewhat lower in the case of the median floor response spectrum, whereas in the case of the third mode, there is practically no difference between the mean and median results, which is quite interesting. In the case of the structure F10, the peak related to the third mode (whose natural period is situated in the very short period range) is significantly lower in the case of the median floor response spectrum.

The errors of the "direct" comparing to the "mean" floor response spectra presented in Figure H.3 are shown in Figure H.4. A negative value of the error indicates that the "direct" spectra are smaller comparing to the "mean" spectra. It should be noted that the size of errors is related to the size of scatter of the applied input, e.g. large scatter in seismic input leads to large errors. In general, the largest errors can be observed in the case of the structure F10.

Figure H.5 shows the CVs for the considered cases of the structures W03, W10, F03 and F10, as well as the CV of the seismic input, previously presented in Figure H.1b. It is interesting to note that in the case of the structures W03 and F03, in a large part of the period range, the CVs of floor response spectra closely follow the CV of the input motions. Large values of the CVs, which indicate large scatter, are evident especially in the low period range. Note a good correlation of the magnitude of the errors in Figure H.4 and the CVs in Figure H.5.

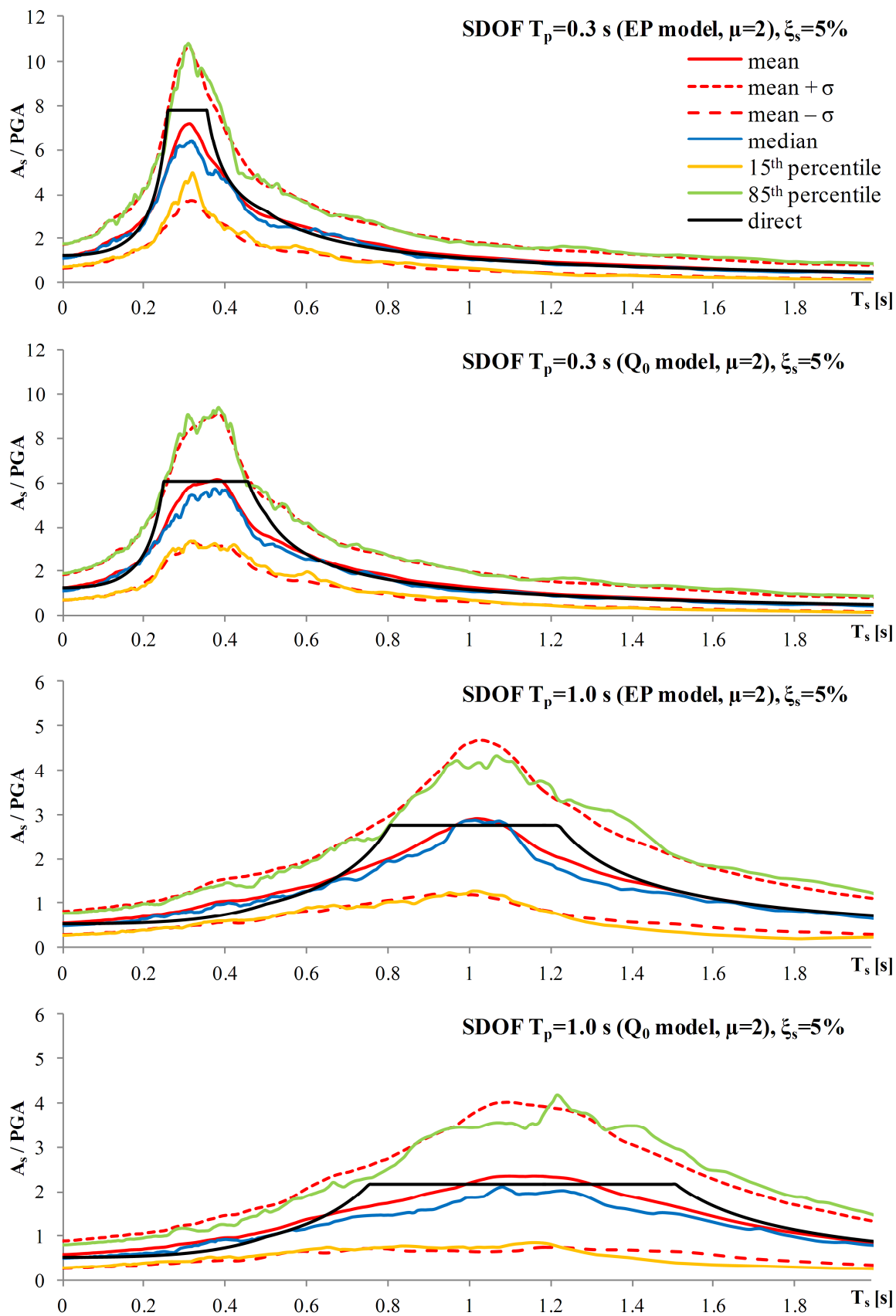


Figure H.2: Normalized floor response spectra for SDOF primary structures

Slika H.2: Normirani etažni spektri odziva za SDOF primarne konstrukcije

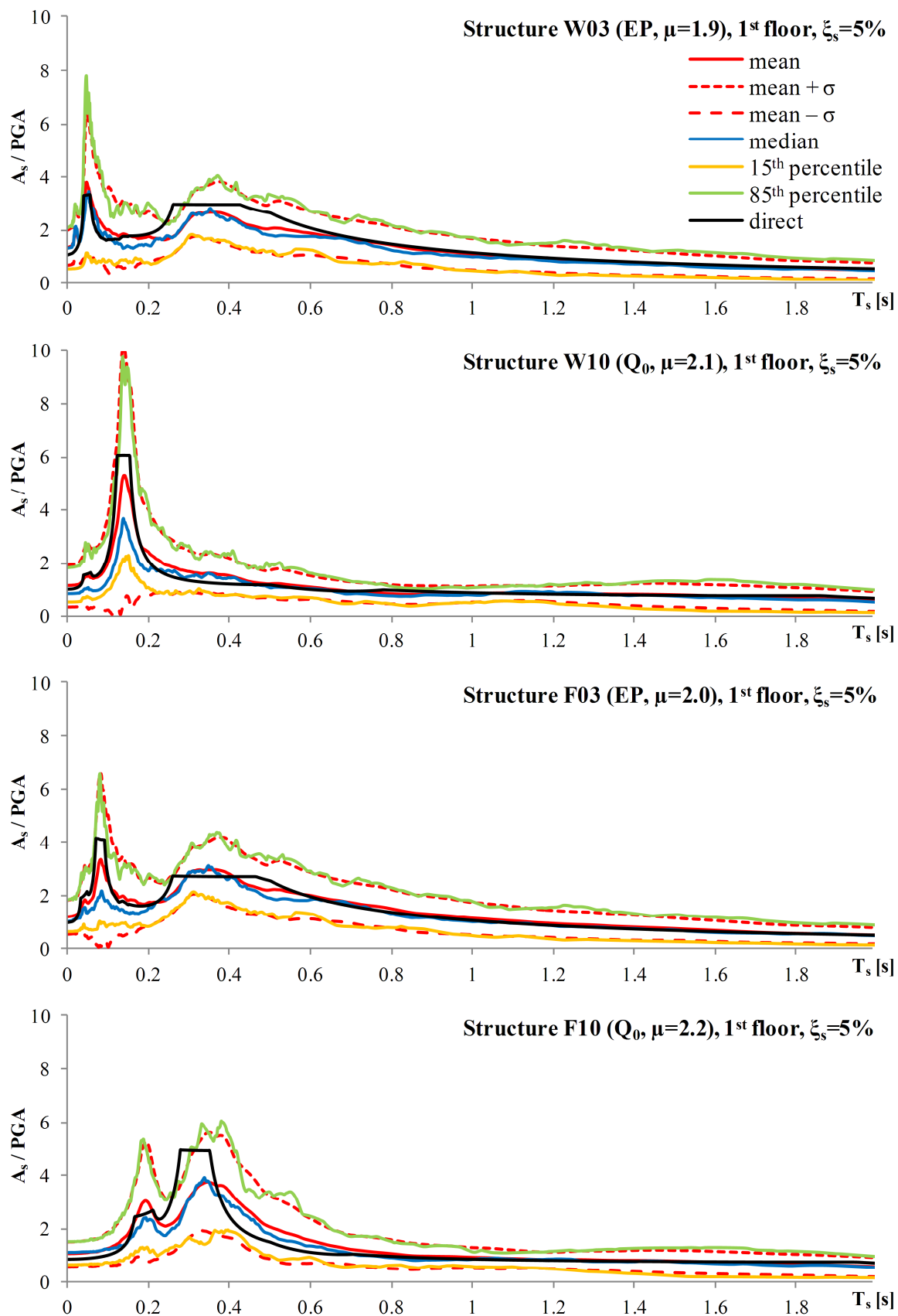


Figure H.3: Normalized floor response spectra at the first storey of the structures W03, W10, F03 and F10

Slika H.3: Normirani etažni spektri odziva v prvi etaži konstrukcij W03, W10, F03 and F10

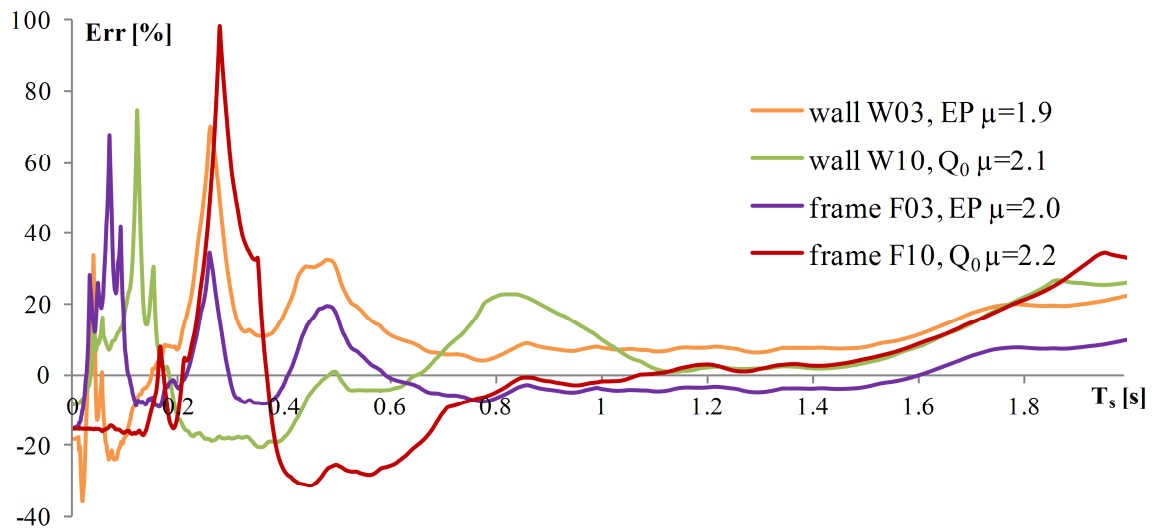


Figure H.4: Errors of the "direct" comparing to the "mean" floor response spectra
Slika H.4: Napake »direktnih« v primerjavi s »povprečnimi« etažnimi spektri odziva

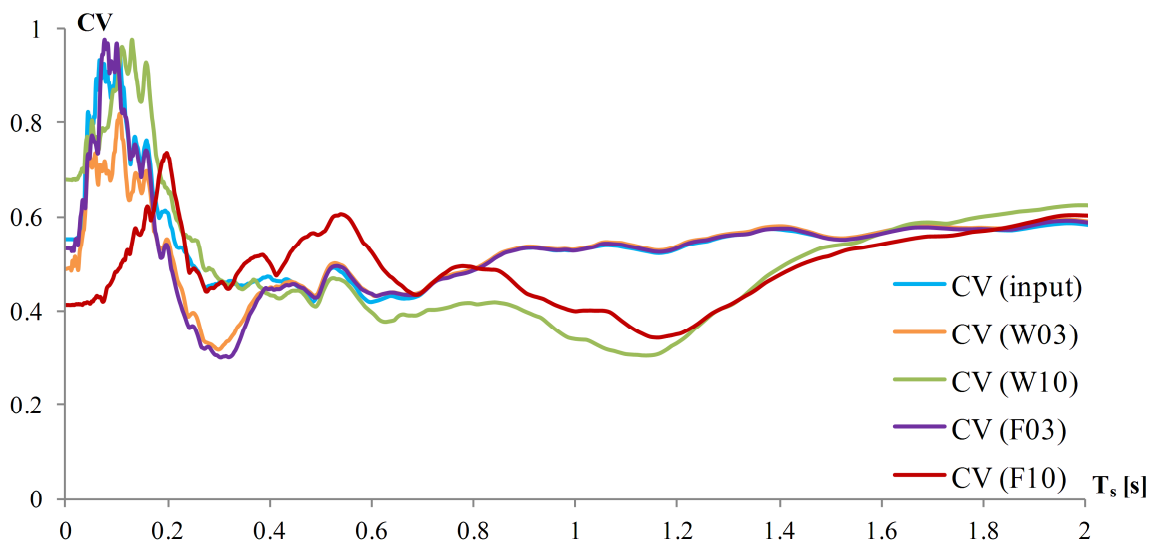


Figure H.5: The coefficient of variation for the considered cases and the seismic input
Slika H.5: Koeficient variacije za obravnavane primere in za potresni input

